AD-774 066

AERODYNAMICS OF AIR CUSHION VEHICLES

V. I. Khanzhonkov

Army Foreign Science and Technology Center
Charlottesville, Virginia

4 October 1973

DEPARTMENT OF THE ARMY
U.S. ARMY FOREIGN SCIENCE AND TECHNOLOGY CENTER
220 SEVENTH STREET, NE.
CHARLOTTESVILLE, VIRGINIA 22901

TRANSLATION

In Reply Refer to:
FSTC HT 23 1556-73
DIA Task No. T70 23 01

Date: 4 Oct 1973

ENGLISH TITLE: AERODYNAMICS OF AIR CUSHION VEHICLES

SOURCE: AERODINAMIKA APPARATOV NA VOZDUSHNOY PODUSHKE
Moscow, "Mashinostroyeniye" Press, 1972, 328 pp.

AUTHOR: V. I. Khanzhonkov

LANGUAGE: Russian

COUNTRY: USSR

REQUESTOR: G. E. Dibbern, 5

TRANSLATOR: Leo Kanner Associates (AC)

ABSTRACT: The book presents the physical fundamentals of the aerodynamics of air cushion vehicles, results of experimental studies on nozzle installations forming the air cushion, and an approximate theory for determining the aerodynamic characteristics of a vehicle from specified geometric parameters of its flow-through section. Functions are derived that determine transverse static stability of an air cushion vehicle with a sectionalized nozzle installation. Relationships are set up between the drag of the flow-through section, the lift properties of the vehicle, and the aerodynamic characteristics of fans. A complex of parameters is outlined for the aerodynamic calculation of a vehicle in the hovering regime. The book is written for engineers and designers working on different kinds of air cushion vehicles.

NOTICE

378

TABLE OF CONTENTS

AUTHOR'S ABSTRACT

Khanzhonkov, V. I. Aerodinamika Apparatov na Vozdushnoy Podushke (Aerodynamics of Air Cushion Vehicles), Moscow, "Mashinostroyeniye" Press, 1972, 328 pp.

In the book are presented the physical fundamentals of the aerodynamics of air cushion vehicles; results of experimental studies on nozzle installations forming the air cushion are set forth; and an approximate theory is given for the determination of aerodynamic characteristics of a vehicle from specific geometric parameters of its flow-through section.

Functions are derived that determine transverse static stability of a vehicle with a sectionalized nozzle installation. The effect of the principal geometric parameters on the aerodynamic and energy characteristics of a vehicle is examined. Relationships are set up between the drag of the flow-through section, the lift properties of the vehicle, and the aerodynamic characteristics of fans. The principal methods of varying the hovering regime of the vehicle over a solid support surface are investigated. A complex of parameters is outlined for the aerodynamic calculation of a vehicle in the hovering regime.

The book is intended for engineers and designers designing different kinds of air cushion vehicles. 72 illustrations; 85 bibliographic entries.

INTRODUCTION

Approximately 40 years ago pilots noted, during tests of the first helicopters, that in direct proximity to the ground during landing an additional lift acting on the helicopter is produced. A kind of cushion is formed between the helicopter and the ground surface, softening the landing. This phenomenon is a consequence of the aerodynamic effect of ground proximity on the jet of air expelled by the lift propeller. Thus the term "air cushion" appeared for the first time.

The principle of air cushion travel at the present time is finding increasing application in varied fields of technology.

As the result of theoretical and experimental studies of air cushion vehicles and tests of different models, serving various functions, conducted in the Soviet Union and abroad, fields of application are being found in which the air cushion is an extremely effective and sometimes the only means for imparting to a given vehicle or technological process new qualities, properties, and specifications.

Attempts to utilize the air cushion in making new kinds of means of conveyance are quite natural. Air cushion vehicles have the following advantages compared to other kinds of transport:

the possibility of obtaining by means of air jets a lift force many times exceeding the reaction force of these jets at some distance from the support surface. This advantageously differentiates air cushion flight vehicles from other kinds of aircraft;

the absence of direct contact of the air cushion vehicle with the support surface, which severely lowers the drag and permits a transport conveyance with high translational velocity to be built;

the possibility of using as a support the underlying surface with any degree of viscosity. This makes it possible to produce all-terrain transport conveyances capable of moving over solid ground, boggy swamp, snow, sand, shallow water, and deep water; and

high shock-absorbing properties of the air cushion through which the weight of the vehicle is very evenly transmitted to the support surface. Small roughnesses of the support surface here have practically no effect on the smoothness of movement of the vehicle both at low and high speeds.

A modern air cushion transport vehicle is a complicated machine, combining the achievements of many fields of technology. Fans and compressors are used to produce the air cushion, while the thrust giving the vehicle its translational movement is produced by air or water propellers, water-jet, or air-jet engines. Piston and jet engines are used as the drive for the fans and propulsors. High requirements are imposed on transmissions converting torque. The vehicle hull is given advantageous aerodynamic and hydrodynamic contours. Its flow-through section often is a complicated system of channels and nozzles supplying air to the bottom section of the vehicle to produce the air cushion. The vehicle is provided with installations ensuring the requisite stability and controllability during takeoff, flight, and landing. Designing and constructing these vehicles would be impossible without scientific research studies in aerohydrodynamics.

Experience shows that air cushion vehicles can find wide application as vessels for travelling over water surface and especially over shallow water. The possibility of hovering and flight over water surface, floating, and passing over sand bars and shoals, emerging on a sloping bank, and travelling over land imparts new qualities to these vessels. These vessels can travel over impassable swamps, marshes, and driftwood, where neither water-displacement vessels nor wheeled and tracked machines can traverse. Neither piers or wharves are required for air cushion vehicles. Exiting onto a solid bank, they can receive passengers and cargo. The achieved speed of 120-170 km/hr is not the maximum for these vessels. It is not precluded that year-around operation of these vessels on rivers is possible, since they can travel over sand and ice. All this advantageously distinguishes air cushion vehicles from water-displacement vessels and hydrofoil craft.

Building prototypes of overland air cushion vehicles travelling at a shallow height above ground, in view of their considerable disadvantages, thus far cannot compete with existing means of land transportation. Severe dust formation and poor controllability hamper the operation of these machines.

Large forces for acceleration and braking of a vehicle and restraining it from side slip are required for executing maneuvers, overcoming even shallow elevations and descents, and for travelling obliquely. These forces can be produced at the penalty of a large power outlay of engines and the employment of complicated control devices.

Maintaining contact of an air cushion vehicle with the ground surface by means of wheels or tracks makes it possible to build land transport vehicles with new properties. If some of the weight of the vehicle is transferred to the ground in a dispersed manner by means of air cushion, then the traversability of wheeled and tracked vehicles can be appreciably increased and machines can be built with high load capacity that is beyond known kinds of conveyances.

The problem of aerodynamic control disappears for air cushion vehicles in which the support units (wheels, tracks) are partially unloaded, and it becomes possible to operate these machines on roads and in populated places.

Employing partial unloading of the support units makes it possible to build a machine with more advantageous power characteristics, since it becomes possible to appreciably reduce the required air flow and to simplify the devices forming the air cushion. Problems associated with aerodynamic achievement of stability of travel fade away. This, in turn, leads to the possibility of using fans at low pressure, which appreciably lowers the aerodynamic noise. Dust and splash formation are also reduced, since the escape velocity of the air jets for a vehicle with partial unloading of the support units is less than in a vehicle with total separation from the ground, given the same overall dimensions.

Bright vistas unfold for the air cushion principle applied to the building of high-speed transport conveyances travelling over specially prepared roads. By maintaining a rail car on an air cushion over a rail bed or over a route made in the form of support rails, channel-trough, or tunnel, and by producing thrust with an air propeller, jet engine, or special electric motor, it becomes possible to produce a ground transport conveyance with a velocity several times greater than the speed of a railway train.

At the present time another important field of use for the air cushion has been noted -- its employment in the metallurgical industry for the heat treatment of roll and sheet metal, especially light alloy metal.

The use of the air cushion makes it possible to introduce radical changes into the design of furnaces and to appreciably improve the technological process of heat treatment. It becomes possible to assign to the air cushion two functions simultaneously: heating (cooling) of the sheet and its transporting.

Rapid and uniform heating or cooling of sheet and roll strip with jets producing an air cushion yields a homogeneous metal structure with small grain, strictly regulated cooled working, and a narrow range of mechanical properties both in the longitudinal and the transverse sheet directions. The sheet is supported in the furnace with the same jets in the suspended state, which permits retaining its high surface properties, since the sheet has no direct contact with furnace parts over the entire route of its travel during heat treatment. The high rate of sheet heating and cooling combined with the transporting operation makes it possible to build a high-capacity furnace with small overall dimensions and with a high efficiency.

Methods of air cushion production are being steadily improved, and the scope of its application for the most diverse technical purposes is broadening. Aircraft with air cushion landing gear are being tested for takeoffs from a landing on unprepared ground. The first successful experiments in transporting drilling rigs in petroleum fields on air cushions are a matter of record. Transport platforms on air cushions are being employed in moving freight and equipment within rooms during installation work. The air cushion is used in metalworking machines and manipulators for supplying machining stock; support towers are put into place more easily with the aid of air cushions. Asbocement slabs, motion picture film during manufacture, and food products at warehouses are being conveyed on air cushions. Electric cars in intrashop transportation operate on air cushions; severely sick patients are conveyed on air cushions in clinics.

The first concepts of the possibility of increasing ship speed by supplying air under its bottom section were advanced as far back as the 19th century. In 1875 the British scientist Froude raised to the prospect of reducing the resistance of water to ship motion by introducing a thin air interlayer between its hull and the water. In 1882 the Swedish inventor Laval patented it, and then built on models and in a prototype craft the so-called "water lubricant." At the same time attempts to achieve this effect were unsuccessful. Research work on practical implementation of this principle often was halted and then resumed.

The principle of air cushion travel was most completely and clearly substantiated in 1927 by K. E. Tsiolkovskiy [58], who was the first to express the idea that by supplying compressed air under the bottom of a means of conveyance it can be raised by some height into the air above the ground surface and maintained in this position, and by imparting the necessary thrust it can be given extremely rapid speeds of translational motion at relatively small power outlay.

K. E. Tsiolkovskiy established that the friction of a train is nearly entirely eliminated by excess air pressure between the flow of rail car and the railroad bed adjoining it, and the pumped air raises the train by several millimeters and is expelled along the edges of the base of the car. Several proposals to implement this principle advanced by K. E. Tsiolkovskiy were implemented in natural structures and designs for present-day machines.

The first air cushion vehicle built in the Soviet Union was the L-1 craft, built and tested by V. I. Levkov in 1934. This two-seater with a water displacement of 1.85 tons had two 110 hp M-11 engines, driving propeller-fans, and could travel over water, sand, plowland, and snow at speeds up to 60 km/hr. V. I. Levkov had begun his work on building it air cushion vehicles as early as 1927 in the aerodynamic laboratory of the Novocherkassk Aviation Institute. There he conducted extensive experimental studies on various models, the first of which was tested in 1931. Under the supervision of V. I. Levkov an entire series of air cushion

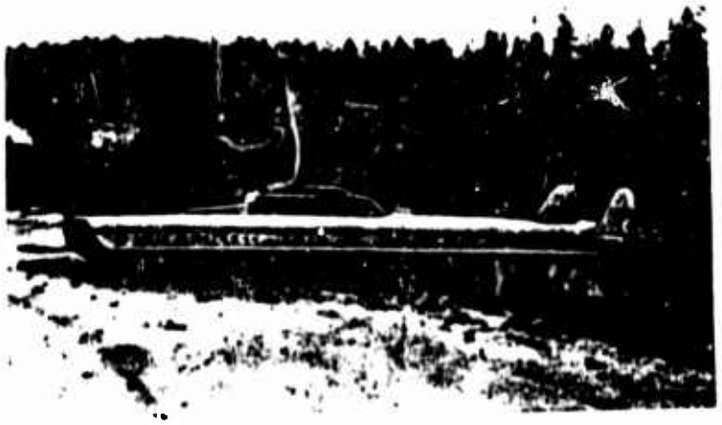

Fig. 1. L-5 air cushion craft (designed by V. I. Levkov, 1935

craft were built, capable of travelling over deep water, shallows, crossing sand bars and shoals, and on emerging onto a bank, of travelling over dry land. One of these craft (Fig. 1) with a water displacement of 8.6 tons and equipped with two 890 hp M-25 engines, built in 1935, displayed a speed over water that was unprecedented for that time -- 155 km/hr.

Late in the 1930's an attempt was made in the Soviet Union to employ an air cushion device on an aircraft in place of landing gear for takeoffs and landings on unprepared soil. This device was built under the supervision of A. D. Nadiradze on the UT-2 aircraft in 1941 and was tested by test pilot I. I. Shelest. The approval of this installation pointed to the theoretical possibility of giving aircraft new takeoff and landing capabilities.

In 1953 G. S. Turkin proposed the design for an all-terrain nonwheel transport vehicle with a nozzle system of air cushion formation. During the two subsequent years he built several models of air cushion vehicles, and then a light experimental machine equipped with two motorcycle engines driving axial bands to supply air to the nozzles. In this vehicle the nozzles were arranged along the perimeter of its bottom. Tests were made of this vehicle in 1955. In 1957 the first single-place all terrain air cushion vehicle was also tested, built under the supervision of V. N. Kozhokhin.

In the 1950's interest in air cushion vehicles rose sharply both in the Soviet Union as well as abroad. From 1953-1954 air cushion vehicles began to be investigated in Great Britain and the United States, and in recent years, especially after the construction in 1959, on the proposal of British designer C. C. Cockerell, of the experimental Hovercraft air cushion vehicle, the SR. N-1, also in many other countries.

In recent years several experimental air cushion transport vessels have been built in the Soviet Union.

The year 1962 saw the completion of the building of the experimental Neva air cushion passenger vessel (Fig. 2). The platform of this vessel, equipped with two floater-side bodies and with bow and stern flaps installed between them, forms the chamber for the air cushion. The following are situated in the superstructure on the platform: the wheelhouse -- in the bow section, compartments for the fan and for fan engines -- in the central amidships, and two 38 passenger-place lounges -- along the sides. The air cushion is produced with two 2-m diameter axle fans, and the thrust for the translational motion is provided with a 2.5-m diameter air propeller. A 225 hp piston aircraft engine drives each fan, and the air propeller is driven with a 285 hp piston engine. The ship is controlled with rudders installed behind the air propeller, and with rotary plenum chamber flaps. The ship length is 17.3 m, its width is 6.6 m, its height from the base line is 2.6 m, and its water displacement is 8.5 tons.

Full-scale tests revealed adequate stability and controllability of the vessel when travelling on its air cushion. The ship showed a speed of about 60 km/hr over quiet waters. It freely emerges onto sloping banks and traverses sandbars. Wind-driven waves up to about 0.5 m in height do not impede its motion at any heading with respect to the wave direction.

In 1961 workers at the Krasnoye Sormovo Plant and the TsAGI [Central Institute of Aerohydrodynamics imeni N. Ye. Zhukovskiy] developed an aero-hydrodynamic layout and in 1962 built the Soviet Union's first air cushion river craft, the Raduga (Fig. 3), with nozzle configuration. The craft is a planform oval platform on which is situated a streamlined superstructure. The nozzle section is built into the platform, consisting of a single-pass nozzle, two longitudinal and two transverse stability nozzles. To improve the seaworthy qualities, the bow formations of the craft were profiled according to smooth curves.

The following are situated in the superstructure: the deckhouse with places for the pilot and four passengers, and 1800-mm diameter axle fan, and a 215 hp aircraft piston engine driving the fan. The thrust for movement is provided with a reversible two-blade 2450-mm diameter air propeller with a shaft-mounted 240 hp engine. The water displacement of the craft when empty is 2.3 tons. It is 9360 mm in length, 4120 mm in width, and 3420 in height (including the air propeller). Craft control is provided with two air rudders mounted aft of the air propeller.

Trial launches were held in the autumn of 1962, and stand, mooring, and run tests -- in 1963. The greatest speed over quiet water was about 110 km/hr, and about 60 km/hr for travel over icy snow-covered surface. The craft rose to 120 mm over hard ground, and up to 150-170 mm when travelling over water surface at speeds upwards of 80 km/hr. The craft emerges onto sloping banks, travels over sandbars and, without slowing down, moves from the beach to the water. In 1965 an elastic enclosure was installed at the nozzle section of the craft, permitting greater craft traversability. The craft freely passes over driftwood in the river.

Fig. 2. Neva air cushion passenger vessel (1962)

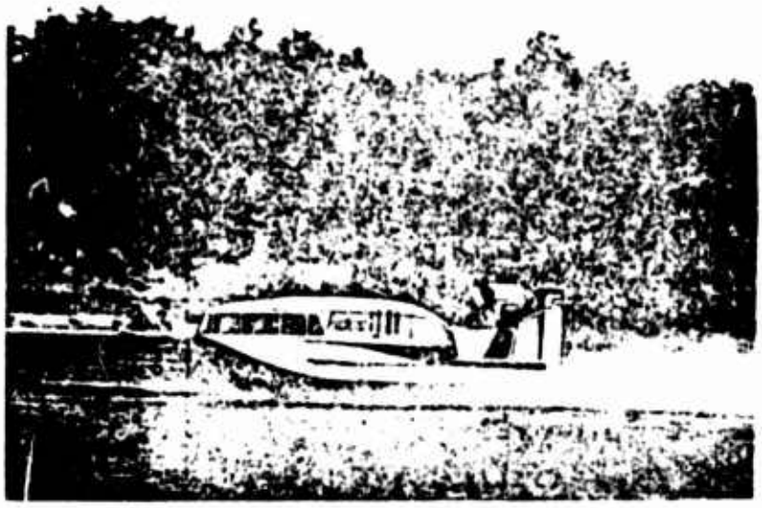

Fig. 3. Raduga air cushion craft (1963)

In 1963 designers of the Krasnoye Sormovo Plant, jointly with scientific personnel of the TsAGI developed plans and in 1965 launched the Sormovich air cushion passenger vessel, built by the Krasnoye Sormovo Plant (Fig. 4). It consists of a lift platform and a zigzag-shaped superstructure mounted thereon. The deckhouse is in the bow section of the superstructure, a 50-passenger lounge is amidships, and a machine complex consisting of a turboprop engine, axial fan, and two four-blade air propellers in rings is in the stern.

The platform is equipped with float bodies giving the ship its required water displacement. The air cushion is produced with jets of air exiting from the nozzle section built into the platform and the float bodies. This arrangement consists of a contoured nozzle and two longitudinal stability nozzles. A fan and air propellers with rotating blades are employed on the ship, which makes it possible to redistribute the power supplied from the motor to the fan and to the air propellers, depending

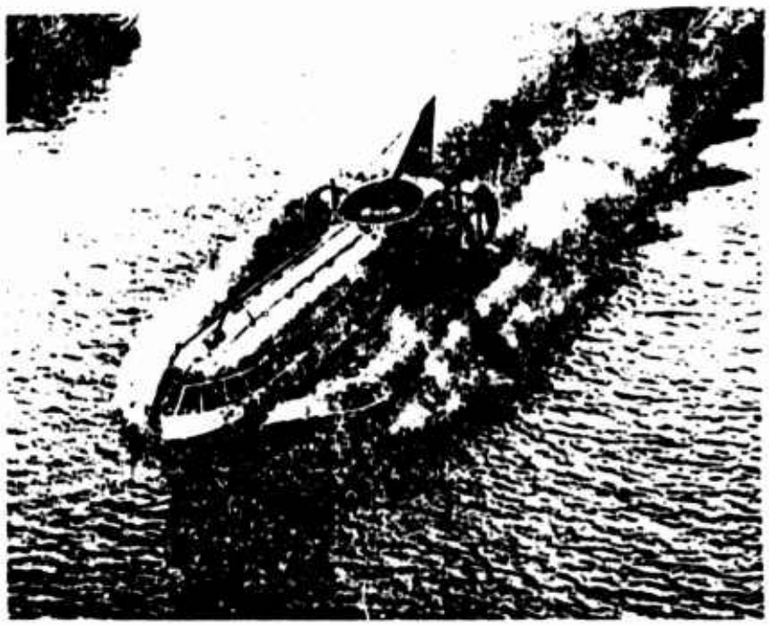

Fig. 4. Sormovich air cushion passenger vessel (1967)

on the ship travel mode. The ship is controlled with air rudders mounted aft of the air propellers and with bow and stern rotary nozzles. The water displacement of the vessel is 29 tons. Its length is 29 m, width 10 m, and height 6 m. A 3.4-m diameter fan is installed on the ship.

In stillwater tests, the ship demonstrated a speed of 120 km/hr. It is lifted above the ground surface to a height of 250-200 mm. The ship easily overcomes shallow water, exits onto sloping banks, and stops thereon.

During the past decade, in the Soviet Union and abroad, interest in air cushion vehicles has risen sharply and the number of scientific research and design-project studies in this area has corresponding risen.

In recent years Soviet scientists (G. Yu. Stepanov, Yu. Yu. Benua, K. P. Vashkevich, I. P. Lyubomirov, A. P. Biryulin, I. T. Yegorov, G. N. Sirotina, V. I. Andryutin, V. K. D'yachenko, B. N. Kolyzayev, V. A. Litvinenko, I. V. Ozimov, and S. A. Smirnov), and the designers (A. A. Zhivotovskiy, V. R. Shenberg, A. A. Smolin, and V. K. Voroastrov) investigated a number of problems in aerohydrodynamics, stability, and controllability of air cushion vehicles and have built experimental transport craft serving various functions.

CHAPTER ONE
PRINCIPAL METHODS OF AIR CUSHION FORMATION

At the present time air cushion vehicles of the most varied forms and designs are being designed and built. Various methods of air cushion formation are also employed. However, with all their diversity, general features can still be examined. For example, known craft can be divided into four main kinds in terms of the method of air cushion formation: plenum chamber, channel flow, nozzle, and vacuum chamber scheme.

1. Plenum Chamber Scheme

Craft built according to the plenum chamber scheme have a dome-shaped form in their lower section (Fig. 5 a). Into the plenum chamber formed by the dome of the craft and the ground surface a fan pumps air, which sustains excess pressure compared to the atmospheric pressure. This pressure is transmitted to the bottom of the craft and as a result a lift is produced. When the lift becomes equal to the weight of the craft as the pressure is raised, the margins of the craft cease exerting a pressure on the support surface and the entire weight of the craft is transmitted to the ground via the air cushion.

A further, extremely slight rise in excess pressure causes a lift-off from the support surface and the transition of the craft into the free hovering regime. Between the lower margin of the craft dome and the ground surface is formed an annular slit and the escape of air from the chamber outward commences. Here the value of the excess pressure in the air cushion at the moment of craft lift-off from the ground surface and in the hovering regime is determined by the weight of the craft and does not depend on the height of the lift. The lift height is only a function of the flow of air supplied under the craft.

A key advantage of craft with this configuration of air cushion formation is the relative simplicity of their execution. The dome-shaped chamber is usually formed by the craft load-bearing platform and side walls projecting below. Air enters the chamber directly from the fan without the use of air-distributing ducts and nozzles.

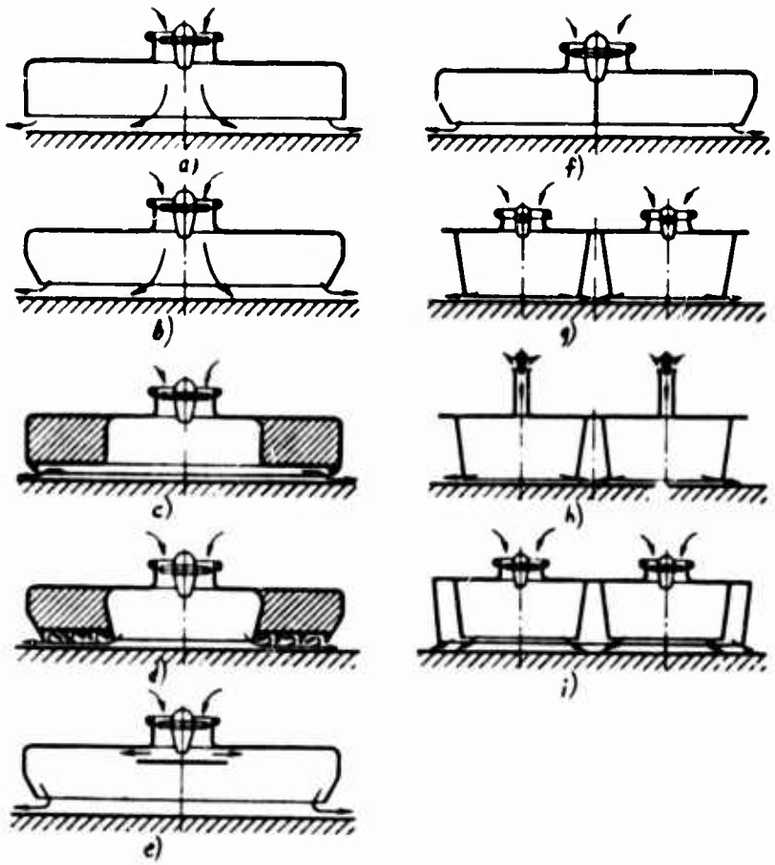

Fig. 5. Schemes for air cushion formation
a -- plenum chamber with vertical sidewalls
b -- plenum chamber with inward-inclined sidewalls
c -- plenum chamber with floaters
d -- plenum chamber with labyrinth seal
e -- plenum chamber with shield at fan exit
f -- plenum chamber with vertical partition
g -- multi-plenum chamber with fans
h -- multi-plenum chamber with ejectors
i -- multi-plenum chamber with enclosing sidewalls

.. drawback of these craft is the necessity of installing relatively high-capacity fans of relatively large overall size with the correspondingly higher power outlay, since air flow for air cushion formation rises rapidly as the craft clearance height increases. The use of craft built in this configuration becomes desirable only for very low clearance heights.

An ideal scheme of this kind of craft can be one in which air enters the chamber in a dispersed manner, and the escape of air through the annular slit occurs as if from a reservoir of very large volume when the air velocity in it is close to zero. In actual craft designs this does not appear

of execution. Usually air enters the chamber from the fan in the form of a jet with relatively small diameter. This jet streams over the support surface and is directed toward the annular slit. As the result, the kinetic energy of the jet to a large extent is lost within the chamber, the uniformity of pressure distribution over the chamber surface deteriorates, and the flow coefficient of the annular slit rises under the effect of the escaping jet. This leads to a drop in lift, higher required air pressure and volume flow, and a corresponding rise in the required power.

There are several modifications of craft built according to the plenum chamber scheme of air cusion formation. To reduce air volume flow, the side walls of the craft are given an inclination toward the interior of the chamber (Fig. 5 b). Thanks to this inclination, it becomes possible to intensify the compression of the jet escaping from beneath the side walls for the same value of the clearance between the lower margin of these walls and the support surface, and thus to reduce the volume flow coefficient.

For the case when the craft is designed as a transport vessel for overwater travel, its side walls are often made in the form of buoyancy tanks [floaters] (Fig. 5 c). These floaters give the craft its required water displacement, impart stability in the floating state, promote higher floating stability when the craft is travelling, and also serve as an enclosure of the air cushion. The lower section of the floaters are given a configuration that permits intensifying the compression of the air jet beneath the floaters and thus reducing the air volume flow required to form the air cushion.

Serving the same purpose, the side walls of the craft in their lower section are fitted with a series of projections with acute edges, which in combination with the support surface form a labyrinth seal (Fig. 5 d). In this seal the air jet encounters a series of successive compressions and expansions, due to which the resistance to the exiting of air from beneath the floaters to the exterior becomes greater and the required excess pressure, for a small air volume flow, is produced beneath the craft.

Another method capable of reducing the air volume flow in the craft is the technique of imparting an advantageous direction to air current within the chamber itself. Thus, by installing a shield close to the fan exit, it becomes possible to direct the air stream leaving the fan toward the side walls in the form of jets (Fig. 5 e). These jets, on flowing off the outlet edges of the side walls downward at an acute angle to the reference surface intensify the effect of compressing the stream as it exits from the annular slit toward the exterior and thus reduce the volume of air flow for the same craft clearance above the support surface.

Air cushion craft in the plenum chamber configuration have a substantial disadvantage: as the clearance height is increased, static stability is very rapidly lost. To enhance stability, the subdome section of the

craft is divided with a vertical partition into separate compartments (Fig. 5 f). When this craft heels, the pressure in the dome compartment located on the depressed side rises, while the pressure in the compartment on the elevated side drops. This causes a righting moment in the air cushion.

A still greater effect of enhanced static stability can achieved by installing under the craft base a group of chambers with independent air supply to each of them, for example, with fans (Fig. 5 g) or by ejectors driven from the same compressor (Fig. 5 h). A disadvantage of craft built in these configurations is the relatively low load-bearing capacity, since much of the base area outside the chambers is under a pressure that is near-atmospheric and participates virtually not at all in lift production.

This drawback can be eliminated to a large extent by installing a common chamber with side walls arranged along the perimeter of the craft base and enveloping a group of small chambers (Fig. 5 i). Air passing through the interior chambers in this craft reaches the common chamber, and then via the gap between the side walls of the common chamber and the support surface exits externally. Two zones with different pressures are formed beneath the craft: one -- within the small chambers, and the others — outside these chambers, enclosed by the side walls of the common chamber.

A craft built in this configuration has relative high lift and is marked by a fairly high longitudinal and transverse static stability. When both the common chamber and the small chambers are made of an elastic material, the craft can be given enhanced traversability.

3. Channel-Flow Scheme

A characteristic structural element of craft built in the channel-flow scheme is a longitudinal channel formed by the craft bottom and the support surface for removal of air from the fan and its discharge predominantly toward the stern (Fig. 6 a). The stream of air exiting through this channel can simultaneously also form the air cushion, supporting the craft at some height above the support surface, as well as producing the thrust that gives the craft translational movement. The excess pressure within the channel forming the lift is produced by further compression of the channel opening with adjustable flaps, while the thrust is induced from the reaction of the exiting jet stream.

The movement of this kind of craft is controlled with stern flaps, and also with a rudder mounted in the jet of air aft of the discharge opening of the channel (in Fig. 6 a the rudders are not shown). If the adjustable flaps are opened wide, the stream of air leaving the fan ejects air from the bow section of the channel and entrains it toward the stern. If the flaps are opened only slightly, some of the air supplied by the

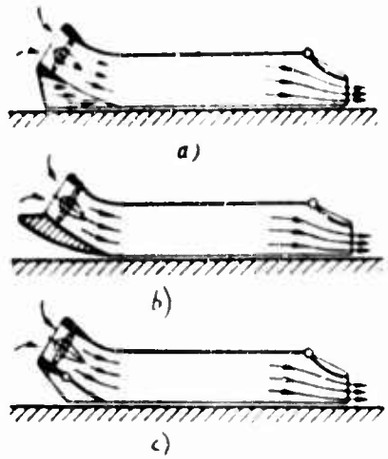

Fig. 6. Schemes of air cushion formation:
a -- channel flow
b -- channel flow with dead-end bowl formation
c -- channel flow with rotary bow flap

fan stream toward the bow opening of the channel and exits externally. When the craft is travelling under the effects of free-stream flow, the escape of air through the bow opening is weakened, and beginning at some velocity the free-stream air flow at the craft passes beneath it.

An advantage of a craft built in this scheme is the possibility of providing with the same propulsion (fan) both craft lift and craft propulsion. This makes it possible to reduce to the minimum the momentum drag on the craft associated with overcoming forces of resistance of the still external air sucked into the craft. In addition, in craft built according to the scheme it becomes possible to achieve the accelerated movement of the flow along the path from the fan to the exit of the channel by profiling of the channel and in this way to markedly lower the pressure losses occurring in the expansion of the flow, that are inevitable in nearly all other schemes of air cushion formation.

Craft built in this scheme exhibit increased traversability, since it becomes possible to make an opening in the bow section of the craft hull for surmounting relatively large surface irregularities, including waves, when the craft is travelling over space water.

A disadvantage of these craft is the displacement of the point of application of the resultant of pressure forces to their bottom section in relation to the position of the adjustable flap in the discharge

opening of the channel and in relation to the change in the fan operating regime and, as a result, difficulty in ensuring stability of craft propulsion and its controllability.

Another craft variant built in the flow-channel scheme of air cushion formation is shown in Fig. 6 b. In this craft the inlet opening of the flow channel is covered with the bow section, reducing the escape of air toward the side of craft motion, and flaps are installed in the exit opening of the channel just as in the scheme shown in Fig. 6 a, permitting adjustment of the thrust in the horizontal direction, and rudders serving to induce a moment relative to the vertical axis, turning the craft toward the desired side, are also installed at the exit opening of the channel. In this case the pressure distribution at the craft bottom depends to a large extent on the position of the adjustable flaps and the fan operating regime.

The installation in the bow section of the channel of a rotary flap (Fig. 6 c) permits more flexible craft control.

f. Nozzle Scheme

The distinguishing feature of a craft built in the nozzle scheme of air cushion formation is that its bottom section is provided with a peripherally arranged slit-like nozzle for discharging the air jet toward the ground surface (Fig. 7 a). Air from the fan is brought to the nozzle by means of a receiver or profiled channels located in the craft hull. Excess pressure in the air cushion in this case is produced by the reaction force of the jet exiting from the nozzle and streaming over the ground surface in radial directions from the craft. To enhance the air cushion pressure, the air stream is directed beneath the craft at some acute angle to the ground surface. In these craft, when in the hovering regime, the excess pressure in the air cushion is always less than the total pressure expanded in producing the jet.

The lift force sustaining the craft at some height above the ground surface is composed of the pressure forces acting at the craft bottom on the air cushion side and the vertical component of the reaction force produced by the air jet exiting downward. At small clearance values, the pressure forces acting on the craft bottom are the fundamental forces raising the craft into the air. The vertical component of the reaction force of the jet is small in this instance. As the craft clearance is increased, the role of these forces changes: the pressure forces of the air cushion decrease while the reaction force becomes greater. Thus, the lift force is reduced for craft with nozzles having a small flow-channel width with increase in clearance height.

Use of the nozzle configuration makes it possible to build air cushion craft with relatively large flight height for small power outlay. The advantage of using this scheme is due to the fact that by employing a

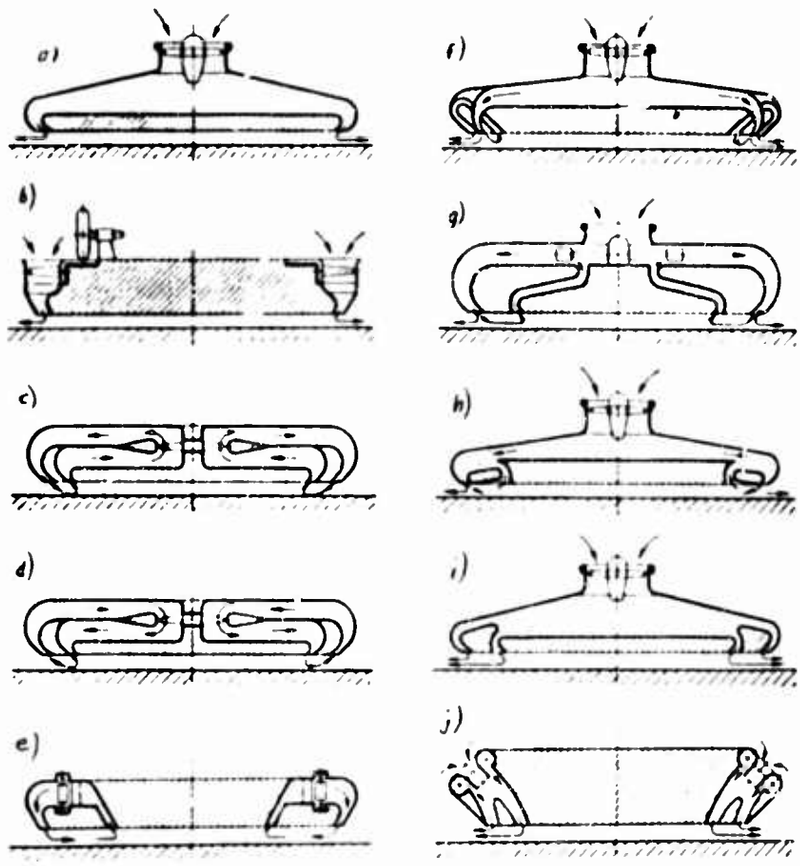

Fig. 7. Schemes of air cushion formation

a -- single-pass nozzle
b -- nozzle with built-in fan
c -- nozzle arrangement with recirculation from outer nozzle to inner
d -- nozzle arrangement with recirculation from inner nozzle to outer
e -- nozzle arrangement with recirculation through built-in belt fan
f -- nozzle arrangement with partial recirculation through additional delivery nozzle
g -- nozzle arrangement with partial recirculation through fan
h -- nozzle arrangement with partial ejector recirculation
i -- two-pass nozzle arrangement
j -- two-pass nozzle arrangement with ejector

nozzle with a narrow channel opening and directing the air jet toward the air cushion side, the required clearance height can be provided for a craft of specified weight and overall dimensions, for small air volume flows.

To produce the air cushion for a craft built in this configuration, a flow of air at relatively greater pressure and small volume expenditure is required, along with relatively high-head fans of low capacity. This permits employing fans of relatively small size on the craft.

At the present time these craft have gained the greatest acceptance. Depending on the purpose of the craft and the requirements imposed on it, the most diverse craft variants and modifications are employed. Let us look at several of the most typical.

In craft built in the nozzle configuration, air from the fan is brought to the nozzle installation through channels laid in its hull. The hydraulic resistance of these channels to the passing air stream is detrimental, since it is not directly related to the effect of air cushion formation and makes it necessary to employ a fan with higher head and additional power expenditure.

A craft with a nozzle installation not employing air ducting is known. Fig. 7 b shows a scheme of this kind of craft. Its fan is built into the hull and the nozzle in such a way that the working vanes are located directly in the entrance of the annular nozzle and the hub serves as the actual base of the craft. External air is sucked into the nozzle directly from the ambient atmosphere and exits from the nozzle in the form of an annular jet directed under the craft bottom.

This installation permits not only bypassing the use of air ducting and associated detrimental resistances, but also the superior use of dynamic pressure built up by the fan.

A key disadvantage of this kind of craft is the necessity of employing large fans. The complexity of design of the fan as well as the transmission to it renders these craft unsuitable for transport vehicles. This scheme can be used in building small craft with small clearance heights.

In craft with a single-pass nozzle installation (cf. Fig. 7 a), the entire volume of the external air sucked in by the fan exits at high velocity through the nozzle into the surrounding atmosphere and its kinetic energy is completely lost. When this craft is travelling, additional drag is produced, caused by the forces of inertia of the still external air sucked in, referred to as momentum drag. The value of this drag is directly proportional to the amount of air passing through the craft and to the craft velocity and is comparable in value to other main kinds of drag.

Craft built in the nozzle configurations with air recirculation (Fig. 7 c and d) permit a reduction in the kinetic energy losses of the jets and lower momentum drag by trapping the exiting air streams and using them again to form an air cushion.

Variants of nozzle configurations with air recirculation are differentiated, differing by the method of arranging the delivery and suction nozzles in the craft base. In the first variant a delivery nozzle serves as the external nozzle located in the base periphery, and a suction nozzle serves as the internal nozzle. In the second variant a suction nozzle is the external nozzle, and a delivery nozzle is the internal. Accordingly, in the first variant jets are directed from the periphery toward the center of the base, and in the second -- from the base center toward its periphery. In craft whose schemes are shown in Fig. 7 c and d, recirculation air is moved by an axial fan located in the craft hull.

One design solution of these craft is the use of a belt fan built directly into the nozzle installation (Fig. 7 c). The blades of this fan are secured to special belts moving on guides along the nozzle. Depending on the position of the blades on the belts, a given variant of flow direction of recirculation air in the nozzle installation can be attained.

Experience shows that nozzle installations with air recirculation are less efficient compared to ordinary single-pass nozzles with air discharged externally, since a smaller excess pressure in the air cushion and a weak lift are achieved. The necessity of installing a suction nozzle and auxiliary ducting in a craft in order to achieve recirculation produces additional drag, exceeding the dynamic pressure of the air jet exiting from the delivery nozzle and bringing to naught the apparent possibility of employing the kinetic energy of the jet.

A nozzle installation whose scheme is shown in Fig. 7 d, for very small clearance heights, has a property of adhering to the surface, that is, has a negative lift. When at the ground surface a craft fitted with this kind of nozzle installation cannot rise independently when the fan is operating.

There are nozzle installations with partial recirculation in which the air jet splits into two parts on exiting from the delivery nozzle: one part streams out, and the other is diverted beneath the craft and then via additional ducting again enters the air cushion.

Nozzle installations whose schemes are shown in Fig. 7 f, g, and h can serve as examples.

In the installation built according to the scheme of Fig. 7 f, air is bled directly from the air cushion and via auxiliary ducting built in the craft hull is discharged toward the ground surface via auxiliary delivery nozzles. Air leakage from the air cushion is replenished by jets splitting off from the main air jets. Flow in the auxiliary ducting is maintained by the excess pressure in the air cushion.

The installation built according to the scheme in Fig. 7 h differs in that some of the air splitting away from the main jet toward the air cushion is sucked in by the fan through additional ducting, and is then

brought to the delivery nozzle and together with the externally escaping air is discharged toward the support surface.

In the nozzle installation (Fig. 7 h) partial recirculation of air is achieved directly in the delivery nozzle. It is assumed that the pressure rise in the air cushion results from the diffuser effect as air flows toward the air cushion in the gap formed by the profiled section of the nozzle bottom and the support surface. The recirculation flow in this installation is produced by the ejecting action of the stream of air fed by the fan into the upper section of the delivery nozzle.

Nozzle installations with partial recirculation, shown in Figs. 7 f and g, are aerodynamically also less advantageous than ordinary single-pass nozzles, since their suction ducts produce high additional drag. Local pressure losses in the bending of the recirculation air stream and also pressure losses in the ejector when the active stream merges with the recirculation stream render the nozzle installation shown in Fig. 7 h inefficient.

Nozzle installations with complete as well as partial recirculation are complex in design, take up a large fraction of the area of the craft base, and require expanded hull volume to house the reverse ducting. These installations have thus far not gained practical acceptance. Nozzle installations employing air recirculation that are advantageous from the aerodynamic point of view and that are feasible as to design have thus far not been found. Nozzle installations with a recirculation system are generally unsuitable for application on transport craft, since they suck in dust, snow, and splashing water through the channel flow of the craft, which rapidly renders them inoperative.

Experience shows that craft with single-pass nozzles exhibit very low stability. Raising this kind of craft by a height of 1.5-2 percent of the nozzle width already causes heeling. Increasing hovering height leads to total loss of stability and the craft rests on the lower edge of one side against the ground. This is caused by the fact that the nozzles on the depressed and elevated sides, during heeling, are at different heights above the support surface and the jets exiting from the sides produce reaction forces directed toward the air cushion differing in magnitude, and thus dissimilar excess pressures.

All this results in the air jet on the depressed side close to the surface splitting into two and some of it moving toward the elevated side. As this takes place, at the depressed side the reaction force of the jet directed toward the air cushion weakens and the ejecting action caused by recirculation of air in the cushion rises. As the result, the pressure in this cushion zone falls off, and thus the pressure over the section of the bottom near the elevated side is also somewhat reduced. A tipping moment acting on the craft is thus induced.

To augment stability, the single-pass nozzle installation is sectionalized into individual sections with additional nozzles -- stability nozzles. Fig. 7 i shows a two-pass nozzle arrangement of an air cushion vehicle. When this kind of craft yields under the effect of the external moment, the pressure rises over the section of the bottom between the outer and the inner nozzles near the depressed side, while the pressure is reduced over the symmetrical section of the bottom at the elevated side. As a result, a righting moment is induced in the air cushion, restoring the craft to the horizontal position after elimination of the external moment applied on the craft. Air is usually fed from the fan to this kind of nozzle installation by means of a receiver.

In several cases, when for some reason it is desired to appreciably reduce the capacity of the fan installed on a craft, nozzle installations with built-in ejector are used (Fig. 7 j). Ejection air is supplied in nozzle arrangements of this configuration at high pressure via slitlike nozzles mounted directly in the nozzle installation. The externally ejected air arrives via a slitlike header located between the ejecting nozzles. Discharge of air in the form of jets takes place through nozzles located in the craft bottom.

Excess pressure in the air cusion is produced by the reaction of the ejecting and ejected air escaping externally. This factor appreciably raises the efficiency of the ejector, however the efficiency of the craft's power plant when this device is used drops off, overall. The nozzle installation employing an ejector requires the use of a high-head fan or compressor.

There are several variants of stability nozzle placement in the craft bottom. They can be located in the longitudinal and transverse directions, in the diametral plane of the craft, near the sides, and in crosswise fashion. The determining conditions include achieving the desired craft stability and satisfying configuration requirements -- the possibility of a contingent arrangement of ducting feeding air from the fan to the stability nozzles, for small hydraulic resistance values of the stability nozzles.

In designing air cushion vehicles, one must bear in mind that the single-pass nozzle installation has the greatest load-bearing capacity. Any sectionalizing of the nozzle installation, with the same total area of the passage opening of a nozzle maintained and with unchanged parameters of the air stream fed to the nozzle, reduces the lift. In other words, introducing auxiliary nozzles into the nozzle installation to augment stability somewhat degrades its load-bearing properties. In spite of this drawback, two-pass and other methods of sectionalizing nozzles have gained the greatest acceptance and are used for craft of the most dissimilar function.

The nozzle installation in craft with the nozzle scheme of air cushion formation and side walls in craft with the plenum chamber and channel-flow configurations, built in the form of rigid metal structures, have a substantial disadvantage -- they do not permit contact with a solid support surface during propulsion. In chance incursions on surface irregularities and projections are often waves strike during propulsion over water, these devices become deformed and rapidly malfunction.

An important step in improving transport air cushion vehicles was the use of elastic air cushion enclosures. By making nozzles and side walls in the form of flexible skirts of thin elastic material (vulcanized rubber, rubberized fabric, nylon, and other synthetic materials), the most important ability of air cushion vehicles -- their traversability -- can be markedly enhanced. Flexible enclosures become kneaded upon striking obstacles and then again acquire their initial shape. Short-term change in the shape of the elastic enclosure has a neglible effect on the aerodynamic qualities of the craft.

Elastic enclosures reduce the requirements imposed on air cushion vehicles with respect to flight height. The possibility of reducing the clearance between the craft and the support surface without detracting from its traversability improves the power capabilities of the craft and permits employing fans of smaller size and power to achieve the same lift.

Aerodynamic requirements imposed on nozzles and side walls made of elastic material remain the same as for their rigid design. By imparting the shape of nozzles to the exiting areas of elastic enclosures, aerodynamically advantageous air cushion formation configurations are achieved. The main regularities of air escape from these devices achieved with respect to rigid structures can be considerably extended also to flexible enclosures serving the same purpose and of similar contours.

4. Vacuum Chamber Scheme

A method of producing lift based on inducing rarefaction between the load-bearing system of the craft and the support surface is possible. Here, to produce the lift sustaining a craft of given weight in the regime of hovering and propulsion, the load-bearing system of the craft is located beneath the support surface. This method has substantial advantages over methods based on sustaining excess pressure under the craft bottom and can be used in making transport conveyances travelling over specially prepared roads, for example, vehicles intended for monorail travel [65-66].

A schematic of air cushion formation using a vacuum chamber is shown in Fig. 8 a. The chamber of this scheme is formed by an upper load-bearing plate, vertical side walls, and (beneath) outward projecting, horizontally arranged strips rigidly connected to the walls. The opening

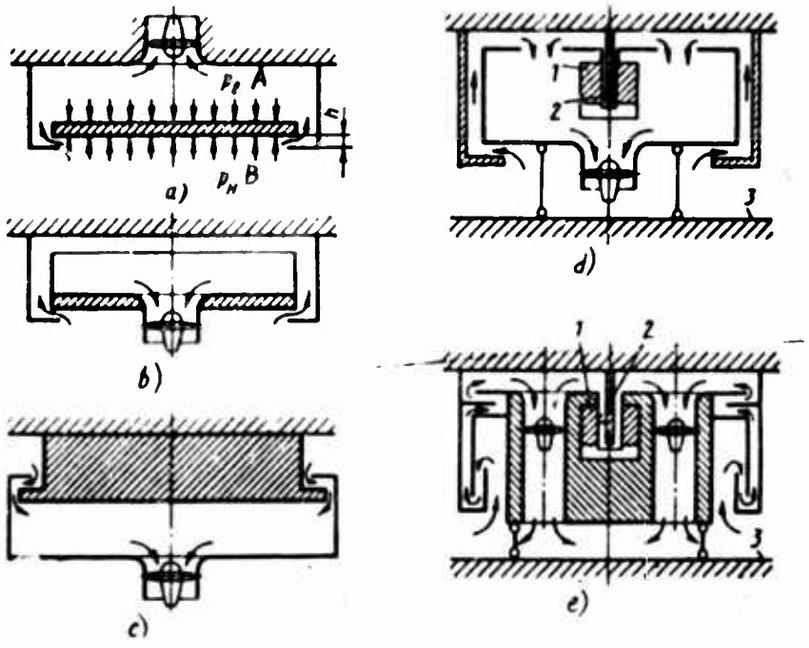

Fig. 8. Schemes of air cushion formation employing vacuum chambers:

a -- with fan built-in to support
b -- with internal support strips
c -- with external support strips
d -- with fan and linear electric motor
e -- with labyrinth seal, fans, and linear electric motor:
1 -- stator
2 -- rotor
3 -- roof of car

between the support strips is covered with a plate to which freight can be suspended. The chamber is equipped with a fan.

The working fan produces within the chamber a rarefaction, extending to its entire internal surface, including the upper surface of the plate. The drop between the atmospheric (external) pressure $p_н$ [н = external] and rarefaction within the chamber $p_в$ [в = internal] produces a force tending to lift the plate. When there are weak rarefactions within the chamber, the plate rests on the support strips. As the rarefaction is intensified, this force increases and the moment arrives when it becomes equal to the weight of the plate and the freight attached to it. In this case the plate is supported by an air cushion and ceases to exert pressure on the support strips. A further rise in rarefaction brings about the liftoff of the plate from the support strips and it rises. External air rushes into the gaps formed by the plate and strips. In this air flow, two positions of the plate in the chamber are possible:

when with rising of the plate and the corresponding increase of the jet between its edges and the support strips the rarefaction drops off, but still remains high enough so that the forces produced by the rarefaction exceeds the weight of the plate, the plate tends to move upward and then is sucked against the upper wall of the chamber -- the load-bearing plate; and

when with increase in the gap the rarefaction in the chamber drops off and the moment of equilibrium arises between the forces of rarefaction and the plate weight, the plate rises within the chamber only to a specific of height about the support strips and remains in the state of free hovering, without mechanical contact with its walls.

The second position is of practical interest in designing transport vehicles. The vacuum air cushion arrangement is built in the form of box-section beams secured to support masts, constituting a distinctive rail spur, and the load-bearing system is in the form of a carriage travelling along this spur bearing a suspended rail car.

The load-bearing system built in the scheme shown in Fig. 8 a has a key disadvantage: the fan is connected directly with the housing. To maintain the required rarefaction as the carriage is in translational motion, the housing must have fans arranged in series of its entire extent, switched on and off depending on the position of the carriage in the housing. The load-bearing system built according to the scheme in Fig. 8 b is free of this drawback. The fan is located directly on the travelling plate, and to reduce the air volume flow and to maintain the required vacuum vertical walls are formed along the plate periphery, forming a clearance with the housing supported by the plate.

The system built according to the scheme shown in Fig. 8 c differs in that the support strips are extended outward, while the side walls of the vacuum chamber in the upper section are equipped with inward-projecting horizontal flanges, which restrain the chamber on the support strips. The ducts for passage of atmospheric air within the chamber have a large number of turns and, therefore, produce great resistance to air passage. This permits producing in the chamber a rarefaction of the same value, but with smaller air flow and correspondingly lower power outlay in order to maintain the load-bearing system in the suspended state.

The air volume flow for a given clearance height of the load-bearing system over the support strips can be achieved by using a system with a labyrinth seal between the walls of the vacuum chamber and the support. By extending the ducts and introducing additional turns into them (Fig. 8 d), one can increase the resistance of the flow-through section to passage of external air within the chamber and make the load-bearing system more economical.

A linear electric motor (Fig. 8 d and e) can be used as a power plant imparting translational motion to the load-bearing system. The principle of its operation is based on the use of the effect of a running electromagnetic field. This motor consists of stator 1, which is a system of windings located on a magnetic conductor, and rotor 2 made of steel or aluminum bar arranged along the spur in the interval between the working surface of the stator, with small air gaps. The stator is mechanically connected to the load-bearing system of the rail car, and the rotor is rigidly connected to the structural elements of the spur -- the support housing. Power is supplied to the motor from ground-based electric traction substations via a contact network using current receivers.

The load-bearing system employing a vacuum chamber must not only produce the requisite lift, but also exhibit adequate stability with respect to angular displacements and side slip. An advantage of the method of producing an air cushion with a vacuum chamber is the fact that the center of gravity of the entire system (carriage and rail car) is appreciably below the point at which the lift is applied. In the event of external moments causing heeling, this system, on the effect of the moment formed by the force of gravity tends to occupy the initial vertical position.

Load-bearing systems shown in Fig. 8 a, b, and c are unstable with respect to transverse shifts caused by the action of external side forces, for example, when the carriage is moving along rail line curves, and so on. By imparting to the channels formed by the side wall of a carriage and the support wall of the housing the shape shown in Fig. 8 e, a side force can be produced that tends to restore the carriage to the center of the support housing.

With respect to aerodynamics and power considerations, the air cushion produced with a vacuum chamber is advantageous in that it permits introducing substantial hydraulic resistances along the route of external air to travel toward the vacuum chamber; these resistances produce the requisite lift for relatively small air volume flows. This not only reduces power outlays in sustaining the equipment in the air above the support surface, but also permits using small fans.

CHAPTER TWO
EXPERIMENTAL CHARACTERISTICS OF AIR CUSHION VEHICLE NOZZLES

5. Nozzles

Nozzles are the most important component (the principal working part) of an air cushion flight vehicle, whose lift qualities are produced by means of jets of air discharged mainly beneath the craft. The nozzle installation forms these jets. As the result of air jets interacting with the support surface beneath the craft, a pressure is produced that is in excess compared to the atmospheric pressure, and this excess pressure by acting on the craft bottom produces the required lift sustaining the craft over the support surface by some height both in the hovering regime as well as in flight.

By giving the nozzle installation different planform contours, arranging the nozzle slits in it in a definite fashion, and giving these nozzle slits different sizes and profiles, one can substantially affect the aerodynamic characteristics of the nozzle installation and thus, the characteristics of the craft with respect to its lift properties as well as its stability. By varying the geometrical parameters of nozzle slits during hovering and flight, to some extent one can assign the functions of craft control devices to the nozzle installation.

The necessity of a continuous supply of air beneath the craft through the nozzles to produce the air cushion involves a constant power outlay. This power is expended directly in producing the air jets as well as in overcoming detrimental resistances in the nozzles and the ducts supplying air to them. These power outlays often exceed the power outlays in overcoming craft drag and are the principal factors determining the energy characteristics of an air cushion vehicle. Therefore setting up a relationship between geometrical parameters of nozzles and the aerodynamic parameters of the air cushion, as well as selecting rational nozzle configurations exhibiting high lift qualities while satisfying the requirements of craft stability is of paramount importance.

6. Single-Pass Annular Nozzles With Profiled Generatrices

A single-pass annular nozzle is the simplest nozzle arrangement and at the same time the most advantageous as to power, since it exhibits the greatest lift capacity for assigned parameters of the air stream fed to it.

By imparting advantageous dimensions and profile to the entrance of a nozzle (rounded entrance edges) and to the guide section (usually straight walls), the total pressure of the stream of air fed to the nozzle can be transformed into dynamic pressure for extremely small total pressure loss. In a properly profiled nozzle installation, these losses amount to 1.5-2 percent of the available total pressure and they are expended mainly in the friction of the stream against the nozzle walls. Owing to the profiled nozzle, it is possible to produce a stream of air of required width with stable flow direction.

A single-pass nozzle installation can serve as a kind of reference standard in evaluating the lift capabilities of nozzle arrangements of other systems.

Annular nozzles. In an experimental determination of the aerodynamic characteristics of the air cushion produced with annular jets, three series of single-pass annular nozzles were built, differing in the width of the passage opening (b = 8, 20, and 40 mm) and in the angle of inclination of the nozzle generatrix to its axis (φ = 0, 30°, and 45°), with an identical inside bottom diameter $D_в$ [в = inside] = 400 mm (Fig. 9), for all nine nozzles tested. One of these nozzles had a passage opening with width b = 25 mm and the generatrix angle of inclination φ = 30°. Each nozzle arrangement (Fig. 10) consisted of an internal section -- bottom 2, and external — tapered rim 3 encompassing this bottom. The bottom and the tapered rim were connected with adjustable rods 2 in such a way that an annular slit was formed — a nozzle with constant width b. The exit edges of this nozzle lay in the same plane.

The bottom of each of the tested nozzles, in turn, consisted of two sections: an upper section 4 profiling the annular nozzle, and a lower section, which consisted of a circular disk 5 with drainage openings to measure pressure distribution. Twenty five drainage openings 1 mm in diameter and spaced at 15 mm intervals were made in this disk along its diameter. Three more additional openings of the same form were drilled near the edges of the disk at a distance of 15 mm from the principal series. The pressure from each orifice was transmitted via a connecting piece secured to the inner side of the disk. The same disk 5 secured to the upper part of the craft bottom was used for all the nozzle arrangements tested. The edges of the entry openings of the annular nozzles with width b = 8 mm were rounded to a radius of 5 mm; the edges of the entry openings for annular nozzles having width b = 20 mm and 25 mm were rounded to a radius of 12.5 mm; and to a radius of 25 mm --

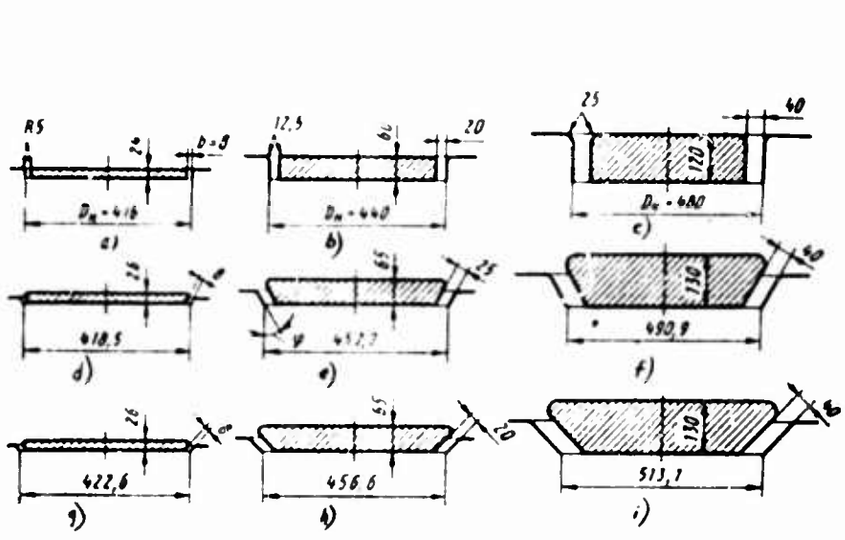

Fig. 9. Configuration of annular nozzles tested
a, b, c -- for $\varphi = 0$
d, e, f -- for $\varphi = 30^{\circ}$
g, h, i -- for $\varphi = 45^{\circ}$

for annular nozzles having width b = 40 mm. The nozzles were made of duralumin. Cast nozzle blanks were machined, and the surfaces of the nozzle walls facing the air stream were ground.

The shield over which the annular air jet streamed was a flat 950 mm diameter circular disk (Fig. 11). The side of the disk facing the stream was made smooth, and the other side was made with stiffness ribs. The shield had a hinged suspension. By using a set of rigid push rods and adjustable bolts, the shield could be given the required position with respect to the nozzle installation. On the flat side of the shield 125 drainage openings 1 mm in diameter were made along two mutually perpendicular diameters, with a spacing of 15 mm. On other side of the shield, the drainage openings terminated in connecting pipes.

experimental stand. Streaming of the annular jet on the shield was investigated on a stand (Fig. 10) consisting of a stabilizing chamber 2, replaceable measuring header 3, convergent duct 6, test nozzle arrangement 10, and sliding flat shield 11 at which the annular jet of air escaping from the nozzle collided. The flow of air in the stand was produced with a special duct connected to the entrance opening of the stabilizing chamber. In this chamber the air was uniformly distributed over the cross-section by means of metal screens 1. Screens 7 were installed in the outlet section of the convergent duct for this same purpose.

The nozzle arrangement 10 was secured to the flange of the convergent duct 6 with bolts. The pressure at the bottom of the nozzle arrangement, taken up by the drainage openings, was diverted by means of rubber hoses through a common header to the outside, to alcohol micromanometer 8.

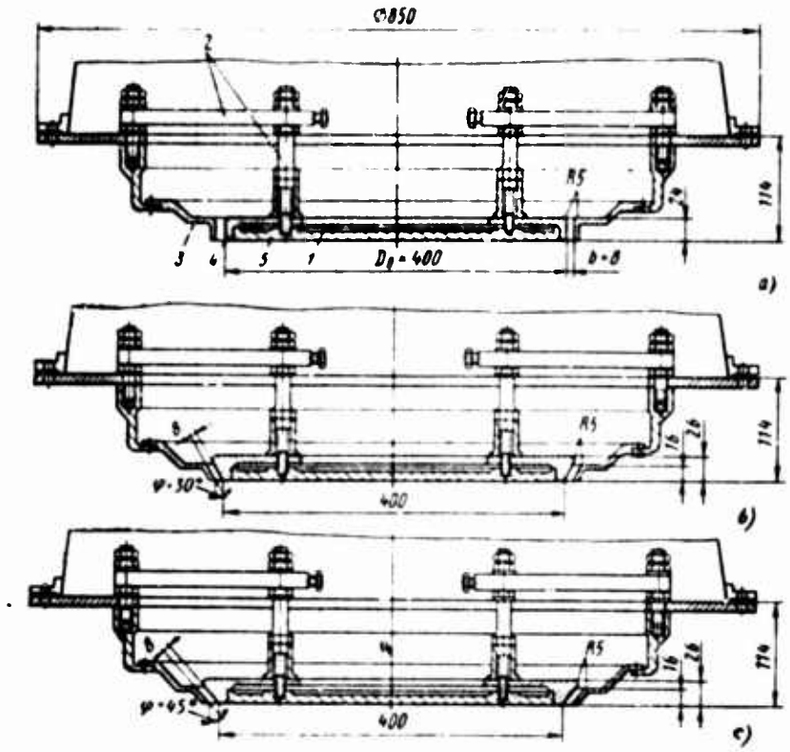

Fig. 10. Annular nozzles tested at b/D_B = 0.02:
a -- for φ = 0
b -- for φ = 30°
c -- for φ = 45°

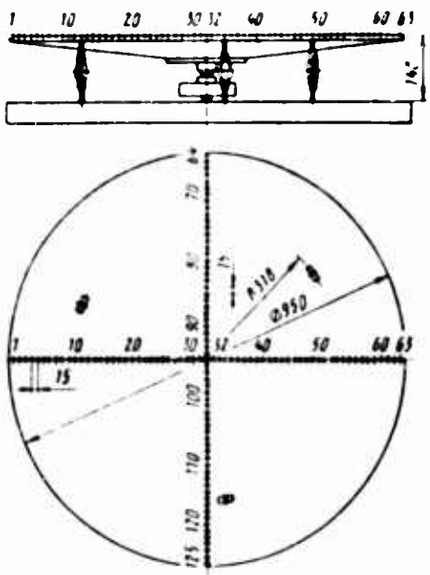

Fig. 11. Arrangement of drain openings on shield

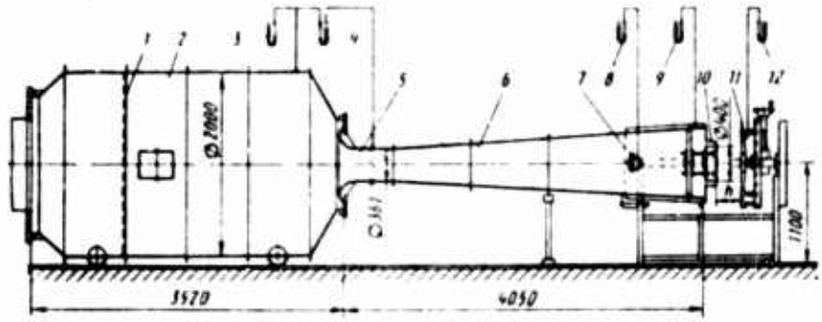

Fig. 12. Experimental stand for testing streaming of annular jet on shield:
1 and 7 -- metal screens
2 -- stabilizing chamber
3, 4, 8, 9, and 12 -- micromanometers
5 -- measuring header
6 -- convergent duct
10 -- test nozzle arrangement
11 -- shield

The shield 11 was secured on a special travelling device in such a way that the centers of the bottom of the annular jet and of the shield lay along the longitudinal axis of the experimental stand, and their drainage openings (one of two shield series) were arranged in the same plane. The travelling shield of the device consisted of a base 12 (Fig. 12) with two cylindrical guides 7 80 mm in diameter, at a distance of 1000 mm from each other, and a carriage 11 travelling along these guides by means of worm mechanism 12 driven by steering wheel 10. The terminal section of the convergent duct containing the test nozzle and the base of the travelling device were rigidly secured to each other by means of a common frame 16.

During the experiments, the shield was positioned at several distances h from the cut-off of the nozzle by means of the travelling device. The distance h was measured on the scale of a coordinate spacer, whose push rod 14 was connected to the sliding shield, and scale 13 was connected to the fixed base of the travelling device. The pressure distribution at the shield was determined with an alcohol micromanometer 9.

The volume for air fed to the nozzle was measured by a replaceable measuring header profiled along the arc of a lemniscate, installed in the stabilizing chamber. A header provided with a connecting pipe 139 mm in diameter was used for nozzles with flow-through opening b = 8 mm; and a header with a connecting pipe of 178 and 261 mm in diameter, respectively, was used for nozzles in which the flow-through opening b was 20 and 40 mm. Micromanometer 4 (cf. Fig. 12) was used to determine the pressure difference between the stabilizing chamber and the header connecting pipe, from

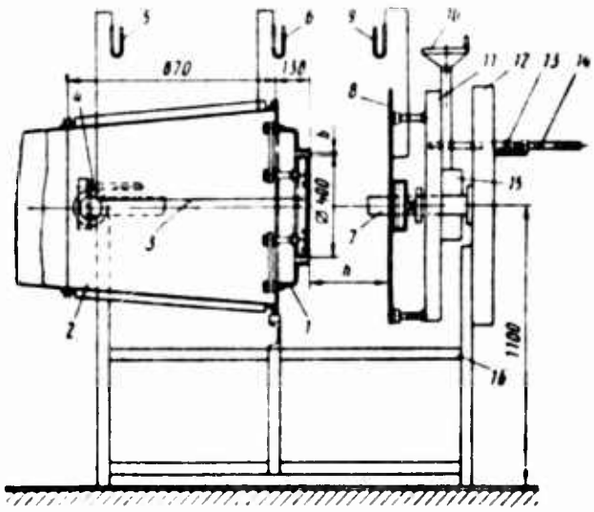

Fig. 13. Experimental stand for testing streaming of annular jet on shield

1 -- test nozzle arrangement
2 -- convergent duct
3 -- rubber hoses
4 -- common header of rubber hoses
5, 6, and 9 -- micromanometers
7 -- cylindrical guide
8 -- shield
10 -- steering wheel
11 -- carriage
12 -- base
13 -- scale
14 -- push rod
15 -- worm mechanism
16 -- frame

which the volume of air flow was calculated. The readings of micromanometer 3 were used to enter corrections in calculating the volume of air flow.

The excess pressure in front of the nozzle causing the escape of the air jet from the nozzle was measured with micromanometer 9 using a connecting pipe installed at the terminal section of the convergent duct.

Tests of nozzle arrangements were conducted by varying the mean escape velocity of air from nozzles in the range 3-55 m/sec, which corresponded to a change in Reynolds number, given in terms of the doubled width of the flow-through opening of the nozzle, in the range 10,000-280,000.

A general view of the experimental stand for nozzle testing is shown in Fig. 14.

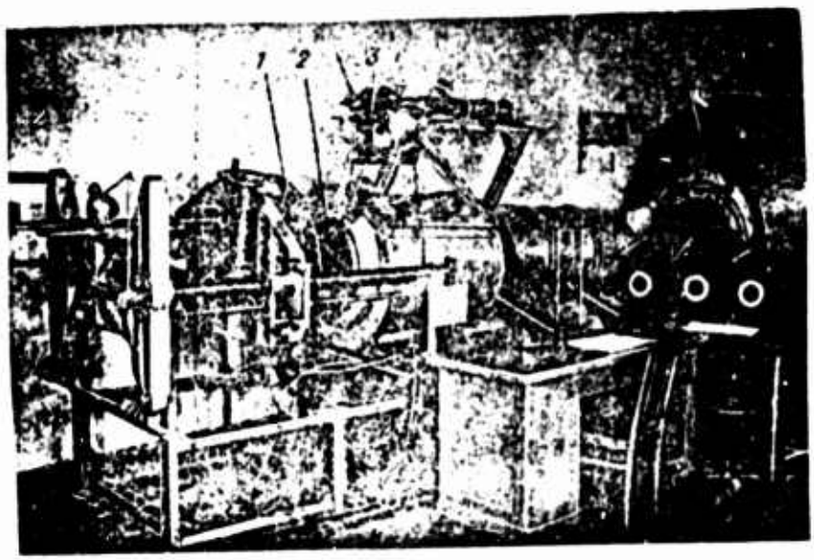

Fig. 14. General view of experimental stand for testing annular nozzles

1 -- movable shield
2 -- nozzle arrangement
3 -- coordinate spacer with pneumometric tube
4 -- stabilizing chamber

Interpretation of test results. The results of measuring the pressure distribution along the bottom of the nozzle arrangement and the shield over which the annular air jet streamed were represented as the dimensionless coefficient of the air cushion pressure:

$$\bar{p} = \frac{p_1 - p_н}{p_0 - p_н}, \qquad (1)$$

where p_1 is the pressure at the test point on the bottom of the nozzle or the shield; p_0 is the pressure in the receiver [header] (terminal section of the convergent duct) ahead of the nozzle; $p_н$ [н = external] is the atmospheric pressure (in the external space surrounding the annular jet).

The discharge coefficient of the annular jet is

$$\alpha = \frac{Q}{F\sqrt{\frac{2}{\rho}(p_0 - p_н)}}, \qquad (2)$$

where Q is the volume flow of air measured with the header of the experimental stand; F is the area of the flow-through opening of the annular nozzle; and ρ is the air density.

Note some arbitrariness in the determination of the area F of the flow-through opening of the annular nozzle for angles of inclination of the generatrix $\varphi > 0$. This arbitrariness lies in the fact that the product of the area of the exit opening (cut-off) of the nozzle by the cosine of the angle of inclination of a generatrix was adopted as the area of the flow-through opening, that is,

$$F = \frac{\pi}{4}(D_н^2 - D_в^2)\cos\varphi = \pi D_в b\left(1 + \frac{b}{D_в\cos\varphi}\right) =$$
$$= \pi D_н b\left(1 - \frac{b}{D_н\cos\varphi}\right), \qquad (3)$$

where $D_н$ is the diameter of the annular nozzle measured at the external exit edge; and $D_в$ is the diameter of the annular nozzle measured at the internal exit edge (diameter of the bottom). The geometric characteristics of the nozzle arrangements tested are as follows:

φ, град A	b, мм B	D_e, мм B	$D_н$, мм B	b/D_e	$b/D_н$	F, м² C	$S = \frac{\pi D_н^2}{4}$, м² C
0	8	400	416,0	0,0200	0,0192	0,01025	0,13592
30	8	400	418,5	0,0200	0,0191	0,01028	0,13756
45	8	400	422,6	0,0200	0,0189	0,01033	0,14026
0	20	400	440,0	0,0500	0,0454	0,02638	0,15205
30	25	400	457,7	0,0625	0,0546	0,03367	0,16453
45	20	400	456,6	0,0500	0,0438	0,02630	0,16374
0	40	400	480,0	0,1000	0,0833	0,05526	0,18096
30	40	400	490,9	0,1000	0,0815	0,05604	0,18927
45	40	400	513,1	0,1000	0,0780	0,05734	0,20677

KEY: A -- in degrees
B -- in mm
C -- in m²

The Reynolds number with reference to the equivalent diameter of the annular nozzle is

$$\mathrm{Re} = \frac{\overset{B}{d_э} v_{ср}}{\nu}, \qquad (4)$$

KEY: A -- $v_{ср}$
B -- $d_э$

where $v_{ср}$ is the mean (with respect to volume flow) escape velocity of the air from the annular nozzle; $d_э$ is the equivalent diameter of the annular nozzle; and ν is the kinematic coefficient of air viscosity.

The equivalent diameter, which is equal to four hydraulic radii of the exit aperture of the annular nozzle, is

$$d_э = 4\frac{F}{\Pi}, \qquad (5)$$

where Π is the wetted perimeter of the exit aperture,

$$\Pi = 2\pi D_e\left(1 + \frac{b}{D_e\cos\varphi}\right) = 2\pi D_н\left(1 - \frac{b}{D_н\cos\varphi}\right). \qquad (6)$$

By inserting Eqs. (3) and (6) in Eq. (5), we get $d_э = 2b$, and therefore

$$Re = \frac{2bv\gamma\rho}{\mu}.$$

The Reynolds numbers used in plotting the aerodynamic characteristics of annular nozzles were determined by this formula.

Effect of Reynolds number on pressure and discharge coefficients. Experiments conducted with annular nozzles show that the nature of pressure distribution along the nozzle bottom and along the shield, as well as the value of the coefficients of pressure p and discharge α, for a specified arrangement of the nozzle installation with respect to the shield, have practically no dependence on the escape velocity of air from the nozzle in the tested velocity range. In Figs. 15 and 16, by way of example results are presented from a determination of the effect that the Re number has on the coefficients of pressure p and discharge α for one of the nozzle arrangements tested, namely for a nozzle with an angle of inclination of the generatrix $\varphi = 45^\circ$, relative width of flow-through aperture $b/D = 0.05$, for an angle of shield inclination to the nozzle $\gamma = 0$, and for various values of the parameter b/h. In these tests the variation in the Re number was attained by varying the escape velocity of air from the nozzle, and the variation in the parameter b/h was achieved by placement of a shield at several distances h from the nozzle cut-off. The pressure coefficient p was determined for the central point of the nozzle bottom.

The pressure coefficient $\bar{p}$ and the discharge coefficient α remain constant in the range of velocity change v 5-35 m/sec, which corresponds to change of Re numbers 13,000 to 90,000. These and similar experiments afforded grounds for assuming that the flow pattern of the annular jet on the flat shield over a wide range of Re numbers remains practically automodeling, and aerodynamic characteristics of annular nozzles do not depend, within wide limits, on the linear dimension of the nozzle.

Pressure distribution along the bottom of annular nozzles. Results of measuring pressure distribution along the bottom of annular nozzles with a relative passage opening width $b/D_\beta = 0.02$ for angles of generatrix $\varphi = 0$, 30, and 45°, are presented in Figs. 17 and 18, 19 and 20, 21 and 22, respectively. These results are presented in the form of the function $p = f(x/D_\beta)$ for various values of the parameter b/h and angles of nozzle inclination with respect to the shield ($\gamma = 0$ and 4°). The central point of the nozzle bottom was adopted as the origin of coordinates. The distance from the center of the bottom to the drainage point at which the pressure p_g was measured corresponded to the x values. Similar functions are presented in Figs. 23-30 for nozzle arrangements with relative width of passage aperture $b/D_\beta = 0.05$ and 0.0625, and for $b/D_\beta = 0.1$ -- in Figs. 31-34.

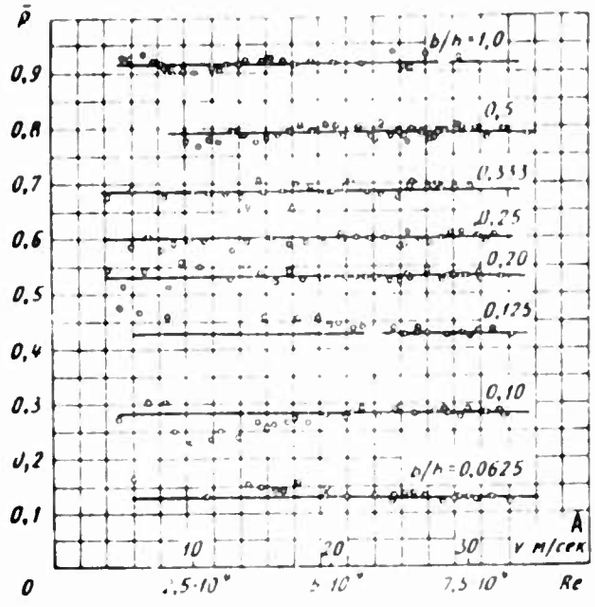

Fig. 15. Pressure coefficient at bottom of annular nozzle as a function of Reynolds number for different values of the parameter b/h ($\gamma = 0$; $\varphi = 45^\circ$; $b/D_\beta = 0.05$)
KEY: A -- v, m/sec

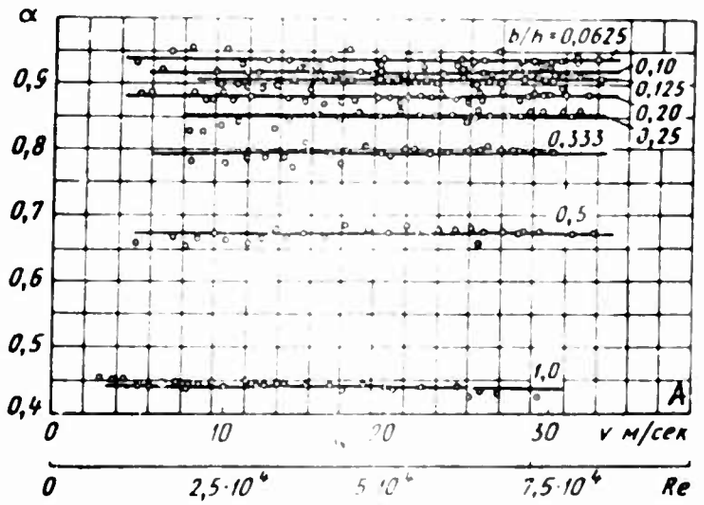

Fig. 16. Discharge coefficient of annular nozzle as a function of Reynolds number for different values of the parameter b/h ($\gamma = 0$; $\varphi = 45^\circ$; $b/D_\beta = 0.05$)
KEY: A -- v, m/sec

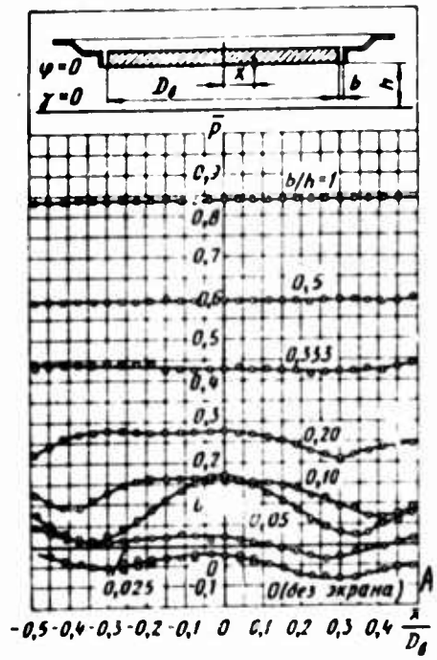

Fig. 17. Pressure distribution along nozzle bottom ($\gamma = 0$, $\varphi = 0$, and $b/D_\beta = 0.02$)
KEY: A -- (without shield)

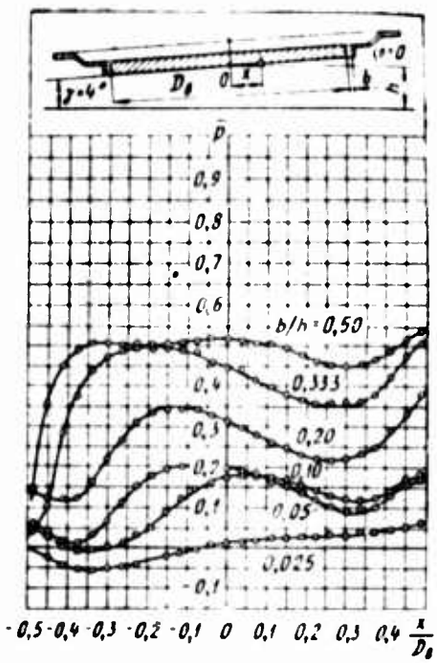

Fig. 18. Pressure distribution along nozzle bottom ($\gamma = 4^\circ$, $\varphi = 0$, and $b/D_\beta = 0.02$)

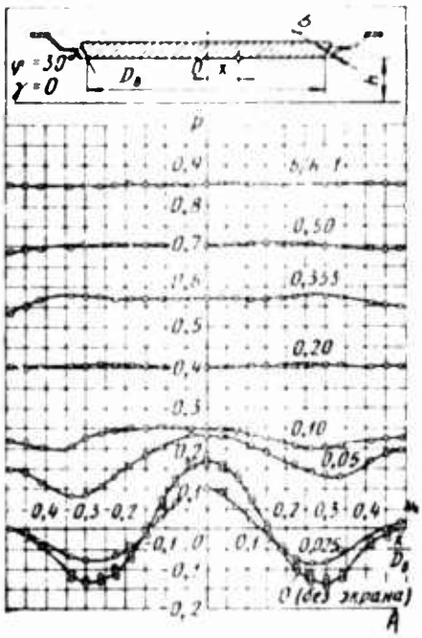

Fig. 19. Pressure distribution along nozzle bottom ($\gamma = 0$, $\varphi = 30^{\circ}$, and $b/D_g = 0.02$)
KEY: A -- (without shield)

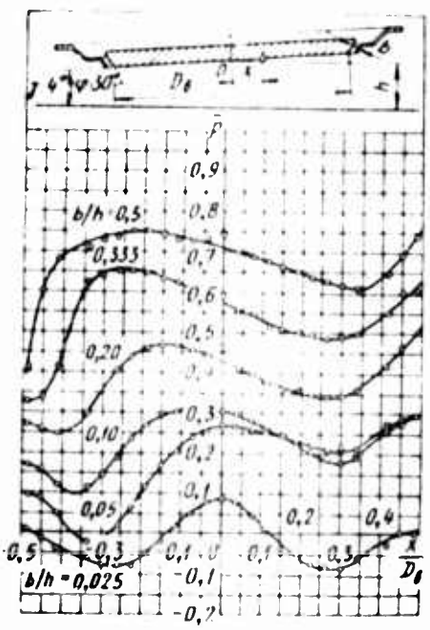

Fig. 20. Pressure distribution along nozzle bottom ($\gamma = 4^{\circ}$, $\varphi = 30^{\circ}$, and $b/D_g = 0.02$)

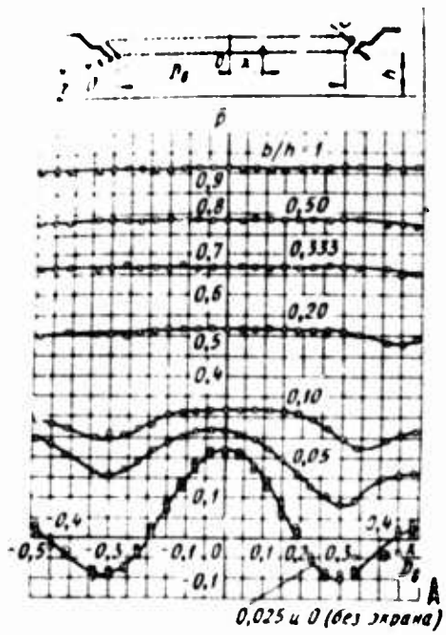

Fig. 21. Pressure distribution along nozzle bottom ($\gamma = 0, \varphi = 45^{\circ}$, and $b/D_{\beta} = 0.02$)
KEY: A -- 0.025 and 0 (without shield)

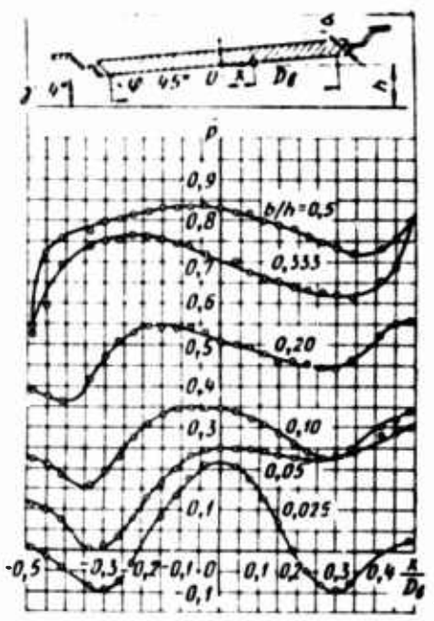

Fig. 22. Pressure distribution along nozzle bottom ($\gamma = 4^{\circ}, \varphi = 45^{\circ}$, and $b/D_{\beta} = 0.02$)

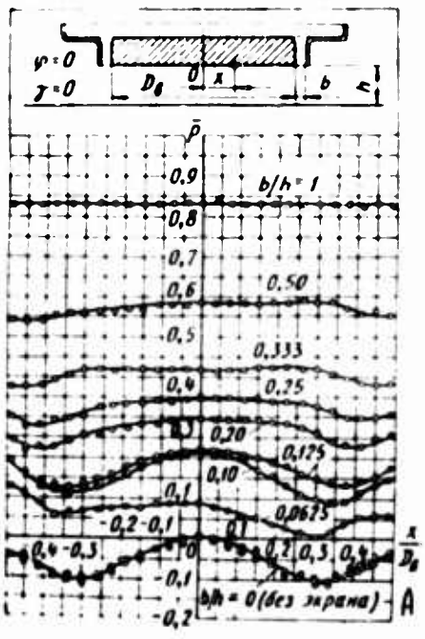

Fig. 23. Pressure distribution along nozzle bottom ($\gamma = 0, \varphi = 0$, and $b/D_{\beta} = 0.05$)
KEY: A -- (without shield)

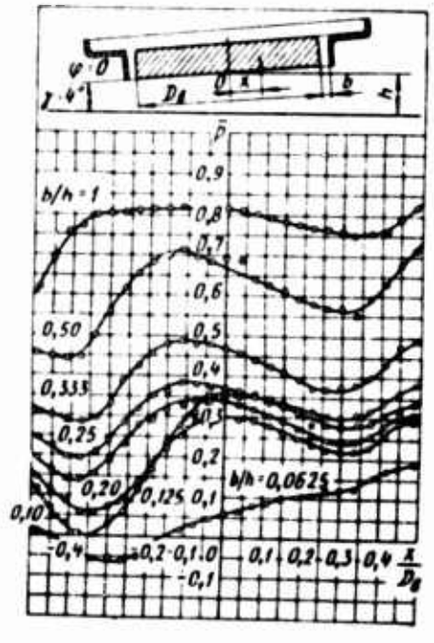

Fig. 24. Pressure distribution along nozzle bottom ($\gamma = 4^{\circ}, \varphi = 0$, and $b/D_{\beta} = 0.05$)

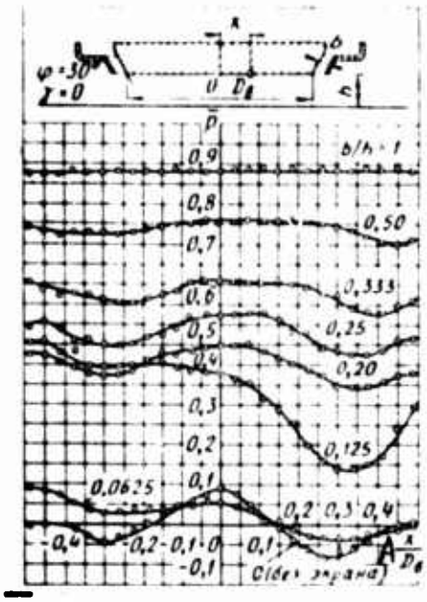

Fig. 25. Pressure distribution along nozzle bottom ($\gamma = 0, \varphi = 30^{\circ}$, and $b/D_{\beta} = 0.0625$)
KEY: A -- (without shield)

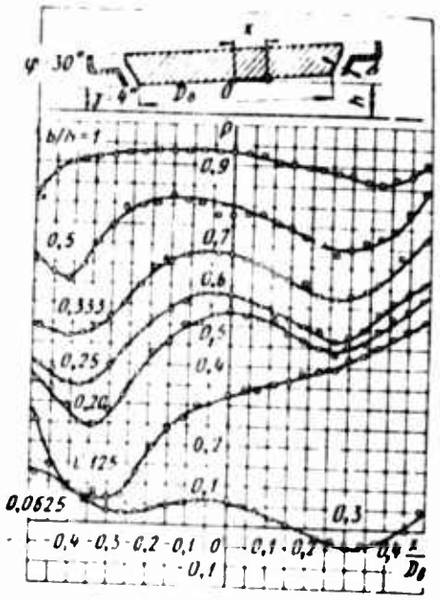

Fig. 26. Pressure distribution along nozzle bottom ($\gamma = 4^{\circ}, \varphi = 30^{\circ}$, and $b/D_{\beta} = 0.0625$)

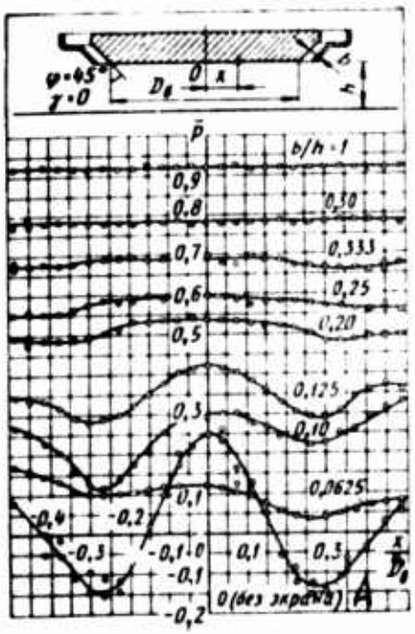

Fig. 27. Pressure distribution along nozzle bottom ($\gamma = 0, \varphi = 45^{\circ}$, and $b/D_{\beta} = 0.05$)
KEY: A -- (without shield)

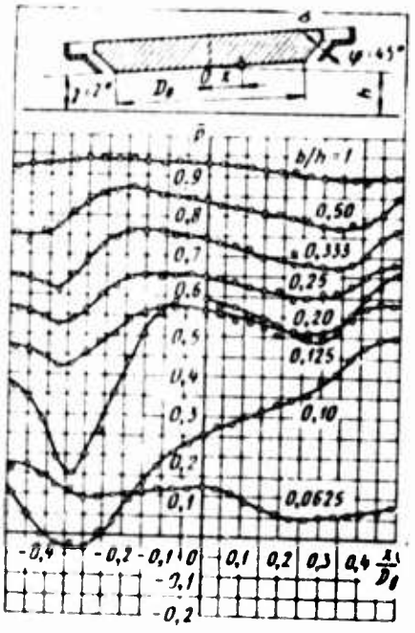

Fig. 28. Pressure distribution along nozzle bottom ($\gamma = 2^{\circ}, \varphi = 45^{\circ}$, and $b/D_{\beta} = 0.05$)

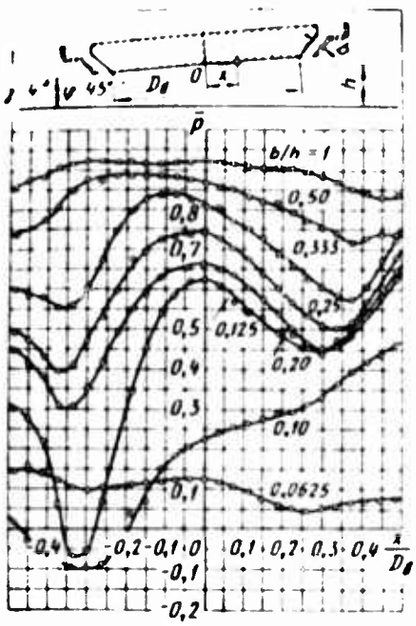

Fig. 29. Pressure distribution along nozzle bottom ($\gamma = 4^\circ$, $\varphi = 45^\circ$, and $b/D_g = 0.05$)

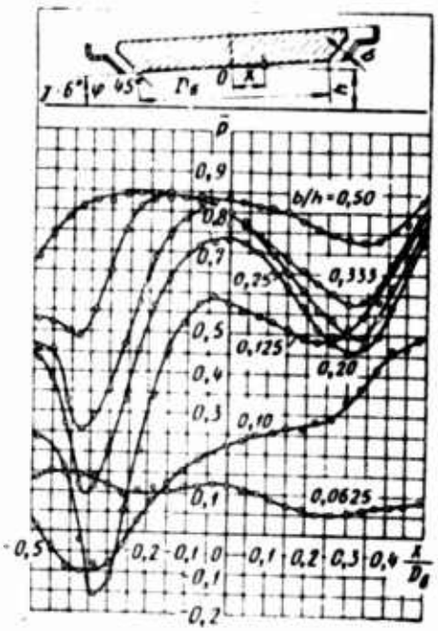

Fig. 30. Pressure distribution along nozzle bottom ($\gamma = 6^\circ$, $\varphi = 45^\circ$, and $b/D_g = 0.05$)

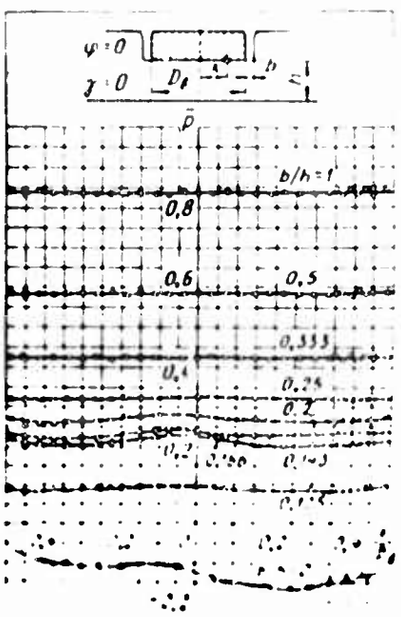

Fig. 31. Pressure distribution along nozzle bottom ($\gamma = 0$, $\varphi = 0$, and $b/D_g = 0.1$)

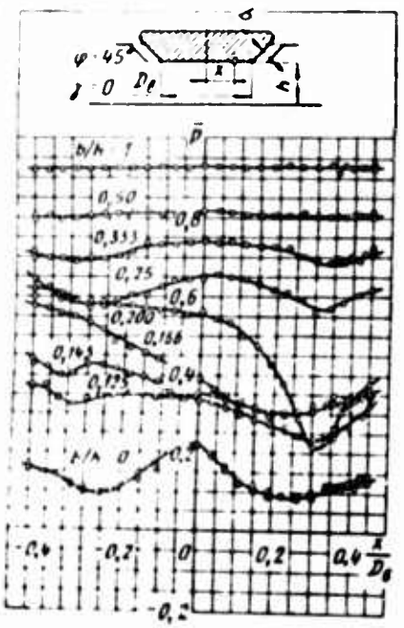

Fig. 32. Pressure distribution along nozzle bottom ($\gamma = 0$, $\varphi = 45^\circ$, and $b/D_g = 0.1$)

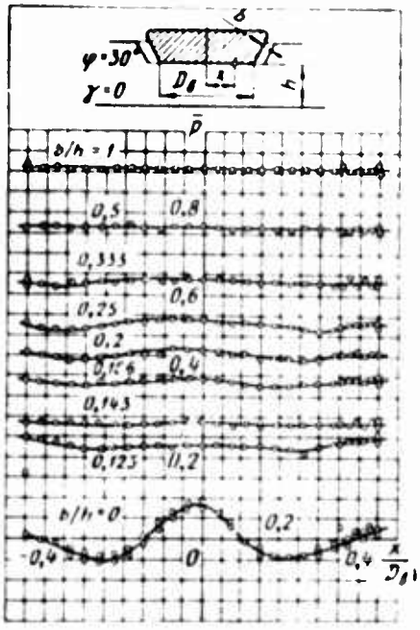

Fig. 33. Pressure distribution along bottom of annular jet for $\gamma = 0$, $\varphi = 30^{\circ}$, and $b/D_\beta = 0.1$ for various values of the parameter b/h

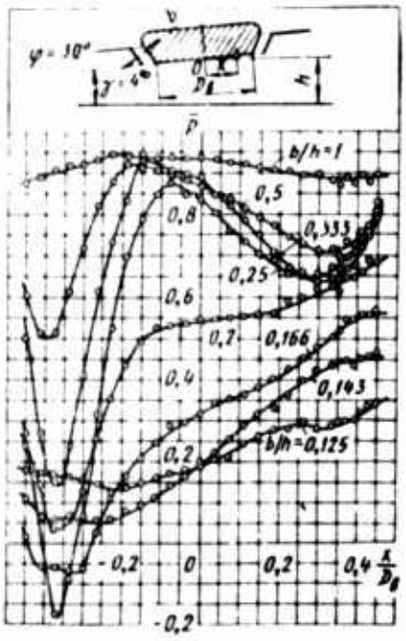

Fig. 34. Pressure distribution along bottom of annular nozzle for $\gamma = 4^{\circ}$, $\varphi = 30^{\circ}$, and $b/D_\beta = 0.1$ for various values of the parameter b/h

For free escape into a still medium not confined by a shield (b/h = 0), on exiting from the nozzle the annular jet gradually becomes constricted and at some distances from the nozzle cut-off merges into a single general jet travelling in the direction of the nozzle axis (Figs. 35 and 36). Due to the ejecting action of the jet in the internal space bounded on the side by the jet, and on the side of the annular nozzle by its bottom, circulation air currents are induced in the shape of an annular vortex. The central jetlets of this vortex will move in the direction of the nozzle bottom. As the result of the ejection effect in this internal space, in the shape of a cone, rarefaction is induced. The presence of a difference between the atmospheric pressure and the pressure in the interior space encompassed by the annular jet also leads to the curved trajectory of the jetlets at the nozzle exit.

If there is no shield along the path of jet travel (b/h = 0), then both rarefaction as well as excess pressure compared to the atmospheric can arise at the surface of the nozzle bottom. This depends on the angle of jet exit with respect to the angle of the nozzle determined by the angle of inclination φ of the nozzle generatrix. When $\varphi = 0$, rarefaction (cf. Figs. 17, 23, and 31) is observed over the entire surface of the bottom of the nozzles tested. Thus, for a nozzle with a relative exit width $b/D_\beta = 0.2$, the pressure coefficient $\bar{p} = -0.08$, and for a nozzle width $b/D_\beta = 0.05$ and 0.1, these values are, respectively, $\bar{p} = -0.1$ and $\bar{p} = -0.17$.

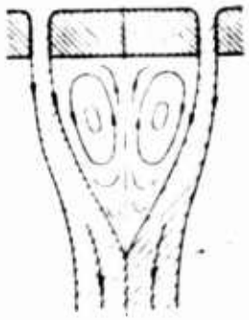

Fig. 35. Pattern of jet flow from nozzle ($\varphi = 0$)

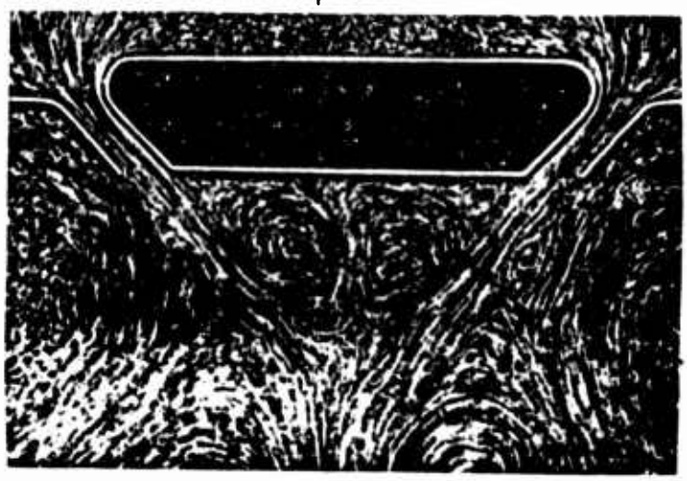

Fig. 36. Spectrum of jet flow from nozzle ($\varphi = 45^{\circ}$)

Increasing the angle of inclination φ of the nozzle generatrix reduces the size of the zone exhibiting circulation currents and markedly increases the pressure in the central area of the bottom, and a reduction of this pressure — at its periphery. For example, for a nozzle with angle of inclination $\varphi = 45^{\circ}$ and having the parameters $b/D_s = 0.2$, 0.05, and 0.1, the pressure coefficients for the central point of the bottom are, respectively, $\bar{p} = 0.23$, 0.25, and 0.22, and over the peripheral area, respectively, $\bar{p} = -0.1$, -0.14, and 0.09 (cf. Figs. 21, 27, and 32). This regularity of pressure distribution at the nozzle bottom is caused by the circulation flow of air in the space bounded by the nozzle bottom and the annular jet. Owing to retardation of the air jetlets striking the nozzle bottom, a head is induced and some excess (compared with atmospheric) pressure occurs in this region.

The presence of a flat shield along the path of jet travel leads to a qualitative change in the pattern of annular jet flow. Figs. 37 and 38 present photographs [1] revealing the flow over a cross-section of the annular jet for this instance. The jet is deflected by the shield toward the sides and streams over it in radial directions. The jet remains annular over the section between the nozzle and the shield, but streaming over the shield it becomes radial. In the interior region bounded from above by the bottom of the annular nozzle, and from beneath — by the shield, and from the sides — by the annular jet, a pressure increase compared with the atmospheric is induced. This rise is caused by the reactive effect of the radial jet.

Circulation flow in the form of a system of concentrically arranged annular vortices determining the nature of pressure distribution along the bottom of the annular nozzle and the shield is induced in the interior region.

When the shield is placed parallel to the nozzle bottom ($\gamma = 0$), and for extremely small distances between the nozzle and the shield, the pressure is distributed evenly over the bottom and in magnitude is close to the total pressure in the air stream ahead of the nozzle. As $h \to 0$, the pressure coefficient $\bar{p} \to 1$.

As the distance between the nozzle and the shield is increased, the excess pressure at the nozzle bottom rapidly drops off, while a fairly high degree of pressure distribution uniformity along the bottom radius is retained. At relatively large distances between the nozzle and the shield, beginning roughly at values of the parameter $b/h \approx 0.2$, for nozzles with relative jet exit width $b/D_g = 0.02$, and beginning with values of $b/h \approx 0.5$ for nozzles having width $b/D_g = 0.05$ and 0.1, the uniformity of pressure distribution rapidly deteriorates.

Experiments show that even a slight inclination of the nozzle with respect to the field leads to an abrupt redistribution of pressure over the bottom surface. A substantial pressure drop is induced over the section of the bottom on the depressed nozzle side, while in the opposite section of the bottom the pressure remains relatively weak. As the angle of inclination rises, the intensity of the pressure drop builds. Rarefaction even occurs in some areas of the bottom. We note that as the angle of inclination of the nozzle generatrix φ is increased, this pressure redistribution becomes more abrupt.

These properties of single-pass annular nozzles are responsible for the inadequate static stability of air cushion craft designed with single-pass nozzles. Even at a relatively low clearance height a tipping moment is induced, acting on the craft in the direction of the depressed side. As the results, the craft touches the support surface with its side.

---

[1] The photographs were obtained in experiments with a flat model in a flow channel. To render the flow visible, the surface of the water was sprinkled with aluminum powder.

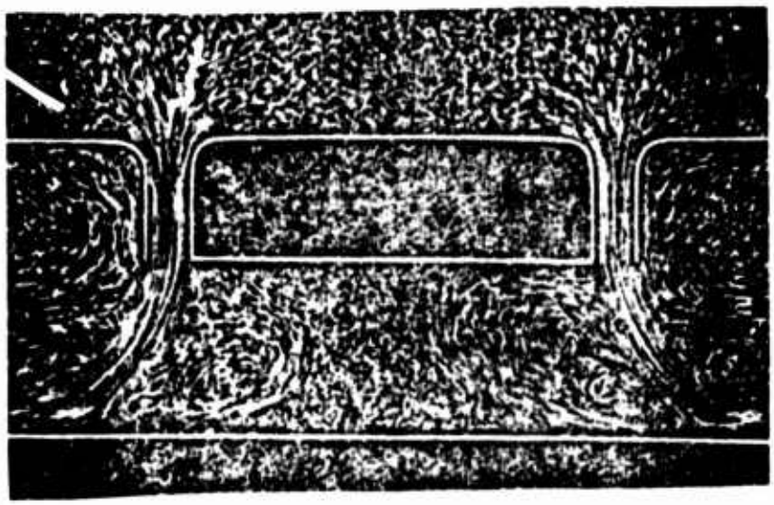

Fig. 37. Spectrum of jet streaming on shield ($\varphi = 0^{\circ}$)

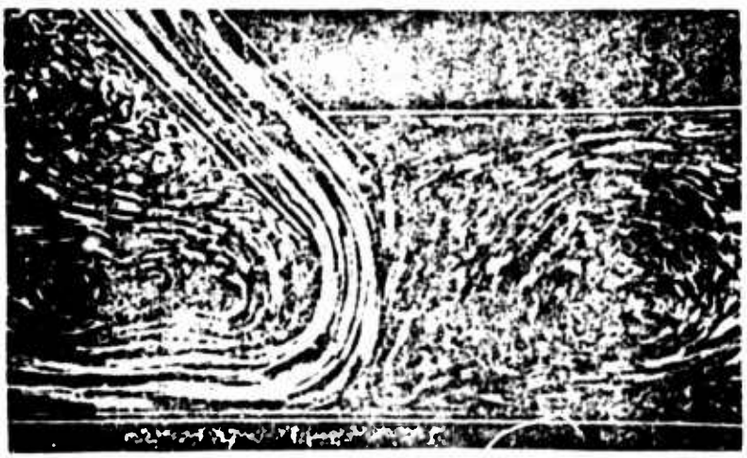

Fig. 38. Spectrum of jet streaming on shield ($\varphi = 45^{\circ}$)

Pressure distribution along the shield. The results of measuring pressure distribution along the shield for various distances between nozzle and shield are given in Figs. 39 and 40 in the form of pressure fields recorded in a plane passing through the center of the nozzle bottom. These pressure fields were obtained for the outflow of jets from nozzles with relative exit width $b/D_g = 0.02$ and angles of inclination of nozzle generatrix $\varphi = 0$ and 45°. The nozzle bottom in these experiments was positioned parallel to the shield ($\gamma = 0$). The variation in the parameter b/h was obtained by varying the distance h for constant b.

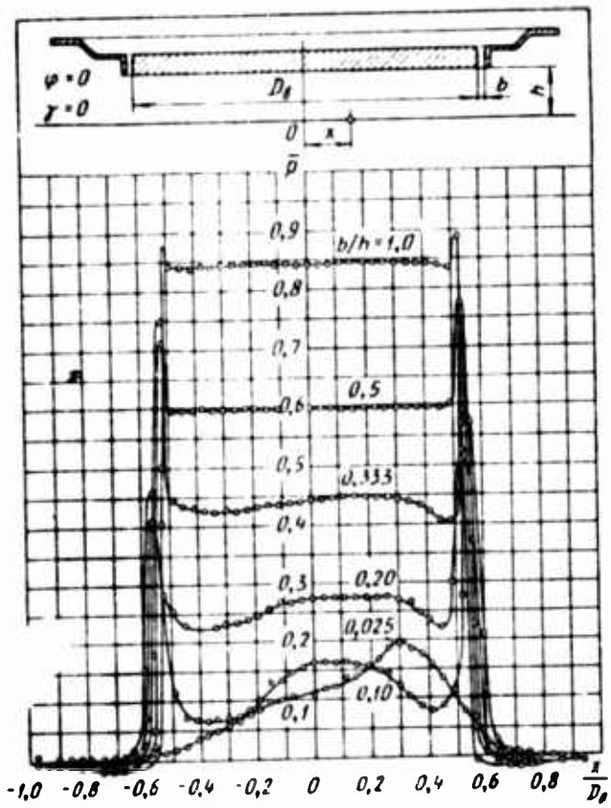

Fig. 39. Pressure distribution along shield when annular jet streams over it ($\gamma = 0, \varphi = 0$, $b/D_\beta = 0.02$)

Thus, the annular jet streaming along the shield produces over its surface a planform circular zone of increased pressure. At small distances h and correspondingly large values of the parameter b/h, the diameter of this zone is approximately equal to the diameter of the nozzle bottom, while the excess pressure in it is evenly distributed and is equal in magnitude to the excess pressure at the nozzle bottom for corresponding values of the parameter b/D_β .

With increase in the distance h, the dimensions of the planform circular zone of increased pressure decrease and, beginning with the value $b/h \approx 0.3$, the pressure in the zone is unevenly distributed. For large distances h, the annular jet, without even reaching the shield, can merge into a single common jet, causing the corresponding pressure distribution over the shield.

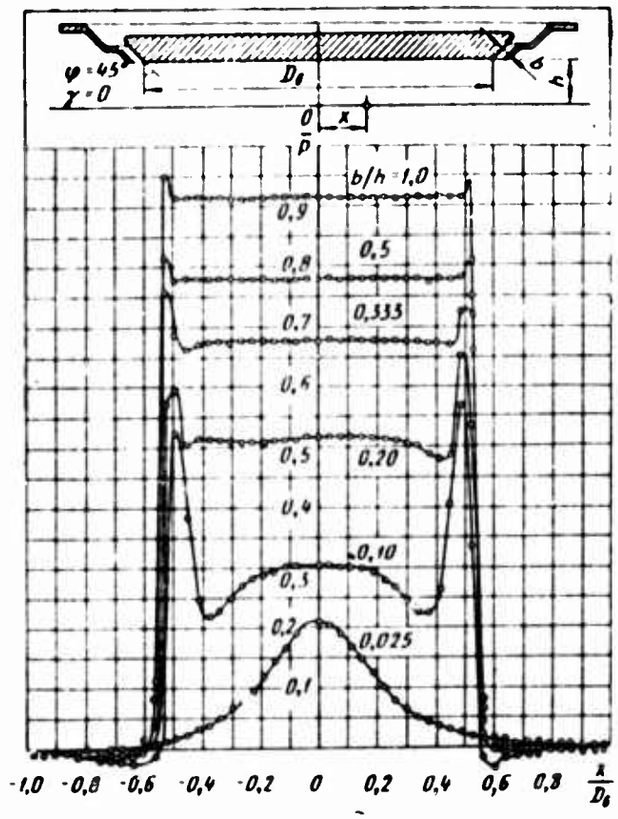

Fig. 40. Pressure distribution along shield when annular jet streams over it ($\gamma = 0, \varphi = 45^\circ$, $b/D_\beta = 0.02$)

In addition, an annular zone with abruptly higher pressure is induced at the shield surface, located over the section of the shield lying opposite the exit of the annular nozzle. The mean radius of this zone is approximately $x/D_\beta = 0.4$-0.6. With increase in the distance x/D_β beyond the value indicated above, the pressure in the direction of the radius falls off rapidly and becomes equal to atmospheric pressure for $x/D_\beta = 0.8$-1.

A splitting of the flow masses streaming over the shield occurs in the annular zone of increased pressure. The volume of air exiting from the annular jet departs to the outside, while masses of air ejected from the interior volume encompassed by the annular jet are directed toward the axis of the annular jet (cf. Fig. 38). A critical annular line corresponding to the streamline dividing the main mass of the annular jet from the attached mass is induced on the shield. Total stagnation of the splitting elementary jetlet occurs along this line.

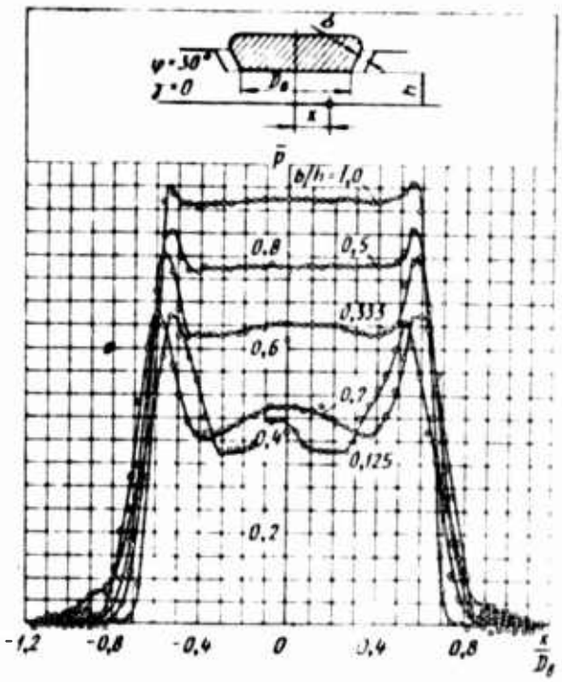

Fig. 41. Pressure distribution along shield when annular jet streams over it ($\gamma = 0$, $\varphi = 30^\circ$, $b/D_\beta = 0.1$)

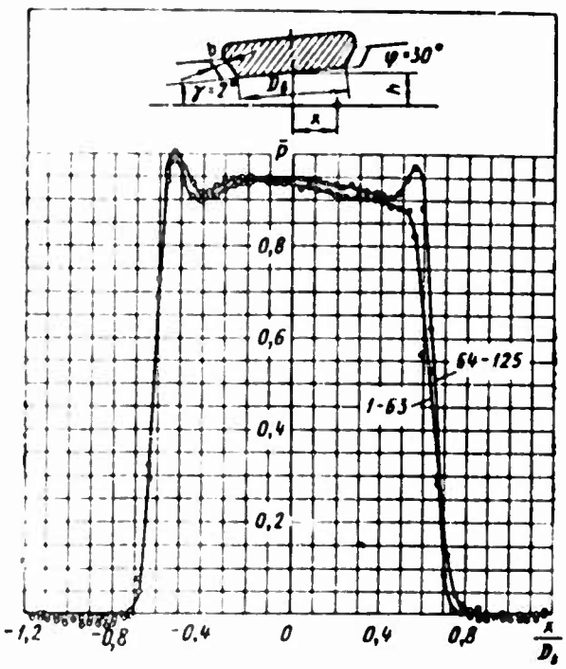

Fig. 42. Pressure distribution along shield when annular jet streams over it ($\gamma = 2^\circ$, $\varphi = 30^\circ$, $b/D_\beta = 0.1$, $b/h = 1$)

The effect of the angle of inclination gamma of the nozzle on the pressure distribution is shown in Figs. 4 -44, where the curves of pressure distribution along two mutually perpendicular axes are presented, one of which -- lying in the plane of nozzle inclination -- bears the drainage points 1-63, and the other -- the drainage points 64-125 (cf. Fig. 11). Inclining the nozzle results in the annular zone of increased pressures at the shield breaking up. The pressure rises in the area of the critical annular zone lying near the nozzle cut-off, while it drops off rapidly over the section distant from the nozzle. The symmetry of pressure distribution is retained along the axis of the shield that is normal to the plane of nozzle inclination. This pattern of pressure distribution at the shield is caused by the variation in the direction of travel of the circulation air currents within the volume bounded by the annular jet.

When the nozzle is inclined, some of the mass of the annular jet streams into the interior space in the direction from the narrow clearance between the nozzle and the shield to the broad clearance, sweeps off the annular vortices, and exits to the exterior from beneath the elevated edge of the nozzle (Fig. 45). A circulation flow is induced in the interior space, which is characterized by the fact that the flow separating from the annular jet will travel along the shield surface, while the attached

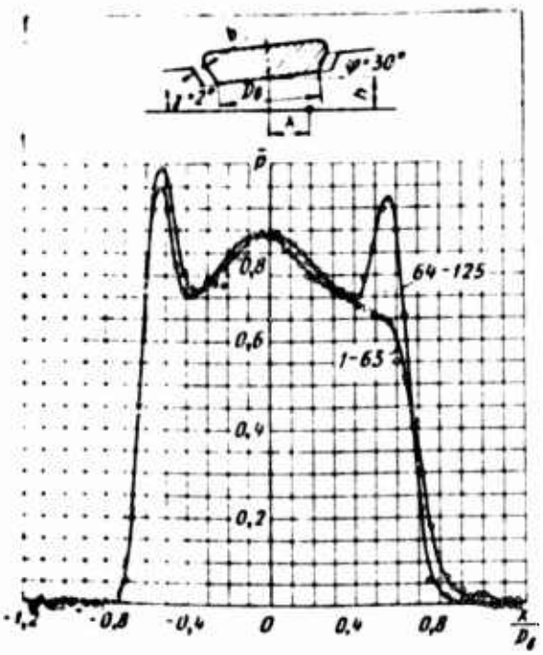

Fig. 43. Pressure distribution along shield when annular jet streams over it ($\gamma = 2^{\circ}, \varphi = 30^{\circ}$, $b/D_g = 0.1$, $b/h = 0.5$)

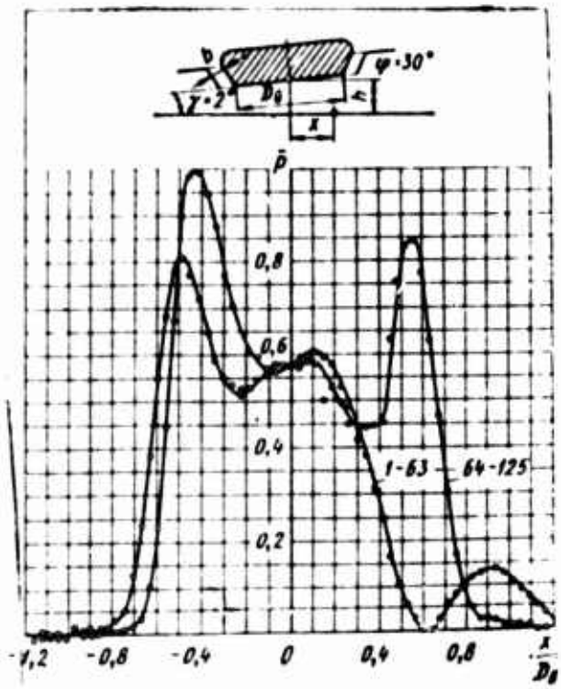

Fig. 44. Pressure distribution along shield when annular jet streams over it ($\gamma = 2^{\circ}, \varphi = 30^{\circ}$, $b/D_g = 0.1$, $b/h = 0.2$)

masses caused by the ejecting action of the active jets are directed along the nozzle bottom in the opposite direction. The local pressure rise at the shield side close to the nozzle is caused by the fact that stagnation of the elementary jetlet of the active flow exhibiting high kinetic energy occurs in this area. The local pressure drop at the shield on the side of the elevated nozzle section is caused by the fact that the active flow passing over the shield is partially deflected upward as it approaches the jet and is sucked into the jet, tending to separate from the shield.

It must be noted that zones of increased pressure at the shield surface lie in the region of zones of abrupt pressure drop at the bottom of the annular jet.

Pressure coefficient and discharge coefficient of annular nozzles. The pressure coefficients p at the bottom of the annular nozzle (the pressure coefficients of the air cushion) and the discharge coefficients α, as functions of the parameter b/h for nozzles with relative exit width $b/D_g = 0.02$, are presented in Figs. 46-48, in Figs. 49-51 -- for nozzles with $b/D_g = 0.05$ and 0.0625, and in Figs. 52-54 -- for nozzles with

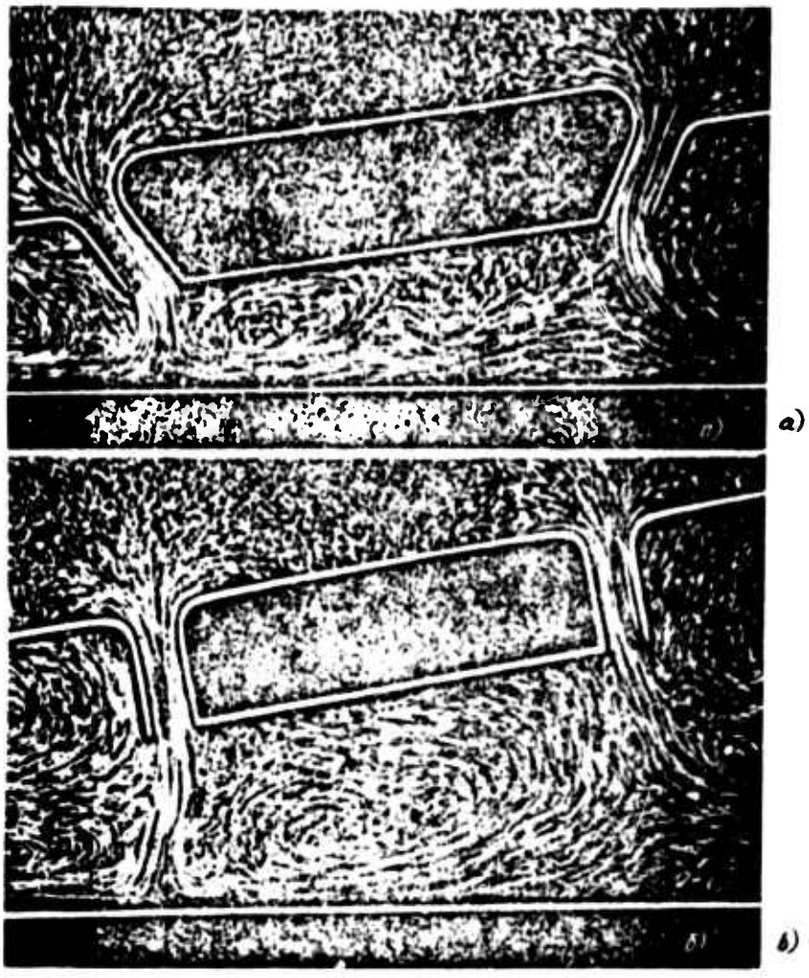

Fig. 45. Flow pattern of inclined annular jet along shield: a and b — for small and large distances between nozzle and shield, respectively

$b/D_0 = 0.1$. Changes in the parameter b/h in the experiments were achieved by varying the distance h between the nozzle and the shield. For the case b/h = 0, the points of the curve were obtained by testing nozzles without using a shield. The pressure coefficient p was determined from measurements at the point lying in the center of the bottom of the annular nozzle.

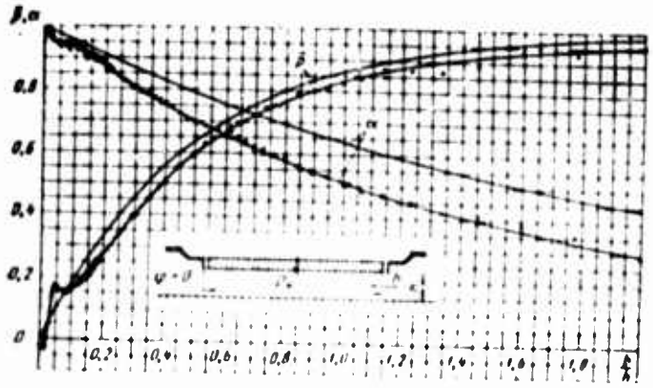

Fig. 46. Coefficient of air cushion pressure and flow coefficient of annular nozzle for $\varphi = 0$ and $b/D_\beta = 0.02$ as theoretical and experimental functions of the parameter b/h

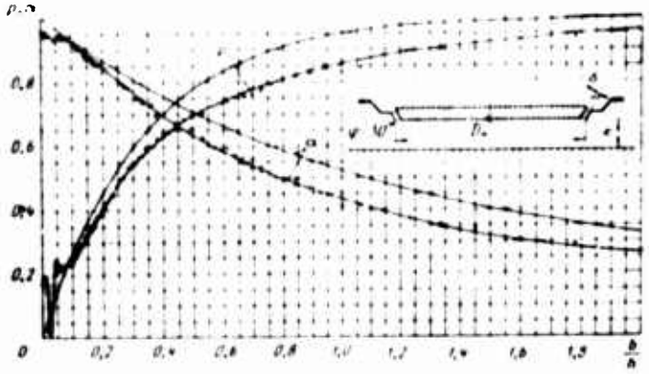

Fig. 47. Coefficient of air cushion pressure and flow coefficient of annular nozzle for $\varphi = 30^\circ$ and $b/D_\beta = 0.02$ as theoretical and experimental functions of the parameter b/h

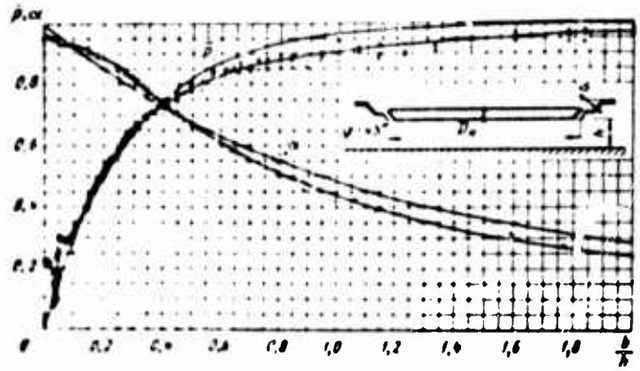

Fig. 48. Coefficient of air cushion pressure and flow coefficient of annular nozzle for $\varphi = 45^{\circ}$ and $b/D_{\beta} = 0.02$ as theoretical and experimental functions of the parameter b/h

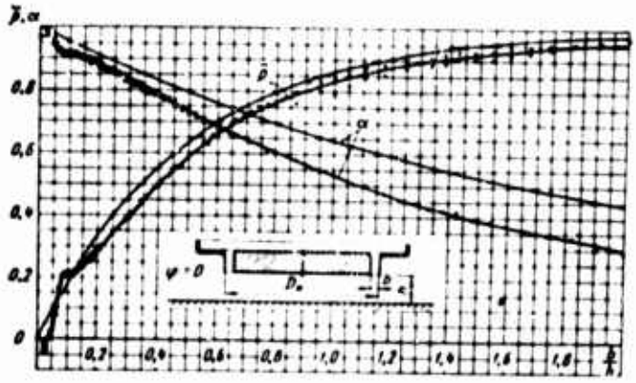

Fig. 49. Coefficient of air cushion pressure and flow coefficient of annular nozzle for $\varphi = 0$ and $b/D_{\beta} = 0.05$ as theoretical and experimental functions of the parameter b/h

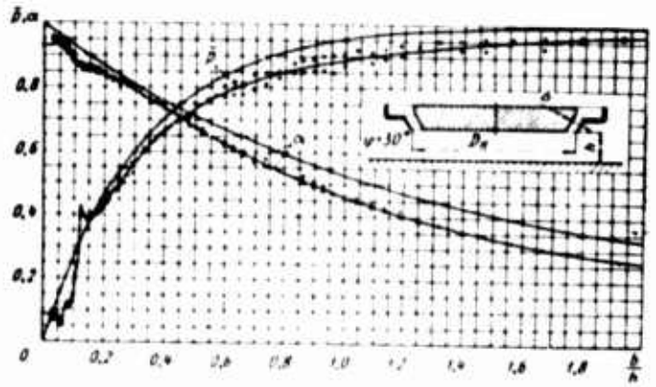

Fig. 50. Coefficient of air cushion pressure and flow coefficient of annular nozzle for $\varphi = 30^{\circ}$ and $b/D_0 = 0.0625$ as theoretical and experimental functions of the parameter b/h

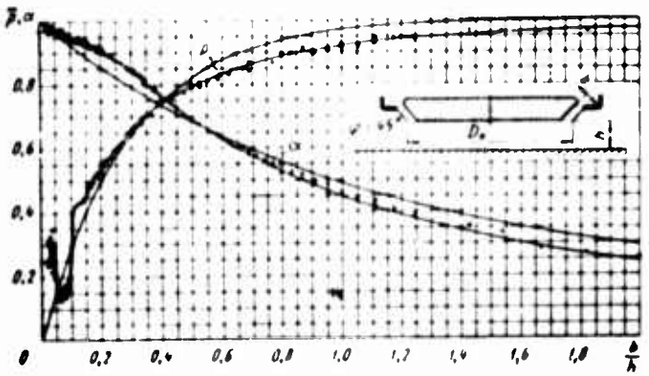

Fig. 51. Coefficient of air cushion pressure and flow coefficient of annular nozzle for $\varphi = 45^{\circ}$ and $b/D_0 = 0.05$ as theoretical and experimental functions of the parameter b/h

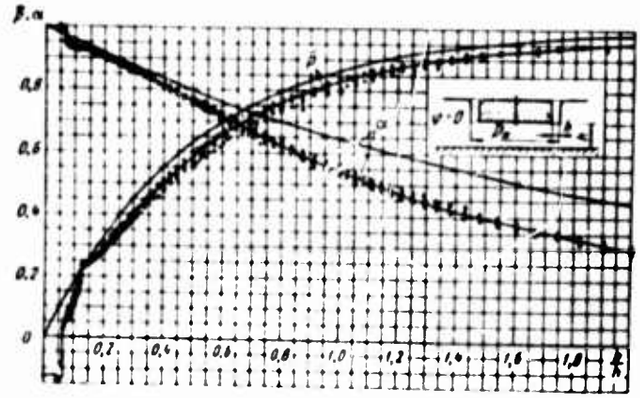

Fig. 52. Coefficient of air cushion pressure and flow coefficient of annular nozzle for $\varphi = 0$ and $b/D_\beta = 0.1$ as theoretical and experimental functions of the parameter b/h

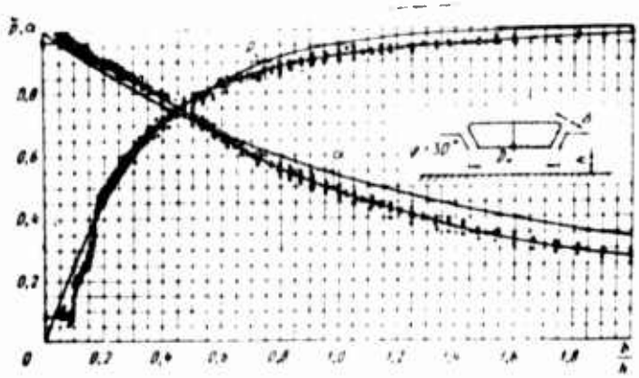

Fig. 53. Coefficient of air cushion pressure and flow coefficient of annular nozzle for $\varphi = 30^\circ$ and $b/D_\beta = 0.1$ as theoretical and experimental functions of the parameter b/h

In the investigation, the range of variation in b/h covered three characteristic regimes of annular jet streaming along the shield. One corresponded to the case of small distances h between the nozzle and the shield. At these distances the annular jet, encountering the shield in its path, streams along it in radial directions. Increased pressure caused by the reaction of the radially streaming jet is induced in the space bounded by the bottom of the nozzle, shield, and by the annular jet -- along the sides, that is, an air cushion is formed (Fig. 55 a). With increase in the distance between the nozzle and the shield, corresponding to a reduction in the parameter b/h, the excess pressure beneath the nozzle is reduced and the air cushion gradually disappears.

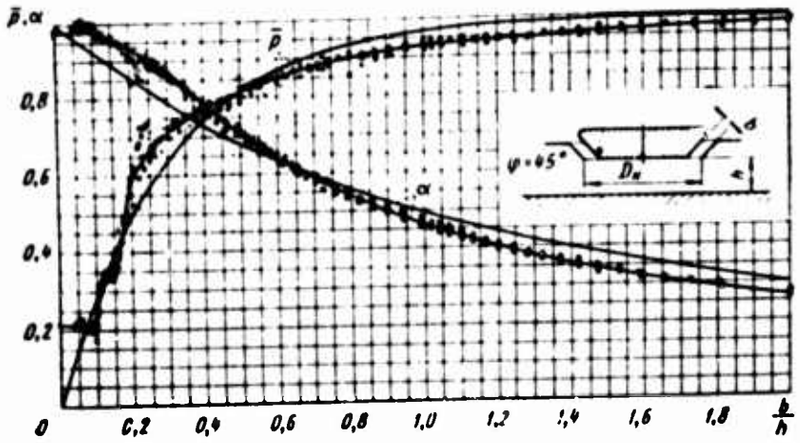

Fig. 54. Coefficient of air cushion pressure and flow coefficient of annular nozzle for $\varphi = 45^{\circ}$ and $b/D_a = 0.1$ as theoretical and experimental functions of the parameter b/h

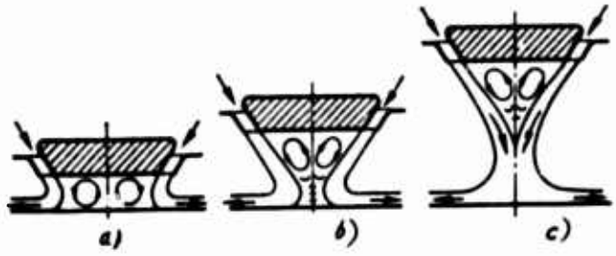

Fig. 55. Typical cases of annular jet streaming over shield: a -- flow with air cushion formation; b -- transient flow regime; c -- outflow without the effect of ground proximity

Beginning at some distance h, a transient flow regime sets in. This second case is characterized by the fact that the annular jet in direct proximity to the shield tends to merge into a single common stream, and the shield itself ceases to serve as the surface bounding the air cushion (Fig. 55 b). In this case the cushion is enclosed between the nozzle bottom and the tapered converging annular jet.

The third case of flow occurs at large distances h at which the annular jet is able along its path to the shield of merging into a single general circular stream, while the shield itself has no aerodynamic effect on the escape of the jet from the nozzle and the distribution of pressure along the nozzle bottom (Fig. 55 c). In this case the pressure and its

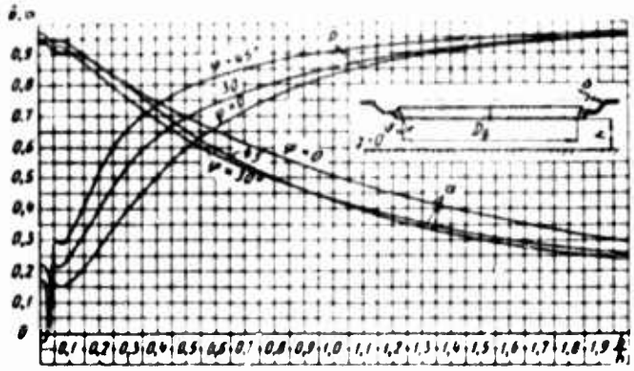

Fig. 56. Effect of slope φ of annular nozzle generatrix on pressure and flow coefficients for $\gamma = 0$ and $b/D_\beta = 0.2$

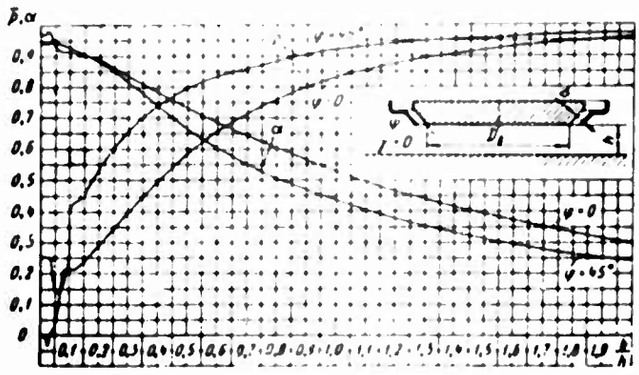

Fig. 57. Effect of slope φ of annular nozzle generatrix on pressure and flow coefficients for $\gamma = 0$ and $b/D_\beta = 0.05$

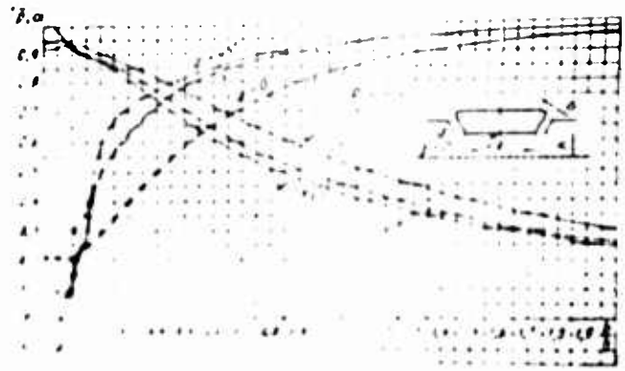

Fig. 58. Effect of slope φ of annular nozzle generatrix on pressure and flow coefficients for $\gamma = 0$ and $b/D_\beta = 0.1$

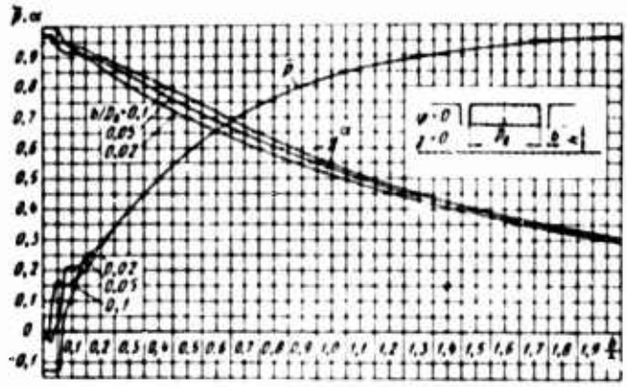

Fig. 59. Effect of relative width b/D_g of flow-passage opening of annular nozzle on pressure and flow coefficients for $\gamma = 0$ and $\varphi = 0$

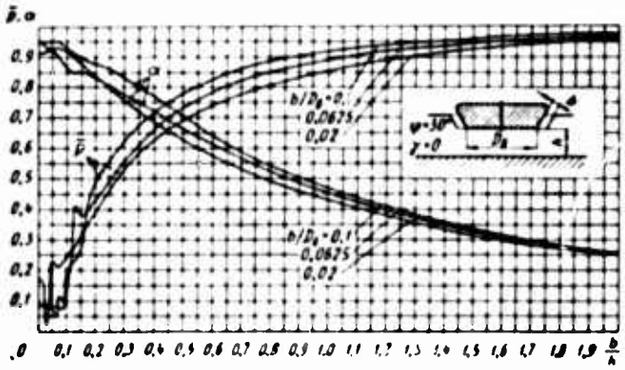

Fig. 60. Effect of relative width b/D_g of flow-passage opening of annular nozzle on pressure and flow coefficients for $\gamma = 0$ and $\varphi = 30^\circ$

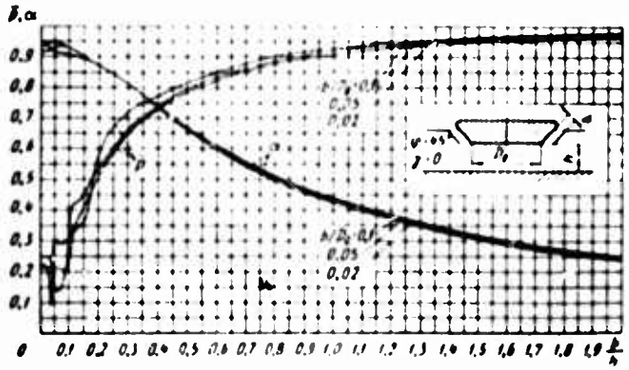

Fig. 61. Effect of relative width b/D_g of flow-passage opening of annular nozzle on pressure and flow coefficients for $\gamma = 0$ and $\varphi = 45^\circ$

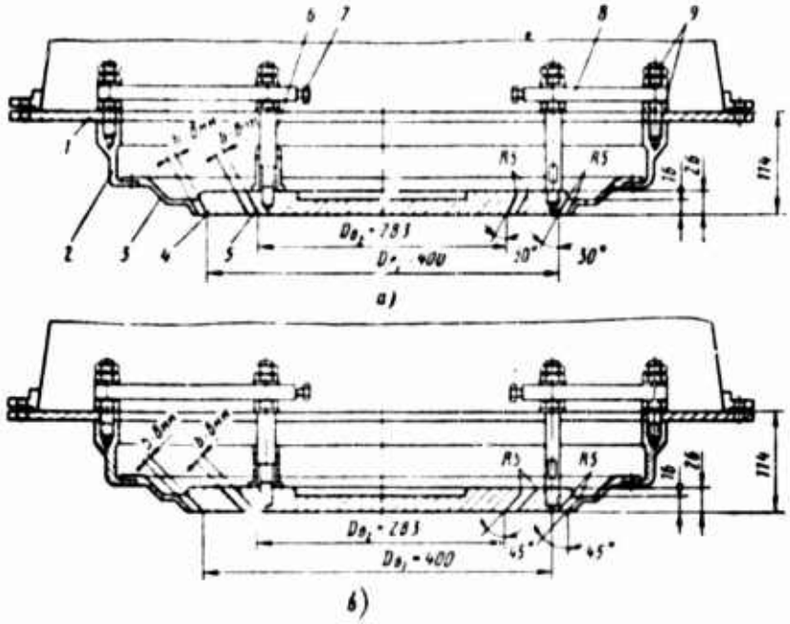

Fig. 62. Two-pass nozzle installations:
1 -- disk
2 -- cylindrical connecting piece
3 -- tapered connecting piece
4 -- annular insert
5 -- circular insert
6 -- pin
7 -- set screw
8 -- push rod
9 -- adjusting screw

distribution along the bottom are determined only by the width and the angle of jet exit from the nozzle and by circulation air currents in the space enveloped by the annular jet.

For nozzles with relative exit width $b/D_\beta = 0.02$, the first case of flow occurs in the region of values of parameter $b/h > 0.1$, the second case -- in the 0.025-0.1 b/h range, and the third case -- in the 0-0.025 b/h range. For nozzles with large relative exit width, the limits of these ranges correspond to somewhat greater values of the parameter b/h. Figs. 56-58 show curves characterizing the effect of the angle of inclination φ of the nozzle generatrix on the pressure coefficeint p and discharge coefficient α as a function of change in parameter d/h for nozzles with relative exit width $b/D_\beta = 0.02$, 0.05, and 0.1.

Tests reveal that increasing the angle of inclination φ appreciably raises the pressure coefficient of the air cushion for all nozzles tested. An especially large rise in the pressure coefficient p occurs in the

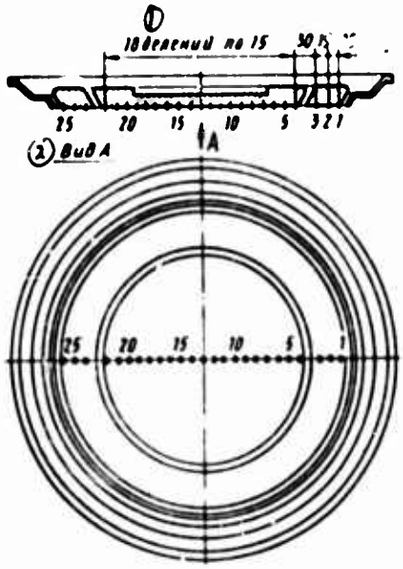

Fig. 63. Arrangement of drainage openings on two-pass nozzle insulation

KEY: 1 -- 18 divisions of 15 [mm] each

2 -- View A

range b/h = 0.25-1.0, which is the working range for air cushion vehicles. The discharge coefficient α, in contrast, decreases with increase in the angle φ.

The effect of the relative exit width of annular nozzle on the coefficients p and α for identical angles of inclination φ of the nozzle generatrices is clear from an examination of Figs. 59-61. The parameter b/D_g, varying during the experiments in the range 0.02-0.1, relatively weakly affects the values of p and α.

7. Two-pass Annular Nozzles

Air cushion flight vehicles with single-pass nozzle installations, as shown by full-scale and model tests, do not exhibit the required static stability. Even a slight heeling of this kind of craft at a relatively small clearance leads to a qualitative change in the motion of the principal and the circulation air currents in the space bounded by the annular jet. An abrupt pressure drop is observed at the bottom of the craft, on the heeled side, resulting in a tipping moment.

The static stability of nozzle type craft can be appreciably augmented by sectionalizing the bottom with additional nozzles. By articulating the craft bottom with nozzles into separate sections, the discharge of air jets forming the air cushion can be organized in such a way that even for large craft heelings higher pressure is induced at the bottom section adjoining the heeling side, and a righting moment will appear, restoring the craft to its initial position after the perturbing.

Several methods of sectionalizing the bottom are known, among which the simplest is based on dividing the bottom into two sections with concentrically arranged nozzles. This method has practical application for air cushion flight craft, and thus finding its aerodynamic qualities in a systematized form is of definite interest.

Studies of the streaming of two coaxial annular jets along a flat shield oriented in different ways relative to the nozzle installation aimed at finding the physical flow pattern of jets and circulation air currents in the air cushion, discovering regularities of pressure distribution over the surface of the bottom of the nozzle installation and the shield, and determining the dependence of pressure coefficient and discharge coefficient of two-pass nozzle installations on their geometrical parameters.

Two-pass annular nozzles. A study of the streaming of two coaxial annular nozzles over a flat shield was carried out on nozzle installations differing by the angle of inclination of the nozzle generatrices: in one case, the angles $\varphi_1 = \varphi_2 = 30^\circ$ (Fig. 62 a), and in the other, $\varphi_1 = \varphi_2 = 45^\circ$ (Fig. 62 b). Each arrangement had two nozzles: external nozzle with diameter $D_{\beta 1} = 400$ mm, and internal nozzle with diameter $D_{\beta 2} = 283$ mm (the dimensions were measured along the inner edges of the nozzles). The width of the exit opening of the external b_1 and internal b_2 nozzles were identical and were equal to $\sim$ 8 mm. The entrance edges of the nozzles were rounded to a radius of 5 mm.

The nozzle installation consisted of a disk 1, cylindrical connecting piece 2, tapered connecting piece 3, annular insert 4 (external section of bottom), and circular insert 5 (inner section of bottom). These parts were cast of aluminum, turned on a lathe, and ground within the limits of the nozzle working surfaces. Parts 2 and 3 were joined together with bolts. Parts 4 and 5 were independently connected to disk 1 by means of three pins 6 and three push rods 8. Screws 7 and washers 9 provided the coaxiality of parts 1-5 and the possibility of installing them in such a way that the exit edges of the nozzles would be in the same plane. In an adjusted nozzle installation prepared for tests, the width of the annular slits, as shown, differed by not more than $\pm$ 0.05 mm in their measurements.

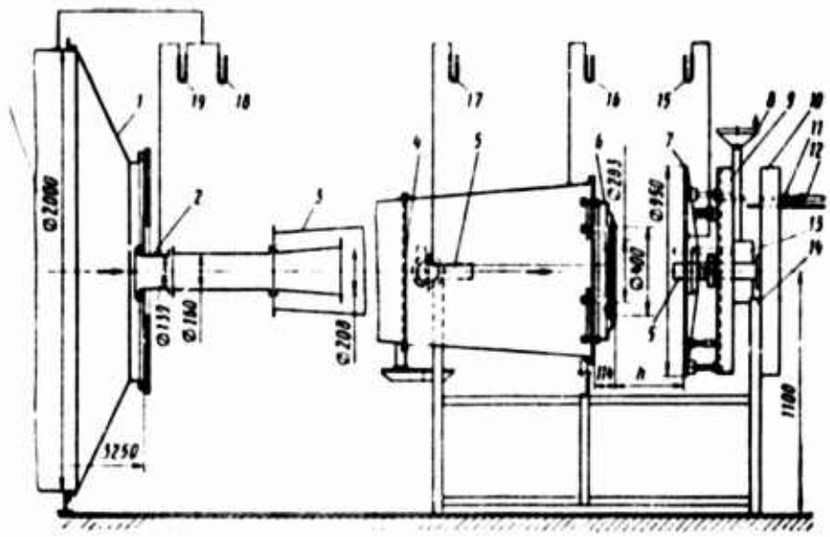

Fig. 64. Experimental stand for investigating streaming of coaxial annular jets over shield:
1 -- stabilizing chamber
2 -- measuring header
3 -- converging duct
4 -- metal screen
5 -- cylindrical guide
6 -- test nozzle installation
7 -- flat screen
8 -- steering wheel
9 -- carriage
10 -- base of travelling device
11 -- scale
12 -- push rod
13 -- worm mechanism
14 -- support frame
15-19 -- micromanometers

Twenty five drainage openings 1 mm in diameter at a spacing of 15 mm were made along a diametral line in the bottom of the nozzle installation (Fig. 63). From each drainage opening the pressure was transmitted along a rubber hose to an alcohol micromanometer through a connecting piece secured to the inner side of the bottom.

Two-pass nozzle installations were tested on the same experimental stand used to test single-pass nozzles (cf. Fig. 12). Part of the stand on which the two-pass nozzle was mounted is shown in Fig. 64, while Fig. 65 clarifies the installation of the nozzle and the shield.

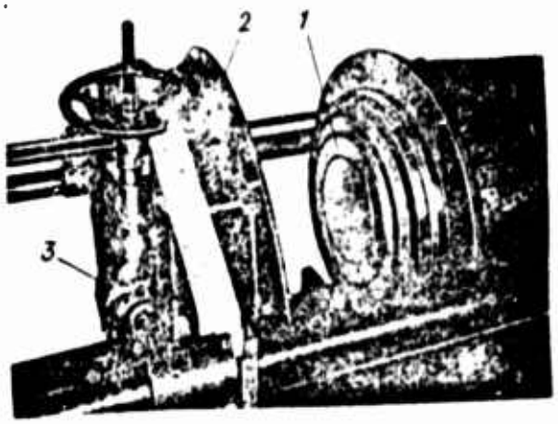

Fig. 65. Assembly of experimental stand
1 -- two-pass nozzle installation
2 -- sliding shield
3 -- worm mechanism

Interpretation of test results. Results of testing two-pass nozzle installations were represented as the dimensionless pressure coefficient p and discharge coefficient α, calculated by formulas (1) and (2). In the determination of the discharge coefficient α for a two-pass nozzle, the areas of the passage openings of the external and internal nozzles were as follows:

$$F = \pi D_{\text{м}} b \left(1 - \frac{b}{D_{\text{м}} \sin\varphi}\right),$$

where $D_{\text{м}}$ is the diameter determined from the external edge of the exit aperture of the nozzle in question.

Therefore, when using the above-derived aerodynamic characteristics of two-pass nozzle installations, we must remember that the discharge coefficient α determines the throughput capacity of the nozzle installation as a whole, that is, both the external and the internal nozzles.

The areas (in m^2) of the components of the nozzle installations tested are as follows.

	$\varphi = 30^\circ$	$\varphi = 45^\circ$
Exit opening of external nozzle	0.01028	0.01033
Exit opening of internal nozzle	0.00734	0.00739
Total area of nozzle exit openings	0.01762	0.01772
External section of bottom	0.05429	0.05229
Internal section of bottom	0.06287	0.06287
Total area of bottom (excluding area of nozzle exit openings)	0.11716	0.11516
Area of bottom along outer margin of external nozzle	0.13749	0.14019

The Re number used in plotting the aerodynamic characteristics of two-pass nozzle arrangements was calculated by Eq. (4). The equivalent diameter, equal to four times the ratio of the area of the nozzle exit openings to the wetted perimeter, is

$$d_1 = 4\frac{\sum f}{\sum \Pi} = 2b,$$

where Π is the wetted parameter of the nozzle exit, calculated by Eq. (6).

Effect of Reynolds number on pressure and discharge coefficients. Results of experiments to determine the effect of the Re number on the pressure coefficient at the external and internal sections of the bottom of one of the tested variants of the nozzle arrangement for different relative widths b/h of nozzle exit are given in Fig. 66 a and b. In the tests the variation in the Re number was achieved by varying the escape velocity v_{ef} of air from the nozzles, and the variation in the parameter b/h was achieved by installing a shield at various distances h from the bottom of the nozzle installation. The pressure coefficient p_1 was determined by the central drain opening of the external section of the bottom (points 2 and 24, cf. Fig. 63), while the pressure coefficient p_2 was determined from the central drain opening of the internal section of the bottom (point 13).

Test reveals that for nozzles with angles $\varphi = 30^\circ$ and 45° and for all the variants of shield placement relative to the nozzle, the pressure coefficients p_1 and p_2 and the discharge coefficient α are practically independent of velocity v_{ef}, which was varied in the range 4-30 m/sec, which corresponds to a variation in the Re number [illegible] to the equivalent diameter of the exit openings of a two-pass nozzle, from ~ 4000 to 32,000. This suggests that streaming of two coaxial annular jets over the flat shield even at Re numbers > 32,000 remains practically automodeling, and the flow characteristics are independent within wide limits of the geometrical dimensions of the nozzle installation.

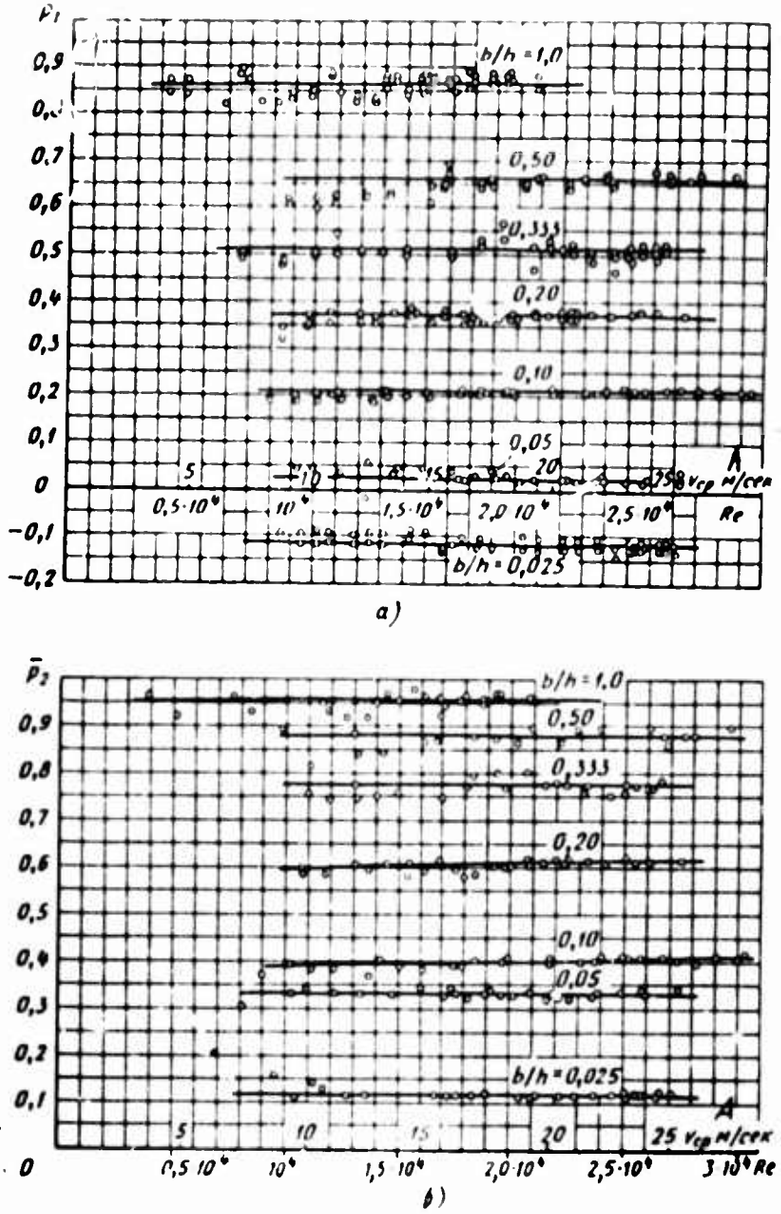

Fig. 66. Pressure coefficients for a section of the bottom of a two-pass nozzle installation as a function of Reynolds number Re for different values of parameter b/h:
a -- external
b -- internal ($\gamma = 0$, $\varphi_1 = \varphi_2 = 30^\circ$; $b_1/D_{61} = b_2/D_{61} = 0.02$)
KEY: A -- v_{av}, m/sec

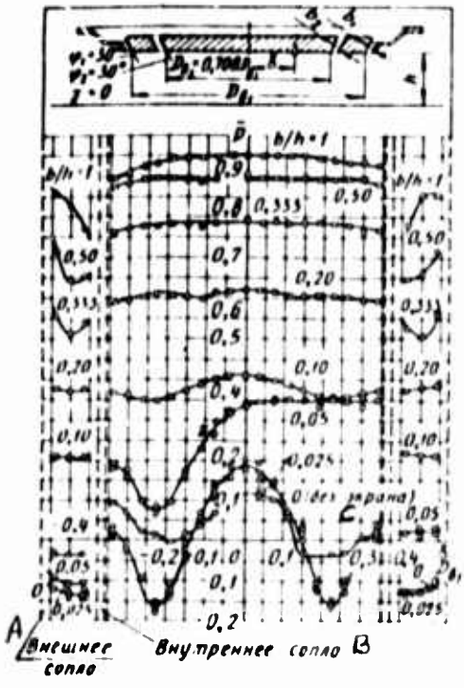

Fig. 67. Pressure distribution along bottom of two-pass annular jet for $\gamma = 0$ and several values of the parameter b/h ($\varphi_1 = \varphi_2 = 30^\circ$; $b_1/D_{\beta 1} = b_2/D_{\beta 1} = 0.01$)

KEY: A -- External nozzle
B -- Internal nozzle
C -- (without shield)

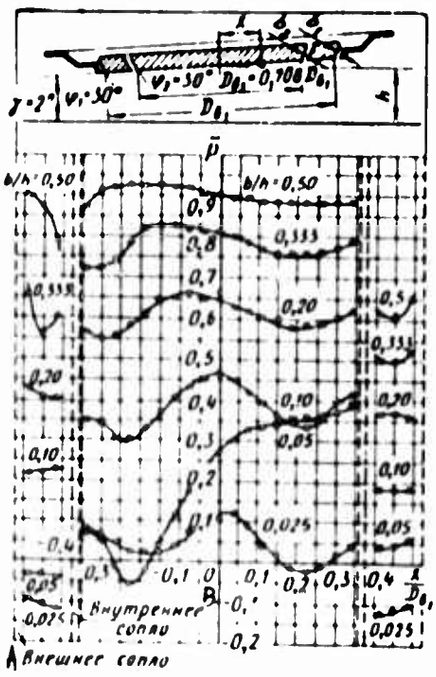

Fig. 68. Pressure distribution along bottom of two-pass annular jet for $\gamma = 2^\circ$ and several values of the parameter b/h ($\varphi_1 = \varphi_2 = 30^\circ$; $b_1/D_{\beta 1} = b_2/D_{\beta 1} = 0.02$)

KEY: A -- External nozzle
B -- Internal nozzle

Pressure distribution over the bottom of the nozzle installation. Figs. 67-70 give the results of measurements of pressure distribution over the bottom of a nozzle installation with nozzle angle inclination $\varphi = 30^\circ$ in the form of the function $p = f(x/D_\beta)$, for various values of parameter b/h for nozzles of shield inclination relative to the nozzle installation $\gamma = 0$, 2°, 4°, and 6°; and Figs. 71-74 give the analogous functions for nozzles with generatrix slope $\varphi = 45^\circ$. The central point of the bottom of the nozzle installation (point 13 -- cf. Fig. 63) was taken as the origin of coordinates. The distance from the central point of the bottom to the drainage point at which pressure p_β was measured corresponded to the x values.

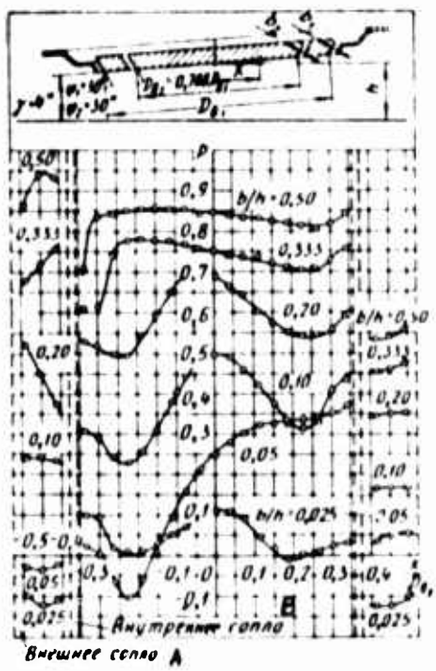

Fig. 69. Pressure distribution along bottom of two-pass annular jet for $\gamma = 4^{\circ}$ and several values of the parameter b/h ($\varphi_1 = \varphi_2 = 30^{\circ}$; $b_1/D_{\beta 1} = b_2/D_{\beta 1} = 0.02$)

KEY: A -- External nozzle
B -- Internal nozzle

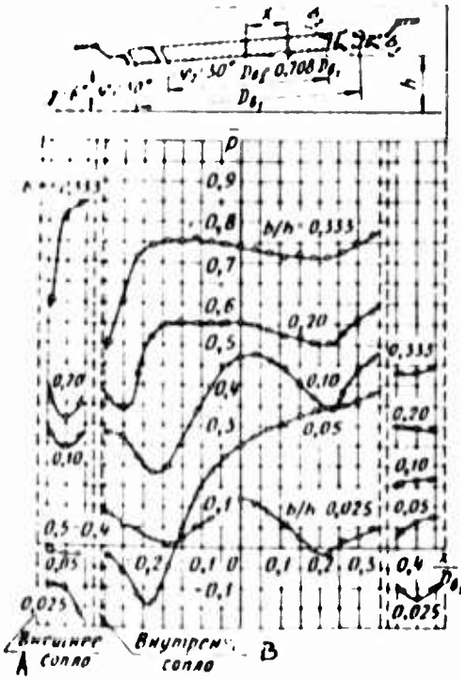

Fig. 70. Pressure distribution along bottom of two-pass annular jet for $\gamma = 6^{\circ}$ and several values of the parameter b/h ($\varphi_1 = \varphi_2 = 30^{\circ}$; $b_1/D_{\beta 1} = b_2/D_{\beta 1} = 0.02$)

KEY: A -- External nozzle
B -- Internal nozzle

Observations showed that jets of air on exiting from a nozzle in free escape, not confined by a shield (b/h = 0), gradually became narrow and at some distance from the nozzle cut-off merging to a single common stream flowing in the direction of the nozzle axis (Fig. 75). Rarefaction is observed in the external section of the bottom of the nozzle installation. For a nozzle installation with nozzle inclination angle $\varphi = 30^{\circ}$ and 45°, this rarefaction is 10-14 percent and 7-12 percent of total pressure in the stream ahead of the nozzle installation, respectively, which can be seen by inspecting the function $p = f(x/D_{\beta 1})$ for b/h = 0 in the section $x/D_{\beta 1} = \pm (0.38\text{-}0.5)$ shown in Figs. 67 and 71.

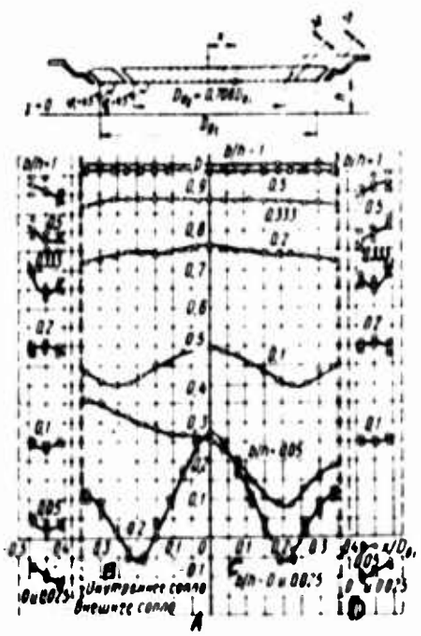

Fig. 71. Pressure distribution along bottom of two-pass annular jet for $\gamma = 0$ and several values of the parameter b/h ($\varphi_1 = \varphi_2 = 45^\circ$; $b_1/D_{\delta 1} = b_2/D_{\delta 1} = 0.02$)

KEY: A -- External nozzle
B -- Internal nozzle
C -- b/h = 0 and 0.025
D -- 0 and 0.025

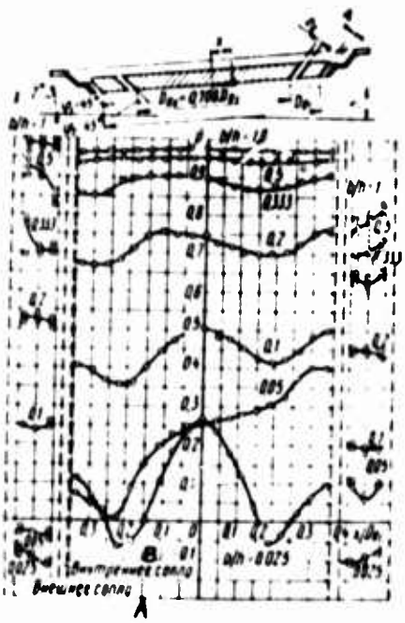

Fig. 72. Pressure distribution along bottom of two-pass annular jet for $\gamma = 2^\circ$ and several values of the parameter b/h ($\varphi_1 = \varphi_2 = 45^\circ$; $b_1/D_{\delta 1} = b_2/D_{\delta 1} = 0.02$)

KEY: A -- External nozzle
B -- Internal nozzle

In the internal section of the bottom rarefaction it is observed only over some annular section of the bottom, where the pressure coefficient takes on values extending to $\bar{p} = -0.16$ for a nozzle installation with angle $\varphi = 30^\circ$, and up to $\bar{p} = -0.06$ for a nozzle installation with angle $\varphi = 45^\circ$. Excess pressure is induced in the central section of this area of the bottom and along the periphery. Here the pressure coefficient rises to $\bar{p} = 0.18$ and $\bar{p} = 0.27$.

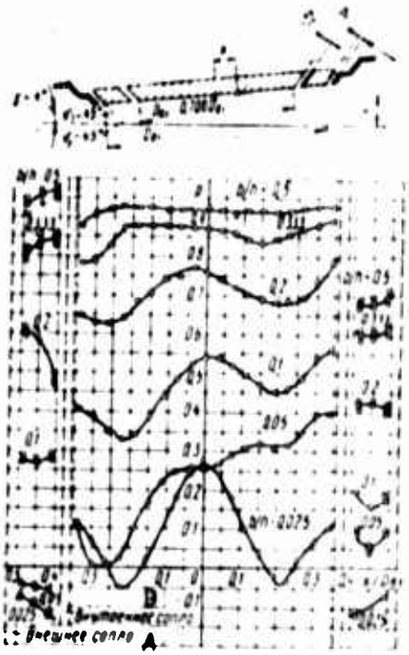

Fig. 73. Pressure distribution along bottom of two-pass annular jet for $\gamma = 4^{\circ}$ and several values of the parameter b/h ($\varphi_1 = \varphi_2 = 45^{\circ}$; $b_1/D_{c.} = b_2/D_{c.} = 0.02$)

KEY: A -- External nozzle
B -- Internal nozzle

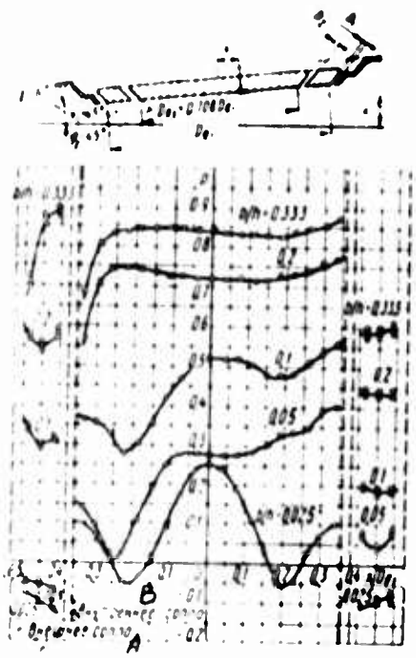

Fig. 74. Pressure distribution along bottom of two-pass annular jet for $\gamma = 6^{\circ}$ and several values of the parameter b/h ($\varphi_1 = \varphi_2 = 45^{\circ}$; $b_1/D_{c1} = b_2/D_{c1} = 0.02$)

KEY: A -- External nozzle
B -- Internal nozzle

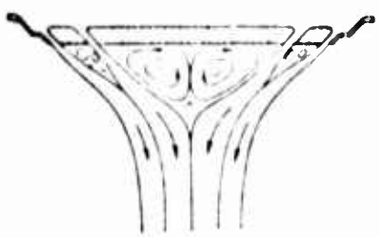

Fig. 75. Free escape from nozzle of two coaxial annular jets

This nonuniformity in pressure distribution over the bottom of a nozzle installation is a consequence of the intense circulation air currents induced in the inner-annular space, caused by the ejecting action of the annular jets.

The flat shield in the path of jet flow leads to a qualitative variation in flow pattern. For large distances between shield and nozzle ($b/h < 0.025$), a single common stream flows along the shield, resulting from the merger of annular jets. In these cases the aerodynamic effect of the shield on the inner-annular space is weak, and the pattern of pressure distribution over the bottom of the nozzle remains nearly the same as for the case of flow without a shield.

As the shield is brought closer to the nozzle, the effect of the shield on flow in the inner-annular space becomes more intense, and the moment is reached when the flow of annular jets changes abruptly: the inner-annular space is enclosed on the shield and the annular jets streaming over the shield are converted into radial. At this critical distance the pressure distribution over the bottom of the nozzle installation becomes particularly nonuniform. This critical distance $b/h = 0.04-0.1$ for two-pass nozzles tested.

With further approach of the shield to the nozzle, the uniformity of pressure distribution over the bottom is substantially improved and the excess pressure over the bottom surface rises. A system of annular vortices is induced in the inner-annular space. The pressure at the surface of the external section of the bottom remains always much weaker than the pressure in its internal section. Fig. 76 shows photographs taken during experiments with a flat model of a nozzle in a flow channel. They clarify the streaming of coaxial annular jets over the shield when the bottom of the nozzle installation is positioned parallel to the shield ($\gamma = 0$) and when it is in the heeled position ($\gamma \neq 0$).

The effect of the angle of shield inclination γ on the pressure distribution over the external and internal sections of the bottom of the nozzle installation can be determined by comparing the functions $p = f(x/D_{\beta 1})$ for the corresponding values of parameter b/h (cf. Figs. 67-74).

As the nozzle of inclination γ at the external section of the bottom is increased in the zone lying near the shield, a pressure rise is observed, while in the same bottom section, but now in a zone located far from the shield, at the opposite of the installation, the pressure drops. When this takes place the intensity of the pressure change in these bottom zones, as a function of the angle of inclination, will be the more intense, the shorter the distance between the nozzle and the shield, that is, the larger the parameter b/h. Figs. 77-80 present -- for several values of parameter

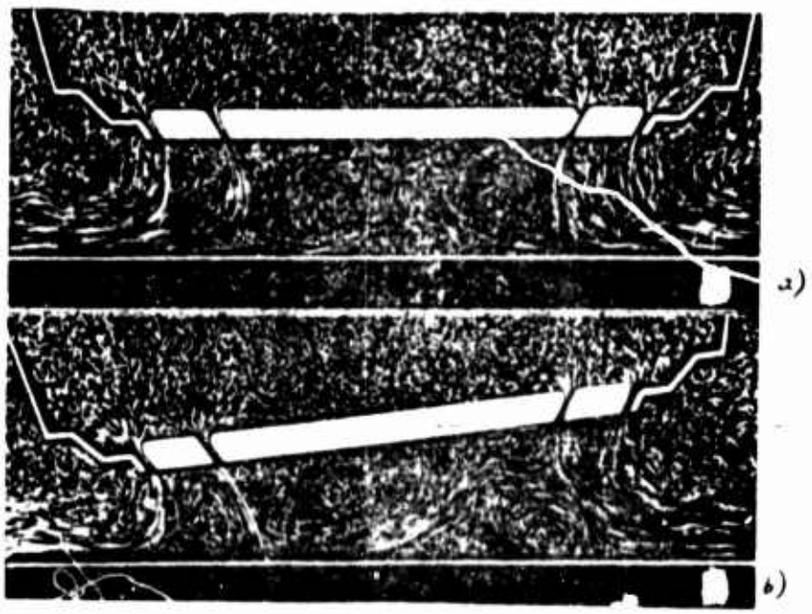

Fig. 76. Streaming of two-pass annular jet over shield
a -- nozzle in horizontal position
b -- nozzle in heeling position

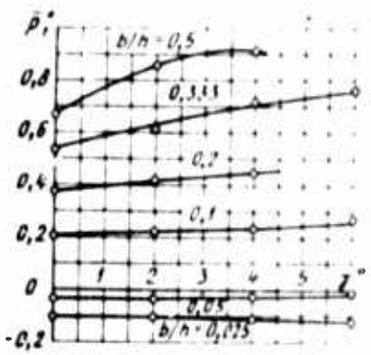

Fig. 77. Pressure coefficient for external section of bottom at depressed nozzle side as a function of angle of heel and parameter b/h ($\varphi = 30^{\circ}$, $b/D_{\beta 1} = 0.02$)

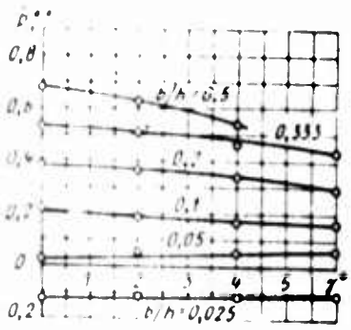

Fig. 78. Pressure coefficient for external section of bottom at elevated nozzle side as a function of angle of heel and parameter b/h ($\varphi = 30^{\circ}$; $b/D_{\beta 1} = 0.02$)

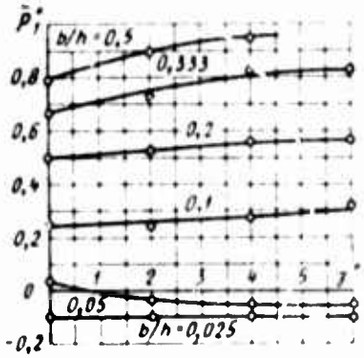

Fig. 79. Pressure coefficient for external section of bottom at depressed nozzle side as a function of angle of heel and parameter b/h (φ = 45°; b/D_{β} = 0.02)

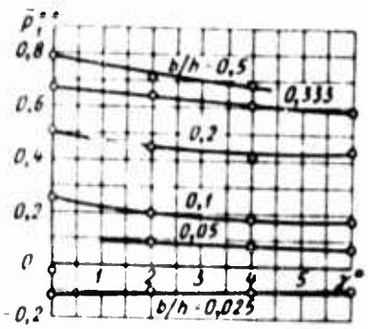

Fig. 80. Pressure coefficient for external section of bottom at elevated nozzle side as a function of angle of heel and parameter b/h (φ = 45°; b/D_{β} = 0.02)

Fig. 81. Pressure distribution over shield in the streaming of a two-pass annular jet (l = 0; $\varphi_1 = \varphi_2$ = 45°; $b_1/D_{\beta 1} = b_2/D_{\beta 1}$ = 0.02)

KEY: A — External nozzle
B — Points 65 and 128
C — Internal nozzle
D — Points 1 and 64

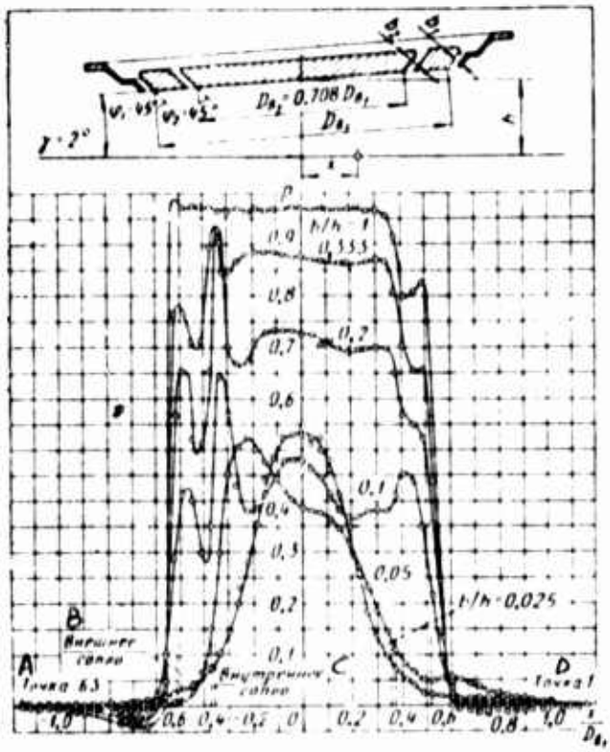

Fig. 82. Pressure distribution over shield in the streaming of a two-pass annular jet ($\gamma = 2°$; $\varphi_1 = \varphi_2 = 45°$; $b_1/D_{в1} = b_2/D_{в1} = 0.02$)

KEY: A -- Point 65
B -- External nozzle
C -- Internal nozzle
D -- Point 1

b/h -- the functions $\bar{p}_1^* = f(\gamma)$ for the near-shield zone, and the function $\bar{p}_1^{**} = f_2(\gamma)$ for the zone that is distant from the shield. These functions were obtained from test results shown in Figs. 67-74. Thus, Figs. 77 and 78 show that when $b/h = 0.5$ and when the angle is varied from 0 to 4°, the pressure coefficient p_1^* rises from 0.67 to 0.91, that is, by about 36 percent, and the pressure coefficient $\bar{p}_1^{**}$ decreases from 0.67 to 0.54, that is, by about 19 percent; but when $b/h < 0.1$, the rise in $\bar{p}_1^*$ and the decrease in $\bar{p}_1^{**}$ are virtually nonexistent as the angle of inclination γ is increased.

Therefore, as the distance between the shield and the nozzle is increased (with decrease in b/h), the pressure difference $p_1^* - p_2^{**}$ decreases, and this means that the righting moment acting on the nozzle

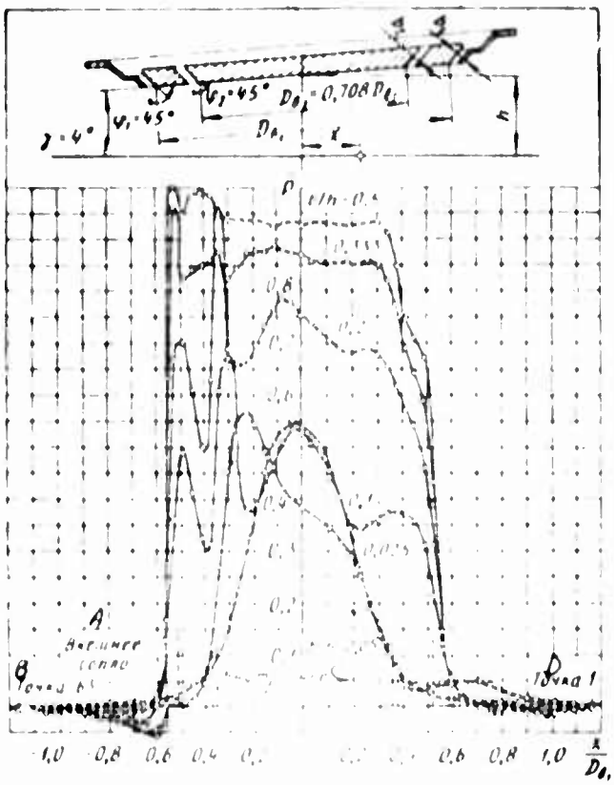

Fig. 85. Pressure distribution over shield in the streaming of a two-pass annular jet ($\gamma = 4^\circ$; $\varphi_1 = \varphi_2 = 45^\circ$; $b_1/D_{\beta 1} = b_2/D_{\beta 1} = 0.02$)

KEY: A -- External [illegible]
B -- Point [illegible]
C -- Internal [illegible]
D -- Poin[illegible]

is also reduced. For [illegible] between the nozzle and the shield, this pressure distance is near-zero.

Pressure distribution along the shield. The results of measuring pressure distribution along a shield from two coaxial annular jets streaming over it, exiting from a nozzle installation with nozzle inclination angle $\varphi = 45^\circ$ are presented in Figs. 85-87. Just as in the preceding experiments, variation in the parameter b/h was achieved by varying distance h between the shield and the nozzle installation.

Test results are presented in the form of the function $\bar{p} = f(x/D_{\beta 1})$, where x is the distance from the draining point tested on the shield at which the pressure p_β was measured to the axis of the nozzle installation

(shield axis), and D_{g1} is the diameter of the bottom of the nozzle installation determined with respect to the interior edge of the external nozzle. The pressure distribution was measured along two mutually perpendicular shield diameters.

The escape of air jets at the inclination angle $\gamma = 0$ of the nozzle installation with respect to the shield is shown in Fig. 81. As we can see, for values of the parameter $b/h = 1-0.1$ a considerable excess pressure is observed at the surface of the shield surrounded by annular jets. The pressure at the surface bounded by the inner jet is markedly higher than the pressure at the surface enclosed between the external and the internal jets. In this range of values of parameter b/h, the pressure distribution along the shield remains symmetric relative to its axis.

For the critical distance between the nozzle installation and the shield, that is, when $b/h = 0.04-0.1$, the symmetry of pressure distribution along the shield is disturbed. Just as in the case of pressure distribution along the bottom of the nozzle installation, the pressure distribution along the shield at this critical distance becomes especially nonuniform (the curve for $b/h = 0.05$). With further increase in the distance between the nozzle installation and the shield, the pattern of pressure distribution along the shield becomes the pattern that would obtain if not an annular, but a single, continuous cross-section jet of air impinged at the shield (the curve for $b/h = 0.25$). Inclining the nozzle installation leads to asymmetry of the pressure distribution along the shield. Increased pressure is observed at the side of the shield adjoining the bottom of the nozzle installation compared to the pressure at the side that is distant from the bottom. The nonuniformity of pressure distribution becomes greater as the angle of inclination γ is increased.

Especially significant nonuniformity of pressure distribution along the shield occurs for critical distances between the nozzle installation and the shield. For example, when $b/h = 0.05$ the pressure sharply drops off nearly to zero at the side of the shield that is distant from the nozzle installation (cf. Figs. 82 and 83). For distances between shield and nozzle installation that are greater than the critical value, for example when $b/h = 0.025$, the pressure distribution along the shield becomes similar to the distribution of pressure when a single continuous cross-section air jet flows along the shield.

Pressure coefficient and discharge coefficient of two-pass annular nozzle. Results of determining the pressure coefficients p_1 and p_2, respectively, at the external and internal sections of the bottom of the nozzle installation, and the discharge coefficient α of the nozzle installation as a whole, as a function of parameter b/h, are presented in Figs. 84 and 85 for the angle of inclination $\gamma = 0$. These functions were determined with constant value of the nozzle exit widths $b_1 = b_2 = 8$ mm and with the distance to the shield varied from 8 to 850 mm, and

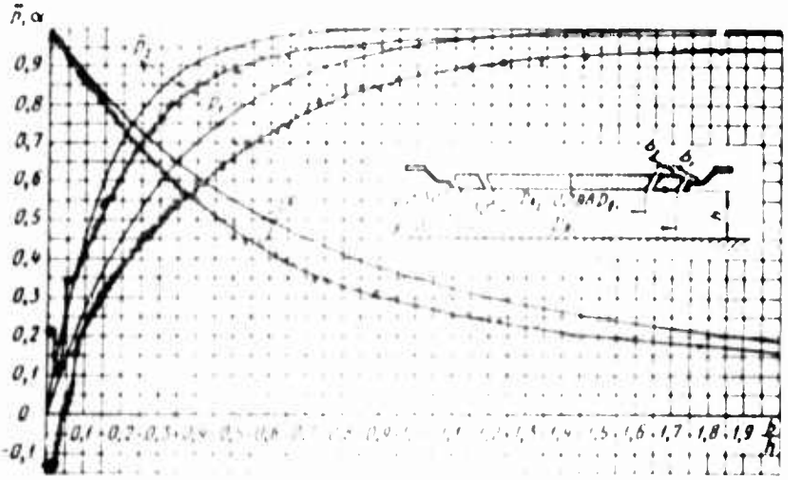

Fig. 84. Pressure coefficient and discharge coefficient as theoretical and experimental functions of parameter b/h for a two-pass annular nozzle when $\varphi_1 = \varphi_2 = 30^0$

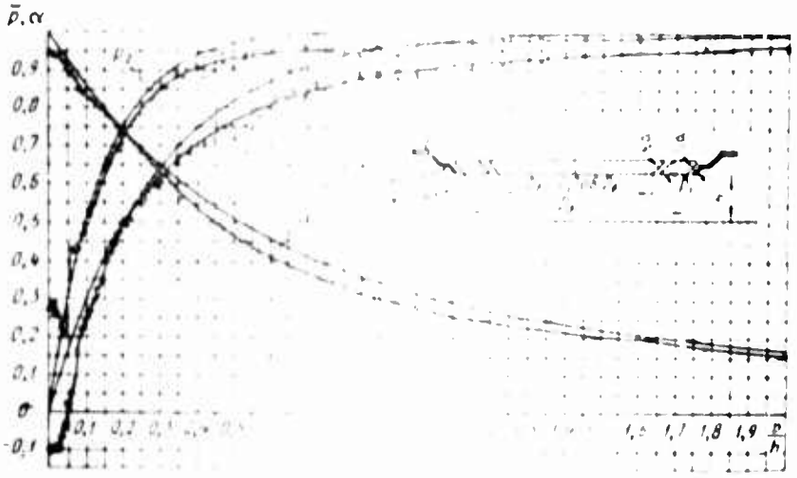

Fig. 85. Pressure coefficient and discharge coefficient as theoretical and experimental functions of parameter b/h for a two-pass annular nozzle when $\varphi_1 = \varphi_2 = 45^0$

also in testing the nozzle installation without placement of a shield (b/h = 0). The pressure coefficients $\bar{p}_1$ and $\bar{p}_2$ were found from the results of measuring pressure at the drainage points 2 and 24 and at drainage point 15, respectively, (cf. Fig. 65) and concerned the case of air escaping from a nozzle installation which the ratio of the exit width to the diameter of the bottom determined with respect to the inner edge of the external nozzle, $b/D_1 = 8/400 = 0.02$.

As the parameter b/h was reduced from 2 to 0.075 (cf. Figs. 84 and 85), that is, as the distance between the nozzle installation and the shield was increased, a monotonic reduction in the pressure coefficients $\bar{p}_1$ and $\bar{p}_2$ was observed. When $b/h < 0.075$, the change in the function $\bar{p} = f(b/h)$ was severely disrupted: the pressure at the external and the internal sections of the bottom of the nozzle installation dropped off sharply. At these critical distances between the nozzle installation and the shield, at first the external annular jet, not reaching the shield, merges with the internal annular jet, and then the common annular jet merges into a continuous jet flowing over the shield.

Tests showed that the pressure at the internal section of the bottom is considerably higher than the pressure of the external section. Thus, the ratio $p_2/p_1 = 1.07$ for a nozzle installation in which the inclination of the nozzle generatrix $\varphi = 45^\circ$ for $b/h = 1$, and the ratio $\bar{p}_2/\bar{p}_1 = 2.05$ -- when $b/h = 0.1$. As the distance between the nozzle installation and the shield was made greater, that is, as the parameter b/h was reduced, the pressure at the interior section of the bottom dropped more rapidly than in the exterior. For free discharge of annular jets, that is, in the case of flow without a shield ($b/h = 0$) the pressure coefficients $\bar{p}_1 = -0.13$ and $\bar{p}_2 = 0.21$ for a nozzle installation with angle of generatrix inclination $\varphi = 30^\circ$, and $\bar{p}_1 = -0.1$ and $\bar{p}_2 = 0.28$ -- for a nozzle installation in which the angle of generatrix inclination $\varphi = 45^\circ$.

The discharge coefficient of the nozzle installation for free air discharge $\alpha = 0.94$-0.97. The presence of a shield along the flow path of the jets reduces coefficient α. This is accounted for by the fact that the presence of the shield near the nozzle installation boosts the pressure at the interior side of the annular jets, intensifies the nonuniformity of a velocity distribution at the nozzle exits, and appreciably lowers the discharge of air for the same total pressure in the flow of air flowing into the nozzle installation. When $b/h = 0.15$-2 and for the same b/h values for nozzle installations inwwhich the angle of nozzle generatrix inclination $\varphi = 30$ and 45°, the discharge coefficients α are practically identical.

Experimental studies showed that the discharge coefficient α of the nozzle installation as a whole is practically independent of the angle of inclination γ of the shield with respect to the nozzle installation in the range of γ values 0-60° for a given distance between shield and center of the bottom, defined by parameter b/h. Therefore, as the parameter b/h and the angle of inclination γ are varied, the discharge coefficient α must take on the corresponding value of parameter b/h and $\gamma \approx 0$.

CHAPTER THREE
THEORETICAL STUDIES OF NOZZLE INSTALLATIONS IN AIR CUSHION VEHICLES

8. Characteristics of Peripheral Jets

One of the principal characteristics in the theory of air cushion vehicles is the dependence of excess pressure in the air cushion on the geometrical parameters of a nozzle installation, its position relative to the support surface, and the total pressure of the air flow fed to this installation. This function is advantageously expressed in the form of a dimensionless pressure coefficient characterizing the ratio of the excess pressure in the cushion to the total pressure of the stream of air fed to the nozzle installation. All other principal air dynamic characteristics, as for example, the discharge coefficient, drag coefficient, lift coefficient, torque coefficient, and coefficient of static stability are to some extent derivatives of this fundamental relationship.

There are several studies presenting a theoretical treatment of the air cushion and establishing a relationship between aerodynamic characteristics and geometrical parameters of the nozzle installation. Let us examine the results of the principal work done in this field and compare them with experimental data.

1. The first and simplest theory of the jet method of air cushion formation was proposed in 1936 by Boehler [67, 68], examining the case of discharge in which the jet of air exiting from a horizontally positioned two-dimensional peripheral [annular] nozzle is directed normal to the ground surface (Fig. 86 a). Boehler assumed air to be an inviscid and incompressible fluid, regarded the distribution of velocity $v_н$ and pressure $p_н$ in the plane of nozzle cut-off to be uniform and invariant along the length of the jet and, by applying the momentum equation to this flow, derived a relationship between the jet width b and height h of the nozzle with respect to the ground surface:

$$\rho v_н^2 b = (p_в - p_н) h,$$

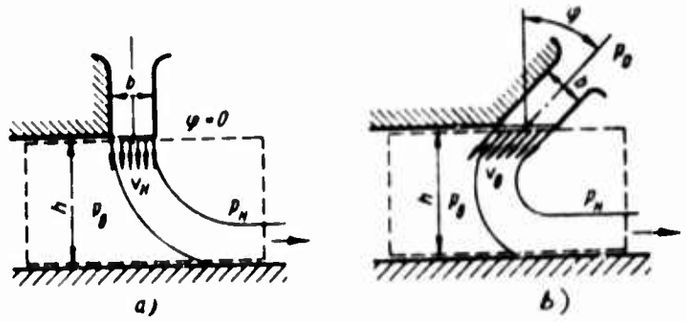

Fig. 86. Determining the air cushion pressure coefficient

where $p_в$ is the pressure in the air cushion.

The pressure coefficient of the air cushion is

$$\bar{p} = \frac{p_в - p_н}{\rho \frac{v_н^2}{2}} = 2\frac{h}{h}. \qquad (7)$$

Boehler [67] observed that this same formula for the pressure coefficient of air cushion was derived independently of him by Chaplin [69] in 1957 and was then expanded for use in the case a jet flowing from a nozzle at the angle φ to the ground surface. With reference to the angle φ, formula (7) becomes

$$\bar{p} = 2\frac{h}{h}(1 + \sin\varphi). \qquad (8)$$

Boehler and Chaplin extended Eqs. (7) and (8) to the case of a three-dimensional (annular) nozzle when the ratio of the exit width b to the diameter $D_н$ of the annular nozzle is extremely small.

In these studies [67, 69] it was assumed that the velocity in the plane of the nozzle cut-off is uniformly distributed and equal to the velocity $v_н$ of the exterior bounding jetlet. Therefore, the discharge coefficient of the nozzle in this case $\alpha = 1$. This assumption means that the effect of ground proximity on the pattern of flow of an air jet from a nozzle was neglected.

The function $\bar{p} = f(b/h)$ plotted by Eq. (8) is given in Fig. 87, curve 1. Here also was plotted the external function $\bar{p} = f(b/h)$ we obtained for an annular jet having parameters $b/D_в = 0.02$ and $\varphi = 45^\circ$ (curve 12).

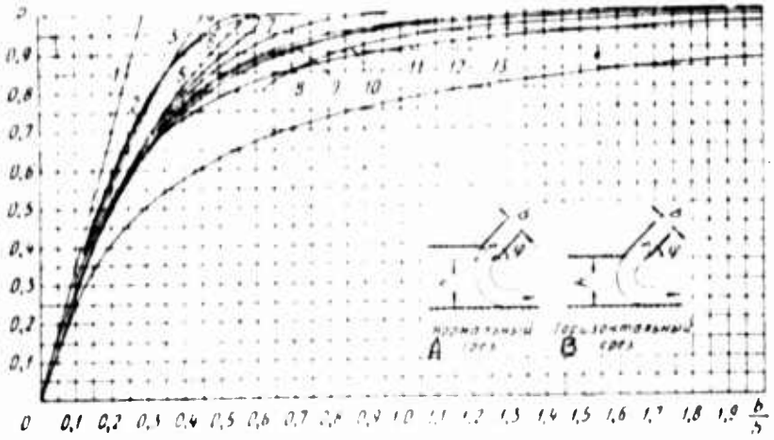

Fig. 87. Functions of air cushion pressure coefficients obtained by various theories:

1 -- according to Boehler-Chaplin ($v = v_н$; $p = p_н$)
2 -- according to Stanton Jones (horizontal cut-off; $R = R_н$)
3 -- according to Alexander
4 -- according to Pinnes (horizontal cut-off)
5 -- according to Stanton Jones ($p = (p_н + p_в)/2$) and for dp/dv = const
6 -- according to Cohen
7 -- according to Pinnes and according to Grewe and Eggington
8 -- according to Stepanov
9 -- according to Strand and Rechou
10 -- according to Stanton Jones (horizontal cut-off, $R = R_в$)
11 -- according to Ehrich
12 -- experimental curve for annular nozzle with horizontal cut-off ($b/D_в = 0.02$ and $\varphi = 45^\circ$)
13 -- based on calculations with $v = v_в$ and $p = p_в$

KEY: A -- Normal cut-off
B -- Horizontal cut-off

As we can see, Eq. (8) satisfactorily reflects the trend of the experimental curve only for very small values of b/h, that is, only for very high clearance heights h of the nozzle above the support surface, this means that Eq. (8) is suitable for very "thin" jets. For the case $\varphi = 45^\circ$, the coefficient $\bar{p} = 0$ already when $b/h = 0.295$. At larger b/h values, this theory becomes meaningless, since the pressure under the nozzle bottom can never exceed the total pressure of the jet. As applied to transport air cushion vehicles, the range of variation in clearance height from $h = 0$ to $h \approx (3\text{-}4)b$ is of interest. Therefore the practical applications of Eq. (8) are very restricted.

2. We can consider another case, which we offer as an extreme case, if we adopt the velocity and pressure in the jet in the plane of nozzle cut-off to be uniformly distributed and equal to the velocity v_δ and pressure p_δ at the inner boundary of the jet (cf. Fig. 86 b). If we assume that the velocity v_δ and the related volume flow of air $Q = v_\delta b$ remain constant along the length of the jet, the momentum equation for this curve will become

$$(1 + \sin\varphi)\rho v_\delta^2 b = (p_\delta - p_n)h.$$

According to the Bernoulli equation, the total pressure brought to the jet is

$$H = p_0 - p_n = p_\delta - p_n + \frac{\rho v_\delta^2}{2},$$

where p_0 is the total pressure in the receiver at the nozzle entrance.

Solving these equations jointly, we get

$$p = \frac{p_\delta - p_n}{H} = \frac{2b/h(1+\sin\varphi)}{1 + 2b/h(1+\sin\varphi)}. \qquad (9)$$

In this case the discharge coefficient of the nozzle is

$$\alpha = \frac{Q}{v_n b}$$

Using the Bernoulli equation, we will write

$$\frac{v_\delta}{v_n} = \sqrt{1 - \frac{p_\delta - p_n}{\frac{\rho v_n^2}{2}}} = \sqrt{1 - p},$$

$$\alpha = \frac{v_\delta}{v_n}\sqrt{1 - \frac{2b/h(1+\sin\varphi)}{1 + 2b/h(1+\sin\varphi)}} = \sqrt{\frac{1}{1 + 2b/h(1+\sin\varphi)}}. \qquad (10)$$

As we can see, when $\bar{h} = 0$ the pressure coefficient of the air cushion $\bar{p} = 1$, and when $\bar{h} \to \infty$, $\bar{p} \to 0$, that is, Eq. (9) gives valid limiting values of the coefficient $\bar{p}$.

Curve 13 plotted by Eq. (9) for the case $\varphi = 45^{\circ}$ is shown in Fig. 87. This formula gives appreciably smaller values of the air cushion pressure coefficient p compared with the values obtained experimentally.

The zone of possible values of the air cushion pressure coefficient is bounded by these two limiting cases, characterized by curves 1 and 13 plotted by Eqs. (8) and (9). Actually, the air velocity in the plane of nozzle cut-off decreases from v_{∞} to v_{β} in the direction from the outer edge to the inner, while the static pressure rises from the atmospheric value p_{∞} to the pressure p_{β} in the air cushion.

All other theoretical studies in this field aimed at finding regularities of the pressure and the velocity distribution in the plane of the nozzle cut-off and the subsequent determination of the air cushion pressure coefficient employing more or less crude assumptions.

5. In 1959 Stanton-Jones [70, 71] made a revision of the "thin" jet theory proposed by Boehler, assuming the pressure in the jet to be the arithmetic mean of the pressures at the boundaries of the jet, that is, $p = (p_{\beta} + p_{\infty})/2$. Accordingly, the momentum equation becomes

$$(1 - \sin\varphi)\rho\bar{v}^2 b = (p_{\beta} - p_{\infty})h,$$

and the Bernoulli equation is

$$H = \frac{p_{\beta} + p_{\infty}}{2} + \frac{\rho\bar{v}^2}{2}, \tag{11}$$

where $\bar{v}$ is the averaged velocity in the jet.

After the joint solution of these equations, the air cushion pressure coefficient was obtained:

$$\bar{p} = \frac{p_{\beta} - p_{\infty}}{H} = \frac{2b(1 - \sin\varphi)}{h + 2b(1 - \sin\varphi)}, \tag{12}$$

where $H = \frac{\rho v_{\infty}^2}{2}$ is the total pressure brought to the air jet.

The discharge coefficient of the nozzle can be represented in the form $\alpha = \frac{\bar{v}b}{v_{\infty}b} = \frac{\bar{v}}{v_{\infty}}$. From Eq. (11), we have

$$\frac{\bar{v}}{v_{\infty}} = \sqrt{1 - \frac{\frac{p_{\beta} - p_{\infty}}{2}}{\frac{\rho v_{\infty}^2}{2}}} = \sqrt{1 - \frac{\bar{p}}{2}}.$$

By replacing the air cushion pressure coefficient with its value taken from Eq. (12), we get

$$\alpha = \frac{v}{v_*} \left| \frac{1}{1 - b/h\,(1 + \sin q)} \right. \qquad (13)$$

Curve 5 (cf. Fig. 87) was plotted by Eq. (12) for the case $q = 45^\circ$. As we can see, the refinement of the pressure coefficient p proposed by Stanton Jones leads to a somewhat better agreement with experimental curve 1?. However, the pressure coefficient obtained by the Stanton Jones method, even when $b/h = 0.586$, gives the value $p = 1$. At larger b/h, Eq. (12) becomes meaningless, since $p > 1$.

4. As already stated, the pressure rises from $p_н$ to p_0 in the cross-section of the jet, in the direction toward the air cushion. To determine, to the first approximation, the aerodynamic characteristics of air cushion it is natural to assume that the pressure in the plane of the nozzle cut-off is linearly distributed [49]. Assuming the static pressure gradient to be constant, we get

$$\frac{b_x}{b} = \frac{p_x - p_н}{p_0 - p_н}, \qquad (14)$$

where b_x is the distance from the outer edge of the nozzle to the point in question; and p_x is the pressure at the point x under study.

The total pressure at each point of the cross-section of a jet is constant, therefore, by using the Bernoulli equation, we will write

$$\frac{\rho v_x^2}{2} + p_x = \frac{\rho v_0^2}{2} + p_0 = \frac{\rho v_н^2}{2} + p_н = \text{const},$$

where v_x is the velocity at this point.

From this equality it follows that

$$\frac{p_x - p_н}{\frac{\rho v_н^2}{2}} = 1 - \left(\frac{v_x}{v_н}\right)^2$$

and

$$p = \frac{p_0 - p_н}{\frac{\rho v_н^2}{2}} = 1 - \left(\frac{v_0}{v_н}\right)^2.$$

By using these functions, we can represent Eq. (14) in the form

$$\frac{b_x}{b} = \frac{1-\left(\frac{v_x}{v_m}\right)^4}{1-\left(\frac{v_e}{v_m}\right)^4}.$$

Hence the velocity field in the nozzle cut-off plane is

$$\frac{v_x}{v_m} = \sqrt{1-\frac{b_x}{b}\left[1-\left(\frac{v_e}{v_m}\right)^4\right]} = \sqrt{1-\frac{b_x}{b}\bar{p}}. \qquad (15)$$

Let us express the pressure coefficient $\bar{p}$ of the air cushion in terms of the geometrical parameters of the nozzle installation and the clearance height h of the craft above the ground surface. By employing the momentum equation to the contour enclosing the air jet, we will write

$$\int_0^b (1+\sin\varphi)\cos\varphi\rho v_x^2 db_x = h(p_e - p_n).$$

Then, by using Eq. (15), we finally get

$$\bar{p} = \frac{2b/h(1+\sin\varphi)}{1+b/h(1+\sin\varphi)}. \qquad (16)$$

With reference to Eq. (15), the discharge coefficient is

$$\alpha = \frac{Q_n}{Q_p} = \frac{\int_0^b v_x db}{v_m b} = \frac{1}{v_m b}\int_0^b v_m\sqrt{1-\frac{b_x}{b}\bar{p}}\,db.$$

After integrating, we get

$$\alpha = \frac{2}{3}\cdot\frac{1}{\bar{p}}\left[1-(1-\bar{p})^{3/2}\right]. \qquad (17)$$

The function $\bar{p} = f(b/h)$, plotted by Eq. (16) for the angle $\varphi = 45^\circ$, is shown in Fig. 87 (curve 5). Note that Eq. (16) for the pressure coefficient we obtained in 1960 independently of the studies of Stanton

Jones [70, 71] agree with Eq. (12) he proposed earlier. The only difference lies in the expressions of the discharge coefficient. Stanton Jones determined the discharge based on the mean escape velocity of the jet from the nozzle, while we use the approach of integrating the velocity field.

5. A paper by Pinnes [72] published in 1959 presents the determination of the air cushion pressure coefficient with reference to the variation in the velocity field in the nozzle cut-off plane caused by the pressure drop at the jet boundary. By examining the conditions of equilibrium of the centrifugal forces and the force of pressure acting on an elementary particle in a jet exerted by the air cushion, and assuming that on exiting from the nozzle the jetlets -- streaming over the ground surface -- will move along the arcs of a circle, and that the total pressure at each point in the jet cross-section remains constant, Pinnes concluded that the velocity in the cross-sections of a jet is distributed just as in a free vortex:

$$v_x R_x = v_\beta R_\beta = v_n R_n = \text{const},$$

where v_x is the velocity in the nozzle cut-off plane with coordinate R_x; R_x is the radius of the arc of a circle, where the velocity is v_x; R_β is the radius of the arc of a circle tangent to the exit edge of the inner side of the nozzle and the ground surface; R_n is the radius of the arc of a circle tangent to the outer edge of the outer wall of the nozzle; $R_\beta - R_n = b$, where b is the nozzle exit width (Fig. 88 a).

Fig. 88. For determining the air cushion pressure coefficient

Here the clearance height of the nozzle installation above the ground surface, with reference to the angle of inclination of the nozzle generatrix, is

$$h = R_n(1 - \sin\varphi) - b$$

Employing the symbols adopted and transforming the equations derived by Pinnes, we can represent them as follows.

The relative velocity at the nozzle exit is

$$\frac{v_x}{v_n} = \frac{R_n}{R_x} = \frac{1}{1 + \frac{b_x}{b}\cdot\frac{b/h}{1-b/h}(1+\sin\varphi)} = \frac{1-\frac{b/h}{h}}{1-\frac{b}{h}+\frac{b_x}{b}x},$$

where b_x is the distance from the outer edge of the nozzle exit to the point x of interest in the nozzle cut-off plane, where the velocity is b_x.

The relative excess static pressure in the nozzle cut-off plane is

$$\frac{p_x - p_n}{\frac{\rho v_n^2}{2}} = 1 - \left(\frac{R_n}{R_x}\right)^2 = 1 - \frac{1}{\left[1+\frac{b_x}{b}\cdot\frac{b/h}{1-b/h}(1+\sin\varphi)\right]^2},$$

where p_x is the static pressure at this point in the nozzle cut-off with coordinate b_x. The pressure coefficient of the air cushion (curve 7, cf. Fig. 87) is

$$p = \frac{p_e - p_n}{\frac{\rho v_n^2}{2}} = 1 - \left(\frac{R_n}{R_e}\right)^2 = 1 - \left(\frac{1-\frac{b/h}{h}}{1-\frac{b}{h}\sin\varphi}\right)^2. \qquad (18)$$

The discharge coefficient of the nozzle installation is

$$\alpha = \frac{\int_0^b v_x\,dy_x}{v_n b} = \frac{1-\frac{b/h}{h}\sin\varphi}{\frac{b}{h}(1-\sin\varphi)}\ln\frac{\frac{b}{h}\sin\varphi}{1-\frac{b}{h}}. \qquad (19)$$

In these formulas the height h is the distance between the exit edge of the outer nozzle wall and the support surface.

If we assume that the nozzle cut-off lies in the plane of the vehicle bottom and that the clearance height is equal to the distance between the bottom and the support surface (cf. Fig. 88 b), that is,

$$h = R_e(1-\sin\varphi) = (R_n - b)(1-\sin\varphi),$$

then the formulas for the air cushion pressure coefficient (curve 4, cf. Fig. 87) and for the nozzle discharge coefficient will become:

$$\bar{p} = 1 - \left[1 - \frac{b}{h}(1 + \sin\varphi)\right]^2; \qquad (20)$$

$$\alpha = \frac{1 - \frac{b/h(1 + \sin\varphi)}{b/h(1 + \sin\varphi)}}{1 - \frac{1}{b/h(1 + \sin\varphi)}}. \qquad (21)$$

If we expand Eq. (20) and neglect the term $[b/h\ (1 + \sin\varphi)]^2$, since it is small, we get Eq (8), proposed by Chaplin [69].

6. Grewe and Eggington proposed in a paper [73] published in 1960 that at the nozzle exit the jet is in the form of an arc of a circle in the vertical plane with constant width b, which is comparable to the mean radius of curvature of a jet equal to $R_m + b/2$, where R_m is the radius of the outer boundary of the jet.

Examining the forces acting on the elementary air particle, Grewe and Eggington assumed that the pressure gradient along the width of the jet is equalized by the centrifugal forces induced in the turning of the jet,

$$\frac{dp}{db_x} = \frac{\rho v^2}{R} = \frac{\rho v^2}{R_m + b_x}. \qquad (22)$$

By the Bernoulli equation, we have

$$p + \frac{\rho v^2}{2} = H,$$

where p and v are variables; and H is the total pressure required for jet formation.

With reference to the Bernoulli equation, Eq. (22) can be represented in the form

$$\frac{d(p/H)}{1 - p/H} = -2\frac{d(1 - b_x/R_m)}{1 - b_x/R_m}.$$

Integrating within the limits from p_m (the pressure at the outer boundary of the jet) to p_s (pressure at the inner boundary of the jet, equal to the pressure in the air cushion), and from $b_x = 0$ to $b_x = b$, we get the air cushion pressure coefficient

$$\bar{p} = \frac{p_s}{H} = \frac{1 + 2R_m b}{(1 + R_m/b)^2}. \qquad (23)$$

From the adopted geometrical form of the jet it follows that $h = b + R_н(1 + \sin\varphi)$, whence we have the parameter

$$\frac{R_н}{b} = \frac{1}{b/h(1 - \sin\varphi)}.$$

The nozzle discharge coefficient is

$$\alpha = \frac{\int v_x db_x}{v_x F_c} \qquad (24)$$

where v_x is the velocity at the instantaneous point in the nozzle cut-off plane; $Q_н$ is the volume flow of air under conditions of ground proximity; and Q_p is the volume flow of air when the jet escapes freely (no shield is present).

The Bernoulli equation in differential form is $dp = -v\,dv$. Inserting this expression into Eq. (22), we get

$$\frac{dv}{v} = \frac{db_x}{R_н - b_x}.$$

Integrating the left-hand side of this equation within the limits $v_н$ the velocity of the outer boundary of the jet to v_x -- the velocity at the point in question with coordinate b_x, we get an expression for the velocity field in the jet

$$\frac{v}{v_н} = \frac{1}{1 - b_x/R_н}. \qquad (25)$$

Replacing velocity v_x in Eq. (24) by its expression from Eq. (25), we get

$$\alpha = \frac{1}{b/R_н}\left[1 - \frac{R_н}{b}\ln\left(1 + \frac{b}{R_н}\right)\right]. \qquad (26)$$

Eqs. (25) and (26) proposed by Grewe and Eggington, if they are expressed as a function of b/h, agree with Eqs. (18) and (19) of Pirnes (curve 7, Fig. 87). On inspecting Eq. (25), we can see that the velocities in the cross-sections of the jet adopted by Grewe and Eggington are distributed the same as in a free vortex.

7. In his work [71], in addition to revising the Boehler-Chaplin "thin" jet theory [68, 69], Stanton Jones proposed an exponential function for a wide range of values for the jet thickness-craft elevation ratio, that is, for a "thick" jet. Stanton Jones assumed that on exiting from a nozzle the jet is curved at the shield along the arc of a circle, without modifying its thickness, while the pressure in the air cushion is reduced by centrifugal forces caused by the movement of the jet along a curved trajectory. In this case the simplified equation of the equilibrium of forces acting on an elementary jet mass is

$$\frac{dp}{dh} = \frac{p}{R}$$

or, when the Bernoulli formula $\left(p = \frac{\rho v^2}{2}\right)$, is used,

$$\frac{d(pH)}{pH} = 2\frac{dh}{R}.$$

Stanton Jones, in contrast to Crewe and Eggington [73] considers the radius R as a constant and, after integration, obtains

$$p = \frac{p_0}{H}\left(p_a - \left(p_a - H\right)e^{-\frac{h}{R}}\right).$$

Assuming that radius R appearing in this formula is equal to the radius of the streamline bounding the air cushion and bearing in mind the adopted jet scheme (Fig. 88 b), Stanton Jones found $R = R_\beta = h/(1 + \sin\varphi)$, and then

$$p = \frac{p_0}{H}\left(p_a - \left(p_a - H\right)e^{-\frac{(1+\sin\varphi)h}{h}}\right). \qquad (27)$$

Assuming that radius R is equal to the radius of the streamline bounding the ambient atmosphere (Fig. 88 c), Stanton Jones obtains $R = R_a = (h - b)/(1 + \sin\varphi)$, and thus,

$$p = \frac{p_0}{H}\left(p_a - \left(p_a - H\right)e^{-\frac{(1+\sin\varphi)h}{h-b}}\right). \qquad (28)$$

These formulas were derived for a nozzle with horizontal cut-off in which the exit edges lie in the same plane with the bottom of the nozzle installation.

Comparison showed that curve 10 (cf. Fig. 87) derived by Eq. (27) agrees better with experimental data then curve 2 determined by Eq. (28). Eq. (27) has been used by numerous authors [42, 74-78].

8. In his work [79] published in 1966, Alexander examines the functions $p = 2x/(1 + x)$ and $p = 1 - e^{-1.4x}$, where $x = b/h\,(1 + \sin\varphi)$ and states that none of these expressions can be accepted as satisfactory when $b/h > 1$, since underlying the derivation of these equations with the condition of constant momentum along the jet length on the assumption that the jet width b over the entire path of its travel remains invariant. Under these assumptions, as Alexander maintains, the condition of continuity is violated.

Alexander suggested that the momentum equation be applied to this case of flow as follows:

$$\rho \bar{v}^2 b \sin\varphi = \rho v_n^2 b_n - (p_a - p_n) h, \qquad (29)$$

where $\bar{v}$ is the mean jet velocity at the nozzle exit; v_n is the nozzle of the jet exiting toward one side of the air cushion, where the pressure in the jet cross-section is equal to the atmospheric; and b_n is the jet width at atmospheric pressure.

Assuming the mean pressure in the nozzle cut-off plane $p = (p_c + p_n)/2$ and using the Bernoulli equation, we can write

$$H = \frac{p_c - p_n}{2} + \frac{\rho \bar{v}^2}{2} + \frac{p_a - p_n}{2}, \qquad (30)$$

$$\rho \bar{v}^2 = [2H - (p_a - p_n)]\,b.$$

With reference to the continuity condition

$$\qquad (31)$$

and Eqs. (30) and (31), the momentum of the departing stream is

$$\rho v_n^2 b_n = \rho \bar{v}^2 b \sin\varphi = [2H + 2H - (p_a - p_n)] =$$
$$= 2Hb \left[1 - \frac{p_c - p_n}{4H} - \left(\frac{p_a - p_n}{4H} \right)^2 \right].$$

Neglecting the term $[(p_c - p_n)/4H]^2$ because of its smallness, we get

$$\rho v_n^2 b_n = \frac{\rho}{2} [4H - (p_a - p_n)]$$

After these transformations, Eq. (29) can be represented as

$$(p_* - p_\infty)\,h = -[2H - (p_* - p_\infty)]\,b\sin\varphi + \frac{b}{2}\,[4H - (p_* - p_\infty)].$$

Then the air cushion pressure coefficient is

$$\bar{p} = \frac{p_* - p_\infty}{H} = \frac{2x}{1 + x} - \frac{b}{2h}\,\frac{2x}{1 - x}\left[1 - \frac{1}{2(1 + \sin\varphi)}\right]. \qquad (32)$$

Using the assumptions presented and referring to the absence of adequate experimental data, Alexander assumed that the actual pressure in an air cushion must be higher than the values expressed by formulas $\bar{p} = 2x/(1 + x)$ and $\bar{p} = 1 - e^{-2x}$. However, experimental data refuted this conclusion of Alexander's. Fig. 87 presents the function (curve 5) $\bar{p} = f(b/h)$ plotted by Eq. (32) for $\varphi = 45^\circ$.

9. Considering the escape of an air jet from a flat nozzle against a shield, using the velocity hodograph method, and introducing simplifying assumptions, Stepanov [41] obtained the following approximate relationship: $v_1 = (v_2 v_3)^{\frac{1}{2}}$, according to which the mean velocity v_1 in the nozzle exit is equal to the geometric mean of the velocities at the exterior v_2 and the interior v_3 limits of the jet.

Applying the momentum theorem to a control contour enclosing a curved section of a jet and using the continuity equation and the Bernoulli equation, Stepanov derived an equation relating the geometric and aerodynamic parameters of a jet:

$$\frac{h}{b} = \frac{v_2 v_3 - v_1^2}{v_2^2 - v_3^2}\cos\alpha + \frac{2v_2\sqrt{v_1 v_3}}{v_2^2 - v_3^2}$$

or

$$\frac{h}{b} = \frac{1}{2}\,x(x - 1) + x - 1\cos\alpha + 2\,|\,x\,|\,\sqrt{x(x - 1)}, \qquad (33)$$

where

$$x = \frac{p^*}{p_1} = \frac{p_2}{p_3} = \frac{v_3}{v_2} < 1 \qquad (34)$$

and

$$x = 1 - \frac{p^* - p_3}{p_2 - p_3} = \frac{v_1^2}{v_2^2 - v_3^2}. \qquad (35)$$

Here p_2 is the pressure at the outer boundary of the jet; p_3 is the pressure at the inner boundary of the jet (air cushion pressure); p^* is the total pressure in the jet (pressure of stagnant stream); and α is the angle of inclination of the nozzle generatrix to the horizontal.

Converting to our symbols, eq. (35) can be represented as

$$\frac{h}{h} = \frac{p}{2\left(1 - p\right)\left(1 - \bar{p}\right)\sin\varphi}, \qquad (36)$$

since

$$p = \frac{p_2 - p_3}{\rho v_2^2} = \frac{1}{x} = \frac{p_2 - p_3}{p^* - p_3}.$$

Let us find the discharge coefficient of a flat nozzle, using the function $v_1 = (v_2 v_3)^{\frac{1}{2}}$. The discharge of a flat nozzle is

$$Q = 2lb = \mu b \int_0^{\frac{2}{\rho}} (p^* - p),$$

from whence

$$\mu = \frac{Q}{b \int_0^{\frac{2}{\rho}} (p^* - p)}$$

Using the equality [illegible] and eqs. (34) and (35), we get $\mu = (1 - 1/x)^{\frac{1}{4}}$ or, in our symbols, $\mu = (1 - \bar{p})^{\frac{1}{4}}$.

With reference to eq. (36), the discharge coefficient of a flat nozzle can be determined from the formula

$$\mu = \frac{1 - \bar{p}^4}{\left(1 - \bar{p}\right)\left(1 - \bar{p}\right)\sin\varphi} \qquad (37)$$

The function $\bar{p} = f(b/h)$, plotted by eq. (36) for $\varphi = 45^\circ$, is given in Fig. 87 (curve 8).

10. In 1959, Strand [80, 81] examined the streaming along a shield of a flat peripheral [annular] jet exiting from a nozzle with normal exit cut-off. Desiring to find the characteristics of an air cushion over wide range of variation in the relative jet width to craft hovering height, including also for the so-called "thick" jets characterized by high values of this ratio ($b/h > 0.3$), Strand employed the method of functions of a complex variable for his study, using the Schwarz-Christoffel transformations, and obtained solutions expressible in terms of first-order elliptical integrals.

The results of numerical calculations were represented as plots expressing the dependence of the pressure coefficient p of an air cushion on parameter b/h for values of the angle of nozzle inclination to the ground surface $\varphi = 0$, 30, and 60°. Fig. 87 (curve 9) presents the function $p = f(b/h)$ for the case $\varphi = 45^{\circ}$, obtained by graphical interpolation of curves calculated by Strand.

11. F. Ehrich [82] examined two characteristic cases of the flow of a peripheral jet from a nozzle onto a shield. In the first case, streaming along the shield, the jet splits, one part of the stream moves toward the increased-pressure region, while the other departs to the outside away from the air cushion. In the second case the entire jet moves to the exterior. F. Ehrich studied flow from a nozzle with an arbitrary exit cut-off angle. In solving the problem, used conformal mappings, the velocity hodograph, and the Schwarz-Christoffel transformations. The resulting equations proved to be extremely complex, and their solution was possible only by the method of numerical integration.

Calculations showed that increasing the angle of inclination of nozzle generatrix in the region $\varphi = 0$-45° leads to a rise in the pressure coefficient p of the air cushion both for the split jet as well as for the jet completely deflected to the outside. Here the coefficient p takes on larger values for the jet deflected to the outside.

The discharge coefficient of a nozzle increases as the angle φ is increased for a split jet, but it decreases for the jet completely deflected to the outside. For identical clearances of the nozzle above the shield (in the range $h/b = 0$-1), the coefficient c is greater for the split jet than for the jet deflected to the outside.

Reducing the height of the exit edge of the inner wall of the nozzle while the elevation height of the nozzle above the shield is kept constant, which corresponds to varying the exit cut-off angle of the nozzle, brings about a drop in the air cushion pressure coefficient for the split jet, but increases the pressure coefficient p for the jet deflected to the outside. In other words, the nozzle with horizontal wall cut-off is more advantageous compared to the nozzle variant with a normal cut-off. Fig. 87 (curve 11) presents the dependence of the air cushion pressure coefficient p on parameter b/h, taken from the work of Ehrich, for a nozzle with normal cut-off and angle of generatrix inclination $\varphi = 45^{\circ}$.

·2. In his work [85], published in 1966, Cohen examined, using the hodograph method, the flow of a peripheral two-dimensional jet near the support surface and obtained in closed form the characteristics of the jet over some range of variation of three main design parameters -- jet thickness b, angle φ of nozzle generatrix inclination, and clearance height h of the nozzle over the support surface. The effect of the angle of nozzle exit cut-off on air cushion characteristics was determined.

The trend of the solution to the problem led to first-order elliptical integrals. By introducing simplifications and approximating several expressions appearing in the elliptical integral, Cohen obtained the following approximate functions associating nozzle geometry with jet parameters.

The form of the internal free streamline of the jet (on the air cushion side) is well approximated by the arc of a circle having the radius

$$R = \frac{\frac{v_0}{v_2} b}{\ln \frac{v_1}{v_2}} \tag{38}$$

and with its center lying along a normal to the nozzle wall.

The slope of the nozzle cut-off taper (angle between a line connecting the exit edges of the nozzle and the normal to the nozzle walls) is

$$\operatorname{tg} \psi = \frac{\ln \frac{1-\zeta}{1+\zeta}}{\pi}, \tag{39}$$

where

$$\zeta = \sin\left[\frac{\pi}{2}\left(1 - \frac{2 \ln \frac{v_1}{v_0}}{\ln \frac{v_1}{v_2}}\right)\right]. \tag{40}$$

Here v_0 is the mean air velocity within the nozzle (velocity at large distances from the exit cross-section); v_1 is the velocity at the free streamline at the outer boundary of the jet; and v_2 is the velocity at the free streamline at the inner boundary of the jet.

Cohen determined the lift of an air cushion vehicle and analyzed the change in the ratio of lift near the ground surface to the thrust at large distances from the ground. In his paper, Cohen does not present functions expressing the pressure change in the air cushion. Let us find this function, by replacing in Eqs. (38) and (39) the relative velocity v_1/v_0 and the coefficient ζ with the corresponding pressure ratio.

The radius of curvature of the internal free streamline of the jet, in accordance with the assumed geometrical parameters of the nozzle and the jet discharging from it is

$$R = \frac{h + b(\sin\varphi + \cos\varphi \operatorname{tg}\psi)}{1 + \sin\psi}, \tag{41}$$

where h is the clearance height of the nozzle (exit edge of the outer nozzle wall) above the support surface.

The total pressure in the plane of the nozzle cut-off is kept constant, and therefore,

$$\frac{p_3 - p_1}{\frac{\rho v_1^2}{2}} = \bar{p} = 1 - \left(\frac{v_2}{v_1}\right)^2.$$

Further, using Eqs. (38)-(41), let us represent the air cushion pressure coefficient in the form

$$\bar{p} = 1 - e^{-c(1-\bar{p})^a}. \tag{42}$$

Here

$$c = \frac{b\,h(1 + \sin\varphi)}{1 + b\,h(\sin\varphi + \cos\varphi \operatorname{tg}\psi)}$$

and

$$a = \frac{1}{4} + \frac{\arctg \zeta}{2\pi},$$

where

$$\zeta = \frac{1 - e^{\pi \operatorname{tg}\psi}}{1 + e^{\pi \operatorname{tg}\psi}}.$$

For a nozzle installation with normal nozzle cut-off ($\psi = 0$), we have

$$\bar{p} = 1 - e^{-2\frac{c}{\sqrt{1-\bar{p}}}},$$

and in the case $\varphi = 0$ and $\psi = 0$, we have

$$\bar{p} = 1 - e^{-2\frac{b/h}{\sqrt{1-\bar{p}}}}.$$

Fig. 87 (curve 6) presents the function $\bar{p} = f(b/h)$, plotted by Eq. (42) for $\varphi = 45^{\circ}$.

15. In his work [84] presented at the International Congress on Applied Mechanics in 1964 and published in 1966, Rechou examined the plane problem of the discharge of a peripheral [annular] jet onto a shield, employing functions of a complex variable for his study. The nozzle had a normal exit cut-off. Using Fourier series, being limited to the first terms of the expansion and making several assumptions, Rechou arrived at the following approximate expressions relating nozzle geometry to jet aerodynamic parameters:

$$\frac{b}{\varepsilon} = \frac{e^{a}-1}{a}; \quad \frac{h}{\varepsilon} = 1 + \operatorname{cth} a - \frac{\cos\varphi}{a}; \quad \frac{h}{b} = \frac{a(1 + \operatorname{cth} a) + \cos\varphi}{e^{a}-1}, \quad (43)$$

where ε is the jet thickness at a distance tending to infinity.

In this case the air cushion pressure coefficient is

$$\bar{p} = \frac{p_2}{p_1} = 1 - e^{-a}, \quad (44)$$

where

$$a = \ln \frac{v_1}{v_2}.$$

It must be noted that a quantity that is the reciprocal of b/ε is the discharge coefficient of the nozzle, the ratio of the actual volume flow q of air to the volume flow q_p where there is uniform velocity distribution at the nozzle cut-off, that is,

$$\alpha = \frac{q}{q_p} = \frac{v_1 b}{v_1 b} = \frac{\varepsilon}{b} = \frac{a}{e^{a}-1}.$$

A function plotted according to Eq. (44) coincides with high accuracy with curve $\bar{p} = f(b/h)$ calculated by Strand (cf. curve 9 in Fig. 87).

These theoretical studies on the determination of aerodynamic characteristics of peripheral jets can be conventionally divided into two groups. The first includes the works of Boehler, Chaplin, Stanton Jones, Pinnes, and so on, in which simplified models of the physical phenomenon associated with the discharge of air jets onto a shield serve as a basis of theoretical generalizations. This enables the authors to derive for the air cushion pressure coefficient simple functions expressed in explicit form, and agreeing quite satisfactorily with experimental results only in a narrow range of geometrical parameters.

The other group encompasses the works of Strand, Ehrich, Cohen, and Keehou. The authors of these works examined the discharge of peripheral jets from nozzles onto a shield more rigorously, employing methods of the theory of functions of a complex variable. However, the solutions obtained in these investigations require complex and laborious calculations or else are given in the form of implicit functions, which markedly complicates their use for practical purposes, particularly in subsequent analysis of aerodynamic and energy characteristics of air cushion vehicles.

In all these studies the air jet streaming along the shield is considered as a flow devoid of viscosity. Such an ideal flow naturally differs from the motion of an actual air jet and the analytical functions obtained reflect only to some degree of approximation the actual pattern of the streaming of an air jet over the shield. Allowing for viscosity even further complicates the final formulas used in calculating aerodynamic characteristics.

Therefore, it appears to us desirable to derive functions in which -- with allowance for the principal features of the physical phenomenon of the discharge of a jet onto a shield — relate in explicit form aerodynamic characteristics of an air cushion with the geometrical parameters of the nozzle installation and its position relative to the support surface in the entire range of variation of the craft hovering regime. It is also desirable that these functions be convenient for practical use in calculating both single-pass as well as sectionalized nozzle installations.

9. Nozzle Installation With Normal Nozzle Cut-off

Let us find functions [1] relating the geometric parameters of a nozzle installation, its clearance height above the support surface, and the aerodynamic parameters of the air stream brought to this installation. Let us determine the air cushion pressure coefficient, discharge coefficient, and drag coefficient of the nozzle installation, and set up relationships between them.

---

[1] The theory proposed was developed by the author in 1961 for single-pass nozzles with horizontal cut-off and was employed in calculations of an air cushion vehicle designed and built in 1961-1962. In 1963 this theory was extended to single-pass nozzles with normal and oblique cut-offs, and in 1964 -- to sectionalized (two-pass) nozzle installations with arbitrary placement of external and internal nozzles. Further consideration yielded, in 1966, analytic expressions of characteristics for sectionalized nozzle installations inclined with respect to the support surface.

Let us examine the discharge of air from the nozzle installation onto the shield (cf. Figs. 37 and 89). Under the effect of the excess pressure $p_0 - p_H$ maintained constant in the receiver, the air is brought into the nozzle and exits from it in the form of jets directed downward. On encountering the shield along their path, the jets become curved and stream along it to either side. With increasing separation from the axis of the nozzle installation, the jet thickness is reduced, as is the jet curvature. At some distance from the nozzle the compression of the jets ends and they travel along the shield surface. Owing to the viscosity and the consequently induced ejection effect, a boundary layer is formed at the jet boundaries. Air sucked from the exterior space is entrained by a jet in the direction of its motion. The air ejected from the inner space, on approaching the shield, is separated from the jet and exits to the side opposite the direction of the main mass of the jet. A circulation flow is induced in the inner space.

In the region bounded by the bottom of the nozzle, shield, and jets, excess pressure -- an air cushion -- is induced as the result of the reaction effect of the jets. As this takes place, in the plane of the nozzle cut-off, the pressure drops from atmospheric p_H to the air cushion pressure p_δ in a direction from the outer trailing edge of the nozzle to the inner, and therefore, there is a transverse pressure gradient in the jet in the plane of nozzle cut-off. The nonuniformity of velocity distribution in the nozzle cut-off plane corresponds to this nonuniformity in pressure distribution: the greatest velocity is near the external exit edge of the nozzle; while the least, determined by the counter pressure [back pressure] produced by the air cushion -- is near the inner edge.

The excess pressure in the air cushion causes pressure forces to become evident, acting on the shield, nozzle bottom, and the jet, and maintaining the latter on a curved trajectory. It can be noted that with the nozzle position kept unchanged relative to the shield, the air cushion pressure varies in proportion to the momentum of the jets ($\Delta p \sim \rho v^2$), while with the momentum kept constant the pressure in the air cushion is inversely proportional to the distance between the nozzle and the shield ($\Delta p \sim 1/h$). With these factors taken into account, the pressure in the nozzle cut-off plane can be expressed as follows for the particular nozzle installation with normal cut-off:

$$\frac{dp}{dx} = \frac{\rho v^2 (1 + \sin\varphi)}{h + x \sin\varphi}, \qquad (45)$$

that is, we will assume that at the nozzle cut-off there is a static pressure gradient that is dependent on the angle of jet inclination with respect to the shield and that varies in direct proportional to the momentum of the elementary jetlet in the plane of nozzle cut-off and inversely proportional to the distance from the exit location of this jetlet issuing from the nozzle to the shield.

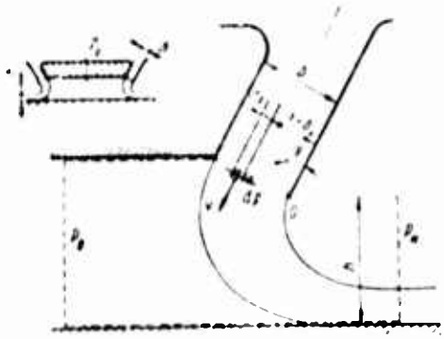

Fig. 89. For calculating the aerodynamic characteristics of air cushion produced by a jet escaping from a nozzle with normal cut-off

If we neglect the friction of air against the nozzle wall and assume the air to be an ideal fluid, then we can assume that the total pressure at each point in the jet in the nozzle cut-off plane remains constant, equal to the excess pressure in the receiver ahead of the nozzle installation, that is $p + \frac{\rho v^2}{2} = p_0 - p_н = \text{const}$, where p and v are the static pressure and air velocity, respectively, at the point in question. Therefore for the nozzle cut-off, by Bernoulli's equation, we have

$$dp = -\rho v\, dv. \tag{46}$$

Inserting this expression into Eq. (45), we get

$$\frac{dv}{v} = -\frac{v(1+\sin\varphi)}{h + x\sin\varphi}. \tag{47}$$

Thus, in the plane of nozzle cut-off in the direction to its inner edge there is a velocity gradient dependent on the angle of jet inclination with respect to the shield and varying in direct proportion to the velocity at the given point and in inverse proportion to the distance from this point to the shield.

Velocity field in nozzle cut-off plane. To obtain the velocity distribution in the nozzle cut-off plane, let us solve differential equation (47). After separation of variables, we get

$$\int_{v_н}^{v_x} \frac{dv}{v} = -(1+\sin\varphi)\int_0^{b_x} \frac{dx}{h + x\sin\varphi}$$

and, therefore,

$$\ln \frac{v_x}{v_м} = -\frac{(1+\sin\varphi)}{\sin\varphi} \ln\left(1+\frac{b_x}{b}\cdot\frac{b}{h}\sin\varphi\right). \qquad (48)$$

Converting from the logarithm to the exponential function, this result can be represented as

$$\frac{v_x}{v_м} = e^{-\left(1+\frac{1}{\sin\varphi}\right)\ln\left(1+\frac{b_x}{b}\cdot\frac{b}{h}\sin\varphi\right)}$$

or

$$\frac{v_x}{v_м} = \left(1+\frac{b_x}{b}\cdot\frac{b}{h}\sin\varphi\right)^{-\left(1+\frac{1}{\sin\varphi}\right)}. \qquad (49)$$

Assigning the instantaneous coordinate b_x/b various values within the limits from 0 to 1 and using this formula, without difficulty we can construct the velocity field as a function of parameter b/h and the slope of the generatrix to the axis of the nozzle installation. When $b_x = b$, we get the formula

$$\frac{v_\beta}{v_м} = \left(1+\frac{b}{h}\sin\varphi\right)^{-\left(1+\frac{1}{\sin\varphi}\right)},$$

enabling us to calculate the velocity v_β of the jetlet travelling from the inner edge of the nozzle at the boundary with the air cushion.

When the slope $\varphi = 0$, Eq. (49) becomes meaningless, since the function $v_x/v_м = f(\varphi)$ expressed by this formula is analogous to the function $y = (1+x)^{\frac{1}{x}}$, defining the Napier number e, has an apparent discontinuity for $\varphi = 0$. Actually, this formula, as $\varphi \to 0$, tends to its limit and is continuous also at the point $\varphi = 0$.

Let us find the expression for the velocity field of the nozzle cut-off when the generatrix slope $\varphi = 0$. As applied to this case, Eq. (45) becomes simplified and takes on the form

$$\rho v^2\, dx = h\, dp.$$

Replacing the pressure drop dp with its expression by Eq. (46), we get

$$\frac{dx}{h} = -\frac{dv}{v}.$$

Integrating this expression within the same limits as for the case $\varphi \neq 0$, we find

$$\frac{v_x}{v_H} = e^{-\frac{b_x}{h}} = e^{-\frac{b_x}{b}\cdot\frac{b}{h}}. \tag{50}$$

Eq. (50) determines in dimensionless form the velocity field in the cut-off plane of a nozzle having the generatrix slope $\varphi = 0$. Fig. 90 presents in dimensionless form theoretical velocity fields in a jet as it exits from nozzles with generatrix slope $\varphi = 30$, 45, 60, and 90°, and for various values of parameter b/h. The velocity fields were plotted by Eq. (49).

Therefore, the greatest nonuniformity in pressure distribution in the nozzle cut-off plane obtains for large values of parameter b/h. Here the velocity field profile faces the nozzle cut-off with its concavity. With decrease in parameter b/h, which can be obtained either by reducing the nozzle exit width b or by increasing height h of its elevation above the ground surface, the velocity field is rapidly equalized, approaching the linear distribution. Moreover, with increase in the slope φ of the nozzle generatrix for identical values of parameter b/h, the nonuniformity of velocity distribution in the nozzle cut-off plane increases somewhat.

Pressure field in nozzle cut-off plane. If we use the Bernoulli equation as applied to the nozzle cut-off in each point of which the total pressure remains constant, then

$$p_x + \frac{\rho v_x^2}{2} = p_H + \frac{\rho v_H^2}{2}.$$

Then

$$\frac{p_x - p_H}{\frac{\rho v_H^2}{2}} = 1 - \left(\frac{v_x}{v_H}\right)^2. \tag{51}$$

Replacing in Eq. (51) the ratio v_x/v_H with the corresponding value from Eq. (49), we get

$$\frac{p_x - p_H}{\frac{\rho v_H^2}{2}} = 1 - e^{-2\left(1+\frac{1}{\sin\varphi}\right)\ln\left(1+\frac{b_x}{b}\cdot\frac{b}{h}\sin\varphi\right)} \tag{52}$$

or

$$\frac{p_x - p_H}{\frac{\rho v_H^2}{2}} = 1 - \left(1 + \frac{b_x}{b}\cdot\frac{b}{h}\sin\varphi\right)^{-2\left(1+\frac{1}{\sin\varphi}\right)}$$

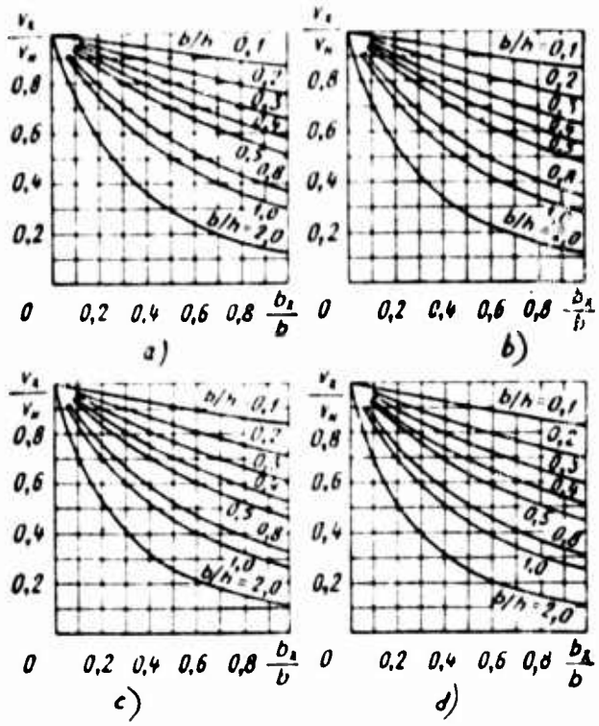

Fig. 90. Theoretical velocity fields in the exit cross-section of a nozzle with normal cut-off for various values of angle φ:
a -- $\varphi = 30^\circ$
b -- $\varphi = 45^\circ$
c -- $\varphi = 60^\circ$
d -- $\varphi = 90^\circ$

For the case $\varphi = 0$, with reference to Eq. (50), the pressure field in the nozzle cut-off plane is

$$\frac{p_x - p_\infty}{\frac{\rho v_\infty^2}{2}} = 1 - e^{-2\frac{b_x}{b}\frac{b}{h}}. \qquad (53)$$

Eqs. (52) and (53) enable us, by specifying values from 0 to 1 to the instantaneous coordinate b_x/b, to construct in the dimensionless form the pressure field in the air jet as it exits from the nozzle as a function of the parameter b/h and the slope φ of the generatrix with respect to the nozzle axis.

In dimensionless form the theoretical pressure fields in the air jet as it exits from a nozzle with normal cut-off and when the generatrix slope φ = 30, 45, 60, and 90° for different parameter b/h values are shown in Fig. 91. Eq. (52) was used in plotting these fields. As we can see, when the exit width v of the nozzle is close to the values of the distance h between the nozzle and the ground surface, the excess pressure in the jet increases rapidly in the direction from the outer edge of the nozzle to the inner, while the pressure gradient is gradually decreasing. The profile of the pressure field in accordance with the nature of the variation in the pressure gradient faces the ground surface with its convexity. With increase in distance h, that is, with decrease in parameter b/h, the excess pressure in the nozzle cut-off plane decreases, while the pattern of the distribution of this pressure in the nozzle cut-off plane approaches the linear.

Air cushion pressure coefficients. Setting in Eqs. (52) and (53) the instantaneous coordinate $b_x = b$, we get

$$\frac{p_\theta - p_н}{\frac{\rho v_н^2}{2}} = 1 - e^{-2\left(1+\frac{1}{\sin\varphi}\right)\ln\left(1+\frac{b}{h}\sin\varphi\right)}. \qquad (54)$$

For the case when $\varphi = 0$

$$\frac{p_\theta - p_н}{\frac{\rho v_н^2}{2}} = 1 - e^{-2\frac{b}{h}}. \qquad (55)$$

Eqs. (54) and (55) determine the excess pressure $p_\theta - p_н$ at the boundary of the jetlet travelling from the inner edge of the nozzle exit. This excess pressure propagates in the space bounded from above by the bottom of the nozzle installation, from below by the ground surface, and from the sides by the air jets escaping from the nozzles. The dynamic pressure $\rho v_\theta^2/2$ of the boundary air jetlet travelling from the exit edge of the outer nozzle wall is equal to the pressure $(p_0 - p_н)$ of the air jet fed to the nozzle installation. Therefore Eqs. (54) and (55), represented as

$$\bar{p} = \frac{p_\theta - p_н}{p_0 - p_н} = 1 - e^{-2\left(1+\frac{1}{\sin\varphi}\right)\ln\left(1+\frac{b}{h}\sin\varphi\right)},$$

$$\bar{p} = 1 - \left(1 + \frac{b}{h}\sin\varphi\right)^{-2\left(1+\frac{1}{\sin\varphi}\right)} \qquad (56)$$

and in the case $\varphi = 0$

$$\bar{p} = \frac{p_\theta - p_н}{p_0 - p_н} = 1 - e^{-2\frac{b}{h}},$$

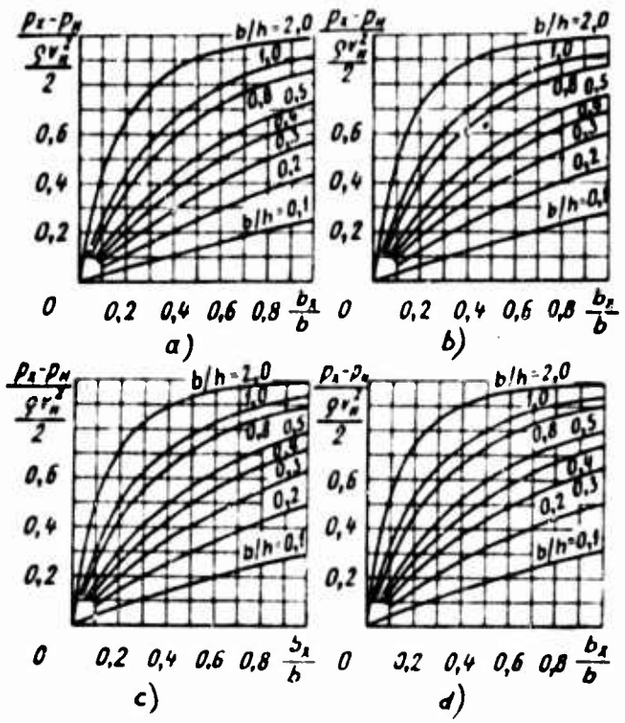

Fig. 91. Theoretical fields of static pressures in exit cross-section of a nozzle with normal cut-off for various values of the angle φ:
a -- $\varphi = 30^\circ$
b -- $\varphi = 45^\circ$
c -- $\varphi = 60^\circ$
d -- $\varphi = 90^\circ$

express the dimensionless air cushion pressure coefficient.

These coefficients determine the fraction of transformation of the total pressure of the air current in front of the nozzle installation into the static pressure in the air cushion, expressed in terms of the geometric parameters of the nozzle: width b of the nozzle exit, slope φ of the generatrix, and height h of the position of the nozzle installation relative to the support surface.

The air cushion pressure can be determined also in another way if we know the velocity field in the nozzle cut-off plane. Let us enclose the jet forming the air cushion in the contour shown in Fig. 89 with a dashed line. Let us extend the upper section of the contour in direct proximity to the bottom of the nozzle installation, and in the section intersecting the jet -- in the nozzle cut-off plane we will locate the outer section of the contour parallel to the ground surface at the level of the nozzle

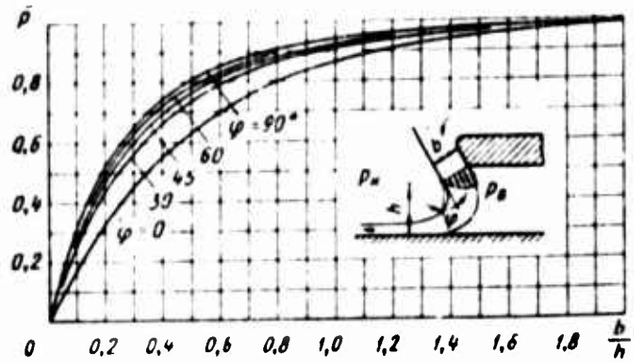

Fig. 92. Pressure coefficient of air cushion of nozzle with normal cut-off as a function of the parameter b/h for various values φ of generatrix slope

exit edge. Let us draw the lower section of the contour in direct proximity to the ground surface. We position the vertical boundaries far from the nozzle cut-off, where the perturbing action of the jets can be neglected and where we can assume the pressure at these contour sections to be constant and equal to $p_в$ and $p_н$.

Let us project onto the axis parallel to the ground surface the forces acting on the isolated contour. The equation of momentum for this contour is

$$-(1+\sin\varphi)\int_0^b \rho v_x^2\,db_x + p_в(h+b\sin\varphi) - \sin\varphi\int_0^b p_x\,db_x - p_н h = 0. \quad (57)$$

With reference to Eq. (5) relating velocity v_x with pressure p_x, we can represent Eq. (57) in the form

$$\frac{p_в - p_н}{\frac{\rho v_н^2}{2}} = \frac{2(1+\sin\varphi)}{h+b\sin\varphi}\int_0^b \left(\frac{v_x}{v_н}\right)^2 db_x + \frac{\sin\varphi}{h+b\sin\varphi}\int_0^b \left[1-\left(\frac{v_x}{v_н}\right)^2\right] db_x. \quad (58)$$

where $v_x/v_н$ is the velocity ratio at the nozzle cut-off, determined by Eq. (49).

The integral appearing in Eq. (58) is

$$\int_0^b \left(\frac{v_x}{v_м}\right)^2 db_x = \int_0^h \left(1 + \frac{b_x}{h}\sin\varphi\right)^{-2\left(1+\frac{1}{\sin\varphi}\right)} db_x =$$

$$\frac{h}{2-\sin\varphi}\left[1 - \left(1 + \frac{b}{h}\sin\varphi\right)\left(1 + \frac{b}{h}\sin\varphi\right)^{-2\left(1+\frac{1}{\sin\varphi}\right)}\right].$$

Inserting the value of this integral in Eq. (58) and transforming it, we get

$$\frac{p_в - p_м}{\frac{\rho v_м^2}{2}} = 1 - \left(1 + \frac{b}{h}\sin\varphi\right)^{-2\left(1+\frac{1}{\sin\varphi}\right)}.$$

This equation corresponds to the earlier derived Eq. (56) expressing the air cushion pressure coefficient for a nozzle with normal cut-off.

The air cushion pressure coefficient $\bar{p}$ as functions of variation in geometrical parameters of a nozzle installation is shown in Fig. 92. The functions simultaneously express the pressure field at the nozzle cut-off in generalized form. Each point lying on these curves specifies the excess pressure at the exit edge of the inner nozzle wall or, which amounts to the same thing, the excess pressure in the air cushion. The section of the curve lying in the region from 0 to the selected b/h value characterizes the pressure field in the cut-off plane for all nozzles with the selected values of parameters b/h and φ. As we can see, an increase in the angle φ leads to a marked rise in the air cushion pressure coefficient.

Discharge coefficient of nozzle installation. For the case of discharge from a large volume when pressure $p_м$ at the outer side of the jet is equal to the pressure $p_в$ at its inner side, and the friction of the flow against the nozzle wall is absent, the discharge of air through a nozzle with a smooth entry section is

$$Q = Fv = F\sqrt{\frac{2}{\rho}(p_o - p_м)}.$$

The difference $p_0 - p_м$ is the drop in total pressures between the receiver into which the nozzle is built, and the surrounding atmosphere. The velocity v in this case is uniformly distributed over the nozzle cross-section and is the mean velocity $v_{ср}$ of the jet at its exit. Approximately the same discharge conditions are observed for the nozzle installation in the case of free -- not confined with a shield -- exit of jet from its nozzles which have a small width compared to the overall width of the nozzle installation. The "thin" jets exiting from this kind of installation during their travel, on being unable to merge into a single

common jet, trail off to the surrounding space. Because of this, the pressure in the volume enclosed by the jets and in the atmosphere is approximately the same ($p_в = p_н$).

The presence of a shield along the jet travel path causes the appearance of the pressure difference $p_в - p_н$ between the inner space enclosed by the jets and the external atmosphere surrounding the jets. This difference is responsible for the uneven distribution of velocity at the nozzle exits. The mean velocity $v_{ср}$ of discharge differs from the velocity $v_н$ by a greater amount, the greater the difference in the pressures $p_в - p_н$. In this case the minimum discharge velocity occurring near the inner wall of a nozzle is

$$v_в = \sqrt{\frac{2}{\rho}(p_0 - p_в)},$$

and the maximum discharge velocity -- near the outer wall is:

$$v_н = \sqrt{\frac{2}{\rho}(p_0 - p_н)}.$$

An increase in the excess pressure in the air cushion reduces the volume flow of air exiting from the nozzle installation.

The volume flow of air when there is a uniform velocity field at the nozzle cut-off is

$$Q_р = Fv_н = F\sqrt{\frac{2}{\rho}(p_0 - p_н)}. \qquad (59)$$

Let us denote the ratio of the mean velocity to the maximum velocity by $v_{ср}/v_н = \alpha$ and let us represent the volume flow of air when there is uneven velocity distribution at the nozzle cut-off in the form

$$Q_н = Fv_{ср} = \alpha Fv_н = \alpha F\sqrt{\frac{2}{\rho}(p_0 - p_н)}. \qquad (60)$$

Dividing the left and right sides of Eq. (60) by the corresponding sides of Eq. (59), we get an expression for determining the discharge coefficient of the nozzle in the conditions when a shield has an effect, [illegible].

The discharge coefficient for a nozzle in the case of uneven velocity distribution in the cut-off plane caused by the presence of a shield along the jet travel path is

$$\alpha = \frac{Q_н}{Q_р} = \frac{L\int_0^b v_x\,db_x}{bLv_н} = \frac{v_н\int_0^b \left(1 - \frac{b_x}{h}\sin\varphi\right)^{\left(1-\frac{1}{\sin\varphi}\right)} db_x}{bv_н}.$$

Integrating this expression, we find

$$\alpha = \frac{h}{b}\left[1 - \left(1 + \frac{b}{h}\sin\varphi\right)^{-\frac{1}{\sin\varphi}}\right].$$

or

$$\alpha = \frac{h}{b}\left[1 - e^{-\frac{1}{\sin\varphi}\ln\left(1+\frac{b}{h}\sin\varphi\right)}\right]. \qquad (61)$$

For the case $\varphi = 0$, the discharge coefficient of a nozzle with normal cut-off is

$$\alpha = \frac{h}{b}\left(1 - e^{-\frac{b}{h}}\right). \qquad (62)$$

The volume flow of air passing through the nozzle is

$$Q = \alpha F\sqrt{\frac{2}{\rho}(p_0 - p_н)},$$

where F = bL is the nozzle exit area.

The variation in the discharge coefficient α for a plane nozzle as theoretical functions of parameter b/h for different slopes φ, based on Eqs. (61) and (62), are shown in Fig. 45. As we can see, an increase in the angle φ leads to a marked reduction in the discharge coefficient, while the degree of decrease becomes the greater, the shorter the distance h between the nozzle and the ground surface, that is, the greater the parameter b/h.

Drag coefficient of nozzle installation. By the aerodynamic drag of a nozzle installation we will mean the total pressure losses associated with the entrance of air from the receiver into the nozzle, flow in the flow-through section, and exiting into the surrounding atmosphere. These losses can be characterized by the local drag coefficient ζ, which is the ratio of the total pressure expended in producing the jet streaming over the shield to the dynamic pressure of the jet determined from the mean velocity $v_{ср}$ of the air in the nozzle exit, that is,

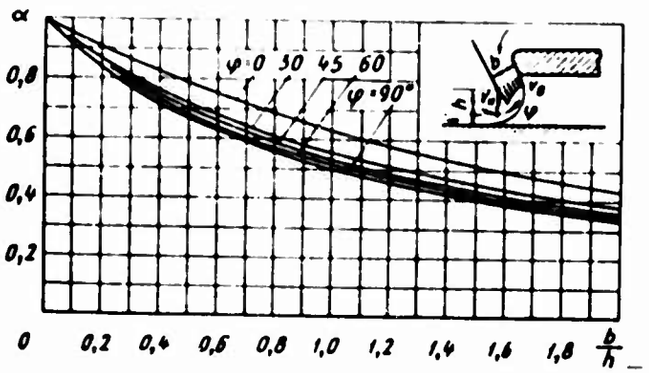

Fig. 93. Discharge coefficient of nozzle with normal cut-off as a function of parameter b/h for various values φ of generatrix slope

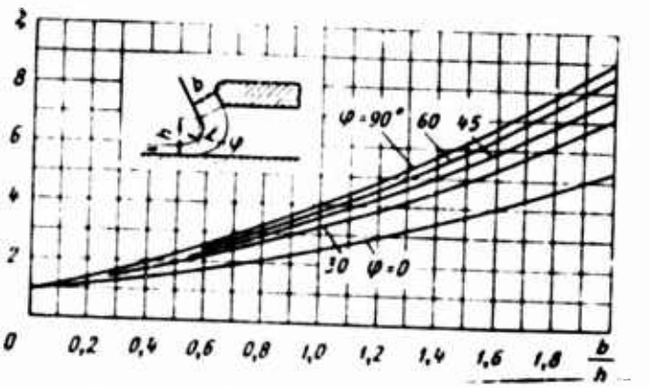

Fig. 94. Drag coefficient of nozzle with normal cut-off as a function of parameter b/h for various angles φ of generatrix slope

$$\zeta = \frac{p_0 - p_н}{\frac{\rho w_{cp}^2}{2}}.$$

In the case of an ideal flow when local pressure losses at the entrance into the nozzle and losses due to friction of the air stream against the nozzle walls are absent, we have

$$\zeta = \frac{p_0 - p_н}{\frac{\rho}{2}\left(\frac{Q_н}{Lb}\right)^2}.$$

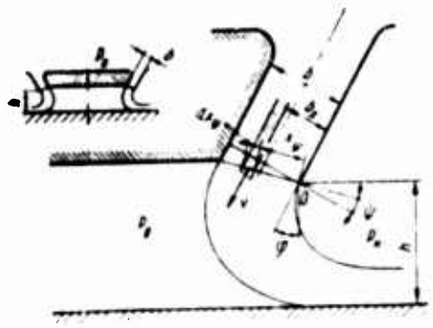

Fig. 95. For calculating aerodynamic characteristics of air cushion produced by jet exiting from a nozzle with oblique cut-off

In accordance with Eq. (60), the volume flow of air passing through the nozzle $Q_н = \alpha Q_р = \alpha bL\sqrt{\frac{2}{\rho}(p_0 - p_н)}$, therefore

$$\zeta = \frac{1}{\alpha^2}. \tag{63}$$

As the function of the geometrical parameters of a nozzle installation, we have

$$\zeta = \frac{(b/h)^2}{\left[1 - \left(1 - \frac{b}{h}\sin\varphi\right)^{-\frac{1}{\sin\varphi}}\right]^2}. \tag{64}$$

The function $\zeta = f(b/h, \varphi)$ or a plane nozzle based on Eq. (64) is shown in Fig. 94.

10. Nozzle Installation With Oblique Nozzle Cut-off

Let us examine air flow in a nozzle installation with oblique nozzle cut-off when the nozzle exit edges lying in a plane at the angle ψ to the normal nozzle cross-section (Fig. 95). For this case the pressure gradient in the jet in the nozzle cut-off plane is

$$\frac{dp}{dx_\psi} = \frac{\rho v^2 \cos\psi (1 - \sin\varphi)}{h + x_\psi \sin(\varphi - \psi)}$$

or, since $dp = -\rho v dv$,

$$\frac{dv}{dx_\psi} = -\frac{v\cos\psi (1 - \sin\varphi)}{h + x_\psi \sin(\varphi - \psi)}.$$

After separation of variables, we get

$$-(1+\sin\varphi)\cos\psi\int_0^{x_\psi}\frac{dx_\psi}{h+x_\psi\sin(\varphi-\psi)}=\int_{v_н}^{v_x}\frac{dv}{v}.$$

After integrating and the required transformations with reference to $x_\beta = b/\cos\psi$, we get

$$\frac{v_x}{v_н}=\left[1+\frac{x_\psi}{x_\beta}\cdot\frac{b}{h}\cdot\frac{\sin(\varphi-\psi)}{\cos\psi}\right]^{-\frac{(1+\sin\varphi)\cos\psi}{\sin(\varphi-\psi)}}. \qquad (65)$$

The function (65) characterizing the velocity distribution in the exit plane of a nozzle with oblique cut-off can be represented also as

$$\frac{v_x}{v_н}=e^{-\frac{(1+\sin\varphi)\cos\psi}{\sin(\varphi-\psi)}\ln\left[1+\frac{x_\psi}{x_\beta}\frac{b}{h}\cdot\frac{\sin(\varphi-\psi)}{\cos\psi}\right]}.$$

Using the above-presented definitions and methods, the aerodynamic characteristics of a nozzle installation with oblique nozzle cut-off can be expressed by the following formulas.

The pressure field in the nozzle exit is

$$\frac{p_x-p_н}{\frac{\rho v_н^2}{2}}=\frac{p_x-p_н}{p_0-p_н}=$$

$$=1-\left(1+\frac{x_\psi}{x_\beta}\cdot\frac{b}{h}\cdot\frac{\sin(\varphi-\psi)}{\cos\psi}\right)^{-2\frac{(1+\sin\varphi)\cos\psi}{\sin(\varphi-\psi)}} \qquad (66)$$

or

$$\bar{p}=\frac{p_x-p_н}{p_0-p_н}=1-e^{-2\frac{(1+\sin\varphi)\cos\psi}{\sin(\varphi-\psi)}\ln\left(1+\frac{x_\psi}{x_\beta}\cdot\frac{b}{h}\cdot\frac{\sin(\varphi-\psi)}{\cos\psi}\right)}.$$

The air cushion pressure coefficient, given the condition $p_x = p_\beta$ and $x_\psi = x_\beta$ is

$$\bar{p}=\frac{p_\beta-p_н}{p_0-p_н}=1-\left(\frac{v_\beta}{v_н}\right)^2=$$

$$=1-\left(1+\frac{b}{h}\cdot\frac{\sin(\varphi-\psi)}{\cos\psi}\right)^{-2\frac{(1+\sin\varphi)\cos\psi}{\sin(\varphi-\psi)}} \qquad (67)$$

or

$$\bar{p} = 1 - e^{-2k_1 \ln k_2}, \tag{68}$$

where

$$k_1 = \frac{(1 + \sin\varphi)\cos\psi}{\sin(\varphi - \psi)} \; ; \; k_2 = 1 + \frac{b}{h} \cdot \frac{\sin(\varphi - \psi)}{\cos\psi}.$$

The discharge coefficient of a nozzle in terms of its exit area is

$$\alpha = \frac{l\cos\psi \int_0^{x_a} v_x \, dx_\psi}{x_a \cos\psi \, l v_H}$$

$$= \frac{1}{b/h} \cdot \frac{1 - \left[1 - \frac{b}{h} \cdot \frac{\sin(\varphi - \psi)}{\cos\psi}\right]^{\frac{(1+\sin\varphi)\cos\psi}{\sin(\varphi-\psi)}+1}}{\frac{\sin(\varphi-\psi)}{\cos\psi}\left[\frac{(1+\sin\varphi)\cos\psi}{\sin(\varphi-\psi)} - 1\right]}$$

or

$$\alpha = \frac{1}{b/h} \cdot \frac{1 - k_2^{-(k_1+1)}}{\frac{\sin(\varphi-\psi)}{\cos\psi}(k_1 - 1)}. \tag{69}$$

The nozzle drag coefficient ζ is associated with the discharge coefficient α by Eq. (65).

For $\psi = 0$, when the nozzle cut-off plane coincides with the plane that is normal to the generatrix, Eqs. (65), (66), (67) and (69) are transformed into expressions determining the corresponding aerodynamic characteristics of a nozzle installation with normal nozzle cut-off.

As the angle ψ is increased, the inclination of the nozzle cut-offs with respect to the plane of the bottom of the nozzle installation decreases, and when $\psi = \varphi$, the nozzle installation with oblique nozzle cut-off is converted into a nozzle installation with horizontal nozzle cut-off in which the exits lie in the plane of the bottom. However, when $\psi = \varphi$, the quantity $\sin(\varphi - \psi) = 0$ and Eqs. (65), (66), (67), and (69) become meaningless, since the functions $v_x/v_H = f_1(\psi)$, $v_a/v_H = f_1(\psi)$, $\frac{p_a - p_H}{\rho v_H^2/2} = f_2(\psi)$, $\bar{p} = f_2(\psi)$, and $\alpha = f_3(\psi)$ have an apparent discontinuity. Actually, these functions, as $\psi \to \varphi$, tend to their limit and are continuous functions also at the point $\sin(\varphi - \psi) = 0$. This factor must be borne in mind when determining the aerodynamic characteristics of a nozzle installation with horizontal nozzle cut-off.

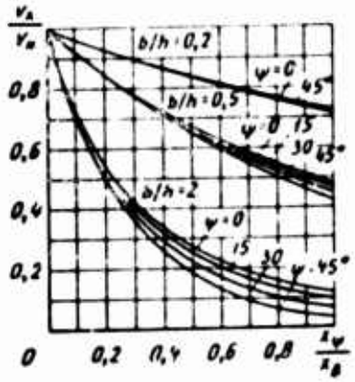

Fig. 96. Effect of nozzle cut-off angle ψ on velocity field profile in exit ($\varphi = 45^\circ$)

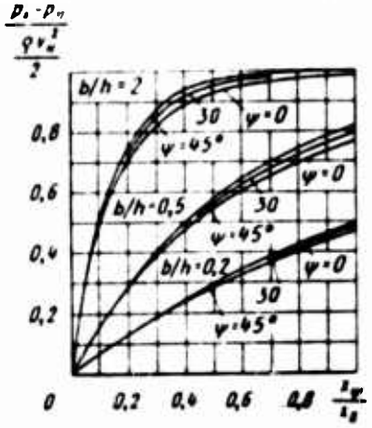

Fig. 97. Effect of nozzle cut-off angle ψ on profile of static pressure field in exit ($\varphi = 45^\circ$)

The effect of the nozzle cut-off angle ψ on the profile of the velocity field and the profile of the static pressure field in the exit is shown in Figs. 96 and 97, respectively. These fields were plotted, respectively, by Eqs. (65) and (66) for a constant angle of nozzle generatrix inclination $\varphi = 45^\circ$. In Fig. 96 we see that the angle ψ strongly affects the profile of the velocity field for small elevations of the nozzle installation above the support surface (for large values of the parameter b/h). As the elevation h is increased, this effect is weakened, and when $b/h \approx 0.2$, that is, when the nozzle is at an elevation that is equal to five times its exit width, the effect of the nozzle cut-off angle ψ practically disappears. The angle ψ of nozzle cut-off also similarly affects the profile of the static pressure field in the nozzle exit (Fig. 97).

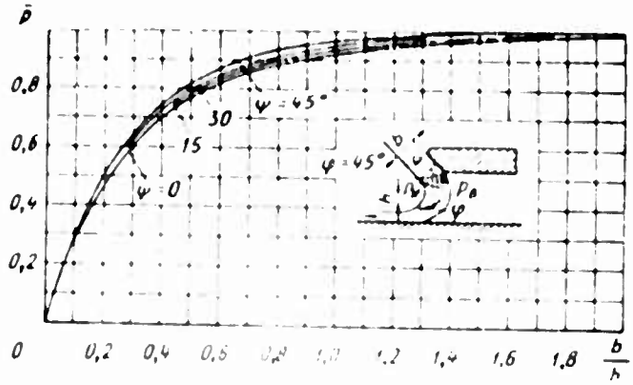

Fig. 98. Effect of nozzle cut-off angle ψ on air cushion pressure coefficient

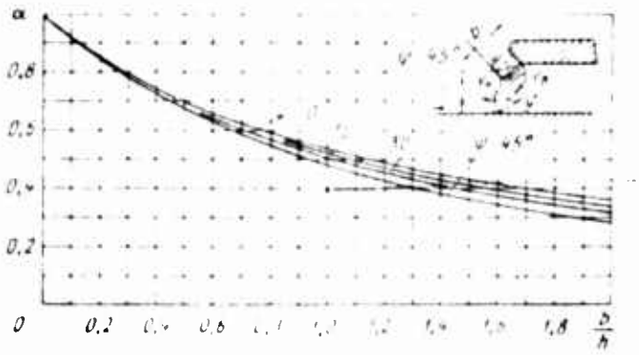

Fig. 99. Effect of nozzle cut-off angle ψ on discharge coefficient of flat nozzle

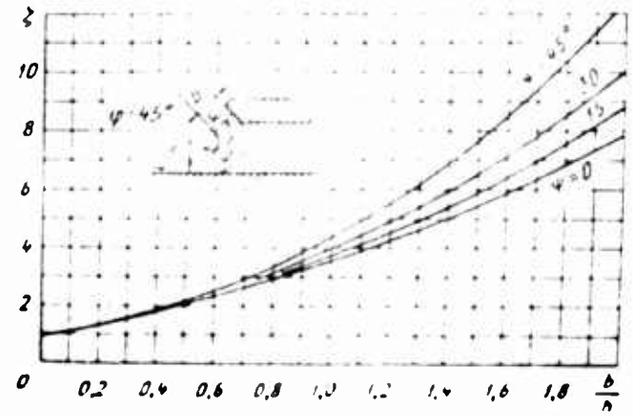

Fig. 100. Effect of nozzle cut-off angle ψ on drag coefficient of flat nozzle

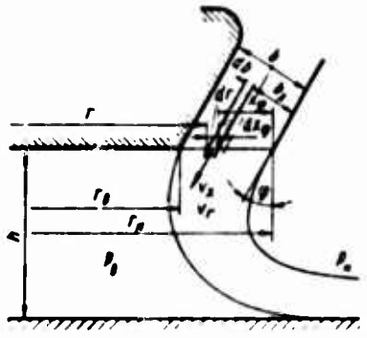

Fig. 101. For calculating aerodynamic characteristics of air cushion produced by jet exiting from nozzle with horizontal cut-off

The results of determining the effect of the angle ψ on the air cushion pressure coefficient, discharge coefficient, and drag coefficient of a nozzle installation with oblique nozzle cut-off are shown in Figs. 98-100, respectively. These functions were plotted according to Eqs. (68), (69), and (63), respectively. As we can see, an increase in the angle ψ leads to a marked increase in the pressure coefficient $\bar{p}$, a reduction in the discharge coefficient α, and an increase in the drag coefficient ζ.

11. Nozzle Installation With Horizontal Nozzle Cut-off

Let us find the aerodynamic characteristics of a nozzle installation with horizontal nozzle cut-off. The pattern of air discharge from this installation and the symbols adopted are shown in Fig. 101. If we examine this nozzle installation as a plane device, the pressure gradient is

$$\frac{dp}{dx_q} = \frac{\rho v^2 \cos\varphi (1 + \sin\varphi)}{h}.$$

Using the Bernoulli equation $dp = -\rho v dv$ expressing in differential form the constancy of the total pressure at each jetlet in the nozzle cut-off plane, we get

$$\frac{dv}{dx_q} = -\frac{v\cos\varphi (1 + \sin\varphi)}{h}.$$

Let us determine the velocity fields in the nozzle exit, by solving this differential equation. We can write

$$\int_{v_x}^{v_x} \frac{dv}{v} = -(1+\sin\varphi)\cos\varphi \frac{1}{h} \int_{0}^{x_\varphi} dx_\varphi$$

and, therefore

$$\ln\frac{v_x}{v_\infty} = -\frac{x_\varphi}{h}(1+\sin\varphi)\cos\varphi. \qquad (70)$$

Since the nozzle exit width in the plane of nozzle cut-off $x_\beta = b/\cos\varphi$, Eq. (70) can be represented as

$$\frac{v_x}{v_\infty} = e^{\int_{x_\varphi}^{x_\beta} -\frac{1}{h}(1+\sin\varphi)\cos\varphi} = e^{-\frac{x_\beta}{h}(1+\sin\varphi)\cos\varphi}. \qquad (71)$$

Assigning to the instantaneous coordinate x_φ different values within the limits from $x_\varphi = 0$ to $x_\varphi = x_\beta$ and using this formula, it is not difficult to plot the velocity field in the nozzle cut-off plane as a function of parameter b/h and the angle φ of generatrix inclination to the nozzle axis. When $x_\varphi = x_\beta$, we get

$$\frac{v_\beta}{v_\infty} = e^{-\frac{b}{h}(1+\sin\varphi)}. \qquad (72)$$

Eq. (72) allows us to calculate the velocity v_β of a jetlet travelling from the inner edge of the nozzle at the boundary with the air cushion.

The pressure field in the nozzle cut-off plane is

$$\frac{p_x - p_\infty}{p_0 - p_\infty} = \frac{p_x - p_\infty}{\frac{\rho v_\infty^2}{2}} = 1 - \left(\frac{v_x}{v_\infty}\right)^2 = 1 - e^{-2\int_{x_\varphi}^{x_\beta}\frac{1}{h}(1+\sin\varphi)}. \qquad (73)$$

The air cushion pressure coefficient is

$$P = \frac{p_\beta - p_\infty}{p_0 - p_\infty} = 1 - \left(\frac{v_\beta}{v_\infty}\right)^2 = 1 - e^{-2\frac{b}{h}(1+\sin\varphi)}. \qquad (74)$$

The discharge coefficient of the plane nozzle given in terms of its exit area is

$$\alpha_n = \frac{L\cos\varphi \int_0^{x_\varphi} v_x\, dx_\varphi}{bLv_n} = \frac{\cos\varphi}{b} \int_0^{b/\cos\varphi} e^{-\frac{x_\varphi}{h}(1+\sin\varphi)\cos\varphi} dx_\varphi =$$

$$= \frac{1 - e^{-\frac{b}{h}(1+\sin\varphi)}}{b/h\,(1+\sin\varphi)}. \qquad (75)$$

The discharge coefficient of the annular nozzle is

$$\alpha_\kappa = \frac{Q_\kappa}{Q_p} = \frac{\int_{r_0}^{r_\kappa} 2\pi r v_r \cos\varphi\, dr}{\pi\left(r_\kappa^2 - r_0^2\right) v_\kappa \cos\varphi} = \frac{2\pi v_\kappa \cos\varphi \int_{r_0}^{r_\kappa} re^{-\frac{r_\kappa - r}{r_\kappa - r_0}\frac{b}{h}(1+\sin\varphi)} dr}{\pi\left(r_\kappa^2 - r_0^2\right) v_\kappa \cos\varphi}. \qquad (76)$$

Since

$$\int_{r_0}^{r_\kappa} re^{-\frac{r_\kappa - r}{r_\kappa - r_0}\frac{b}{h}(1+\sin\varphi)} dr = \frac{(r_\kappa - r_0)^2}{\frac{b}{h}(1+\sin\varphi)} +$$

$$+ \left[r_0(r_\kappa - r_0) - \frac{(r_\kappa - r_0)^2}{\frac{b}{h}(1+\sin\varphi)}\right] \frac{1 - e^{-\frac{b}{h}(1+\sin\varphi)}}{\frac{b}{h}(1+\sin\varphi)},$$

$$r_\kappa - r_0 = \frac{b}{\cos\varphi} \text{ и } r_\kappa = \frac{D_\kappa}{2},$$

Eq. (76), after uncomplicated transformations, will become

$$\alpha_\kappa = \frac{2\frac{h}{D_\kappa}}{(1+\sin\varphi)\left(\cos\varphi - \frac{b}{D_\kappa}\right)} + \left[\frac{\cos\varphi - 2\frac{b}{D_\kappa}}{\cos\varphi - \frac{b}{D_\kappa}} - \right.$$

$$\left. - \frac{2\frac{h}{D_\kappa}}{(1+\sin\varphi)\left(\cos\varphi - \frac{h}{D_\kappa}\right)}\right] \frac{1 - e^{-\frac{b}{h}(1+\sin\varphi)}}{\frac{b}{h}(1+\sin\varphi)}.$$

Introducing the notation $b/D_\kappa = \bar{b}$ and $b/D_\kappa = \bar{h}$, we obtain a formula for determining the discharge coefficient of an annular nozzle with reference to axial symmetry:

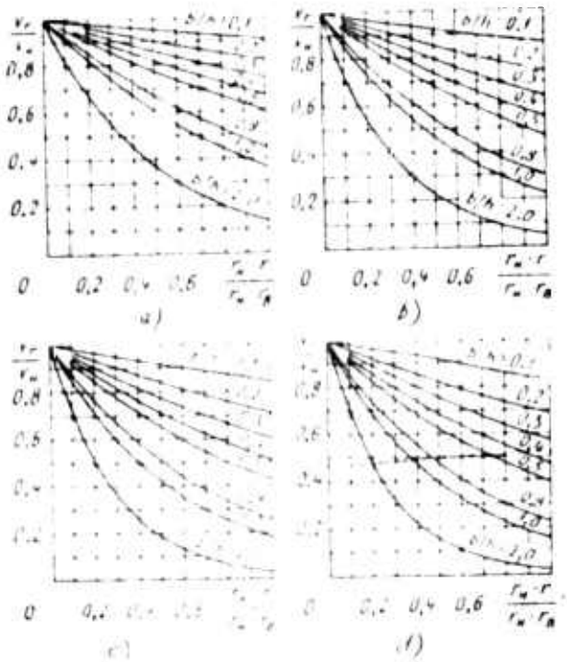

Fig. 10. Theoretical velocity fields in air jet at nozzle cut-off as a function of parameter b/h:

a -- $\varphi = 0$
b -- $\varphi = 30^{\circ}$
c -- $\varphi = 45^{\circ}$
d -- $\varphi = 60^{\circ}$

$$\alpha_x = \frac{2h}{(1+\sin\varphi)(\cos\varphi - b)} \left[\frac{\cos\varphi}{\cos\varphi} - \frac{2b}{b} \right] \alpha_n. \qquad (77)$$

Eq. (77) can be represented with reference to Eq. (7), in the form of the function

$$\alpha_x = \frac{2h}{(1+\sin\varphi)(\cos\varphi - b)} \left[\frac{\cos\varphi}{\cos\varphi} - \frac{2b}{b} \right] \alpha_n.$$

relating the discharge coefficient of the annular nozzle with the discharge coefficient of a plane nozzle.

The volume flow of air in an annular nozzle with angle of generatrix inclination φ and with exit edges lying in the same plane with the nozzle bottom is

$$Q = \alpha_н F \sqrt{\frac{2}{\rho}(p_в - p_н)},$$

where:

$F = F_c \cos\varphi = \pi (r_н^2 - r_в^2) \cos\varphi$; F_c is the nozzle exit area in the cut-off plane.

The drag coefficient of a plane nozzle installation is

$$\zeta = \left[\frac{b\,h\,(1 + \sin\varphi)}{1 - e^{-b\,h\,(1+\sin\varphi)}}\right]^2 = \left[\frac{\frac{b}{h}\frac{D_н}{D_н}(1+\sin\varphi)}{1 - e^{-\frac{b}{h}\frac{D_н}{D_н}(1+\sin\varphi)}}\right]^2. \qquad (73)$$

The theoretical velocity fields in an air jet as it exits from nozzles with horizontal cut-off and with angle of generatrix inclination φ = 0, 30, 45, and 60° for different values of the parameter b/h are shown in dimensionless form in Fig. 102. These velocity fields were plotted by Eq. (71). By comparing the curves in Fig. 102 with those shown in Fig. 90, we can see that the general pattern of variation in the velocity profile as a function of parameter b/h and φ for a nozzle with horizontal cut-off remains the same as for a nozzle with normal cut-off. The only difference is that for the same b/h and φ values, the nozzles with horizontal cut-off have a lesser nonuniformity of velocity distribution in the nozzle exit.

Using Eq. (72), we can readily find the effect of the angle of inclination φ on the velocity distribution in the air jet at the nozzle cut-off. Fig. 103 shows the dependence of $v_в/v_н$ on the parameter b/h for nozzles with angle of generatrix inclination φ = 0, 30, 45, 60, and 90°. As we can see, for a nozzle with contant relative exit width b/h, the relative velocity $v_в/v_н$ at a point with coordinate $x_\varphi = b_x/\cos\varphi$ decreases with increase in the angle of inclination φ, and the nonuniformity of velocities distribution at the nozzle cut-off correspondingly rises. It must be noted that φ = 90°, Eq. (72) becomes meaningless, since in this case the nozzle exit width $x_\varphi = \infty$

The theoretical velocity field in the air jet in the nozzle cut-off plane plotted by Eq. (72) as the dependence of the relative velocity $v_в/v_н$ on the generalizing parameter b/h (1 + sin φ) is shown in Fig. 104. By means of the generalizing parameter, it appears possible to characterize the entire diversity of the velocity fields in the jet at the nozzle cut-off determined by its exit width b, height h of nozzle position relative

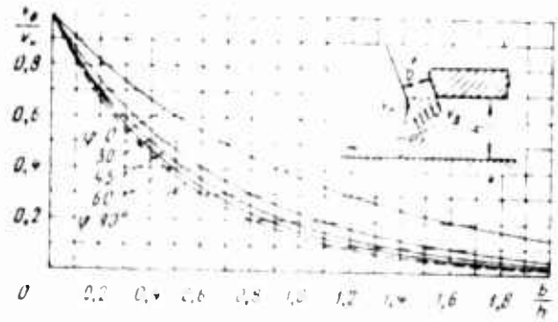

Fig. 03. Theoretical velocity fields in air jet at nozzle cut-off as a function of parameter b/h for various angles φ of generatrix slope

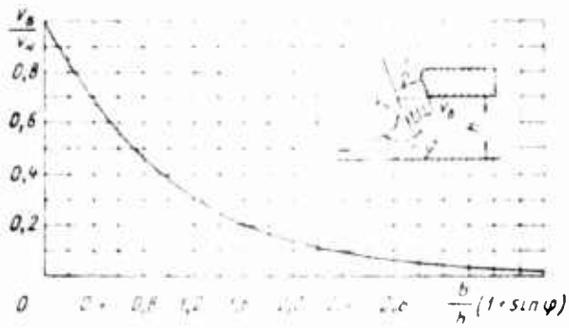

Fig. 04. Theoretical velocity fields in jet at nozzle cut-off as a function of generalizing parameter $b/h(1 + \sin\varphi)$

to the ground surface, and angle φ is the inclination of the nozzle generatrix to the nozzle [illegible] curve. Thus, for example, for a nozzle with an exit [illegible] the angle of inclination $\varphi = 30^\circ$, and the distance [illegible] the ground surface, the air velocity of the bounding jet [illegible] from the inner edge of the nozzle $v_\delta = 0.55v_н$, since

$$\frac{b}{h}(1 + \sin\varphi) = 0.6$$

The velocity field in the nozzle cut-off plane in this case is characterized by the section of the curve line within the limits $b/h(1 + \sin\varphi) = 0$–0.6. For all other values of b, φ, and h, a combination of which makes the parameter $b/h(1 + \sin\varphi) = 0.6$, the velocity field will be similar to that found in this example.

The theoretical pressure fields in the air jet as it exits from a nozzle with an angle of generatrix inclination φ = 0, 30, 45, and 60° for different values of parameter b/h are shown in dimensionless form in Fig. 105. These fields were plotted by Eq. (73). For a nozzle with horizontal cut-off, just as for a nozzle with normal cut-off, the profile of the pressure field faces the ground surface with its convexity. As the distance h is decreased (by a reduction in the parameter b/h), the excess pressure in the nozzle cut-off plane becomes less.

The variation in the relative excess pressure $(p_\beta - p_H)/(p_0 - p_H) = (p_\beta - p_H)/(\rho v_H^2/2)$ in the nozzle cut-off plane, as a function of the ratio b/h for different angles φ, is shown in Fig. 106. These curves plotted by Eq. (74) consist of the dependences of the air cushion pressure coefficient $\bar{p}$ on the geometric parameters of the nozzle installation and simultaneously expressed in generalized form the pressure field at the nozzle cut-off. Each point lying on these curves determines the excess pressure at the exit edge of the inner wall of the nozzle or, which amounts to the same thing, the excess pressure in the air cushion. The reflection of the curve lying in the range from 0 to the reflected b/h value characterizes the pressure field in the cut-off plane for all nozzles with selected values of the parameters b/h and φ.

As we can see, an increase in the angle φ leads to a marked increase in the pressure and the nozzle cut-off plane. Here, even when φ = 90°, Eq. (74) becomes meaningless, since at this angle the nozzle exit width $b_\varphi = \infty$.

Theoretical pressure fields in a jet as it exits from a nozzle, on analogy with pressure fields, can be expressed in terms of the generalizing parameter $b/h(1 + \sin\varphi)$. The dependence of the distribution of relative pressure in the jet in the nozzle cut-off plane on this parameter, plotted by Eq. (74), is shown in Fig. 107, from which it is not difficult to determine the excess pressure at any point lying in the plane of nozzle cut-off. For example, for a nozzle with b = 0.1 m, φ = 30°, and h = 0.25 m, the excess pressure at the exit edge of the inner wall $p_\beta - p_H = 0.7(\rho v^2/2)$, since the generalizing parameter $b/h(1 + \sin\varphi)$ takes on the value 0.6. The pressure field in this case is characterized by the section of the curve within the limits $b/h(1 + \sin\varphi)$ = 0-0.6.

Changes in the pressure coefficient $\bar{p}$ of the air cushion as functions of the relative elevation h/D_H of the nozzle installation above the ground surface for different relative nozzle exit widths and for the generatrix angles of inclination φ = 0 and 45° are presented in Figs. 108 and 109, respectively. These functions were plotted by the equation

$$\bar{p} = 1 - e^{-\frac{b}{h}(1+\sin\varphi)} = 1 - e^{-\frac{b/D_H}{h/D_H}(1+\sin\varphi)},$$

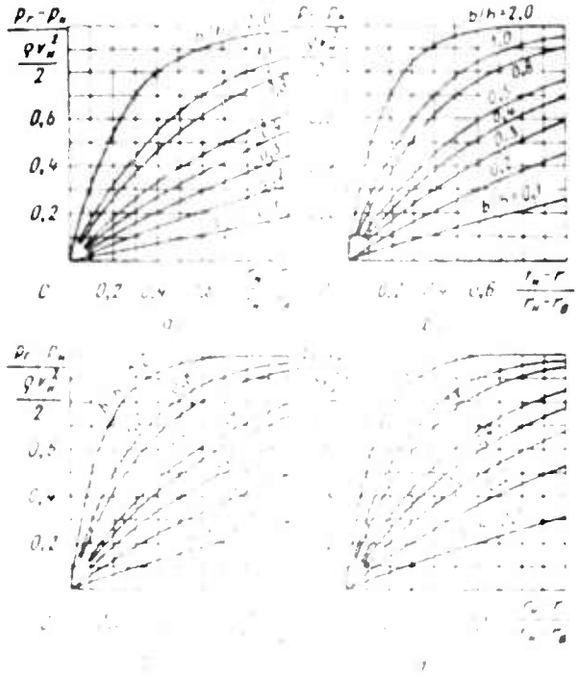

Fig. 0[illegible]. [illegible] fields in air [illegible] function of

a -- φ = [illegible]
b -- φ = [illegible]
c -- φ = [illegible]
d -- φ = [illegible]

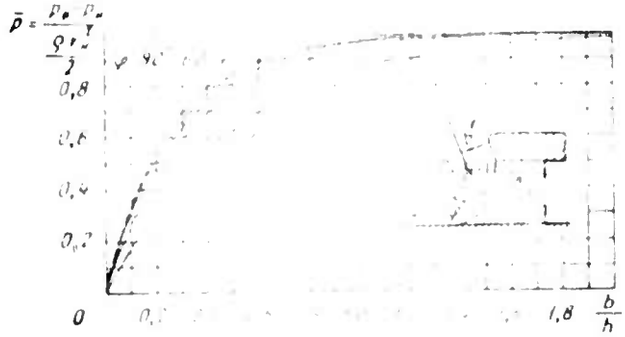

Fig. 0[illegible]. [illegible] fields in air jet at no[illegible] [illegible] parameter b/h for various [illegible]

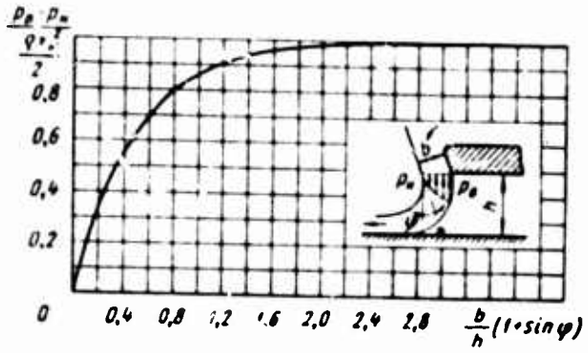

Fig. 107. Theoretical static pressure fields in air jet at nozzle cut-off as a function of generalizing parameter b/h (1 + sin φ)

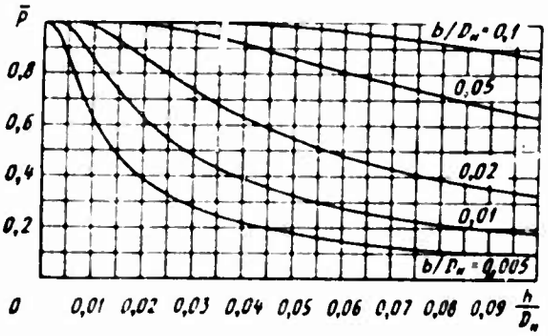

Fig. 108. Pressure coefficient of air cushion of annular jet as a function of clearance above shield for different nozzle exit widths and generatrix slope $\varphi = 0$

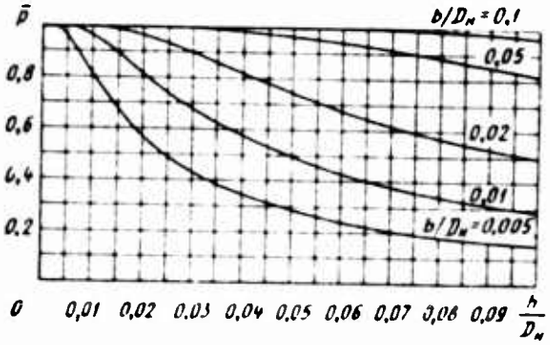

Fig. 109. Pressure coefficient of air cushion of annular jet as a function of elevation above shield for various nozzle exit widths and generatrix slope $\varphi = 45^{\circ}$

where $D_н$ is the diameter (width) of the nozzle installation, determined with respect to the exit edges of the outer wall of the nozzles.

As we can see, with increase in the elevation of the nozzle installation above the ground surface, the pressure coefficient $\bar{p}$ decreases, and does so the more rapidly, the smaller the relative width $b/D_н$ of the nozzle exit. By comparing analogous curves in Figs. 108 and 109, we see that an increase in the angle of inclination of the nozzle generatrix leads, for the same elevation values, to greater values of the air cushion pressure coefficient.

Changes in the discharge coefficient $\alpha_п$ for a plane nozzle as theoretical functions of the parameter b/h, plotted by Eq. (75) for different values of inclination angle φ, are presented in Fig. 110. As we can see, an increase in angle φ leads to a marked reduction in the discharge coefficient, where the degree of reduction becomes the greater, the smaller the distance h between the nozzle and the ground surface, that is, the greater the parameter b/h. The effect of variation in the annular nozzle exit width in the range $b/D_н = 0$–0.1 on the discharge coefficient $\alpha_к$ for the angles $\varphi = 0$ and 45° is shown in Fig. 111. These functions were plotted by Eq. (77), the effect of the parameter $b/D_н$ on the value of $\alpha_к$ also for other angles of generatrix inclination φ is readily limited.

Variations in the discharge coefficient $\alpha_к$ of an annular nozzle as functions of the elevation $h/D_н$ for different exit widths $b/D_н$, plotted by Eq. (77), are shown in Fig. 112, where the analogous functions determined by Eq. (75) for the plane nozzle are given with dashed lines. By comparing the corresponding curves, we see that allowing for the axisymmetricity of the flow weakly affects the discharge coefficient. There is some difference in the values of the coefficients $\alpha_п$ and $\alpha_к$ when $b/D_н > 0.02$. When $b/D_н < 0.02$, the coefficients $\alpha_п$ and $\alpha_к$ are practically the same. For air cushion vehicles, the utilized range of values of the nozzle exit width $b/D_н = 0$–0.05, while the range of the parameter $b/h = 0.2$–1.0, therefore the simpler formula (75) can be used for practical calculations.

The function $\zeta = f(b/h, \varphi)$ for a plane nozzle plotted by Eq. (78) is shown in Fig. 113. The dependence of the coefficient ζ on the relative elevation $h/D_н$ of the nozzle installation above the ground surface is shown in Fig. 114 for different relative nozzle exit widths $b/D_н$.

2. Two-Pass Nozzle Installation with Horizontal Nozzle Cut-off

Earlier we found functions that enable us, for a known geometry, to determine the aerodynamic characteristics of a single-pass nozzle -- the velocity field and the pressure field in the nozzle cut-off plane and the air cushion pressure coefficient, discharge coefficient, and

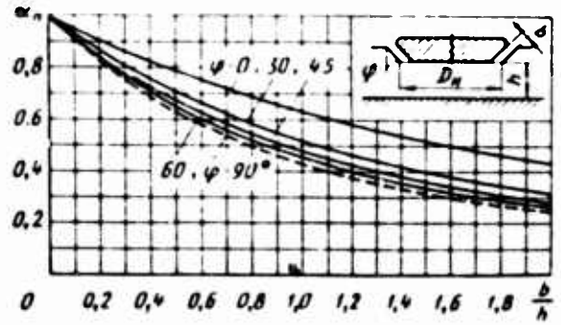

Fig. 110. Discharge coefficient of flat nozzle as a function of parameter b/h for various angles φ of generatrix slope

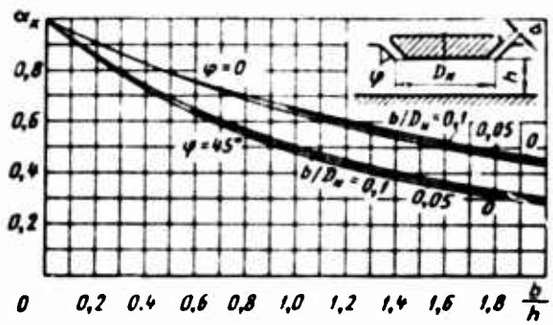

Fig. 111. Discharge coefficient of annular jet as a function of parameter b/h for various relative widths $b/D_н$ of nozzle exit

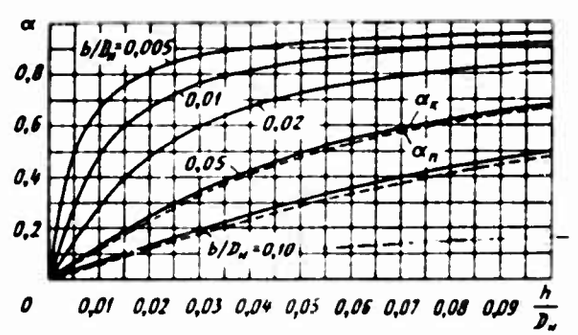

Fig. 112. Discharge coefficients of annular and flat nozzles as a function of relative nozzle clearances above shields for various relative nozzle exit widths and generatrix slope $\varphi = 45^0$

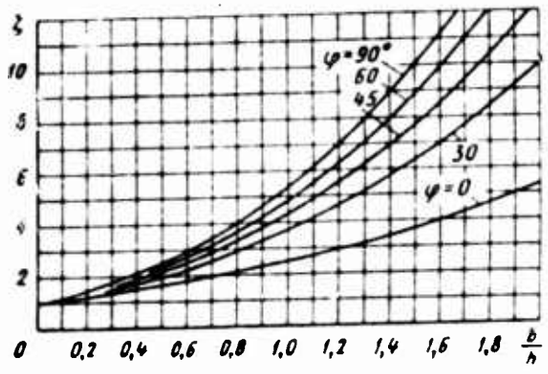

Fig. 13. Drag coefficient of flat nozzle as a function of parameter b/h for various angles φ of generatrix slope

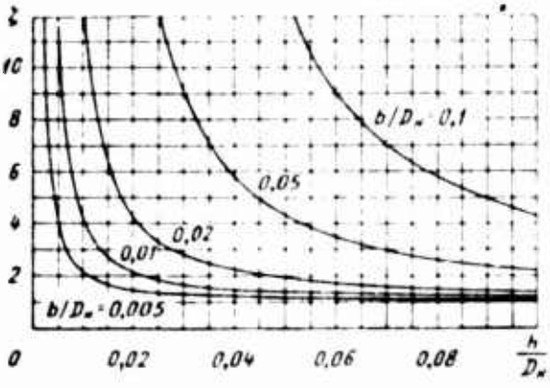

Fig. 14. Drag coefficient of flat nozzle as a function of relative clearance above shield for several relative nozzle exit widths and generatrix slope $\varphi = 45^\circ$

drag coefficient as functions of the elevation of the nozzle above this support surface. Thus, for a single-pass nozzle with horizontal cut-off of the exit edges, for known b, φ, and h, the relative air velocity at a point in question in the nozzle cut-off plane is

$$\frac{v_x}{v_н} = e^{-\frac{x_\varphi}{x_\theta}\frac{h}{h}(1+\sin\varphi)} \cdot e^{-\frac{x_\varphi}{h}(1+\sin\varphi)\cos\varphi}, \qquad (79)$$

while the relative excess pressure is

$$\bar{p} = \frac{p_x - p_н}{\frac{\rho v_н^2}{2}} = 1 - e^{-2\frac{x_\varphi}{x_\theta}\frac{b}{h}(1+\sin\varphi)} \cdot 1 - e^{-2\frac{x_\varphi}{h}(1+\sin\varphi)\cos\varphi}. \qquad (80)$$

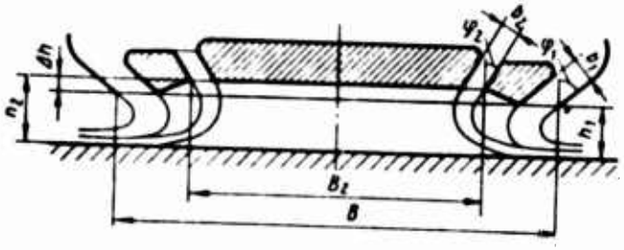

Fig. 115. Arrangement of nozzles in two-pass nozzle installation

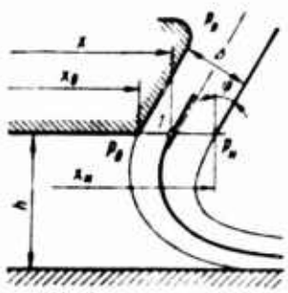

Fig. 116. Scheme of two-pass jet form from a single-jet

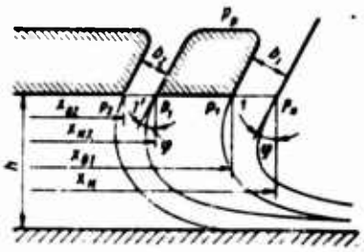

Fig. 117. Streaming of two-pass jet over shield

For the case when the coordinate of the point in question coincides with the coordinate of the inner edge of the nozzle exit ($x_\varphi = x_\delta$), the excess pressure at this point is the excess pressure in the boundary jetlet travelling from the inner edge of the nozzle. This excess pressure propagates in the space bounded from above by the bottom of the nozzle installation, from beneath by the ground surface, and from the sides by the air jets, and constitutes the excess pressure in the air cushion. In this case the drag coefficient is determined by Eq. (78), the air cushion pressure coefficient is

$$\bar{p} = \frac{p_\delta - p_н}{\frac{\rho v_н^2}{2}} = 1 - e^{-2\frac{b}{h}(1+\sin\varphi)}, \qquad (81)$$

while the discharge coefficient is

$$\alpha = \frac{1 - e^{-\frac{b}{h}(1+\sin\varphi)}}{b/h\,(1+\sin\varphi)}. \qquad (82)$$

If we know the total pressure H_c in the air stream ahead of the nozzle installation, equal to the dynamic pressure $\rho v^2/2$, then by using Eqs. (65), (81), and (82) we can determine the excess pressure in the air cushion $p_g - p_н$ and the volume flow of air q in the jet exiting from the nozzle.

Let us determine the aerodynamic characteristics of a two-pass nozzle installation with horizontal nozzle cut-off (Fig. 115). Let us mentally draw in the jet of the single-pass nozzle installation a surface along the streamline through point 1 (Fig. 116) and let us divide the jet and the exit section of the nozzle with this surface into two parts. Let us shift the left part of the jet and the nozzle section relating to it to one side in the horizontal direction and thus let us form two jets with their own nozzles and bottom section line between these nozzles, that is, let us form a two-pass nozzle installation (Fig. 117).

We will assume, as inthe case of the single-pass nozzle, that an invisced and incompressible fluid is brought to the nozzles and, therefore, we can neglect the effect of circulation currents in the space between these jets. Given this assumption, the excess pressure both at points 1 and 1', as well as over the entire section of the bottom between the given points, will be identical and equal to the excess pressure produced by the external air jet, while the excess pressure in the section of the bottom bounded by the internal nozzle will be determined by the overall reaction effect of two jets -- external and internal. This action of two jets can be replaced by the reaction effect of a single jet exiting from a nozzle and with a width equal to the total width of the external and internal nozzles.

Calculating a nozzle installation when $\varphi = \varphi_1 = \varphi_2$ and $\Delta h = 0$. The coefficients of drag, pressure, and discharge of a plane two-pass nozzle installation with identical angles of generatrix inclination of the external and internal nozzles $\varphi = \varphi_1 = \varphi_2$ can be determined, respectively, by Eqs. (65), (81), and (82) with reference to the new geometry of the nozzle installation. The coefficient of air cushion pressure for the section of the bottom between the outer and inner nozzles is

$$\bar{p}_1 = \frac{p_1 - p_н}{\frac{\rho v_н^2}{2}} = 1 - e^{-\frac{b_1}{h}(1+\sin\varphi)},$$

and for the section of the bottom bounded by the internal nozzles, it is

$$\bar{p}_2 = \frac{p_2 - p_н}{\frac{\rho v_н^2}{2}} = 1 - e^{-2\frac{b_1+b_2}{h}(1+\sin\varphi)}.$$

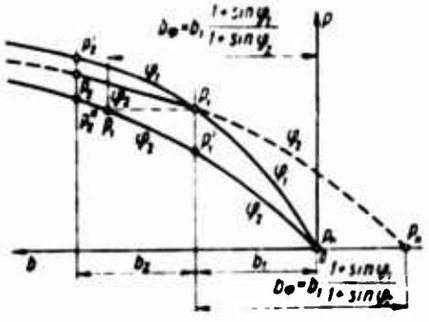

Fig. 118. Scheme for reducing the air cushion pressure for different angles of generatrix inclination of the external and internal nozzles

The total discharge coefficient of a two-pass nozzle installation, given with respect to the overall exit areas of the external and internal nozzles, is

$$\alpha = \frac{1 - e^{-\frac{b_1 + b_2}{h}(1 + \sin\varphi)}}{\frac{b_1 + b_2}{h}(1 + \sin\varphi)}. \qquad (83)$$

The discharge coefficient of the external nozzle, with respect to its exit area, is

$$\alpha_1 \quad \frac{1 - e^{-\frac{b_1}{h}(1 + \sin\varphi)}}{b_1/h\,(1 + \sin\varphi)}. \qquad (84)$$

The discharge coefficient of the internal nozzle, given with respect to its exit area, is

$$\alpha_2 = \alpha + (\alpha - \alpha_1)\frac{b_1}{b_2}. \qquad (85)$$

Eqs. (83) - (85) are real for a plane nozzle installation in which both the generatrix slopes of the external and internal nozzles as well as the length of their nozzle slits are identical.

The total drag coefficient of a two-pass nozzle installation with respect to the overall exit area of the external and internal nozzles $\zeta = \zeta'/\alpha'$.

Calculating a nozzle installation when $\varphi_1 \neq \varphi_2$ and $h = 0$. Let us examine the case of the more complex geometry of a nozzle installation when both the nozzle generatrix slopes and the length of the nozzle slits are different, and the nozzle cut-off lie in the same plane ($\Delta h = 0$). Let us denote the generatrix slope of the external nozzle by φ_1 and that of the internal nozzle by φ_2, and the corresponding length of the exits of these nozzles by l_1 and l_2.

Obviously, the pressure coefficient $\bar{p}_1$ for the external nozzle does not differ in any way from the coefficient $\bar{p}$ for the single-pass nozzle and by Eq. (81) is

$$\bar{p}_1 = 1 - e^{-\frac{b_1}{h}(1+\sin\varphi_1)} \tag{86}$$

The determination of the coefficient $\bar{p}_2$ directly by Eq. (81) does not yield the correct result, since in the transition from the external nozzle to the internal, owing to the change in the angle φ_1 by φ_2 for the same values of b_1 and h, the function (81) gives different values of $\bar{p}$ for the points 1 and 1', that is, different pressures in the air cushion formed by the external and internal jets, which is physically impossible.

For a unique solution to the problem, let us reduce the pressure in the air cushion formed by the internal nozzle to the pressure formed by the external nozzle, by introducing the fictitious exit width φ_1 of the internal nozzle. For the adopted values of b_1, h, and φ_1 the pressure coefficient $\bar{p}_1$ at point 1 can be determined by Eq. (86). The same pressure coefficient $\bar{p}_2$ can be obtained also for a nozzle with a generatrix slope φ_2 if we make the nozzle exit width equal to b_φ. In this case

$$\bar{p}_2 = 1 - e^{-\frac{b_\varphi}{h}(1+\sin\varphi_2)}. \tag{87}$$

By equating the right sides of Eqs. (86) and (87), we get $b_1(1 + \sin\varphi_1) = b_\varphi(1 + \sin\varphi_2)$. Then

$$b_\varphi = b_1 \frac{1+\sin\varphi_1}{1+\sin\varphi_2}. \tag{88}$$

Thus, for an identical elevation h of the nozzles above the shield, the nozzle with the generatrix slope φ_2 and the fictitious exit width b_φ also gives the same initial pressure coefficient $\bar{p}_1$ as does the nozzle with the generatrix slope φ_1 and exit width b_1. The method of reducing the pressure in the air cushion formed by the internal nozzle of a two-pass nozzle installation to the pressure produced by the external nozzle is graphically clarified in Fig. 118.

A curve plotted along points $p_н$, p_1, and p_2' characterizes the variation in pressure in the cut-off plane of the external and internal nozzles with identical angles φ_1 of generatrix inclination and identical exit widths b_1 and b_2.

The curve plotted along points $p_н$, p_1', and p_2'' characterize the pressure variation in the cut-off plane of the external and internal nozzles that have identical angles φ_2 of generatrix inclination and identical exit widths b_1 and b_2.

The curve plotted along points $p_н$, p_1, and p_2 characterizes pressure variation in the cut-off plane of nozzles with angle of inclination φ_1 for the external nozzle and φ_2 for the internal nozzle.

Thus, the pressure coefficient for the section of the bottom bounded by the internal nozzle of a two-pass nozzle installation is

$$\bar{p}_2 = \frac{p_2 - p_н}{\frac{\rho v_н^2}{2}} = 1 - e^{-2\frac{b_\varphi + b_2}{h}(1+\sin\varphi_2)},$$

and with reference to Eq. (88)

$$\bar{p}_2 = 1 - e^{-2\frac{b_1\frac{1+\sin\varphi_1}{1+\sin\varphi_2} + b_2}{h}(1+\sin\varphi_2)}$$

or

$$\bar{p}_2 = 1 - e^{-2\left[\frac{b_1}{h}(1+\sin\varphi_1) + \frac{b_2}{h}(1+\sin\varphi_2)\right]}. \qquad (89)$$

Let us determine the discharge coefficients of a two-pass nozzle with different generatrix slopes and different nozzle slit length. The total volume flow of air passing through the two-pass nozzle installation is equal to the volume flows of air in the external and internal nozzles, that is, $Q = Q_1 + Q_2$. The volume flow of air in the external nozzle is

$$Q_1 = \alpha_1 f_1 \sqrt{\frac{2H_c}{\rho}}. \tag{90}$$

The discharge coefficient α_1 of the external nozzle determined on analogy with the coefficient of a single-pass nozzle installation by Eq. (82) is

$$\alpha_1 = \frac{1 - e^{-\frac{b_1}{h}(1+\sin\varphi_1)}}{b_1 h (1+\sin\varphi_1)}. \tag{91}$$

This coefficient is related to the exit area of the external nozzle

$$f_1 = x_1 l_1 \cos\varphi_1 + b_1 l_1,$$

where x_1 is the exit width of the external nozzle in the cut-off plane.

The volume flow of air in the internal nozzle is

$$Q_2 = \alpha_2 f_2 \sqrt{\frac{2}{\rho} H_c}, \tag{92}$$

where $f_2 = x_2 l_2 \cos\varphi_2 + b_2 l_2$, x_2 is the exit width of the internal nozzle in the cut-off plane.

By Eq. (92) and with reference to the uneven distribution of velocity in the nozzle cut-off plane, the discharge coefficient of the internal nozzle is

$$\alpha_2 = \frac{Q_2}{f_2 \sqrt{\frac{2H_c}{\rho}}} \qquad \frac{\int_{x_{\varphi 2}}^{x_\Phi} x_2 l_2 \cos\varphi_2 \, dx_{\varphi 2}}{x_2 l_2 \cos\varphi_2}. \tag{93}$$

When determining the discharge coefficient for an internal nozzle with a generatrix slope differing from that of the external nozzle, it is necessary, as in the case when we were determining the coefficient p_2, to take into account the disparity in pressures in the air cushion for different generatrix slopes and for identical values of b_1 and h,

that is, to introduce the fictitious width b_φ into the velocity equation. As applied to this particular case, Eq. (79) for an internal nozzle will become

$$\frac{v_{x_2}}{v_m} = \frac{x_\varphi}{h}(1 + \sin\varphi_1)\cos\varphi_2 =$$

$$= \frac{x_\phi + x_{\varphi_2}}{h}(1 + \sin\varphi_1)\cos\varphi_2 = \frac{b_\phi + b_{x_2}}{h}(1 + \sin\varphi_2). \qquad (94)$$

Inserting this expression for the velocity into Eq. (93), integrating within the limits from $x_{\varphi 2} = 0$ to $x_{\varphi 2} = b_2/\cos\varphi_2$, and carrying out the necessary transformations, we get the discharge coefficient of the internal angle with respect to its area:

$$\alpha_2 = e^{-\frac{b_1}{h}(1+\sin\varphi_1)} \frac{1 - e^{-\frac{b_2}{h}(1+\sin\varphi_2)}}{b_2/h\,(1+\sin\varphi_2)}. \qquad (95)$$

The total discharge coefficient of the two-pass nozzle installation with respect to the overall exit areas of the external and internal nozzles is

$$\alpha = \frac{\alpha_1 F_1 + \alpha_2 F_2}{F_1 + F_2}. \qquad (96)$$

The total volume flow of air passing through the two-pass nozzle installation is

$$Q = \alpha F \sqrt{\frac{2}{\rho} H_0}, \qquad (97)$$

where $F = F_1 + F_2 = b_1 l_1 + b_2 l_2$.

General case of the calculation of a nozzle installation when $\varphi_1 \neq \varphi_2$ and $h_1 \neq h_2$. Let us consider the general case of nozzles located in a two-pass nozzle installation when the internal nozzle differs from the external not only by the angle of generatrix inclination φ, exit width b and length l, but also by the height h relative to the principal plane of the nozzle installation coinciding with the cut-off plane of the external nozzle (cf. Fig. 115).

Determining the pressure coefficient $\bar{p}_1$ for an external nozzle in this case does not differ at all from its determination for a single-pass nozzle installation. The coefficient is

$$\bar{p}_1 = 1 - e^{-2\frac{b_1}{h_1}(1+\sin\varphi_1)}.$$

Let us find the expression for the coefficient $\bar{p}_2$. In order to maintain the condition of constancy of pressure p, bounded by jets and the section of the nozzle installation bottom enclosed between them, and to derive the formula for coefficient $\bar{p}_2$ that is structurally similar to the formula for the coefficient $\bar{p}_1$, let us find the fictitious exit width b_φ of the internal nozzle. We can write

$$\bar{p}_1 = 1 - e^{-2\frac{b_1}{h_1}(1+\sin\varphi_1)} = 1 - e^{-2\frac{b_\varphi}{h_1}(1+\sin\varphi_1)},$$

whence

$$b_\varphi = b_1 \frac{h_2}{h_1} \cdot \frac{1+\sin\varphi_1}{1+\sin\varphi_2}. \tag{98}$$

Accordingly, the air cushion pressure coefficient for the section of the bottom bounded by the internal nozzle of a two-pass nozzle installation is

$$\bar{p}_2 = 1 - e^{-2\frac{b_1\frac{h_2}{h_1}\cdot\frac{1+\sin\varphi_1}{1+\sin\varphi_2}-h_1}{h_1}(1+\sin\varphi_1)}$$

or

$$\bar{p}_2 = 1 - e^{-2\frac{b_1}{h_1}(1+\sin\varphi_1)\left(1-\frac{h_2}{b_1}\cdot\frac{h_1}{h_2}\cdot\frac{1+\sin\varphi_2}{1+\sin\varphi_1}\right)}.$$

With reference to $h_2 = h_1 \pm \Delta h$, the coefficient is

$$\bar{p}_2 = 1 - e^{-2\frac{b_1}{h_1}(1+\sin\varphi_1)\left(1-\frac{h_2}{b_1}\cdot\frac{1+\sin\varphi_2}{1+\sin\varphi_1}\cdot\frac{1}{1\pm\frac{\Delta h}{h_1}}\right)}, \tag{99}$$

where Δh is the distance along the vertical between the cut-offs of the internal and external nozzles.

From Eq. (99) it is not difficult to obtain an expression for the coefficient $\bar{p}_2$ corresponding to the particular case when the profile of the internal nozzle differs from the external only by the exit width b and height h of the nozzle cut-off relative to the principal plane of the nozzle installation. Thus, when $\varphi = \varphi_1 = \varphi_2$, Eq. (99) will become

$$\bar{p}_2 = 1 - e^{-2\frac{b_1}{h_1}(1+\sin\varphi)\left(1-\frac{h_2}{b_1}\cdot\frac{1}{1\pm\frac{\Delta h}{h_1}}\right)}. \tag{100}$$

For the case $b_1 \neq b_2$; $\varphi_1 \neq \varphi_2$, and $\Delta h = 0$, Eq. (99) transforms into the earlier-derived Eq. (89), and then in the case of $b_2 = 0$ -- into the formula for the single-pass nozzle installation.

The discharge coefficient of the external nozzle in the general case of the placement of internal nozzles in the nozzle installation we are considering, that is, when $b_2 \neq b_1$; $\varphi_2 \neq \varphi_1$, and $h_2 \neq h_1$, is determined in the same way as for a single-pass nozzle based on Eq. (91). Let us determine the discharge coefficient α_2 of the internal nozzle in this installation just as we did for the derivation of Eq. (95). Using Eq. (93) and Eq. (94) for the velocity in the cut-off plane of the internal nozzle, we get

$$\alpha_2 = e^{-\frac{h_\varphi}{h_1}(1+\sin\varphi_2)} \frac{1 - e^{-\frac{b_2}{h_2}(1+\sin\varphi_2)}}{b_2/h_2(1+\sin\varphi_2)};$$

then, with reference to Eq. (98) determining the fictitious exit width b_φ of the internal nozzle, we finally find

$$\alpha_2 = e^{-\frac{h_1}{h_1}(1+\sin\varphi_1)} \frac{1 - e^{-\frac{b_2}{h_2}(1+\sin\varphi_2)}}{b_2/h_2(1+\sin\varphi_2)}. \qquad (101)$$

The coefficient α_2 is related to the exit area of the internal nozzle $F_2 = b_2 l_2$. The total discharge coefficient of the nozzle installation with respect to the overall exit of the external and internal nozzles is determined by Eq. (96).

13. Double-Pass Nozzle Installation With Oblique Nozzle Cut-off

Let us determine the aerodynamic characteristics of a two-pass nozzle installation with oblique nozzle cut-off (Fig. 119), by using the same method of calculation that was adopted for the nozzle installation with horizontal nozzle cut-off (cf. Fig. 115). For a single-pass nozzle installation with oblique nozzle cut-off, the instantaneous relative air velocity in the nozzle cut-off plane is

$$\frac{v_\psi}{v_\infty} = \left(1 + \frac{b_x}{h} \cdot \frac{\sin(\varphi - \psi)}{\cos\psi}\right)^{-\frac{(1+\sin\varphi)\cos\psi}{\sin(\varphi-\psi)}} =$$

$$= \left[1 + \frac{x_\psi}{h}\sin(\varphi - \psi)\right]^{-\frac{(1+\sin\varphi)\cos\psi}{\sin(\varphi-\psi)}},$$

and the instantaneous relative excess pressure in this same plane is

$$\frac{p_\psi - p_\infty}{\frac{\rho v_\infty^2}{2}} = 1 - \left(1 + \frac{b_x}{h}\frac{\sin(\varphi - \psi)}{\cos\psi}\right)^{-2\frac{(1+\sin\varphi)\cos\psi}{\sin(\varphi-\psi)}} =$$

$$= 1 - \left[1 + \frac{\Delta\varphi}{h}\sin(\varphi - \psi)\right]^{-2\frac{(1+\sin\varphi)\cos\psi}{\sin(\varphi-\psi)}},$$

where x_ψ is the instantaneous coordinate in the nozzle cut-off plane.

These formulas can be used in determining characteristics of the external nozzle as well as the internal if we allow for the geometry of these nozzles. To derive the characteristics of the internal nozzle, we must also introduce into these formulas the values of the fictitious width and fictitious height of the internal nozzle in the nozzle installation.

Two-pass nozzle installation with normal nozzle cut-off. Let us examine the simplest scheme of a two-pass nozzle installation when the angles of nozzle generatrix inclination $\varphi_1 = \varphi_2 = \varphi$, the cut-off nozzles are $\psi_1 = \psi_2 = 0$, and the external edges of the internal nozzles and the internal edges of the external nozzles are at the same distance $\Delta h = b_1 \sin\varphi$ from the principal plane of the nozzle installation, that is, let us consider the characteristics of one of the special cases of a two-pass nozzle installation with normal nozzle cut-off. The method of forming this nozzle installation and the symbols adopted are shown in Fig. 120.

The air cushion pressure coefficient for the external nozzle is

$$\bar{p}_1 = \frac{p_1 - p_\infty}{\frac{\rho v_\infty^2}{2}} = 1 - \left(1 + \frac{b_1}{h_1}\sin\varphi\right)^{-2\frac{1+\sin\varphi}{\sin\varphi}},$$

since when $b_x = b$, the pressure $p_\psi = p_1$.

The air cushion pressure coefficient for the internal nozzle is

$$\bar{p}_2 = \frac{p_2 - p_\infty}{\frac{\rho v_\infty^2}{2}} = 1 - \left(1 + \frac{b_1 + b_2}{h_1}\sin\varphi\right)^{-2\frac{1+\sin\varphi}{\sin\varphi}},$$

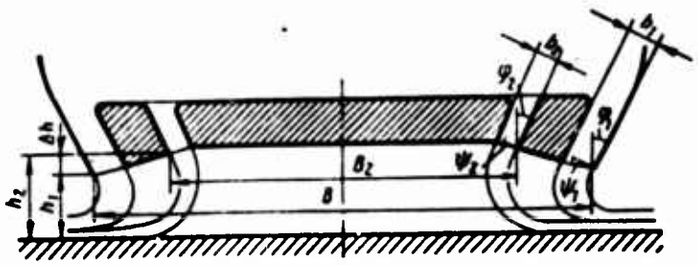

Fig. 119. Arrangement of nozzles in two-pass nozzle installation with oblique nozzle cut-offs

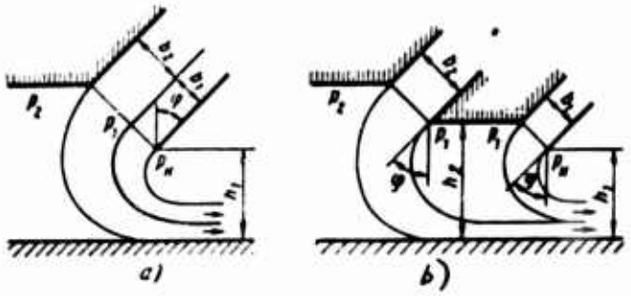

Fig. 120. Formation of two-pass nozzle installation with normal nozzle cut-off:
a -- initial variant
b -- final variant

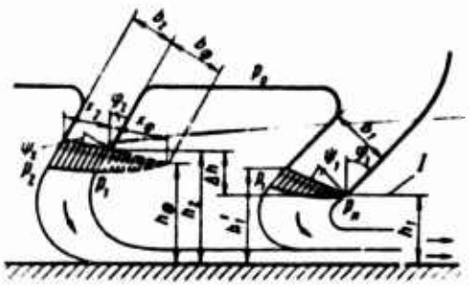

Fig. 121. Design scheme of two-pass nozzle installation with oblique nozzle cut-off:
1 -- principal plane of nozzle installation

since when $b_x = b_1 + b_2$, the pressure $p_\psi = p_2$.

The discharge coefficient of the external nozzle given with respect to its exit area is

$$\alpha_1 = \frac{\int_0^{b_1} v_\psi l_1 \, db_x}{b_1 l_1 v_н},$$

where $v_\psi / v_н$ is the relative air velocity in the nozzle cut-off plane;

$$\frac{v_\psi}{v_н} = \left(1 + \frac{b_x}{h_1} \sin\varphi\right)^{-\frac{1+\sin\varphi}{\sin\varphi}}.$$

After integration, we get

$$\alpha_1 = \frac{h_1}{b_1}\left[1 - \left(1 + \frac{b_1}{h_1}\sin\varphi\right)^{-\frac{1+\sin\varphi}{\sin\varphi}}\right].$$

The discharge coefficient of the internal nozzle given with respect to its exit area is

$$\alpha_2 = \frac{\int_{b_1}^{b_1+b_2} v_\psi l_1 \, db_x}{b_2 l_1 v_н} = \frac{1}{b_2}\int_{b_1}^{b_1+b_2}\left(1 + \frac{b_x}{h_1}\sin\varphi\right)^{-\frac{1+\sin\varphi}{\sin\varphi}} db_x.$$

Integrating this expression, we get

$$\alpha_2 = \frac{h_1}{b_2}\left[\left(1 + \frac{b_1}{h_1}\sin\varphi\right)^{\frac{1}{\sin\varphi}} - \left(1 + \frac{b_2}{h_1}\sin\varphi\right)^{-\frac{1}{\sin\varphi}}\right].$$

The total air discharge coefficient related to total exit area of the nozzle installation is

$$\alpha = \frac{\int_0^{b_1+b_2} v_\psi l_1 \, db_x}{(b_1+b_2) l_1 v_н} = \frac{1}{b_1+b_2}\int_0^{b_1+b_2}\left(1 + \frac{b_x}{h_1}\sin\varphi\right)^{-\frac{1+\sin\varphi}{\sin\varphi}} db_x.$$

Finally,

$$\alpha = \frac{h_1}{b_1 + b_2}\left[1 - \left(1 + \frac{b_1 + b_2}{h_1}\sin\varphi\right)^{-\frac{1}{\sin\varphi}}\right].$$

The drag coefficients of the nozzles are associated with the discharge coefficients by the relationship $\zeta = 1/\alpha_2$.

Two-pass nozzle installation with oblique nozzle cut-off. Let us examine the general case of the placement of internal nozzles in the nozzle installation with oblique nozzle cut-off (Fig. 121). The pressure coefficient of the air cushion formed by jets of air exiting from the external nozzles is determined as in the case of the single-pass nozzle installation:

$$\bar{p}_1 = 1 - \left(1 + \frac{b_1}{h_1}\cdot\frac{\sin(\varphi_1 - \psi_1)}{\cos\psi_1}\right)^{-2\frac{(1+\sin\varphi_1)\cos\psi_1}{\sin(\varphi_1 - \psi_1)}} \qquad (102)$$

or

$$\bar{p}_1 = 1 - e^{-2k_1 \ln k_2}, \qquad (103)$$

where

$$k_1 = \frac{(1+\sin\varphi_1)\cos\psi_1}{\sin(\varphi_1 - \psi_1)}; \quad k_2 = 1 + \frac{b_1}{h_1}\cdot\frac{\sin(\varphi_1 - \psi_1)}{\cos\psi_1}.$$

Let us find the analytic expression for the pressure coefficient of the internal nozzle, which for arbitrarily specified values of b_2, h_2, φ_2, and ψ_2 of the internal nozzle satisfies the condition of equality of pressures $\bar{p}$ at the internal and external edges of the external and internal nozzles, respectively. By maintaining the function $\bar{p}_2 = f(b_2, h_2, \varphi_2, \psi_2)$ structurally singular to the function for the coefficient of the external nozzle, and bearing in mind the conditions specified above, we can express the pressure coefficient for the internal nozzle in the form

$$\bar{p}_2 = 1 - \left(1 + \frac{b_\varphi + b_2}{h_\varphi}\cdot\frac{\sin(\varphi_2 - \psi_2)}{\cos\psi_2}\right)^{-2\frac{(1+\sin\varphi_2)\cos\psi_2}{\sin(\varphi_2 - \psi_2)}}. \qquad (104)$$

The fictitious exit width b_φ of the internal nozzle and the fictitious height h_φ of the placement of this nozzle relative to the support surface appearing in this expression are unknown. The fictitious elevation expressed in terms of the distance between the outer edge of the internal nozzle and the support surface is

$$h_\varphi = h_2 - x_\varphi \sin(\varphi_2 - \psi_2) = h_2 - b_\varphi \frac{\sin(\varphi_2 - \psi_2)}{\cos\psi_2}. \qquad (105)$$

Let us determine the expression for the fictitious width b_φ. By setting the width $b_2 = 0$ in Eq. (04) and equating the right sides of the resulting equation and of Eq. (02), we will have

$$1 - \left[1 + \frac{b_\varphi}{h_\varphi} \cdot \frac{\sin(\varphi_2 - \psi_2)}{\cos\psi_2}\right]^{-2\frac{(1+\sin\varphi_2)\cos\psi_2}{\sin(\varphi_2 - \psi_2)}} =$$

$$= 1 - \left[1 + \frac{b_1}{h_1} \cdot \frac{\sin(\varphi_1 - \psi_1)}{\cos\psi_1}\right]^{-2\frac{(1+\sin\varphi_1)\cos\psi_1}{\sin(\varphi_1 - \psi_1)}}.$$

By replacing h_φ in this expression with its value from Eq. (05), and by carrying out the necessary transformations, we get

$$b_\varphi = \frac{h_2 \cos\psi_2}{\sin(\varphi_2 - \psi_2)} \cdot \frac{A_\psi - 1}{A_\psi}, \qquad (106)$$

where

$$A_\psi = \left[1 + \frac{b_1}{h_1} \cdot \frac{\sin(\varphi_1 - \psi_1)}{\cos\psi_1}\right]^{\frac{1+\sin\varphi_1}{1+\sin\varphi_2} \cdot \frac{\sin(\varphi_2 - \psi_2)}{\sin(\varphi_1 - \psi_1)} \cdot \frac{\cos\psi_1}{\cos\psi_2}}.$$

Inserting into Eq. (04) the values of h_φ and b_φ determined based on Eqs. (105) and (106), and carrying out the transformations, we get

$$\bar{p}_2 = 1 - \left[A_\psi \left(1 + \frac{b_2}{h_2} \cdot \frac{\sin(\varphi_2 - \psi_2)}{\cos\psi_2}\right)\right]^{-2\frac{(1+\sin\varphi_2)\cos\psi_2}{\sin(\varphi_2 - \psi_2)}}$$

or

$$\bar{p}_2 = 1 - \left(\frac{v_g}{v_w}\right)^2 \left[1 + \frac{b_2}{h_2} \cdot \frac{\sin(\varphi_2 - \psi_2)}{\cos\psi_2}\right]^{-2\frac{(1+\sin\varphi_2)\cos\psi_2}{\sin(\varphi_2 - \psi_2)}},$$

where v_g / v_w is the relative velocity of the jetlet travelling from the internal edge of the external nozzle or from the external edge of the internal nozzle,

$$\frac{v_e}{v_M} = \left[1 + \frac{b_1}{h_1} \cdot \frac{\sin(\varphi_1 - \psi_1)}{\cos\psi_1}\right]^{-\frac{(1+\sin\varphi_1)\cos\psi_1}{\sin(\varphi_1-\psi_1)}}.$$

With reference to the equality $\bar{p}_1 = 1 - \left(\frac{v_e}{v_M}\right)^2$, the pressure coefficient of the air cushion produced by the external nozzle is

$$\bar{p}_2 = 1 - (1 - \bar{p}_1)\left[1 + \frac{b_2}{h_2} \cdot \frac{\sin(\varphi_2 - \psi_2)}{\cos\psi_2}\right]^{-2\frac{(1+\sin\varphi_2)\cos\psi_2}{\sin(\varphi_2-\psi_2)}}$$

or, since $h_2 = h_1 + \Delta h$,

$$\bar{p}_2 = 1 - (1 - \bar{p}_1)\left[1 + \frac{b_2/h_1}{1 + \frac{\Delta h}{h_1}} \cdot \frac{\sin(\varphi_2 - \psi_2)}{\cos\psi_2}\right]^{-2\frac{(1+\sin\varphi_2)\cos\psi_2}{\sin(\varphi_2-\psi_2)}},$$

or in the form

$$\bar{p}_2 = 1 - (1 - \bar{p}_1)e^{-2k_3 \ln k_4}, \qquad (107)$$

where

$$k_3 = \frac{(1+\sin\varphi_2)\cos\psi_2}{\sin(\varphi_2 - \psi_2)} \quad \text{and} \quad k_4 = 1 + \frac{b_2/h_1}{1 + \frac{\Delta h}{h_1}} \cdot \frac{\sin(\varphi_2 - \psi_2)}{\cos\psi_2}.$$

Eqs. (103) and (104) are used to determine the pressure coefficients $\bar{p}_1$ and $\bar{p}_2$ of the air cushion produced by the external and internal nozzles for their arbitrarily specified position in the two-pass nozzle installation.

The air discharge coefficient of the external nozzle of the two-pass nozzle installation with oblique nozzle cut-off given with respect to its exit area is

$$\alpha_1 = \frac{\int_0^{x_{\psi_1}} v_\psi \cos\psi_1 l_1 \, dx_\psi}{x_{\psi_1}\cos\psi_1 l_1 v_M} = \frac{1}{x_{\psi_1}} \int_0^{x_{\psi_1} = \frac{b_1}{\cos\psi_1}} \frac{v_\psi}{v_M} dx_\psi.$$

where

$$\frac{v_\psi}{v_n} = \left[1 + \frac{x_\psi}{h_1} \sin(\varphi_1 - \psi_1)\right]^{-\frac{(1+\sin\varphi_1)\cos\psi_1}{\sin(\varphi_1-\psi_1)}};$$

$$x_{\psi 1} = \frac{b_1}{\cos\psi_1}$$

is the exit width of the nozzle in the cut-off plane.

After substitution and integration, we get

$$\alpha_1 = \frac{h}{h_1} \cdot \frac{1 - \left[1 - \frac{b_1}{h} \cdot \frac{\sin(\varphi_1-\psi_1)}{\cos\psi_1}\right]^{-\frac{(1+\sin\varphi_1)\cos\psi_1}{\sin(\varphi_1-\psi_1)}+1}}{\frac{\sin(\varphi_1-\psi_1)}{\sin\psi_1}\left[\frac{(1+\sin\varphi_1)\cos\psi_1}{\sin(\varphi_1-\psi_1)} - 1\right]},$$

or, which amounts to the same thing,

$$\alpha_1 = \frac{h}{h_1} \cdot \frac{1 - \left[\quad\right]}{\cos\psi_1 \left[\quad\right]}, \qquad (108)$$

where

$$k_1 = \frac{(1+\sin\varphi_1)\cos\psi_1}{\sin(\varphi_1-\psi_1)} \quad ; \quad k_2 = 1 + \frac{b_1}{h} \cdot \frac{\sin(\varphi_1-\psi_1)}{\cos\psi_1}. \qquad (109)$$

The discharge coefficient of the internal nozzle given with respect to its exit area is

$$\alpha_2 = \frac{\int_0^{x_{\psi 2}} v_{\psi 2} \cos\psi_2 l_2 \, dx_\psi}{x_{\psi 2} \cos\psi_2 l_2 v_n} = \frac{1}{x_{\psi 2}} \int_0^{x_{\psi 2} = \frac{b_2}{\cos\psi_2}} \frac{v_{\psi n}}{v_i} dx_\psi. \qquad (110)$$

where

$$\frac{v_{\psi_2}}{v_M} = \left[1 + \frac{x}{h_\phi}\sin(\varphi_2 - \psi_2)\right]^{-\frac{(1+\sin\varphi_2)\cos\psi_2}{\sin(\varphi_2-\psi_2)}}$$

is the relative velocity in the cut-off plane of the internal nozzle and $x_2 = \frac{b_2}{\cos\psi_2}$ is the exit width in the cut-off plane.

Here,

$$x = x_\phi + x_{\psi 2} = \frac{b_\phi}{\cos\psi_2} + \frac{b_{x2}}{\cos\psi_2};$$

$$h_\phi = h_2 - x_\phi \sin(\varphi_2 - \psi_2) = h_2 - b_\phi \frac{\sin(\varphi_2 - \psi_2)}{\cos\psi_2}.$$

Replacing the fictitious width b_φ with its value from Eq. (106) and using the notations in (109), after transformations we derive an expression for the instantaneous relative velocity in the cut-off plane of the internal nozzle of a two-pass nozzle installation:

$$\frac{v_{\psi_2}}{v_M} = k_2^{-k_1}\left[1 + \frac{x_{\psi_2}}{h_2}\sin(\varphi_2 - \psi_2)\right]^{-\frac{(1+\sin\varphi_2)\cos\psi_2}{\sin(\varphi_2-\psi_2)}}. \quad (111)$$

Inserting function (111) into Eq. (110) and carrying out the integration, we get

$$\alpha_2 = \frac{h_2}{b_2}\cdot\frac{k_2^{-k_1}\left[1-\left(1+\frac{b_2\sin(\varphi_2-\psi_2)}{h_2\cos\psi_2}\right)^{-\frac{(1+\sin\varphi_2)\cos\psi_2}{(\sin\varphi_2-\psi_2)}+1}\right]}{\frac{\sin(\varphi_2-\psi_2)}{\cos\psi_2}\left[\frac{(1+\sin\varphi_2)\cos\psi_2}{\sin(\varphi_2-\psi_2)}\right]-1}$$

or,

$$\alpha_2 = \frac{h_2 k_2^{-k_1}\left|1-k_4^{-(k_3-1)}\right|}{b_2\frac{\sin(\varphi_2-\psi_2)}{\cos\psi_2}(k_3-1)},$$

where

$$k_3 = \frac{(1+\sin\varphi_2)\cos\psi_2}{\sin(\varphi_2-\psi_2)}; \quad k_4 = 1 + \frac{b_2}{h_2}\cdot\frac{\sin(\varphi_2-\psi_2)}{\cos\psi_2}.$$

Moreover, since $h_2 = h_1 + \Delta h$,

$$\alpha_2 = \frac{1 + \frac{\Delta h}{h_1}}{b_2/h_1} \cdot \frac{k_2^{-k_3}\left|1 - k_4^{-(k_3-1)}\right|}{\frac{\sin(\varphi_2 - \psi_2)}{\cos\psi_2}(k_3 - 1)}. \qquad (112)$$

Eqs. (108) and (112) are used to determine the discharge coefficient of the external and internal nozzles for their arbitrarily specified position in a two-pass nozzle installation.

CHAPTER FOUR
DETERMINING THE LIFT OF AN AIR CUSHION VEHICLE

To produce an air cushion under a vehicle in the free hovering state at some elevation above the support surface, one must continually feed air by means of fans. External air is sucked through receiver openings usually located in the upper section of the vehicle and is fed to the nozzle installation placed in its lower section -- in the bottom. Owing to the reaction of air jets escaping from the nozzle installation and streaming over the ground surface to either side of the craft in directions radial from it, under the bottom is produced a pressure that is greater compared with the atmospheric, that is, the air cushion effect is achieved. In the upper section of the craft at the outer surface of the air intakes and the adjoining sections of the craft roof rarefaction is produced due to the effect of the suction action of the fan.

The lift sustaining the craft in the air is composed of vertical component forces of excess pressure and rarefaction acting on its hull, and the vertical composite reaction forces of the entering and exiting air streams.

The forces of excess pressure acting on the bottom can be determined quite accurately if we know the air dynamic characteristics of the nozzle insulation used on the craft and the air cushion it produces. Direct determination of the rarefaction forces induced due to the effect of air being sucked into the craft and acting on its hull encounters major difficulties, since we must know the regularities of the distribution of rarefaction over the entire surface of the craft roof and especially near the suction opening of the fan. Usually large areas and the small value of the rarefaction do not permit these forces to be determined experimentally with accuracy sufficient for practical use. Let us find in general form the lift produced by the air flowing through the craft.

To find what effect the suction of air has on the lift, let us examine the flow in a vehicle that is in the hovering regime at a considerable distance from the support surface, that is, at a distance

for which the surface has no aerodynamic effect on the discharge air jets from the vehicle and does not bring about an air cushion under the craft bottom.

For simplicity, we will also assume that the vehicle has a single suction opening and a single exit opening. This vehicle (Fig. 122) consists of a vertical duct III, intake header I, and exit nozzle IV. In the duct is mounted a fan II with a drive sucking air through the header and discharging it through the nozzle in the form of a continuous jet aimed vertically downward. The header and the nozzle are profiled along smooth curves, and the entrance edge of the header is separated from the duct axis by a distance that is much greater than the duct diameter.

To determine the lift of the craft, let us enclose it in the contour 1-2-3-4-1 and let us apply the momentum equation. Let us project onto the vertical axis y of craft symmetry forces acting on the craft and on the surface of the isolated contour. If the contour dimensions are taken so that over all sections the pressure is equal to the atmospheric p_H, and the air velocity through the contour $v = 0$ (with the exception of the section where the jet exit velocity is v), we get

$$Y = mv = \rho v^2 F.$$

Thus, the lift acting on the vehicle is numerically equal to the momentum of the jet exiting from the craft to the exterior, is determined only by the velocity v of jet discharge, its density ρ, and the exit area F, and does not depend either on the rarefaction induced at the surface of the craft under the effect of suction, along the configuration of the craft, where the shape of its air intake section and the adjoining structural members. This familiar determination of the thrust from a jet reaction was given as early as 1882 by N. Ye. Zhukovskiy [22, 23, 24].

Let us examine at which craft structural members and to what extent this lift is realized, and let us also determine the power outlays to produce this lift force.

14. Craft With Inlet Header and Exit Nozzle

Let us assume that the header provides a continuous nonseparation entry of air into the duct. We will assume the air to be an ideal fluid -- inviscid and incompressible. Accordingly, we will assume that friction of air against the wall of the header, duct, and nozzle is absent, and also that there are no local pressure losses throughout the flow-through section. Let us assume that the fan has an infinite number of blades and is a kind of disk in which thrust and velocity are distributed evenly over its entire area, including the hub, and that twisting of the

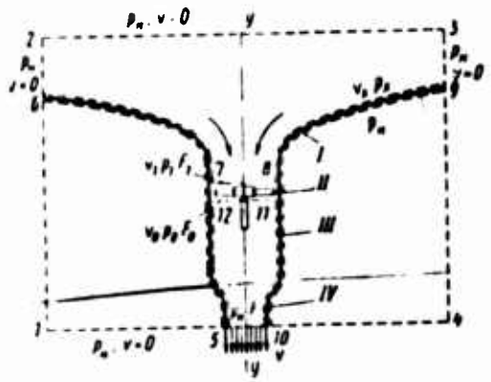

Fig. 122. Control contour for determining the lift of a flight craft with header and nozzle

stream is absent. Let us also assume that the velocity v_1 in the duct cross-section behind the header, v_c -- in the section of the duct behind the fan, and v -- in the nozzle exit are distributed uniformly.

Since the diameter of the header inlet is much larger than the duct parameter, we can assume that the velocity v_x of the air at the edges of this inlet is negligibly small compared with the velocity v_1 at the entrance into the duct, and that the pressure p_x near these edges is equal to the pressure p_H far from the duct inlet, that is, the atmospheric pressure. The velocity v_x of the air jetlet increases in the direction to the duct inlet, and the pressure p_x at the inner surface of the header is reduced. Atmospheric pressure acts on the outer surface of the header. The pressure difference $p_H - p_x$ produces a lift that is applied at the header.

Let us enclose this craft in the control contour 5-6-7-8-9-10-11-12-5 and to determine the lift let us use the equation of momentum. We will draw the contour in direct proximity to the external and internal surfaces of the duct and the header, and over the horizontal sections of the contour, within the duct in front of the fan and behind it -- in the sections where the velocities v_1 and v_0 are uniformly distributed.

Let us project onto the vertical axis y of craft symmetry the forces acting on the craft and on the surface of the adopted contour. By the equation of momentum, we will have

$$Y = mv_0 - mv_1 + p_0F_0 - p_1F_1 + R_н - R_в + \\ + p_н(F_0 - F) - R_c. \qquad (113)$$

where mv_0 is the momentum of the air stream in the section 11-12 behind the fan; mv_1 is the momentum of the air stream behind the fan in the section 7-8; p_0F_0 are the pressure forces in the duct section behind the fan; p_1F_1 are the pressure forces in the duct section ahead of the fan; $R_н$ is the vertical component of the pressure forces acting on the lower surface of the header; $R_в$ is the vertical component of the pressure forces acting on the upper surface of the header; $p_н(F_0 - F)$ is the vertical component of the pressure forces acting on the outer surface of the nozzle; and R_c is the vertical component of the pressure forces acting on the inner surface of the nozzle.

With reference to $F_1 = F_0$ and $v_1 = v_0$, Eq. (113) becomes

$$Y = (p_0 - p_1)F_1 + R_н - R_в + p_н(F_1 - F) - R_c.$$

In this equation the unknowns are pressure p_0 in the duct section behind the fan, pressure $\bar{p}_1$ behind the curved section of the header in front of the fan, and the vertical components $R_н$, $R_в$, and R_c.

The projection on the vertical of the pressure forces acting on the header is

$$R_н - R_в = \int_I (p_н - p_x)dF.$$

Here the pressure drop $p_н - p_x$ depends on the coordinates of the elementary area dF. However this force difference can be determined also without knowing the law of pressure distribution over the surface of the header we use the contour 2-5-9-8-7-6-2 and apply the momentum equation to it. For this contour, since in its section 6-2-5-9 the pressure p = const and v = 0, we have

$$mv_1 + p_1F_1 - p_нF_1 + R_в - R_н = 0.$$

Then the lift acting on the header is

$$Y_к = R_н - R_в = \rho v_1^2 F_1 - (p_н - p_1) F_1,$$

since $m = \rho v_1 F_1$.

We can write for the stream of air between the header, in accordance with Bernoulli's equation

$$p_н - p_1 = \frac{\rho v_1^2}{2}. \quad (114)$$

Then

$$Y_к = R_н - R_в = \rho v_1^2 F_1 - \frac{\rho v_1^2}{2} F_1 = \frac{\rho v_1^2}{2} F_1 = \frac{F}{2F_1} \rho v^2 F,$$

since from the continuity equation $v_1/v = F/F_1$.

The vertical component of the pressure forces acting on the header, expressed in the fraction of the total craft lift, is

[illegible]

Let us determine the pressure forces acting on the nozzle. To do this, let us use the contour 5-12-11-10-5 and apply the equation of momentum to it. Since in the section 11-12 behind the fan the velocity field is uniform, we will write

[illegible]

Using Bernoulli's equation for the air stream passing between the sections 11-12 and 5-10,

$$p_в + \frac{\rho v_0^2}{2} = p_н + \frac{\rho v^2}{2}, \quad (115)$$

it is not difficult to derive an expression for the vertical component of the pressure forces acting on the nozzle,

$$Y_c = p_н (F_0 - F) - R_c = \left(1 - \frac{F_0}{2F} - \frac{F}{2F_0}\right) \rho v^2 F.$$

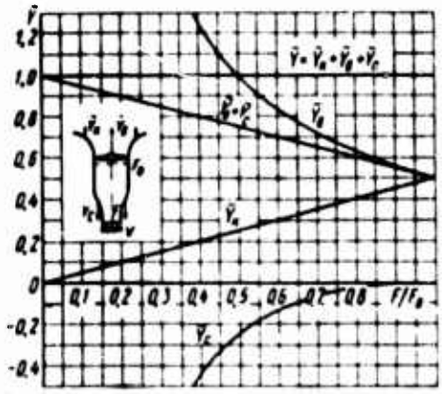

Fig. 123. Craft lift and its components as functions of nozzle relative exit width

The component Y_c when $F/F_0 < 1$ is always negative, that is, it is directed downward and reduces the craft lift. Relating this projection of pressure forces to the total craft lift, we get

$$\bar{Y}_c = \frac{Y_c}{Y} = 1 - \frac{F_0}{2F} - \frac{F}{2F_0}.$$

The vertical component of the pressure forces acting on the fan is

$$Y_e = (p_0 - p_1) F_0.$$

Replacing the pressure p_0 behind the fan with its value based on Eq. (1.5), and the pressure p_1 in the section in front of the fan by its value from Eq. (1.4), and considering that $v_1 = v_0$, we get

$$Y_e = \frac{\rho v^2}{2} F_0$$

or, in fractions of total lift,

$$\bar{Y}_e = \frac{Y_e}{Y} = \frac{1}{2} \cdot \frac{F_0}{F}.$$

The force $\bar{Y}_\beta$ acting on the fan is realized ultimately in the form of the pressure forces acting on its blades and hub. Thus, the craft lift is

$$Y = Y_\kappa + Y_\beta + Y_\varepsilon = \left[\frac{F}{2F_0} + \frac{F_0}{2F} - \frac{F}{2F_0} - \frac{F_0}{2F} + 1\right]\rho v^2 F = \rho v^2 F.$$

The nature of the change in the lift and its components as a function of the relative area F/F_0 of the nozzle exit is shown in Fig. 123, from whence we can see that a change in this area strongly affects the lift components. When the area F/F_0 is reduced, the forces acting on the header become less, while the forces acting on the fan rise. Also increasing in absolute value is the vertical component of the pressure forces on the nozzle wall, but it is directed downward. The algebraic sum of these components always remain unchanged and equal to the reaction of the exiting air jet.

15. Craft With Ideal Header

In the particular case when the nozzle exit area equals the area of the duct cross-section ($F = F_0$), that is, the craft consists of duct, header, and fan with drive, the vertical component of the pressure forces on the header is

$$Y_\kappa = \frac{F}{2F_0}\rho v^2 F = \frac{1}{2}\rho v^2 F,$$

the vertical component of the pressure forces on the fan is

$$Y_\beta = \frac{1}{2}\cdot\frac{F_0}{F}\rho v^2 F = \frac{1}{2}\rho v^2 F$$

and the vertical component of the pressure forces on the nozzle walls is

$$Y_\varepsilon = 1 - \frac{F_0}{2F} - \frac{F}{2F_0} = 1 - \frac{1}{2} - \frac{1}{2} = 0.$$

The lift of the craft for this case is

$$Y = Y_\kappa + Y_\beta = \frac{1}{2}\rho v^2 F + \frac{1}{2}\rho v^2 F = \rho v^2 F,$$

that is, it is numerically equal to the momentum of the jet as it exits from the craft (jet reaction). Here half of the lift component is induced by the action of the pressure forces on the header walls, while the other half of the component comes from the action of pressure forces on the fan. Though that the total drag of the flow-through section of the craft is equal to the dynamic pressure of the air stream as it exits from the craft, that is, $H_c = \rho v^2/2$.

16. Craft With Acute Inlet Edge

Let us examine another characteristic case when the header and the exit nozzle are absent, and the duct has an acute inlet edge (Fig. 124). If we use the contour 1-2-3-4-1 and apply to it the equation of momentum, we will have

$$Y = mv = \rho v^2 F. \qquad (116)$$

Let us determine in this case the point at which the lift is applied. To do this, let us use the contour 5-6-7-8-9-10-11-12-5. The projection on the y axis of the pressure forces acting normally to the duct walls are equal to zero, therefore the equation of momentum is

$$[illegible]$$

With reference to $v_0 = v_1$, we get

$$Y = (p_0 - p_1) F. \qquad (117)$$

The lift Y ultimately is realized in the form of pressure forces acting on the fan blades and hub.

From the joint solution of Eqs. (116) and (117), we have

$$p_0 - p_1 = \rho v^2.$$

The velocities in the sections 7-8 and 11-12 are identical, therefore the dynamic pressures are also equal and, therefore, the pressure difference $p_0 - p_1 = \rho v^2$ is the total pressure built up by the fan in the network. This total pressure is expended in overcoming the network drag. The losses of the dynamic pressure of the flow as it exits from the craft ($\rho v^2/2$) are smaller than the total pressure built up by the fan (ρv^2), therefore the flow in this craft can exist only in the case when local pressure losses are present in the flow-through section. These losses exist and

result from the separation of the flow as it enters a duct with an acute edge, as the result of compression of the jet formed here, and as the result of its subsequent expansion. Let us express the pressure losses in the network in terms of the drag coefficients.

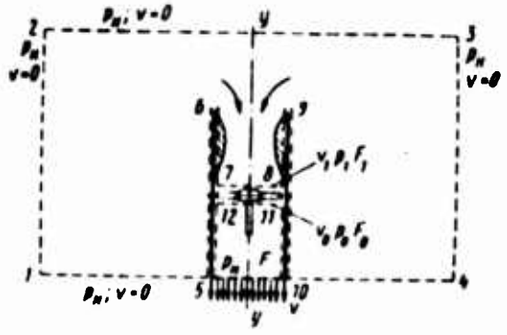

Fig. 124. Contour loop for determining the lift of a flight craft with acute entrance edge

The pressure losses in the delivery network (if we assume that the flow is ideal and that there is no friction of air against the duct walls) consists of the losses of the dynamic pressure of the stream during its exit, that is,

$$H_н = \frac{\rho v^2}{2}.$$

These losses can be expressed as the local drag coefficient

$$\zeta_н = \frac{H_н}{\frac{\rho v^2}{2}} = \frac{\frac{\rho v^2}{2}}{\frac{\rho v^2}{2}} = 1.$$

The atmospheric pressure occurs not only in the duct exit plane but also within it over the section from the duct cut-off to the fan, therefore in the section 11-12 the pressure $p_0 = p$ [illegible].

To determine pressure losses in the suction network, let us apply the Bernoulli equation to the air stream entering the duct:

$$p_н = p_1 + \frac{\rho v_1^2}{2} + \zeta_{вс}\frac{\rho v_1^2}{2}.$$

Since the velocity $v_0 = v$, the coefficient is

$$\zeta_{вс} = \frac{p_н - p_1}{\frac{\rho v^2}{2}} - 1.$$

To determine the pressure difference $p_н - p_1$, let us use the momentum equation. For the contour 1-2-3-4-10-9-8-7-6-5-1, we can write $mv_1 + p_1F - p_нF = 0$. Whence

$$p_н - p_1 = \frac{mv}{F} = \frac{\rho v^2 F}{F} = \rho v^2$$

and

$$\zeta_{вс} = \frac{p_н - p_1}{\frac{\rho v^2}{2}} - 1 = \frac{\rho v^2}{\frac{\rho v^2}{2}} - 1 = 1.$$

As we know, the pressure losses at the entrance into a duct with acute edge are characterized by the coefficient $\zeta_{вс}$.

The total drag of the network is

$$H = H_{вс} + H_н = (\zeta_{вс} + \zeta_н)\frac{\rho v^2}{2} = (1 + 1)\frac{\rho v^2}{2} = \rho v^2.$$

Here we note that for the same lift the drag of the flow-through section of a craft with a duct that has an acute entry edge is twice as great as the drag of the flow-through section of the craft provided with an ideal collector in its duct, since in this case the drag coefficient of the network as a whole is $\zeta = \zeta_{вс} + \zeta_н = 1 + 1 = 2$.

17. Craft With Header Having a Small Radius of Curvature

When a small header is installed in a duct (Fig. 125), introducing additional drag into the flow-through section, the vertical components of the pressure forces acting on the collector is

$$Y. \quad R_н - R_в = mv_1 - (p_н - p_1)F = \rho v_1^2 F - (p_н - p_1)F.$$

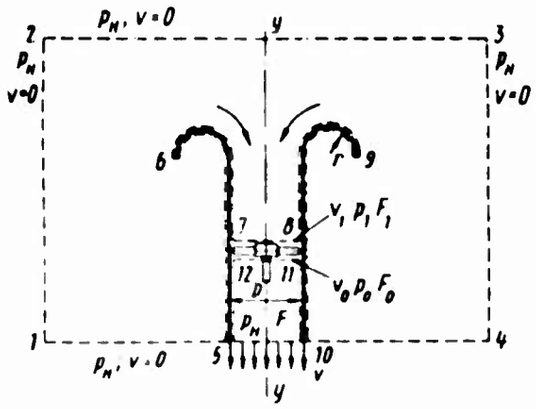

Fig. 125. Contour loop for determining the lift of a flight craft provided with a header

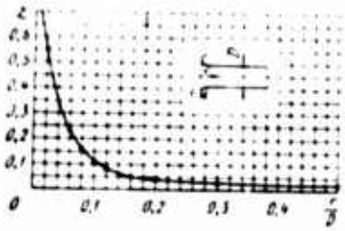

Fig. 126. Dependence of drag coefficient of entrance to header on relative radius of curvature of entrance edge

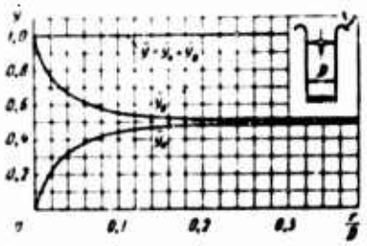

Fig. 127. Relative lift $\bar{Y}$ of craft and its component $\bar{Y}_к$ and $\bar{Y}_\beta$ as functions of the relative header radius of curvature

Expressing the pressure losses in the header in terms of the local drag coefficient ζ, for the air stream entering the duct we can write, in accordance with Bernoulli's equation,

$$p_0 = p_1 + \frac{\rho v_1^2}{2} + \zeta \frac{\rho v_1^2}{2}.$$

Then

$$Y_к = \frac{1-\zeta}{2} \rho v_1^2 F$$

or, in terms of fraction of craft lift,

$$\bar{Y}_к = \frac{Y_к}{Y} = \frac{1-\zeta}{2}.$$

The vertical component of the lift induced by the pressure forces at the fan is

$$Y_в = (p_0 - p_1)F = (p_к - p_1)F = \frac{1+\zeta}{2}\rho v_1^2 F$$

or

$$\bar{Y}_в = \frac{Y_в}{Y} = \frac{1+\zeta}{2}.$$

Thus, even for this case

$$\bar{Y} = \bar{Y}_к + \bar{Y}_в = \frac{1-\zeta}{2} + \frac{1+\zeta}{2} = 1.$$

If in the craft duct we install a header profiled along the arc of a curve and use the experimental dependence of the local drag coefficient ζ on the relative radius of curvature r/D (Fig. 126), the relative lift $\bar{Y}$ and its components $\bar{Y}_k$ and $\bar{Y}_\beta$ can be represented as the curves shown in Fig. 127. As we can see, reducing the header radius of curvature reduces the component $\bar{Y}_k$ and increases the component $\bar{Y}_\beta$ by the same amount. When r/D = 0, that is, when we are dealing with an acute inlet edge of the duct to which ζ = 1 corresponds, the craft lift is determined only by the component acting on the fan ($\bar{Y} = \bar{Y}_\beta$, and $\bar{Y}_k = 0$). But now when r/D = 0.2, the component of the header lift is

$$\bar{Y}_к = \frac{1-\zeta}{2} = \frac{1-0{,}04}{2} = 0{,}48,$$

and the component of the fan lift is

$$\bar{Y}_в = \frac{1+\zeta}{2} = \frac{1+0{,}04}{2} = 0{,}52.$$

Increasing the header diameter by a factor of 2 (when r/D = 0.4) increases the component Y_k by only ~ 1.5 percent.

18. Aerodynamic and Energy Characteristics of Craft

The lift of a craft is

$$Y = \rho v^2 F = \rho v_o^2 F \left(\frac{F_o}{F}\right)^2. \tag{118}$$

The volume flow of air is

$$Q = vF = v_o F_o. \tag{119}$$

The drag of the suction network, equal to the pressure losses as the air enters the header, is

$$H_{sc} = \zeta \frac{\rho v_o^2}{2}. \tag{120}$$

The drag of the delivery network, equal to the losses of the dynamic pressure of the air flow as it exits from the craft, is

[illegible] (121)

The total drag of the flow-through section of the craft is

$$H = H_{sc} + H_n = \left[\zeta + \left(\frac{F_o}{F}\right)^2\right] \frac{\rho v_o^2}{2} = \\ = \left[\zeta + \left(\frac{F_o}{F}\right)^2\right] \frac{\rho}{2} \left(\frac{Q}{F_o}\right)^2. \tag{122}$$

The required power is

$$N = \frac{QH}{75} = \frac{v_o F_o}{75} \left[\zeta + \left(\frac{F_o}{F}\right)^2\right] \frac{\rho v_o^2}{2} = \frac{F_1}{75} \left[\zeta + \left(\frac{F_o}{F}\right)^2\right] \frac{\rho v_o^3}{2}. \tag{123}$$

From Eq. (118), $v_0 = \sqrt{\frac{Y}{\rho F_0 \frac{F_0}{F}}}$. inserting this expression into

Eq. (123) and considering that the density of air is

$$\rho = \rho_H \frac{\rho}{\rho_H} = \rho_H \Delta = \frac{\Delta}{8}, \tag{124}$$

where ρ_H is the density of air at normal atmospheric conditions ($\rho_H = 0.125$ kg · sec^{2}m^4), we get the power N expressed in terms of the lift

$$N = \frac{\sqrt{2}}{75\sqrt{\Delta}} \cdot \frac{\zeta + \left(\frac{F_0}{F}\right)^2}{\sqrt{\left(\frac{F_0}{F}\right)^3}} \sqrt{\frac{Y}{F_0}} Y. \tag{125}$$

Eq. (125), represented in the form

$$K = \frac{N}{Y}\sqrt{\frac{Y}{F_0}} = \frac{75\sqrt{\Delta}}{\sqrt{2}} \cdot \frac{\sqrt{\left(\frac{F_0}{F}\right)^3}}{\zeta + \left(\frac{F_0}{F}\right)^2}, \tag{126}$$

expresses the power ratio of the craft.

For a comparison of the power ratio of craft under consideration, two curves plotted by Eq. (126) are given in Fig. 128. Curve 1 characterizes the power ratio of a craft consisting of a fan, ideal header ($\zeta = 0$), duct, and exit nozzle, and curve 2 characterizes the energy ratio of the same craft, but now without a header -- and with a duct that has an acute inlet edge ($\zeta = 1$).

For a craft consisting of a fan and an ideal header, when $F = F_0$, the power ratio reaches its maximum:

$$K_{\max} = \frac{75\sqrt{\Delta}}{\sqrt{2}} \cdot \frac{\sqrt{\left(\frac{F_0}{F}\right)^3}}{1 + \left(\frac{F_0}{F}\right)^2} = \frac{75\sqrt{\Delta}}{\sqrt{2}} \cdot \frac{1}{0+1} \quad 53.$$

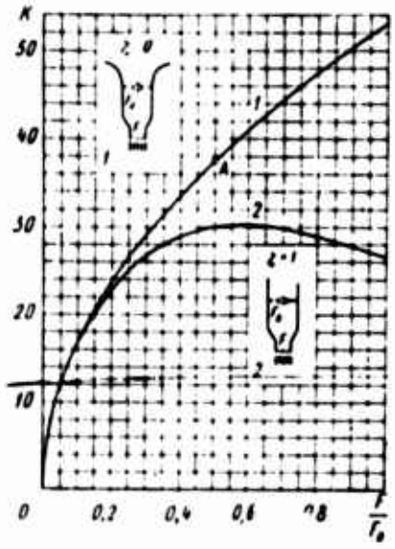

Fig. 128. Power ratio of craft as functions of relative nozzle exit area and inlet header drag coefficient
1 -- for $\zeta = 0$
2 — for $\zeta = 1$

As the relative nozzle exit area F/F_0 is reduced, the power ratio drops off (cf. curve 1). Plotted on this same curve is point A characterizing the familiar power ratio $K_\theta = 37.5$ of an ideal isolated air propeller. For this propeller, the relative area of the compressed section of the jet is $F/F_0 = \frac{1}{2}$, and the drag coefficient of the "flow-through" section related to the velocity directly behind the propeller $\zeta = 4$.

For a craft consisting of a fan and a duct with an acute inlet [entry] edge, when $F = F_0$ (with no exit nozzle), the power ratio is

$$K_0 = \frac{75\sqrt{\Delta}}{\sqrt{2}} \cdot \frac{\sqrt{\left(\frac{F_0}{F}\right)^3}}{\zeta + \left(\frac{F_0}{F}\right)^2} =$$

$$= \frac{75 \cdot 1}{\sqrt{2}} \cdot \frac{1}{1+1} = 26{,}5.$$

Examining Eq. (126) and Fig. 128, we can see that when $F = F_0$, the power ratio of a craft consisting of a fan and a smoothly contoured header is twice as great as for the same craft, but lacking a header, and is 1.41 times greater than for a craft with an isolated air propeller.

For the same lift ($Y_u = Y_0$), the power ratio $\frac{N_u}{N_0} = \frac{K_0}{K_u} = \frac{26,5}{53} = \frac{1}{2}$,

that is, the required power for a craft with a smooth header is half that for a craft with an acute inlet edge.

For the identical power consumption ($N_u = N_0$), the lift ratio $\frac{Y_u}{Y_0} = \left(\frac{K_u}{K_0}\right)^{2/3} = \left(\frac{53}{26,5}\right)^{2/3} = 1.59$, that is, installing a smooth header in a duct with an acute inlet edge increases the lift by $\sim$ 59 percent.

This is dictated by the fact that the installation of a smooth header in the craft reduces the drag of the flow-through section by a factor of 2, reducing to nought local pressure losses caused by the contraction of the jet, that is, by the contraction of the jet at its entrance into the duct with an acute edge and [illegible] by its expansion in the duct.

Inlets made in the form of a smooth header and an acute edge produce the following (extreme) cases of streaming of air to the craft fan: in one nonimpact air entrance is ensured, while in the other -- the greatest local pressure losses caused by compression of the jet. The zone enclosed between curves 1 and 2 (cf. Fig. 128) to determine the power ratio of a craft provided with a collector with relatively small radius of curvature.

For a craft with a header in which the curvature of the inlet edges relatively small, the maximum power ratio occurs for relative exit nozzle width $F/F_0 = 1/(3\zeta)^{\frac{1}{2}}$ and can be expressed, when $\Delta = 1$, in the form

$$K_0 = \frac{75}{\sqrt{2}} \cdot \frac{1}{\zeta} \frac{(\sqrt{3\zeta})^3}{(\sqrt{3\zeta})^3} = \frac{30,2}{\sqrt{\zeta}}.$$

The maximum power ratio occurs when $\zeta \geq 1/3$.

For a craft that has a duct with an acute inlet edge ($\zeta = 1$), the optimal relative nozzle exit width $F/F_0 = 1/(3)^{\frac{1}{2}} = 0.597$ and the maximum ratio of $K = 30.2$.

Using Eqs. (118) - (125), for these craft we can derive the following relationships between pressure, volume flow, power, and lift.

The pressure is

$$H = \left[\zeta + \left(\frac{F_0}{F}\right)^2\right] \frac{\Delta}{16}\left(\frac{Q}{F_0}\right)^2 = \frac{\zeta + \left(\frac{F_0}{F}\right)^2}{2F_0\frac{F_0}{F}} Y =$$

$$= \left(\frac{75\sqrt{\Delta}}{4} \cdot \frac{\sqrt{\zeta + \left(\frac{F_0}{F}\right)^2}}{F_0} N\right)^{2/3}. \qquad (127)$$

The volume flow of air is

$$Q = \frac{4F_0}{\sqrt{\Delta}} \sqrt{\frac{H}{\zeta + \left(\frac{F_0}{F}\right)^2}} = 2\sqrt{\frac{75 \cdot 16}{\Delta} \cdot \frac{F_0^2}{\zeta + \left(\frac{F_0}{F}\right)^2} N} =$$

$$= \frac{2\sqrt{2}}{\sqrt{\Delta}} \sqrt{Y F_0 \frac{F}{F_0}}. \qquad (128)$$

The power required is

$$N = \frac{4}{75\sqrt{\Delta}} \cdot \frac{F_0}{\sqrt{\zeta + \left(\frac{F_0}{F}\right)^2}} \sqrt{H^3} = \frac{\sqrt{2}}{75\sqrt{\Delta}} \cdot \frac{\zeta + \left(\frac{F_0}{F}\right)^2}{\sqrt{\left(\frac{F_0}{F}\right)^3}} \cdot \frac{\sqrt{Y^3}}{\sqrt{F_0}} =$$

$$= \frac{1}{75 \cdot 16} \cdot \frac{\zeta + \left(\frac{F_0}{F}\right)^2}{F_0} Q^3. \qquad (129)$$

The lift force is

$$Y = \left(\frac{75\sqrt{\Delta}}{\sqrt{2}} \cdot \frac{\sqrt{F_0}\sqrt{\left(\frac{F_0}{F}\right)^3}}{\zeta + \left(\frac{F_0}{F}\right)^2} N\right)^{2/3} =$$

$$= \frac{2F_0\frac{F_0}{F}}{\zeta + \left(\frac{F_0}{F}\right)^2} H = \frac{\Delta}{8} \cdot \frac{Q^2}{F_0} \cdot \frac{F_0}{F}. \qquad (130)$$

Let us compare the characteristics of two craft: one with an inlet header and an exit nozzle, and the other equipped only with a header. Let us assume that the fan diameters of these craft are identical and their collectors are executed along smooth curves ($\zeta = 1$). Let us denote with the subscript "K" the characteristics of the craft provided only with a header (without a nozzle). Let us unc Eqs. (127) - (130) to determine the characteristics.

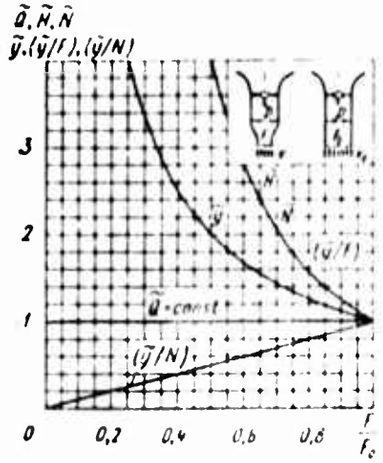

Fig. 129. Craft characteristics for constant air volume flow as functions of relative nozzle exit area

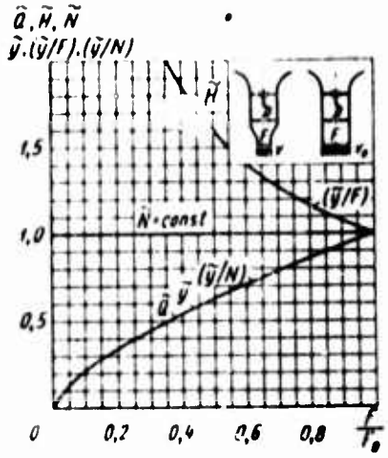

Fig. 130. Craft characteristics for constant power consumption as functions of relative nozzle exit area

For identical air volume flows in the flow-through section of the craft ($\tilde{Q} = Q/Q_K = 1$)

$$\frac{H}{H_K} = \frac{N}{N_K} = \frac{\frac{Y}{F}}{\left(\frac{Y}{F}\right)_K} = \left(\frac{F_0}{F}\right)^2 \quad \text{or} \quad \tilde{H} = \tilde{N} = \left(\frac{\tilde{Y}}{F}\right) = \left(\frac{F_0}{F}\right)^2;$$

$$\frac{\frac{Y}{N}}{\left(\frac{Y}{N}\right)_K} = \left(\frac{Y}{N}\right) = \frac{F}{F_0}; \quad \frac{Y}{Y_K} = \tilde{Y} = \frac{F_0}{F}.$$

For identical power outlay ($\tilde{N} = N/N_K = 1$), we get

$$\frac{Q}{Q_K} \quad \frac{Y}{Y_K} = \frac{\frac{Y}{N}}{\left(\frac{Y}{N}\right)_K} = \left(\frac{F}{F_0}\right)^{2/3}$$

$$\text{or} \quad Q = \tilde{Y} = \left(\frac{Y}{N}\right) = \left(\frac{F}{F_0}\right)^{2/3};$$

$$\frac{H}{H_K} \quad \frac{\frac{Y}{F}}{\left(\frac{Y}{F}\right)_K} = \left(\frac{F_0}{F}\right)^{2/3} \quad \text{or} \quad H = \left(\frac{\tilde{Y}}{F}\right) = \left(\frac{F_0}{F}\right)^{2/3}.$$

The effect of installing a nozzle on the aerodynamic characteristics of a craft with identical air volume flow in the flow-through section is shown in Fig. 129, from whence we can see that reducing the ratio of areas F/F_0 for the nozzle exit leads to an increase in the lift $\tilde{Y}$, an appreciable increase in the required pressure $\tilde{H}$, required power N, and required load over the area $\tilde{Y}/F$, and to a reduction of the load for the power $\tilde{Y}/N$.

The effect of installing a nozzle on the aerodynamic characteristics of a craft is shown in Fig. 130, for identical power outlays. In this case reducing the ratio of areas F/F_0 leads to an increase in the pressure $\tilde{H}$ and the load over the area Y/F and reduces the air volume flow $\tilde{Q}$, lift $\tilde{Y}$, and the load for power $\tilde{Y}/N$.

Let us compare the characteristics of a craft with a small header with the characteristics for the same craft, but now provided with a header that does not produce pressure losses ($\zeta = 0$). Here we will use the experimental dependence of the drag coefficients ζ of the header on the radius of curvature r/D. Let us denote with the index K the characteristics of the craft with a smooth header and, with reference to Eqs. (127) - (130), we get:

for identical air volume flow in the craft $\left(\tilde{Q} = \frac{Q}{Q_к} = 1\right)$

$$\tilde{H} = \tilde{N} = 1 + \zeta, \quad \tilde{Y} = \left(\frac{\tilde{Y}}{F}\right)_к = 1; \quad \left(\frac{\tilde{Y}}{N}\right) = \frac{1}{1+\zeta};$$

for identical total pressure $\left(\tilde{H} = \frac{H}{H_к} = 1\right)$

built up by the fan in the flow-through section of the craft,

$$\tilde{Q} = \tilde{N} = \left(\frac{\tilde{Y}}{N}\right) = \frac{1}{\sqrt{1+\zeta}}; \quad \tilde{Y} = \left(\frac{\tilde{Y}}{F}\right) = \frac{1}{1+\zeta}.$$

for identical power outlay $\left(\tilde{N} = \frac{N}{N_к} = 1\right)$

$$\tilde{Q} = \frac{1}{\sqrt[3]{1+\zeta}}; \quad \tilde{Y} = \left(\frac{\tilde{Y}}{F}\right) = \left(\frac{\tilde{Y}}{N}\right) = \frac{1}{\sqrt[3]{(1+\zeta)^2}}; \quad \tilde{H} = \sqrt[3]{1+\zeta}.$$

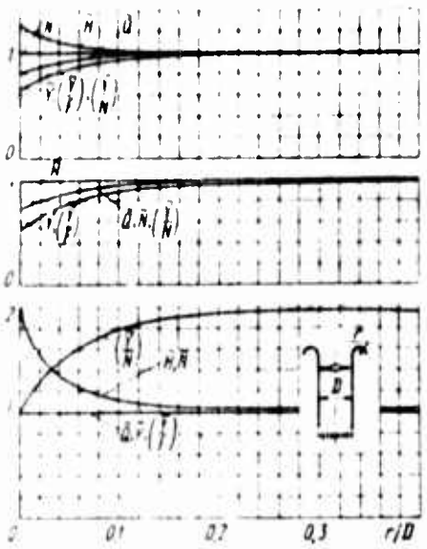

Fig. 151. Aerodynamic and power characteristics of craft as functions of relative header radius of curvature (with respect to the characteristics of a craft provided with an ideal header)

For the case of identical air supply $\left(Q = \frac{Q}{Q_*} = 1\right)$ in a craft with a header having a small radius of curvature compared with the craft with an ideal header, it is necessary (Fig. 151), for the same lift ($\tilde{Y} = 1$) and for unchanged load over area ($Y/F = 1$) to use the fan to sustain an increased pressure ($H > 1$) and to expend additional power ($\tilde{N} > 1$). Here, the smaller the header radius of curvature, the lower will be the specific load on the power ($\tilde{Y}/N$) < 1.

If the fan independently of the header radius of curvature builds up the same total pressure ($\tilde{H} = 1$) in the flow-through section of the craft, then as this radius is reduced, the air volume flow, power, and specific load on power become less. As this takes place, the lift is reduced even more sharply, and so is the load over the area.

For identical power outlay ($\tilde{N} = 1$), as the header radius of curvature is reduced, the total pressure rises, and the air volume flow correspondingly is reduced. Here, the lift is identically reduced to the same extent, as is the load over the area and the load on the power.

Thus, analysis of craft characteristics shows that the use of an inlet header is advantageous not only in that it causes the formation of additional lift in response to the reactive force produced by the air jets exiting from the craft, but also in that by ensuring a smooth intake of air into the craft, the header appreciably reduces the drag of the flow-through section and thereby improves the power ratio of the craft as a whole.

In actual conditions, the presence of local pressure losses in craft structures, especially behind the fan in the delivery network, and the friction of air against the walls of the flow-through section channels reduces the positive effect achieved with the header, and does so the more strongly, the greater the overall drag of the flow-through section. The lift of this kind of craft, independently of the pressure losses in the flow-through section, is equal to the reaction of the air jet exiting from the craft.

CHAPTER FIVE
LIFT OF AN AIR CUSHION VEHICLE IN THE HORIZONTAL HOVERING REGIME

19. Craft With Normal Nozzle Cut-off

The lift of air cushion vehicles is one of the most important characteristics determining not only the principal air dynamic qualities of such craft, but also their power features. This is caused by the fact that to sustain a craft at some elevation over the ground surface both in the hovering regime as well as during flight require a continuous power outlay, since air must be continually supplied under the craft bottom by means of jets to form the air cushion. The hovering regime is one of the design regimes, therefore let us continue for this case the streaming of jets over the ground surface and establish a relationship between the lift produced by the air cushion, the geometry of the nozzle installation, and the aerodynamic parameters of the air stream fed to the nozzle.

Let us determine the lift of the air cushion vehicle [illegible] a flat nozzle with normal nozzle cut-off. For this purpose, let us isolate a section with length l from this craft by using two parallel cross-sections normal to the craft's longitudinal axis (Fig. 152), enclosed in the control contour, and apply to this contour the equation of momentum. We will position the upper and side boundaries of the contour at a distance from the craft at which the velocity v of air streaming can be regarded as zero, and the pressure along these boundaries as constant, equal to the atmospheric pressure p_a. We will position the lower boundary of the contour in direct proximity to the bottom of the craft, parallel to the ground surface, and at the nozzle sections -- in their cut-off plane.

Let us project onto the y axis the forces acting on the craft and on the surface of the isolated contour. The forces acting on the lateral surfaces of a loop are normal to the surfaces and their projections on the y axis are equal to zero. Therefore the momentum equation for this contour is

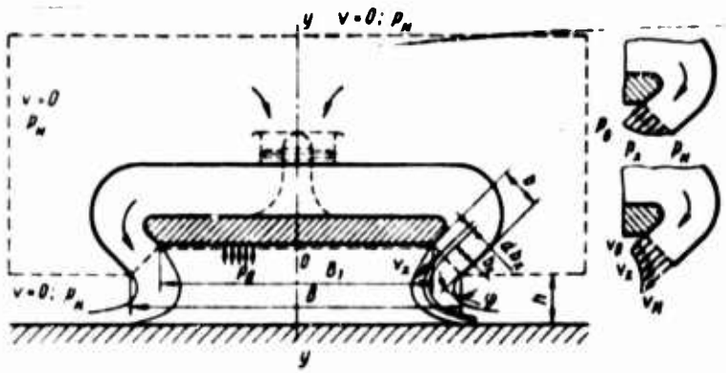

Fig. 132. Control contour for determining the lift of an air cushion vehicle with a plane nozzle provided with normal cut-off

$$Y = 2\rho L \cos\varphi \int_0^b v_x^2\, db_x +$$

$$+ 2L\cos\varphi \int_0^b (p_x - p_н)\, db_x + B_1 L\,(p_в - p_н). \qquad (131)$$

where L is the length of the nozzle slit; and B_1 is the width of the nozzle installation with respect to the inner edges of the external nozzles.

The first term of the right side of Eq. (131)

$$Y_1 = 2\rho L \cos\varphi \int_0^b v_x^2\, db_x \qquad (132)$$

is the projection on the y axis of the momentum of the plane air jets, with reference to the nonuniformity of distribution of velocity v_x at the nozzle exit, that is, the component of the lift due to the reaction of the air jets. The second term of the right side of Eq. (131)

$$Y_2 = 2L\cos\varphi \int_0^b (p_x - p_н)\, db_x \qquad (133)$$

is the projection of the pressure forces acting in the nozzle exit plane, with reference to the nonuniformity of pressure p_x distribution, that is, the component of the lift arising from the forces of excess pressure in the nozzle exit. The last term of the right half of Eq. (131)

$$Y_n = B_1 L (p_{\text{ж}} - p_a)$$

is the projection of the forces of excess pressure acting at the craft bottom, that is, the component of the lift due to the air cushion.

Let us express these forces as a function of the geometrical quantities of the nozzle installation and the aerodynamic parameters of the air jet producing the air cushion. Let us use the equation determining the regularity of velocity distribution in the nozzle exit,

$$\frac{v_x}{v_{\text{ж}}} = \left(1 + \frac{b_x}{h} \sin\varphi\right)^{-\left(1+\frac{1}{\sin\varphi}\right)}, \qquad (134)$$

where v_x is the air velocity at the point lying in the nozzle cut-off plane; $v_{\text{ж}}$ is the discharge velocity of the bounding jetlet at the outer edge of the nozzle$_x$ [sic] exit; b_x is the instantaneous coordinate of the point at which the velocity is equal to v_x; and φ is the angle of generatrix inclination of the plane nozzle with respect to the vertical axis of the craft.

Replacing the instantaneous velocity v_x in Eq. (132) with its expression from Eq. (134), we get

$$Y_p = 2\rho v_{\text{ж}}^2 L \cos\varphi \int_0^h \left(1 + \frac{b_x}{h} \sin\varphi\right)^{-2\left(1+\frac{1}{\sin\varphi}\right)} db_x.$$

The integral appearing in this equation is

$$\int_0^b \left(1 + \frac{b_x}{h} \sin\varphi\right)^{-2\left(1+\frac{1}{\sin\varphi}\right)} db_x = \frac{h}{2 + \sin\varphi} \times$$

$$\times \left(1 - \left(1 + \frac{b}{h} \sin\varphi\right)\left[1 - \left[1 - \left(1 + \frac{b}{h} \sin\varphi\right)^{-2\left(1+\frac{1}{\sin\varphi}\right)}\right]\right]\right), \qquad (135)$$

and the coefficient

$$p = \frac{p_a - p_{\text{ж}}}{\rho \frac{v_{\text{ж}}^2}{2}} = 1 - \left(1 + \frac{b}{h} \sin\varphi\right)^{-2\left(1+\frac{1}{\sin\varphi}\right)} \qquad (136)$$

is the air cushion pressure coefficient, therefore the component of the lift due to the reaction of the air jet exiting from the nozzle is

$$Y_p = 4hL\frac{\cos\varphi}{2+\sin\varphi}\left[\left(1+\frac{b}{h}\sin\varphi\right)\bar{p}-\frac{b}{h}\sin\varphi\right]\frac{\rho v_н^2}{2}. \quad (137)$$

Let us express the lift produced by the forces of excess pressure in the nozzle cut-off plane also in terms of the geometrical dimensions of the nozzle and the aerodynamic parameter of the air jet. The total pressure at each point lying in the nozzle cut-off plane is identical, and by Bernoulli's equation,

$$p_в + \frac{\rho v_в^2}{2} = p_н + \frac{\rho v_н^2}{2}.$$

Therefore, Eq. (135) can be represented as

$$Y_c = 2L\cos\varphi\int_0^h\left(\frac{\rho v_н^2}{2}-\frac{\rho v_в^2}{2}\right)db_в =$$

$$= 2Lb\frac{\rho v_н^2}{2}\cos\varphi - 2L\frac{\rho v_н^2}{2}\cos\varphi\int_0^h\left(1+\frac{b_в}{h}\sin\varphi\right)^{-\left(1+\frac{1}{\sin\varphi}\right)}db_в.$$

Replacing the integral appearing in this equation with its value from the solution (135) and using Eq. (136), we get the component of the lift due to the excess pressure in the nozzle cut-off plane

$$Y_c = \left\{2bL\cos\varphi - 2hL\frac{\cos\varphi}{2+\sin\varphi}\left[\left(1+\frac{b}{h}\sin\varphi\right)\bar{p}-\right.\right.$$

$$\left.\left.-\frac{b}{h}\sin\varphi\right]\right\}\frac{\rho v_н^2}{2} \quad (138)$$

The component of the lift due to excess pressure in the air cushion is

$$Y_п = B_1L(p_c - p_н) = B_1L\frac{p_c-p_н}{\frac{\rho v_н^2}{2}}\cdot\frac{\rho v_н^2}{2} = B_1L\bar{p}\frac{\rho v_н^2}{2}. \quad (139)$$

The total lift of an air cushion vehicle with plane nozzle $Y = Y_p + Y_c + Y_n$ and, by Eqs. (137), (138), and (139),

$$Y = \left\{ 2bL\cos\varphi + 2hL\frac{\cos\varphi}{2+\sin\varphi}\left[\left(1+\frac{b}{h}\sin\varphi\right)\bar{p} - \right.\right.$$

$$\left.\left. - \frac{b}{h}\sin\varphi\right] + B_1 L\bar{p}\right\}\frac{\rho v_n^2}{2}.$$

Denoting the overall area of the nozzle exits by $F = 2bL$, and the area of the bottom of the nozzle insulation bounded by the inner edges of the nozzles as $S_1 = B_1 L$, and carrying out uncomplicated transformations, we get

$$Y = \left\{ F\frac{\cos\varphi}{2+\sin\varphi}\left[2+\left(\frac{h}{b}+\sin\varphi\right)p\right] + S_1\bar{p}\right\}\frac{\rho v_n^2}{2}.$$

The lift of an air cushion vehicle can be represented as

$$Y = c_y S H_c, \tag{140}$$

where c_y is the lift coefficient; S is the characteristic area of the craft nozzle installation; and H_c is the characteristic pressure in the air stream producing the air cushion.

Adopting as the characteristic area the area of the nozzle installation bounded by the external exit edge of the nozzles, $S = BL$, adopting as the characteristic pressure the total pressure in the air stream required to produce the jets, $H_c = \rho v^2/2$, and using the definition (140), we derive a formula for the coefficient of an air cushion vehicle with a single-pass nozzle

$$c_y = F\frac{\cos\varphi}{2+\sin\varphi}\left[2+\left(\frac{h/B}{b/B}+\sin\varphi\right)\bar{p}\right] + \bar{S}_1\bar{p}, \tag{141}$$

where

$$F = \frac{F}{S}\ ;\ S_1 = \frac{S_1}{S}.$$

The first term of the right side of this equation

$$c_{yx} = c_{yp} = c_{yc} = F\frac{\cos\varphi}{2+\sin\varphi}\left[2+\left(\frac{h/B}{b/B}+\sin\varphi\right)\bar{p}\right]$$

is the component of the lift determined by the momentum of the air jet exiting from the nozzle and by the pressure forces acting at its cross-section, and the second term $c_{yn} = \bar{S}_1\bar{p}$ is the component of the lift acting in the air cushion over the section of the craft bottom bounded by the internal edges of the nozzles.

For an air cushion vehicle with a single-pass annular nozzle, Eq. (141) becomes

$$c_y = \bar{F}_c \frac{\cos\varphi}{2 + \sin\varphi}\left[2 + \left(\frac{h/D_н}{b/D_н} + \sin\varphi\right)\bar{p}\right] + (1 - \bar{F}_c\cos\varphi)\bar{p}, \quad (142)$$

where $\bar{F}_c = 4\frac{b}{D_н}\left(1 - \frac{b}{D_н}\cos\varphi\right)$ is the relative cut-off area of the annular

nozzle, found as the lateral surface of a truncated cone, whose base perimeters are circles formed by the external and internal edges of the nozzle.

The air cushion pressure coefficient appearing in Eq. (142) is

$$\bar{p} = 1 - \left(1 + \frac{b/D_н}{h/D_н}\sin\varphi\right)^{-\left(1 + \frac{1}{\sin\varphi}\right)}.$$

The dependence of a lift coefficient c_y of the plane nozzle installation with normal nozzle cut-off on the relative elevation h_b for different relative nozzle exit width b_B and constant angle of inclination of its generatrices ($\varphi = 45^\circ$) is given in Fig. 133. When the nozzle installation rests on the support surface ($h/B = 0$), the lift coefficient $c_y = 1$. The discharge of air from the nozzle is absent in this case and the excess pressure in the air cushion is equal to the total pressure in front of the inlet into the nozzle installation.

When the craft rises above the support surface, the nature of the variation in the coefficient c_y is predetermined by the relative nozzle exit width b/B. For small b/B values, the coefficient c_y decreases rapidly with increase in elevation h/B. For a relatively large exit width b/B, we have maximum values of the function $c_y = f(b_h, b_B)$, where with an increase in the parameter b/B the maximum c_y values are displaced toward the larger h/B values.

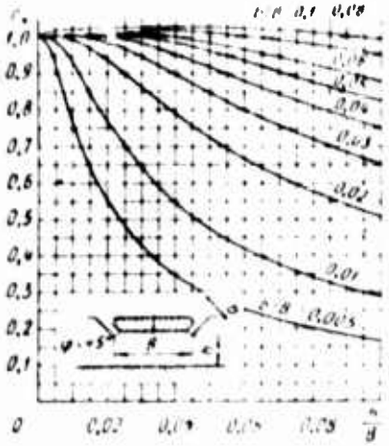

Fig. 133. Lift coefficient c_y of plane nozzle installation with normal nozzle cut-off as functions of relative elevation h/B for different relative nozzle exit width b/B

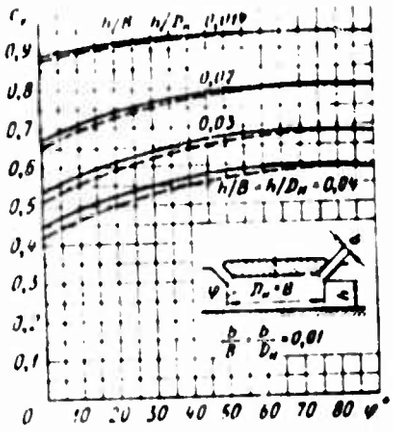

Fig. 134. Lift coefficient c_y of plane and annular nozzles as functions of the angle φ of inclination of nozzle generatrix (dashed curves correspond to a plane nozzle, and continuous curves -- to an annular nozzle)

The lift coefficient c_y for a plane and an annular nozzle, with identical exit width ($b/D = b/D_\mu = 0.01$) as functions of the angle φ of nozzle generatrix are determined by Eqs. (141) and (142) and they are shown in Fig. 134. As we can see, the effect of the angle φ on the coefficient c_y is appreciable for small angle values ($\varphi = 0\text{-}45^\circ$). In the range $\varphi = 45\text{-}90^\circ$, the coefficient c_y changes only slightly. When $\varphi = 60\text{-}80^\circ$, there is a mildly pronounced maximum of c_y values. Calculations show that for identical exit width, the annular nozzle has a somewhat larger c_y value than the plane nozzle.

20. Craft With Oblique Nozzle Cut-off

Let us examine the general case when the cut-offs are made at some angle ψ to the normal nozzle cross-section (Fig. 135), assuming as earlier that the problem is a plane one. Let us isolate from this air cushion vehicle a section with length L by means of two parallel cross-sections normal to the longitudinal axis of the craft, let us enclose this section in the control contour, and to this contour let us apply the momentum equation. We will arrange the upper and side bounds of the contour at a distance from the craft for which the air streaming velocity v can be

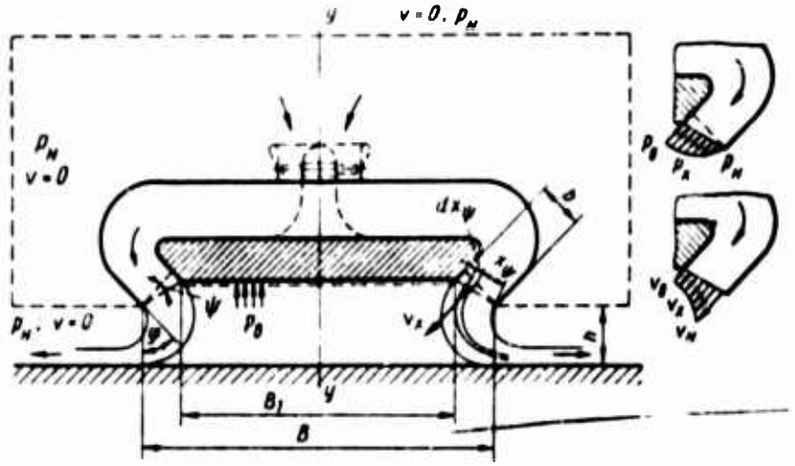

Fig. 135. Control contour for determining the lift of an air cushion vehicle with a plane contour with oblique cut-off

assumed to be zero, and the pressure along the boundaries can be assumed to be constant and equal to the atmospheric pressure $p_н$. Let us draw the lower boundary of the contour in such a way that its first section passes in direct proximity to the craft bottom, parallel to the ground surface, the second lies in the nozzle cut-off plane, and the third, external, passes parallel to the ground surface across the lower nozzle edges.

Let us project on the y axis the forces acting on the craft and the surface of the isolated contour. The forces acting on the vertical surfaces of the isolated contour are normal to the surfaces and their projections on the y axis are equal to zero. The forces acting on the section of the lower surface of the contour projecting beyond the outer edge of the nozzle are equalized by the forces acting on the upper surface of the contour corresponding to it. Therefore the momentum equation for this contour, in accordance with the notation given in Fig. 135, is

$$Y = 2L\cos\varphi\int_0^{x_ψ}\rho v_1^2\cos\psi\,dx_ψ +$$

$$+ 2L\cos(\varphi - \psi)\int_0^{x_ψ}(p_0 - p_н)\,dx_ψ + LB_1(p_0 - p_н). \qquad (143)$$

where v_y is the air velocity at a point lying in the nozzle cut-off plane; p_x is the static pressure at this point; p_β is the air cushion pressure; $p_н$ is the atmospheric pressure; L is the length of the nozzle installation; B_1 is the width of the nozzle installation bottom bounded by the inner edges of the nozzles; φ is the angle of inclination of the nozzle generatrices to the craft axis; and ψ is the angle between the cut-off and the normal nozzle cross-section.

The lift of the craft is

$$Y = c_y S H_c = c_y S \frac{\rho v_н^2}{2},$$

where c_y is the lift coefficient; S is the overall area of the nozzle installation; and H_c is the total pressure in the air stream in front of the nozzle installation.

Eq. (143), with reference for the expression for Y, will become

$$c_y = \frac{2\rho L \cos\varphi \cos\psi}{S \frac{\rho v_н^2}{2}} \int_0^{x_\psi} v_x^2 \, dx_\psi + \frac{2L \cos(\varphi - \psi)}{S \frac{\rho v_н^2}{2}} \int_0^{x_\psi} (p_x - p_н) \, dx_\psi + \cdot \frac{B_1 L}{S} \cdot \frac{p_\beta - p_н}{\frac{\rho v_н^2}{2}}. \qquad (144)$$

Using the equation

$$\frac{v_x}{v_н} = \left[1 + \frac{x_\psi}{h} \sin(\varphi - \psi)\right]^{-\frac{(1+\sin\varphi)\cos\psi}{\sin(\varphi-\psi)}},$$

determining the distribution of velocity in the nozzle cut-off plane, and considering that the pressure distribution in the nozzle cut-off plane is expressed by the function

$$\frac{p_x - p_н}{\frac{\rho v_н^2}{2}} = 1 - \left(\frac{v_x}{v_н}\right)^2,$$

we can represent the lift component appearing in the Eq. (144) by the following expressions.

The lift component due to the reaction of air jets exiting from the nozzles is

$$c_{yp} = \frac{Y}{S\frac{\rho v_n^2}{2}} = \frac{2\rho L\cos\varphi\cos\psi}{S\frac{\rho v_{nm}^2}{2}} \int_0^{x_\psi = \frac{b}{\cos\psi}} v_x^2\, dx_\psi =$$

$$= 2\frac{\bar{F}}{b/h}\cdot\frac{\cos\varphi\cos\psi}{\sin(\varphi-\psi)}\cdot\frac{1-k_2(1-\bar{p})}{2k_1-1},$$

where $\bar{p}$ is the air cushion pressure coefficient; $\bar{t} = 1 - e^{-2k_1 \ln k_3}$ $\bar{F} = 2bl_S$ is the relative nozzle exit area; and k_1 and k_2 are the coefficient of proportionality;

$$k_1 = \frac{(1+\sin\varphi)\cos\psi}{\sin(\varphi-\psi)};\quad k_2 = 1+\frac{b}{h}\cdot\frac{\sin(\varphi-\psi)}{\cos\psi}. \qquad (145)$$

The component of the lift coefficient arising from forces of excess pressure at nozzle cut-offs is

$$c_{yc} = \frac{2L\cos(\varphi-\psi)}{S\frac{\rho v_n^2}{2}} \int_0^{x_\psi = \frac{b}{\cos\psi}} (p_x - p_n)\, dx_\psi =$$

$$= \bar{F}\frac{\cos(\varphi-\psi)}{\cos\psi} - \bar{F}\frac{\cos(\varphi-\psi)}{b/h\sin(\varphi-\psi)}\cdot\frac{1-k_2(1-\bar{p})}{2k_1-1}.$$

The component of the lift arising from pressure forces of the air cushion acting at the bottom of the nozzle installation is

$$c_{yn} = \frac{Y_n}{SH_c} = \frac{B_1 L}{S}\cdot\frac{p_c - p_n}{\frac{\rho v_n^2}{2}} = \frac{S_1}{S}\bar{p} = \left[1 - \bar{F}\frac{\cos(\varphi-\psi)}{\cos\psi}\right]\bar{p}.$$

The lift coefficient of an air cushion vehicle with a plane nozzle installation that has oblique nozzle cut-off is

$$c_y = c_{yc} + c_{yp} + c_{yn} = \bar{F}\left[\frac{\cos(\varphi-\psi)}{\cos\psi} + \right.$$

$$\left. + \frac{\cos(\varphi+\psi)}{\sin(\varphi-\psi)}\cdot\frac{1-k_2(1-\bar{p})}{(2k_1-1)\,b/h}\right] + \left[1 - \bar{F}\frac{\cos(\varphi-\psi)}{\cos\psi}\right]\bar{p}. \qquad (146)$$

The first term of the right side of this equation is

$$c_{y\text{вн}} = \bar{F}\left[\frac{\cos(\varphi-\psi)}{\cos\psi} + \frac{\cos(\varphi+\psi)}{\sin(\varphi-\psi)} \cdot \frac{1-k_2(1-\bar{\rho})}{(2k_1-1)\,b/h}\right]$$

which is the component of the lift due to the reaction of air jets and to excess pressure forces at the nozzle cut-offs. In these formulas $\bar{F}$ is the overall relative nozzle flow-through area. The total nozzle cut-off area is

$$\bar{F}_c = \frac{\bar{F}}{\cos\psi}. \qquad (147)$$

As applied to an air cushion vehicle with a single-pass annular nozzle, Eq. (146) becomes

$$c_y = \bar{F}_c\left[\cos(\varphi-\psi) + \frac{\cos(\varphi+\psi)\cos\psi}{\sin(\varphi-\psi)} \cdot \frac{1-k_2(1-\bar{\rho})}{(2k_1-1)\,b/h\,D_н}\right] + \\ + \left[1 - \bar{F}_c\cos(\varphi-\psi)\right]\bar{\rho}. \qquad (148)$$

where $\bar{F}_c$ is the cut-off area of the annular nozzle;

$$\bar{F}_c = 4\,\frac{b}{D_н}\cdot\frac{1}{\cos\psi}\left[1 - \frac{b}{D_н}\cdot\frac{\cos(\varphi-\psi)}{\cos\varphi}\right].$$

The lift coefficient of a single-pass annular nozzle as functions of the cut-off angle ψ for different relative elevations $h/D_н$ is shown in Fig. 156. These functions $c_y = f(h/D_н, b/D_н, \varphi, \psi)$ were calculated by Eq. (148) for constant angle of nozzle generatrix inclination ($\varphi = 45^\circ$) and for a relative nozzle exit width $b/D_н = 0.005$-0.02. The nozzle installation with normal nozzle cut-off ($\psi = 0$) has the smallest lift coefficient. As the angle ψ is increased, the coefficient c_y increases and takes on the largest value when $\psi = 45^\circ$, which corresponds to a nozzle installation with horizontal nozzle cut-off. The appreciable effect of the angle ψ on the coefficient c_y becomes evident at relatively small elevations of the nozzle installation above the support surface ($h/D_н \approx 0$-0.05), that is, elevations that are typical of transport air cushion vehicles.

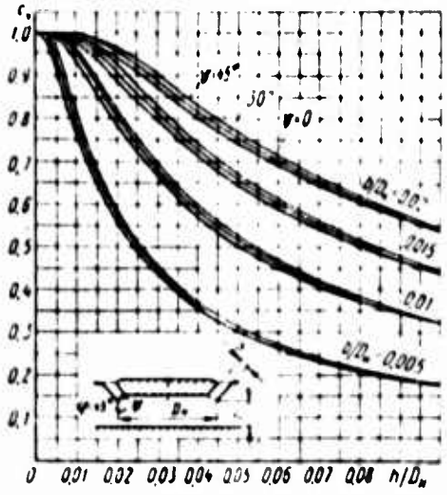

Fig. 136. Lift coefficient c_y of a single-pass annular nozzle as functions of elevation for different nozzle exit widths and different cut-off angles

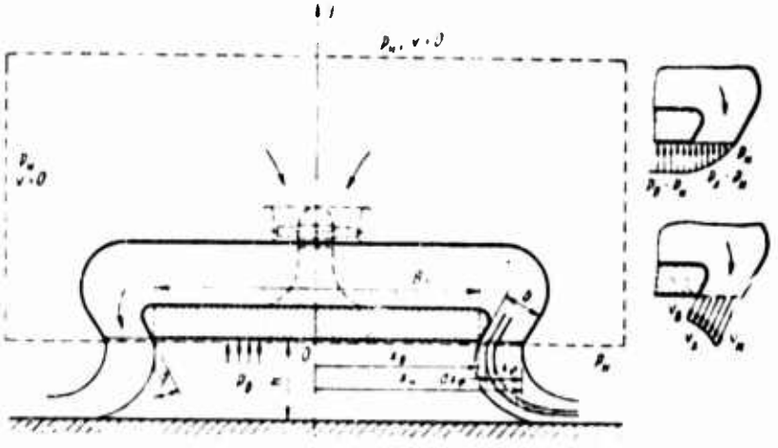

Fig. 137. Control contour for determining the lift of an air cushion vehicle with a plane contour provided with horizontal cut-off

21. Craft With Horizontal Nozzle Cut-off

To determine the lift of an air cushion vehicle with a nozzle installation having exit edges lying in the plane of the craft bottom, let us isolate a section of length L from this craft by means of two parallel cross-sections normal to the craft's longitudinal axis. Let us enclose section L in a control contour (Fig. 137). We will arrange the upper and side boundaries of the contour at a distance from the craft for which the air streaming velocity can be taken as zero, and the pressure along the boundaries as constant and equal to the atmospheric pressure p_H. We will position the lower boundary of the contour in direct proximity to the craft bottom, parallel to the ground surface.

Let us project onto the y axis the forces acting on the craft and the surface of the isolated contour. The forces acting on the lateral surfaces of a contour are normal to the surfaces and their projections onto the y-y axis are equal to zero. Therefore the equation of momentum for this contour, in accordance with the notations given in Fig. 137, will become

$$2\rho L\cos^2\varphi\int_0^{h_\varphi} v_x^2\,dx_\varphi + 2L\int_0^{h_\varphi}(p_x - p_n)\,dx_\varphi + B_1L(p_0 - p_n).$$

Let us express the lift and its components as a function of the geometrical quantities of the nozzle installation and the aerodynamic parameters of the air jet producing the air cushion. For this nozzle installation the velocity field in the nozzle cut-off plane is

$$\frac{v_x}{v_n} = e^{-\frac{h_\varphi}{h}(1+\sin\varphi)\cos\varphi},$$

and the pressure field is

$$\frac{p_x - p_n}{\frac{\rho v_n^2}{2}} = 1 - \left(\frac{v_x}{v_n}\right)^2 = 1 - e^{-2\frac{h_\varphi}{h}(1+\sin\varphi)\cos\varphi}.$$

The air cushion pressure coefficient is

$$\bar{p}_0 = 1 - e^{-2\frac{h}{h}(1+\sin\varphi)}$$

For each nozzle the exit width $x_н - x_в = b/\cos\psi$, the total flow-through area $F = 2bL$, and the relative total flow-through area

$$\bar{F} = \frac{F}{S} = \frac{2bL}{S}.$$

The component of the lift due to the reaction of the air jet is

$$c_{y\rho} = \frac{2\rho L\cos^2\varphi}{S\frac{\rho v_н^2}{2}}\int_0^{x_\psi = \frac{b}{\cos\varphi}} v_x^2\,dx_\psi =$$

$$= \frac{2\rho v_н^2\cos^2\varphi}{S\frac{\rho v_н^2}{2}}\int_0^{x_\varphi = \frac{b}{\cos\varphi}} e^{-2\frac{x_\varphi}{h}(1+\sin\varphi)\cos\varphi}\,dx_\varphi.$$

Integrating this equation and making the appropriate substitutions, we get

$$c_{y\rho} = \frac{\bar{F}}{b/h}\cdot\frac{\cos\varphi}{1+\sin\varphi}\bar{p}.$$

The component of the lift due to the forces of excess pressure acting at the nozzle cut-offs is

$$c_{yc} = \frac{2L}{S\frac{\rho v_н^2}{2}}\int_0^{x_\varphi = \frac{b}{\cos\varphi}} (p_x - p_н)\,dx_\varphi =$$

$$= \frac{2L\frac{\rho v_н^2}{2}}{S\frac{\rho v_н^2}{2}}\int_0^{x_\varphi = \frac{b}{\cos\varphi}} \left[1 - \left(\frac{v_x}{v_н}\right)^2\right]dx_\varphi =$$

$$= 2\frac{L}{S}\int_0^{x_\psi = \frac{b}{\cos\varphi}} \left[1 - e^{-2\frac{x_\varphi}{h}(1+\sin\varphi)\cos\varphi}\right]dx_\varphi.$$

After solution and uncomplicated transformations, we get

$$c_{yc} = \frac{\bar{F}}{\cos\varphi}\left[1 - \frac{1}{(1+\sin\varphi)}\cdot\frac{\bar{p}}{2b/h}\right].$$

The component of the lift due to the reaction of air jets and excess pressure forces acting at the nozzle cut-offs is

$$c_{yn\kappa} = c_{yp} + c_{y\kappa} = \frac{\bar{F}}{\cos\varphi}\left(1 + \frac{2\cos^2\varphi - 1}{1 + \sin\varphi}\cdot\frac{\bar{p}}{2b/h}\right).$$

The component of the lift arising from forces of excess air cushion pressure acting at the bottom section of the nozzle installation is

$$c_{yn} = \frac{B_1 l}{S}\cdot\frac{p_0 - p_\kappa}{\frac{\rho v_\kappa^2}{2}} = \frac{S_1}{S}\bar{p} = \bar{S}_1\bar{p}.$$

The lift coefficient of a nozzle installation with horizontal nozzle cut-off is

$$c_y = c_{yp} + c_{y\kappa} + c_{yn} = \frac{\bar{F}}{\cos\varphi}\left(1 + \frac{2\cos^2\varphi - 1}{1 + \sin\varphi}\cdot\frac{\bar{p}}{2b/h}\right) + \bar{S}_1\bar{p}. \quad (149)$$

When the angle of nozzle generatrix inclination $\varphi = 45^\circ$, Eq. (149) becomes

$$c_y = \bar{F}\left(2 + \bar{S}_1\bar{p}\right).$$

For an air cushion vehicle with a single-pass annular nozzle, Eq. (149) becomes

$$c_y = \bar{F}_c\left(1 + \frac{2\cos^2\varphi - 1}{1 + \sin\varphi}\cdot\frac{\bar{p}}{2\frac{b/D_\kappa}{h/D_\kappa}}\right) + (1 - \bar{F}_c)\bar{p}, \quad (150)$$

where $\bar{F}_c$ is the relative cut-off area of the annular nozzle,

$$\bar{F}_c = 4\frac{b}{D_\kappa\cos\varphi}\left(1 - \frac{b}{D_\kappa\cos\varphi}\right).$$

The air cushion pressure coefficient appearing in Eq. (150) is

$$\bar{p} = 1 - e^{-\frac{b/D_\kappa}{h/D_\kappa}(1+\sin\varphi)}.$$

When Eqs. (149) and (150) are used, it must be remembered that they are real when $\cos\varphi \geq b/D_H$. If $\cos\varphi = 2b/D_H$, the internal walls of the nozzle apparently converge to a single point lying in the center of the nozzle bottom, and the area of the bottom S_1 of the nozzle installation becomes equal to zero. When $\cos\varphi < 2b/D_H$, Eqs. (149) and (150) become meaningless, since the conditions stipulated in the derivation of the lift equations are violated.

The lift coefficients c_y of a single-pass annular nozzle as functions of relative elevation h/D_H of a support surface for various relative nozzle flow-through widths b/D_H and for the nozzle generatrix inclination angles $\varphi = 0$, 30, 45, and 60° are given in Figs. 138-141, respectively. Fig. 142 compares the functions $c_y = f(h/D_H)$ for different angles of inclination for a nozzle with relative widths $b/D_H = 0.01$ and 0.1.

If the nozzle installation rests on the support surface ($h/D_H = 0$), lift coefficient $c_y = 1$. With increase in the relative elevation h/D_H, the coefficient c_y begins to depend on the angle φ of nozzle generatrix inclination. For small angles of inclination ($\varphi < 45°$), we have optimal values of the relative elevation h/D_H of the nozzle installation at which the lift coefficient takes on maximum values, where $c_{y\,max} > 1$. The $c_{y\,max}$ values are the greater, the larger the relative width b/D_H of the nozzle flow-through section. For appreciable angles of generatrix inclination ($\varphi > 45°$), the lift coefficient decreases with increase in elevation and does so more rapidly, the smaller the flow-through width of the nozzle. Here, $c_y < 1$.

The coefficient c_y of a single-pass annular nozzle for small values of b/D_H and for the same elevation h/D_H increases with increase in the angle φ, and for large b/D_H values it decreases (cf. Fig. 142). This is due to the variation in the ratio of the lift components, determined by the reaction of a jet and by the excess pressure in the air cushion.

To verify the proposed method of calculating the lift of an air cushion vehicle in the hovering regime, an experimental study was made of lift by measuring it directly with a graphometric technique. The experiments were conducted with three annular nozzles with angle of generatrix inclination $\varphi = 45°$ and with flow-through widths b = 8, 20, and 40 mm, with the identical inside diameter of the nozzle bottom $D_\delta = 400$ mm (Fig. 143). To these parameters corresponded the b/D_H values of 0.0189, 0.0438, and 0.0780. The nozzles were machined on a lathe, and the surface of the walls of the flow-through section was polished.

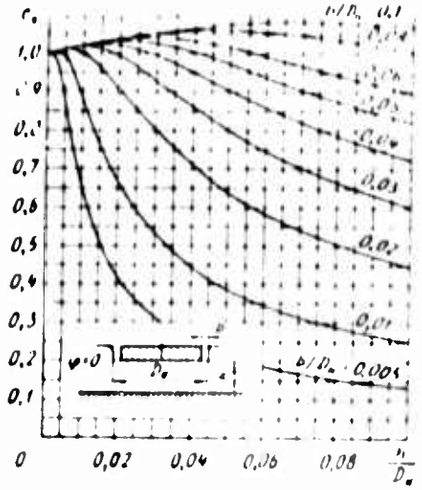

Fig. 138. Lift coefficient of single-pass annular nozzle as functions of relative elevation for different relative nozzle exit widths ($\varphi = 0^{\circ}$)

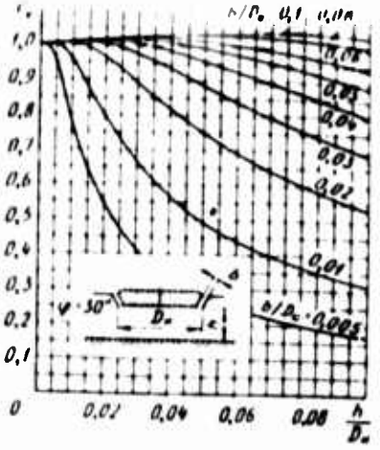

Fig. 139. Lift coefficient of a single-pass annular nozzle as functions of relative elevation for different relative exit nozzle widths ($\varphi = 30^{\circ}$)

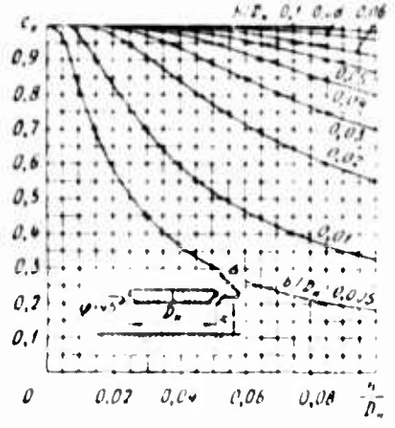

Fig. 140. Lift coefficient of single-pass annular nozzle as functions of relative elevation for different relative nozzle exit widths ($\varphi = 45^{\circ}$)

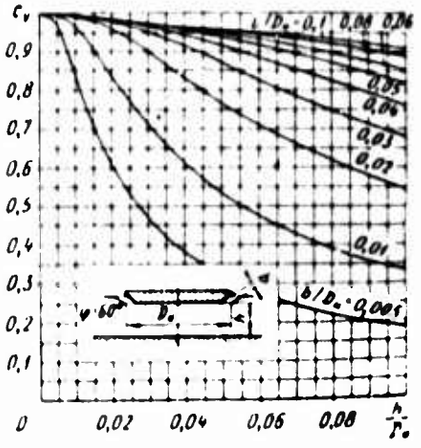

Fig. 141. Lift coefficient of single-pass annular nozzle as functions of relative elevation for different relative nozzle exit widths ($\varphi = 60^{\circ}$)

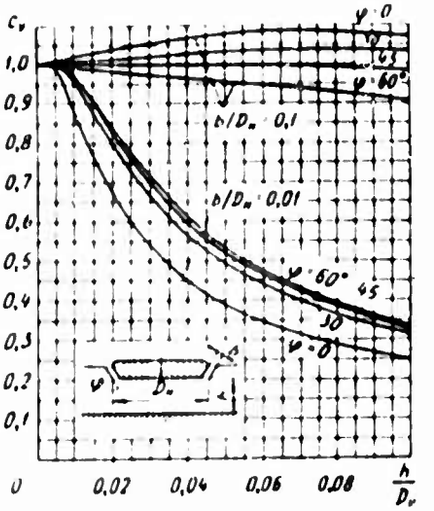

Fig. 142. Lift coefficient as functions of relative elevation and slope of generatrix of single-pass nozzle for constant relative nozzle exit widths

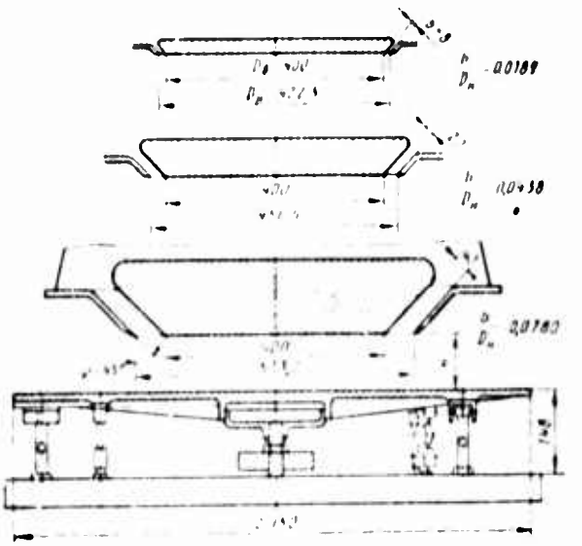

Fig. 143. Schemes of annular nozzles and shield-scales tested

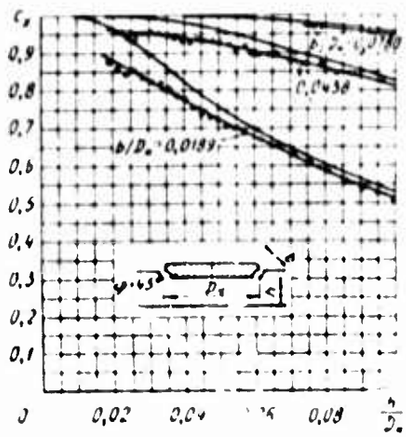

Fig. 144. Theoretical and experimental dependences of the lift coefficient of annular single-pass nozzles on parameter $h/D_к$

A 250 mm diameter metal disk served as the shield over which the annular jet of air streamed. The side of the disk facing the jet was made smooth, and the other side was provided with stiffness ribs and special hinges for annular strain gauges. This disk served two functions: it modeled the support surface and simultaneously served as a three-component strain gauge instrument for measuring the nozzle lift, equal to the pressure forces of the annular jet and the air cushion at the shield.

On an experimental stand[1] the nozzle installation and the shield were positioned coaxially, and the vertical surface of the shield was positioned in parallel to the plane of the nozzle bottom. The shield bearing the annular strain gauges can be shifted along its axis on two cylindrical guides and secured at various distances from the plane of the bottom of the annular nozzle tested, which corresponds to different elevations of the craft above the ground surface. The pressure force of the annular jet at the shield, equal to the lift acting at the nozzle installation, was determined by the deformation of the annular strain gauges measured with a special instrument — an electronic strain meter. Investigations of the lift were conducted at a moderate discharge velocity of air issuing from the annular nozzles $v_{ср}$ = 50-70 m/sec.

[1] The stand layout and the description are given in Section 6.

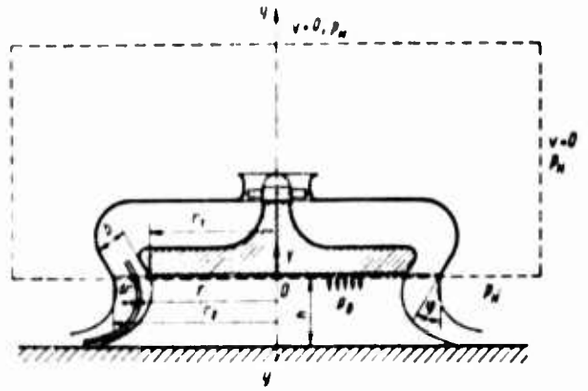

Fig. 145. Control contour for determining the lift of an air cushion vehicle with horizontal nozzle cut-off

The results of theoretical calculations of the lift of an air cushion vehicle in the hovering regime were compared with experimental values (Fig. 144). The theoretical curves were calculated based on Eq. (150), while the experimental curves were obtained by measuring the lift with a gravimetric technique.

Experiments showed that the proposed method of calculating the lift agrees closely enough with experiment. At small elevations ($h/D_H = 0.02$-0.04), the difference between the data of calculation and experiment does exceed 5-7 percent of the calculated value of the lift, while for large elevations ($h/D_H = 0.06$-0.08), it is even reduced to 2-5 percent of the calculated c_y value.

22. Craft With Annular Nozzle

Let us find the functions determining the lift of an air cushion vehicle provided with an annular nozzle and let us estimate the effect of axial symmetry of the jet on the lift of a nozzle installation with horizontal nozzle cut-off.

Suppose y axis is the axis of symmetry of this kind of craft (Fig. 145). Let us isolate some large enough cylindrical region encompassing the craft, whose boundaries are beyond the limits of the perturbed section of the air streams entering and leaving the craft. The lateral and upper surfaces of the cylindrical contour will be positioned at a distance from the craft for which the velocity of air streaming toward the craft can be regarded as zero, and the pressure can be taken as equal to the atmospheric value. We will position the lower surface of the contour at the cut-off level of the annular nozzle in parallel to

the ground surface. By projecting onto the y axis the forces acting on the craft and at the surface of the isolated contour, let us write

$$Y = Y_p + Y_c + Y_n = 2\pi \int_{r_1}^{r_2} v_r^2 r\,dr + 2\pi \int_{r_1}^{r_2} p_r r\,dr - \pi (r_2^2 - r_1^2) p_\infty + \pi r_1^2 (p_0 - p_\infty),$$

where Y_p is the lift due to the reaction of the annular jet;

$$Y_p = 2\pi\rho \cos^2\varphi \int_{r_1}^{r_2} v_r^2 r\,dr; \tag{151}$$

Y_c is the lift produced by the pressure forces in the nozzle cut-off plane

$$Y_c = 2\pi \int_{r_1}^{r_2} p_r r\,dr - \pi (r_2^2 - r_1^2) p_\infty; \tag{152}$$

and Y_n is the lift due to the excess pressure in the air cushion acting at the nozzle bottom;

$$Y_n = \pi r_1^2 (p_0 - p_\infty). \tag{153}$$

Let us express these forces as a function of the geometrical quantities of the nozzle installation and the aerodynamic parameters of the air jets producing the air cushion. The velocity field in a jet at the nozzle cut-off as applied to this nozzle installation can be expressed in the form

$$\frac{v_r}{v_a} = e^{-\frac{r_2 - r}{h}(1 + \tan\varphi \cos\varphi)}, \tag{154}$$

where v_r is the air velocity at a point lying in the nozzle cut-off plane (with coordinate r); v_a is the discharge velocity of the boundary jetlet at the outer edge of the nozzle exit; r is the coordinate of a point lying in the nozzle cut-off plane at which the velocity is v_r; r_2 is the radius of the nozzle installation determined with respect to the external edge of the nozzle exit; h is the distance between the nozzle cut-off and the ground surface; and φ is the angle of nozzle generatrix inclination to the craft axis.

Replacing velocity v_r in Eq. (151) with its value from Eq. (154), we can write

$$Y_p = 2\pi\rho v_н^2 \cos^2\varphi \int_{r_1}^{r_2} re^{-2\frac{r_2 - r}{h}(1+\sin\varphi)\cos\varphi} dr.$$

Solving the integral appearing in this equation, we get

$$\int_{r_1}^{r_2} re^{-2\frac{r_2-r}{h}(1+\sin\varphi)\cos\varphi} dr = \frac{h}{2(1+\sin\varphi)\cos\varphi} \times$$

$$\times \left[r_2 - r_1 + \left(r_1 - \frac{h}{2(1+\sin\varphi)\cos\varphi} \right) \left(1 - e^{-2\frac{r_2-r_1}{h}(1+\sin\varphi)\cos\varphi} \right) \right].$$

Considering that

$$r_2 - r_1 = \frac{b}{\cos\varphi}, \quad r_2 = \frac{D_н}{2} \tag{155}$$

and the air cushion pressure coefficient is

$$\bar{p} = \frac{p_0 - p_н}{\frac{\rho v_н^2}{2}} = 1 - e^{-2\frac{r_2 - r_1}{h}(1+\sin\varphi)\cos\varphi} \left(1 - e^{-2\frac{b}{h}(1+\sin\varphi)} \right), \tag{156}$$

we find

$$\int_{r_1}^{r_2} re^{-2\frac{r_2-r}{h}(1+\sin\varphi)\cos\varphi} dr = \frac{\frac{h}{D_н} \cdot D_н^2}{4(1+\sin\varphi)\cos^2\varphi} \times$$

$$\times \left[2b/D_н + \left(\cos\varphi - 2b/D_н - \frac{h/D_н}{1+\sin\varphi} \right) \bar{p} \right]. \tag{157}$$

Then lift due to the reaction of the annular jet is

$$Y_p = \frac{\pi D_н^2}{1+\sin\varphi} \cdot \frac{h}{D_н} \left[2b/D_н + \left(\cos\varphi - 2b/D_н - \frac{h/D_н}{1+\sin\varphi} \right) \bar{p} \right] \frac{\rho v_н^2}{2}. \tag{158}$$

Let us express the lift produced by the pressure forces in the nozzle cut-off plane and also as a function of the geometrical quantities of the nozzle installation and the aerodynamic parameters of the air jets. The total pressure at each point lying in the nozzle cut-off plane is constant and by Bernoulli's equation

$$p_r + \frac{\rho v_r^2}{2} = p_н + \frac{\rho v_н^2}{2}; \qquad (159)$$

Therefore Eq. (154) determining the lift becomes

$$Y_c = 2\pi \int_{r_1}^{r_2} \left(\bar{p}_н + \frac{\rho v_н^2}{2} - \frac{\rho v_r^2}{2} \right) r\, dr - \pi (r_2^2 - r_1^2) p_н =$$

$$= \pi (r_2^2 - r_1^2) \frac{\rho v_н^2}{2} - \pi \rho v_н^2 \int_{r_1}^{r_2} r e^{-2\frac{r_2 - r}{h}(1+\sin\varphi)\cos\varphi} dr.$$

Replacing the integral appearing in this expression with its solution (157) and carrying out the required transformations, we finally get

$$Y_c = \frac{\pi D_н h D_н}{\cos\varphi} \left(1 - \frac{b}{\cos\varphi} \frac{D_н}{2}\right) \frac{\rho v_н^2}{2} - \frac{\pi D_н^2 h D_н}{2(1+\sin\varphi)\cos^2\varphi} \times$$

$$\times \left[\left(\cos\varphi - 2\frac{b}{D_н}\right) - \left(1 - \frac{h}{D_н}\cos\varphi\right) e^{-\frac{D_н}{h}\cos\varphi} \right] \frac{\rho v_н^2}{2}. \qquad (160)$$

The lift due to the action of excess air cushion pressure at the nozzle bottom, with reference to Eqs. (155), (155), and (156), is

$$Y_н = \pi r_1^2 \frac{p_н - p_н}{\frac{\rho v_н^2}{2}} \cdot \frac{\rho v_н^2}{2} = \frac{\pi D_н^2}{4} \left(1 - \frac{2\frac{b}{D_н}}{\cos\varphi}\right)^2 \bar{p} \frac{\rho v_н^2}{2}. \qquad (161)$$

Then by Eqs. (158), (160), and (161), the lift of an air cushion vehicle with single-pass annular nozzle is

$$Y = \left\{F_c + 4 \cdot \frac{b}{D_н} \cdot \frac{h}{D_н} kS + \left[\left(\cos\varphi - 2b/D_н - \right.\right.\right.$$

$$\left.\left.\left. - \frac{h/D_н}{1 + \sin\varphi}\right) 2h/D_н kS + S_1\right] \bar{p}\right\} \frac{\rho v_н^2}{2}, \qquad (162)$$

where F_c is the nozzle exit (cut-off) area,

$$F_c = \frac{\pi D_н^2 b/D_н}{\cos\varphi}\left(1 - \frac{b/D_н}{\cos\varphi}\right);$$

S_1 is the area of the bottom bounded by the internal nozzle edge,

$$S_1 = \frac{\pi D_н^2}{4}\left(1 - \frac{2b/D_н}{\cos\varphi}\right)^2;$$

S is the area of the nozzle installation with respect to the outer nozzle edges,

$$S = \frac{\pi D_н^2}{4};$$

k is the coefficient of proportionality,

$$k = \frac{2\cos^2\varphi - 1}{(1 + \sin\varphi)\cos^2\varphi}.$$

Let us establish yet another relationship. We will determine the total energy of a jet as it exits from a nozzle, with respect to the volume flow in one second, that is, we will find the total pressure required to produce a jet with specified nonuniform velocity and pressure distribution in the nozzle cut-off plane. If we neglect the forces of friction of the jet against the nozzle wall, the total pressure of the jet at the nozzle cut-off, equal to the total pressure in the receiver in front of the nozzle, is

$$H_c = p_0 - p_н = \frac{p_н - p_0}{Q} = \frac{\int_0^m \frac{v_r^2}{2}\, dm_м \int_0^Q (p_r - p_н)\, dQ}{\int_0^F v_r\, dF}. \qquad (163)$$

The kinetic energy of a jet in the nozzle cut-off plane is

$$e_к = \int_0^m \frac{v_r^2}{2}\, dm = \int_{r_1}^{r_2} \frac{v_r^2}{2}\, \rho v_r 2\pi r \cos\varphi\, dr = \pi\rho\cos\varphi \int_{r_1}^{r_2} v_r^3 r\, dr.$$

Replacing the velocity v_r with its corresponding value from Eq. (154) and integrating, we get

$$e_к = \pi\rho v_н^3 \cos\varphi \int_{r_1}^{r_2} r \cdot e^{-3\frac{r_2 - r}{h}(1+\sin\varphi)\cos\varphi}\, dr =$$

$$= \frac{1}{3} \cdot \frac{\pi D_н^2 h / D_н v_н}{(1+\sin\varphi)\cos\varphi} \times$$

$$\times \frac{\rho v_н^2}{2}\left[2\frac{b}{D_н} + \left(\cos\varphi - 2\frac{b}{D_н} - \frac{2h/D_н}{3(1+\sin\varphi)}\right) \times \right.$$

$$\left. \times \left(1 - e^{-3\frac{b}{h}(1+\sin\varphi)}\right)\right]. \qquad (164)$$

The work done by the pressure forces in the section from the nozzle cut-off to the jet exiting into the atmosphere is

$$e_п = \int_0^V (p_r - p_н)\, dQ = \int_{r_1}^{r_2} (p_r - p_н)\, 2\pi r v_r \cos\varphi\, dr.$$

Using Eqs. (159) and (154) and integrating, we find

$$e_п = \frac{\pi D_н^2 h / D_н v_н}{(1+\sin\varphi)\cos\varphi} \cdot \frac{\rho v_н^2}{2}\left[2\frac{b}{D_н} + \left(\cos\varphi + 2\frac{b}{D_н} - \frac{2h/D_н}{(1+\sin\varphi)}\right) \times \right.$$

$$\left. \times \left(1 - e^{-\frac{b}{h}(1+\sin\varphi)}\right)\right] - \frac{1}{3} \cdot \frac{\pi D_н^2 \cdot h / D_н \cdot v_н}{(1+\sin\varphi)\cos\varphi} \times$$

$$\times \frac{\rho v_н^2}{2}\left[2\frac{b}{D_н} + \left(\cos\varphi - 2\frac{b}{D_н} - \frac{2h/D_н}{3(1+\sin\varphi)}\right) \times \right.$$

$$\left. \times \left(1 - e^{-3\frac{b}{h}(1+\sin\varphi)}\right)\right]. \qquad (165)$$

The volume flow of air in one second is

$$Q = \int_0^F v_r\,dF = \int_{r_1}^{r_2} v_r \cdot 2\pi r \cos\varphi\,dr =$$

$$\ldots \left[2\frac{b}{D_n} \ldots \left(\cos\varphi - 2\frac{b}{D_n} - \frac{2h/D_n}{1+\sin\varphi}\right) \times \right.$$

$$\left. \ldots \left(1 \ldots e^{-\frac{b}{b}\ldots\cos\varphi}\right)\right]. \qquad (166)$$

After replacing the values of ξ_k, ξ_n, and Q found by Eqs. (164), (165), and (166), in Eq. (165) we get

$$H_c = \frac{\rho v_n^2}{2}. \qquad (167)$$

Thus, the theoretical total pressure required to produce the annular jet forming the air cushion, when excess pressure is present at the inner side of a jet, is equal to the dynamic pressure of the stream determined from the velocity v of the bounding jetlet at the external side of the jet with atmospheric pressure. Eq. (167) allows us to write the following formula for determining the lift as a function of the geometrical parameters of a nozzle installation and the total air stream pressure:

$$Y = \left\{F_c + 4\frac{b}{D_n} \cdot \frac{h}{D_n} kS + \right.$$

$$\left. + \left[\left(\cos\varphi - 2\frac{b}{D_n} - \frac{h/D_n}{1+\sin\varphi}\right) 2\frac{h}{D_n} kS + S_1\right] \bar{p}\right\} H_c. \quad (168)$$

Bearing in mind that $Y = c_y S H_c$, we get the lift coefficient of a craft with a single-pass annular nozzle

$$c_y = \bar{F}_c + 4\frac{b}{D_n} \cdot \frac{h}{D_n} k + \ldots$$

$$+ \left[\left(\cos\varphi - 2\frac{b}{D_n} - \frac{h/D_n}{1+\sin\varphi}\right) 2\frac{h}{D_n} k + \bar{S}_1\right] \bar{p}, \quad (169)$$

where $\bar{F}_c$ is the relative nozzle exit (cut-off) area

$$\bar{F}_c = \frac{F_c}{S} = \frac{\pi(r_2^2 - r_1^2)}{\pi r_2^2} = 4\frac{b/D_n}{\cos\varphi}\left(1 - \frac{b/D_n}{\cos\varphi}\right);$$

$\bar{S}_1$ is the relative area of the bottom of the nozzle installation bounded by the inner edge of the annular nozzle,

$$\bar{S}_1 = \frac{S_1}{S} = \frac{\pi r_1^2}{\pi r_2^2} = \left(1 - \frac{2b/D_н}{\cos\varphi}\right)^2.$$

The component of the lift coefficient due to the jet reaction is

$$c_{yp} = -\frac{4h/D_н}{1+\sin\varphi}\left[2\frac{b}{D_н} + \left(\cos\varphi - 2\frac{b}{D_н} - \frac{h/D_н}{1+\sin\varphi}\right)\bar{p}\right]. \quad (170)$$

The component of the lift coefficient produced by the pressure forces in the nozzle cut-off plane is

$$c_{yc} = 4\frac{b/D_н}{\cos\varphi}\left(1 - \frac{h/D_н}{\cos\varphi}\right) -$$
$$- \frac{2h/D_н}{(1+\sin\varphi)\cos^2\varphi}\left[2\frac{b}{D_н} + \left(\cos\varphi - 2\frac{b}{D_н} - \frac{h/D_н}{1+\sin\varphi}\right)\bar{p}\right]. \quad (171)$$

The component of the lift coefficient due to the forces of the air cushion pressure against the bottom of the nozzle installation is

$$c_{yn} = \left(1 - \frac{2b/D_н}{\cos\varphi}\right)^2 \bar{p}. \quad (172)$$

Results of theoretical calculations of the lift coefficients and its components based on Eqs. (169) and (170) - (171) for a single-pass annular nozzle with angle of generatrix inclination $\varphi = 45^\circ$ are presented in Figs. 146-149, respectively. These results are given in the form of the coefficients c_y, c_{yp}, c_{yc}, and c_{yn} as functions of relative elevation $h/D_н$ of the craft of the ground surface for different relative nozzle exit width $b/D_н$. As we can see, for small elevation the pressure forces acting at the craft bottom are the principal forces lifting the craft into the air. The vertical component of the reactive force of the jet in this case is small. With increase in elevation, the pressure forces acting at the craft bottom become less, while the reactive force increases. An increase in the relative flow-through width of the nozzle installation for the same elevation leads to a very marked increase in the component of lift due to the reaction of the annular jet.

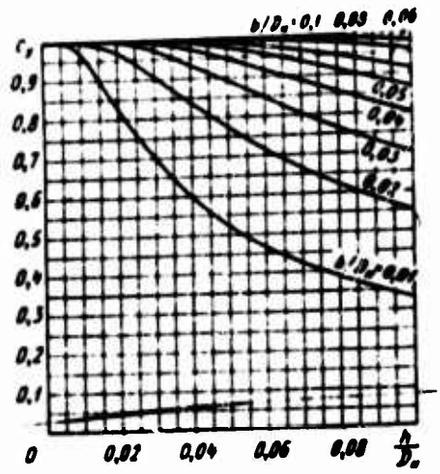

Fig. 146. Lift coefficient c_y as functions of relative elevation $h/D_н$ of craft for different relative flow-through widths $b/D_н$ of annular nozzle ($\varphi = 45°$)

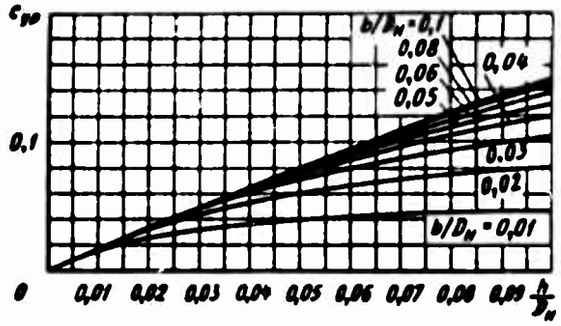

Fig. 147. Component c_{yp} (due to reaction of annular jet) of lift as functions of the parameters $h/D_н$ and $b/D_н$ ($\varphi = 45°$)

A comparison of results from calculating the lift coefficients of a single-pass annular nozzle based on Eq. (169), derived with reference to the axial symmetry of the annular jet and based on the formula

$$c_y = \bar{F}_c\left(1 + \frac{2\cos^2\varphi - 1}{1 + \sin\varphi} \cdot \frac{\bar{p}}{2\frac{b/D_н}{h/D_н}}\right) + (1 - \bar{F}_c)\,\bar{p}, \qquad (173)$$

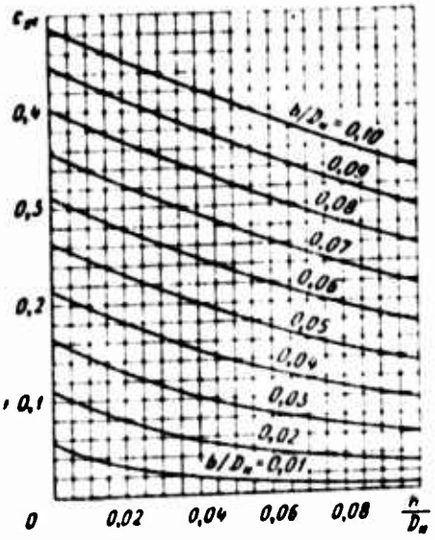

Fig. 148. Component c_{yc} (due to pressure in the nozzle cut-off plane) of lift coefficient as functions of parameters h/D_H and b/D_H ($\varphi = 45^\circ$)

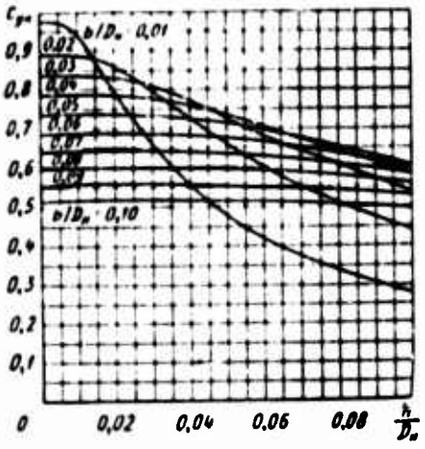

Fig. 149. Component c_{yn} (due to pressure forces at craft bottom) of lift coefficient as functions of parameters h/D_H and b/D_H ($\varphi = 45^\circ$)

obtained for a plane nozzle and extended to the case of an annular nozzle, affords the conclusion that both formulas yield nearly identical numerical values. Thus, in the ranges of variation of parameters $b/D_H = 0.001$-0.1, $h/D_H = 0$-0.1, and $\varphi = 0$-45° observed in practice, the values of the coefficient c_y differed by not more than 0.1 percent.

Considering the simplicity of the solution and the quite satisfactory convergence of calculation results with experimental data, we can recommend Eq. (173) for practical use in determining the lift of plane and contour-closed nozzle installations with horizontal nozzle cut-off.

23. Craft With Double-Pass Nozzle Installation Provided with Horizontal Nozzle Cut-Off

Lift of a plane nozzle installation. Let us determine the lift of an air cushion vehicle with plane double-pass nozzle installation consisting of an annular external nozzle and internal nozzles — stability nozzles. Let us examine the general case when the internal nozzles differ from the external both in the flow-through width and by the angle of generatrix inclination, as well as by their height relative to the plane of the bottom of the nozzle installation (Fig. 150).

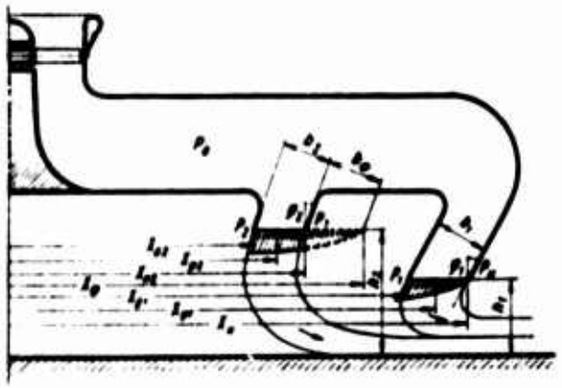

Fig. 150. Air cushion vehicle with two-pass nozzle installation with horizontal nozzle cut-off

Let us determine the lift for this nozzle installation as the sum of components acting on its individual structural members:

$$Y = Y_{p1} + Y_{c1} + Y_{n1} + Y_{p2} + Y_{c2} + Y_{n2}$$

or in terms of the lift coefficients:

$$Y = c_y S H_c = (c_{yp1} + c_{yc1} + c_{yn1} + c_{yp2} + c_{yc2} + c_{yn2}) S H_c.$$

Let us express the lift coefficient and its components in terms of the geometrical parameters of the nozzle installation, the elevation above the support surface, and the aerodynamic parameters of the air stream supplied. In the derivation, let us take account of the non-uniformity of velocity and pressure distribution in the cut-off planes of the external and internal nozzles.

Let us employ the following equations determining the distribution of velocity and pressure in the nozzle cut-off plane.

For the external nozzles, we have

$$\frac{v_x}{v_n} = e^{-\frac{x_n - x_{\varphi 1}}{x_n - x_{01}} \cdot \frac{b_1}{h_1}(1+\sin\varphi_1)}$$

and

$$\frac{p_x - p_n}{\frac{\rho v_n^2}{2}} = 1 - e^{-2\frac{x_n - x_{\varphi 1}}{x_n - x_{01}} \cdot \frac{b_1}{h_1}(1+\sin\varphi_1)}.$$

For the internal nozzles, we have

$$\frac{v_x}{v_н} = e^{\frac{x_ф - x_{ф2}}{x_ф - x_{ф1}} \cdot \frac{b_ф + b_2}{h_1}(1 + \sin\varphi_1)}$$

and

$$\frac{p_x - p_н}{\frac{\rho v_н^2}{2}} = 1 - e^{-2\frac{x_ф - x_{ф2}}{x_ф - x_{ф1}} \cdot \frac{b_ф + b_2}{h_1}(1+\sin\varphi_1)},$$

where

$$b_ф = b_1 \frac{h_2}{h_1} \cdot \frac{1 + \sin\varphi_1}{1 + \sin\varphi_2}.$$

The air cushion pressure coefficient for the section of the bottom between the external and the internal nozzles is

$$\bar{p}_1 = \frac{p_{ф1} - p_н}{\frac{\rho v_н^2}{2}} = 1 - e^{\frac{b_1}{h_1}(1+\sin\varphi_1)},$$

and for the section between the internal nozzles, it is

$$\bar{p}_2 = \frac{p_{ф2} - p_н}{\frac{\rho v_н^2}{2}} = 1 - e^{-2\frac{b_ф - b_2}{h_1}(1+\sin\varphi_1)}.$$

The component of the lift due to the reaction of the air jets exiting from the external nozzles is

$$c_{y\varphi 1} = \frac{Y_{\varphi 1}}{SH_c} = \frac{\int_{x_{ф1}}^{x_н} 2\rho L \cos^2\varphi_1 v_x^2 \, dx_{\varphi 1}}{SH_c} =$$

$$= \frac{2\rho v_н^2 L \cos^2\varphi_1}{SH_c} \int_{x_{ф1}}^{x_н} e^{-2\frac{x_н - x_{\varphi 1}}{x_н - x_{ф1}} \cdot \frac{b_1}{h_1}(1+\sin\varphi_1)} dx_{\varphi 1}.$$

Considering that the coordinate

$$x_{01} = x_n - \frac{b_1}{\cos\varphi_1}, \tag{174}$$

the general flow-through area of the external nozzles is

$$F_1 \quad 2b_1L; \tag{175}$$

the relative flow-through area of the external nozzles is

$$\bar{F}_1 \quad \frac{F_1}{S}. \tag{176}$$

and the dynamic pressure of the bounding jet issuing from the external nozzle is equal to the total pressure of the air stream flowing into the nozzle installation, that is,

$$H_c = \frac{\rho w_n^2}{2}, \tag{177}$$

the component $c_{yp\ 1}$ can be represented as

$$c_{yp1} = \frac{\bar{F}_1}{b_1/h_1} \cdot \frac{\cos\varphi_1}{1 + \sin\varphi_1} \bar{p}_1.$$

The component of the lift coefficient due to the forces of excess pressure acting at the external nozzle cut-offs is

$$c_{yc1} = \frac{Y_{c1}}{SH_c} = \frac{\int_{x_{01}}^{x_n} 2L(p_x - p_n)\,dx_{\varphi 1}}{SH_c} =$$

$$= \frac{2L\frac{\rho w_n^2}{2}}{SH_c} \int_{x_{01}}^{x_n} \left[1 - e^{-2\frac{x_n - x_{\varphi 1}}{x_n - x_{01}} \cdot \frac{b_1}{h_1}(1+\sin\varphi_1)}\right] dx_{01}.$$

Using Eqs. (174) - (177), we find

$$c_{yc1} = \frac{\bar{F}_1}{\cos\varphi_1}\left(1 - \frac{1}{1+\sin\varphi_1} \cdot \frac{\bar{p}_1}{2b_1/h_1}\right).$$

The overall component of the lift coefficient due to the forces of pressure against the cut-offs of the external nozzles and the reaction forces of the jets is

$$c_{y\varphi 1} = c_{y\varphi 1} + c_{y\varphi 1} = \frac{F_1}{\cos\varphi_1}\left(1 + \frac{2\cos^2\varphi_1 - 1}{1 + \sin\varphi_1}\cdot\frac{\bar{p}_1}{2b_1/h_1}\right).$$

The component of the lift due to the pressure forces of the air cushion over the sections of the bottom bounded by the external and internal nozzles is

$$c_{yn1} = \frac{Y_{n1}}{SH_c} \quad 2\frac{(x_{\varphi 1} - x_{n2})\,L\,(p_{n1} - p_H)}{SH_c} = \bar{S}_1\bar{p}_1, \qquad (178)$$

where $\bar{S}_1$ is the relative area of the sections of the bottom of the nozzle installation lying between the external and internal nozzles,

$$\bar{S}_1 \quad \frac{2(x_{\varphi 1} \quad x_{n2})\,L}{SH_c}. \qquad (179)$$

The component of the lift due to the reaction of the air jets flowing from the internal nozzles is

$$c_{y\varphi 2} = \frac{Y_{\varphi 2}}{SH_c} = \frac{1}{SH_c}\int_{x_{n2}}^{x_{\varphi 2}} 2\rho L\cos^2\varphi_2\, v_x^2\, dx_{\varphi 2} =$$

$$= \frac{2\rho v_n^2 L\cos^2\varphi_2}{SH_c}\int_{x_{n1}}^{x_{n2}} e^{-2\frac{x_\phi - x_{\varphi 2}}{x_\phi - x_{n1}}\cdot\frac{b_\phi + b_2}{h_2}(1+\sin\varphi_2)}\, dx_{\varphi 2}.$$

Since the overall flow-through area of the internal nozzles is

$$F_2 \quad 2b_2L, \qquad (180)$$

the relative flow-through area of the internal nozzles is

$$\bar{F}_2 = \frac{F_2}{S}, \qquad (181)$$

and the coordinates are

$$x_{n2} = x_\phi - \frac{b_\phi}{\cos\varphi_2} \quad \text{and} \quad x_{\varphi 2} = x_\phi - \frac{b_\phi + b_2}{\cos\varphi_2},$$

we can represent the component $c_{yp\,2}$ as

$$c_{yp2} = \frac{\bar{F}_2}{\cos\varphi_2} \cdot \frac{\cos\varphi_2}{1 + \sin\varphi_2} \cdot \frac{\bar{p}_2 - \bar{p}_1}{b_2/h_2}.$$

The component of the lift due to the forces of excess pressure acting at the internal nozzle cut-offs is

$$c_{yp2} = \frac{Y_{c2}}{SH_c} = \frac{1}{SH_c} \int_{x_{c2}}^{x_{n2}} 2L\,(p_x - p_n)\,dx_{\varphi 2} =$$

$$= \frac{2L\,\frac{\rho v_n^2}{2}}{SH_c} \int_{x_{c2}}^{x_{n2}} \left[1 - e^{-2\frac{x_\phi - x_{\varphi 2}}{x_\phi - x_{c2}} \cdot \frac{b_\phi + b_2}{h_2}(1+\sin\varphi_2)}\right] dx_{\varphi 2}.$$

Using Eqs. (179) - (181), we get

$$c_{yp2} = \frac{\bar{F}_2}{\cos\varphi_2}\left(1 - \frac{1}{1+\sin\varphi_2} \cdot \frac{\bar{p}_2 - \bar{p}_1}{2b_2/h_2}\right).$$

The overall components of the lift coefficient due to pressure forces acting at the internal nozzle cut-offs and the reaction forces of the jets flowing from these nozzles is

$$c_{yp\Sigma 2} = c_{yp1} + c_{yp2} = \frac{\bar{F}_2}{\cos\varphi_2}\left(1 + \frac{2\cos^2\varphi_2 - 1}{1+\sin\varphi_2} \cdot \frac{\bar{p}_2 - \bar{p}_1}{2b_2/h_2}\right).$$

The components of the lift coefficient due to the pressure forces of the air cushion over the section of the bottom bounded by the internal nozzles is

$$c_{yn2} = \frac{Y_{n2}}{SH_c} = 2\,\frac{(x_{n2} - x_{c2})\,L\,(p_{c2} - p_n)}{SH_c} = \bar{S}_2\bar{p}_2,$$

where $\bar{S}_2$ is the relative area at the section of the nozzle installation bottom line between the internal nozzles

$$\bar{S}_2 = \frac{2x_{c2}L}{S}. \qquad (182)$$

Thus, the lift coefficient of an air cushion vehicle with a plane two-contour nozzle installation provided with angles of generatrix inclination of the external φ_1 and internal φ_2 nozzles, the flow-through width b_1 and b_2, respectively, and different placements of nozzles with respect to the height of the nozzle installation, is

$$c_y = \frac{\bar{F}_1}{\cos\varphi_1}\left(1 + \frac{2\cos^2\varphi_1 - 1}{1 + \sin\varphi_1}\cdot\frac{\bar{p}_1}{2b_1/h_1}\right) + \\ + \frac{\bar{F}_2}{\cos\varphi_2}\left(1 + \frac{2\cos^2\varphi_2 - 1}{1 + \sin\varphi_2}\cdot\frac{\bar{p}_2 - \bar{p}_1}{2b_2/h_2}\right) + \bar{S}_1\bar{p}_1 + \bar{S}_2\bar{p}_2, \quad (183)$$

where

$$\bar{p}_1 = 1 - e^{-2\frac{h_1}{b_1}(1+\sin\varphi_1)}; \quad (184)$$

$$\bar{p}_2 = 1 - e^{-2\frac{b_1}{h_1}(1+\sin\varphi_1)\left(1+\frac{b_2}{b_1}\cdot\frac{h_1}{h_2}\cdot\frac{1+\sin\varphi_2}{1+\sin\varphi_1}\right)}. \quad (185)$$

The parameters $\bar{F}_1$, $\bar{F}_2$, $\bar{S}_1$, and $\bar{S}_2$ appearing in Eq. (183) are determined in accordance with the adopted nozzle installation geometry based on Eqs. (176), (181), (179), and (182).

When $\varphi_1 = \varphi_2 = 45^\circ$, Eq. (183) becomes

$$c_y = \bar{F}_1\sqrt{2} + \bar{F}_2\sqrt{2} + \bar{S}_1\bar{p}_1 + \bar{S}_2\bar{p}_2, \quad (186)$$

and when $\varphi_1 = \varphi_2 = 30^\circ$, we have

$$c_y = \frac{2\bar{F}_1}{\sqrt{3}}\left(1 + \frac{1}{3}\cdot\frac{\bar{p}_1}{2b_1/h_1}\right) + \\ + \frac{2\bar{F}_2}{\sqrt{3}}\left(1 + \frac{1}{3}\cdot\frac{\bar{p}_2 - \bar{p}_1}{2b_2/h_2}\right) + S_1\bar{p}_1 + S_2\bar{p}_2.$$

Experimental data are compared in Fig. 151 with the results of theoretical calculations of the lift coefficient for a two-pass annular nozzle with angle of generatrix inclination $\varphi_1 = \varphi_2 = 45^\circ$ and flow-through width $b_1 = b_2 = 8$ mm. The lift in this experiment was determined by direct measurement on a gravimetric instrument. As we can see, the proposed method of calculation agrees quite satisfactorily with experiment. The difference between the calculation and experimental data does not exceed ~ 6 percent.

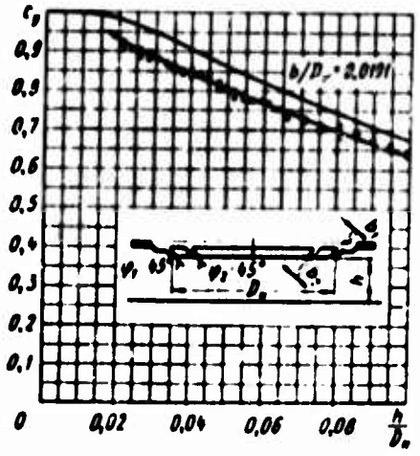

Fig. 151. Lift coefficient of two-pass annular nozzle as theoretical and experimental functions of parameter $h/D_н$ for $b_1/D_б = b_2/D_б = 0.02$ and $\varphi_1 = \varphi_2 = 45^\circ$

The lift of a plane and an annular nozzle installation. Let us examine the effect of the elevation of a plane two-contour nozzle installation above a solid support surface and the placement of the stability nozzles in this installation on the lift characteristics. We will assume that the exit edges of the external and internal nozzles lie in the same plane, and that the angles of inclination of their generatrices and the flow-through widths are identical. We will assume $\varphi_1 = \varphi_2 = 45^\circ$ and $b_1/B = b_2/B = 0.01$. We will vary the parameter b_2/B within the limits $b_2/B = 0.972$-0.2. We note that the value $b_2/B = 0.972$ corresponds to the case when the stability nozzles merge with the external nozzle into a single general nozzle, forming a single-pass nozzle installation, since

$$\frac{B_2}{B} = \frac{B - 2\frac{b_1}{\cos\varphi_1}}{B}$$

$$= 1 - 2\frac{b_1}{B\cos\varphi_1}$$

$$= 1 - 2\frac{0,01}{\cos 45^\circ} = 0,972.$$

We will vary the elevation of the craft within the range $h/B = 0$-0.1.

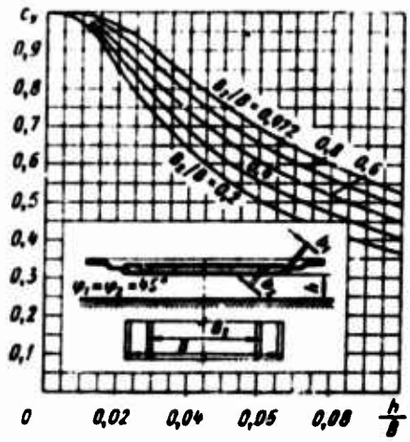

Fig. 152. Coefficient c_y of lift as functions of elevation of air cushion vehicle with plane two-pass nozzle installation ($b_1/B = b_2/B = 0.01$) for different placement of stability nozzles

For the particular nozzle installation, the relative cut-off area of the external and internal nozzles is

$$\bar{F}_{c1} = 2\frac{b_1}{B\cos\varphi_1} \quad \text{and} \quad \bar{F}_{c2} = 2\frac{b_2}{B\cos\varphi_2}, \tag{187}$$

and the relative area of the section of the bottom bounded by these nozzles is

$$\bar{S}_1 = 1 - \frac{B_2}{B} - 2\frac{b_1}{B\cos\varphi_1} \quad \text{and} \quad \bar{S}_2 = \frac{B_2}{B} - 2\frac{b_2}{B\cos\varphi_2}. \tag{188}$$

Specifying various values for the parameter b_2/B, let us determine based on Eqs. (187) and (188) relative areas $\bar{F}_{c1}$, $\bar{F}_{c2}$, $\bar{S}_1$, and $\bar{S}_2$, and by Eqs. (184) and (185), when $h/B = \text{const}$ -- the air cushion pressure coefficients $\bar{p}_1$ and $\bar{p}_2$. Then by Eq. (186) let us find the corresponding values of the coefficient c_y of the lift. We will perform the calculations for various values of the elevation h/B of the nozzle installation over the support surface.

The results of the calculations are given in Fig. 152, from which we can see that the single-pass nozzle installation (the curve for $B_2/B = 0.972$) has the top load-bearing capacity. Building a two-pass nozzle installation with the same overall areas and with the same flow-through area and the same angles of nozzle generatrix inclination, as well as employing any other method of sectionalizing for the specified conditions leads to a reduction in the lift coefficient. Degradation of the load-bearing qualities of a nozzle installation due to sectionalizing is the more marked, the higher the elevation of the craft above the support surface.

Let us determine the effect that placement of the nozzle installations has on the lift characteristics of a planform round two-pass nozzle installation for different elevations above the support surface. As in the case of a plane nozzle installations, we will assume $\varphi_1 = \varphi_2 = 45^\circ$ and $b/D_н = b_2/D_н = 0.01$.

We will characterize the position of an internal nozzle in the nozzle installation with the diameter $D_{н2}$, and the overall dimensions of the nozzle installation -- by the diameter $D_н$. We will vary the diameter $D_{н2}/D$ within the limits $D_{в2}/D_н = 0.972$-0.2, and the elevation of the craft — within the limits $h/D_н = 0$-0.1. Let us determine the lift coefficient for this nozzle installation by Eq. (186). The relative cut-off areas of the external and internal nozzles appearing in this formula are

$$\bar{F}_{c1} = 4\frac{b}{D_н\cos\varphi}\left(1-\frac{b}{D_н\cos\varphi}\right) \tag{189}$$

and

$$\bar{F}_{c2} = 4\frac{D_{н2}}{D_н}\cdot\frac{b}{D_н\cos\varphi}\left(1-\frac{b}{D_{н2}}\frac{D_н}{D_н\cos\varphi}\right), \tag{190}$$

and the relative areas of the external and internal sections of the bottom of the nozzle installation are

$$\bar{S}_1 = 1-\left(\frac{D_{в1}}{D_н}\right)^2 - 4\frac{b}{D_н\cos\varphi_1}\left(1-\frac{b}{D_н\cos\varphi_1}\right) \tag{191}$$

and

$$\bar{S}_2 = \left(\frac{D_{н2}}{D_н}\right)^2 - 4\frac{D_{н2}}{D_н}\cdot\frac{b}{D_н\cos\varphi}\left(1-\frac{b}{D_{н2}}\frac{D_н}{D_н\cos\varphi}\right). \tag{192}$$

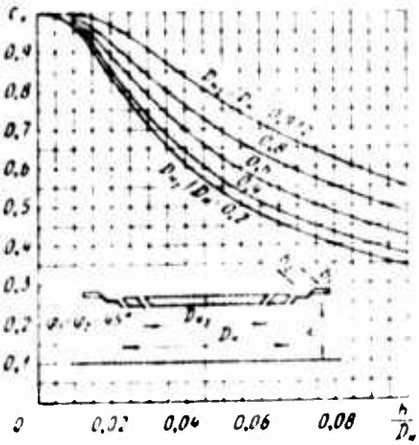

Fig. 153. Coefficient c_y of lift as functions of elevation of air cushion vehicle with annular two-pass nozzle installation ($b_1/D_H = b_2/D_H = 0.01$) for different placement of stability nozzles

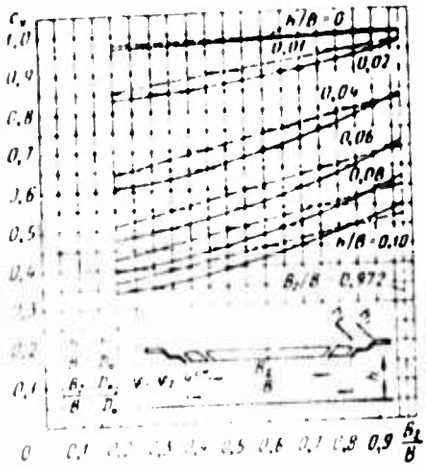

Fig. 154. Coefficient c_y of lift as functions of placement of stability nozzles in two-pass nozzle installation for different elevations above support surface (solid curves -- for annular nozzle installation, and dashed curves -- for plane installation)

The air cushion pressure coefficients pertaining to this case are as follows, in accordance with Eqs. (184) and (185):

$$p_1 = 1 - e^{-2\frac{b/D_H}{h/D_H}(1+\sin\varphi)} \tag{193}$$

and

$$p_2 = 1 - e^{-4\frac{b/D_H}{h/D_H}(1+\sin\varphi)}. \tag{194}$$

The results of determining the effect of elevation of a craft with an annular two-pass nozzle installation on the lift coefficient for different placement of stability nozzles are given in Fig. 153. By comparing Fig. 153 and Fig. 152, we see that the overall pattern of variation of the function $c_y = f(h/D_H, D_{H2}/D_H)$, for an annular two-pass nozzle installation, remains the same as for a plane two-pass nozzle installation. There is only a numerical difference in the lift coefficients.

The lift coefficient as functions of where the stability nozzles are placed in a two-pass nozzle installation, for different elevations of the nozzle installation above the support surface, is shown in Fig. 154. As we can see, increasing the separation between the internal and external nozzles very appreciably reduces the lift coefficient c_y, especially for relatively large elevations $h/B = h/D_H$. And the coefficient c_y decreases more rapidly for an annular nozzle installation than for a plane one.

For large values of the parameter $B_2/B = D_{H2}/D_H$, the annular nozzle installation has a greater load-bearing capacity compared with a plane installation, but for small values of $B_2/B = D_{H2}/D_H$, in contrast, the plane two-pass nozzle installation achieves a greater lift than the annular.

24. Craft With Two-Pass Nozzle Installation Provided With Oblique Nozzle Cut-Offs

The lift of an air cushion vehicle with a two-pass nozzle installation having external and internal nozzles with oblique cut-off is

$$Y = c_y S H_c (c_{yp1} + c_{yc1} + c_{yn1} + c_{yp2} + c_{yc2} + c_{yn2}) S \frac{\rho v_H^2}{2}.$$

When determining the components of the lift coefficients, let us use the following equations that determine the distribution of velocity and pressure in the nozzle cut-off plane.

For the external nozzles, the velocity field is

$$\frac{v_{\psi_1}}{v_H} = \left[1 + \frac{x_{\psi_1}}{x_1} \cdot \frac{b_1}{h_1} \cdot \frac{\sin(\varphi_1 - \psi_1)}{\cos\psi_1}\right]^{-\frac{(1+\sin\varphi_1)\cos\psi_1}{\sin(\varphi_1-\psi_1)}}$$

and the pressure field is

$$\frac{p_{\psi_1} - p_H}{p_0 - p_H} = 1 - \left[1 + \frac{x_{\psi_1}}{x_1} \cdot \frac{b_1}{h_1} \cdot \frac{\sin(\varphi_1 - \psi_1)}{\cos\psi_1}\right]^{-2\frac{(1+\sin\varphi_1)\cos\psi_1}{\sin(\varphi_1-\psi_1)}}.$$

For the internal nozzles, the velocity field is

$$\frac{v_{\psi_2}}{v_H} = \frac{v_{e1}}{v_H}\left[1 + \frac{x_{\psi_2}}{x_2} \cdot \frac{b_2/h_1}{1 - \Delta h/h_1} \cdot \frac{\sin(\varphi_2 - \psi_2)}{\cos\psi_2}\right]^{-\frac{(1+\sin\varphi_2)\cos\psi_2}{\sin(\varphi_2-\psi_2)}}, \quad (195)$$

where

$$\frac{v_{e1}}{v_a} = \left[1 + \frac{b_1}{h_1} \cdot \frac{\sin(\varphi_1 - \psi_1)}{\cos\psi_1}\right]^{\frac{(1+\sin\varphi_1)\cos\psi_1}{\sin(\varphi_1-\psi_1)}},$$

and the pressure field is

$$\frac{p_{\psi_2} - p_a}{p_c - p_a} = 1 - (1 - \bar{p}_1)\left[1 + \frac{\varphi_{\psi_2}}{\varphi_1} \cdot \frac{b_2 h_1}{b_1 h_2}\left(1 - \frac{\sin(\varphi_1 - \psi_2)}{\cos\psi_2}\right)\right]^{\frac{(1+\sin\varphi_1)\cos\psi_1}{\sin(\varphi_1-\psi_1)}},$$

where

$$\bar{p}_1 = 1 - \left[1 + \frac{b_1}{h_1} \cdot \frac{\sin(\varphi_1 - \psi_1)}{\cos\psi_1}\right]^{\frac{(1+\sin\varphi_1)\cos\psi_1}{\sin(\varphi_1-\psi_1)}}.$$

The components of the lift coefficient due to the reaction of air jets $c_{yp\,1}$ and the pressure forces at the cut-offs of the external nozzles $c_{yc\,1}$ of a two-pass nozzle installation can be determined from the formulas for a single-pass nozzle installation, namely:

$$c_{yp1} = 2\bar{F}_1 \frac{\cos\varphi_1 \cos\psi_1}{b_1 h_1 \sin(\varphi_1 - \psi_1)} \cdot \frac{1 - k_2(1 - \bar{p}_1)}{2k_1 - 1}$$

and

$$c_{yc1} = \bar{F}_1 \left[\frac{\cos\varphi_1}{\cos\psi_1} - \frac{\cos\varphi_1 \cos\psi_1}{\sin(\varphi_1 - \psi_1)} \cdot \frac{1 - k_2(1 - \bar{p}_1)}{(2k_1 - 1) b_1 / h_1}\right],$$

where

$$\bar{p}_1 = 1 - e^{-2k_1 \ln k_2}$$

is the air cushion pressure coefficient

$$\bar{F}_1 = \frac{2b_1 l_1}{S} \tag{196}$$

is the relative total flow-through area of the external nozzles, and

$$k_1 = \frac{(1 + \sin\varphi_1)\cos\psi_1}{\sin(\varphi_1 - \psi_1)} \quad \text{and} \quad k_2 = 1 + \frac{b_1}{h_1} \cdot \frac{\sin(\varphi_1 - \psi_1)}{\cos\psi_1}$$

are the coefficients of proportionality.

The overall component of the lift due to the reaction of jets and pressure forces at the external nozzle cut-off is

$$c_{yR1} = c_{yR1} + c_{y\bar{n}1} = I_1 \left[\frac{\cos(\varphi_1 - \psi_1)}{\cos\psi_1} + \frac{\cos(\varphi_1 - \psi_1)}{\sin(\varphi_1 - \psi_1)} \cdot \frac{1 - k_2(1 - \bar{p}_1)}{(2k_1 - 1)\, b_1/h_1} \right].$$

The component of the lift due to the pressure forces of the air cushion over the sections of the bottom bounded by the external and internal nozzles is

$$c_{y\bar{n}1} = \frac{S_1}{S} \bar{p}_1 = \left[1 - \bar{F}_1 \frac{\cos(\varphi_1 - \psi_1)}{\cos\psi_1} \right] \bar{p}_1.$$

The coefficient of the reactive forces of jets acting at the cut-offs of the internal nozzles is

$$c_{yR2} = \frac{2\rho L_2 \cos\psi_2 \cos\varphi_2}{S \frac{\rho v_H^2}{2}} \int_{x_{\psi 2}=0}^{x_{\psi 2}=x_2} v_{\psi 2}^2 \, dx_{\psi 2}.$$

Replacing in this equation velocity $v_{\psi 2}$ in the nozzle cut-off plane with its value from Eq. (195) and integrating the resulting expression, we find

$$c_{yR2} = 2 \frac{\bar{F}_2}{b_2/h_2} \cdot \frac{\cos\varphi_2 \cos\psi_2}{\sin(\varphi_2 - \psi_2)} \cdot \frac{(1 - \bar{p}_1) - k_4(1 - \bar{p}_2)}{2k_3 - 1},$$

where

$$\bar{F}_2 = \frac{2b_2 L_2}{S} \tag{197}$$

is the relative total flow-through area of the internal nozzles,

$$k_3 = \frac{(1 - \sin\varphi_2)\cos\psi_2}{\sin(\varphi_2 - \psi_2)}$$

and

$$k_4 = 1 + \frac{b_2/h_1}{1 - \frac{\Delta h}{h_1}} \cdot \frac{\sin(\varphi_2 - \psi_2)}{\cos\psi_2}$$

are the coefficients of proportionality.

The coefficient of the external pressure forces acting at the internal nozzle cut-offs is

$$c_{yc2} = \frac{2l_2 \cos(\psi_2 - \psi_2)}{S \frac{\rho v_\infty^2}{2}} \int_{x_{\psi 2}=0}^{x_{\psi 2}} (p_\psi - p_\infty)\, dx_\psi. \qquad (198)$$

Referring to the equality

$$p_\psi - p_\infty = \frac{\rho v_\infty^2}{2}\left[1 - \left(\frac{v_{\psi 2}}{v_\infty}\right)^2\right],$$

and Eq. (195), we represent the solution to Eq. (198) in the form

$$c_{yc2} = F_2\left[\frac{\cos(\psi_2 - \psi_2)}{\cos\psi_2} - \frac{\cos(\psi_2 - \psi_2)}{\sin(\psi_2 - \psi_2)} \cdot \frac{(1 - \bar{p}_1) - k_1(1 - \bar{p}_2)}{(2k_1 - 1)\bar{b}_2 \bar{h}_2}\right].$$

The overall coefficient of reactive forces and the excess pressure forces acting at the internal nozzle cut-offs is

$$c_{yn2} = c_{yp2} + c_{yc2} = F_2\left[\frac{\cos(\psi_2 - \psi_2)}{\cos\psi_2} - \right.$$

$$\left. - \frac{\cos(\psi_2 - \psi_2)}{\sin(\psi_2 - \psi_2)} \cdot \frac{(1 - \bar{p}_1) - k_1(1 - \bar{p}_2)}{(2k_1 - 1)\bar{b}_2 \bar{h}_2}\right].$$

The coefficient of air cushion pressure forces over the section of the nozzle installation bottom enclosed between the internal nozzles is

$$c_{yn2} = \frac{S_2}{S}\bar{p}_2 = S_2\bar{p}_2 \quad \left[\frac{B_2 l_2}{S} - F_2 \frac{\cos(\psi_2 - \psi_2)}{\cos\psi_2}\right]\bar{p}_2$$

or

$$c_{yn2} = \left[1 - S_1 - F_1 \frac{\cos(\psi_1 - \psi_1)}{\cos\psi_1} - F_2 \frac{\cos(\psi_2 - \psi_2)}{\cos\psi_2}\right]\bar{p}_2.$$

The lift coefficient of a two-pass nozzle installation with oblique nozzle cut-off is

$$c_u = \bar{F}_1 \left[\frac{\cos(\varphi_1 - \psi_1)}{\cos \psi_1} + \frac{\cos(\varphi_1 + \psi_1)}{\sin(\varphi_1 - \psi_1)} \cdot \frac{1 - k_2(1 - \bar{p}_1)}{(2k_1 - 1)\, b_1/h_1} \right] +$$

$$+ \bar{F}_2 \left[\frac{\cos(\varphi_2 - \psi_2)}{\cos \psi_2} + \frac{\cos(\varphi_2 + \psi_2)}{\sin(\varphi_2 - \psi_2)} \cdot \frac{(1 - \bar{p}_1) - k_2(1 - \bar{p}_2)}{(2k_2 - 1)\, b_2/h_2} \right] +$$

$$+ \bar{S}_1 \bar{p}_1 + \bar{S}_2 \bar{p}_2. \qquad (199)$$

In these formulas the flow-through areas of the external $\bar{F}_1$ and the internal $\bar{F}_2$ nozzles can be determined by Eqs. (196) and (197).

CHAPTER SIX
AERODYNAMIC CHARACTERISTICS OF HEELING AIR CUSHION VEHICLE

As we know, air cushion vehicles with a single-pass nozzle installation do not exhibit desired static stability. Experience shows that these craft [7] have a very small neutral hovering height (2-2.5 percent of nozzle installation width), and rising above this height causes total loss of static stability. Since the craft must be in a quite stable hovering regime, the elevation to which it can rise in practice above a support surface, determined by some reserve of static stability, is taken to be much less than the neutral hovering height. The low stability of these craft is dictated by the fact that even a slight heeling of the craft causes marked qualitative changes in the flow pattern of the main and circulation air currents under its bottom. This causes the pressure to be redistributed over the bottom and even at low elevations causes a tipping moment, acting on the craft in the direction of the lowered side.

The static stability of a craft with a single-pass nozzle installation can be augmented by introducing auxiliary nozzles -- stability nozzles. By compartmentalizing the craft bottom with additional nozzle into individual sections, it is possible to markedly boost the neutral hovering height, within whose limits increased pressure can be achieved over the sections of the bottom on the lowered side even when the craft has large angles of heeling, and thus produce the requisite restoring moment returning the craft to the horizontal position after the elimination of the perturbing force.

However, introducing auxiliary nozzles into a single-pass nozzle installation diminishes the lift per unit power input, that is, degrades the power characteristics of the nozzle installation. The point is that this single-pass nozzle installation has the highest load-bearing capacity compared with sectionalized nozzle installations with the same flow-through nozzle area and the same overall installation areas for the identical volume flow of air and the identical total pressure expended. This is caused by the fact that in a single-pass nozzle installation the entire air stream participates in producing the excess

pressure under the entire area of the nozzle installation bottom, while in a sectionalized installation air jets flowing from the auxiliary nozzles augment the pressure only over some sections of the bottom.

One of the sectionalized nozzle installations gaining acceptance is an installation that consists of a rectangular or planform oval single-pass nozzle with two longitudinal nozzles. In development of this installation, the goal was, by using longitudinal nozzles, to augment the transverse stability and to build a nozzle installation with approximately identical degree of stability both in the longitudinal and transverse directions. Experiments showed that this nozzle installation has a neutral hovering height that is roughly 4-5 times greater than a single-pass nozzle.

Since the lift and the degree of static stability depend heavily on the dimensions and position of the auxiliary nozzles in the sectionalized nozzle installation, functions relating these parameters are of practical interest, as well as an evaluation of the effect that heeling has on the efficiency of these installations.

25. Design Model of a Nozzle Installation

In examining the experimental characteristics of the pressure distribution over the bottom of two-pass annular nozzle installations, we can see that for small heeling angles ($\gamma = 0\text{-}2^{\circ}$) and for small relative elongation of the nozzle installation over the support surface ($h/b = 0.2$), the pressure over the surface of the nozzle installation bottom section bounded by the internal nozzle is distributed virtually uniformly (the greatest deviation does not exceed $\pm$ 2.5 percent of the mean pressure). The mean pressure is virtually equal to the pressure when $\gamma = 0$, while the pressure over the bottom sections bounded by the external and internal nozzles depends strongly on the heeling angle γ. For example, for a nozzle installation with angles $\varphi_1 = \varphi_2 = 30^{\circ}$, when $b/h = 0.5$ and when the angle γ is varied within the limits $0\text{-}2^{\circ}$, the pressure coefficient p_1 at the lowered craft side rises from 0.67 to 0.86, that is, by 28 percent, while on the opposite side it decreases from 0.67 to 0.62, that is, by 8 percent.

These regularities suggest a method for approximate calculation of forces and moments acting on a heeling sectionalized nozzle installation from the air cushion, by adopting the following assumptions:

the pressure over the section of the nozzle installation bottom bounded by the internal nozzles, for small angles of heeling γ and for limited related elevation h/v, does not depend on the angle of heeling and remains equal to the pressure for $\gamma = 0$ and for the same mean elevation h of the nozzle installation over the support surface; and

the pressure over the bottom sections between the nozzles is uniformly distributed areawise.

This method of calculation can be used to determine the effect that heeling has on the paramount aerodynamic characteristics of a nozzle installation: the air cushion pressure coefficient, discharge coefficient, and drag coefficient of individual nozzles as well as the nozzle installation as a whole; the lift coefficient and the side coefficient; the coefficients of air cushion moments; and the coefficients of transverse static stability. If we know these characteristics, it appears possible to find the optimum layout of internal nozzles (stability nozzles) in a sectionalized nozzle installation, assuming the condition of a large enough restoring moment without appreciable loss of lift, and also it appears possible to find the balancing angles as functions of the moment of external forces acting on the nozzle installation.

26. Lift and Side Force of Heeling Nozzle Installation

Let us examine functions determining the lift and side force of a plane sectionalized nozzle installation consisting of external nozzles and internal nozzles arranged parallel to them (Fig. 155). The resultant force acting from the air cushion against the craft with this sectionalizing scheme is determined by the sum of the components acting on individual installation members (of the cut-offs of the external nozzles and the stability nozzles, and also over the bottom sections enclosed between these nozzles).

When the craft is in the horizontal position, the resultant forces directed normally to the bottom surface and tends to raise the craft above the support surface. In the heeled craft position, the reaction forces of air jets leaving the nozzles are directed at an angle to the nozzle installation bottom and differ in magnitude for different angles. Therefore the direction of the resultant force in this case does not coincide with the normal to the bottom. However, in practice since the fraction of the reaction forces in the resultant is very small compared with the forces of excess air cushion pressure, even for a heeling craft we can assume the resultant force to be directed normally to the nozzle installation bottom. The resultant force tends to lift the craft above the support surface and to shift it toward the depressed side.

The lift determined in terms of the resultant R is

$$Y = R\cos\gamma = c_y S H_c \cos\gamma \approx c_y S H_c, \qquad (200)$$

where c_R is the coefficient of the resultant force; c_y is the lift coefficient; S is the area of the nozzle installation bounded by the external edge of the external nozzle; and H_c is the total pressure of the air stream fed to the nozzle installation to produce the jets forming the air cushion.

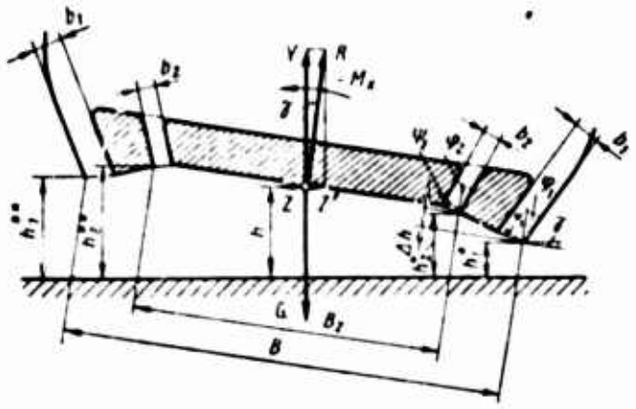

Fig. 155. Calculation scheme of sectionalized nozzle installation at small heeling angles

At small heeling angles varied within the limits $\gamma = 0\text{-}2^{\circ}\ 30'$, $\cos\gamma$ lies within the limits 1-0.9990, therefore we can assume $Y \approx R$ and, accordingly, $c_y \approx c_R$, with practical accuracy.

The side force produced by craft heeling is

$$Z = c_z S H_c = R\sin\gamma = c_R S H_c \sin\gamma.$$

For the indicated heeling angles, $\sin\gamma$ lies within the limits 0-0.0456. Therefore in actual calculations we can assume

$$Z = R\sin\gamma \approx Y\,\mathrm{tg}\,\gamma \approx Y\gamma \qquad (201)$$

and, thus $c_z = c_R \sin\gamma \approx c_y\,\mathrm{tg}\,\gamma \approx c_y\gamma$, since at small angles $\sin\gamma \approx \mathrm{tg}\,\gamma \approx \gamma$.

The effect of air cushion craft heeling on its aerodynamic characteristics is dictated by the fact that as the heeling angle γ is varied, both the elevation h of the individual nozzles as well as the angles φ of air jet outflow relative to the support surface change. As the result of craft heeling, the escape velocity of air jets, the pressure at nozzle cut-off, air volume flows, and air cushion pressure change. Ultimately, all this causes the forces acting at the craft bottom to be redistributed and a moment to be induced in the air cushion.

We must remember that when the nozzle installation heels by the angle γ, for a moderate elevation h above the support surface, the exit edges of the external nozzle walls are displaced and will be at different elevations:

for the external nozzle of the depressed side

$$h_1^* = h - \frac{B}{2}\sin\gamma, \tag{202}$$

for the internal nozzle of the depressed side

$$h_2^* = h_2 - \frac{B_2}{2}\sin\gamma \approx h + \Delta h - \frac{B_2}{2}\sin\gamma; \tag{203}$$

for the external nozzle of the elevated side

$$h_1^{**} = h + \frac{B}{2}\sin\gamma; \tag{204}$$

for the internal nozzle of the elevated side

$$h_2^{**} = h_2 + \frac{B_2}{2}\sin\gamma \approx h + \Delta h + \frac{B_2}{2}\sin\gamma. \tag{205}$$

Here and in the following, the symbol (*) will denote quantities pertaining to the depressed [lower] side of the nozzle installation, while the symbol (**) will refer quantities pertaining the elevated side.

The limiting value of the angle $\gamma_{пр}$ for which one of the nozzle installation sides touches the support surface is

$$\gamma_{пр} = \arcsin 2\frac{h}{B}. \tag{206}$$

Heeling of the craft increases the angle of generatrix inclination φ of the nozzles at the lowered side with respect to the support surface by the angle γ and reduces the angle φ of generatrix inclination of the nozzles on the elevated side by the same angle γ.

7. Air Cushion Pressure Coefficients of a Heeling Nozzle Installation

When a sectionalized nozzle installation is horizontal, the air cushion pressure coefficients are:

for the external nozzle

$$\bar{p}_1 = 1 - e^{-2k_1 \ln k_3}; \tag{207}$$

for the internal nozzle

$$\bar{p}_2 = 1 - (1 - \bar{p}_1) e^{-2k_2 \ln k_4}, \tag{208}$$

where

$$k_1 = \frac{(1 + \sin \varphi_1) \cos \psi_1}{\sin (\varphi_1 - \psi_1)}; \tag{209}$$

$$k_2 = 1 + \frac{b_1}{h_1} \cdot \frac{\sin (\varphi_1 - \psi_1)}{\cos \psi_1}; \tag{210}$$

$$k_3 = \frac{(1 - \sin \varphi_2) \cos \psi_2}{\sin (\varphi_2 - \psi_2)}; \tag{211}$$

$$k_4 = 1 + \frac{b_2 \frac{h_1}{\Delta h}}{1 - \frac{h_1}{\Delta h}} \cdot \frac{\sin (\varphi_2 - \psi_2)}{\cos \psi_2}. \tag{212}$$

Replacing in Eqs. (210) and (212) the elevation $h_1 = h$ of nozzles over the support surface with its value from Eqs. (202) and (203) for the lowered side, and by Eqs. (204) and (205) for the elevated side, and the angle of nozzle generatrix inclination — with the angle $\varphi + \gamma$ of the jet exit for the depressed side, and with the angle $\varphi - \gamma$ of the jet exit for the elevated side, we arrive at the following formulas for determining the air cushion pressure coefficient of a heeling nozzle installation.

For the external nozzle of the lowered side we have

$$\bar{p}_1^{\circ} = 1 - e^{-2k_1^{\circ} \ln k_3^{\circ}}; \tag{213}$$

for the internal nozzle of the lowered side

$$\bar{p}_2^{\circ} = 1 - (1 - \bar{p}_1^{\circ}) e^{-2k_3^{\circ} \ln k_4^{\circ}}, \tag{214}$$

where

$$k_1^{\bullet} = \frac{[1 + \sin(\varphi_1 + \gamma)]\cos\psi_1}{\sin(\varphi_1 + \gamma - \psi_1)}; \tag{215}$$

$$k_2^{\bullet} = 1 + \frac{2b_1/B}{2\frac{h}{B} - \sin\gamma} \cdot \frac{\sin(\varphi_1 + \gamma - \psi_1)}{\cos\psi_1}; \tag{216}$$

$$k_3^{\bullet} = \frac{[1 + \sin(\varphi_2 + \gamma)]\cos\psi_2}{\sin(\varphi_2 + \gamma - \psi_2)}; \tag{217}$$

$$k_4^{\bullet} = 1 + \frac{2b_2/B}{2\frac{h}{B}\left(1 + \frac{\Delta h}{h}\right) - \frac{B_2}{B}\sin\gamma} \cdot \frac{\sin(\varphi_2 + \gamma - \psi_2)}{\cos\psi_2}. \tag{218}$$

For the external nozzle of the elevated side, we have

$$\bar{p}_1^{\bullet\bullet} = 1 - e^{-2k_1^{\bullet\bullet}\ln k_2^{\bullet\bullet}}; \tag{219}$$

for the internal nozzle of the elevated side, we have

$$\bar{p}_2^{\bullet\bullet} = 1 - (1 - \bar{p}_1^{\bullet\bullet})\, e^{-2k_3^{\bullet\bullet}\ln k_4^{\bullet\bullet}}, \tag{220}$$

where

$$k_1^{\bullet\bullet} = \frac{[1 - \sin(\varphi_1 - \gamma)]\cos\psi_1}{\sin(\varphi_1 - \gamma - \psi_1)}; \tag{221}$$

$$k_2^{\bullet\bullet} = 1 + \frac{2b_1/B}{2\frac{h}{B} + \sin\gamma} \cdot \frac{\sin(\varphi_1 - \gamma - \psi_1)}{\cos\psi_1}; \tag{222}$$

$$k_3^{\bullet\bullet} = \frac{[1 + \sin(\varphi_2 - \gamma)]\cos\psi_2}{\sin(\varphi_2 - \gamma - \psi_2)}; \tag{223}$$

$$k_4^{\bullet\bullet} = 1 + \frac{2b_2/B}{2\frac{h}{B}\left(1 - \frac{\Delta h}{h}\right) + \frac{B_2}{B}\sin\gamma} \cdot \frac{\sin(\varphi_2 - \gamma - \psi_2)}{\cos\psi_2}. \tag{224}$$

28. Air Volume Flow in a Heeling Nozzle Installation

The air volume flow in a nozzle installation or in some of its nozzles is

$$Q = \alpha F \sqrt{\frac{2}{\rho} H_c},$$

where α is the discharge coefficient of the nozzle installation (nozzle) given with respect to its flow-through area, F is the flow-through area of the nozzle installation (nozzle); H_c is the total pressure of the air current flowing into the nozzle installation; and ρ is the density of the air.

For a sectionalized nozzle installation that is horizontal relative to the support surface, the discharge coefficients of the individual nozzles are as follows:

for the external nozzle

$$\alpha_1 = \frac{h_1}{b_1} \cdot \frac{1 - k_2^{(k_1 - 1)}}{\frac{\sin(\varphi_1 - \psi_1)}{\cos\psi_1}(k_1 - 1)}; \tag{225}$$

for the internal nozzle

$$\alpha_2 = \frac{1 - \frac{\Delta h}{h_1}}{\frac{b_2}{h_1}} \cdot \frac{k_2^{k_3}\left[1 - k_4^{-(k_3 - 1)}\right]}{\frac{\sin(\varphi_2 - \psi_2)}{\cos\psi_2}(k_3 - 1)}, \tag{226}$$

where k_1, k_2, k_3, and k_4 are the coefficients determined by Eqs. (209) - (212).

Using Eqs. (225) and (226) for the case of a heeling nozzle installation and considering the variation in the elevation of individual nozzles relative to the support surface and the jet exit angle, we derive the following formulas for the discharge coefficients:

for the external nozzle of the depressed side

$$\alpha_1^{\cdot} = \frac{2\frac{h}{B} - \sin\gamma}{2b_1/B} \cdot \frac{1 - k_2^{-(k_1^{\cdot} - 1)}}{\frac{\sin(\varphi_1 - \gamma - \psi_1)}{\cos\psi_1}(k_1^{\cdot} - 1)}; \tag{227}$$

for the internal nozzle of the depressed side

$$\alpha_2^{\cdot} = \frac{2\frac{h}{B} - 2\frac{\Delta h}{B} - \frac{B_2}{B}\sin\gamma}{2b_2/B} \cdot \frac{k_2^{-k_1^{\cdot}}\left[1 - k_4^{\cdot -(k_3^{\cdot} - 1)}\right]}{\frac{\sin(\varphi_2 - \gamma - \psi_2)}{\cos\psi_2}(k_3^{\cdot} - 1)}; \tag{228}$$

for the external nozzle of the elevated side

$$\alpha_1^{\cdot\cdot} = \frac{2\frac{h}{B} + \sin\gamma}{2b_1/B} \cdot \frac{1 - k_2^{\cdot\cdot -(k_1^{\cdot\cdot} - 1)}}{\frac{\sin(\varphi_1 + \gamma - \psi_1)}{\cos\psi_1}(k_1^{\cdot\cdot} - 1)}; \tag{229}$$

for the internal nozzle of the elevated side

$$\alpha_2^{\cdot\cdot} = \frac{2\frac{h}{B} + 2\frac{\Delta h}{B} + \frac{B_2}{B}\sin\gamma}{2b_2/B} \cdot \frac{k_2^{\cdot\cdot}\sqrt{k_1^{\cdot\cdot}\left|1 - k_4^{\cdot\cdot}\left(k_3^{\cdot\cdot} - 1\right)\right|}}{\frac{\sin(\varphi_2 - \gamma - \psi_2)}{\sin\psi_2}\left(k_3^{\cdot\cdot} - 1\right)}. \qquad (230)$$

The coefficients $k_1^{\cdot}$, $k_2^{\cdot}$, $k_3^{\cdot}$, and k_4^{*} for the depressed side and the coefficients $k_1^{\cdot\cdot}$, $k_2^{\cdot\cdot}$, $k_3^{\cdot\cdot}$, and k_4^{**} for the elevated side are determined, respectively, by Eqs. (215) - (218) and by (221) - (224). The discharge coefficients $\alpha_1^{\cdot}$, $\alpha_2^{\cdot}$, $\alpha_3^{\cdot}$, and α_4^{*} each relate to the flow-through area of a particular nozzle.

The total discharge coefficient of the nozzle installation is

$$\alpha = \frac{\alpha_1^{\cdot}F_1^{\cdot} + \alpha_2^{\cdot}F_2^{\cdot} + \alpha_1^{\cdot\cdot}F_1^{\cdot\cdot} + \alpha_2^{\cdot\cdot}F_2^{\cdot\cdot}}{F_1^{\cdot} + F_2^{\cdot} + F_1^{\cdot\cdot} + F_2^{\cdot\cdot}}, \qquad (231)$$

where $F_1^{\cdot}$, $F_2^{\cdot}$, $F_1^{\cdot\cdot}$, and F_2^{**} are the flow-through areas of the external and internal nozzles of the depressed and elevated sides.

For a plane sectionalized nozzle installation in which the length of the external and internal nozzles is the same, we have

$$\alpha = \frac{(\alpha_1^{\cdot} + \alpha_1^{\cdot\cdot})b_1 + (\alpha_2^{\cdot} + \alpha_2^{\cdot\cdot})b_2}{2(b_1 + b_2)}, \qquad (232)$$

since for this nozzle installation $F_1^{\cdot}$ $F_1^{\cdot\cdot}$ b_1L and $F_2^{\cdot}$ $F_2^{\cdot\cdot}$ b_2L.

Analysis shows that the position of the internal nozzles in the plane sectionalized nozzle installation having approximately the same flow-through width of the external and internal nozzles ($b_1 \approx b_2$) and identical angles of inclination of their generatrices ($\varphi_1 \approx \varphi_2$), when $\Delta h = 0$, affects the total discharge coefficient only very slightly. Therefore in practical calculations it is useful to neglect the effect of the position of the stability nozzles and to determine the total discharge coefficient of the sectionalized nozzle installation as for a single-pass nozzle installation, regarding the flow-through width of the nozzle to be equal to the overall width of the external and internal nozzles.

Approximate working formulas in this case will become

$$\alpha = \frac{\alpha^* + \alpha^{**}}{2}; \quad \alpha^* = \frac{1 - e^{-k^*}}{k^*}; \quad \alpha^{**} = \frac{1 - e^{-k^{**}}}{k^{**}};$$

$$k^* = \frac{2\frac{b_1 + b_2}{B}\left[1 + \sin(\varphi + \gamma)\right]}{2\frac{h}{B} - \sin\gamma_w};$$

$$k^{**} = \frac{2\frac{b_1 - b_2}{B}\left[1 + \sin(\varphi - \gamma)\right]}{2\frac{h}{B} + \sin\gamma}.$$

The discharge coefficient α calculated by these formulas corresponds to the case $B_2/B = 0.972$, where the stability nozzles merge with the external nozzles into a single general nozzle.

29. Lift Coefficients of a Heeling Nozzle Installation

When determining the lift coefficients of a heeling nozzle installation, let us use results from theoretical studies made of the aerodynamic characteristics of a sectionalized nozzle installation for the case when the craft is horizontal relative to the support surface (cf. Chapters Three and Five). In this case the lift coefficient of the air cushion vehicle is

$$c_y = c_{yp1} + c_{yc1} + c_{yn1} + c_{yp2} + c_{yc2} + c_{yn2}. \tag{233}$$

The component of the lift coefficient arising from the reaction forces of the air jets flowing from the external nozzles is

$$c_{yp1} = 2\frac{l_1}{b_1 h_1}\cdot\frac{\cos\varphi_1\cos\psi_1}{\cos(\varphi_1 - \psi_1)}\cdot\frac{1 - k_2(1 - \bar{p}_1)}{2k_1 - 1}. \tag{234}$$

The component of the lift coefficient arising from the forces of excess pressure at the external nozzle cut-offs is

$$c_{yc1} = \bar{F}_1\left[\frac{\cos(\varphi_1 - \psi_1)}{\cos\psi_1} - \frac{\cos(\varphi_1 - \psi_1)}{\sin(\varphi_1 - \psi_1)}\cdot\frac{1 - k_2(1 - \bar{p}_1)}{(2k_1 - 1)\,b_1/h_1}\right]. \tag{235}$$

The overall component of the lift coefficient arising from the reaction forces of jets and the pressure forces at the external nozzle cut-offs is

$$c_{y\pi 1} = c_{y\pi 1}' + c_{y\pi 1}'' = \bar{F}_1 \left[\frac{\cos(\varphi_1 - \psi_1)}{\cos\psi_1} + \right.$$

$$\left. + \frac{\cos(\varphi_1 + \psi_1)}{\sin(\varphi_1 - \psi_1)} \cdot \frac{1 - k_2(1 - \bar{p}_1)}{(2k_1 - 1)\, b_1/h_1} \right]. \qquad (236)$$

The component of the lift coefficient arising from the reaction forces of air jets flowing from the internal nozzles is

$$c_{y\pi 2} = 2 \frac{\bar{F}_2}{b_2/h_2} \cdot \frac{\cos\varphi_2 \cos\psi_2}{\sin(\varphi_2 - \psi_2)} \cdot \frac{(1 - \bar{p}_1) - k_4(1 - \bar{p}_2)}{2k_3 - 1}. \qquad (237)$$

The component of the lift coefficient arising from the forces of excess pressure at the internal nozzle cut-offs is

$$c_{yc2} = \bar{F}_2 \left[\frac{\cos(\varphi_2 - \psi_2)}{\cos\psi_2} - \frac{\cos(\varphi_2 - \psi_2)}{\sin(\varphi_2 - \psi_2)} \cdot \frac{(1 - \bar{p}_1) - k_4(1 - \bar{p}_2)}{(2k_3 - 1)\, b_2/h_2} \right]. \qquad (238)$$

The overall component of the lift coefficient arising from the jet reaction forces and the pressure forces at the internal nozzle cut-offs is

$$c_{y\pi c2} = \bar{F}_2 \left[\frac{\cos(\varphi_2 - \psi_2)}{\cos\psi_2} + \frac{\cos(\varphi_2 + \psi_2)}{\sin(\varphi_2 - \psi_2)} \cdot \frac{(1 - \bar{p}_1) - k_4(1 - \bar{p}_2)}{(2k_3 - 1)\, b_2/h_2} \right]. \qquad (239)$$

The overall component of the lift coefficient arising from the air cushion pressure forces at the external and internal sections of the nozzle installation bottom is

$$c_{yn} = c_{yn1} + c_{yn2} = \bar{S}_1 \bar{p}_1 + \bar{S}_2 \bar{p}_2. \qquad (240)$$

The lift coefficient of an air cushion vehicle with a sectionalized nozzle installation provided with oblique nozzle cut-off is

$$c_y = \bar{F}_1 \left[\frac{\cos(\varphi_1 - \psi_1)}{\cos\psi_1} + \frac{\cos(\varphi_1 + \psi_1)}{\sin(\varphi_1 - \psi_1)} \times \right.$$

$$\left. \times \frac{1 - k_2(1 - \bar{p}_1)}{(2k_1 - 1)\, b_1/h_1} \right] + \bar{F}_2 \left[\frac{\cos(\varphi_2 - \psi_2)}{\cos\psi_2} + \right.$$

$$\left. + \frac{\cos(\varphi_2 + \psi_2)}{\sin(\varphi_2 - \psi_2)} \cdot \frac{(1 - \bar{p}_1) - k_4(1 - \bar{p}_2)}{(2k_3 - 1)\, b_2/h_2} \right] + \bar{S}_1 \bar{p}_1 + \bar{S}_2 \bar{p}_2. \qquad (241)$$

where $\bar{F}_1$ is the total flow-through area of the external nozzles, $\bar{F}_1 = b_1 \Pi_1 / S$; $\bar{F}_2$ is the total flow-through area of the internal nozzles, $\bar{F}_2 = b_2 \Pi_2 / S$; $\bar{S}_1$ is the total area of the external bottom sections bounded by the exit edges of the external and internal nozzles, $\bar{S}_1 = S_1 / S$; $\bar{S}_2$ is the area of the internal section of the bottom bounded by the exit edge of the internal nozzles, $\bar{S}_2 = S_2 / S$.

The air cushion pressure coefficient $\bar{p}_1$ and $\bar{p}_2$ appearing in Eqs. (234) - (241) are determined by Eqs. (207) and (208). In the special case for a sectionalized nozzle installation with horizontal nozzle cut-off ($\varphi_1 = \psi_1$ and $\varphi_2 = \psi_2$), the lift coefficients are determined by the following formulas.

The overall components of the lift force arising from the jet reaction forces and the pressure forces of the external nozzle cut-offs is

$$c_{y\text{пс}1} = \frac{\bar{F}_1}{\cos\varphi_1}\left(1 + \frac{2\cos^2\varphi_1 - 1}{1 + \sin\varphi_1} \cdot \frac{\bar{p}_1}{2b_1/h_1}\right).$$

The overall component of the lift coefficient arising from the jet reaction forces and the pressure forces at the internal nozzle cut-offs is

$$c_{y\text{пс}2} = \frac{\bar{F}_2}{\cos\varphi_2}\left(1 + \frac{2\cos^2\varphi_2 - 1}{1 + \sin\varphi_2} \cdot \frac{\bar{p}_2 - \bar{p}_1}{2b_2/h_2}\right).$$

The overall component of the lift coefficient arising from air cushion pressure forces at the external and internal sections of the nozzle installation bottom is

$$c_{yn} = c_{yn1} + c_{yn2} = \bar{S}_1\bar{p}_1 + \bar{S}_2\bar{p}_2. \qquad (242)$$

The lift coefficient of an air cushion vehicle with horizontal nozzle cut-off is

$$c_y = \frac{\bar{F}_1}{\cos\varphi_1}\left(1 + \frac{2\cos^2\varphi_1 - 1}{1 + \sin\varphi_1} \cdot \frac{\bar{p}_1}{2b_1/h_1}\right) + \frac{\bar{F}_2}{\cos\varphi_2}\left(1 + \frac{2\cos^2\varphi_2 - 1}{1 + \sin\varphi_2} \cdot \frac{\bar{p}_2 - \bar{p}_1}{2b_2/h_2}\right) + \bar{S}_1\bar{p}_1 + \bar{S}_2\bar{p}_2. \qquad (243)$$

where

$$p_1 = 1 - e^{-\frac{b_1 l_1}{h_1 B}(1+\sin\varphi_1)}; \quad (244)$$

$$p_2 = 1 - e^{-\frac{b_1 l_1}{h_1 B}(1+\sin\varphi_1)\left(1+\frac{b_2}{b_1}\frac{1+\sin\varphi_2}{1+\sin\varphi_1}\frac{h_1}{h_2}\right)}; \quad (245)$$

$\bar{S}_1$ and $\bar{S}_2$ are the relative areas of the nozzle installation bottom bounded by the exit edges of the nozzles.

When the discharge of air jets from the nozzle installation can be viewed as a plane discharge,

$$\bar{F}_1 = \frac{2b_1 L}{BL} = 2b_1/B; \quad \bar{F}_2 = \frac{2b_2 L}{BL} = 2b_2/B;$$

$$\bar{S}_1 = 1 - \frac{B_2}{B} = \frac{2b_1/B}{\cos\varphi_1}; \quad \bar{S}_2 = \frac{B_2}{B} = \frac{2b_2/B}{\cos\varphi_2}.$$

For the heeling nozzle installation, the lift coefficient is

$$c_y = c^{\bullet}_{yp1} + c^{\bullet}_{yc1} + c^{\bullet}_{yn1} + c^{\bullet}_{yp2} + c^{\bullet}_{yc2} + c^{\bullet}_{yn2} + c^{\bullet\bullet}_{yp1} + c^{\bullet\bullet}_{yc1} + c^{\bullet\bullet}_{yn1} + c^{\bullet\bullet}_{yp2} + c^{\bullet\bullet}_{yc2} + c^{\bullet\bullet}_{yn2}. \quad (246)$$

Referring to these functions determining the variation in the elevation of nozzles and the jet exit angle during the heeling of a nozzle installation, the coefficients appearing in the right side of Eq. (246) can be represented by the following expressions.

The coefficient of the reaction force of a jet exiting from the external nozzle of the lowered side is

$$c^{\bullet}_{yc1} = 2\bar{F}^{\bullet}_1 \frac{\cos(\varphi_1+\gamma)\cos\varphi_1}{\sin(\varphi_1+\gamma-\varphi_1)} \cdot \frac{2h/B - \sin\gamma}{2b_1/B} \cdot \frac{1-k^{\bullet}_{-}(1-\bar{p}^{\bullet}_1)}{2k^{\bullet}_1 - 1}. \quad (247)$$

The coefficient of the excess pressure forces acting at the cut-off of the external nozzle of the lowered side is

$$c_{yc1}^{\cdot} = \bar{F}_1^{\cdot}\left[\frac{\cos(\varphi_1 + \gamma - \psi_1)}{\cos\psi_1} - \right.$$

$$\left. - \frac{\cos(\varphi_1 + \gamma - \psi_1)}{\sin(\varphi_1 + \gamma - \psi_1)} \cdot \frac{2h/B - \sin\gamma}{2b_1/B} \cdot \frac{1 - k_2^{\cdot}(1 - \bar{p}_1^{\cdot})}{2k_1^{\cdot} - 1}\right]. \qquad (248)$$

The coefficient of the reaction force of a jet and the excess pressure forces acting at the cut-off of the external nozzle at the lower side is

$$c_{yp.1}^{\cdot} = c_{yp1}^{\cdot} + c_{yc1}^{\cdot} = \bar{F}_1^{\cdot}\left[\frac{\cos(\varphi_1 + \gamma - \psi_1)}{\cos\psi_1} + \right.$$

$$\left. + \frac{\cos(\varphi_1 + \gamma - \psi_1)}{\sin(\varphi_1 + \gamma - \psi_1)} \cdot \frac{2h/B - \sin\gamma}{2b_1/B} \cdot \frac{1 - k_2^{\cdot}(1 - \bar{p}_1^{\cdot})}{2k_1^{\cdot} - 1}\right]. \qquad (249)$$

The coefficient of the air cushion pressure forces at the section of the nozzle installation bottom bounded by the external and internal nozzles of the lowered side is

$$c_{cm1}^{\cdot} = \frac{S_1}{2}\bar{p}_1^{\cdot} =$$

$$= \left[1 - \frac{B_2 l_c}{S} \cdot (\bar{F}_1^{\cdot} + \bar{F}_1^{\cdot\cdot}) \cdot \frac{\cos(\varphi_1 - \psi_1)}{\cos\psi_1}\right] \frac{\bar{p}_1^{\cdot}}{2}. \qquad (250)$$

The coefficient of the reaction force of a jet exiting from the internal nozzle of the lowered side is

$$c_{yp2}^{\cdot} = 2\bar{F}_2^{\cdot} \frac{\cos(\varphi_2 + \gamma)\cos\psi_2}{\sin(\varphi_2 + \gamma - \psi_2)} \cdot \frac{2\frac{h}{B}\left(1 + \frac{\Delta h}{h}\right) - \frac{B_2}{B}\sin\gamma}{2b_2/B} \times$$

$$\times \frac{(1 - \bar{p}_1^{\cdot}) - k_4^{\cdot}(1 - \bar{p}_2^{\cdot})}{2k_3^{\cdot} - 1}. \qquad (251)$$

The coefficient of the excess pressure forces acting at the cut-off of the internal nozzle of the lowered side is

$$c_{yc2}^{\cdot} = \bar{F}_2^{\cdot} \frac{\cos(\varphi_2 + \gamma - \psi_2)}{\cos\psi_2} - \frac{\cos(\varphi_2 + \gamma - \psi_2)}{\sin(\varphi_2 + \gamma - \psi_2)} \times$$

$$\times \frac{2\frac{h}{B}\left(1 + \frac{\Delta h}{h}\right) - \frac{B_2}{B}\sin\gamma}{2b_1/B} \cdot \frac{(1 - \bar{p}_1^{\cdot}) - k_4^{\cdot}(1 - \bar{p}_2^{\cdot})}{2k_3^{\cdot} - 1}. \qquad (252)$$

The coefficient of the jet reaction force and the excess pressure forces acting at the cut-off of the internal nozzle of the lower side is

$$c^{\cdot}_{yрс2} = c^{\cdot}_{yр2} + c^{\cdot}_{yс2} = \bar{F}^{\cdot}_2 \left[\frac{\cos(\varphi_2 - \gamma - \psi_2)}{\cos\psi_2} + \right.$$

$$+ \frac{\cos(\varphi_2 + \gamma + \psi_2)}{\sin(\varphi_2 + \gamma - \psi_2)} \cdot \frac{2\frac{h}{B}\left(1 + \frac{Mh}{h}\right) - \frac{B_2}{B}\sin\gamma}{2b_2/B} \times$$

$$\left. \times \frac{(1 - \bar{p}^{\cdot}_1) - k^{\cdot}_4 (1 - \bar{p}^{\cdot}_2)}{2k^{\cdot}_3 - 1} \right]. \qquad (253)$$

The coefficient of the air cushion pressure forces at the section of the nozzle installation bottom enclosed between the internal nozzles is

$$c_{yп2} = c^{\cdot}_{yп2} + c^{\cdot\cdot}_{yп2} = \frac{S_2}{S}\bar{p}_2 =$$

$$= \left[\frac{B_2 l_c}{S} - (\bar{F}^{\cdot}_2 + \bar{F}^{\cdot\cdot}_2) \cdot \frac{\cos(\varphi_2 - \psi_2)}{\cos\psi_2} \right] \bar{p}_2. \qquad (254)$$

The coefficient of the reaction force of a jet exiting from the external nozzle of the elevated side is

$$c^{\cdot\cdot}_{yр1} = 2\bar{F}^{\cdot\cdot}_1 \frac{\cos(\varphi_1 - \gamma)\cos\psi_1}{\sin(\varphi_1 - \gamma - \psi_1)} \cdot \frac{2\frac{h}{B} + \sin\gamma}{2b_1/B} \times$$

$$\times \frac{1 - k^{\cdot\cdot}_2 (1 - \bar{p}^{\cdot\cdot}_1)}{2k^{\cdot\cdot}_1 - 1}. \qquad (255)$$

The coefficient of the external pressure forces acting at the cut-off of the external nozzle of the elevated side is

$$c^{\cdot\cdot}_{yс1} = \bar{F}^{\cdot\cdot}_1 \left[\frac{\cos(\varphi_1 - \gamma - \psi_1)}{\cos\psi_1} - \frac{\cos(\varphi_1 - \gamma - \psi_1)}{\sin(\varphi_1 - \gamma - \psi_1)} \times \right.$$

$$\left. \times \frac{2\frac{h}{B} + \sin\gamma}{2b_1/B} \cdot \frac{1 - k^{\cdot\cdot}_2 (1 - \bar{p}^{\cdot\cdot}_1)}{2k^{\cdot\cdot}_1 - 1} \right]. \qquad (256)$$

The coefficient of the jet reaction force and the excess pressure forces acting at the cut-off of the external nozzle of the elevated side is

$$\bar{c}^{\bullet\bullet}_{yp1} = \bar{c}^{\bullet\bullet}_{yp1} + \bar{c}^{\bullet\bullet}_{yc1} = \bar{F}^{\bullet\bullet}_1 \left[\frac{\cos(\varphi_1 - \gamma - \psi_1)}{\cos\psi_1} \cdot \right.$$

$$\left. \cdot \frac{\cos(\varphi_1 - \gamma - \psi_1)}{\sin(\varphi_1 - \gamma - \psi_1)} \cdot \frac{2\frac{h}{B} + \sin\gamma}{2b_1/B} \cdot \frac{1 - k^{\bullet\bullet}_2(1 - \bar{p}^{\bullet\bullet}_1)}{2k^{\bullet\bullet}_1 - 1} \right]. \quad (257)$$

The coefficient of the air cushion pressure forces at the section of the nozzle installation bottom bounded by the external and internal nozzles of the elevated side is

$$\bar{c}^{\bullet\bullet}_{yc1} = \frac{\bar{S}_1}{2}\bar{p}^{\bullet\bullet}_1 = \left[1 - \frac{B_2 l}{S} - (\bar{F}^{\bullet}_1 + \bar{F}^{\bullet\bullet}_1) \cdot \frac{\cos(\varphi_1 - \psi_1)}{\cos\psi_1}\right] \frac{\bar{p}^{\bullet\bullet}_1}{2}. \quad (258)$$

The coefficient of the reaction force of a jet exiting from the internal nozzle of the elevated side is

$$\bar{c}^{\bullet\bullet}_{yp2} = 2\bar{F}^{\bullet\bullet}_2 \frac{\cos(\varphi_2 - \gamma)\cos\psi_2}{\sin(\varphi_2 - \gamma - \psi_2)} \cdot \frac{2\frac{h}{B}\left(1 + \frac{\Delta h}{h}\right) + \frac{B_2}{B}\sin\gamma}{2b_2/B} \times$$

$$\times \frac{(1 - \bar{p}^{\bullet\bullet}_1) - k^{\bullet\bullet}_4(1 - \bar{p}^{\bullet\bullet}_2)}{2k^{\bullet\bullet}_3 - 1}. \quad (259)$$

The coefficient of the excess pressure forces acting at the cut-off of the internal nozzle of the elevated side is

$$\bar{c}^{\bullet\bullet}_{yc2} = \bar{F}^{\bullet\bullet}_2 \left[\frac{\cos(\varphi_2 - \gamma - \psi_2)}{\cos\psi_2} - \frac{\cos(\varphi_2 - \gamma - \psi_2)}{\cos(\varphi_2 - \gamma - \psi_2)} \times \right.$$

$$\left. \times \frac{2\frac{h}{B}\left(1 + \frac{\Delta h}{h}\right) + \frac{B_2}{B}\sin\gamma}{2b_2/B} \cdot \frac{(1 - \bar{p}^{\bullet\bullet}_1) - k^{\bullet\bullet}_4(1 - \bar{p}^{\bullet\bullet}_2)}{2k^{\bullet\bullet}_3 - 1} \right]. \quad (260)$$

The coefficient of the jet reaction force and the excess pressure forces acting at the cut-off of the internal nozzle of the elevated side is

$$c''_{yp\Sigma} = c''_{yp2} + c''_{yc2} = \bar{F}''_2 \left[\frac{\cos(\varphi_2 - \gamma - \psi_2)}{\cos\psi_2} + \frac{\cos(\varphi_2 - \gamma + \psi_2)}{\sin(\varphi_2 - \gamma - \psi_2)} \times \right.$$

$$\left. \times \frac{2\frac{h}{B}\left(1 + \frac{\Delta h}{h}\right) + \frac{B_2}{B}\sin\gamma}{2\bar{b}_2/B} \cdot \frac{(1-\bar{p}''_1) - \bar{s}''(1-\bar{p}''_2)}{2\bar{k}''_3 - 1} \right]. \quad (261)$$

The pressure coefficients $\bar{p}^{*}_1$, $\bar{p}^{*}_2$, $\bar{p}^{**}_1$, and $\bar{p}^{**}_2$, and the coefficients k'_1, k'_2, k'_3, k'_4, k''_1, k''_2, k''_3, and k^{**}_4 appearing in these formulas are determined by Eqs. (215) - (224). The pressure coefficient $\bar{p}_2$ in Eq. (254), according to the assumption adopted, does not depend on the heeling angle γ. For a two-pass nozzle installation with oblique nozzle cut-off, this coefficient is determined by Eq. (208), and for a two-pass nozzle installation with horizontal nozzle cut-off -- by Eq. (245); $\bar{F}'_1 = \bar{F}''_1 = \bar{F}_1/2$ and $\bar{F}'_2 = \bar{F}''_2 = \bar{F}_2/2$.

Knowing the geometrical parameters of a sectionalized nozzle installation, that is, the flow-through width b_1 of the external nozzle and b_2 of the internal nozzle, angles φ_1 and φ_2 of their generatrix inclinations, cut-off angles ψ_1 and ψ_2, nozzle installation width b, and the distance b_2 between stability nozzles, as well as the elevation of the nozzle installation above the support surface and its heeling angle γ, let us determine by Eqs. (249), (250), (253), (254), (257), (258), and (261) the components of the lift coefficients. Then by Eq. (246) we find the lift coefficient c_y of the heeling nozzle installation. For a known total pressure p_c of the air stream fed to the nozzle installation, let us calculate by Eq. (200) the lift, and then the side force -- by Eq. (201).

30. Moments Induced in the Air Cushion of a Heeling Nozzle Installation

Let us look at functions determining the heeling moment of a plane sectionalized nozzle installation consisting of external nozzles and stability nozzles (cf. Fig. 155). Suppose that when acted on by moments induced by external forces and the air cushion, this nozzle installation heels and is balanced at a heeling angle γ_δ at elevation h from the support surface. Let us find relationships between the restoring moment, the geometrical parameters of the nozzle installation, its heeling angle, and its elevation.

The heeling moment related to the width B of the nozzle installation is:

$$M_x = m_x BSH_c \qquad (262)$$

where m_x is the dimensionless coefficient of the heeling moment.

Let us set up an equation of moments induced by the air cushion relative to the longitudinal axis x of the nozzle installation:

$$M_x = z_{p1}Y''_{p1} + z_{c1}Y''_{c1} + z_{p2}Y''_{p2} + z_{c2}Y''_{c2} + z_{n1}Y''_{n1} + z_{n2}Y''_{n2} - z_{p1}Y'_{p1} - z_{c1}Y'_{c1} - z_{p2}Y'_{p2} - z_{c2}Y'_{c2} - z_{n1}Y'_{n1} - z_{n2}Y'_{n2}, \qquad (263)$$

where z represents the distances from the x axis to the points at which the vertical components of forces Y are applied to the corresponding structural members of the nozzle installation.

The positive terms appearing in the right side of Eq. (263) are the moments of the jet reaction forces, the pressure forces at the external and internal nozzle cut-offs, and the air cushion pressure forces over the sections of the nozzle installation bottom of the elevated side, while the negative terms correspond to the moments of forces acting at the corresponding structural members of the nozzle installation on the depressed side.

In expanding Eq. (263), we will bear in mind that the bottom section bounded by the internal nozzles and the x axis are identical in area and equidistant from this axis, and the pressure over their surface areas, according to the calculation scheme adopted, is uniformly distributed. Therefore the moments of forces acting at these sections become equalized and, therefore, $z_{n2}Y''_{n2} - z_{n2}Y'_{n2} = 0$.

Note that owing to the nonuniformity of velocity and pressure distribution in the nozzle cut-off plane, the points at which the resultant reaction forces and the pressure forces are applied are somewhat shifted toward either side of the nozzle midline. For the pressure forces, the point at which the resultant is applied is shifted toward the inner wall of the nozzle, and for the reaction forces of the jet -- toward the outer wall of the nozzle. Since these forces are displaced from the nozzle midline to the different sites, but the displacement itself is very small compared with the distance from the midline to the x axis of the nozzle installation, we can assume -- with precision adequate for practical calculations -- that the point at which the resultant of the reaction forces and the pressure forces is applied lies along the midline of the nozzle cut-off. Accordingly,

$$z_{c1} \approx z_{p1} = z_{pc1} \quad \text{and} \quad z_{c2} \approx z_{p2} = z_{pc2}.$$

Referring to the foregoing and denoting

$$Y^{\cdot}_{p1} + Y^{\cdot}_{c1} = Y^{\cdot}_{pc1}; \quad Y^{\cdot}_{p2} + Y^{\cdot}_{c2} = Y^{\cdot}_{pc2}; \quad Y^{\cdot\cdot}_{p1} + Y^{\cdot\cdot}_{c1} = Y^{\cdot\cdot}_{pc1};$$
$$Y^{\cdot\cdot}_{p2} + Y^{\cdot\cdot}_{c2} = Y^{\cdot\cdot}_{pc2},$$

we can represent Eq. (265) as

$$M_x = z_{pc1}(Y^{\cdot\cdot}_{pc1} - Y^{\cdot}_{pc1}) + z_{pc2}(Y^{\cdot\cdot}_{pc2} - Y_t$$

In this equation the distance from the x ax to the middle of the external nozzle cut-off, expressed in terms of th eometrical parameters of a nozzle installation, is

$$z_{pc1} = \frac{B}{2}\left(1 - \frac{b_1}{B} \cdot \frac{\cos(\varphi_1 - \ }{\cos\psi_1} \right. \quad ; \qquad (265)$$

the distance from the x axis to the middle of the in al nozzle cut-off is

$$z_{pc2} = \frac{B}{2}\left(\frac{B_2}{B} - \frac{b_2}{B} \cdot \frac{\cos(\varphi_2 - \psi_2)}{\cos\psi_2}\right); \qquad (266)$$

and the distance from the x axis to the middle of the bottom section bounded by the external and internal nozzles is

$$z_{n1} = \frac{B}{4}\left(1 + \frac{B_2}{B} - 2\frac{b_1}{B} \cdot \frac{\cos(\varphi_1 - \psi_1)}{\cos\psi_1}\right). \qquad (267)$$

Expressing the forces Y appearing in Eq. (265) by the corresponding lift coefficients c_y, the nozzle installation area S, and the total pressure H_c related by the equality

$$Y = c_y S H_c,$$

and using Eq. (264), we get the heeling moment of the nozzle installation

$$M_x = \left[\frac{z_{pc1}}{B}(c^{\cdot\cdot}_{ypc1} - c^{\cdot}_{ypc1}) + \frac{z_{pc2}}{B}(c^{\cdot\cdot}_{ypc2} - c^{\cdot}_{ypc2}) + \right.$$
$$\left. + \frac{z_{n1}}{B}(c^{\cdot\cdot}_{yn1} - c^{\cdot}_{yn1})\right] BSH_c.$$

Referring to Eq. (267), we get the coefficient of the heeling moment

$$m_x = \frac{z_{pc1}}{B}(c^{\cdot\cdot}_{ypc1} - c^{\cdot}_{ypc1}) + \frac{z_{pc2}}{B}(c^{\cdot\cdot}_{ypc2} - c^{\cdot}_{ypc2}) + \frac{z_{n1}}{B}(c^{\cdot\cdot}_{yn1} - c^{\cdot}_{yn1}).$$

Representing the heeling moment coefficient in the form of its components

$$m_x = m_{xpc1} + m_{xpc2} + m_{xn1}, \tag{268}$$

we get the coefficient of the heeling moment due to the jet reaction and the pressure forces acting at the external nozzle cut-offs,

$$m_{xpc1} = \frac{z_{pc1}}{B}(c^{\cdot\cdot}_{xpc1} - c^{\cdot}_{ypc1}); \tag{269}$$

the coefficient of the heeling moment induced by the jet reaction and the pressure forces acting at the internal nozzle cut-offs is

$$m_{xpc2} = \frac{z_{pc2}}{B}(c^{\cdot\cdot}_{ypc2} - c^{\cdot}_{ypc2}), \tag{270}$$

and the coefficient of the heeling moment induced by the air cushion pressure forces acting at the bottom sections enclosed between the external and internal nozzles is

$$m_{xn1} = \frac{z_{n1}}{B}(c^{\cdot\cdot}_{yn1} - c^{\cdot}_{yn1}). \tag{271}$$

The relative distances $z_{pc\ 1}/B$, $z_{pc\ 2}/B$, and $z_{n\ 1}/B$ appearing in Eqs. (269) - (271) are calculated based on Eqs. (265) - (267), respectively; the lift coefficients $c^{\cdot}_{ypc1}$, $c^{\cdot}_{ypc2}$ and $c^{*}_{yn\ 1}$ for the depressed side -- based on Eqs. (249), (253), and (250); and the lift coefficients $c^{**}_{ypc\ 1}$, $c^{**}_{ypc\ 2}$, and $c^{**}_{yn\ 1}$ for the elevated side -- based on Eqs. (257), (261), and (258).

Analysis of Eq. (268) shows that the components of the moment coefficient $m_{xpc\ 1}$ and $m_{xpc\ 2}$ are very small -- one-three orders of magnitude smaller than the component $m_{xn\ 1}$. For transport air cushion vehicles, the relative flow-through width of external nozzles as well as stability nozzles usually does not exceed 1-1.5 percent of the nozzle installation with B, while the nozzle inclination angles φ = 50-60°. When the stability

nozzle situated at a distance 0.1B from the external nozzles ($B_2/B = 0.8$), the sum of the components $m_{xpc\ 1} + m_{xpc\ 2}$ is equal to 3-4 percent of the moment coefficient m_x. For values of parameter $b_2/B < 0.8$, which usually occurs in practice, the fraction of the total $m_{xpc\ 1} + m_{xpc\ 2}$ in the moment coefficient m_x decreases rapidly. Therefore, without introducing a large error into the determination of the coefficient m_x, in Eq. (268) we can neglect the components $m_{xpc\ 1}$ and $m_{xpc\ 2}$ and adopt

$$m_x \approx m_{xn1} \approx \frac{z_{n1}}{B}(c''_{yn1} - c'_{yn1}).$$

since

$$c'_{yn1} = \frac{1}{2} \cdot \frac{S_1}{S} \bar{p}'_1 \quad \text{and} \quad c''_{yn1} = \frac{1}{2} \cdot \frac{S_1}{S} \bar{p}''_1,$$

the coefficient of the transverse moment induced in the air cushion can be expressed as

$$m_x \approx \frac{1}{2} \cdot \frac{S_1}{S} \cdot \frac{z_{n1}}{B}(\bar{p}''_1 - \bar{p}'_1); \tag{272}$$

here the area of the section of the nozzle installation bottom enclosed between the external and internal nozzles on the depressed (elevated) side is

$$\frac{1}{2} \cdot \frac{S_1}{S} = \frac{1}{2}\left[1 - 2\frac{b_1}{B} \cdot \frac{\cos(\gamma_1 - \psi_1)}{\cos\psi_1} - \frac{B_2}{B}\right]. \tag{273}$$

Replacing in Eq. (272) the relative area $(\frac{1}{2})(S_1/S)$ and the relative distance z_{n1}/B by their functions (273) and (267), we get

$$m_x = \frac{1}{8}\left[\left(1 - 2\frac{b_1}{B} \cdot \frac{\cos(\gamma_1 - \psi_1)}{\cos\psi_1}\right)^2 - \left(\frac{B_2}{B}\right)^2\right](\bar{p}''_1 - \bar{p}'_1), \tag{274}$$

where $\bar{p}'_1$ and $\bar{p}''_1$ are the air cushion pressure coefficients, dependent on the heeling angle γ of the nozzle installation relative to the support surface.

§1. Coefficients of Transverse Static Stability

In examining the stability of air cushion vehicle, it is convenient -- in addition to the dimensionless moment coefficient $m_x = f(\gamma)$ -- to use the coefficient of the static stability of the nozzle installation, which is the derivative of the moment coefficient with respect to the heeling angle

$$\frac{dm_x}{d\gamma} = m_x^{\gamma},$$

taken at the balance point of the craft ($\sum M = 0$).

Let us find an analytic expression for the coefficient m_x^{γ} of the transverse static stability of a plane sectionalized nozzle installation. By inserting into Eq. (274) the values of the coefficients p_1^* and p_1^{**} by eqs. (215) and (219), taking the derivative with respect to angle γ, and making the necessary transformations, we derive an expression for the coefficient of transverse static stability

$$m_x^{\gamma} = 2A\left[(1-\dot{p_1})\left(c_1 \ln k_2^{*} - c_2 \frac{\dot{k_1}}{\dot{k_2}}\right) + (1-\ddot{p_1})\left(c_3 \ln k_2^{**} - c_4 \frac{\ddot{k_1}}{\ddot{k_2}}\right)\right], \tag{275}$$

where

$$A = \frac{1}{8}\left[\left(1 - 2\frac{b_1}{B}\cdot\frac{\cos(\varphi_1 - \psi_1)}{\cos\psi_1}\right)^2 - \left(\frac{B_2}{B}\right)^2\right];$$

$$c_1 = \frac{[\sin\psi_1 - \cos(\varphi_1 - \gamma - \psi_1)]\cos\psi_1}{\sin^2(\varphi_1 - \gamma - \psi_1)};$$

$$c_2 = \frac{2b_1/B\,[\sin(\varphi_1 - \psi_1) + 2h/B\cos(\varphi_1 - \gamma - \psi_1)]}{(2h/B - \sin\gamma)^2\cos\psi_1};$$

$$c_3 = \frac{[\sin\psi_1 - \cos(\varphi_1 - \gamma - \psi_1)]\cos\psi_1}{\sin^2(\varphi_1 - \gamma - \psi_1)};$$

$$c_4 = \frac{2b_1/B[\sin(\varphi_1 - \psi_1) + 2h/B\cos(\varphi_1 - \gamma - \psi_1)]}{(2h/B - \sin\gamma)^2\cos\psi_1}.$$

The coefficients $\dot{p_1}$, $\ddot{p_1}$, $\dot{k_1}$, $\dot{k_2}$, $\ddot{k_1}$, and k_2^{**} are determined by Eqs. (215), (219), (215), (216), (221), and (222), respectively.

Eq. (275) is a general expression enabling us to determine the coefficient of transverse static stability of a nozzle installation with an arbitrarily selected nozzle cut-off.

This formula is real when $\varphi_1 + \gamma - \psi_1 \neq 0$ and $\varphi_1 - \gamma - \psi_1 \neq 0$.

In two particular cases when $\varphi_1 - \psi_1 = \gamma$ and $\varphi_1 - \psi_1 = -\gamma$, when the cut-off of one of the nozzles is assigned the horizontal position (parallel to the support surface), Eq. (275) becomes meaningless since for the values of the sum of angles $\varphi_1 - \gamma - \psi_1 = 0$ and $\varphi_1 + \gamma - \psi_1 = 0$, the value of the coefficient $\bar{p}^*$ or $\bar{p}_1^{**}$ becomes indeterminate.

This indeterminacy is expanded by the familiar L'Hopital's rule.

Setting the angle $\psi_1 = 0$, we can find the function $m_x^\gamma = f(\gamma)$ for a nozzle installation with normal nozzle cut-off, and adopting $\psi_1 = \varphi_1$, we can determine $m_x^\gamma = f(\gamma)$ for a nozzle installation with horizontal nozzle cut-off.

For a nozzle installation with normal nozzle cut-off ($\psi_1 = 0$), the formulas for m_x^γ, $\bar{p}_1^*$, and $\bar{p}_1^{**}$ remain the same [(275), (215), and (219)], but the coefficients appearing in them are replaced with the following expressions:

$$A = \frac{1}{8}\left[\left(1 - 2\frac{b_1}{B}\cdot\frac{1}{\cos\varphi_1}\right)^2 - \left(\frac{B_2}{B}\right)^2\right]; \qquad (276)$$

$$k_1^* = 1 + \frac{1}{\sin(\varphi_1 + \gamma)}; \quad k_1^{**} = 1 + \frac{1}{\sin(\varphi_1 - \gamma)};$$

$$k_2^* = 1 + 2\frac{b_1}{B}\cdot\frac{\sin(\varphi_1 + \gamma)}{2h/B - \sin\gamma}; \quad k_2^{**} = 1 + 2\frac{b_1}{B}\cdot\frac{\sin(\varphi_1 - \gamma)}{2h/B - \sin\gamma};$$

$$c_1 = -\frac{\cos(\varphi_1 + \gamma)}{\sin^2(\varphi_1 + \gamma)}; \quad c_2 = 2\frac{b_1}{B}\cdot\frac{\sin\varphi_1 + \frac{2h}{B}\cos(\varphi_1 + \gamma)}{(2h/B - \sin\gamma)^2};$$

$$c_3 = -\frac{\cos(\varphi_1 - \gamma)}{\sin^2(\varphi_1 - \gamma)}; \quad c_4 = 2\frac{b_1}{B}\cdot\frac{\sin\varphi_1 + \frac{2h}{B}\cos(\varphi_1 - \gamma)}{(2h/B - \sin\gamma)^2}.$$

For a nozzle installation with horizontal nozzle cut-off ($\varphi_1 = \psi_1$), the formulas for m_x^γ, $\bar{p}_1^*$, and $\bar{p}_1^{**}$ also remain unchanged [(275), (215), and (219)]. The coefficients appearing in them are determined by the following expressions:

$$k_1^{\cdot} = \frac{[1 + \sin(\varphi_1 + \gamma)]\cos\varphi_1}{\sin\gamma}; \quad k_1^{\cdot\cdot} = -\frac{[1 + \sin(\varphi_1 - \gamma)]\cos\varphi_1}{\sin\gamma}; \quad (277)$$

$$k_2^{\cdot} = 1 + \frac{2b_1/B}{2h/B - \sin\gamma} \cdot \frac{\sin\gamma}{\cos\varphi_1}; \quad k_2^{\cdot\cdot} = 1 - \frac{2b_1/B}{2h/B + \sin\gamma} \cdot \frac{\sin\gamma}{\cos\varphi_1}; \quad (278)$$

$$c_1 = c_3 = \frac{(\sin\varphi_1 + \cos\gamma)\cos\varphi_1}{\sin^2\gamma}; \quad (279)$$

$$c_2 = \frac{4\frac{b_1}{B} \cdot \frac{h}{B}\cos\gamma}{\left(2\frac{h}{B} - \sin\gamma\right)^2 \cos\varphi_1}; \quad c_4 = \frac{4\frac{b_1}{B} \cdot \frac{h}{B}\cos\gamma}{\left(2\frac{h}{B} + \sin\gamma\right)^2 \cos\varphi_1}. \quad (280)$$

The coefficient a even in the case of horizontal nozzle cut-off is determined by Eq. (276).

If an air cushion vehicle with a nozzle installation provided with horizontal nozzle cut-off ($\psi_1 = \varphi_1$) is balanced horizontally ($\gamma_\delta = 0$) relative to the support surface, Eq. (275) also loses meaning, since for these angle values it becomes indeterminate. Let us find the expression for the coefficient m_x^γ of transverse static stability for this case. Inserting into Eq. (275) the values of the coefficients A, $k_1^{\cdot}$, $k_1^{\cdot\cdot}$, $k_2^{\cdot}$, $k_2^{\cdot\cdot}$, c_1, c_2, c_3, and c_4 by Eqs. (276) and (277) - (280), expanding the resulting indeterminacies of the form 0/0 and $\infty - \infty$, and carrying out the requisite transformations, we get

$$m_x^\gamma = -2cA(1 - \bar{p}_1), \quad (281)$$

where

$$c = \frac{b_1/B}{(h/B)^2}\left[1 + \sin\varphi_1 + 2\frac{h}{B}\cos\varphi_1 - \frac{1 + \sin\varphi_1}{\cos\varphi_1} \cdot \frac{b_1}{B}\right];$$

$$\bar{p}_1 = 1 - e^{-2\frac{b_1/B}{h/B}(1+\sin\varphi_1)};$$

a is a coefficient determined by Eq. (276).

Formula (281) expresses the coefficient of transverse static stability of air cushion vehicle (with nozzle installation provided with horizontal nozzle cut-off) balanced horizontally relative to the support surface.

Analysis of formula (281) shows that there is an optimal elevation h/B of the craft above the support surface at which the static stability becomes the greatest. Equating the first derivative of function (281) taken with respect to the independent variable h/B = 0, solving the resulting equation for h/B, we get

$$\left(\frac{h}{B}\right)_{onm} = \frac{1 + \sin\varphi_1}{2\cos\varphi_1}\left[2\frac{b_1}{B}\cos\varphi_1 + \frac{b_1/B}{\cos\varphi_1} - 1 + \right.$$
$$\left. + \sqrt{\left(1 - \frac{b_1/B}{\cos\varphi_1}\right)^2 + \left(2\frac{b_1}{B}\cos\varphi_1\right)^2}\right], \qquad (282)$$

determining the optimal elevation $(h/B)_{onm}$ of the craft for which the coefficient m_x^γ of the transverse static stability takes on the smallest value.

In the radicand of Eq. (282), the second term is very small compared with the first. Thus, in transport air cushion vehicles the flow-through width b_1 of the external nozzle usually does not exceed 2 percent of the width B of the sectionalized nozzle installation, and the angles at which these nozzles are placed $\varphi_1 = 30\text{-}60^\circ$. Therefore the ratio

$$\frac{(2b_1/B\cos\varphi_1)^2}{\left(1 - \frac{b_1/B}{\cos\varphi_1}\right)^2} = \frac{(2\cdot 0{,}02\cdot\cos 30^\circ)^2}{\left(1 - \frac{0{,}02}{\cos 30^\circ}\right)^2} \approx \frac{1}{1000}.$$

Therefore, without making an error that is noticeable in practice, we can assume

$$\left(2\frac{b_1}{B}\cos\varphi_1\right)^2 = 0,$$

and the optimal elevation of a craft, expressed by Eq. (282), can be represented as

$$\left(\frac{h}{B}\right)_{onm} \approx (1 + \sin\varphi_1)\frac{b_1}{B}. \qquad (283)$$

[onm = optimal]

Then the minimum coefficient of transverse static stability for which there is the greatest degree of stability is

$$(m_x^\gamma)_{min} = 2cA(\bar{p} - 1) = -\frac{2A}{c^2} \cdot \frac{\frac{1}{b_1/B} + 2\cos\varphi_1 - \frac{1}{\cos\varphi_1}}{1 + \sin\varphi_1} \quad (284)$$

or

$$(m_x^\gamma)_{min} = -0{,}27A \frac{\frac{1}{b_1/B} + 2\cos\varphi_1 - \frac{1}{\cos\varphi_1}}{1 + \sin\varphi_1}. \quad (285)$$

Since when $\varphi_1 = 45^\circ$, the difference $2\cos\varphi_1 - \frac{1}{\cos\varphi_1} = 0$, and when $\varphi_1 = 50\text{-}60^\circ$, this difference is only hundredths of the term $1/(b_1/B)$ (when $b_1/B \leqslant 0.02$, it is not more than 2 percent), we can assume $2\cos\varphi_1 - \frac{1}{\cos\varphi_1} \approx 0$, then the minimum value of the coefficient of transverse static stability when the craft is horizontal is

$$(m_x^\gamma)_{min} = -\frac{0{,}27A}{(1 + \sin\varphi_1) b_1/B} = -0{,}27 \frac{A}{\left(\frac{b_1}{B}\right)_{опт}}, \quad (286)$$

where A is a coefficient determined by Eq. (276).

From Eq. (282) it follows that the optimal elevation $(h/B)_{опт}$ at which there is the greatest static stability for a craft in the horizontal position is expressed only in terms of the flow-through width b_1/B of the external nozzles and the angle φ_1 of their inclination and is independent of the stability nozzle placement in the nozzle installation, determined by the parameter B_2/B.

These coefficients of transverse static stability are given with respect to the angle γ, expressed in radians. The coefficient m_x^γ has the dimension rad^{-1}. In practical calculations it is convenient also to use the coefficient of transverse static stability m_x^γ related to the heeling angle of 1°. These coefficients are related with each other by the equality $m_x^{\gamma^\circ} = \frac{m_x^\gamma}{57{,}3^\circ}$ and has the dimension deg^{-1}.

The absolute value of the coefficient m_x^{γ} characterizes the static stability (or instability) of an air cushion vehicle. The conditions of static stability on air cushion vehicle are expressed by the inequality $m_x^{\gamma} < 0$, the condition of static instability -- by the function $m_x^{\gamma} > 0$, and the condition of neutrality -- by the equality $m_x^{\gamma} = 0$.

5. Balancing Angles

When acted on by external moments, an air cushion vehicle heels. If in a heeling craft the required restoring moment is induced in the air cushion, the craft balances at some angle $\gamma_б$ relative to the support surface. Let us determine the balancing angle, one of the most important elements in the aerodynamic calculation of this craft.

For equilibrium of a craft relative to the heeling angle, it is necessary that

$$m_x + m_{x_в} = 0. \tag{287}$$

Since the coefficient of the sum of external moments is

$$m_x = \frac{\sum M_x}{BSH_c}, \quad \text{where} \quad H_c = \frac{G_0}{c_{\varphi\gamma} S},$$

and the moment coefficient m_x is determined by Eq. (272), Eq. (287) can be represented as

$$m_x = -\frac{c_{\varphi\gamma} \sum M_x}{BG_0} = \frac{1}{2} \cdot \frac{z_{m1}}{B} \cdot \frac{S_1}{S} (\bar{p}_1' - \bar{p}_1''). \tag{288}$$

In this equation $\bar{p}_1' = f_1(\gamma)$; $\bar{p}_1'' = f_2(\gamma)$; $c_{\varphi\gamma} = f_3(\gamma)$. The sum of the external moments $\sum M_б$ in the general case is also a function of the heeling angle. To find the dependence of the balancing angle on the moments acting on the craft, in explicit form, does not appear possible owing to the complexity of their determining equations. Eq. (288) can be solved for the angle γ by the method of successive approximations.

For cases when the moment of external forces is independent of the heeling angle or depends so weakly that this function can be neglected, the balancing angle can be estimated in explicit form. For an approximate solution, let us simplify Eq. (288) with respect to this angle.

Analysis of Eqs. (215) and (219) shows that as the angle γ is increased, the air cushion pressure coefficient $\bar{p}_1^*$ for the lowered side increases, while the coefficient $\bar{p}_1^{**}$ for the elevated side becomes smaller. These increments are approximately identical in magnitude, but different in sign. If we assume $\bar{p}_1^* - \bar{p}_1 = \bar{p}_1 - \bar{p}_1^{**}$, where $\bar{p}_1$ is the air cushion pressure coefficient when $\gamma = 0$, then

$$\bar{p}_1^* - \bar{p}_1^{**} = 2\,(\bar{p}_1^* - \bar{p}_1). \tag{289}$$

Let us introduce yet another simplification dealing with the air cushion pressure coefficient $\bar{p}_1^*$. The variation in this coefficient when acted on by heeling of the nozzle installation is dictated by the change in the elevation of the nozzle as well as in the air jet exit angle relative to the support surface. Let us estimate the extent of the effect these factors have on the pressure coefficient $\bar{p}_1^*$. The contribution introduced by varying only the jet exit nozzle into the general increment of coefficient $\bar{p}_1^*$, caused by varying the heeling angle, can be expressed by the relationship

$$\frac{\bar{p}_1^* - \bar{p}_{1h}^*}{\bar{p}_1^* - \bar{p}_1} = \frac{\left(1 - e^{-2k_1^* \ln k_2^*}\right) - \left(1 - e^{-2k_{1h}^* \ln k_{2h}^*}\right)}{\left(1 - e^{-2k_1^* \ln k_2^*}\right) - \left(1 - e^{-2k_1 \ln k_2}\right)}, \tag{290}$$

where $\bar{p}_1^*$ is the air cushion pressure coefficient of the external nozzle of the heeling nozzle installation, with reference to the variation in the nozzle elevation and in the jet exit angle; $\bar{p}_{1h}^*$ is the air cushion pressure coefficient of the external nozzle of a heeling nozzle installation, with reference only to variation in the nozzle elevation; $\bar{p}_1$ is the air cushion pressure coefficient of the external nozzle when the nozzle installation is in the horizontal position ($\gamma = 0$);

$$k_{1h}^* = \frac{(1 + \sin\varphi_1)\cos\psi_1}{\sin(\varphi_1 - \psi_1)};$$

$$k_{2h}^* = 1 + \frac{2b_1/B}{2h/B - \sin\gamma} \cdot \frac{\sin(\varphi_1 - \psi_1)}{\cos\psi_1};$$

k_1, k_2, k_1^*, and k_2^* are coefficients determined by Eqs. (209), (210), (215), and (216), respectively.

Calculations show that the main factor determining the effect of heeling on the coefficient $\bar{p}^*$ is the nozzle elevation. The effect of the jet exit nozzle is manifested relatively weakly. For example, for a nozzle installation with parameters b_1/B 0,0[illegible], φ_1 45°, ψ_1 0, h/B 0.05 and $\gamma = 2^\circ$, the proportion of the increment caused by varying only the jet exit nozzle when the installation is heeling, $\frac{\bar{p}_1^* - p_{1h}^*}{\bar{p}_1^* - p_1^*} \approx 0{,}01$, while the proportion of the increment produced by varying only the nozzle elevation height is $1 - \frac{\bar{p}_1^* - p_{1h}^*}{\bar{p}_1^* - p_1^*} \approx 0{,}99$.

Thus, we can assume the following approximate expressions of the pressure coefficient for nozzle installations:

with oblique nozzle cut-offs ($\psi_1 \neq 0$)

$$\bar{p}_1^* \approx 1 - \left[1 + \frac{2b_1/B}{2h/B - \sin\gamma} \cdot \frac{\sin(\varphi_1 - \psi_1)}{\cos\psi_1}\right]^{-2\frac{(1+\sin\varphi_1)\cos\psi_1}{\sin(\varphi_1 - \psi_1)}}; \quad (291)$$

with horizontal nozzle cut-offs ($\varphi = \psi_1$)

$$p_1^* \approx 1 - e^{-2\frac{2b_1/B(1+\sin\varphi_1)}{2h/B - \sin\gamma}}. \quad (292)$$

Let us make one more assumption. Analysis of Eq. (246) and its component terms shows that in the actually observed ranges of variation in the flow-through width of external and internal nozzles ($b_1/B = b_2/B = 0.005 - 0.02$), their angles of inclination ($\varphi_1 = \varphi_2 = 30\text{-}60^\circ$), the stability nozzle placement ($B_2/B = 0.2\text{-}0.8$), and the craft elevation ($h/B = 0\text{-}0.05$), a variation in the heeling angle has a relatively weak effect on the lift coefficient $c_{y\gamma}$ of the nozzle installation: deviations do not exceed ± 5 percent of the lift coefficient c_y of the horizontally arranged nozzle installation. Therefore, we can assume that the coefficient $c_{y\gamma}$ does not depend on the heeling angle. Then for the case of oblique nozzle cut-off

$$c_{yv} \approx c_y - F_1\left[\frac{\cos(\varphi_1-\psi_1)}{\cos\psi_1} + \frac{\cos(\varphi_1-\psi_1)}{\sin(\varphi_1-\psi_1)}\cdot\frac{1-k_2(1-\bar{p}_1)}{(2k_1-1)\,b_1/h_1}\right] +$$

$$+ F_2\left[\frac{\cos(\varphi_2-\psi_2)}{\cos\psi_2} + \frac{\cos(\varphi_2-\psi_2)}{\sin(\varphi_2-\psi_2)}\cdot\frac{(1-\bar{p}_1)-k_1(1-\bar{p}_2)}{(2k_2-1)\,b_2/h_2}\right] +$$

$$+ S_1\bar{p}_1 + S_2\bar{p}_2$$

and in the case of horizontal nozzle cut-off

$$c_y = F_{c1}\left(1 + \frac{2\cos^2\varphi_1 - 1}{1+\sin\varphi_1}\cdot\frac{\bar{p}_1}{2b_1/h_1}\right) +$$

$$+ F_{c2}\left(1 + \frac{2\cos^2\varphi_2 - 1}{1+\sin\varphi_2}\cdot\frac{\bar{p}_2-\bar{p}_1}{2b_2/h_2}\right) + S_1\bar{p}_1 + S_2\bar{p}_2.$$

Replacing in Eq. (288) the difference in coefficients $\bar{p}_1^* - \bar{p}_1^{**}$ with their approximately values by Eq. (289), with reference to $c_{yt} \approx c_y$ and using Eqs. (291) and (292), we get:

for a nozzle installation with oblique nozzle cut-off

$$\bar{p}_1^* = 1 - \left[1 + \frac{2b_1/B}{2h/B - \sin\gamma}\cdot\frac{\sin(\varphi_1-\psi_1)}{\cos\psi_1}\right]^{-2\frac{(1+\sin\varphi_1)\cos\psi_1}{\sin(\varphi_1-\psi_1)}} =$$

$$= \bar{p}_1 + \frac{m_a}{\frac{z_{n1}}{B}\cdot\frac{S_1}{S}}; \qquad (293)$$

for a nozzle installation with horizontal nozzle cut-off

$$\bar{p}_1^* = 1 - e^{-2\frac{\frac{b_1}{B}(1+\sin\varphi)}{2h/B - \sin\gamma}} = \bar{p}_1 + \frac{m_a}{\frac{z_{n1}}{B}\cdot\frac{S_1}{S}}. \qquad (294)$$

Solving Eqs. (293) and (294) for the angle γ, we get the following for a nozzle installation with oblique nozzle cut-off

$$\gamma_\delta = \arcsin\left[2\frac{h}{B} + \frac{2\frac{b_1}{B}\cdot\frac{\sin(\varphi_1-\psi_1)}{\cos\psi_1}}{1-\left(1-\bar{p}_1-\bar{m}_e\right)^{-\frac{\sin(\varphi_1-\psi_1)}{2(1+\sin\varphi_1)\cos\psi_1}}}\right], \quad (295)$$

where

$$m_e = \frac{m_e}{\frac{z_{n1}}{B}\cdot\frac{S_1}{S}} \quad (296)$$

and

$$\bar{p}_1 = 1 - \left[1 + \frac{b_1}{h}\frac{B}{B}\cdot\frac{\sin\varphi_1}{\cos\psi_1}\right]^{-2\frac{(1+\sin\varphi_1)\cos\psi_1}{\sin(\varphi_1-\psi_1)}};$$

for a nozzle installation with horizontal nozzle cut-off

$$\gamma_\delta = \arcsin\left[2\frac{h}{B} + \frac{4b_1/B(1+\sin\varphi_1)}{\ln(1-\bar{p}_1-\bar{m}_e)}\right], \quad (297)$$

where

$$\bar{p}_1 = 1 - e^{-2\frac{b_1/B}{h/B}(1+\sin\varphi_1)};$$

let us determine $\bar{m}_e$ by Eq. (296).

The coefficient of the moment of external forces appearing in Eq. (296) is

$$m_e = \frac{\sum M_e}{BSH_c} = \frac{c_0\sum M_e}{BG_0}.$$

By Eqs. (295) and (297) we can determine, in approximate terms, the balancing angle of an air cushion vehicle with sectionalized nozzle installation if the overall moment of external forces $\sum M_e$ is assumed to be independent of heeling angle γ.

3. Aerodynamic Characteristics of Heeling Sectionalized Nozzle Installation

Let us determine the effect that the heeling angle has on aerodynamic characteristics of a plane sectionalized nozzle installation consisting of a single-contour annular nozzle with two internal longitudinal stability nozzles (Fig. 156), for different stability nozzle placement and different elevation of the craft above the support surface.

The flow-through widths of the external and internal nozzles, the angles of their generatrix inclinations, and their cut-off angles will be assumed to be identical: $b_1/B = b_2/B = 0{,}01$; $\varphi_1 = \varphi_2 = 45°$ and $\psi_1 = \psi_2 = 45°$. We will vary the placement of the internal nozzles within the limits from $B_2/B = 0{,}2$ to $B_2/B = 1 - \frac{2b_1/B}{\cos\varphi_1} = 0{,}972$, that is, to the position at which the internal nozzles are in contact with the external, forming a single-contour nozzle installation. We will vary the heeling angle within the limits $\gamma = 0°$–$3°30'$, and the elevation of the craft above the support surface -- within the limits $h/B = 0$–$0{,}05$.

Specifying the angle γ to take on different values for discrete values of parameters B_2/B and h/B, let us calculate the air cushion pressure coefficient and the discharge coefficient of a nozzle installation, and then let us find the lift coefficients, the restoring moment, and the transverse static stability.

Air cushion pressure coefficients. In the case when the nozzle installation is horizontal relative to the support surface ($\gamma = 0$), the air cushion pressure coefficient both for the external as well as the internal nozzles are independent of the stability nozzle placement and are determined by the flow-through width of the nozzle, the angle of inclination of its generatrix, and the elevation of the nozzle installation above the support surface.

Heeling of the nozzle installation leads to a rise in the air cushion pressure coefficient $\bar{p}_1^*$ of the external nozzle of the lowered side and they drop in the pressure coefficient $\bar{p}_1^{**}$ of the external nozzle of the elevated side (Fig. 157). This is caused by variation both in the elevation of the nozzle cut-offs as well as in the air jet exit angle relative to the support surface. The position of the stability nozzles, defined by the parameter B_2/B here has no effect on the pressure coefficients $\bar{p}_1^*$ and $\bar{p}_1^{**}$ of the external nozzles.

The pressure coefficients $\bar{p}_2^*$ and $\bar{p}_2^{**}$ for the internal nozzles (stability nozzles) as functions of the heeling angle, when they are in different placement arrangements in the nozzle installation and for different elevations of the support surface, are shown in Fig. 158.

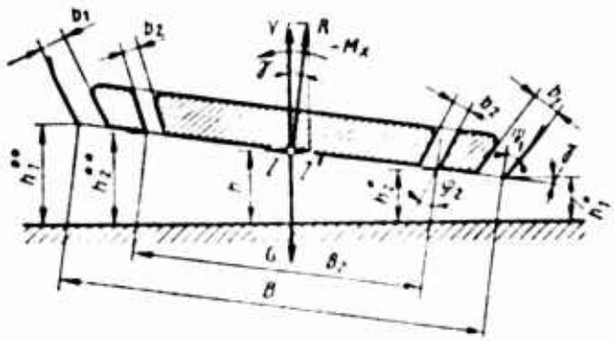

Fig. 156. Calculation scheme of sectionalized nozzle installation with horizontal nozzle cut-off for small heeling angles

When the nozzle installation is heeling, the pressure coefficient $\bar{p}_2^*$ increases and at the moment when a side of the nozzle installation touches the support surface, determined by the limiting value of the heeling angle $\gamma_{np} = \arcsin 2h/B$, has the maximum value: $\bar{p}_1^* = 1$. The coefficient $\bar{p}_2^{**}$ expressing the pressure at the elevated side decreases with increase in angle .

Shifting the internal nozzles toward the side of the longitudinal axis of the nozzle installation, that is, reducing the values of the parameter B_2/B for the same angle γ leads to some decrease in the coefficient $\bar{p}_2^*$ and an increase in the coefficient $\bar{p}_2^{**}$. This is because as the parameter B_2/B is reduced, the cut-off of the internal nozzle on the lowered side is at greater distances from the support surface, the effect of ground proximity on jet discharge is attenuated, and the coefficient $\bar{p}_2^*$ becomes smaller. The cut-off of the internal nozzle on the elevated side, conversely, approaches the support surface as the value B_2/B is reduced, which then leads to a rise in the coefficient $\bar{p}_2^{**}$. The effect of the parameter B_2/B on the coefficients $\bar{p}_2^*$ and $\bar{p}_2^{**}$ is the more marked, the higher the elevation h/B of the nozzle installation of the support surface. This effect shows up to greater extent in the pressure coefficient $\bar{p}_2^{**}$ of the elevated side.

Discharge coefficients. When the nozzle installation is horizontal, the discharge coefficients of the external and internal nozzles, as well as the air cushion pressure coefficients, are independent of the stability nozzle placement in the nozzle installation. As the angle of heeling γ is increased, the discharge coefficient α_1^* of the external nozzle at the

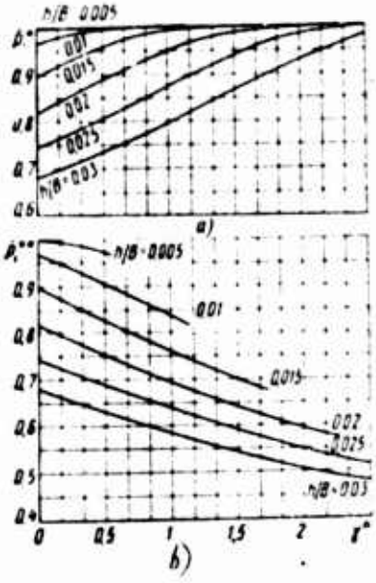

Fig. 157. Air cushion pressure coefficient of external nozzles as functions of heeling angle of plane sectionalized nozzle installation for different elevations above support surface:
a and b -- for lowered and elevated nozzles, respectively

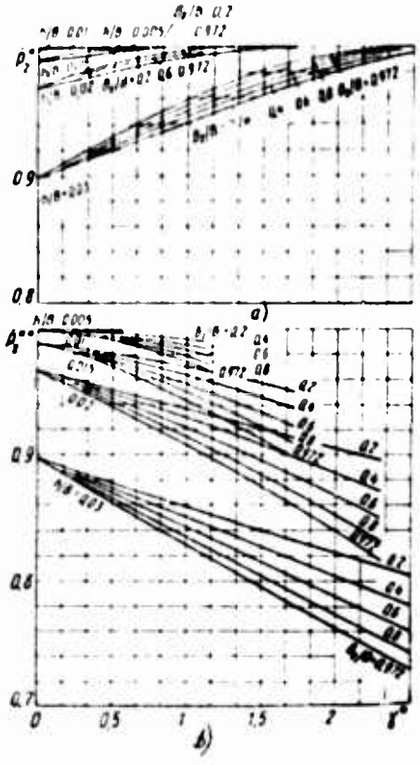

Fig. 158. Air cushion pressure coefficients of internal nozzles as functions of heeling angle of plane sectionalized nozzle installation for different elevations above support surface and different nozzle placements in the nozzle installation:
a and b -- for lowered and elevated nozzles, respectively

lowered side becomes smaller and that the moment the nozzle installation touches the support surface with its side, determined by the limiting value of the heeling angle $\gamma_{пр} = \arcsin 2h/B$, becomes equal to zero (Fig. 159). The discharge coefficient α_1^{**} of the external nozzle at the elevated side, with increase in the angle γ, rises, and does so more rapidly, the smaller the elevation h/B of the nozzle installation above the support surface.

The variation in the total discharge coefficient α_1 of external nozzles as functions of the heeling angle γ, for different elevations h/B of the nozzle installation, are also shown in Fig. 159. This coefficient pertains to the overall flow-through area of the external nozzles. As applied to this particular nozzle installation, by Eq. (252) we have

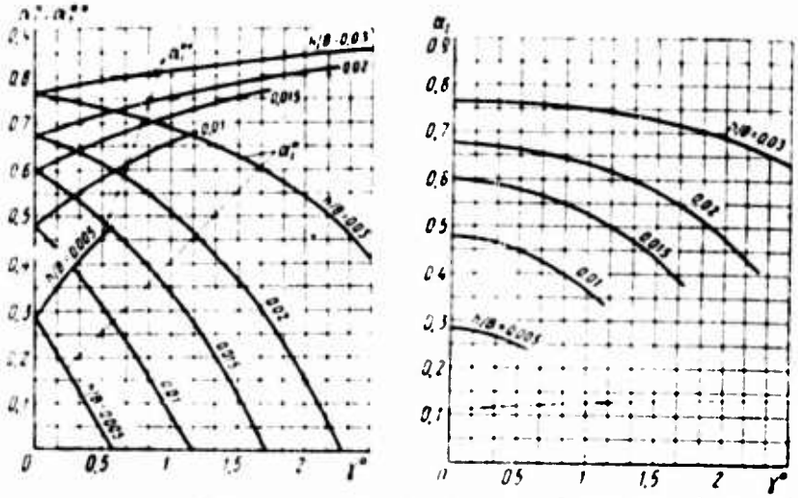

Fig. 159. Discharge coefficients of external nozzles as functions of heeling angle of plane sectionalized nozzle installation for different elevations above support surface ($\varphi_1 = 45^0$; $b_1/B = 0.01$)

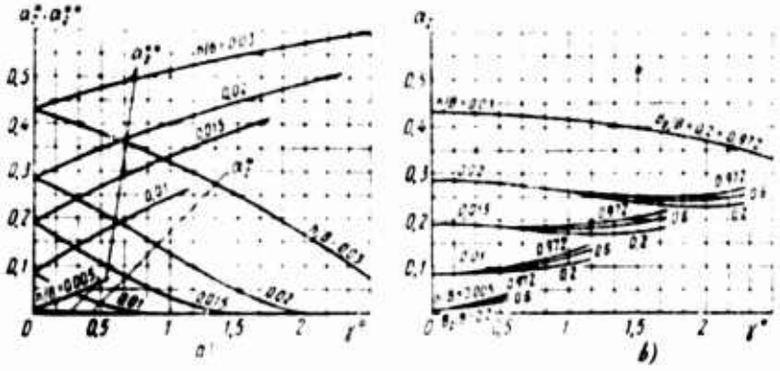

Fig. 160. Discharge coefficients of internal nozzles as functions of heeling angle of plane sectionalized nozzle installation for different elevations above support surface ($\varphi_2 = 45^0$):

a — when $B_2/B = 0.6$

b — when B_2/B = var

$$\alpha_1 = \frac{\alpha_1' + \alpha_1''}{2}.$$

Heeling of a plane nozzle installation, with its elevation from the support surface kept constant (h_p/B = const), leads to a reduction in the total discharge coefficient α_1 of the external nozzles. Fig. 160 shows the effect that the heeling angle γ has on the discharge coefficients α_2' and α_2'' and on the total discharge coefficient α_2 of the internal nozzles for the specified position in the nozzle installation ($B_p/B = 0.6$) and for different elevation h/B above the support surface. The coefficient α_2 is given with respect to the overall flow-through area of the internal nozzles and is determined by the formula

$$\alpha_2 = \frac{\alpha_2' + \alpha_2''}{2}.$$

In Fig. 160 we can see that, like the variation in the discharge coefficients α_1' and α_1'' of the external nozzles, the coefficient α_2' of the internal nozzle on the lowered side decreases most, while the coefficient α_2'' of the internal nozzle on the elevated side increases as the angle of heeling is made greater. The regularity in variation of the overall coefficient α_2 of the internal nozzles as a function of angle γ differs from the pattern of variation of the coefficient α_1 of the external nozzles: with increasing angle γ, the coefficient α_2 decreases only for relatively large elevations h/B, while with small variations ($h/B < 0.015$), the coefficient α_2 increases as the angle γ is made larger.

This pattern of variation in the discharge coefficients α_1 and α_2 as a function of heeling angle γ is due to the varying influence of the support surface on compressing the air jets exiting from the external and internal nozzles. When the installation heels by some angle γ, the compressing action of the support surface on the air jet escaping from the external nozzle on the lowered side shows up to a greater extent than on the jet exiting from the internal nozzle on the same side, since the linear displacements of the exits of these nozzles are different: the external nozzle is closer to the support surface than the internal.

So the coefficient α_1' of the external nozzle on the lowered side decreases more abruptly with variation in the angle γ compared with the coefficient α_2' of the internal nozzle on the same side (cf. Figs. 159 and 160). At the same time, on the elevated side the external and internal nozzles are at relatively greater distance from the support surface, the compressing action of the surface on the air jets shows up less strongly, and the increments in the coefficients α_1'' and α_2'' vary little with

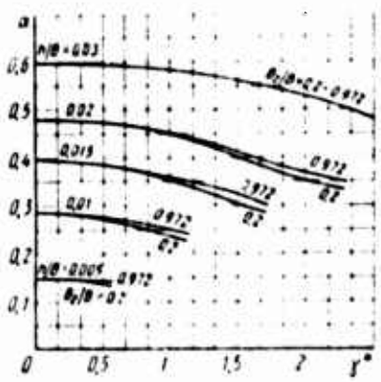

Fig. 161. Total discharge coefficient of plane sectionalized nozzle installation as functions of heeling angle for different elevations above support surface and different stability nozzle placement

change in angle γ. Fig. 160 also shows the effect of stability nozzle position, determined by parameter B_2/B, on the overall discharge coefficient α_2 of the internal nozzles.

The total discharge coefficient α of the nozzle installation as functions of heeling angle for different elevations and for different stability nozzle placements is shown in Fig. 161. As applied to this installation,

$$\alpha = \frac{1}{4}(\alpha_1' + \alpha_1'' + \alpha_2' + \alpha_2'').$$

As we can see, heeling of a plane sectionalized nozzle installation reduces the total discharge coefficient. For the same flow-through width of the external and internal nozzles ($b_1 = b_2$) and identical angles of inclination of their generatrices ($\varphi_1 = \varphi_2$), a variation in the placement of the internal nozzles in the nozzle installation, that is, in the parameter B_2/B, weakly affects the discharge coefficient α. Even in the case when the nozzle installation heels by the maximum angle γ_{max} [γ_{max} = maximum] at which one of the edges of the nozzle installation touches the support surface, the difference in the discharge coefficients α when the stability nozzles are displaced in the range from $B_2/B = 0.972$ to $B_2/B = 0.2$ does not exceed ~ 6 percent for all the elevations h/B considered.

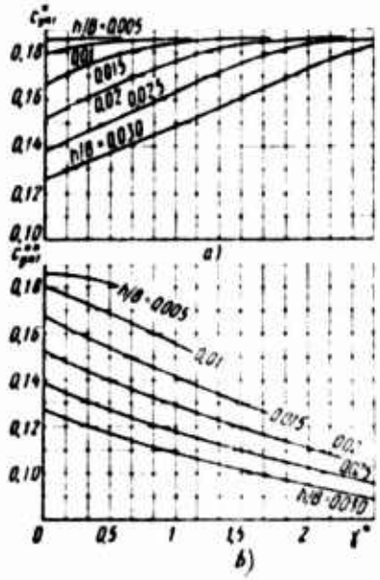

Fig. 10. Components of lift coefficient of air cushion acting at the external bottom sections as functions of the heeling angle of the plane sectionalized nozzle installation ($B_2/B = 0.6$):

a -- for lowered nozzle
b -- for elevated nozzle

Lift coefficients. The heeling angle γ of a plane sectionalized nozzle installation affects the components of the lift coefficient due to reaction forces of air jets exiting from the external nozzles. Analysis shows that a rise in the angle γ reduces the components $c^{*}_{yp\ 1}$ and increases the component $c^{**}_{yp\ 1}$ of the lift in all the elevations h/B of interest. This is because with increase in the heeling of the nozzle installation the support surface exerts a varying compressive action on the air jets exiting from the lowered and elevated external nozzles. As the result, the volume flow of air in the nozzles on the lowered side becomes less, while it increases in the nozzles on the elevated side, reflected in a change in the momentum of the jets and the reaction forces they produce.

For a nozzle on the lowered side, a rise in the angle γ increases the components $c^{*}_{yc\ 1}$, while it reduces the component $c^{**}_{yc\ 1}$ -- for a nozzle on the elevated side. This pattern of variation in these coefficients results from the aerodynamic effect that ground proximity exerts, evidenced in a rise in the excess pressure forces in the nozzle cut-off plane as the distance between the nozzle and the support surface is reduced.

With increase in the angle γ, coefficient $c^{*}_{ypc\,1}$ for the external nozzle on the lowered side initially is reduced, and then reaches its minimum, and further increases, while the coefficient $c^{**}_{ypc\,1}$ for the external nozzle on the elevated side increases throughout the entire range of angles γ. This pattern of variation in the coefficients $c^{*}_{ypc\,1}$ and $c^{**}_{ypc\,1}$ is due to the different values of the increments in the pressure forces and in the jet reaction forces when they are linear and angular displacements of the external nozzles under the effect of variation in the angle γ.

Heeling of the nozzle installation has practically no effect on the coefficient $c^{*}_{ypc\,2}$. The coefficient $c^{**}_{ypc\,2}$ increases somewhat as the angle of heeling becomes greater.

Functions of the coefficients $c^{*}_{yp\,1}$ and $c^{**}_{yp\,1}$ of the lift reduced by the excess air cushion pressure over the bottom sections lying between the external and internal nozzles are shown in Fig. 162. These functions were calculated by Eqs. (250) and (248) for one of the stability nozzle positions ($B_2/B = 0.6$). The lift coefficients $c^{*}_{yn\,1}$ and $c^{**}_{yn\,1}$ are mainly predetermined by the air cushion pressure coefficients $\bar{p}^{*}_{1}$ and $\bar{p}^{**}_{1}$, therefore even the pattern of variation in the lift coefficients as a function of angle γ and elevation h/B remains approximately the same as for the air cushion pressure coefficients: with increase in the angle γ, the coefficient $c^{*}_{yn\,1}$ rises, while the coefficient $c^{**}_{yn\,1}$ decreases h/B for all the elevations considered.

The pressure coefficients $\bar{p}$ appearing in Eq. (254), under the adopted assumption that the air cushion pressure is independent of the heeling angle for bottom sections bounded by the internal nozzles, was calculated based on the average elevation h/B, therefore the coefficient $c_{yn\,2}$ also is independent of the heeling angle and is determined only by this elevation. As shown by calculations, taking account of the variation in the pressure coefficients $\bar{p}^{*}_{2}$ and $\bar{p}^{**}_{2}$ as a function of the angle γ introduces practically no changes in the end results of determining the total coefficients $c_{yn\,2}$: the difference in the coefficients does not exceed ~ 2 percent of $c_{yn\,2}$ determined with reference to variation in the angle γ.

The lift components acting at the nozzle cut-offs and over the external and internal sections of the nozzle installation bottom as functions of the heeling angle for a specified stability nozzle position ($B_2/B = 0.6$) and different elevations h/B of the nozzle installation above the support surface are shown in Fig. 163. These coefficients were determined by the formulas

$$c_{ypc\,1} = c^{\cdot}_{ypc\,1} + c^{\cdot\cdot}_{ypc\,1};\quad c_{ypc\,2} = c^{\cdot}_{ypc\,2} + c^{\cdot\cdot}_{ypc\,2};\quad c_{yn\,1} = c^{\cdot}_{yn\,1} + c^{\cdot\cdot}_{yn\,1}.$$

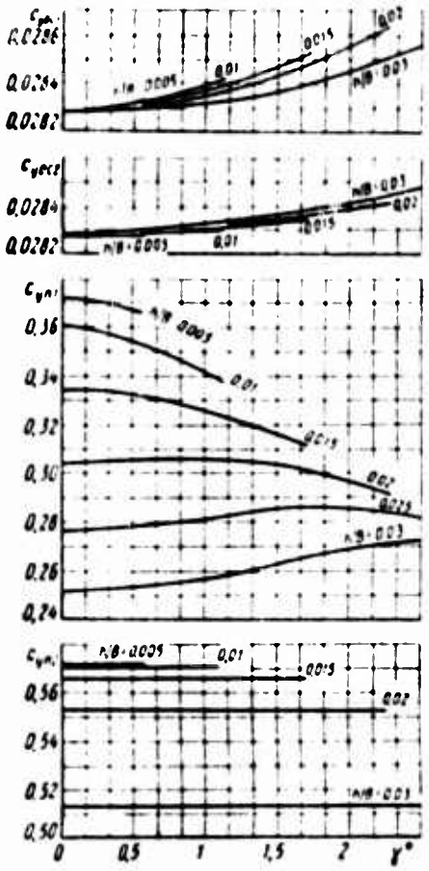

Fig. 163. Lift coefficient components as functions of the heeling angle of the plane sectionalized nozzle installation for different elevations above the support surface ($B_2/B = 0.6$)

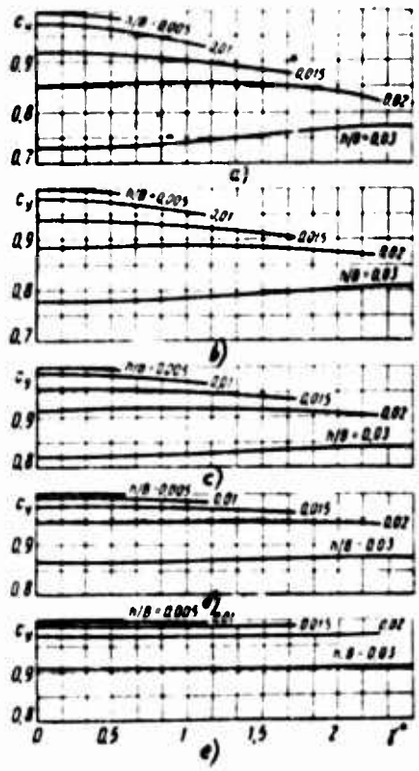

Fig. 164. Lift coefficient of heeling angle of plane sectionalized nozzle installation for different elevations above the support surface and for different stability nozzle placement:

a -- $B_2/B = 0.2$

b -- $B_2/B = 0.4$

c -- $B_2/B = 0.6$

d -- $B_2/B = 0.8$

e -- $B_2/B = 0.972$

In Fig. 163 we can see that heeling of the nozzle installation increases the lift coefficients $c_{ypc\ 1}$ and $c_{ypc\ 2}$ acting at the cut-offs of both the external and the internal nozzles. The smallest value of these coefficients occurs when the nozzle installation is horizontal ($\gamma = 0$) for all its elevations above the ground surface in the range covered. This is due to the fact that as the angle γ is increased, the resultant of the pressure forces and the jet reactions acting at one of the nozzle cross-sections always makes up for the decrease in the resultant force acting at the nozzle cut-off on the opposite side.

In this same graph we can see the effect that the heeling angle has on the lift coefficients $c_{yn\ 1}$ acting over the bottom sections lying between the external and internal nozzles. For small elevations h/B heeling of the nozzle installation leads to a decrease in the coefficient $c^*_{yn\ 1}$. For an elevation h/B = 0.2, a variation in the angle γ relatively weakly affects the coefficients $c_{yn\ 1}$. For relatively large elevations ($h/B \approx 0.3$), heeling of the nozzle installation leads to an increase in the lift. This pattern of variation in the function $c_{yn\ 1} = f(\gamma, h/B)$ is governed by the pattern of variation in the coefficients $\bar{p}_1^*$ and $\bar{p}_1^{**}$ of the air cushion produced by the external nozzles: with increase in the heeling angle γ for small elevations, the coefficient $\bar{p}_1^{**}$ decreases faster for the elevated side than the coefficient $\bar{p}_1^*$ on the lowered side decreases, while for large elevations, conversely, the coefficient $\bar{p}_1^{**}$ decreases more slowly than the coefficient $\bar{p}_1^*$ increases.

Results of determining the dependence of the total lift coefficient c_y of a plane sectionalized nozzle installation on the heeling angle γ for different stability nozzle placements B_c/B and different elevations h/B above the support surface are shown in Fig. 164.

As we can see, when the nozzle installation is horizontal ($\gamma = 0$), we have extremal values of the lift coefficient. For small elevations and for the horizontal position of the nozzle installation, a lift maximum is observed. Heeling of the nozzle installation at these elevations leads to a marked drop in the lift. At relatively large elevations h/B, conversely, the smallest value of the coefficient c_y occurs when the angle $\gamma = 0$. In this case heeling of the nozzle installation is accompanied by an increase in the coefficient c_y, that is, by an increase in the lift.

Coefficients of moments. The moment coefficient $m_{xpc\ 1}$ caused by the pressure forces at the cut-offs of the external nozzles and the air jet reactions as functions of heeling angle γ for a nozzle installation areshown in Fig. 165. These functions were calculated by Eq. (269).

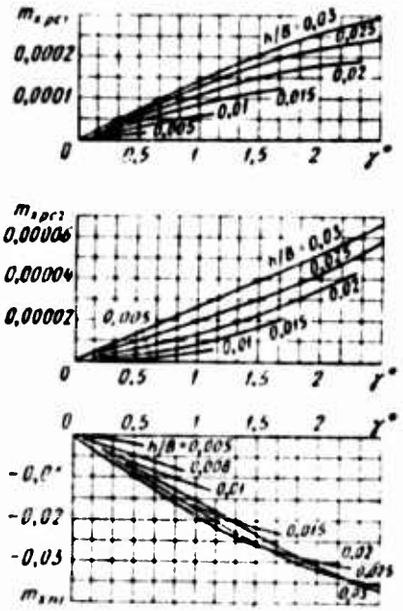

Fig. 165. Components of moment coefficient as functions of the heeling angle of the plane sectionalized nozzle installation ($B_2/B = 0.6$)

From the graph we see that heeling of the nozzle installation caused a tipping moment and one that is the larger, the greater the elevation h/B, though of itself the value of this moment is very slight. The appearance of the tipping (positive) moment is caused by the fact that as the angle γ is increased the lift of the external nozzle on the lowered side becomes less, while the lift of the external nozzle on the elevated side becomes greater. This effect results from the action of the air jet reaction, which is the greater, the farther the nozzle is from the support surface.

Fig. 165 presents in graphical form also the results of calculations based on Eq. (270) of the moment coefficient $m_{xpc\ 2}$ as functions of heeling angle γ. As we can see, heeling of the nozzle installation causes a tipping moment to be induced for all the stability nozzle placements B_2/B and all elevations h/B of the nozzle installation above the support surface considered. Shifting the stability nozzles in the direction toward the external nozzles, that is, increasing the parameter B_2/B, leads to a rise in the coefficient of tipping moment $m_{xpc\ 2}$. The largest value of the coefficient $m_{xpc\ 2}$ is reached when $B_2/B = 0.972$, when the stability nozzles directly abut the external nozzles. The value of the coefficient

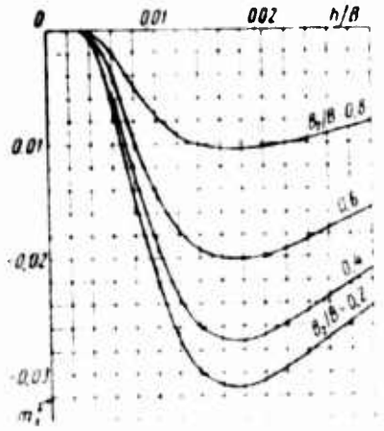

Fig. 166. Coefficient of transverse static stability of a plane sectionalized nozzle installation as functions of the elevation above the support surface for different stability nozzle placement ($b_1/B = b_2/B = 0.8$; $\varphi_1 = \varphi_2 = 45^\circ$; $\psi_1 = \psi_2 = 45^\circ$; $\gamma_\delta = 0$)

$m_{xpc\,2}$ is very small: it is approximately one order of magnitude smaller than the coefficient $m_{xpc\,1}$ for the external nozzles.

The moment coefficient m_{xn}, as functions of the angle γ, calculated by eq. (3.71), is also given in Fig. 166, from whence we can see that heeling of the nozzle installation causes a restoring (negative) moment, induced by the excess air cushion pressure over the bottom sections bounded by the external nozzles and the stability nozzles. At the distance between the stability nozzles and the external nozzles is increased, that is, with decrease in the parameter b_1/B, the coefficient of the restoring moment $m_{xn\,1}$ rises.

The coefficient of the nozzle installation moment $m_x = m_{xpc\,1} + m_{xpc\,2} + m_{xn}$. By separating the factors $m_{xpc\,1} = f_1(\gamma)$, $m_{xpc\,2} = f_2(\gamma)$, $m_{xn\,1} = f_3(\gamma)$, we can see that the coefficients $m_{xpc\,1}$ and $m_{xpc\,2}$ taken together are two-three orders smaller than the values of the moment coefficient $m_{xn\,1}$ for the entire range of variation in the heeling angles ($\gamma = 0$-$2^\circ 30'$) and stability nozzle placements ($b_1/b = 0.2$-0.8). For example, for the case $h/B = 0.5$ when $\gamma = 2^\circ 30'$ and $b_1 = 0.8$, the ratio of these coefficients is

$$\frac{m_{xc1} + m_{xn2}}{m_{xn1}} = \frac{0{,}000295 + 0{,}000092}{0{,}0192} \approx 0{,}02,$$

that is, the sum of the moments induced by the outflow of jets from the external and internal nozzles does not exceed ~2 percent of the coefficient of the moment induced by the action of the air cushion over the bottom sections enclosed between these nozzles. With decrease in both the angle γ as well as parameter B_y/B, this ratio of the moment coefficients decreases the faster.

Therefore, we can neglect the moments induced by the pressure forces at the cut-offs of the external and internal nozzles, as also induced by the reactions of air jets outflowing from these nozzles. And we can assume that the moment acting at the nozzle installation as a whole is equal to the moment induced by the action of the air cushion over the bottom sections enclosed between the external and internal nozzles, that is, $m_y = m_{xn\,1}$.

Coefficients of transverse static stability. Fig. 156 presents the coefficient m_x of the static stability of a plane sectionalized nozzle installation as a function of its elevation h/B above the support surface, for different stability nozzle placements b_y/B in the nozzle installation for the case when the craft is horizontal ($\gamma_\delta = 0$). These functions were determined by Eq. (281) and are given with respect to $\bar{p}_H$.

Therefore, at the moment the craft lifts from the support surface and at very slight elevations the craft is practically neutral. This is because that very small elevations ($h/B < 0.03$), heeling of the craft by some angle $\Delta\gamma$ yields practically no increment in the moment coefficient Δm_x, since for these elevations the air cushion pressure coefficient for the external nozzle on the lowered side ($\bar{p}_1^*$) as well as for the external nozzle on the elevated side ($\bar{p}_1^{**}$) determining the moment coefficient m_x are practically identical ($\bar{p}_1^* \approx \bar{p}_1^{**} \approx$) and their difference is close to zero (cf. Fig. 157).

Beginning at the elevations $h/B \approx 0.002$–0.005, static stability increases rapidly with increase in h/B and at some elevation reaches its maximum, and then gradually decreases as elevation h/B is increased. We note that the optimal elevation $(h/B)_{crit}$ of the craft at which the coefficient m_x takes on the smallest value is independent of the stability nozzle placement in the nozzle installation determined by the parameter

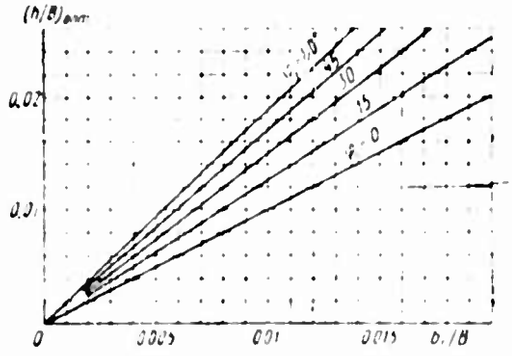

Fig. 167. Optimal (based on the conditions of the greatest static stability) elevation of nozzle installation as functions of flow-through width of external nozzles for different angles of nozzle inclination ($\gamma_\delta = 0$)

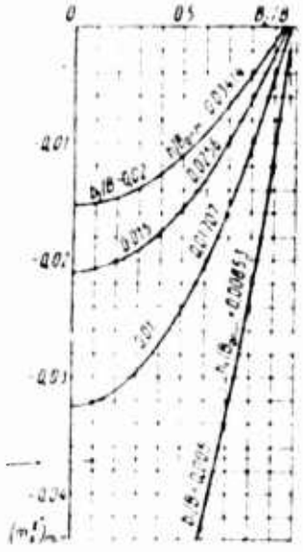

Fig. 168. Minimum coefficient of transverse static stability as functions of stability nozzle placement for different flow-through width of external nozzle ($\varphi_1 = \varphi_2 = 45^\circ$; $\psi_1 = \psi_2 = 45^\circ$; $\gamma_\delta = 0$)

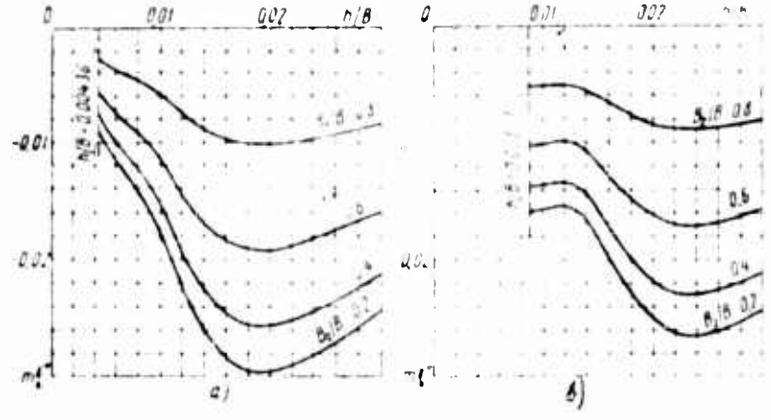

Fig. 169. Coefficient of transverse static stability of plane sectionalized nozzle installation as functions of elevation above support surface for different stability nozzle placement ($b_1/B = b_2/B = 0.01$; $\varphi_1 = \varphi_2 = 45^\circ$; $\psi_1 = \psi_2 = 45^\circ$):

a -- when $\gamma_\delta = 30^\circ$
b -- when $\gamma_\delta = 10^\circ$

B_2/B and is a function only of the flow-through width of the external nozzles and their angle of inclination φ_1.

For this position of the craft relative to the support surface ($\gamma_\delta = 0$), this optimal elevation can be found by Eq. (283), and the minimum coefficient of transverse static stability corresponding to this elevation can be found by Eq. (286).

The optimal elevation $(h/B)_{опт}$ of a craft when it is horizontal, with respect to the support surface is calculated as a function of the relative flow-through width b_1/B of a nozzle for different angles of generatrix inclination φ_1 by Eq. (283) and is presented in Fig. 167. The pattern of variation in minimum values of the coefficient of transverse static stability $(m_x^{\gamma^\circ})_{min}$, as a function of the stability nozzle placement B_2/B for different flow-through width $(b_1/B)_{опт}$ of nozzles and for a constant angle of inclination $\varphi = 45^\circ$ is clear from an inspection of the curves in Fig. 168, plotted by Eq. (286).

The placement of the stability nozzles (cf. Figs. 166 and 168) strongly affects the static stability of a craft. As the parameter B_2/B is varied from 0.8 to 0.6, the coefficient $m_x^{\gamma^\circ}$ increases nearly by a factor of two. The closer the stability nozzles lie to the diametral plane of the craft, the greater stability an air cushion vehicle exhibits. However, a decrease in the parameter B_2/B leads to a reduction in the craft lift.

Fig. 169 a and b present the functions of the coefficient $m_x^{\gamma^\circ}$ of the transverse static stability of a nozzle installation (balanced at heeling angles $\gamma_\delta = 30'$ and 1°), calculated by Eqs. (275), (276), and (277) - (280). In the same figure a dashed line shows the maximum elevation $h/B = (\sin \gamma_\delta)/2$ for which the nozzle installation touches the support surface with an edge of an external nozzle for a specified balancing angle.

As we can see, as the balancing angle is increased, the static stability craft becomes less, and the optimal relative elevation $(h/B)_{опт}$ at which the static stability is the greatest in this case rises somewhat.

In the zone of elevations (h/B) above the support surface of practical interest, the static stability of the sectionalized nozzle installation increases with decrease in the flow-through width (b_1/B) of the contour nozzle for unchanged elevation (h/B). The pattern of the change in this function is graphically shown in Fig. 170 for a nozzle installation balanced in the horizontal position ($\gamma_\delta = 0$), where the family of curves $m_x^{\gamma^\circ} = f(b_1/B, h/B, \varphi_1)$ is plotted by Eq. (281) for the case $\varphi_1 = 45^\circ$,

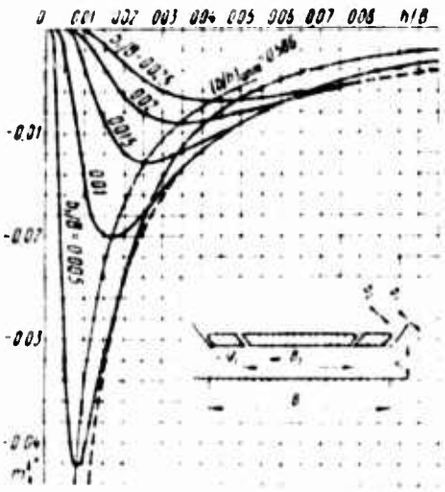

Fig. 170. Coefficient of transverse static stability as functions of elevation of a plane sectionalized nozzle installation for different flow-through widths of external nozzle ($\varphi_1 = 45^\circ$; $B_2/B = 0.6$; the envelope is indicated with a dashed line)

$B_2/B = 0.6$ and different flow-through widths of the contoured nozzle ($b_1/B = 0.005 - 0.025$).

With unchanged relative elevation of the nozzle installation above the support surface ($h/B = 0.02$), a decrease in the flow-through width of the nozzle from $b_1/B = 0.02$ to $b_1/B = 0.01$, that is, by a factor of two, reduces the coefficient of transverse static stability from $m_x^{\gamma^\circ} = -0.0064$ to $m_x^{\gamma^\circ} = -0.0198$, that is, by more than a factor of three. This pattern of variation in the coefficient $m_x^{\gamma^\circ}$ is a direct consequence of determining the coefficient of transverse static stability, which is $\lim_{\gamma \to 0} \frac{\Delta m_x}{\Delta \gamma}$, given for a heeling angle of 1°.

Let us explain this situation. Heeling of nozzle installation differing only in the flow-through width of a contour nozzle (b_M and b_6) for identical elevation ($h = \text{const}$) by some angle $\Delta\gamma$, for example, by 1°, yields identical vertical displacements h^* and h^{**} of the exit edge of the nozzles relative to the support surface (Fig. 171). For this example, we have

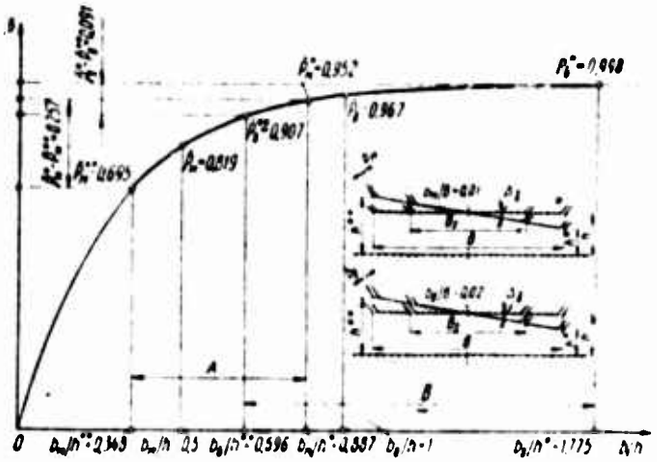

Fig. 171. For determining the coefficients of transverse static stability of nozzle installations with small and large flow-through widths of contour nozzle:

a -- range of variation in parameter b/h when the angle of heeling 1° applies to a small nozzle

b -- as above, for a large nozzle

$$\frac{h^*}{B} = \frac{h}{B} - \frac{\text{tg}\,1^\circ}{2} = 0{,}02 - \frac{0{,}01746}{2} = 0{,}01127$$

and

$$\frac{h^{**}}{B} = \frac{h}{B} - \frac{\text{tg}\,1^\circ}{2} = 0{,}02 - \frac{0{,}01746}{2} = 0{,}02874$$

Here the parameters b/h* and b/h** will have smaller values for a nozzle installation with small flow-through nozzle width than for a nozzle installation with large width. Thus, for a nozzle installation with small flow-through width

$$\frac{b_м}{h} = \frac{b_м/B}{h/B} = \frac{0{,}01}{0{,}02} = 0{,}5;$$

$$\frac{b_м}{h^*} = \frac{b_м/B}{h^*/B} = \frac{0{,}01}{0{,}01127} = 0{,}887$$

and

$$\frac{b_н}{h^{**}} = \frac{b_н/B}{h^{**}/B} = \frac{0{,}01}{0{,}02873} = 0{,}348.$$

For a nozzle installation with large flow-through width, we have

$$\frac{b_б}{h} = \frac{b_б/B}{h/B} = \frac{0{,}02}{0{,}02} = 1;$$

$$\frac{b_б}{h^*} = \frac{b_б/B}{h^*/B} = \frac{0{,}02}{0{,}01127} = 1{,}775$$

and

$$\frac{b_б}{h^{**}} = \frac{b_б/B}{h^{**}/B} = \frac{0{,}02}{0{,}02873} = 0{,}696.$$

The air cushion pressure and the coefficient $\bar{p}$ are determined by the parameter b/h. Therefore, for a nozzle installation with small nozzle flow-through width, the difference in the pressure coefficients $\bar{p}^* - \bar{p}^{**}$ for the lowered and elevated sides will be greater than for a nozzle installation with large flow-through width. The coefficient of the moment acting in the air cushion is found by Eq. (272) as a direct function of the difference $\bar{p}^* - \bar{p}^{**}$, therefore the coefficient of transverse static stability for a nozzle installation with small flow-through width will also be greater.

Actually, for a nozzle installation with small nozzle flow-through width ($b_н/B = 0.01$), the coefficient is

$$m_x^{\gamma^\circ} \approx \frac{\Delta m_x}{\Delta\gamma} = -\frac{A(\bar{p}_н^* - \bar{p}_н^{**})}{1^\circ} = -\frac{0{,}073 \cdot 0{,}257}{1^\circ} = -0{,}0188,$$

where

$$A = \frac{1}{8}\left[\left(1 - 2\frac{b_н}{B}\cdot\frac{1}{\cos\varphi}\right)^2 - \left(\frac{B_1}{B}\right)^2\right] =$$

$$= \frac{1}{8}\left[\left(1 - \frac{2\cdot 0{,}01}{\cos 45}\right)^2 - 0{,}6^2\right] = 0{,}073.$$

For a nozzle installation with large ($b_б/B = 0.02$) nozzle flow-through width, the coefficient is

$$m_z^{\gamma} \approx \frac{\Delta m_z}{\Delta\gamma} = -\frac{A(\bar{p}_0^{\cdot} - \bar{p}_0^{\cdot\cdot})}{1^{\circ}} = -\frac{0{,}0663 \cdot 0{,}091}{1^{\circ}} = -0{,}00603,$$

where

$$A = \frac{1}{8}\left[\left(1 - 2\frac{b_0}{B}\cdot\frac{1}{\cos q}\right)^2 - \left(\frac{B_2}{B}\right)^2\right] =$$

$$= \frac{1}{8}\left[\left(1 - \frac{2 \cdot 0{,}02}{\cos 45}\right)^2 - 0{,}6^2\right] = 0{,}0663.$$

The coefficient A is the product of the area of the bottom section enclosed between the contour nozzle and the stability nozzle, by the arm that is equal to the distance from the center of this bottom section to the longitudinal axis of the nozzle installation.

In other words, when the nozzle installation heels from the horizontal ($\gamma_\delta = 0$) by some extremely small angle ($\Delta\gamma \to 0$), the pattern of air outflow from the contour nozzle onto the shield varies dissimilarly for nozzles with different flow-through widths. Also changing to differing degrees are the forces acting in the air cushion on the nozzle installation, since different values of the parameter b/h, determining the air cushion pressure and ultimately the coefficient of transverse static stability, correspond to the same angular changes $\Delta\gamma$.

Corresponding to each elevation h/B is its optimal contour nozzle flow-through width $(b/B)_{opt}$ for which the coefficient of transverse static stability reaches a minimum. With decrease in the width b/B, the relatively optimal coefficient of static stability increases gradually, that is, the static stability deteriorates.

Let us find the envelope [illegible] curves $m_z^{\gamma} = f\left(\frac{b_1}{B}, \frac{h}{B}, \frac{B_2}{B}, q_1\right)$.

Expanding Eq. (.201) in powers of parameter b/B and neglecting the terms of second, third, and fourth degrees of smallness, let us write

$$m_z^{\gamma} \approx -\frac{1}{4\left(\frac{h}{B}\right)^2}\left(1 + \sin q_1 - 2\frac{h}{B}\cos q_1\right) \times$$

$$\times \left[1 - \left(\frac{B_2}{B}\right)^2\right]\frac{b_1}{B}\, e^{-2\frac{b_1}{h}\frac{h}{B}(1 + \sin q_1)}.$$

Taking the derivative of this function with respect to the variable parameter b_1/B and here assuming that all the remaining quantities are constant, we get

$$\frac{1}{4\left(\frac{h}{B}\right)^3}\left(1+\sin\varphi_1+2\,\frac{h}{B}\cos\varphi_1\right)\left[1-\left(\frac{B_2}{B}\right)^2\right]\times$$

$$\times\left[\frac{h}{B}-2\,\frac{b_1}{B}\,(1+\sin\varphi_1)\right]e^{-2\frac{b_1/B}{h/B}(1+\sin\varphi_1)}=0,$$

from whence

$$\left(\frac{b_1}{B}\right)_{opt}=\frac{h}{2(1+\sin\varphi_1)}. \tag{298}$$

The optimal flow-through width of the contour nozzle in a sectionalized nozzle installation at which the coefficient of transverse static stability takes on the smallest value for the specified elevation h/B and angle φ_1 of nozzle generatrix inclination is determined by this approximate expression.

Replacing in Eq. (281) the relative flow-through width b_1/B of the contour nozzle with its optimal value based on Eq. (298), we get the following for the unknown envelope:

$$m_1^{\gamma}=-\frac{A_0c_0}{4c}=-0{,}092A_0c_0, \tag{299}$$

where

$$A_0=\left(1-\frac{h/B}{(1+\sin\varphi)\cos\varphi}\right)^2-\left(\frac{B_2}{B}\right)^2;$$

$$c_0=\frac{4\cos^2\varphi}{4(1+\sin\varphi)\cos\varphi}+\frac{1}{2h/B}.$$

When the angle of inclination of the contour nozzle generatrix is 45°, Eq. (299) becomes

$$m_1^{\gamma}=-\frac{0{,}092}{57{,}3}\left(0{,}207+\frac{1}{2h/B}\right)\left[\left(1-0{,}83\,\frac{h}{B}\right)^2-\left(\frac{B_2}{B}\right)^2\right].$$

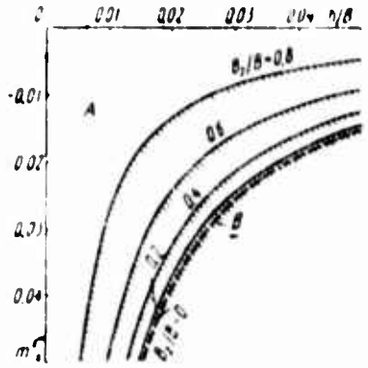

Fig. 171. Theoretical region of transverse static stability of a plane sectionalized nozzle installation as the function of internal nozzle placement ($\varphi_1 = 45^\circ$):

A -- theoretical region of static stability

B -- boundary to region of possible static stability

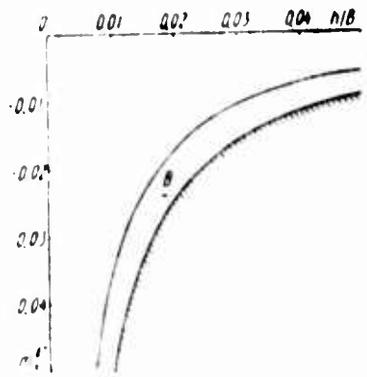

Fig. 172. Theoretical regions of transverse static stability of a plane sectionalized nozzle installation when $\varphi = 45^\circ$ and $B_2/B = 0.6$:

A -- region with increasing stability

B -- region of decreasing stability

The envelope plotted from this equation for a nozzle installation with a parameter $\varphi = 45^\circ$ and $B_2/B = 0.6$ as shown in Fig. 170 with a dashed line. The region bounded by the coordinate axes and the envelope calculated by Eq. (299) is the zone of theoretically possible static stability of a plane sectionalized nozzle installation. To each point lying within this zone there corresponds the values of ΔY and h/B, which can be attained by selecting a nozzle installation with a specific flow-through width b_1/B of the contour nozzle.

As the parameter B_2/B is reduced, that is, as the stability nozzles are brought closer to the longitudinal axis of the nozzle installation, and with the corresponding increase in the area of the bottom sections enclosed between the contour nozzle and these nozzles, the static stability zone is enlarged (Fig. 172). When the stability nozzles are brought closer, forming a single general nozzle with width $2b_2/B \cos\varphi_2$, and the jets exiting from this merging to a single central jet, the static stability zone becomes greatest. The boundary of this zone is conventionally indicated with a dashed curve B, calculated on the assumption that $B_2/B = 2b_2/B \times \cos\varphi = 0$.

Let us inspect the static stability zone of a sectionalized nozzle installation from another point of view. Let us plot in the coordinates h/B and m_x^{γ} the envelope calculated by Eq. (299), and also the curve of minimum values of the transverse static stability coefficient of a nozzle installation, each point of which characterizes the greatest static stability for the corresponding nozzle flow-through width b_1/B (Fig. 175). This curve plotted by Eq. (286) will divide the static stability zone. In one section adjoining the coordinate axes, the static stability of a nozzle installation with a specific b_1/b increases with increase in elevation h/B and becomes the greatest at the points lying on the curve. In the other section enclosed between the envelope and the curve of minimum m_x^{γ} values, the static stability falls off for a given b_1/B.

Since an air cushion vehicle must have a specific reserve of static stability, the section of the zone bounded by the coordinate axes and the curve of minimum m_x^{ζ} values in which, as noted earlier, the static stability increases with increase in elevation is of interest.

Actually, the static stability zone of a sectionalized nozzle installation will be even further restricted compared with the theoretical value shown in Fig. 175. This reduction in the stability zone will depend on the design of the nozzle installation, the method of supplying air to it, the degree of uniformity of air supply both along the perimeter of the contour nozzle, as well as the stability nozzles, and many other aerodynamic and design conditions. The dimensions of the practical stability zone can be revised as the result of experimental studies.

54. Experimental Determination of Characteristics of Static Stability of a Sectionalized Nozzle Installation

To verify the main regularities expressing the static stability of a sectionalized nozzle installation, a schematic operating air cushion vehicle model was tested. The characteristics were recorded on a special stand equipped with six-component aerodynamic balances and a movable shield. These balances were used to measure the forces and moments induced by the air cushion. Variation in the hovering elevation of the model above the shield and its heeling angle in the required ranges was provided with the movable shield, which models the support surface and is 5000 x 6000 mm in size.

An operating model (Figs. 174 and 176), 2200 mm in length, 1600 mm wide, and 740 mm high, consisted of a platform 1, a housing mounted on it 3, forming in conjunction with the platform a receiver 2, axial fan 5 with a rectifying device 6, high-frequency electric motor 7, inlet header 4, and radial-annular diffusor 8.

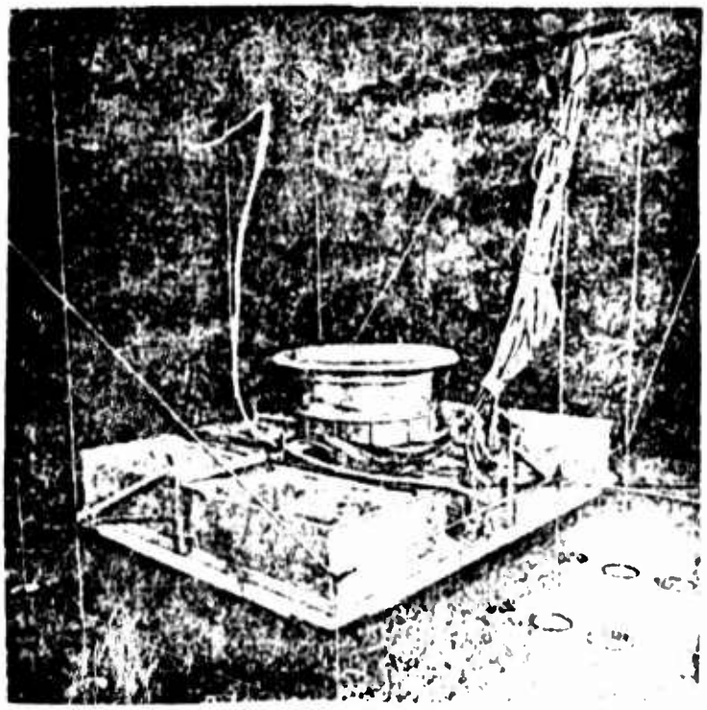

Fig. 174. Model of an air cushion vessel with [illegible] in the tank.

The platform was a [illegible] made in the form of a contour nozzle [illegible] expanding the platform along its perimeter and two internal nozzles -- stability nozzles 9. The distance between the exit edges of the external walls of the stability nozzles was 840 mm, that is, 60 percent of the width of the nozzle installation measured with respect to the external [illegible] of the contour nozzle. The side sections of the contour nozzle [illegible] with b_1 = 50 mm, while the bow and stern sections had a flow-through width b_2 = 60 mm. The flow-through width of the stability nozzles was b_3 = 40 mm. All nozzles had an inclination angle $\varphi = 45^\circ$.

A model UK-2M axial fan from the TsAPI [Central Aero-Hydrodynamic Institute] was mounted on the model. The impeller had a diameter of 615 mm, with a 276 mm hub, fitted with eight profiled blades. The fan fan seated on the shaft of a 9-kw electric motor. The angular speed of the fan was varied smoothly within the limits from 0 to n = 2800 rpm.

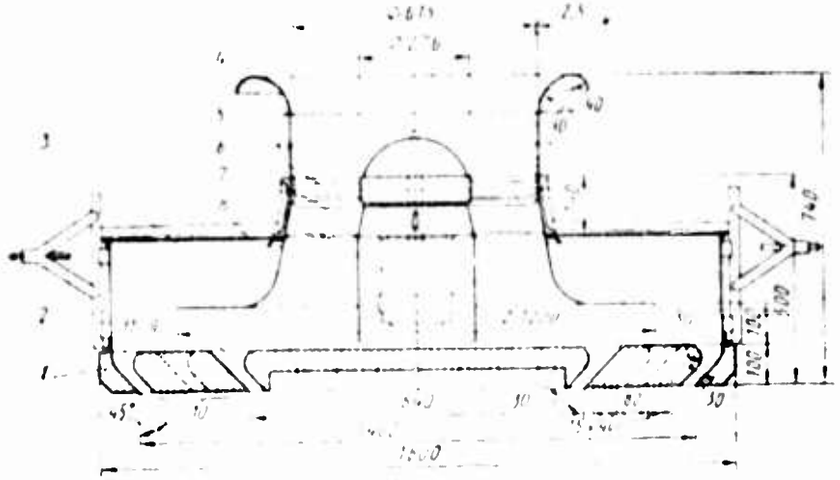

Fig. 1/6. Schematic air cushion vehicle with sectionalized nozzle installation:

1 -- platform
2 -- receiver
3 -- housing
4 -- header
5 -- fan
6 -- rectifying device
7 -- electric motor
8 -- diffuser
9 -- stability nozzle
10 -- drainage openings
11 -- external nozzle

The header provided smooth inlet of the air into the fan and simultaneously served as a device for measuring the volume flow of air passing through the model. The diffuser recovered part of the kinetic energy of the air stream exiting from the fan, converting it into static pressure and feeding air in radial directions.

To find the pattern of pressure distribution over the undersurface of the platform in the air cushion, [illegible] tubes with 1 mm diameter receiver openings, arranged in a longitudinal and two transverse sections (Fig. 1/6), were mounted in the [illegible]. The total pressure in the stream of air entering the receiver was determined with total pressure tubes installed in the exit of the radial-annular diffusor. Four tubes with 1 mm diameter heads connected to a common hose were installed for the measurements. In addition, the pressure on the inner surface of the receiver was measured.

The volume flow of air was measured based on the pressure in the header measured at four drainage openings of its connecting piece. The discharge coefficient of this header was determined by calibration with the fan operating.

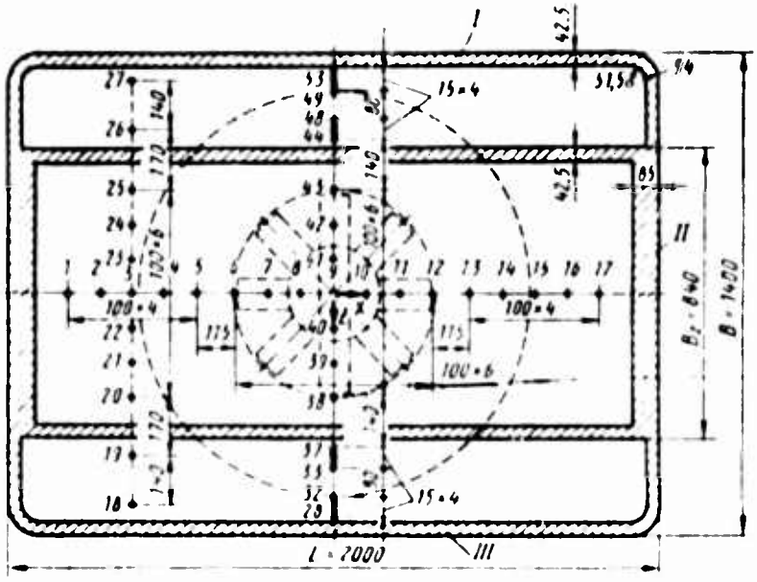

Fig. 176. Layout of drainage openings at model under surface:
1 - 55 -- drainage openings;
I -- left side;
II -- bow;
III -- right side

The housing of the model was made of duralumin, and the nozzle installation was made of foam plastic coated with veneer. The flow-through section of the nozzles was made of wood and was polished.

Results of measuring the pressure distribution along the bottom of the nozzle installation for the case when the nozzle was horizontal with respect to the support surface ($\gamma = 0$), for different relative elevations h/B, are shown in Fig. 177, where the pressure coefficients $\bar{p}$ are plotted along the Y axis, that is, the ratio of the excess pressure at a particular point in the surface of the bottom to the total pressure of the air stream in the receiver, and along the X axis is plotted the relative distance x/L for the longitudinal section, and the relative distance z/B for the transverse section (x and z are the coordinates of the particular point; L and B are the length and width of the nozzle installation, respectively).

For the elevation of the nozzle above the shield measured within the limits h/B = 0-0.0286, the pressure was distributed virtually uniformly both over the internal as well as the external sections of the nozzle installation bottom and reached a maximum ($\bar{p} = 0.99$), when the model rested on the shield (h/B = 0). At relatively greater elevations, the uniformity of pressure distribution deteriorates, and does so especially noticeably over the external bottom sections adjoining the corners of the model.

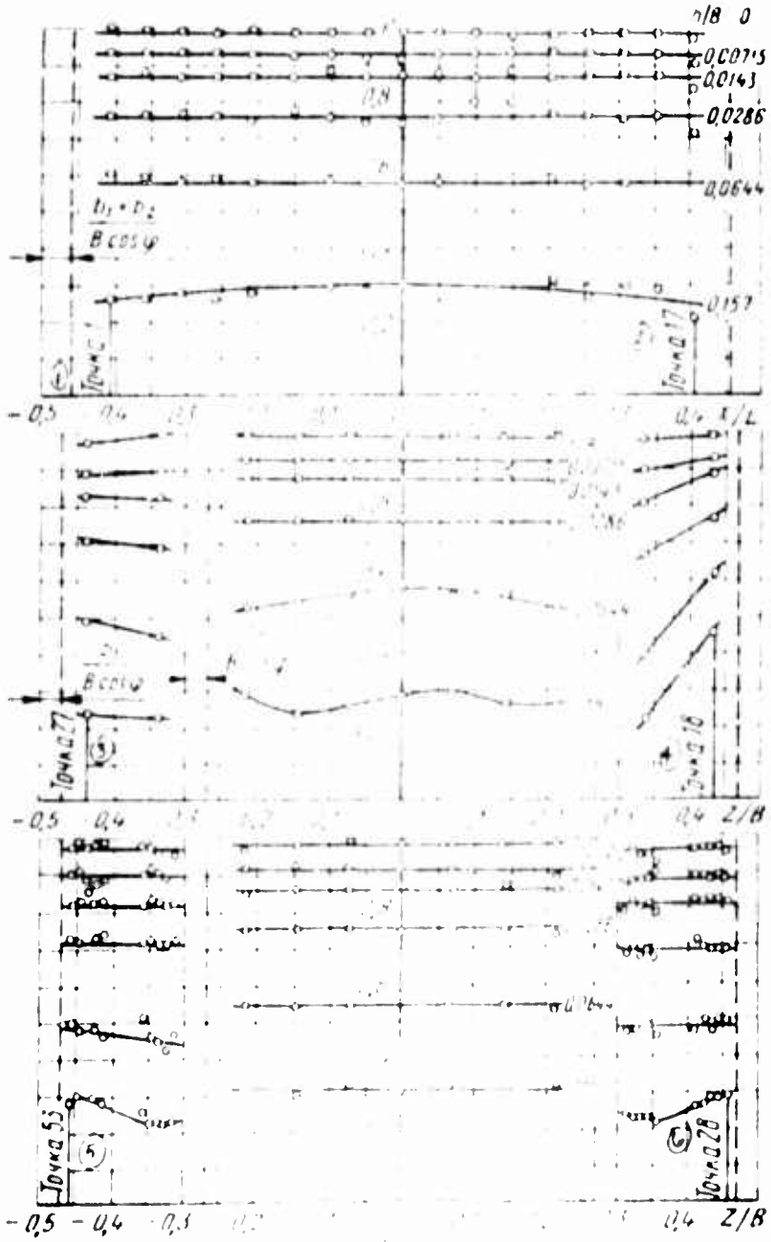

Fig. 177. Pressure [illegible] location of the nozzle installation [illegible] elevation when $b_1/B = b_2/B = \ldots$; $\varphi = \ldots$; $\gamma = 0$

KEY: 1 -- Point [illegible] -- [illegible]
[illegible] -- Point [illegible] -- [illegible]
3 -- Point [illegible] -- [illegible]

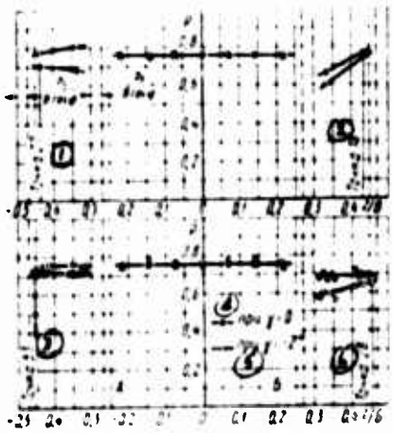

Fig. 178. Pressure distribution along the bottom of the nozzle installation as functions of the heeling angle for $b_1/B = b_2/B = 0.0214$; $B_2/B = 0.6$; $\varphi = 45^0$; $h/B = 0.0286$:

A -- for lowered side
B -- for elevated side
KEY: 1 -- Point 1
2 -- Point 18
3 -- Point 53
4 -- When $\gamma = 0$
5 -- When $\gamma = -2^0$
6 -- Point 28

The effect of model heeling on the pressure distribution over the bottom in the transverse section, with the elevation kept unchanged $h/B = 0.0286$, can be seen in Fig. 178. Measurements show that increasing the heeling angle from $\gamma = 0$ to $\gamma = 2^0$ has practically no effect on the pressure in the middle of the bottom bounded by the stability nozzles. At the same time, the pressure rises over the external bottom sections, on the lowered side, while it becomes less on the elevated side. This causes a restoring moment to appear, acting on the model from the air cushion.

Measurement of the transverse moment induced in the air cushion when the model heels was made with the elevation above the shield varied from $h = 10$ mm to $h = 220$ mm, that is, in the range $h/B = 0.00715 - 0.157$. The transverse moment coefficient was calculated by the formula

$$m_x = \frac{M_x}{BSH_c},$$

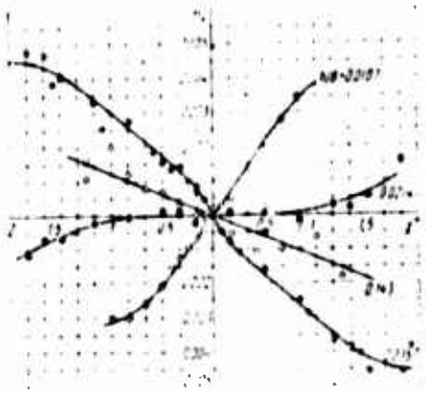

Fig. 179. Moment coefficient as functions of the heeling angle for different relative elevation of craft with sectionalized nozzle installation

where M_x is the transverse moment measured on aerodynamic balances; B is the width of the model nozzle installation measured with respect to the exit edges of the contour nozzle outer walls; S is the area of the nozzle installation measured with respect to the exit edges of the contour nozzle outer walls; and H_c is the total pressure of the air stream arriving at the receiver.

As an example, Fig. 179 presents the results of an experimental determination of the dependence of the heeling moment coefficient m_x on the angle γ for four characteristic elevations of the model above the shield: $h/B = 0.0107$ is the unstable model position; $h/B = 0.0214$ is the model in the neutral position; $h/B = 0.0557$ is the highest static stability; and $h/B = 0.145$ is weak static stability.

For small and moderate elevations ($h/B = 0.06$), the readings on the aerodynamic balances measuring the transverse moment for stable width time. This gave a well-defined regularity of the variation in the moment M_x as a function of elevation h/B and heeling angle γ. With further increase in the elevation, noticeable fluctuations were observed in the measured moment from the mean, and the scatter of the experimental points correspondingly became greater. At relatively large elevations ($h/B \geq 0.1$), these fluctuations became appreciable, and the balances gave readings variable in sign, corresponding to transitions from a negative moment to positive moment and back again, that is, from the stable model state to the unstable. The hovering regime of the model at these elevations must be regarded as in practice unstable, since in this case an air cushion

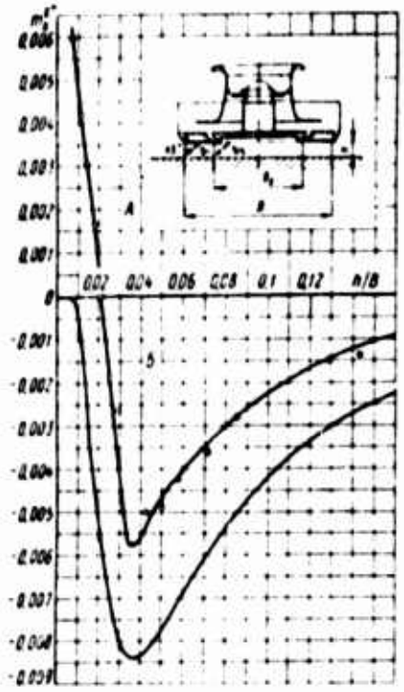

Fig. 180. Coefficient of transverse static stability of model of air cushion vehicle as functions of relative elevation above support surface ($\gamma_f = 0$; $b_1/B = b_2/B = 0.0214$; $\varphi_1 = \varphi_2 = 45^0$; $B_2/B = 0.6$):
A -- region of unstable operation
B -- region of stable operation

vehicle in the free hovering regime would touch the support surface with its side. A similar pattern of variation in the readings with increasing elevation occurred also for alcohol micromanometers used to measure the air cushion pressure.

These effects are accounted for by the fact that at relatively high elevations of the model above the shield the air jets exiting from the contour nozzle and the stability nozzle located on the elevated side, without yet reaching the shield, merging to a single, jet. The pressure over the bottom section enclosed between these jets becomes nonuniform and pulsating, while the outflow of jets as a whole from the nozzle installation is unstable with time.

Based on experimental functions $m_x = f(\gamma)$ for different elevations, similar to those presented in Fig. 179, the coefficients $m_x^{\gamma'}$ of transverse static stability for a model balanced in the horizontal position ($\gamma_f = 0$)

were found. Fig. 180 presents the theoretical and experimental curves characterizing the variation in the coefficient $m_x^{\gamma^\circ}$ of static stability as a function of relative elevation of the model above the support surface.

At the moment of liftoff from the support surface and at lower elevations (h/B = 0-0.02), a vehicle with sectionalized nozzle installation is unstable. With increase in elevation h/B, the degree of static stability rises rapidly, and when h/B = 0.03 - 0.04 it reaches its maximum, but with further increase in elevation it gradually decreases.

A similar pattern of variation in the coefficient of static stability as a function of elevation was found by Frost [85] in testing a round model of air cushion vehicle with central stability nozzle placement. For this kind of nozzle installation, the coefficient of static stability also rises with increase in elevation, and as some value of h/D reaches its maximum, while further increase in elevation h/D becomes less.

The theoretical dependence of the coefficient of transverse static stability $m_x^{\gamma^\circ}$ on the relative elevation h/B, shown in Fig. 180, for a plane sectionalized nozzle installation was calculated by Eq. (281) as applied to the geometrical parameters of the tested model, and specifically for the case b_1/B $b_2/B = 0.0714$, $\varphi = 45^\circ$, and $B_2/B = 0.6$. The theoretical function confirms both the principal trend of the variation in the coefficient $m_x^{\gamma^\circ}$ as a function of elevation h/B, as well as the order of magnitude of $m_x^{\gamma^\circ}$, found as the result of experiments.

When the theoretical and experimental curves are compared, it must be remembered that Eq. (281) was derived for a plane sectionalized nozzle installation, while the model has end nozzles in its bow and stern. In addition, in the derivation of Eq. (281) the uniform distribution of the total pressure in front of the inlets of the nozzles was assumed, which predetermined the uniform supply of air along the perimeter of the nozzles, while the model has a central air supply in the receiver and owing to the different pressure losses in the air jetlets along the paths from the diffusor to individual sections of the nozzles, the model has nonuniformity of total pressure distribution along the perimeter of the nozzles and the corresponding nonuniformity of air supply.

In the range of elevations h/B = 0-0.01, Eq. (281) yields values of the coefficient $m_x^{\gamma^\circ}$ that are close to zero, that is, it characterizes the vehicle as a neutral craft. Experience shows a more abrupt dependence of the coefficient $m_x^{\gamma^\circ}$ on the elevation: in this range of elevations the craft is unstable. The theoretical value of the optimal elevation for which the static stability becomes the greatest agrees quite well with experiment. Thus, for this nozzle installation the theoretical optimal

elevation $(h/B)_{теор} = 0.0562$, while the experimentally obtained value of $(h/B)_{эксп} = 0.035 - 0.04$. In the work arrangement of elevations, Eq. (281) satisfactorily reflects the variation in the function $m_x^{\gamma''} = f(h/b)$ and to the first approximation gives values of $m_x^{\gamma''}$ that are of practical utility.

CHAPTER SEVEN
WORKING PARAMETERS FOR AIR CUSHION VEHICLES

In designing air cushion vehicles, the free hovering regime of a solid support surface is one of the principal design regimes for which aerodynamic qualities of the craft and its power characteristics must be found, to the first approximation, for a known craft weight and for known geometrical parameters of its flow-through section, including the nozzle installation.

1. Lift, Pressure, Air Volume Flow, and Power

The lift Y acting on a craft in the horizontal hovering regime, craft weight G, and the total pressure H_c of the air flow fed to the nozzle installation with S as the area S are related by the equality

$$Y = G = c_y S H_c. \tag{300}$$

From whence the required total pressure in the air stream in front of the nozzle installation is

$$H_c = \frac{1}{c_y} \frac{G}{S}. \tag{301}$$

The drag of the nozzle installation, equal to the total pressure in the passing air stream, is

$$H_c = \zeta \frac{\rho v_p^2}{2} = \zeta \frac{\rho}{2} \left(\frac{Q}{f} \right)^2, \tag{302}$$

where ζ is the drag coefficient of the nozzle installation with respect to the nozzle flow-through area; v_p is the mean air velocity as it leaves the nozzle installation; Q is the air volume flow; f is the nozzle flow-through area; and ρ is the density of air.

The drag of the channels of the flow-through section of the craft over the extent from the external air inlet into the craft to the inlet into the opening of the nozzle installation is

$$H_к = \zeta_к \frac{\rho v_{cp}^2}{2} = \zeta_к \frac{\rho}{2} \left(\frac{Q}{F}\right)^2, \tag{303}$$

where ζ_k is the total drag coefficient of the channels with respect to the flow-through areas F of the nozzle installation.

The total pressure required to overcome the drag of the nozzle installation H_c and the air ducts H_k, that is, the drag of the flow-through section of the craft as a whole equal to the total pressure built up by the fan in the network, is

$$H = H_c + H_к = (\zeta + \zeta_к) \frac{\rho v_{cp}^2}{2} = (\zeta + \zeta_к) \frac{\rho}{2} \left(\frac{Q}{F}\right)^2. \tag{304}$$

The air volume flow passing through the flow-through section, equal to the fan capacity, is

$$Q = \frac{F}{\sqrt{\zeta + \zeta_к}} \sqrt{\frac{2}{\rho} H} \tag{305}$$

or expressed in terms of the total pressure of the air flow in front of the nozzle installation,

$$Q = \alpha F \sqrt{\frac{2}{\rho} H_c} = \frac{F}{\sqrt{\zeta}} \sqrt{\frac{2}{\rho} H_c}, \tag{306}$$

where

$$\alpha = \frac{1}{\sqrt{\zeta}}. \tag{307}$$

The fan shaft power is

$$N = \frac{QH}{75} \quad \frac{\zeta + \zeta_к}{75\eta} \cdot \frac{\rho}{2} \cdot \frac{Q^3}{F^2} = \frac{F}{75\eta \sqrt{\zeta + \zeta_к}} \sqrt{\frac{2}{\rho}} \sqrt{H^3} \tag{308}$$

or, as function of the total pressure in the air flow ahead of the nozzle installation,

$$N = \frac{F\left(1 + \frac{\zeta_к}{\zeta}\right)}{75\eta \sqrt{\zeta}} \sqrt{\frac{2}{\rho}} \sqrt{H_c^3},$$

where η is the fan efficiency.

Denoting $\frac{\gamma_в}{\gamma_н} = \zeta$ and expressing the density of air in these conditions by the density $\rho_н$ of air at normal atmospheric conditions ($t = 15^\circ$ C and $p_н = 760$ mm·Hg·cm),

$$\rho = \frac{\rho}{\rho_н}\rho_н = \Delta\rho_н = \frac{\Delta}{g}, \tag{309}$$

where Δ is the correction coefficient, we get

$$N = \frac{Af}{75\eta\Delta}\cdot\frac{1+\zeta}{\sqrt{\zeta}}\sqrt{H_c^3}.$$

The fan shaft power expressed in terms of the craft weight is

$$N = \frac{A}{75\eta\Delta}\cdot\frac{1+\zeta}{\sqrt{1+\zeta c_y}}\cdot\frac{f}{S}\sqrt{\frac{G}{S}}G. \tag{310}$$

The lift of the craft expressed in terms of the fan shaft power is

$$Y = \left(\frac{75}{A}\cdot\frac{1+\zeta}{1+\zeta}\cdot\frac{c_y}{f}\cdot\frac{\sqrt{S}}{f\sqrt{S}}N\eta\right)^{\frac{2}{3}}. \tag{311}$$

The lift coefficients c_y and ζ of the nozzle installation depend on the geometrical parameters of the nozzle installation, elevation h, and angle of craft inclination relative to the support surface. The coefficient ζ allows for the losses in the dynamic pressure of the stream as it exits into the atmosphere.

The coefficient $\zeta_к$ is determined by the geometrical shape and dimensions of the flow-through channels and is comprised of the coefficients of local drag and the reduced coefficients of friction for the individual members of the flow-through section: diffusor behind the fan, turns, projecting parts, and other constrictions and dilations causing local pressure losses.

The efficiency of the fan η depends on the perfection of the fan and its operating regime in the flow-through section of the craft.

36. Power Ratio of a Craft

Eq. (310) can be represented as

$$K = \frac{G}{N}\sqrt{\frac{G}{S}} = \frac{75}{4}\cdot\frac{\sqrt{2}\,c_y}{1+\zeta}\cdot\frac{\eta\sqrt{\Delta}}{F/S}. \qquad (312)$$

This expression is structurally similar to the familiar expression for the power ratio of a helicopter and can be called the power ratio of an air cushion vehicle.

Eq. (312) allows for the effect of ground proximity and reflects the value of K for which the craft can hover above the support surface. The larger the value of K, the more advantageous is the craft in terms of power: for a specific craft weight lesser power outlays are required, while for a specific power of the craft can carry a greater payload.

This formula also reflects the effect on the power ratio K of the load-bearing properties of the nozzle installation (c_y), the drag of the nozzle installation (ζ), the relative area of the flow-through openings (F/S), the drag of the flow-through section channels (ζ_k), and the efficiency of the fan installed on the craft (η).

Coefficients c_y and ζ depend on the elevation h of the craft above its support surface. The power ratio K of a craft with a nozzle installation expressed as the explicit dependence on elevation is inconvenient owing to the complexity of the expressions $c_y = f(h)$ and $\zeta = f(h)$. Therefore the effect of elevation h on K is more conveniently shown graphically.

For a craft with specified geometrical parameters and unchanged fan speed, reducing elevation h increases the coefficients c_y and ζ and reduces the fan efficiency η. Therefore for each craft K is varied within wide limits and is determined by how strongly the coefficients c_y and ζ depend on elevation h.

The coefficient ζ is organically related to the effect of air cushion formation. When $h = \infty$, $\zeta = 1$. An increase in the coefficient ζ with decrease in elevation results from the compressive action of the excess pressure in the air cushion on the air jets escaping from the nozzles. This increase in ζ shows that the air volume flow required to produce the air cushion has been reduced. Therefore the drag characterized by the coefficient ζ must not be regarded as a detrimental drag. The drag of the channels in the flow-through section of the craft is a detrimental aerodynamic drag. The smaller the coefficient ζ_k, the higher the power ratio of the craft.

An extremely important factor influencing the power ratio of a craft is the relative flow-through area F/S of the nozzle installation. Also essentially determined by this parameter is the gain in using air cushion vehicles compared with craft sustained in air by the reaction forces of air jets expelled from beneath, for example, from helicopters. The smaller the parameter F/S, the higher the power ratio of a craft. However, corresponding to very small values of this parameter will be extremely small relative elevations of the craft above the support surface. Thus, for a planform round nozzle installation, the parameter is

$$\frac{F}{S} = \frac{\pi Db}{\pi D^2/4} = 4\frac{b}{D},$$

where b is the flow-through width of the nozzle and D is the diameter of the nozzle installation.

From the condition of minimum power outlay, the ratio $b/h = (b/D)/(h/D)$ remains nearly unchanged, therefore small values of h/D will also correspond to small values of $F/S = 4b/D$.

When the craft touches the support surface, the outflow of air from the nozzle installation is halted. At this instant the drag coefficient of the nozzle installation $\zeta = \infty$ (the discharge coefficient $\alpha = 0$), the relative coefficient of channel drag $\bar{\zeta} = 0$, the lift coefficient $c_y = 1$, the fan efficiency $\eta = 0$, and Eq. (312) becomes meaningless, since its right hand section becomes indeterminate.

Let us find the power ratio for the case when the weight of the entire craft is transmitted to the ground via the air cushion, while the outflow of air from the nozzle installation does not take place. To do this, let us use the dimensionless aerodynamic characteristics of the fan. The power required by the fan in the regime $q = 0$ is

$$N = \frac{\bar{N} F_0 \rho u^3}{75}, \tag{313}$$

where $\bar{N}$ is the fan power coefficient; F_0 is the area swept by the fan wheel; and u is the fan tip speed.

The total pressure built up by the fan in the network is

$$H = \bar{H}\rho u^2, \tag{314}$$

where $\bar{H}$ is the fan pressure coefficient.

The air cushion pressure equal to the pressure at the inlet into the nozzle installation and thus equal to the fan pressure, completely aerodynamically relieving the craft and transmitting all its weight via the air cushion onto the ground, is

$$H = \frac{G}{S}. \qquad (315)$$

Jointly solving Eqs. (314) and (315), we get

$$u = \sqrt{\frac{G/S}{H\rho}}.$$

Replacing the density of air ρ with its value from formula 309 and inserting the resulting expression for the fan tip speed into Eq. (313), we find

$$N = \frac{2\sqrt{2}}{75\sqrt{\lambda}} \cdot \frac{\lambda}{\eta H^2} \cdot \frac{F_0}{S} \sqrt{\frac{G}{S}}\, G.$$

Then the power ratio of an air cushion vehicle touching the support surface in the total aerodynamic unloading regime is

$$K_k = \frac{G}{N}\sqrt{\frac{G}{S}} = \frac{75}{2\sqrt{2}} \cdot \frac{\sqrt{\lambda}}{F_0/S} \cdot \frac{\eta H^2}{N} = 26{,}52\, \frac{\sqrt{\lambda}}{F_0/S} \cdot \frac{\eta H^2}{N}. \qquad (316)$$

The power ratio of the craft in this case is predetermined by the exceptionally aerodynamic properties of the fan used on the craft, that is, by the ability of the fan to build up high pressure for small power outlay and small overall dimensions. The power ratio of the craft when the elevation h = 0 is one of the vital characteristics, since the numerical value of K_k is a criterion affording an evaluation of the possibility of the craft lifting off from the support surface and entering the hovering regime. The transition of the craft into the hovering regime is possible only when

$$\frac{K}{K_k} \leq 1, \qquad (317)$$

where K is the power ratio of the craft in hovering regime at some elevation h above the support surface.

When a centrifugal fan is installed on a craft, condition (317) is usually maintained, since the pressure $\bar{H}$ built up by the fan, with decrease in elevation and the corresponding drop in air volume flow $\bar{Q}$ increases, and the power coefficient $\bar{N}$ is reduced by several times.

As applied to axial fans, satisfying condition (317) depends on the blade angle θ on the impeller. For small angles θ, the function $\bar{H} = f(\bar{Q})$ rises steadily with decrease in $\bar{Q}$. For large angles θ, as $\bar{Q}$ is reduced discontinuities are observed in the characteristic $\bar{H} = f(\bar{Q})$ along with

an abrupt drop in the pressure built up by the fan. The power coefficient $\bar{N}$, when $\bar{\zeta} = 0$, remains approximately the same as in the calculated regimes of fan operation in a network. Because of this, an abrupt drop in the power ratio of a craft is possible, leading to the inequality $(K/K_{h=0}) < 1$.

Cases are possible when a craft installed with an axial fan with large blade angles on the impeller, on reaching the design fan annular velocity (corresponding to a specific elevation above the support surface) is not able to lift off from the support surface and enter the designed hovering regime. But if an additional lift is applied to this craft with fan operating (for example, the craft is raised with jacks to the designed elevation), and then this force is removed, the craft will remain in the hovering regime over the support surface.

Formula (5.12) can be used not only in estimating the efficiency of the craft as a whole, but also in estimating the efficiency of its nozzle installation. Replacing in this formula the weight of the craft by the lift Y and setting $\bar{\zeta} = 0$, that is, cancelling out the drag of the flow-through section channels, and also assuming $\eta = 1$, we get

$$K = \frac{1}{\Delta}\left|\frac{Y}{S} - \frac{75}{4F_S}\left|\bar{\zeta}\right|\bar{c}_y^2\right|\Delta. \qquad (318)$$

This formula expresses the power ratio of the nozzle installation regarded separately. Here the power is hydraulic power fed to the air flow streaming into the nozzle installation. By using this formula, we can compare the efficiency of various nozzle installations.

The dependence of the power ratio K of a single-pass annular nozzle installation with horizontal nozzle cut-off on elevation $h/D_н$ and angle of generatrix inclination φ, for constant flow-through width $b/D_н = 0.01$, is given in Fig. 181. The curves were calculated by Eq. (318) with $\Delta = 1$, that is, the air density ρ [illegible] kg sec^2/m^4. As we can see, a decrease in the elevation of the nozzle installation of the support surface leads to a rapid rise in the power coefficient, and as $h/D_н \to 0$, $K \to \infty$. For the elevation $h/D_н$ [illegible] $= 0.01$, that is, close to the flow-through nozzle width, the power ratio of single-pass nozzle installation is tens of times greater than the power ratio of an ideal lift air propeller located beyond the aerodynamic influence of ground proximity. Increasing the angle of nozzle generatrix inclination φ markedly raises the power ratio of a nozzle installation.

The dependences of the power ratio on the flow-through width b/D of a nozzle for constant generatrix inclination angle ($\varphi = 45^\circ$) are shown in Fig. 182. At relatively large elevations, the power ratio of a single-pass annular nozzle is the higher, the smaller the flow-through width, while for relatively large elevations -- it is the smaller, the

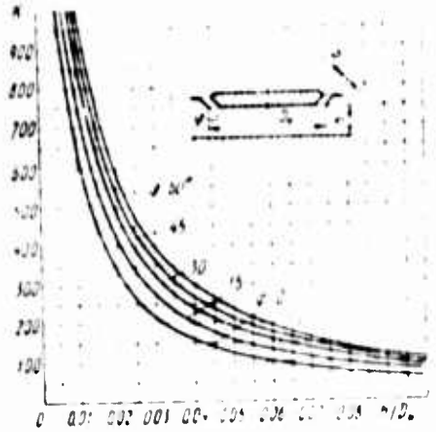

Fig. 18. Power ratio of single-pass annular nozzle installation as functions of elevation for different angles of generatrix inclination ($b/D_н = 0.01$)

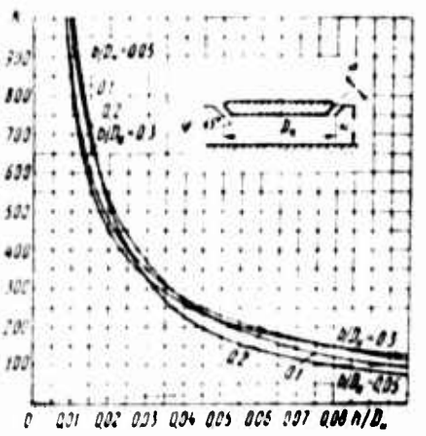

Fig. 18. Power ratio as a function of elevation for different flow-through widths of single-pass annular nozzle ($\varphi = 45^{\circ}$)

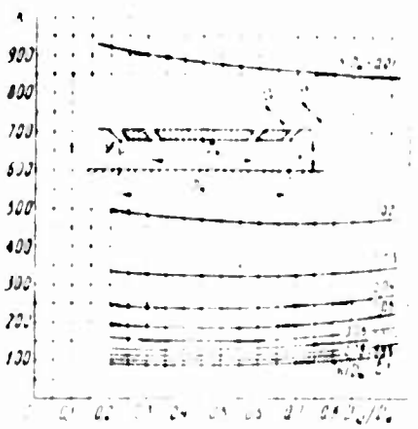

Fig. 19. Power ratio of two-pass annular nozzle installation as functions of stability nozzle displacement for different elevations ($b_1/D_н = b_2/D_н = 0.01$; $\varphi_1 = \varphi_2 = 45^{\circ}$)

smaller the nozzle flow-through width. Fig. 185 shows the power ratio of a two-pass annular nozzle installation with parameters $b_1/D_\mu = b_2/D_\mu = 0.01$ and $\varphi_1 = \varphi_2 = 45^\circ$ as function of stability nozzle placement. The pattern of variation in the power ratio as a function of the parameter D_{μ_2}/D_μ is strongly affected by the elevation of the nozzle installation above the support surface. As the diameter of the stability nozzle is reduced for some high elevation h/D_μ, the power ratio drops off, while at a relatively low elevation -- it increases.

57. Generalized Parameters for Interpreting Craft Test Results

In interpreting the results of testing air cushion vehicles and their individual components or the results of testing their models in laboratory conditions, we must often express the data as functions of dimensionless parameters of air volume flow, pressure, and expended power. Using these parameters, we can take desired generalizations and represent test results in a simple form convenient for further use. To determine these parameters, let us use Eqs. (300) - (308). After necessary transformations, we get the following dimensionless coefficients:

total pressure for the entire craft

$$\bar{H} = \frac{H}{G_1 S} = \frac{\zeta_c + \zeta_n}{\zeta_n} \cdot \frac{1}{c_y^2} + (\zeta_c + \zeta_n)\frac{a^2}{c_y}; \qquad (319)$$

total pressure for the nozzle installation

$$\bar{H} = \frac{H_n}{G_n S} = \frac{1}{c_y^2}; \qquad (320)$$

air volume flow

$$Q = \sqrt{\frac{2}{\rho}}\sqrt{\frac{G_1}{S}}\left(1 + \sqrt{\zeta_n}\right)\frac{a}{\sqrt{c_y}}; \qquad (321)$$

power for the craft with reference to fan efficiency

$$N = \frac{A}{\frac{\eta}{75}\sqrt{\frac{2}{\rho}}\sqrt{\left(\frac{G_1}{S}\right)^3}} = \frac{\zeta_c + \zeta_n}{\eta}\sqrt{2}\,\frac{a\left(1 + \frac{\zeta_n}{\zeta_c}\right)}{\eta\, c_y^2}; \qquad (322)$$

hydraulic power for the entire craft

$$N = \frac{N}{\frac{1}{75}\sqrt{\frac{2}{\rho}}\sqrt{\left(\frac{Q}{S}\right)^3}} = \frac{\zeta + \zeta_a}{\sqrt{2}\,c_y^{3/2}} = \frac{a\left(1 + \frac{\zeta_a}{\zeta}\right)}{c_y^{3/2}}; \quad (323)$$

hydraulic pressure for the nozzle installation

$$\bar{N}_c = \frac{N_c}{\frac{1}{75}\sqrt{\frac{2}{\rho}}\sqrt{\left(\frac{Q}{S}\right)^3}} = \frac{1}{\sqrt{2}\,c_y^{3/2}} = \frac{a}{\sqrt{c_y^3}}. \quad (324)$$

The coefficients α, ζ, c_y, and fan efficiency η are dimensionless quantities and ultimately depend only on the configuration and geometrical parameters of the flow-through section of the craft and the fan installed on it, also the position of the craft relative to the support surface and the terrain of the support surface itself. Therefore the right sides of eqs. (319) - (324) are also dimensionless parameters characterizing the aerodynamic properties of an air cushion vehicle in a generalized form.

The dimensionless coefficients expressed by eqs. (319) - (324) can serve as generalizing parameters interpreting the results of testing operating air cushion vehicles, as well as testing their individual components.

58. Effect of Ground Proximity on the Craft Lift

Lift of a craft touching the ground surface with the exit edges of the nozzle installation. Corresponding to this case is the craft elevation $h = 0$, or which amounts to the same thing, the ratio $b/h = \infty$. Here the air cushion pressure coefficient is

$$\bar{p} = \frac{p_a - p_n}{p_0 - p_n} = 1 - \left(1 + \frac{b}{h}\cdot\frac{\sin(\varphi - \psi)}{\cos\psi}\right)^{-2\frac{(1+\sin\varphi)\cos\varphi}{\sin(\varphi-\psi)}} =$$

$$= 1 - \frac{1}{e^2} = 1,$$

that is, the excess pressure $(p_a - p_H)$ in the air cushion is equal to the total pressure $(p_0 - p_H)$ in the receiver.

The lift coefficient when $b/h = \infty$ is

$$c_{y_0} = f\left[\frac{\cos(\varphi - \psi)}{\cos\psi} + \frac{\cos(\varphi - \psi)}{\sin(\varphi - \psi)} \cdot \frac{1 - k_2(1 - p)}{(2k_1 - 1)\,b/h}\right] \cdot$$

$$\cdot \left[1 - f\frac{\cos(\varphi - \psi)}{\cos\psi}\right] p - f\left[\frac{\cos(\varphi - \psi)}{\cos\psi}\right] \cdot$$

$$\cdot \left[\frac{\cos(\varphi - \psi)}{\sin(\varphi - \psi)(2k_1 - 1)} \cdot 0\right] + \left[1 - f\frac{\cos(\varphi - \psi)}{\cos\psi}\right] \cdot 1 = 1,$$

where

$$k_1 = \frac{(1 - \sin\varphi)\cos\psi}{\sin(\varphi - \psi)} \quad \text{and} \quad k_2 = 1 - \frac{b}{h}\frac{\sin(\varphi - \psi)}{\cos\psi}.$$

In this case the craft lift $Y = c_{y_0} qS$.

Thus, when the craft is on the ground and the external edges of its flexible installation lie correctly against the support surface, the lift force equals to the product of the area S of the nozzle installation by the total pressure $p_0 - p_H$ in front of it or by the total pressure developed by the fan in the network ($H = p_0 - p_H$), since the air volume flow $Q = 0$.

Lift of a craft beyond the aerodynamic effect from ground proximity. With increase in elevation of a craft, the effect of the support surface on the characteristics of jet outflow is attenuated, the air cushion apparently "degenerates", and the lift becomes smaller. To determine the lift of a craft beyond the aerodynamic influence of proximity, let us examine the case when the elevation of a craft is ∞, which amounts to the same thing, $b/h = 0$. Here the air cushion pressure coefficient is

$$\bar{p} = 1 - (1 - \cdot \frac{\sin\varphi\cos\psi}{\sin(\varphi - \psi)} \cdot \frac{1 - \sin\varphi\cos\psi}{\sin(\varphi - \psi)} = 1 - 1 = 0,$$

that is, in this case the pressure under the bottom of the nozzle installation is equal to the atmospheric pressure ($p_0 = p_H$).

The lift coefficient when

$$c_{y_\infty} = f\left[\frac{\cos(\varphi - \psi)}{\cos\psi} + \frac{\cos(\varphi - \psi)}{\sin(\varphi - \psi)} \cdot \frac{1 - k_2(1 - p_0)}{(2k_1 - 1)\,0}\right] \cdot$$

$$\cdot \left[1 - f\frac{\cos(\varphi - \psi)}{\cos\psi}\right] 0 \cdot p - f\left[\frac{\cos(\varphi - \psi)}{\cos\psi}\right] \cdot$$

$$\cdot \left[\frac{\cos(\varphi - \psi)}{\sin(\varphi - \psi)} \cdot \frac{1 - \cdot(1 - 0)}{0} + [1 - f\cos(\varphi - \psi)]\,0 = \frac{0}{0}\right].$$

where

$$k_1 = 1 + \frac{h}{h} \cdot \frac{\sin(\varphi - \psi)}{\cos\psi} = 1.$$

Using L'Hopital's rule for expanding the indeterminacy 0/0, we get

$$\lim_{b/h \to 0} \frac{1 - k_1(1 - \bar{p})}{b/h} = \lim_{b/h \to 0} \frac{[1 - k_1(1 - \bar{p})]'}{(b/h)'} =$$

$$= 2(1 + \sin\varphi) - \frac{\sin(\varphi - \psi)}{\cos\psi}.$$

Thus, the lift coefficient is

$$c_{y\infty} = 2\bar{F}\cos\varphi, \tag{325}$$

where $\bar{F} = b\Pi/S$ is the total relative area of nozzle flow-through openings; and Π is the total length of the nozzle slit.

The right side of the Eq. (325) expresses the projection of the reaction force of an air jet leaving the nozzle installation along the vertical. The maximum value of coefficient $c_{y\infty}$ occurs when $\varphi = 0$. This corresponds to the case when the air jet is directed vertically downward by the nozzle installation.

The effect of ground proximity on the lift. The effect of ground proximity on the lift of an air cushion vehicle is conveniently evaluated by the ratio of the lift coefficient of a craft near the support surface to the maximum value of this coefficient for the same craft, but now elevated to a height where the aerodynamic effect of the surface on the craft ceases to be exerted. With this in mind and using Eqs. (146) and (325), let us write

$$\bar{c}_y = \frac{c_y}{c_{y\infty\max}} = \frac{1}{2}\left[\frac{\cos(\varphi - \psi)}{\cos\psi} + \right.$$

$$\left. + \frac{\cos(\varphi + \psi)}{\sin(\varphi - \psi)} \cdot \frac{1 - k_1(1 - \bar{p})}{(2k_1 - 1)\,b/h}\right] + \left[\frac{1}{F} - \frac{\cos(\varphi - \psi)}{\cos\psi}\right]\frac{\bar{p}}{2}. \tag{326}$$

For a nozzle installation with normal nozzle cut-off ($\psi = 0$), we have

$$\bar{c}_y = \frac{1}{2} \cdot \frac{\cos\varphi}{2 + \sin\varphi}\left[2 + \left(\frac{h/B}{b/B} + \sin\varphi\right)\bar{p}\right] + \frac{1 - \bar{F}\cos\varphi}{F}\,\frac{\bar{p}}{2}.$$

Here $c_{y\,max}^{\infty} = 2\bar{F}$ is the lift coefficient of a craft with relative total area $\bar{F} = n\bar{f}$ of flow-through openings of the nozzle installation when the angle of nozzle generatrix inclination $\varphi = 0$. The coefficients k_1, k_2, and $\bar{p}$ are determined by eqns. (145) and (66).

For a craft with a nozzle installation having horizontal nozzle cut-off plane ($\varphi = \psi$), eq. (5.[illegible]) becomes

$$\bar{c}_y = \frac{1}{2\cos\psi}\left(1 + \frac{2\cos^2\psi - 1}{1 + \sin\psi}\cdot\frac{p}{2b/h}\right) + \left(\frac{1}{p} - \frac{1}{\cos\psi}\right)\frac{\bar{p}}{2},$$

where

$$p = 1 - e^{-\frac{b}{h}(1+\sin\psi)}.$$

In the special case when a craft, being near the support surface, has a nozzle installation of its [illegible] with the cut-off angle $\psi = 0$, the coefficient of [illegible] effect is

$$\bar{c}_y = \frac{1}{2}\left(1 + \frac{p}{2b/h}\right) + \left(\frac{1}{p} - 1\right)\frac{\bar{p}}{2}, \qquad (327)$$

where $\bar{p} = \bar{p}(\bar{z} = t/h)$.

The coefficient $\bar{c}_y$ characterizes the variation in the lift of a craft as a function of its elevation at constant pressure in the air flow fed to the nozzle installation. Let us determine, for this case, the dependence of the variation in the required hydraulic power on the elevation of the craft above the support surface. The power coefficient characterizing the effect of ground proximity is

$$\bar{N}_{H=\text{const}} = \frac{N}{N_\infty} = \frac{\alpha H}{\alpha_\infty H_\infty}\sqrt{\frac{\left(\frac{2}{\rho}H - H\right)_\infty}{\left(\frac{2}{\rho}H - H\right)}} = \frac{a}{a_\infty},$$

since in this case the pressure in front of the nozzle installation is kept constant ($H = H_\infty$).

The discharge coefficient of the nozzle installation near the support surface is

$$\alpha = \frac{1 - \left[1 + \frac{b/B}{h/B} \cdot \frac{\sin(\varphi - \psi)}{\cos\psi}\right]^{-\frac{(1+\sin\varphi)\cos\psi}{\sin(\varphi-\psi)}+1}}{\frac{b/B}{h/B} \cdot \frac{\sin(\varphi-\psi)}{\cos\psi}\left[\frac{(1+\sin\varphi)\cos\psi}{\sin(\varphi-\psi)} - 1\right]}.$$

The discharge coefficient of the nozzle installation of a craft beyond the effect of ground proximity, $\alpha_\infty = 1$, since the air cushion in this case is absent and the air velocity determined by the pressure H_∞ is uniformly distributed in the nozzle exit. Therefore the pressure coefficient is

$$\bar{N}_{H=\text{const}} = \alpha = \frac{1 - \left[1 + \frac{b/B}{h/B} \cdot \frac{\sin(\varphi - \psi)}{\cos\psi}\right]^{-\frac{(1+\sin\varphi)\cos\psi}{\sin(\varphi-\psi)}+1}}{\frac{b/B}{h/B} \cdot \frac{\sin(\varphi-\psi)}{\cos\psi}\left[\frac{(1+\sin\varphi)\cos\psi}{\sin(\varphi-\psi)} - 1\right]},$$

and for a nozzle installation with normal nozzle cut-off ($\psi = 0$), we have

$$\bar{N}_{H=\text{const}} = \frac{h/B}{b/B}\left[1 - \left(1 + \frac{b/B}{h/B}\sin\varphi\right)^{-\frac{1}{\sin\varphi}}\right]. \qquad (328)$$

For a craft with nozzle installation provided with horizontal nozzle cut-off ($\varphi = \psi$), Eq. (228) becomes

$$\bar{N}_{H=\text{const}} = \alpha = \frac{1 - e^{-\frac{b/B}{h/B}(1+\sin\varphi)}}{\frac{b/B}{h/B}(1+\sin\varphi)}. \qquad (329)$$

The variation in coefficients $\bar{c}_y$ and $\bar{N}_{H=\text{const}}$ as functions of elevation h/B of a craft above the support surface, with constant pressure ($H = p_0 - p_H = \text{const}$) in the craft receiver in front of the nozzle installation, is shown in Fig. 184. These functions are calculated by Eqs. (327) and (329) for a nozzle installation with generatrix angle of inclination $\varphi = 0$, nozzle cut-off angle $\psi = 0$, and various relative nozzle flow-through areas $\bar{F} = 2b/B$.

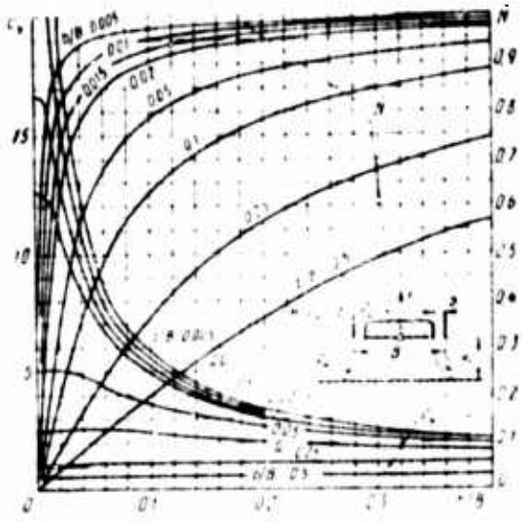

Fig. 184. Effect of ground proximity on lift and expended power of air cushion vehicle for constant pressure in air stream flowing into the nozzle installation

In Fig. 184 we see that as the relative nozzle flow-through width b/B is reduced, the relative lift coefficient c_y increases, and does so the faster, the smaller the relative elevation h/B of the craft above the support surface. Even for a nozzle flow-through width b = 0.05B and elevation h = 0.05B, the lift is approximately five times greater than lift for the same craft located far from the support surface. For smaller flow-through width, the lift increases by several tens of times. With decrease in elevation, this increase is accompanied by an appreciable reduction in the power required to sustain the craft in the air.

However, relatively large flow-through nozzle width ($b/B > 0.25$), the lift does not increase with decrease in elevation, as occurs for small values of b/B, but decreases. In the special case when b/B = 0.5, when both jets merge into a single continuous jet, the lift at the instant when the craft touches the ground surface becomes half the lift of the same craft elevated to a considerable height above the support surface (when h/B = 0, the coefficient $c_y = 1/(4b/B)$; when $h/B = \infty$, the coefficient $c_y = 1$). The effect of ground proximity manifested in increase in the lift for appreciable reduction in the required power for a nozzle with small flow-through width, even dictates the suitability of employing air cushion vehicles for the most diverse applications.

Let us compare the power required to sustain a craft near the ground surface with the power expended in sustaining a craft having the same weight and overall dimensions at a considerable elevation beyond the aerodynamic influence of the ground.

From the condition of constancy of weight $G = Y = Y_\infty$, let us write $c_y SH = c_{y\infty} SH_\infty$. From this we have the ratio of the required total pressures $H/H_\infty = c_{y\infty}/c_y = 1/\bar{c}_y$. The ratio of the required air volume flow is

$$\frac{Q}{Q_\infty} = \frac{aF\sqrt{\frac{2}{\rho}H}}{a_\infty F\sqrt{\frac{2}{\rho}H_\infty}} = \frac{a}{\sqrt{\bar{c}_y}}.$$

In this case, the power coefficient is

$$N = \frac{N}{N_\infty} = \frac{QH}{Q_\infty H_\infty} = \frac{a}{a_\infty}\frac{1}{\sqrt{\bar{c}_y}} = \frac{\alpha}{\sqrt{\bar{c}_y}},$$

where α and $\bar{c}_y$ are coefficients determined by Eqs. (329) and (327).

The variation in relative power, total pressure, and volume flow as functions of relative elevation h/B of a craft with a nozzle installation provided with normal nozzle cut-off ($\psi = 0$), when the angle of generatrix inclination $\varphi = 0$ and for different relative flow-through nozzle widths b/B, is shown in Fig. 185, from which we can see that for unchanged craft weight (constant lift), the required power drops off sharply with decrease in elevation of the craft for all values of the possible flow-through width. Here the required air volume flow also becomes smaller.

The pattern of variation in the required total pressure and the receiver in front of the nozzle installation in this case depends on the nozzle flow-through width: for small width b/B characteristic of air cushion vehicles, the required pressure H/H_∞ also decreases with reduction in elevation h/B, but for relatively large nozzle flow-through width ($b/B > 0.2^{5}$), the required pressure rises.

Let us evaluate the effect of ground proximity on the lift of an air cushion vehicle at constant power expended in producing the jets forming the air cushion. Under this condition ($N = N_\infty$), we can write

$$QH = Q_\infty H_\infty. \tag{330}$$

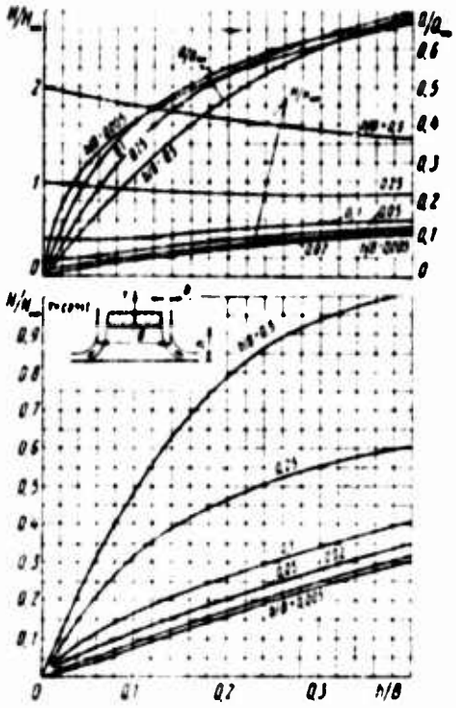

Fig. 185. Effect of ground proximity on required relative power, total pressure, and air volume flow to sustain an air cushion vehicle of specified weight in the hovering regime

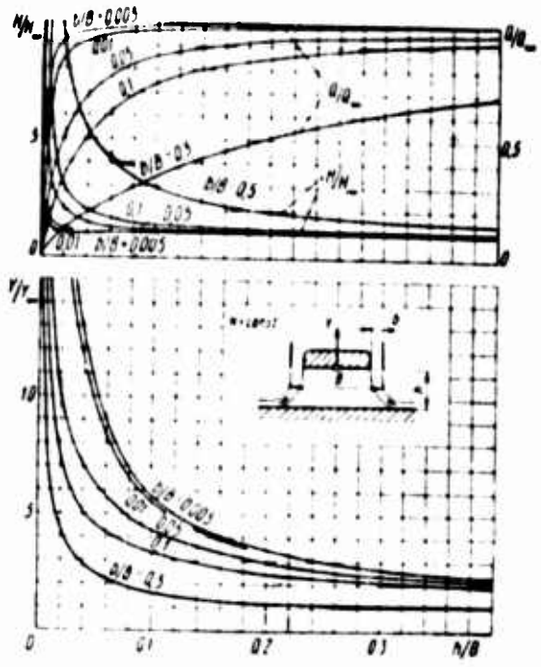

Fig. 186. Effect of ground proximity on lift of an air cushion vehicle, total pressure ahead of the nozzle installation, and air volume flow at constant expended power

Since the required air volume flows are

$$Q = \alpha F \sqrt{\frac{2H}{\rho}}$$

and

$$Q_{\infty} = \alpha_{\infty} F \sqrt{\frac{2H_{\infty}}{\rho}},$$

while the total pressures in the air volume flow in front of the nozzle installation is

$$H = \frac{Y}{c_y S} \quad \text{and} \quad H_{\infty} \quad \frac{Y_{\infty}}{c_{y\infty} S},$$

equality (330) can be expanded in the form

$$\alpha F \sqrt{\frac{2H}{\rho}} H =$$

$$= \alpha_\infty F \sqrt{\frac{2H_\infty}{\rho}} H_\infty$$

or

$$\alpha F \sqrt{\frac{2}{\rho} \cdot \frac{Y}{c_y S}} \cdot \frac{Y}{c_y S} = \alpha_\infty F \sqrt{\frac{2}{\rho} \cdot \frac{Y_\infty}{c_{y\infty} S}} \cdot \frac{Y_\infty}{c_{y\infty} S}.$$

Hence, bearing in mind that $\alpha_\infty = 1$, we get

$$\bar{Y} = \frac{Y}{Y_\infty} = \frac{c_y / c_{y\infty}}{\sqrt[3]{\alpha^2}} = \frac{\bar{c}_y}{\sqrt[3]{\alpha^2}}. \tag{331}$$

Using these functions, it is not difficult to derive expressions for the relative air volume flow

$$\frac{Q}{Q_\infty} = \sqrt[3]{\alpha^2} \tag{332}$$

and the relative total pressure

$$\frac{H}{H_\infty} = \frac{1}{\sqrt[3]{\alpha^2}}, \tag{333}$$

where

$$\alpha = \frac{h/B}{b/B}\left(1 - e^{-\frac{b/B}{h/B}}\right).$$

The functions $\frac{Y}{Y_\infty} = f_1(b/h, b/B), \frac{Q}{Q_\infty} = f_2(b/h, b/B), \frac{H}{H_\infty} = f_3(b/h,$ b/B), calculated by Eqs. (331), (332), and (333), for a craft with nozzle installation having generatrix angle of inclination $\varphi = 0$ and nozzle cut-off angle $\psi = 0$, are shown in Fig. 186. The curves $(Y/Y_\infty) = f(h/B, b/B)$ show by how many times the lift of a craft can increase for the same power expenditure if the craft is in the zone of influence of ground proximity. Here, with decrease in the elevation h/B, the air volume flow drops off rapidly, while the pressure correspondingly rises.

In all the cases considered of the effect that ground proximity has on lift and power, the craft nozzle had an angle of generatrix inclination $\varphi = 0$. When $\varphi > 0$, which is usually observed in practice, the load-bearing qualities of the nozzle installation are improved and the positive effect of the influence of ground proximity becomes augmented.

The advantages of flight air cushion vehicles compared with other means of transportation whose lift is produced by using the reaction of air masses expelled from the craft downward, for example, by the lift propeller of a helicopter, are essentially then predetermined by the functions $\frac{c_y}{c_{y\infty}} = f_1(h/B,\ b/B)$, and $\frac{N}{N_\infty} = f_2(h/B,\ b/B)$. By using the effect of ground proximity, it appears possible for the same power expenditure to produce a greater additional lift, making air cushion vehicles practical.

CHAPTER EIGHT
AERODYNAMIC AND POWER CHARACTERISTICS OF AIR CUSHION VEHICLES IN THE HOVERING REGIME

Let us examine in general form the effect that the geometrical parameters of a nozzle installation have on the aerodynamic and power characteristics of air cushion vehicles. To simplify the calculations, in our analysis the craft is assumed to be planform round and to have a single-pass nozzle installation. Here, the restrictions imposed on the characteristics of the craft by the requirements of static stability will not be taken into account.

In the calculations let us use the following theoretical prerequisites and functions. The lift of a nozzle installation determined by Eq. (300) is equal to the weight of the air cushion vehicle. In Eq. (150) for the lift coefficient, the relative nozzle cut-off area $\bar{F}_c = \frac{F_c}{S} =$

$= 4\frac{b}{D_н \cos\varphi}\left(1 - \frac{b}{D_н \cos\varphi}\right)$, , while the relative area of the bottom of the nozzle installation determined with respect to the internal edge of the nozzle is $\bar{S}_1 = \frac{S_1}{S} = 1 - \bar{F}_c$.

In the special case when $\varphi = 0$, the lift coefficient $c_y = \bar{F} + \bar{S}_1\bar{p}$. The air cushion pressure coefficient and the discharge coefficient of the nozzle installation will be found, respectively, by Eqs. (74) and (75). The air volume flow in the nozzle installation will be calculated by Eq. (306) where the nozzle flow-through area

$$F = F_c \cos\varphi = \pi D_н b\left(1 - \frac{b}{D_н \cos\varphi}\right)$$

and thus its relative area is

$$\bar{F} = \frac{F}{S} = 4\frac{b}{D_н}\left(1 - \frac{b}{D_н \cos\varphi}\right). \qquad (334)$$

The intensity of the air flow streaming into the nozzle installation is

$$N_c = \frac{QH_c}{75} = \frac{1}{75}\alpha F\sqrt{\frac{2}{\rho}}\sqrt{H_c^3} = \frac{1}{75}\cdot\frac{a}{\sqrt{c_y^3}}\cdot\frac{F}{S}\sqrt{\frac{2}{\rho}}\sqrt{\frac{G^3}{S}}. \tag{335}$$

59. Effect of Elevation on Characteristics of a Craft for Specified Craft Weight and Geometrical Parameters of the Nozzle Installation

Let us examine the characteristics of a craft weighing G = 10,000 kg with a nozzle installation having the diameter D_H = 10 m, nozzle flow-through width b = 0.1 m, and angle of generatrix inclination $\varphi = 45^\circ$. Assigning to the elevation of the craft above the ground surface various values, let us determine by Eqs. (74), (75), and (150) the pressure coefficient $\bar{p}$, discharge coefficient α, and lift coefficient c_y. Then by the formulas $\tilde{H}_c = 1/c_y$, $\tilde{Q} = \alpha/\sqrt{c_y}$, and $\tilde{N}_c = \alpha/\sqrt{c_y^3}$, let us find the generalized dimensionless parameters characterizing, respectively, pressure H_c, air volume flow Q, and power N_c to sustain the air cushion vehicle with the assumed geometrical parameters and weight at a specified elevation.

The functions $\tilde{H}_c = f_1(h/D_H)$, $\tilde{Q} = f_2(h/D_H)$, and $\tilde{N}_c = f_3(h/D_H)$ determined in this manner are shown in Fig. 187, which also gives the scales of H_c, Q, and N_c as applied to this craft. The dimensional quantities of pressure, volume flow, and power were calculated based on the following formulas, respectively:

$$H_c = \tilde{H}\frac{G}{S};\quad Q = QF\sqrt{\frac{2}{\rho}}\sqrt{\frac{G}{S}} \quad \text{and}$$

$$N_c = \tilde{N}_c F\sqrt{\frac{2}{\rho}}\sqrt{\left(\frac{G}{S}\right)^3},$$

where ρ is the density of air; and F is the nozzle flow-through area:

$$F = \pi D_n b\left(1 - \frac{b}{D_n\cos\varphi}\right).$$

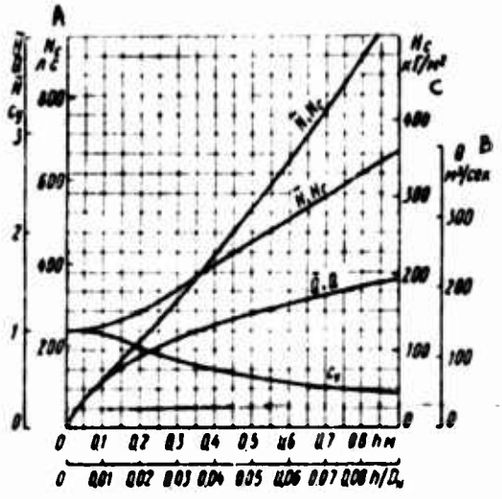

Fig. 187. Aerodynamic characteristics as functions of elevation of craft for specified weight and geometrical parameters of nozzle installation (G = 10,000 kg; D_H = 10 m; b = 0.1 m; φ = 45°)

KEY: A -- N_c, hp
B -- m^3/sec
C -- kg/m^2

The power N_c to produce jets forming the air cushion increases roughly directly proportional to the increase in craft elevation h for specified overall craft parameters and weight. Here it is required that with increase in elevation h both the air volume flow Q and the total pressure H_c to sustain the required discharge velocity of the annular jet from the nozzle increase.

40. Effect of Nozzle Flow-Through Width on the Characteristics of a Craft for Specified Overall Dimensions and Weight

Let us examine the aerodynamic characteristics of an air cushion vehicle weighing G = 10,000 kg, with nozzle installation diameter D_H = 10 m, and angle of nozzle generatrix inclination φ = 45°. Specifying to the nozzle relative flow-through width various values of b/D_H for discrete values of h/D_H of the relative elevation of the nozzle installation above the support surface, and for constant value of the nozzle generatrix angle of inclination φ, let us determine by Eqs. (74), (75), and (150) the pressure coefficient $\bar{p}$, discharge coefficient α, and lift coefficient c_y. Then by the following formulas

$$H_c = \frac{1}{c_y} \cdot \frac{G}{S}; \quad Q = \alpha F \sqrt{\frac{2}{\rho}} \sqrt{H_c} \quad \frac{a}{\sqrt{c_y}} F \sqrt{\frac{2}{\rho}} \sqrt{\frac{G}{S}}$$

and

$$N_c = \frac{QH_c}{75} = \frac{1}{75} \cdot \frac{a}{\sqrt{c_y^3}} F \sqrt{\frac{2}{\rho}} \sqrt{\left(\frac{G}{S}\right)^3}$$

let us find the required pressure, volume flow, and power required to sustain the air cushion vehicle at a specified elevation, for the assumed geometrical craft parameters and weight ($G/S = 127.5$ kg/m^2).

The results of determining the coefficients $\bar{p}$, α, and c_y and the required H_c, Q, and N_c for a single-pass annular nozzle for the values $h/D_H = 0.01$, 0.02, 0.03, 0.04, and 0.05 are presented in Figs. 188 and 189, from which we can see that a reduction in the nozzle flow-through width b increases the pressure H_c in front of the nozzle installation and reduces the air volume flow Q. Here there are optimal widths b for which the power N_c becomes minimum. To each elevation there corresponds its optimal nozzle flow-through width b. As the elevation h is reduced, the optimal values b_{opt} shifted toward the side of small b values. If we plot on Fig. 189 lines of equal values of parameter b/h, then we can see that corresponding to the minimum power values is an approximately constant parameter b/h. For a craft with the particular geometrical parameters and weight we are considering, the value $b_{opt}/h \approx 0.56$ (cf. dashed line).

41. Effect of Angle of Nozzle Generatrix Inclination on Craft Characteristics

Let us consider two typical cases:

let us determine the effect of the angle of generatrix inclination φ of a single-pass annular nozzle on the lift Y, air volume flow Q, and power N_c for different elevations h, specified dimensions of the nozzle installation (D_H = const and b = const), and constant total pressure (H_c = const) of the air stream fed to the nozzle installation;

and let us find the effect that the angle of inclination of nozzle generatrix φ has on the volume flow Q, pressure H_c, and power N_c for specified nozzle installation dimensions (D_H = const and b = const), its elevation (h = const), and constant weight (G = Y = const).

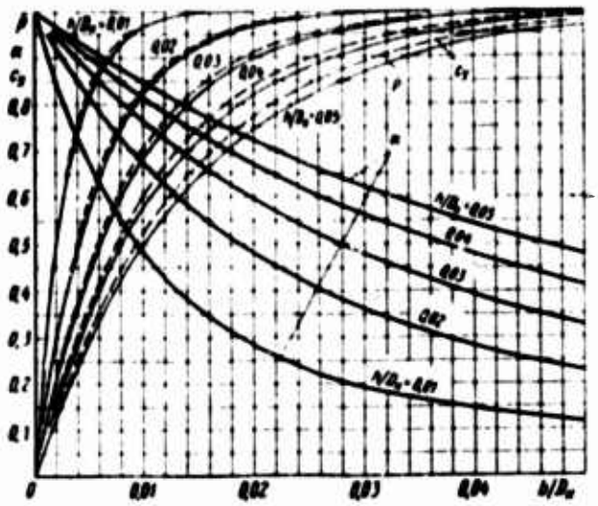

Fig. 188. Pressure coefficient, discharge coefficient, and lift coefficient as functions of flow-through width of a single-pass annular nozzle for different hovering heights ($\varphi = 45^0$; $\bar{p}$ -- indicated with solid lines, and c_y indicated with dashed lines)

1. Let us determine the effect of the angle of nozzle generatrix inclination φ on lift Y, volume flow q, and power N_c by Eqs. (300), (306), and (355), respectively, by first calculating in advance the aerodynamic coefficients $\bar{p}$, α, and c_y appearing in them for constant values of D_H, b, and H_c, and for different values of φ and h. The resulting coefficients $\bar{p}$, α, and c_y as functions of the angle φ are given in Fig. 190. Fig. 191 presents the functions $Y = f_1(\varphi, h/D_H)$, $q = f_2(\varphi, h/D_H)$, and $N_c = f_3(\varphi, h/D_H)$ for a nozzle installation having a diameter $D_H = 10$ m and nozzle flow-through width $b = 0.1$ m, for constant pressure ahead of the nozzle installation, $H_c = 150$ kg/m^2.

As we can see, there are optimal angles of nozzle generatrix inclination $\varphi_{опт}$ for which the lift takes on the greatest values. The optimal value of the angle $\varphi_{опт}$ depends on the elevation h of the nozzle above the support surface. With increase in elevation h, the angle $\varphi_{опт}$ rises. For this particular nozzle installation, the angle $\varphi_{опт} = 50$-63° in the range of relative elevations $h/D_H = 0.01$-0.05.

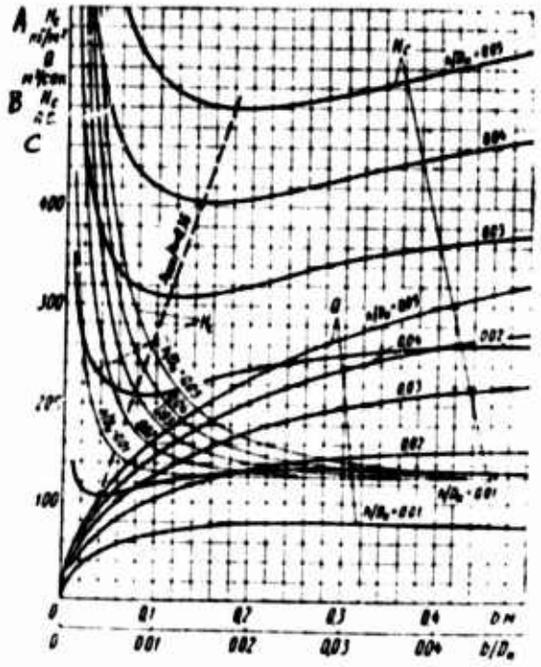

Fig. 189. Aerodynamic characteristics as functions of flow-through width of single-pass annular nozzle (G = 10,000 kg; D_H = 10 m; $\varphi = 45^\circ$; G/S = 127.3 kg/m^2)

KEY: A -- kg/m^2
B — m^3/sec
C — hp

2. Let us determine the effect that the nozzle generatrix angle of inclination φ has on the aerodynamic characteristics H_c, q, and N_c of a nozzle installation for constant craft weight G and for discrete values of elevation h, by using Eqs. (300), (306), and (335), respectively, and the earlier-calculated values of $\bar{p}$, α, and c_y (cf. Fig. 190) for a craft weighing G = 10,000 kg with a nozzle installation having the diameter D_H = 10 m and nozzle flow-through width b = 0.1 m. Figs. 191, 192, and 193 present the results of determining pressure H_c, volume flow q, and power N_c for different angles of inclination φ for the relative elevations h/D = 0.01, 0.02, 0.03, 0.04, and 0.05.

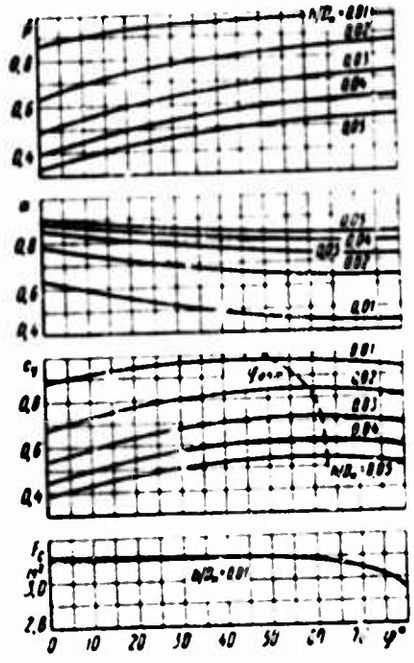

Fig. 190. Pressure coefficient, discharge coefficient, lift coefficient, and nozzle cut-off area as functions of angle of generatrix inclination of a single-pass annular nozzle for different elevations of nozzle above support surface

With increase in angle φ for constant nozzle flow-through width b, the air volume flow decreases throughout this entire range of angles φ, while the pressure and power initially also decrease with rise in the angle φ, but then, on reaching minimum values, begin to climb. Corresponding to different elevations h of the craft above the support surface are various values of $\varphi_{опт}$.

When the elevation of the nozzle installation with the specified dimensions is varied within the limits $h/D_н = 0.01$–0.05 for the pressure H_c, the optimal angles of inclination $\varphi_{опт} = 58$–$62°$, while the angle $\varphi_{опт} = 68°$ for the power. With decrease in the elevation $h/D_н$, the range of extremal values of N_c and H_c becomes less well-defined.

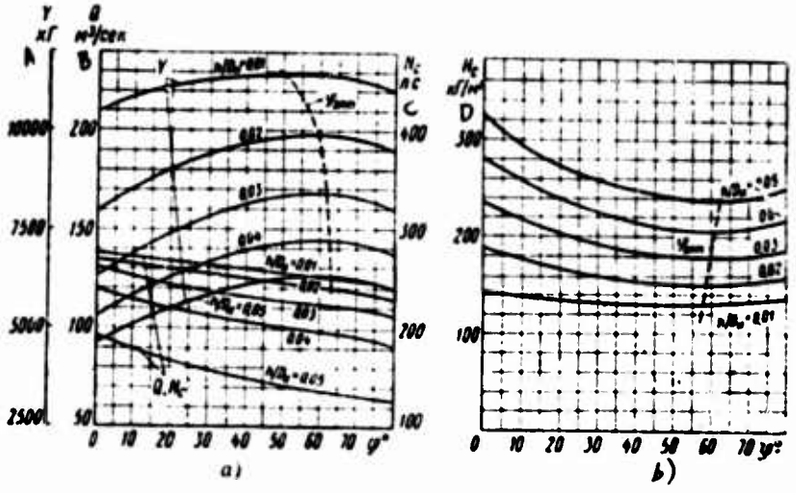

Fig. 191. Effect of angle of generatrix inclination of single-pass annular nozzle for different nozzle elevations, on the following quantities:

a -- lift and air volume flow (D_H = 10 m; b = 0.1 m; H_c = 150 kg/m^2)

b -- required total pressure (D_H = 10 m; b = 0.1; G = 10,000 kg)

KEY: A -- kg
B -- m^3/sec
C -- hp
D -- kg/m^2

42. Effect of Overall Craft Dimensions on Its Characteristics for Specified Elevation and for Different Laws of Variation of Craft Weight

Let us examine the effect that overall craft dimensions has its characteristics as the diameter of the nozzle installation is varied from D_H = 5 m to D_H = 20 m. We will assume the flow-through width of the nozzle installation and the craft elevation to be constants. Let us take b = 0.16 m, h = 0.4 m, and the angle of generatrix inclination φ = 45°. The relative flow-through width of the nozzle in this case lies within the limits b/D_H = 0.032-0.008. The coefficients $\bar{p}$ and α defined by the parameter b/h and the angle of generatrix inclination φ are constant for our calculations, and by Eqs. (74) and (75), $\bar{p}$ = 0.745 and α = 0.726.

Let us examine craft characteristics for the following laws of variation in craft weight as a function of its overall dimensions:

the craft weight is constant (G = 10,000 kg) and is independent of overall dimensions;

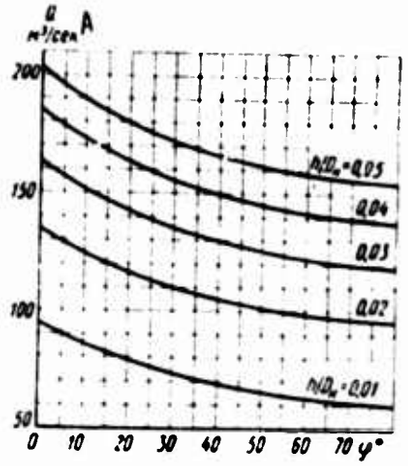

Fig. 192. Required air volume flow as a function of angle of generatrix inclination of single-pass annular nozzle for constant craft weight and different elevations (G = 10,000 kg; $D_н$ = 10 m; b = 0.1 m)
KEY: A -- m^3/sec

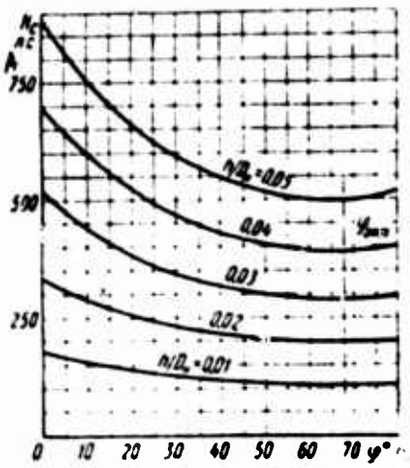

Fig. 193. Required power as function of angle of generatrix inclination of single-pass annular nozzle for constant craft weight and for different elevations (G = 10,000 kg; $D_н$ = 10 m; b = 0.1 m)
KEY: A -- hp

the craft weight varies linearly with variation in diameter $D_н$, and let us take G = 10,000 kg when $D_н$ = 10 m. Therefore

$$G = k_1 D_н = \frac{G}{D_н} D_н = \frac{10\,000 D_н}{10} = 1000 D_н;$$

the craft weight varies linearly with variation in nozzle installation area, where G = 10,000 kg when $S = (\pi D_н^2)/4 = (3.14 \cdot 10^2)/4 = 78.5$ m^2. Therefore

$$G = k_2 S = \frac{G}{\frac{\pi D_н^2}{4}} \cdot \frac{\pi D_н^2}{4} = \frac{10\,000}{\frac{3{,}14 \cdot 10^2}{4}} \cdot \frac{3{,}14 D_н^2}{4} = 100 D_н^2;$$

the craft weight varies according to a cubic function of the craft linear dimension, where G = 10,000 kg when $D_н$ = 10 m. Therefore

$$G = k_3 D_н^3 \quad \frac{G}{D_н^3} D_н^3 \quad \frac{10\,000 D_н^3}{10^3} = 10 D_н^3.$$

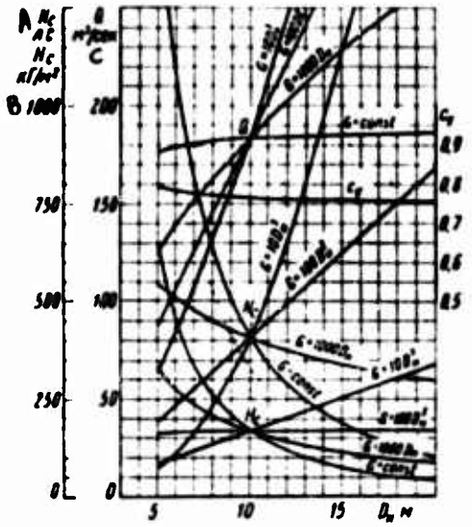

Fig. 194. Aerodynamic characteristics as a function of overall craft weight for specified elevation and for different loss of weight variation (b = 0.16 m; φ = 45°; h = 0.4 m)

KEY: A -- hp
B -- kg/m^2
C -- m^3/sec

Assigning different values of D_H = 5-20 m to the craft diameter and assuming the law of variation in craft weight as a function of its diameter, let us determine by Eqs. (150), (300), (306), and (335) the following craft characteristics: lift coefficient c_y, pressure H_c, air volume flow Q, and power N_c.

The calculation results are given in Fig. 194 in the form of craft characteristics as a function of its diameter for different laws of weight variation. As we can see, the lift coefficient c_y for constant parameter b/h 0.4 decreases somewhat with increase in the craft diameter. This is because with an increase in the overall dimensions of the nozzle installation, the proportion of the lift produced by the reaction of the annular jet in the overall lift, comprised of the reactions of annular jets and the pressure forces at the craft bottom, becomes smaller.

Increasing the craft diameter under any of the indicated laws of weight variation increases the air volume flow required to produce the air cushion. The greatest rise in air volume flow occurs when the craft weight is varied according to the cubic dependence on its linear dimension.

The pressure required to produce the jets forming the air cushion decreases as the craft diameter is increased, under the laws of weight variation G = const and $G = k_1 D_H$. When the craft weight rises proportional to the nozzle installation area, that is, when $G = k_2 D_H^2$, there is a very slight increase in pressure as the diameter is made greater. With variation in the craft weight under the law $G = k_3 D_H^3$, the pressure rises roughly directly proportional to the craft diameter.

The power required to produce the air cushion depends essentially on the law of craft weight variation as its overall dimensions are varied. When the weight is not dependent on the craft overall dimensions (G = const), the power decreases rapidly as the craft linear dimension is increased. The power decreases when craft diameter is increased, also if its weight varies proportional to the diameter. When the craft weight varies directly in proportion to its area ($G = k_2 D_H^2$), the power increases roughly linearly with increase in diameter. The required power rises sharply as a function of craft diameter when its weight variation is proportional to the cube of the craft linear dimension ($G = k_3 D_H^3$).

45. Effect of Ratio of Nozzle Flow-Through width and Elevation on Craft Power for Specified Overall Dimensions and Weight

Let us find the effect that the parameter b/h has on the power N_c when the craft is lifted to some elevation h for specified D_H, angle of generatrix inclination φ = const, and weight G = const. To do this, let us use the function

$$\frac{N_c}{G} = \frac{1}{75} \cdot \frac{\alpha}{c_y \bar{F}} \sqrt{\frac{2}{\rho}} \sqrt{\frac{G}{S}}, \qquad (336)$$

relating the geometrical parameters of the nozzle installation to craft weight and to the intensity of the air stream fed to the nozzle installation. Here $\alpha = f(b/h)$, $c_y = f(b/h)$, and $\bar{F} = f(b/D_H)$. Let us present the calculation results in the form of the function $N_c/G = f(b/h)$ for constant loading G/S on the craft bottom and for different relative nozzle flow-through width b/D_H.

Assigning different values to the parameter b/h when φ = const, let us determine by Eqs. (74) and (75) the pressure coefficient $\bar{p}$ and the discharge coefficient α. Then specifying values for the parameter b/D_H, let us calculate by Eq. (334) the relative nozzle flow-through area $\bar{F}$, and by Eq. (150) — the lift coefficient c_y. Assuming that the loading at the craft bottom G/S = 200 kg/m^2 is constant, let us find N_c/G by Eq. (336).

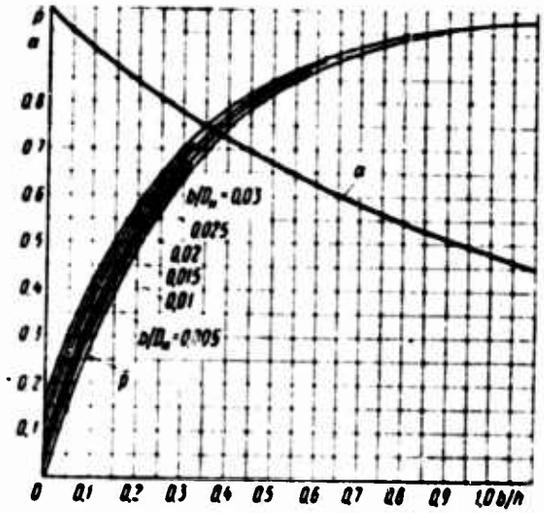

Fig. 195. Pressure coefficient and discharge coefficient of single-pass annular nozzle as functions of parameter b/h (angle of generatrix inclination $\varphi = 45°$)

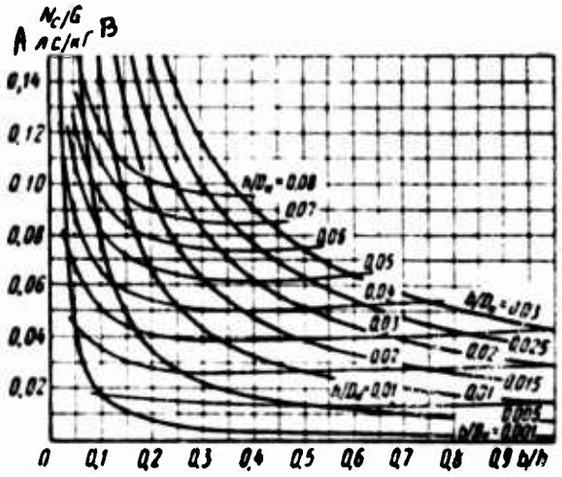

Fig. 196. Required power as a function of parameter b/h for various nozzle flow-through width and craft elevations (G/S = 200 kg/m^2; $\varphi = 45°$)

KEY: A -- hp/kg

The pressure coefficient $\bar{p}$, discharge coefficient α, and lift coefficient c_y as functions of the parameter b/h for a single-pass annular nozzle with angle of generatrix inclination $\varphi = 45^\circ$ are presented in Fig. 195. Fig. 196 shows the functions $N_c/G = f(b/h)$ for different values of the nozzle flow-through relative width b/D_H and also presents the curves when h/D_H = const, characterizing the relative elevation of the nozzle installation above the support surface. On inspecting these functions, we can make the following conclusions:

as the parameter b/h is reduced, achieved by increasing the hovering elevation h/D_H for constant nozzle flow-through width b/D_H, the required power rises rapidly;

for each specified elevation h/D_H of the craft above the support surface there is an optimal nozzle flow-through width b/D_H for which the power outlay per unit craft weight is at a minimum;

for a shallow elevation h/D_H of the craft above the support surface, it is advantageous -- from the standpoint of reducing power outlays -- to use a nozzle installation with small flow-through width; and

the optimal values of the parameter b/h at which the power outlays are at a minimum are b/h = 0.25-0.5, which corresponds to a jet length equal to two-four times its width (h/b = 2-4) -- for actually observed elevations h/D_H and nozzle flow-through width b/D_H.

When designing air cushion vehicles, plotting this kind of function makes it possible in graphical form to estimate, for specified overall craft dimensions and weight, the advantageous nozzle flow-through width required to ensure the necessary craft elevation, with the aim of minimum power outlays.

44. Effect of Craft Weight on Its Elevation for Specified Available Power

Let us assume that the power N_c fed to the air stream arriving at the nozzle installation is constant, and let us determine the dependence of the variation in elevation h and in the aerodynamic characteristics of the craft H_c and ζ on its weight G for specified geometrical parameters of the nozzle installation. We will assume that the nozzle installation has D_H = 10 m, b = 0.16 m, and $\varphi = 45^\circ$. We will carry out the calculations for power values N_c = 200, 300, 400, and 500 hp. We will find the function h = f(G) by carrying out the following calculations based on the formula

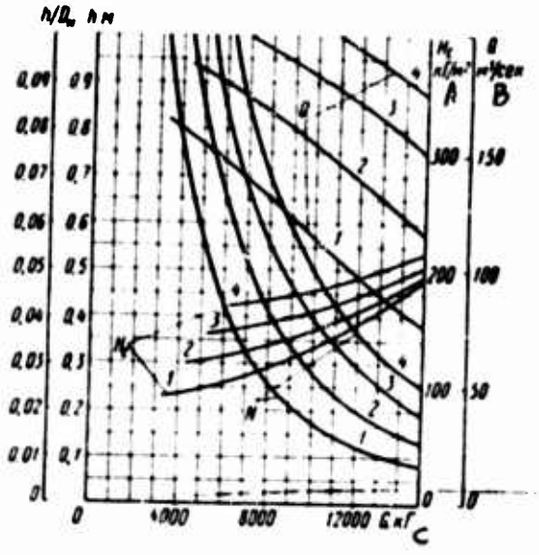

Fig. 197. Elevation of craft, air volume flow, and pressure as functions of craft weight for specified geometrical parameters of nozzle installation and available power ($D_н$ = 10 m; b = 0.16 m; = 45°):

1 -- for N_c = 200 hp

2 -- for N_c = 300 hp

3 -- for N_c = 400 hp

4 -- for N_c = 500 hp

KEY: A -- kg/m^2
B -- m^3/sec
C -- kg

$$G = c_y S \sqrt[3]{\frac{\rho}{2}\left(\frac{75N_c}{aF}\right)^2}. \qquad (337)$$

Setting various values for the elevation h of the craft, let us determine the corresponding values of b/h and then by Eqs. (74), (75), and (150), let us find the coefficients $\bar{p}$, α, and c_y. From known geometrical parameters of the nozzle installation, let us determine the nozzle flow-through area F and the area S of the nozzle installation. By Eq. (337), let us find the values of G corresponding to the adopted values of h and N_c. We calculate the pressure by the formula $H_c = (1/c_y) \cdot (G/S)$ for the resulting values of weight G, and then we determine the volume flow q by Eq. (306).

The results of the calculations for the particular nozzle installation are shown graphically in Fig. 197, where we can see that increasing the weight of a craft with specified geometrical parameters for the same power outlay sharply lowers the possible elevation of the craft above the support surface. When this is done, the air volume flow required to sustain the craft in the hovering regime falls off rapidly, while the pressure correspondingly rises.

45. Effect of Loading at Craft Bottom for Different Relative Elevations on Weight per Unit Power

Let us find the function $G/N_c = f(G/S)$ for a craft with specified geometrical parameters of the nozzle installation, for different relative elevations h/D_H of the craft above the support surface. Here N_c is the power expended in forming the jet producing the air cushion, and G is the weight of the craft, equal to the lift Y produced by the air cushion.

Let us consider, as above, a craft provided with a single-pass annular nozzle. We will assume the external nozzle diameter $D_H = 10$ m and the angle of generatrix inclination $\varphi = 45^\circ$. We will make the calculations for a nozzle with a flow-through width $b = 0.1$ m. Corresponding to these geometrical nozzle parameters is the relative flow-through width $b/D_H = 0.01$. We will determine the function $G/N_c = f(G/S)$ by the formula

$$\frac{G}{N_c} = 75\frac{\sqrt{c_y}}{\alpha}\cdot\frac{\sqrt{\frac{\rho}{2}}}{\frac{F}{S}\sqrt{\frac{G}{S}}},$$

by specifying different values for G/S. Here coefficients α and c_y and the geometrical parameter F/S depend only on the relative nozzle flow-through width b/D_H, relative elevation h/D_H of the craft, and angle of nozzle generatrix inclination φ. By specifying different values for the parameter h/D_H and assuming the values of b/D_H and φ, let us determine the coefficients α and c_y by Eqs. (75) and (150).

The variation in the power loading G/N_c as a function of area loading G/S for different relative elevations h/D_H of the craft is in Fig. 198, from which we can see that an increase in the loading on the craft bottom markedly reduces the power loading. With decrease in the elevation, the parameter G/N_c rises sharply, which makes the application of air cushion vehicles advantageous.

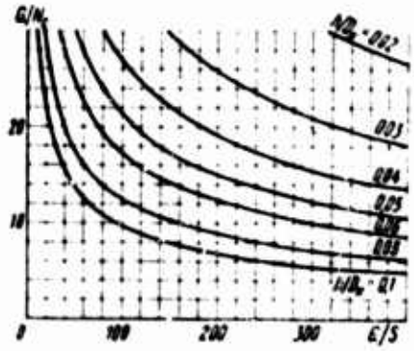

Fig. 198. Craft weight per unit power as a function of weight load on nozzle installation for different elevations (D = 10 m; b = 0.1 m; φ = 45°)

46. Effect of Ambient Air Temperature on Craft Characteristics for Specified Geometrical Parameters and Weight

The characteristics of an air cushion vehicle depend on the temperature of the ambient [external] air sucked into the craft. As the air temperature is changed, the density of air jets outflowing from the nozzle installation changes. This is reflected in the air cushion pressure and thus in the lift of the craft. To sustain a craft with unchanged geometrical parameters ($D_н$ = const, b = const, and φ = const) and constant weight (G = const) at a specified elevation h above the ground surface, the pressure H_c for forming the air cushion, as follows from Eq. (300), must be constant, determined by the assumed geometrical parameters of the craft and its weight.

The air volume flow and power determined by Eqs. (306) and (335) can be expressed as the following ratios, as a function of ambient air temperature:

$$\frac{Q_i}{Q_0} = \frac{N_i}{N_0} = \sqrt{\frac{\rho_0}{\rho_i}} = \sqrt{\frac{T_i}{T_0}},$$

since for constant atmospheric pressure the air density varies inversely proportional to its absolute temperature (the subscript "0" denotes the parameter for a known temperature, and the subscript "i" denotes the parameter for an unknown temperature). Thus, when the ambient air temperature is raised from -20 to 30° C and for constant atmospheric pressure, the air volume flow and the required power to sustain the air cushion vehicle at a specified elevation must be increased by the following number of times:

$$\frac{Q_t}{Q_n} \quad \frac{N_t}{N_n} \quad \sqrt{\frac{273+30}{273-25}} = 1{,}095$$

that is, the air volume flow and power must be raised by 9.5 percent.

Let us determine the effect that the ambient air temperature has on the elevation of the craft above the ground surface for specified geometrical parameters of weight and constant air volume flow fed beneath the craft. Let us examine the craft characteristics with weight G = 10,000 kg for $D_н$ = 10 m, b = 0.1 m, and φ = 45°. Suppose the fan feeds air into the flow-through section of the craft independently of its elevation, in the quantity Q = 150 m^3/sec. It is not possible to represent the dependence of elevation h on these parameters in explicit form. Let us solve this problem graphically. The craft weight $G = c_y S H_c$, while the ratio of the air densities as a function of absolute air temperatures for constant pressure $\frac{\rho_t}{\rho_н} = \frac{T_н}{T_t}$, where $\rho_н$ is the air density for normal atmospheric conditions (for example, when T = 288° K and $p_н$ = 760 mm Hg cm, $\rho_н$ = 0.125 kg·sec^2/m^4). The volume flow equation

$$Q_t = \alpha F \sqrt{\frac{2}{\rho_t}} \sqrt{H_c} = \frac{\alpha}{\sqrt{c_y}} F \sqrt{\frac{2}{\rho_t}} \sqrt{\frac{G}{S}} =$$

$$= \frac{\alpha}{\sqrt{c_y}} F \sqrt{\frac{2}{\rho_н} \cdot \frac{T_t}{T_н}} \sqrt{\frac{G}{S}}$$

can be represented as

$$\frac{\alpha}{\sqrt{c_y}} = \frac{Q_t}{F \sqrt{\frac{2}{\rho_н}} \sqrt{\frac{T_t}{T_н}} \sqrt{\frac{G}{S}}} = \tilde{Q}. \qquad (338)$$

The left side of this equation is a function of the relative elevation $h/D_н$ of the craft, while the right side depends only on the ratio of absolute air temperatures $T_t/T_н$. Both sides of Eq. (338) represent the generalized dimensionless air volume flow $\tilde{Q}$. By calculating the areas F_c, F, S_1, and S, and specifying various values for the parameters $h/D_н$ and T_t/T, let us determine the coefficients α, $\bar{p}$, and c_y and let us find the functions

$$\tilde{Q} = \frac{\alpha}{\sqrt{c_y}} \quad \text{and} \quad \tilde{Q} = \frac{Q_t}{F \sqrt{\frac{2}{\rho_н}} \sqrt{\frac{T_t}{T_н}} \sqrt{\frac{G}{S}}}.$$

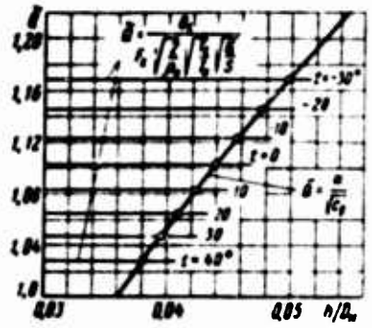

Fig. 199. Graphical determination of effect of air temperature on elevation of craft above support surface

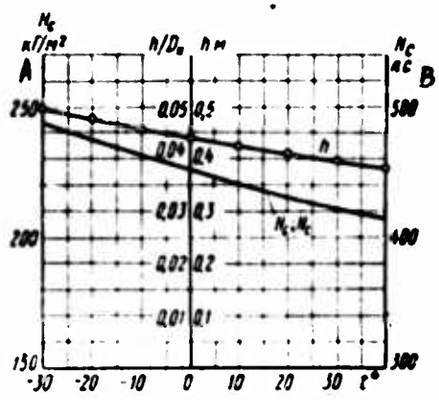

Fig. 200. Elevation of craft above support surface and required pressure and power as functions of air temperature for constant air volume flow (G = 10,000 kg; D_H = 10 m; b = 0.1 m; φ = 45°; Q = 150 m^3/sec)

KEY: A -- kg/m^2
B -- hp

Let us plot these functions in the coordinates $\tilde{Q}$ and h/D_H. The points at which the curves characterizing these functions intersect will be the solutions to Eq. (338). Taking the values of h/D_H for different air temperatures from this graph, we get data characterizing the elevation of a craft above the ground surface for specified geometrical parameters, weight, and air volume flow as functions of the temperature of air streaming through the nozzle installation.

The graphical determination of the air temperature dependence of the craft elevation above the support surfaces shown in Fig. 199. Fig. 200 shows the desired function $h = f(t)$ and also the function of pressure $H_c = f(t)$ and power $N_c = f(t)$ that must be imparted to the air stream in front of the nozzle installation to ensure the supply of air in the quantity Q = 150 m^3/sec. In this case the pressure and power were calculated by the formulas

$$H_c = \frac{Q_t^2}{\alpha^2 F^2 2/\rho_t} \text{ and } N_c = \frac{Q_t H_c}{75} = \frac{1}{75} \cdot \frac{Q_t^3}{\alpha^2 F^2 2/\rho_t}.$$

The discharge coefficient α was determined by Eq. (75) for values of the elevation h/D_H assumed from Fig. 200 for the corresponding air temperature t. Here the air density is

$$\rho_t = \rho_n \frac{T_n}{273 + t}.$$

As we can see, the air temperature very markedly affects both the elevation of the craft above the support surface, as well as the required pressure and power to produce the air cushion. Thus, in feeding the same volume of air and in increasing its temperature from -20 to 30° C, the elevation h of the craft with the specified parameters is reduced by approximately 17 percent. When this is done, the pressure and power are reduced by $\sim$ 30 percent.

47. Effect of Planform Shape of Nozzle Installation on Craft Lift

In designing air cushion vehicles, the problems of selecting the layout and geometrical parameters of the nozzle installation are primary, since this installation is the principal working component producing the air cushion and since its characteristics determine the aerodynamic and power characteristics of the craft as a whole. In addition to the geometrical parameters of the nozzle installation, and specifically the profile of the flow-through section, nozzle flow-through width, angle of nozzle generatrix inclination, and the method of sectionalizing the bottom, the load-bearing qualities of the craft are affected by the planform shape of the nozzle installation. As the shape of the nozzle installation is varied, the length of the nozzle bounded by the perimeter of the craft bottom changes, and depending on circular conditions imposed on the law of variation of the nozzle exit areas, so do the aerodynamic and energy characteristics of the nozzle installations.

Knowing the regularities in the variation of the load-bearing qualities of nozzle installations as a function of changes in their planform shape allows us to impart an advantageous contour to the nozzle installation of a craft being designed and to improve the craft efficiency. It is of practical interest to evaluate various nozzle installation arrangements from this point of view. Below are examined the load-bearing qualities of planform round, square, rectangular, and oval nozzle installations, and they are evaluated from the standpoint of achieving the required lift for a specified hovering elevation above the support surface with minimum power outlay fed to the air stream producing the air cushion.

The evaluation of various nozzle installation layouts is based on theoretical functions determining the lift of these installations as dependent on their geometrical parameters. For simplicity of analysis, in the examination we assumed single-pass nozzle installations with angle of nozzle generatrix inclination $\varphi = 0$. In analyzing the characteristics, the problems of the effect that the shape of nozzle installations has on craft stability were omitted.

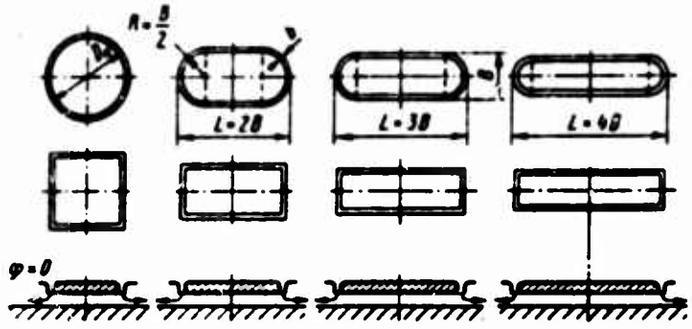

Fig. 201. Nozzle installation arrangements

These nozzle installation layouts are shown in Fig. 201. The oval nozzle installation consists of a middle section with parallel external walls, and also bow and stern sections rounded to a radius that is equal to half of the nozzle installation width. The relative length of the nozzle installations was varied within the range L/B = 1-4. For the case L/B = 1, the oval nozzle intergrades into a round, and the rectangular -- into a square contour.

Characteristics of nozzle installations. In examining the aerodynamic and power characteristics of nozzle installations, the following functions were used. The lift of a nozzle installation equal to the weight G of the air cushion vehicle was determined by Eq. (300). The air volume flow in the nozzle installation was found by Eq. (306). The discharge coefficient of the nozzle installation is

$$\alpha = \frac{1 - e^{-\frac{b}{h}}}{b/h} = \frac{h}{B} \cdot \frac{1 - e^{-\frac{b/B}{h/B}}}{b/B}. \qquad (339)$$

The air cushion pressure coefficient, which is the ratio of the excess pressure $p_в - p_н$ in the air cushion to the total pressure H_c of the air stream fed to the nozzle installation is

$$\bar{p} = 1 - e^{-2\frac{b}{h}} = 1 - e^{-2\frac{b/B}{h/B}}. \qquad (340)$$

The lift coefficient for a single-pass plane nozzle with angle of generatrix inclination $\varphi = 0$ is

$$c_y = \bar{F} + \left(1 - \bar{F} + \frac{\bar{F}}{2b/h}\right)\bar{p}, \qquad (341)$$

where $\bar{F} = F/S$ is the relative nozzle exit area.

In these and subsequent formulas we used: b -- nozzle exit width; h -- elevation of craft above the support surface; B -- width of nozzle installation measured with respect to the outer edge of the nozzle; L -- length of nozzle installation measured with respect to the outer edge of the nozzle; F -- nozzle exit area; S -- area of nozzle installation bounded by external edge of nozzle; and ρ -- air density.

The discharge coefficient α of the nozzle installation and the air cushion pressure p are shown in Fig. 202 as functions of parameter b/h. Fig. 203 presents the dependence of the lift coefficients c_y as a function of parameter b/h, plotted by Eq. (341), for different relative nozzle exit areas $\bar{F}$, and Fig. 204 presents the function $c_y = f(b/D_H;\ b/D_H)$ for an annular nozzle with diameter D_H measured with respect to the outer edge of the exit. In this case the coefficient c_y was determined by Eq. (341), and the relative nozzle exit area was determined by the formula $\bar{F} = 4\frac{b}{D_H}\left(1 - \frac{b}{D_H}\right)$. The intensity of the air stream fed to the nozzle installation was calculated by Eq. (335).

The dependence of the weight (lift) per unit power on the weight loading per unit nozzle installation area is

$$\frac{G}{N_c} = 75\frac{\sqrt{c_y}}{a}\cdot\frac{\sqrt{\frac{F}{2}}}{\frac{F}{S}\sqrt{\frac{G}{S}}}. \qquad (342)$$

The relative exit area, expressed in terms of nozzle perimeter and exit width, is $\bar{F} = \frac{b\Pi_H}{S} \quad \frac{b}{S}\cdot\frac{\Pi_H + \Pi_e}{2}$, where Π_H and Π_e are the perimeters of the nozzle installation determined with respect to the external and internal nozzle edges, respectively. With reference to this expression, the nozzle exit area for a planform oval nozzle installation with rectilinear middle and with bow and stern sections rounded to a radius equal to half the nozzle installation width, we have

$$\bar{F} = \frac{b}{B}\cdot\frac{2\left(\frac{L}{B} - 1\right) + \pi\left(1 - \frac{b}{B}\right)}{L/B + \pi/4 - 1}, \qquad (343)$$

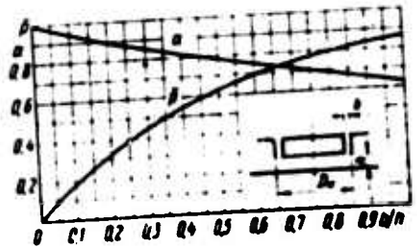

Fig. 202. Discharge coefficient α and air cushion pressure coefficient $\bar{p}$ as functions of parameter b/h for angle of nozzle generatrix inclination $\varphi = 0$

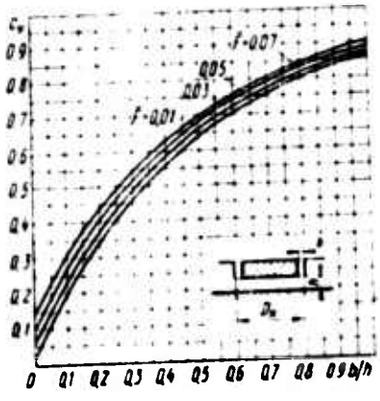

Fig. 203. Lift coefficient of nozzle installation as functions of parameter b/h, when the angle of nozzle generatrix inclination $\varphi = 0$, and for different relative nozzle exit areas

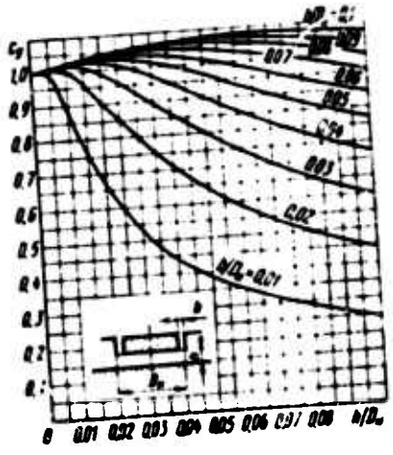

Fig. 204. Lift coefficient of planform round nozzle installation as functions of relative elevation for $\varphi = 0$ and for different relative nozzle exit widths

or, as a function of parameters b, S, and L/B,

$$\bar{F} = \frac{b}{\sqrt{S}} \cdot \frac{2\left(\frac{L}{B} - 1\right) + \pi\left(1 - \frac{b}{\sqrt{S}}\sqrt{\frac{L}{B} + \frac{\pi}{4} - 1}\right)}{\sqrt{\frac{L}{B} + \frac{\pi}{4} - 1}}. \quad (344)$$

For a planform rectangular installation, we have

$$\bar{F} = 2\frac{b}{L}\left(1 + \frac{L}{B} - 2\frac{b}{B}\right), \qquad (345)$$

or, as a function of the parameters b, S, and L/B,

$$\bar{F} = 2\frac{b}{\sqrt{S}} \cdot \frac{1}{\sqrt{L/B}}\left(1 + \frac{L}{B} - 2\frac{b}{\sqrt{S}}\sqrt{\frac{L}{B}}\right). \qquad (346)$$

In the special case for planform round and square nozzle installations, $\bar{F} = 4(b/B)(1 - b/B)$, where B is the side of the square nozzle installation and the diameter of the round nozzle installation. The area of the oval nozzle installation measured with respect to the exit edge of the external nozzle wall is

$$S_0 = B^2\left(\frac{L}{B} + \frac{\pi}{4} - 1\right). \qquad (347)$$

and the area of the rectangular nozzle installation $S_{np} = LB$.

Eq. (341) for the lift coefficient c_y can be extended -- with adequate practical accuracy -- to nozzle installations of various planform shapes -- round, oval, rectangular, and so on, given the condition that the parameter $\bar{F}$ appearing in this formula is replaced with the appropriate value of the relative area of the particular installation.

Effect of shape of nozzle installation on lift for identical nozzle installation area, measured with respect to the exit edge of the external nozzle wall. For all the craft under consideration, we will assume -- independently of their relative elongation*L/B — the overall area of the nozzle installations to be $S = 100\ m^2$, and the elevation of the craft above the ground surface $h = 0.3$ m. We will compare the nozzle installations in terms of the lift (weight) of the craft, per unit required power for two characteristic cases: for identical width b/h, and for identical relative area $\bar{F}$ of nozzle exit. [*also referred to as "aspect ratio"]

The case of identical exit width of particular nozzle installations. Let us assume the nozzle exit width $b = 0.12$ m. To this there corresponds a constant value of the parameter $b/h = 0.12/0.3 = 0.4$. Knowing b/h and finding -- by Eqs. (344) and (346) for each nozzle installation differing by the relative elongation L/B -- its value of $\bar{F}$, let us determine by Eqs. (339), (340), and (341) the values of the coefficient α, $\bar{p}$, and c_y. Further, assigning different values to G/S, by Eq. (342) let us calculate the value of G/N_c. For these same values of the parameter G/S, let us find the pressure

$$H_c = \frac{1}{c_y} \cdot \frac{G}{S},$$

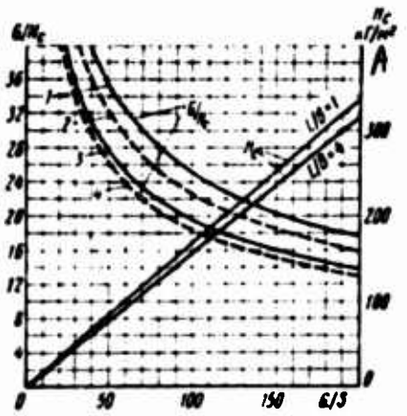

Fig. 205. Weight per unit power, and required pressure as functions of weight load at craft bottom and relative elongation of nozzle installation (S = 100 m^2; b = 0.12 m; h = 0.2):
1 -- for round nozzle when L/B = 1
2 -- for square nozzle when L/B = 1
3 -- for oval nozzle when L/B = 4
4 -- for rectangular nozzle when L/B = 4
KEY: A -- kg/m^2

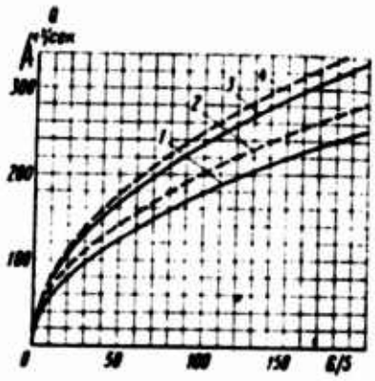

Fig. 206. Required volume flow of air fed to nozzle installation as functions of weight load at craft bottom (S = 100 m^2; b = 0.12 m; h = 0.5 m):
1 -- for round nozzle when L/B = 1
2 -- for square nozzle when L/B = 1
3 -- for oval nozzle when L/B = 4
4 -- for rectangular nozzle when L/B = 4
KEY: A -- m^3/sec

which must be sustained in the air stream in front of the nozzle installation, and then -- by Eqs. (306) and (335) -- air volume flow Q_c and power N_c, respectively.

For these nozzle installations with identical area loading and craft elevation, the parameter G/N_c has its maximum value for a planform round nozzle (curve 1, Fig. 205). As the length of the oval nozzle installation is increased for the same overall area, the value of the parameter G/N_c becomes less (curve 3). A similar effect also occurs for planform square and planform rectangular nozzles (curves 2 and 4, respectively). Here H_c varies only slightly with change in the relative length* L/B of both oval and rectangular nozzle installations. A marked rise in the air volume flow Q_c and an increase in the power N_c are observed (Figs. 206 and 207).

[* also referred to as "aspect ratio"]

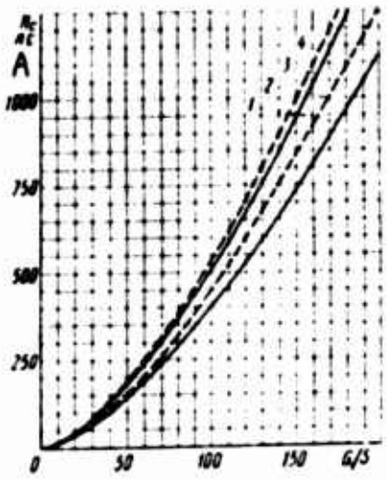

Fig. 207. Required power as functions of weight load at craft bottom (S = 100 m^2; b = 0.12 m; h = 0.3 m):
1 -- for round nozzle when L/B = 1
2 -- for square nozzle when L/B = 1
3 -- for oval nozzle when L/B = 4
4 -- for rectangular nozzle when L/B = 4

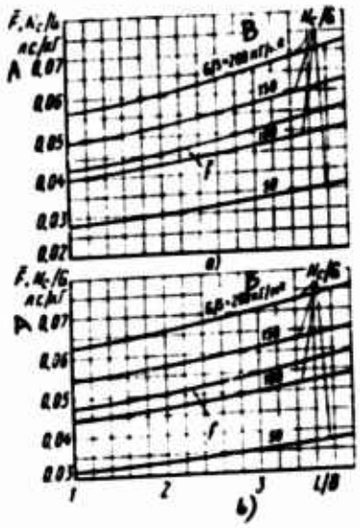

Fig. 208. Power required to raise craft to specified elevation as functions of relative elongation of nozzle installation for different weight loads (S = 100 m^2; h = 0.3 m; b = 0.12 m):
a and b -- for oval and rectangular nozzle installations, respectively
KEY: A -- hp/kg
B -- kg/m^2

Let us examine two cases of variation in the nozzle installation characteristics for the above-indicated geometrical parameters of the installations: for identical craft weight (G/S = const), let us find the variation in the power (N_c/G = var) as a function of the nozzle installation contour; for identical power outlay N_c, let us find the dependence of the variation in the lift coefficient c_y (weight) on the contour [shape] of the nozzle installation.

The dependences of power, per unit weight, on the relative elongation of oval and rectangular nozzle installations for different bottom loading are shown in Fig. 208, which also gives the dependence of the relative area $\bar{F}$ of nozzle installations on their elongation L/B. To determine the relative power, we used Eq. (342), and to determine the relative area -- Eqs. (344) and (346). As we can see, for identical craft weight, identical elevation above the support surface, and identical nozzle flow-through width, there is a gain in power with increase in the relative elongation of the nozzle installation.

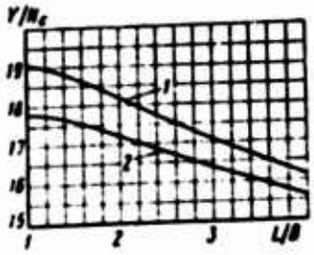

Fig. 209. Lift of air cushion vehicle for identical power outlay as functions of planform shape of nozzle installation ($S = 100\ m^2$; $h = 0.3$ m; $b = 0.12$ m; $N_c = 900$ hp): 1 and 2 -- for oval and rectangular nozzle installations, respectively

The rise in power with increase in relative length L/B is less intense compared with the rise in the nozzle exit area F, or, which amounts to the same thing, with increase in the nozzle exit perimeter, since b and S are identical for all nozzle installations. Thus, for oval nozzles when L/B is increased from 1 to 4, the relative area $\bar{F}$ rises by a factor 1.33, while the power per unit weight increases by only a factor 1.28. Here the increase in N_c/G is nearly independent of the loading of the bottom of the nozzle installation. This is accounted for by the fact that the lift coefficient c_y depends nonlinearly on relative area $\bar{F}$. Similar regularities also hold for rectangular nozzle installation.

Let us examine the case of identical power outlay. Suppose $N_c = 900$ hp. We will assume $S = 100\ m^2$, $b = 0.12$ m, and $h = 0.3$ m. Let us determine the dependence of craft weight (lift) per unit power on the relative elongation [aspect ratio] of the nozzle installation. From the known value of the parameter b/h, let us determine α and p. Using the values of these parameters and knowing the function $\bar{F} = f(L/B, b/\sqrt{S})$, defined by Eqs. (344) and (346), let us calculate the lift coefficient c_y for the corresponding values of L/B. Then by the formula

$$\frac{Y}{N_c} = c_y S \sqrt[3]{\frac{\rho}{2}\left(\frac{75}{\alpha F}\right)^2 \frac{1}{N_c}}, \qquad (348)$$

readily derived from Eq. (342), let us determine the value of Y/N_c.

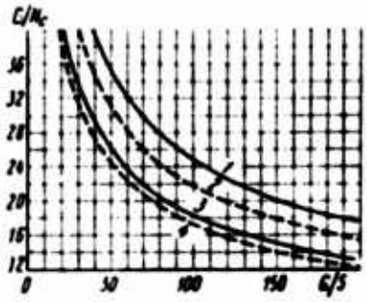

Fig. 210. Weight per unit volume as functions of weight load at craft bottom ($S = 100\ m^2$; $\bar{P} = 0.04$; $h = 0.3$ m):
1 -- for round nozzle when $L/B = 1$
2 -- for square nozzle when $L/B = 1$
3 -- for oval nozzle when $L/B = 4$
4 -- for rectangular nozzle when $L/B = 4$

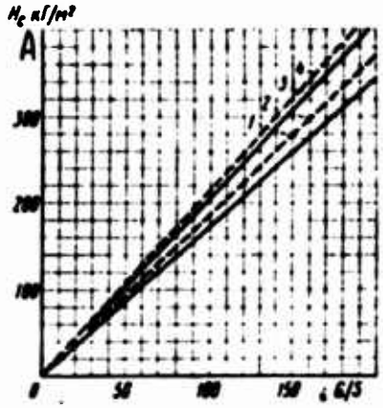

Fig. 211. Required power as functions of weight load at craft bottom and relative elongation of oval nozzle installation ($S = 100\ m^2$; $\bar{P} = 0.04$; $h = 0.3$ m):
1 -- for round nozzle when $L/B = 1$
2 -- for square nozzle when $L/B = 1$
3 -- for oval nozzle when $L/B = 4$
4 -- for rectangular nozzle when $L/B = 4$
KEY: A -- kg/m^2

The function $Y/N_c = f(L/B)$ for planform oval and rectangular nozzle installations is shown in Fig. 209, where we can see that for the same expended power, the lift diminishes with increase in relative length of the nozzle installation. Here planform oval installations exhibit the greater lift, while among these is the round nozzle, producing roughly 7 percent more lift than a square nozzle. As the elongation of the oval nozzle installation is increased to $L/B = 2$, the lift is reduced by approximately 4.7 percent. The elongation of planform oval nozzles up to $L/B = 3$ reduces the lift by about 10.5 percent compared with the round nozzle. For rectangular nozzles, an increase in elongation to $L/B = 2$ and $L/B = 3$ means a reduction in lift of 3.4 and 8 percent compared with the square nozzle, respectively.

Case of identical exit area of particular nozzle installations. For all nozzle installations considered, we will assume that their overall area $S = 100\ m^2$ and the elevation of the craft above the ground surface $h = 0.3$ m is the same. We will assume the nozzle exit area also to be identical and

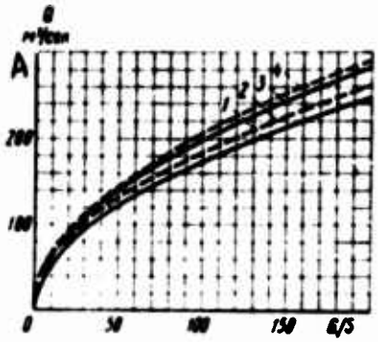

Fig. 212. Volume flow of air fed to nozzle installation as functions of load at craft bottom ($S = 100\ m^2$; $\bar{F} = 0.04$; $h = 0.3$ m):
1 -- for round nozzle when $L/B = 1$
2 -- for square nozzle when $L/B = 1$
3 -- for oval nozzle when $L/B = 4$
4 — for rectangular nozzle when $L/B = 4$
KEY: A -- m^3/sec

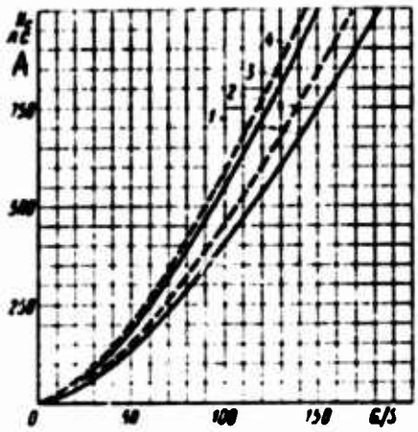

Fig. 213. Required power as functions of load on craft bottom ($S = 100\ m^2$; $\bar{F} = 0.04$; $h = 0.3$ m):
1 -- for round nozzle when $L/B = 1$
2 -- for square nozzle when $L/B = 1$
3 — for oval nozzle when $L/B = 4$
4 — for rectangular nozzle when $L/B = 4$
KEY: A -- hp

equal to 4 percent of the nozzle installation area, that is, $F = 4\ m^2$. Knowing the planform shape of the nozzle installation and the relative exit area $\bar{F}$, let us determine the nozzle flow-through width:

for an oval nozzle installation

$$\frac{b}{\sqrt{S}} = k_1 - \sqrt{k_1^2 - \frac{\bar{F}}{\pi}}, \qquad (349)$$

where

$$k_1 = \frac{\frac{L}{B} + \frac{\pi}{2} - 1}{\pi \sqrt{\frac{L}{B} + \frac{\pi}{4} - 1}};$$

for a rectangular nozzle installation

where

$$\frac{b}{\sqrt{S}} = k_2 - \sqrt{k_2^2 - \frac{\bar{F}}{4}}, \tag{350}$$

$$k_2 = \frac{1 + \frac{L}{B}}{4\sqrt{L/B}}.$$

Since the elevation h is specified, let us find its value b/h for each nozzle installation differing in relative elongation L/B. Then let us determine by Eqs. (339), (340), and (341) the coefficients α, $\bar{p}$, and c_y, respectively. Further, specifying various values for the parameter G/S, let us calculate the values of G/N_c by Eq. (342). For the same G/S values, let us find the total pressure H_c that must be sustained in the air stream in front of the nozzle installation, and then the air volume flows Q and power N_c -- by Eqs. (306) and (335).

By comparing the resulting curves (Figs. 210-213) for the corresponding functions derived earlier (cf. Figs. 205-207), we can see that the pattern of variation in the parameters G/N_c, Q, H_c, and N_c as a function of loading G/S remains approximately the same as in the case of constant exit width of nozzle installations. The only difference is that when F = const, the pressure H_c rises markedly with increase in relative elongation L/B, when there is a small rise in volume flow Q, and in the case when b = const, conversely, the pressure varies weakly with increase in L/B, while the volume flow rises appreciably. With increase in L/B there is a gain in power N_c, in either case.

Let us also determine dependence of power (N_c/G) on nozzle installation shape for constant craft weight (G/S = const) and lift (weight) on the nozzle installation shape for identical power outlay (N_c = const).

To solve the problem, let us use equation (342). Starting from the condition that $\bar{F}$ = 0.04 for all the nozzles considered is a constant, let us determine by Eqs. (349) and (350) the nozzle exit width b for various L/B values. Further, calculating b/h, let us find the coefficients α, $\bar{p}$, and c_y, and then by using Eq. (342), let us determine the unknown value of N_c/G for the corresponding value of L/B.

The dependence of power per unit weight on the relative elongation of a nozzle installation for identical bottom loading is shown in Fig. 214, where the dependence of relative nozzle exit width $b/\sqrt{S}$ on its relative elongation L/B is also plotted. As we can see, for identical nozzle installation weight, identical elevation above support surface, and identical nozzle flow-through width, as the elongation of the nozzle installation is increased the power rises, and it does so more intensely than when the nozzle installation width remains constant.

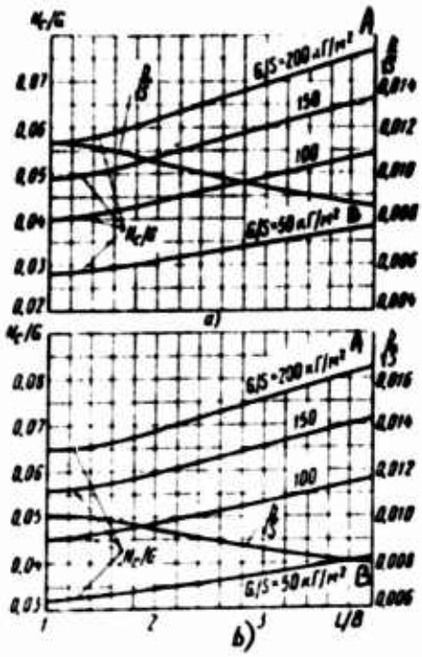

Fig. 214. Required power as functions of relative elongation of nozzle installation for different weight loads ($S = 100\ m^2$; $h = 0.3$ m; $F = 0.4\ m^2$):

a -- for oval nozzle installation

b -- for rectangular nozzle installation

KEY: A -- kg/m^2

B -- kg/m

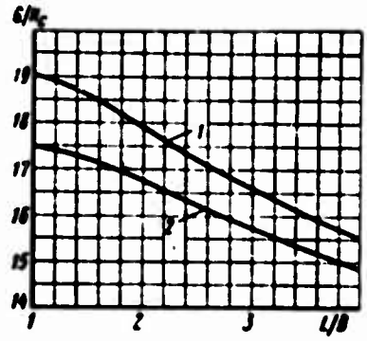

Fig. 215. Power loading as functions of planform shape of nozzle installation for identical nozzle installation area ($S = 100\ m^2$; $F = 4\ m^2$; $N_c = 900$ hp; $h = 0.3$ m):

1 and 2 -- for oval and rectangular nozzles, respectively

To find the dependence of the lift (weight) on nozzle installation shape for identical power outlay, which we assume to be $N_c = 900$ hp, let us use Eq. (348). Employing the values of α and c_y determined in the preceding case for $\bar{F} = 0.04$ as a function of L/B, and also Eq. (348), we get the function $G/N_c = f(L/B)$ shown in Fig. 215 for oval and rectangular nozzle installations. As we can see, for the same expended power, as the relative length of the nozzle installation is increased, the weight power loading becomes less, where in this case, that is, when $\bar{F} = \text{const}$, the decrease in G/N_c (lift per unit power) proceeds more intensely with increase in L/B than when $b = \text{const}$ (cf. Figs. 209 and 215).

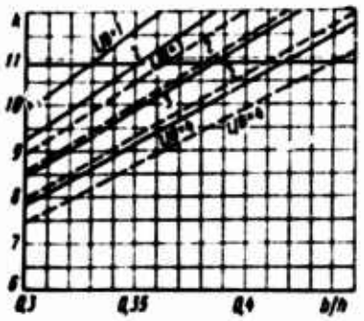

Fig. 216. For graphical determination of parameter b/h for oval and rectangular nozzle installations with different relative elongations (S = 100 m^2; b = 0.12 m; G = 15,000 kg; N_c = 900 hp; the solid curves correspond to oval nozzles, and the dashed curves — to rectangular nozzles)

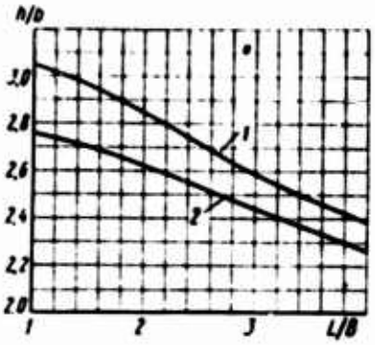

Fig. 217. Effect of planform shape of nozzle installation on craft elevation above support surface (S = 100 m^2; b = 0.12 m; G = 15,000 kg; N_c = 900 hp):

1 and 2 — for oval and rectangular nozzles, respectively

Effect of nozzle installation shape on craft elevation above ground surface. Let us find the dependence of craft elevation above support surface on the relative length of oval and rectangular nozzle installations. For all the particular nozzle installations we will assume the following: S = 100 m^2, b = 0.12m; G = 15,000 kg; and N_c = 900 hp. Since it is not possible to express the dependence of elevation h explicitly on these parameters, let us solve this problem graphically. Eq. (342) can be written as

$$\frac{\sqrt{\bar{c}_y^3}}{\alpha\bar{F}} = \frac{1}{75}\cdot\frac{G}{N_c}\sqrt{\frac{2}{\rho}}\sqrt{\frac{G}{S}}. \qquad (351)$$

The right side of the equation is constant. The coefficients c_y and α appearing in the left side of the equation depend on the relative elevation of the craft, that is, on the parameter b/h. Knowing b and S, and assigning different values to L/B for oval and rectangular nozzle installations, let us determine by Eqs. (344) and (346) the relative exit area $\bar{F}$. Using these values of $\bar{F}$ for each elongation L/B and specifying different values to b/h, let us determine by Eqs. (339), (340), and (341) the values of α, $\bar{p}$, and c_y, and then let us plot the relationship $k\ \frac{\sqrt{\bar{c}_y^3}}{\alpha\bar{F}}$ as a function of b/h.

The point of intersection of the curve $k \frac{|\ \ |}{aF} f(b/h)$ and the straight line $\ \ \ \ f(b/h)$ gives the unknown value of the parameter b/h for the particular relative elongation of the nozzle. Fig. 216 shows the graphical solution of Eq. (351), and Fig. 217 shows the dependence of the relative elevation h/b of the nozzle installation above the support surface on the relative elongation L/B.

For identical nozzle installation area, identical nozzle exit width, identical craft power, and identical power expended in forming the air cushion, planform oval nozzles provide the greater elevation. For the conditions specified above, the elevation of a planform round nozzle is proportionally 10 percent higher than that of a square nozzle. With increase in relative elongation of a nozzle, the elevation difference becomes gradually smaller, however even for the elongation L/B = 2-5, it still is quite appreciable.

Effect of nozzle installation shape on lift for identical length and width of nozzle installation. Let us determine the optimal planform shape of a nozzle installation for specified overall craft dimensions (length L and width B), that is, let us find the form for which the lift Y will be the greatest, and the power N_c supplied to the air streaming producing the air cushion and the elevation h of the craft above the surface will remain identical.

We will assume the area $L \cdot B = 100\ m^2$, the elevation of the nozzle installation h = 0.5 m, and the power of the air stream in front of the nozzle N_c = 900 hp. Let us examine two planform dissimilar nozzle installations -- rectangular and oval over the range of variation in relative elongation L/B from 1 to 4. We will perform the analysis for two cases: for identical relative nozzle exit width b/h; and for identical relative nozzle exit area $\bar{F}$.

The case of identical nozzle exit width. Let us assume the nozzle exit width b = 0.12 m. To this value there corresponds the parameter b/h = 0.12/0.5 = 0.4. Specifying different values for the parameter L/B and using the condition $LB = 100\ m^2$, let us find the corresponding values of B and L. Then by Eqs. (345) and (345) let us determine the relative exit area $\bar{F}$ of oval and rectangular nozzle installations. Further, by Eqs. (339), (340), and (341) let us calculate the coefficients α, $\bar{p}$, and c_y. Using the values found for these coefficients for the various values of the relative craft elongation L/B, let us determine G/N_c by Eq. (348). The air volume flow G and the total pressure H_c required to produce the air cushion can be found by Eqs. (306) and (301).

The resulting functions are shown in Fig. 218, from which it is clear that for small relative elongations, the rectangular nozzle installations have greater power loading, that is, greater lift compared with the oval. Thus, the lift of a square nozzle installation is about 8.5 percent greater than for a round, in spite of the fact that the areas of these installations differ by 27 percent for identical overall dimensions. This difference is due to the fact that a higher total pressure with somewhat less air volume flow must be maintained in front of the round nozzle installation.

With increase in relative elongation L/B of a craft, the efficiency of the oval nozzle installations rises, and then begins to decrease, approaching the efficiency of rectangular nozzle installations. For the relative elongation L/B = 3, the power loading becomes identical, in spite of the fact that the bottom area of oval nozzle installations is less than the bottom area of rectangular nozzle installations. Even in this case somewhat greater total pressure H_c is required for oval nozzle installations.

Case of identical relative nozzle exit area. We will assume the nozzle exit area F to be equal to 4 percent of the area S of the nozzle installation bottom. For each rectangular nozzle installation, the area F -- according to the adopted conditions -- is 4 m^2, and for an oval installation -- $F = 0.04\ S_0$, where we determine S_0 by Eq. (347) as a function of the relative elongation L/B of the nozzle installation. Knowing $\bar{F}$ and S, let us calculate by Eqs. (349) and (350) the values of the parameter $b/\sqrt{S}$ and let us determine the nozzle exit width b. Further, by determining the parameter b/h for the corresponding L/B, let us find the coefficients α, $\bar{p}$, and c_y, and then by Eq. (348) -- the power loading. Using Eqs. (300) and (306), it is not difficult to determine for each calculated L/B value the air volume flow Q and the total pressure H_c required to produce an air cushion. The resulting functions are shown in Fig. 219.

Calculations showed that for the same relative nozzle exit area ($\bar{F}$ = const), there is the same pattern of variation in the functions $H_c = f_1(L/B)$ and $Q = f_2(L/B)$ as in the case of identical nozzle exit width (b = const), in spite of the fact that the coefficients α and $\bar{p}$ differ for the particular nozzle installations. Just as in the preceding case, the increase in the relative elongation L/B of the oval nozzle installation initially leads to a rise in lift, and then to a reduction. The efficiency of the rectangular and the oval nozzle installations becomes identical when $L/B \approx 2.6$.

The calculations afford the following principal conclusions:

planform oval nozzle installations compared with rectangular installations, for identical overall bottom areas and relative elongations, and also for identical elevation above the support surface and power expended in air cushion formation produce the greater lift.

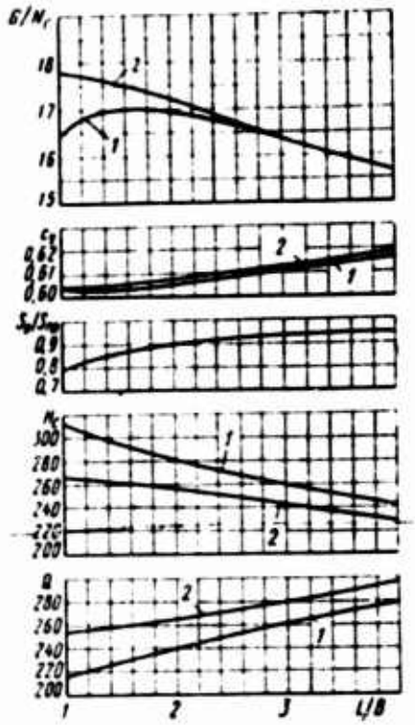

Fig. 218. Characteristics of air cushion vehicle as a function of planform shape of nozzle installation and its relative elongation ($L \cdot B = 100\ m^2$; $b = 0.12$ m; $h = 0.3$ m; $N_c = 900$ hp):

1 and 2 -- for oval and rectangular nozzles, respectively

An increase in the relative elongation of a nozzle installation for the same overall bottom area leads to a reduction in lift both for oval as well as rectangular nozzle installations. Curving of the edges of a planform rectangular nozzle and its conversion into an oval nozzle, with the overall bottom area retained, improves its load-bearing qualities. Under these conditions, oval nozzle installations provide greater hovering height above a support surface than do rectangular.

For specified overall dimensions (length and width) of an air cushion vehicle, the advantage of employing a particular nozzle installation planform shape depends on its relative elongation. For small relative elongations (close to unity), rectangular nozzle installations provide greater lift compared with oval. With increasing relative elongation, the efficiency of oval nozzle installation rises, and when $L/B > 2$, oval and rectangular

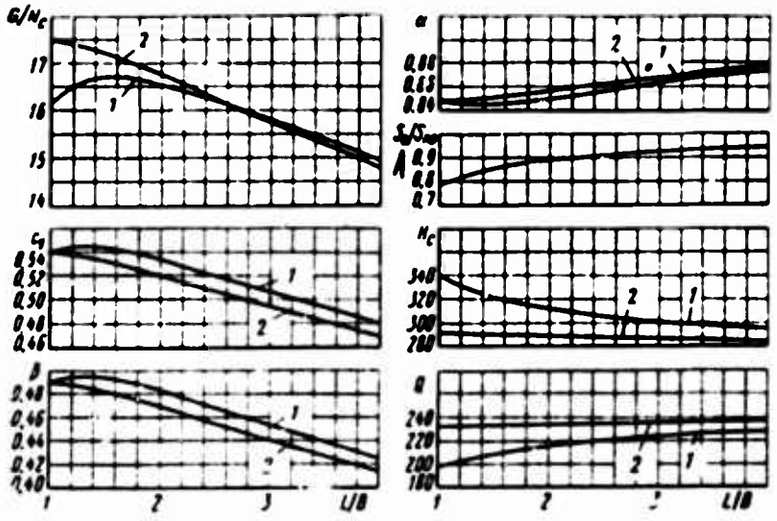

Fig. 219. Characteristics of air cushion vehicle as a function of planform shape of nozzle installation and its relative elongation ($L \cdot B = 100$ m^2; $\bar{F} = 0.04$; $h = 0.3$ m; $N_c = 900$ hp):

1 and 2 -- for oval and rectangular nozzles, respectively

nozzle installations produce approximately the same lift, in spite of the fact that in these cases the area of the oval nozzle installations is less than that of the rectangular.

48. Effect of Stability Nozzle Placement on the Lift of a Two-Pass Nozzle Installation for Constant Power Outlay

Variation in the lift of a plane sectionalized nozzle installation is wholly determined by the pattern of variation in its lift coefficient c_y. The power fed to this nozzle installation is independent of the stability nozzle placement B_2/B, since the flow-through area of the external nozzles F_1 and of the stability nozzles F_2 and their discharge coefficients α_1 and α_2 remain constant with variation in the parameter B_2/B. We can evaluate the pattern of the function $Y = f(B_2/B)$ from the curve $c_y = f(B_2/B, K/B)$ shown in Fig. 152. The lift of this installation is always smaller than the lift of a plane single-pass nozzle constructed with the same overall dimensions, with the same total flow-through area, and with the same angle of generatrix inclination, as well as identical power outlay.

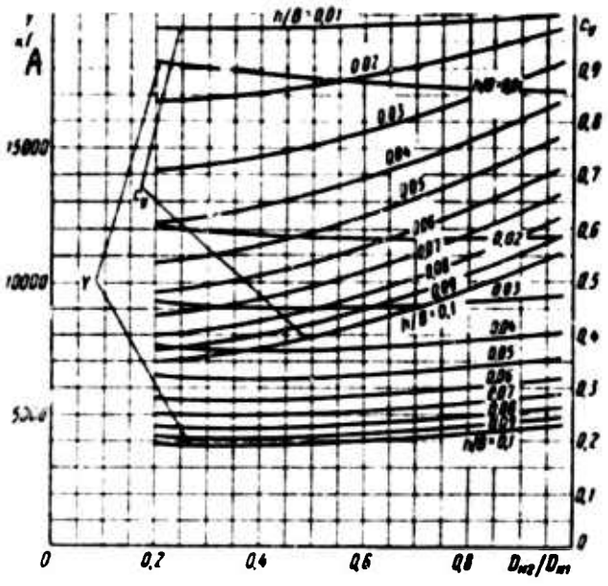

Fig. 220. Load-bearing capacity of two-pass annular nozzle installation as functions of placement of internal nozzle for constant power outlay (D_H = 10 m; $b_1/D_H = b_2/D_H = 0.01$; $\varphi_1 = \varphi_2 = 45°$; N_c = 300 hp)

KEY: A -- kg

Let us determine the pattern of variation in the lift of a double-pass annular nozzle as a function of stability nozzle placement D_{H2}/D_H for the same power outlay expended in producing the air cushion, and with unchanged hovering height above the support surface. In this kind of nozzle installation, as the parameter D_{H2}/D_H is reduced, the stability nozzle flow-through area becomes less, the air volume flow is smaller, and the power required to sustain the craft at a given elevation h above the support surface changes. For a double-pass annular nozzle the nature of variation in the lift coefficient c_y does not directly express the pattern of variation in the lift Y for constant power outlay.

Let us examine the characteristics of a double-pass annular nozzle with horizontal nozzle cut-off having the following parameters: D_H = 10 m, $b_1 = b_2$ = 0.1 m, $\varphi_1 = \varphi_2 = 45°$. We will assume the air density $\rho = 0.125$ kg·sec^2/m^4, and the expended power is taken as constant and equal to N_c = 300 hp. Specifying various values for elevation h, let us

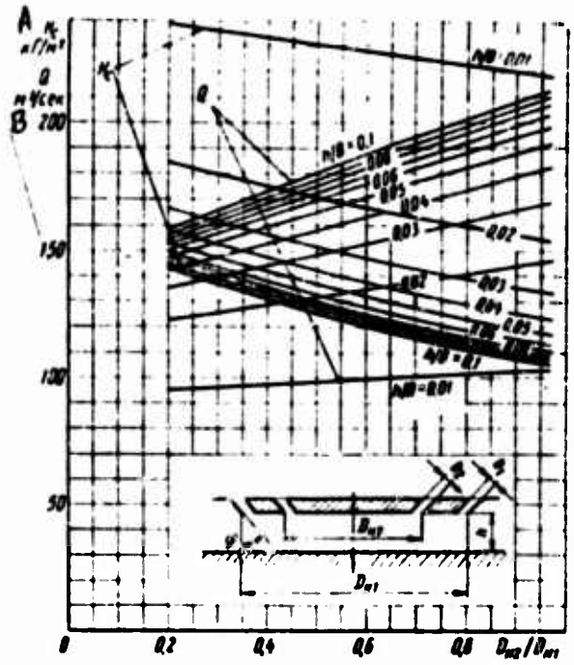

Fig. 221. Air pressure and air volume flow of double-pass annular nozzle installation as functions of placement of internal nozzle for constant power outlay ($D_н$ = 10 m; $b_1/D_н = b_2/D_н = 0.01$; $\varphi_1 = \varphi_2 = 45°$; N_c = 300 hp)

find the corresponding values of the parameter b/h, and then by Eqs. (86), (89), (91), and (95), let us determine the coefficients p_1, p_2, α_1, and α_2. Further, specifying different values to the parameter $D_{н2}/D_н$ and using the familiar geometrical parameters of the nozzle, let us calculate by Eqs. (189), (190), (191), and (192) the areas $\bar{F}_{c1}$ and $\bar{F}_{c2}$ of the nozzle cut-offs, areas of the sections $\bar{S}_1$ and $\bar{S}_2$ of the nozzle installation bottom, and the area of the entire bottom S. Then let us determine the corresponding values of c_y and α by Eqs. (186) and (96), and further, by the following formulas

$$Y = c_y S \sqrt[3]{\frac{\rho}{2}\left(\frac{75N_c}{\alpha F}\right)^2}; \quad H_c = \sqrt[3]{\frac{\rho}{2}\left(\frac{75N_c}{\alpha F}\right)^2}$$

and $$Q = \alpha F \sqrt[3]{\frac{2}{\rho}\cdot\frac{75N_c}{\alpha F}}$$

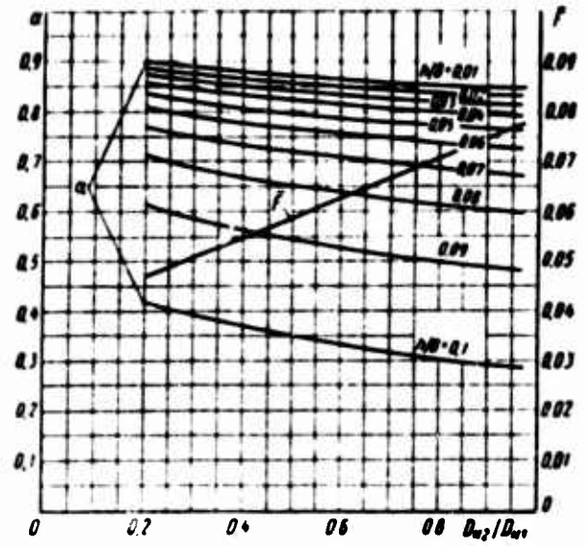

Fig. 222. Discharge coefficient of two-pass annular nozzle installation as functions of internal nozzle placement (D_H = 10 m; $b_1/D_H = b_2/D_H = 0.01$; $\varphi_1 = \varphi_2 = 45°$; N_c = 300 hp)

let us find the corresponding lift, pressure, and air volume flow.

As the diameter of the internal nozzle is reduced (Fig. 220), that is, with decrease in the parameter D_{H2}/D_H, the lift rises for small elevations h/D_H and decreases somewhat for greater elevations, in spite of the fact that the lift coefficient c_y decreases with decrease in the parameter D_{H2}/D_H for all the elevations considered. Here, as we can see in Figs. 221 and 222, the pressure H_c rises with decrease in the parameter D_{H2}/D_H, while the air volume flow -- in spite of the increase in the total discharge coefficient α -- becomes smaller.

Thus, the conversion of the single-pass annular nozzle installation $\left(\frac{D_{H2}}{D_H} \approx 0{,}972\right)$ into a two-pass installation ($D_{H2}/D_H < 0.972$) with the same overall flow-through width ($b = b_1 + b_2$) and the same angle of generatrix inclination ($\varphi = \varphi_1 = \varphi_2$) makes it possible, for the same

power outlay, to produce a greater lift at low elevations. Here it must be remembered that a higher-pressure air flow must be brought to the double-pass nozzle installation. This pattern of variation in the aerodynamic characteristics of a double-pass annular nozzle is due to the appreciable reduction in the overall flow-through area $\bar{F}$ as the diameter D_{H2} of the internal nozzle is made smaller.

With increase in the nozzle installation elongation, that is, with the transformation of the round nozzle installation into an oval installation, the difference in the pattern of variation of lift Y and lift coefficient c_y as a function of parameter B_2/B becomes smoothed over, the load-bearing capacity of oval two-pass nozzle installations deteriorates, and single-pass nozzle installations become more efficient for the same power outlay in sustaining the craft at a specified elevation.

CHAPTER NINE
AERODYNAMIC DRAG OF FLOW-THROUGH SECTION OF AN AIR CUSHION VEHICLE

49. Aerodynamic Characteristics of Flow-Through Section

The flow-through section of flight air cushion vehicles comprises a system of air ducts for sucking in ambient air, channeling it through the craft, and discharging it through the nozzle installation to the exterior toward the ground surface in the form of jets producing the air cushion. The flow-through section is a vital component of these craft: its configuration and dimensions often predetermine the craft arrangement as a whole, and on the aerodynamic qualities of the flow-through section depend not only the efficiency of the nozzle installation but also the power characteristics of the craft.

The principal requirements on the flow-through section are the following: the most uniform possible supply of air as it is fed to the nozzle installation, small hydraulic pressure losses, and small overall duct dimensions. These requirements are contradictory, since satisfying one of them most fully entails degrading other parameters. Therefore, building a rational system of the flow-through section is possible only given a compromise solution.

The flow-through section of an air cushion vehicle differs aerodynamically from the ordinary network in which a fan operates. Its distinction is that at small pressures produced by a fan this network is a closed volume admitting barely any air. This corresponds to the case when an air cushion vehicle rests on the support surface and its nozzle exits proved to be quite tightly sealed by the soil if the craft is on the ground, or by the water if it is afloat. In this condition the craft remains until the critical moment when the forces of excess pressure beneath the craft, increasing with the pressure rise in the network, become equal to the craft weight. A slight excess of the critical pressure leads to the lift of the craft from the support surface and the apparently automatic opening of the valves and the discharge of air from them. At this instant the craft enters the free hovering regime.

With further pressure rise in the network and a corresponding increase in the air volume flow, the elevation rises and so does the distance between the nozzle cut-off and the support surface, while the compressing action of the support surface on the air jets escaping from the nozzles weakens. The drag coefficient of a nozzle installation becomes smaller with increase in the elevation.

Thus, the flow-through section of an air cushion vehicle is a network with variable-area exit openings, whose beginning and degree of opening depend on the pressure built up by the fan. These properties of the flow-through section predetermine the pattern of variation in its drag as a function of the amount of air passed, which introduces the points of distinction into the combined operation of the craft's flow-through section and its fan installation.

50. Drag of the Flow-Through Section

The aerodynamic drag of the flow-through section in an air cushion vehicle is

$$H = H_{вс} + H_н + H_с,$$

where $H_{вс}$ is the drag of the suction network ducts; $H_н$ is the drag of the delivery network ducts; and $H_с$ are the losses in the dynamic pressure of the air jets outflowing from the nozzle installation.

The dynamic pressure of an air jet outflowing from the nozzle installation is directly associated with the effect of air cushion formation beneath the craft. Losses in dynamic pressure are determined by the total pressure expended in producing the jets for required air volume flow in the conditions of air cushion formation. The size of the losses depends strongly on the nozzle installation geometry and the elevation of the nozzle installation above the support surface. This function is manifested in the variation of velocity fields in the nozzle cut-off plane.

The drag of the suction network and the delivery network is associated with the necessity of feeding external air into the nozzle installation and has no direct effect on the excess pressure in the air cushion. Aerodynamically, this drag is detrimental. To overcome the drag in the suction and delivery network, an additional power outlay is required, which degrades the power characteristics of the air cushion vehicle.

Pressure losses in the suction network are especially small, since the extent of the ducts forming this network is limited and its shaped sections do not produce large local drag values. Often the suction network consists only of an air-receiving connecting piece, which is at once the

inlet header of the fan. In this case the pressure losses in the suction network are assumed to be zero, since the air-receiving connecting piece-header is regarded as a component of the fan and the pressure losses it produced are accounted for in the fan characteristic.

Pressure losses in the delivery network can reach large values. They usually consist of pressure losses in the diffusor mounted behind the fan, in the annular and radial turns by which the fan diffusor is conjugated with the air-distributor ducts, in the receiver and its turns guiding the air into the nozzle installation, and also in the narrow constrictions and dilations produced by the presence in the flow-through section of different kinds of projecting parts and installations.

The total drag of the flow-through section in an air cushion vehicle is

$$H = \zeta \frac{\rho v_c^2}{2} + \sum \zeta_i \frac{\rho v_i^2}{2} + \sum \lambda_i \frac{l_i}{d_i} \cdot \frac{\rho v_i^2}{2}, \qquad (352)$$

where ζ is the coefficient of dynamic pressure losses in the stream as it exits from the nozzle installation; ζ_i is the coefficient of local drag in the shaped component of a duct; v_c is the mean air velocity in the flow-through openings of the nozzle installation; v_i is the mean air velocity in a typical section of a particular duct component; l_i is the length of the particular duct section; d_i is the equivalent diameter of the flow-through cross-section of a particular duct section; ρ is the air density; and λ_i is the coefficient of air friction against the walls of the particular duct section.

The first term at the right side of Eq. (352) characterizes the pressure losses in the nozzle installation, and the two others -- the pressure losses in the flow-through section ducts from the point at which the ambient air is sucked into the craft until it enters the nozzle installation. The coefficients ζ, ζ_i, and λ_i depend in the general case on the Reynolds number, velocity field profile in the air stream flowing into the duct element, the roughness of the duct walls, and the stream turbulence.

In practical calculations of the flow-through section in an air cushion vehicle, these coefficients can be determined from the appropriate theoretical or experimental functions for the specified geometry of the duct element and the assumed aerodynamic parameters of the air stream, with allowance for the effect of the Re number and other factors, but upon further examination of the various operating regimes of the flow-through section, these coefficients can be assumed to be constant and independent of these factors if during the variation of the regime these factor do not undergo large changes.

The coefficient of drag ζ in the nozzle installation and the coefficients ζ_i and λ_i of drag in the ducts, appearing in Eq. (352), are different in physical meaning, their values are determined by different factors, and they affect the characteristics of an air cushion vehicle in different ways. Let us determine what effect they have on a craft in the hovering regime.

51. Drag of Nozzle Installation

The pressure losses in a nozzle installation are

$$H_c = \zeta \frac{\rho v_c^2}{2} = \zeta \frac{\rho}{2} \left(\frac{Q}{F}\right)^2, \tag{353}$$

where Q and F are the air volume flow and flow-through area of the nozzle installation, respectively.

The drag coefficient ζ of a nozzle installation reflects the losses and kinetic energy suffered by the air jets producing the air cushion and comprises an outlay of total pressure required to produce these jets, expressed in fractions of the dynamic stream pressure determined from the mean discharge velocity. The size of this coefficient is predetermined by the nozzle installation geometry and by the position of this installation relative to the support surface, that is, on the one hand by shape of the nozzle installation, dimensions of the flow-through openings of its constituent nozzles, angle of generatrix inclination, and by the conditions under which the air flows into the nozzle installation, and on the other hand — by the elevation of the nozzle installation above the support surface, the relief of the surface, and the angle at which the nozzle installation heels with respect to it.

The drag coefficient ζ is associated with the discharge coefficient of the nozzle installation by the relationship $\zeta = 1/\sigma^2$. We can determine this coefficient in several cases theoretically with accuracy that suffices for practical purposes, or else experimentally by full-scale or model tests of nozzle installations in their required ranges of elevation above this support surface and angles of inclination to it.

For a single-pass nozzle installation with a nozzle flow-through width b and angle of generatrix inclination φ, and which is horizontal relative to a smooth solid support surface at elevation h, the drag coefficient is calculated by Eq. (78), or this coefficient is related to the flow-through area of the nozzle installation.

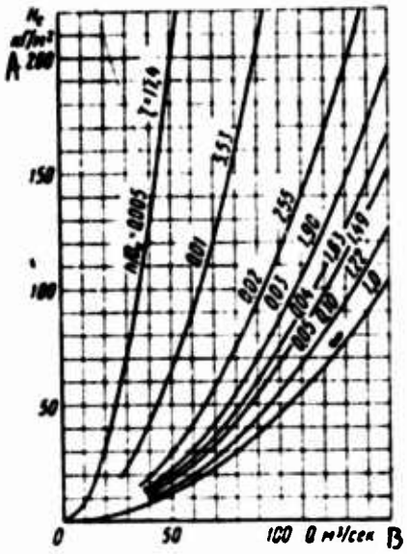

Fig. 223. Drag characteristics of nozzle installation of air cushion vehicle with single-pass annular nozzle as function of air volume flow (D_H = 10 m; b = 0.12 m; φ = 45°; ζ_k = 0)

KEY: A — kg/m^2
B — m^3/sec

The functions clarifying the manner in which the drag H_c of a nozzle installation depends on air volume flow q for different elevations h/D_H above the support surface are defined by Eqs. (353) and (78) for a planform round single-pass nozzle with diameter D_H = 10 m, flow-through width b = 0.12 m, and angle of generatrix inclination φ = 45°, and are shown in Fig. 223. As we can see, an increase in the elevation of the craft above the support surface reduces the drag of the nozzle installation, and when the craft is beyond the aerodynamic influence of ground proximity ($h = \infty$), the drag of the nozzle installation reaches its minimum (ζ = 1). When h = 0, where the craft rests on the ground with its nozzle installation, the drag coefficient $\zeta = \infty$. In this case, the characteristics of the nozzle installation drag coincide with the Y axis.

The drag coefficient ζ for double-pass and sectionalized nozzle installations depends more complexly on the geometrical parameters of the nozzle installation and its position relative to the support surface, above the pattern of variation $H_c = f(q)$ even in these cases remains similar to that shown in Fig. 223.

52. Drag of Flow-Through Section Ducts

Pressure losses in the flow-through section ducts over the area from the ambient air inlet into the air cushion vehicle to the point where air enters the nozzle installation are

$$H_{\kappa} = \sum \zeta_i \frac{\rho v_i^2}{2} + \sum \lambda_i \frac{l_i}{d_i} \cdot \frac{\rho v_i^2}{2};$$

this equation can conveniently be represented as the following, after determining the coefficients appearing in it:

$$H_{\kappa} = \sum (\zeta_i + \zeta_{\lambda i}) \frac{\rho v_i^2}{2},$$

where $\zeta_{\lambda i} = \lambda_i (l_i/d_i) = \text{const}$ is the reduced coefficient of friction.

Upon examining the problems associated with the combined operation of a fan and network, the network comprises of suction and delivery ducts is conveniently characterized by a single overall drag coefficient related to the representative cross-section of the flow-through area:

$$\zeta_{\kappa} = \frac{H_{\kappa}}{\frac{\rho v_c^2}{2}} = \sum (\zeta_i + \zeta_{\lambda i}) \left(\frac{v_i}{v_c}\right)^2,$$

where v_c is the mean air velocity in the nozzle installation exit adopted as the characteristic network cross-section.

The air volume flow in each section of the network ducts is the same, that is, $Q = v_i F_i = v_c F = \text{const}$, therefore $v_i/v_c = F/F_i$ and thus the drag coefficient of the suction and delivery sections of network are represented by

$$\zeta_{\kappa} = \sum (\zeta_i + \zeta_{\lambda i}) \left(\frac{F}{F_i}\right)^2.$$

where F and F_i are the cross-section areas of the exit of the nozzle installation and the particular duct section, respectively.

Thus, the pressure losses in the flow-through section ducts are

$$H_{\kappa} = \zeta_{\kappa} \frac{\rho v_c^2}{2}.$$

The drag coefficient ζ_k appearing in this formula characterizes the pressure losses associated with the phenomenon of stream separation from the walls of the flow-through section ducts, with the constrictions of the stream and its subsequent expansions, and also with the friction of the stream against the walls of the flow-through section ducts. This coefficient is determined by the duct geometry and the aerodynamic properties of the stream and is independent of the placement of the nozzle installation relative to the support surface.

53. Characteristics of Network Drag

Total pressure losses in the flow-through section of an air cushion vehicle, including the losses in dynamic pressure of the stream exits from the nozzle installation are

$$H = (\zeta + \zeta_{вх}) \frac{\rho v_c^2}{2}$$

or, with reference to $v_c = Q/F$,

$$H = (\zeta + \zeta_{вх}) \frac{\rho}{2} \left(\frac{Q}{F}\right)^2. \qquad (354)$$

In several cases it appears useful to characterize the total drag in the network

$$H = (\zeta + \zeta_{вх}) \frac{\rho v_c^2}{2} = \zeta_0 \frac{\rho}{2} \left(\frac{Q}{F}\right)^2 = kQ^2$$

by a single overall drag coefficient $k = (\rho/2) \cdot (\zeta + \zeta_k)/F^2$, which has the dimension $[кг \cdot сек^2/м^8]$.

Sometimes it is worthwhile expressing the drag of the craft flow-through section in terms of the drag coefficients given with respect to the exit area F_θ of the fan housing or with respect to the area $F_{ом}$ swept by the fan impeller. In these cases the drag coefficients are

$$\zeta_0 \quad \zeta_0 \left(\frac{F_\theta}{F}\right)^2 \quad \text{and} \quad \zeta_0' = \zeta_0 \left(\frac{F_{ом}}{F}\right)^2,$$

and the pressure losses in the flow-through section are

$$H = \zeta_0 \frac{\rho v_\theta^2}{2} \quad \text{and} \quad H = \zeta_0' \frac{\rho v_{ом}^2}{2},$$

where v_θ is the mean air velocity at the fan discharge; $v_{ом}$ is the mean air velocity in the imaginary opening, whose area is equal to the area swept by the fan impeller.

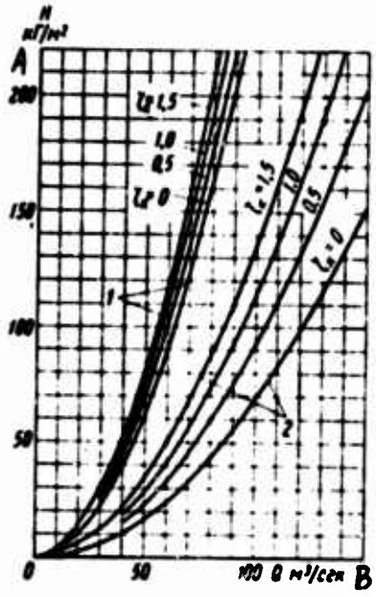

Fig. 224. Drag characteristics of network of air cushion vehicle with single-pass annular nozzle as function of air volume flow ($D_н$ = 10 m; b = 0.12 m; φ = 45°):

1 -- when $h/D_н$ = 0.01 and ζ = 5.53

2 -- when $h/D_н$ = 0.05 and ζ = 1.49

KEY: A -- kg/m^2
B -- m^3/sec

For a single-pass nozzle installation above the solid support surface by the height h, the pressure losses in the craft flow-through section are

$$H = \frac{1}{1}\left[\frac{b\,h\,(1+\sin\varphi)}{1-e^{-b\,h\,(1+\sin\varphi)}}\right]^2 + \\ + \zeta_н \frac{1}{1}\frac{\rho}{2}\left(\frac{Q}{F}\right)^2. \qquad (355)$$

This equation is the network characteristic expressed as the function $H = f(Q)$ relating the geometrical parameters of the craft flow-through section with its elevation above the support surface.

As an example, in Fig. 224 are given the drag characteristics of the flow-through section in an air cushion vehicle with a single-pass nozzle, with $D_н$ = 10 m, b = 0.12 m, and φ = 45°. These characteristics were plotted

by Eq. (355) for two craft elevations above the support surface ($h/D_н$ = 0.01 and 0.05) for different values of the drag coefficient ζ_k of the flow-through section ducts. The drag of the ducts is strongly reflected in the overall drag of the network at relatively high elevations of the craft above the support surface. At shallow elevations, the contribution of the drag introduced by the ducts into the overall drag of the network becomes less, in spite of the fact that the duct drag coefficients are of the same value. This is accounted for by the increase in the fraction of the drag introduced by the nozzle installation. The curves for $\zeta_k = 0$ correspond to the case when the network drag is determined only by the drag of the nozzle installation.

The network characteristics of craft with sectionalized nozzle installation can be determined in similar fashion. To do this, we need to replace the coefficient ζ appearing in Eq. (354) with an expression for it as the function of geometrical parameters of the nozzle installation and its elevation above the support surface, and when more complicated cases are considered -- also as a function of the heeling and pitching angles.

54. Craft Drag Characteristics

Let us find the relationship between craft weight, the load-bearing properties of its nozzle installation, and the drag of the flow-through section. In the free hovering regime the craft weight can be expressed in terms of the total pressure H_c in the air stream in front of the nozzle installation, lift coefficient c_y, and area S of the nozzle installation, that is,

$$G = c_y S H_c.$$

The pressure H_c is expended in forming the jets producing the air cushion, and with respect to the craft flow-through section is completely lost, that is, it consists of the drag in the nozzle installation:

$$H_c = \frac{G}{c_y S} = \zeta \frac{\rho v_c^2}{2} = \zeta \frac{\rho}{2} \left(\frac{Q}{F}\right)^2.$$

Accordingly, the total drag of the flow-through section of air cushion vehicle is

$$H = (\zeta + \zeta_н) \frac{\rho v_c^2}{2} = \frac{G}{c_y S} + \zeta_н \frac{\rho v_c^2}{2}$$

or

$$H = \frac{G}{c_y S} + \zeta_н \frac{\rho}{2} \left(\frac{Q}{F}\right)^2. \qquad (356)$$

Replacing the lift coefficient c_y by its dependence on the geometrical parameters of the nozzle installation, elevation h, and heeling and pitching angles, we will have the characteristic of the craft drag, represented in the form $H = f(Q)$, relating the craft weight, geometrical parameters of the flow-through section including the nozzle installation, and the altitude [position] of the craft relative to the support surface.

Thus, for a single-pass planform round nozzle installation with flow-through width b and angle of generatrix inclination $\varphi = 45°$ when $\gamma = \alpha = 0$, the lift coefficient is

$$c_y = \bar{F}_c + \bar{S}\bar{p}, \tag{357}$$

where $\bar{F}_c$ is the relative cut-off area,

$$\bar{F}_c = \frac{F_c}{S} =$$

$$4\frac{b}{D_н \cos\varphi}\left(1 - \frac{b}{D_н \cos\varphi}\right);$$

$\bar{S}$ is the relative area of the nozzle installation bottom measured with respect to the inner edge of the nozzle exit,

$$\bar{S} \quad \frac{S_1}{S} = 1 - \bar{F}_c;$$

$\bar{p}$ is the air cushion pressure coefficient determined by Eq. (74).

In the similar way we can express the lift coefficient of a craft with a sectionalized nozzle installation and determine its drag characteristics.

Fig. 225 presents the drag characteristics of an air cushion vehicle at different elevations $h/D_н$ above the support surface. This craft has a single-pass annular nozzle with parameters $D_н = 10$ m, $b = 0.12$ m, and $\varphi = 45°$, and flow-through section ducts for supplying external air into the nozzle. The duct resistance is defined by the coefficient $\zeta_к = 0.5$ related to the nozzle flow-through area. These craft characteristics are plotted by Eq. (356), with the use of Eq. (357).

On examining Fig. 225, we can conclude that in a craft resting on a support surface ($h/D_н = 0$), the discharge of air from the nozzle installation is impossible until the pressure beneath it $H \leq G/S$. As the pressure beneath the craft is increased, that is, as $H > G/S$, the craft rises to some elevation $h/D_н$. To sustain the craft weighing G in the hovering regime at this elevation we must expand a total pressure equal to the sum of the pressure $H_c = G/(c_y S)$ to produce the necessary lift and the pressure

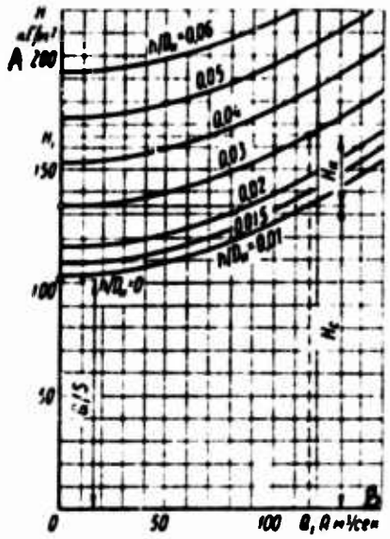

Fig. 225. Drag characteristics of air cushion vehicle as function of air volume flow for constant craft elevation (G = 8000 kg; D_M = 10 m; b = 0.12 m; φ = 45°; ζ_k = 0.5; $H_c = G/c_y S$; $H_k = \zeta_k \times (\rho/2)\cdot(Q/F)^2$)

KEY: A -- kg/m^2

B -- m^3/sec

$$H_k = \zeta_k \frac{\rho}{2}\left(\frac{Q}{F}\right)^2$$

to overcome the drag in the ducts exerted on the air passing through them. For this particular nozzle installation, as the elevation h is increased, the lift coefficient c_y becomes continually less, therefore the required pressure H_c must correspondingly rise.

The drag characteristics of the craft taken separately (356), as well as the network characteristics (354) do not uniquely determine the required pressures and air volume flows to raise a craft of a given weight to the specified elevation, since the drag characteristics of the craft do not allow for the pattern of variation in the nozzle installation drag, while the network characteristics do not allow for the weight of the craft and the load-bearing properties of its nozzle installation.

55. Characteristics of Required Pressures and Volume Flows

Let us find the characteristics of the required pressures and volume flows of air needed to raise a craft with a given weight to a specified elevation. For known craft weight, geometrical parameters of the flow-through section, and elevation above the support surface, by Eqs. (354) and (356) the air volume flow is

$$Q = \frac{F}{\sqrt{\zeta + \zeta_м}} \sqrt{\frac{2}{\rho}} \sqrt{H} = \frac{F}{\sqrt{\zeta + \zeta_м}} \sqrt{\frac{2}{\rho}} \sqrt{\frac{G}{c_y S} + \zeta_м \frac{\rho}{2} \left(\frac{Q}{F}\right)^2}.$$

After uncomplicated transformations, we have

$$Q = \frac{F}{\sqrt{\zeta}} \sqrt{\frac{2}{\rho}} \sqrt{\frac{G}{c_y S}}. \tag{358}$$

Knowing the required air volume flow, it is not difficult to determine the required total pressure needed to overcome the flow-through section drag:

$$H = \frac{G}{c_y S} + \zeta_м \frac{\rho}{2} \left(\frac{Q}{F}\right)^2 = \frac{G}{c_y S} +$$

$$+ \zeta_м \frac{\rho}{2} \cdot \frac{1}{F^2} \left(\frac{F}{\sqrt{\zeta}} \sqrt{\frac{2}{\rho}} \sqrt{\frac{G}{c_y S}}\right)^2,$$

from whence

$$H = \frac{\zeta + \zeta_м}{\zeta} \cdot \frac{G}{c_y S}. \tag{359}$$

Eqs. (358) and (359) allow us to determine the required air volume flow and total pressure that must be provided by the fan installation to overcome the drag in the flow-through section and to raise the air cushion vehicle to the specified elevation h, for known craft weight G and flow-through section geometry. Thus, by plotting on the graph $H = f(Q)$ the points corresponding to the values of Q and H calculated by Eqs. (358) and (359), we get a curve that is the characteristic of the required pressures and volume flows with reference to the craft weight and variation in its elevation above the support surface.

This same characteristic can also be defined as the geometrical locus of the points at which the craft characteristic (356) intersect with the drag characteristics of its network (354), for the appropriate elevations h of the craft above the support surface.

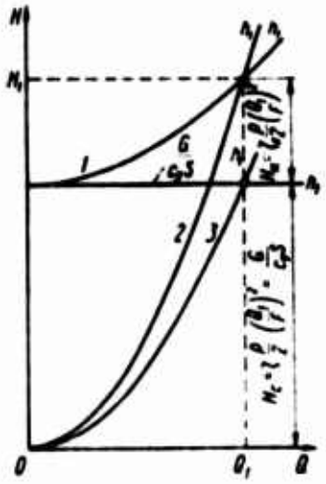

Fig. 226. Graphical determination of required pressure H_1 and volume flow Q_1 to sustain an air cushion vehicle with specified geometrical parameters and weight at an assumed elevation h_1:

1 — craft characteristics
2 — network characteristics
3 — function $H_c = \frac{\rho}{2}\left(\frac{Q}{F}\right)^2$

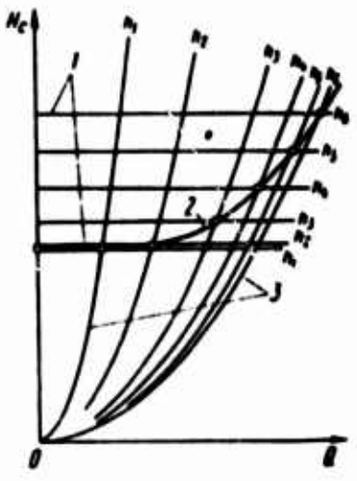

Fig. 227. Graphical determination of required pressures and air volume flows for an air cushion vehicle when $\zeta_k = 0$:

1 — craft characteristics
2 — characteristics of required H_c and Q
3 — network characteristics

The determination of the point characterizing the required pressure H_1 and the air volume flow Q_1 for the specified elevation h_1, by superimposing the craft characteristic on its network characteristic, is clarified in Fig. 226. Fig. 227 presents the construction of the characteristic of the required pressure and air volume flows for a craft having a specified weight and specified geometry of the nozzle installation in the particular case when the drag of the flow-through section ducts is equal to zero ($\zeta_k = 0$). Fig. 228 gives the construction of the analogous characteristic for the general case when $\zeta_k > 0$. To each point of these characteristics there corresponds a specific elevation h of the craft above the support surface.

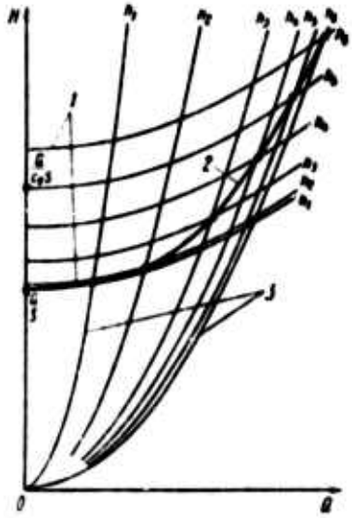

Fig. 228. Graphical determination of required pressures and air volume flows for air cushion vehicle when $\zeta_k > 0$:

1 -- craft characteristics
2 -- characteristics of required H and Q
3 -- network characteristics

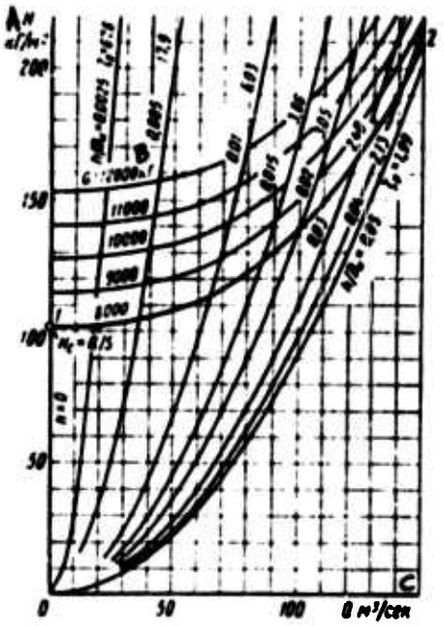

Fig. 229. Characteristics of required pressure and air volume flows of an air cushion vehicle with single-pass annular nozzle ($D_н$ = 10 m; b = 0.12 m; φ = 45°; ζ_k = 0.5)

KEY: A -- kg/m^2
B -- kg
C -- m^3/sec

The craft weight strongly affects the characteristics of the required pressures and air volume flows. As an example, Fig. 229 presents the characteristics of the required pressure and volume flows for an air cushion vehicle of different weights, with the same single-pass annular nozzle having the parameters $D_н$ = 10 m, b = 0.12 m, and φ = 45°. The drag coefficient of the flow-through section ducts over the area from the fan to the inlet into the nozzle installation, given with respect to the nozzle flow-through area, ζ_k = 0.5.

To get these characteristics, by assigning various values to the craft elevation h, we determine the coefficient of the nozzle installation drag ζ, the coefficient $\bar{p}$ of air cushion pressure, and the lift coefficient c_y by Eqs. (78), (74), and (357), respectively. Then, by using these values,

we calculate by Eqs. (358) and (359) the required air volume flows Q and the total pressures H to sustain a craft with given weight at the elevations h assumed in the calculation. In addition to the functions $H = f(Q)$ thus derived, Fig. 229 also presents the network drag characteristics calculated by Eq. (355) for various craft elevations above the support surface.

Let us examine the characteristic $H = f(Q)$ for a constant-weight craft. As the pressure in the flow-through section is varied from 0 to $H = G/S$, the craft remains immobile on the support surface ($h = 0$). When $H = G/S$, a critical state sets in -- the craft touches down. In this case all of the craft weight is transmitted to the support surface via the air cushion, since the elevation still remains equal to zero, the discharge of air from beneath the craft is absent ($Q = 0$). When $H > G/S$, the craft lifts from the support surface and enters the free hovering regime, rising to some elevation h. To increase the elevation, it is required to increase not only the total pressure H, but also the air volume flow Q regardless of the fact that the load per unit nozzle installation area remains constant. This is because as the elevation h is increased, the lift coefficient c_y is reduced, that is, the load-bearing ability of the nozzle installation becomes smaller. The rise in the craft weight leads to a rise both in the required pressure as well as in the required air volume flow to sustain the craft at a specified elevation h.

In actual conditions when an air cushion vehicle is on uneven soil, the exit edges of its nozzle installation do not lie tightly against the support surface. The different kinds of depressions and projections on this support surface, as well as the deflections of the exit nozzle edges from the bottom plane caused by the imperfection of craft manufacture, and some elastic deformation of its housing and the nozzle installation under its own weight produce gaps between the exit edges of the nozzle installation and the support surface through which air supplied to produce the air cushion can exit outward even when the craft rests on the ground.

In these conditions, the discharge of air from beneath the craft begins simultaneously with the rise in pressure in the flow-through section and occurs for operating regimes of the fan installation, that is, not only when the craft is hovering freely above the support surface, but even when the craft rests on the ground.

If we evaluate the height of the gaps by some arbitrary value and assume that the pressure losses therein vary in proportion to the square of the discharge velocity, in this case the network drag $\parallel (\zeta_0 + \zeta_\text{н}) \frac{\rho}{2} \left(\frac{Q}{F}\right)^2$

or when applied to a craft with a single-pass annular nozzle,

$$H = \left\| \left[\frac{b/h_0 (1 + \sin\varphi)}{1 - e^{-b/h_0 (1+\sin\varphi)}} \right] + \zeta_\text{н} \right\| \frac{\rho}{2} \cdot \left(\frac{Q}{F}\right)^2, \qquad (360)$$

where ζ_{co} is the drag coefficient of the nozzle installation on a support surface given the presence of a gap with height h_0.

The characteristic of required pressures and air volume flows in the coordinates H and Q in this case is defined by the broken line shown in Fig. 230. The section 0-1 of the curve calculated by Eq. (360) characterizes the required H and Q for the case when the craft rests on the ground. The section 1-2 of the curve calculated by Eqs. (358) and (359) corresponds to the craft hovering regime over a support surface. The point 1 of intersection of the curves characterizes the transitional regime in which the craft lifts off on the support surface and enters the free hovering regime.

The similar pattern of variation in the required pressures and volume flows, but more strongly pronounced, occurs for air cushion vehicles in which the exit edges of individual sections of the nozzle installation are above its sections that simultaneously fulfill the functions of support devices, such as for example, in craft with elevated bow and stern nozzles.

Characteristics of required pressures and volume flows make it possible to graphically represent the relationship between craft weight, geometrical parameters of nozzle installation and flow-through section, and also the aerodynamic parameters of the air stream producing the air cushion and the elevation of the craft above the support surface.

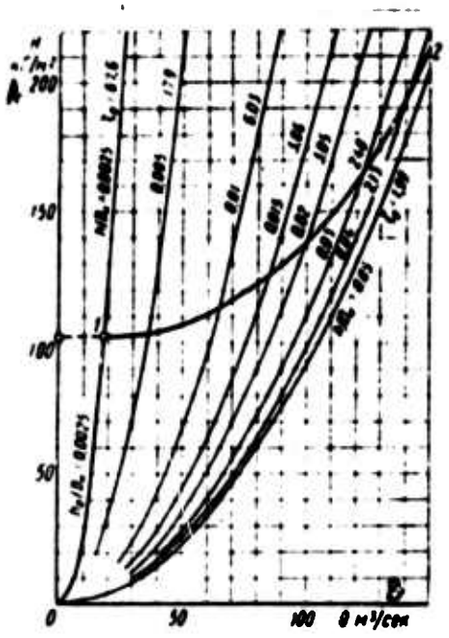

Fig. 250. Characteristics of required pressures and air volume flows for an air cushion vehicle with single-pass annular nozzle, when the clearance between the nozzle edges and the support surface is h_0 (G = 8000 kg; $D_н$ = 10 m; b = 0.12 m; $\varphi = 45°$; $\zeta_к = 0.5$; h_0 = 0.025 m)

KEY: A -- kg/m^2

B -- m^3/sec

CHAPTER TEN
EFFECT OF OPERATING REGIME OF FAN INSTALLATION ON AIR CUSHION CHARACTERISTICS

Let us examine the effect that the operating regime of a fan installation has on the aerodynamic and power characteristics of an air cushion vehicle when the craft is freely hovering above the support surface. This influence can be shown in convenient and graphic form by using the characteristics of the required pressures and air volume flows for an air cushion vehicle for specified geometrical parameters and weight and specified aerodynamic characteristics of the fan. By superimposing the characteristics of craft pressures and air volume flows $[H = f(Q)]$ over the fan characteristics, we can select the optimal fan installation, evaluate the possible fan operating regimes in the craft, and select the rational method of regulation. Then we can follow the variation in the attitude [position] of the craft above the support surfaces by varying the method of fan operation or the parameters of the craft flow-through section.

56. Effect of Fan rpm on Craft Characteristics

We will assume the geometrical parameters of a craft, that is, the shape and size of its nozzle installation and its flow-through section to be specified, and the type, dimensions, and characteristics of the fan installed on the craft to be known. Suppose a craft with weight $G = 8000$ kg has a nozzle installation made in the form of a single-pass annular nozzle, with diameter $D_H = 10$ m, flow-through width $b = 0.12$ m, and angle of nozzle generatrix inclination $\varphi = 45°$. The drag coefficient of the flow-through section ducts $\zeta_k = 0.5$. A model K-06 TsAGI axial fan is installed on the craft, with a wheel having the diameter $D_\beta = 3.0$ m, with number of blades $z = 12$, and with blade angle $\theta_k = 20°$.

Let us use Eqs. (359) and (358) and determine the characteristic of required air pressures and volume flows for this craft (Fig. 251). Specifying various values for the craft elevation h, by Eqs. (78), (74), and

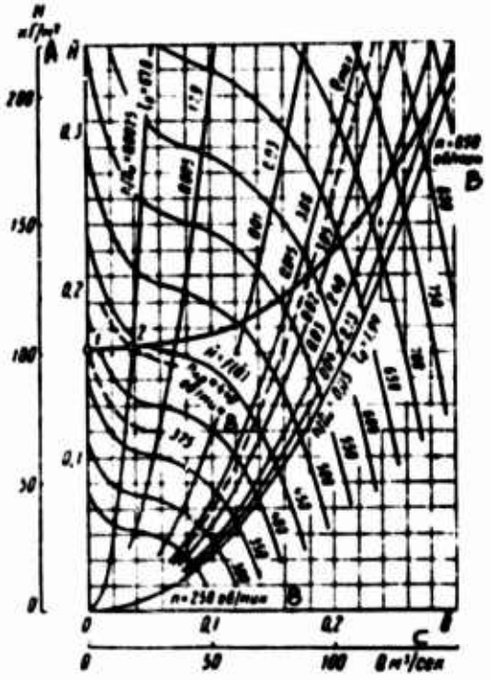

Fig. 251. Effect of fan annular velocity on air cushion vehicle characteristics (G = 8000 kg; D = 10 m; b = 0.12 m; φ = 45°; ζ_k = 0.5; D_k = 3 m; z = 12; θ_k = 20°)

KEY: A -- kg/m^2
B -- rpm
C -- m^3/sec

(357) we determine the coefficients ζ, $\bar{p}$, and c_y. Then by Eqs. (359) and (358) we calculate, respectively, the required air pressures H and volume flows Q to sustain a craft having a given weight at the elevations h assumed in all calculations.

Further, let us use the dimensionless aerodynamic characteristic of the fan $\bar{H} = f(\bar{Q})$ shown in the form of the curve coinciding with the dimensional characteristic when n = 450 rpm, and the expressions for the pressure coefficient and the capacity coefficient:

$$\bar{H} = \frac{H}{\rho u^2}; \quad (361)$$

$$\bar{Q} = \frac{Q}{F_k u}, \quad (362)$$

where u is the tip velocity of the outer radius of the fan wheel, $u = (\pi D_k n/60)$; F_k is the fan wheel area, $F_k = \pi D_k^2/4$; D_k is the diameter of the fan wheel; and n is the wheel rpm.

Then, let us determine the dimensional characteristics of the fan for different rpm values n of its wheel and let us plot these characteristics on the characteristic of the required craft pressures and air volume flows. Let us also plot the characteristics of network resistance for different elevations h/D_H of the craft above the support surface calculated by Eq. (354).

The points at which the fan characteristics intersect with the characteristic of the required pressures and air volume flows will also be the working points determining the fan operation in the craft with specified parameters and weight for the corresponding elevation h/D_H of the craft above the support surface.

Fig. 231 shows that for small fan rpm when the total pressure builds up by the fan and transmitted via the flow-through section underneath the craft is still inadequate to produce the required lift, that is, when $H < G/S$, the craft rests on the support surface ($h = 0$). With increase in fan rpm, the pressure beneath the craft rises, and for some critical value of fan rpm (n_{kp} = 575 rpm [kp = critical]) the moment is reached when the entire craft weight is transmitted to the soil via the air cushion. To this corresponds the total pressure value $H = G/S$. With further rise in the fan rpm, the craft lifts from the support surface and rises to some elevation h determined by the amount of air fed into the flow-through section and by the corresponding pressure buildup by the fan in the flow-through section. We must remember that up to the moment of craft liftoff from the ground $c_y = 1$, but after liftoff $c_y \neq 1$.

In addition, it is quite clear that with increase in fan rpm in the range from $n = 0$ to $n = n_{kp}$, the working point shifts from the extreme left point of the fan characteristic, and then with further rise in the rpm it shifts along the fan characteristic downward, passing all of its points lying in the range from $Q = 0$ to Q_n -- the air volume flow corresponding to the particular fan rpm.

Variation in craft rpm and craft aerodynamic parameters as typical functions of fan rpm, with constant craft weight, are shown in Fig. 232. These functions were plotted from data determined by the working points of the curves shown in Fig. 231.

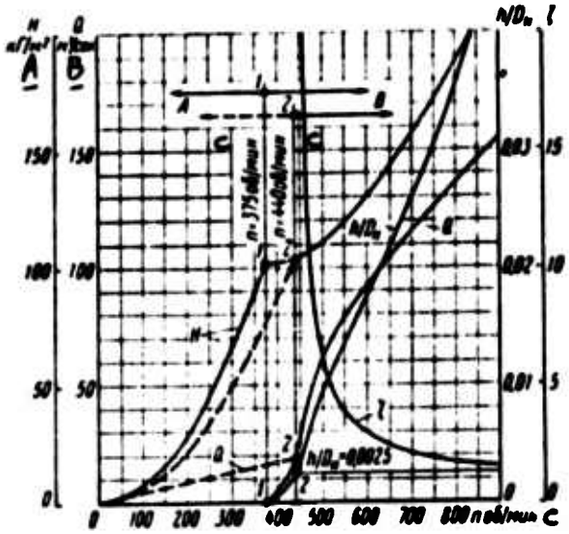

Fig. 232. Elevation of air cushion vehicle and its aerodynamic characteristics as functions of fan angular velocity:
A -- craft on ground
B -- craft in free hovering regime
KEY: A -- kg/m^2
B -- m^3/sec
C -- rpm

The section of the total pressure curve H lying between the points 0 and 1 corresponds to the case when the craft rests on the bottom, and the edges of its nozzle installation fit tightly against the support surface. The total pressure over the section is

$$H = H_{кр}\left(\frac{n}{n_{кр}}\right)^2,$$

where $H_{кр}$ is the total pressure generated by the fan at fan wheel rpm $n_{кр}$ = 375 rpm.

The section of the curve H = f(n) lying to the right of point 1 and corresponding to the values n > 375 rpm characterizes the regime of craft free hovering above the support surface. The pattern of variation in the air volume flow Q, elevation $h/D_н$, and drag coefficient ζ of the nozzle installation as functions of fan rpm n is determined by the corresponding curves shown in this same figure.

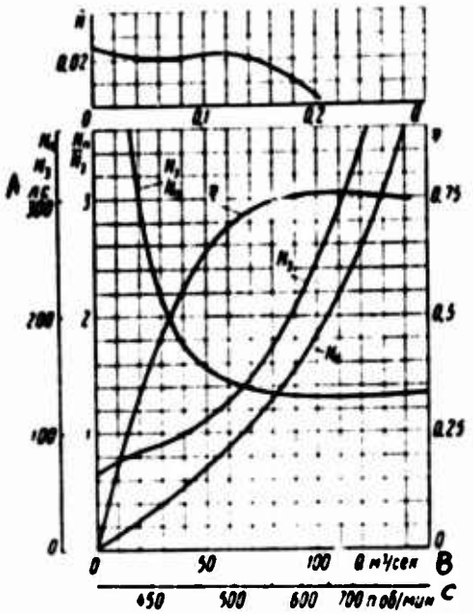

Fig. 233. Required and expended power as functions of air supplied to flow-through section of craft, determined by fan angular velocity
KEY: A -- hp
B — m^3/sec
C -- rpm

In actual conditions when an air cushion vehicle is on uneven ground, clearances of various heights are formed. In this situation, the discharge of air from beneath the craft begins simultaneously with the pressure rise in the craft flow-through section and beneath the craft caused by the operating fan. These clearances can be estimated roughly by the elevation h_0, and the drag coefficient can be expressed as

$$\zeta_{\text{вн}} = \left[\frac{b/h_0(1+\sin\varphi)}{1-e^{-b/h_0(1+\sin\varphi)}}\right]^2.$$

If we assume that $h_0/D_M = 0.0025$, the dependence of total pressure H and air volume flow Q on fan rpm h when the craft is on the ground will have the form of curves 0-2 (cf. Figs. 231 and 232). The critical value of the fan wheel rpm in this case is n'_{kp} = 440 rpm. Over the range of fan wheel rpm values from n = 0 to $n = n'_{kp}$ = 440 rpm, the air volume flow is

$$Q = Q_{кр} \frac{n}{n_{кр}},$$

where $Q_{кр}$ is the air volume flow when $n'_{кр}$ = 440 rpm.

Let us trace the power outlays as a function of changes in fan operating regime in the flow-through section of the craft defined by the working points lying at the intersections of fan characteristics with the characteristic of required pressures and air volume flows. In Fig. 233 we plotted the dimensionless characteristics of the expended power $\bar{N} = f_1(\bar{Q})$, and also the fan efficiency η, required power $N_п$, expended power $N_с$, and the ratio $N_з/N_п$ as functions of air volume flow. These power values are defined by the following expressions:

$$N = \frac{75N_з}{\rho u^3 F_к} \quad \text{and} \quad N_п = \frac{HQ}{75},$$

where $N_з$ is the expended power corresponding to the power measured on the balancing stand when the fan characteristic was recorded; u is the tip velocity at the outer radius of the fan wheel; H is the total pressure built up by the fan in the craft flow-through section; and Q is the fan capacity.

As the fan angular velocity n is reduced, that is, in the transition from the calculated regimes (corresponding to the maximum efficiency or near-maximum efficiency) to the regimes with low craft hovering height above the support surface, the expended power with respect to the required power rises markedly. This is accounted for by the specific characteristic of required pressures and air volume flows intrinsic to air cushion vehicles, which result -- as the fan rpm is reduced -- to the shifting of the working point upward along the fan characteristic in the region of low efficiencies.

Therefore, the method of varying the craft elevation above the support surface that is based on regulating the fan operating regime by varying its wheel rpm over a wide range is energetically nonoptimal. By this method of regulation, prolonged operation of the fan in the nondesigned regimes at low elevations is inexpedient from the standpoint of fuel economy.

Another important factor that must be remembered when selecting the axial fan for an air cushion vehicle relates to the shifting of the working point along the fan characteristic over the entire section from Q = 0 to the design value Q as the rpm is varied. To reduce fan size, axial fans with large blade placement angles are used. With these blade angles, the characteristics of axial fans have a trough or even discontinuities in the low-capacity section. When a craft enters the free hovering regime, the working point always passes through the zone of this trough and extremely undesirable unstable fan operating regimes in the network are possible.

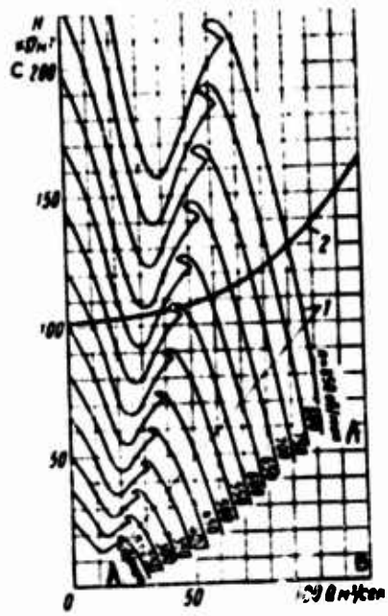

Fig. 234. Graphical determination of the effect of an angular velocity on stability of fan operation in an air cushion vehicle:
1 -- fan characteristics
2 -- characteristic of required H and Q
KEY: A -- rpm
B -- m^3/sec
C -- kg/m^2

Typical characteristics of an axial fan with large blade placement angle for different wheel rpms are shown in Fig.234, where the characteristic of the required pressures and air volume flows of an air cushion vehicle is plotted. As we can see, for both small as well as large fan rpms the working points lie on the steeply-dropping branches of the fan characteristic, to which corresponds the completely stable fan performance in the flow-through section of the craft. At moderate angular velocity lying in the range $n \approx 600$-690 rpm, the characteristic of required pressures and air volume flows of the craft and the fan characteristics intersect in the trough section, where there is an abrupt variation in the fan operating regime: the air supplied into the flow-through section of the craft and the craft elevation above the support surface changes in jumps. Here the critical angular velocity at which an abrupt variation in the fan

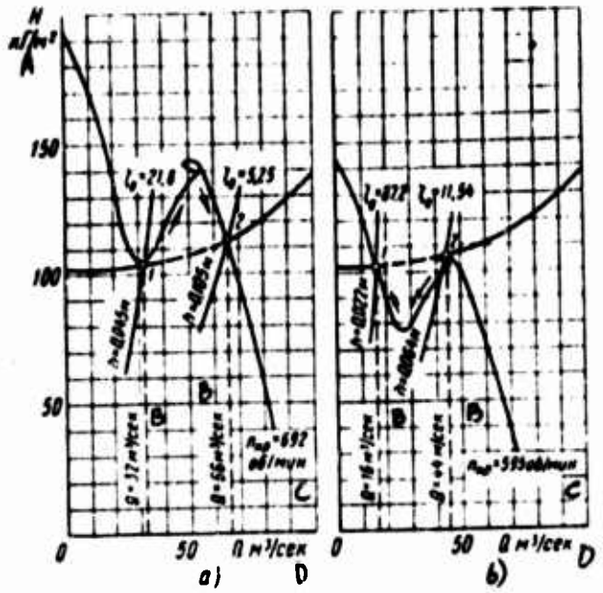

Fig. 235. Effect of changes in fan angular velocity in an air cushion vehicle on the transition of the working point through the zone of instable performance:
a and b -- with increase and decrease in angular velocity, respectively
KEY: A -- kg/m^2
B -- m^3/sec
C -- rpm
D -- m^3/sec

operating regime sets in depends on the method by which the working point is approached toward the zone of unstable fan operation.

Two representative cases of the transition of the working points through the zone of unstable fan operation are shown in Fig. 235, a and b. In the first case, characterized by a gradual rise in the angular velocity, the critical velocity sets in when n_{kp} = 692 rpm. Even the slight rise in the angular velocity compared with the critical results in the working point 1 shifting discontinuously along the right steeply-dropping branch of the fan characteristic to point 2, the air volume flow rising discontinuously from 52 to 66 m^3/sec, and the elevation of the craft above the support surface rising similarly from 0.045 to 0.105 m. With further increase in the angular velocity, the working point shifts downward along the right branch of the characteristic as the fan operates quite stably.

In the second case characterized by a gradual decrease in the angular fan wheel velocity, the critical velocity sets in when n_{kp} = 595 rpm. A slight drop in the angular velocity compared with the critical value also causes a discontinuous transition of the working point to the other steeply-falling branch of the fan characteristic. In this case the air volume flow decreases discontinuously from 44 to 16 m^3/sec, while the craft descends from the elevations 0.064 to 0.022 m.

These transitions of the working points through the zone of unstable fan operation as the fan wheel angular velocity is varied can lead to large aerodynamic loads on the fan wheel and even to its breakdown. Impacts of the craft against the ground are possible, for example, when the fan angular velocity is reduced and in the transition from the working point 2 to the working point 1, when the craft passes through the elevation h = 0.022 m and drops to h = 0 under the effect of the inertial forces induced as the craft drops from the elevation h = 0.064 m.

Employing special antisurge devices in the fan, the trough in the fan characteristic can be reduced or even completely eliminated and the fan operation can be made stable even when using the method of regulation based on varying the angular velocity of the fan wheel.

57. Variation in Fan Characteristics by Throttling the Air Stream in the Flow-Through Section

One of the simplest, designwise, methods of varying the characteristics of an air cushion vehicle by varying the operating regime of its fan installation is the technique of throttling the air stream in the craft flow-through section. With this technique, a throttling unit comprised of swivel dampers, baffles, diaphragms, and so on is installed in the duct of the flow-through section, is put in its narrow cross-section. By varying smoothly the duct flow-through cross-section and thus producing additional drag, the amount of air passing through the craft flow-through section can be regulated. Here an effort is made to install the throttle unit at a sufficient distance from the nozzle installation in order that the perturbations in the air stream caused by the throttling unit can be damped along the path to the nozzle installation and not have a detrimental aerodynamic effect on the latter (degrading the uniformity of air distribution as the nozzle installation is approached).

The aerodynamic drag produced by the throttle unit is

$$H_\partial = \zeta_\partial \frac{\rho v_\partial^2}{2} = \zeta_\partial \frac{\rho}{2} \left(\frac{Q}{F_\partial}\right)^2$$

$$\zeta_\partial \left(\frac{F}{F_\partial}\right)^2 \frac{\rho}{2} \left(\frac{Q}{F}\right)^2 \quad \zeta_\partial \frac{\rho}{2} \left(\frac{Q}{F}\right)^2,$$

where $\zeta_д$ is the drag coefficient of the throttle unit related to the representative duct cross-section; $\zeta_д'$ is the drag coefficient of the throttle unit related to the flow-through area of the nozzle installation; $v_д$ is the air velocity in the representative duct cross-section; $F_д$ is the area of the representative duct cross-section; and F is the exit area of the nozzle installation.

The value of the coefficient $\zeta_д'$ appearing in this expression is determined by the degree of throttle opening and for convenience in analysis can be represented as the function $\zeta_д' = f(\delta)$, where δ is the angle by which the throttle damper is rotated or else the value of the scale division characterizing the displacement of the damper. In this case the total drag in the flow-through section is

$$H = (\zeta + \zeta_к + \zeta_д') \frac{\rho}{2} \left(\frac{Q}{F}\right)^2. \qquad (363)$$

and the craft characteristic is

$$H = \frac{G}{c_y S} + (\zeta_к + \zeta_д') \frac{\rho}{2} \left(\frac{Q}{F}\right)^2. \qquad (364)$$

Solving jointly Eqs. (363) and (364), we derive the formulas for the required air volume flow

$$Q = \frac{F}{\sqrt{\zeta}} \sqrt{\frac{2}{\rho}} \sqrt{\frac{G}{c_y S}} \qquad (365)$$

and for the required pressure

$$H = \frac{\zeta + \zeta_к + \zeta_д'}{\zeta} \cdot \frac{G}{c_y S}.$$

In these formulas the lift coefficient c_y and the drag coefficient ζ of the nozzle installation depend on the geometrical parameters of the nozzle installation and its elevation h above the support surface. The drag coefficient $\zeta_к$ of the flow-through section ducts for specified geometrical parameters is a constant, while the drag coefficient $\zeta_д'$ of the throttle unit is a variable, dependent on the opening of the throttle damper and is characterized, for example, by its angular displacement δ. The drag produced by the throttle unit, by increasing the drag of the flow-through section, does not vary the drag of the nozzle installation.

The characteristic of the required pressures and volume flows corresponding to the different angles of throttle damper opening (Fig. 236) was determined by Eqs. (364) and (365) in the following order. Assigning

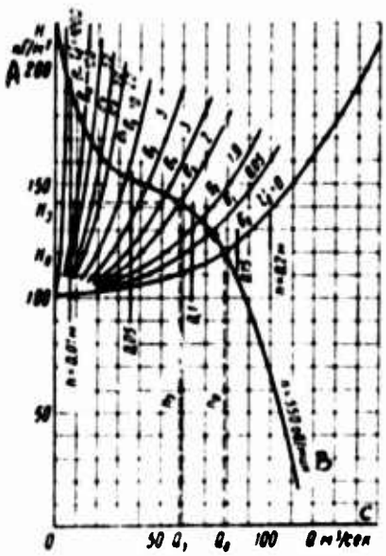

Fig. 256. Effect of throttling of air stream in flow-through section on air cushion vehicle characteristics (G = 8000 kg; D_M = 10 m; b = 0.12 m; φ = 45°; ζ_k = 0.5; D_k = 3 m)

KEY: A -- kg/m^2
B -- rpm
C -- m^3/sec

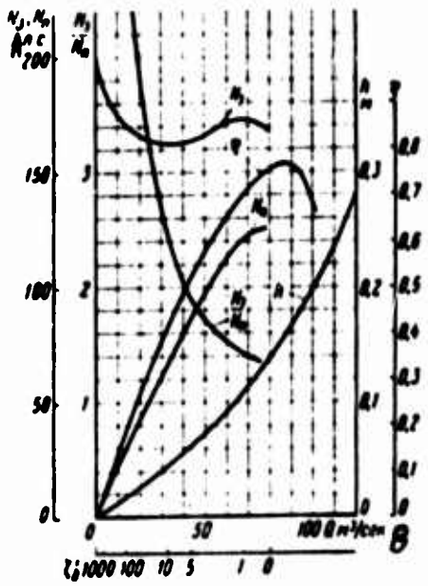

Fig. 257. Required and expended power as functions of air supplied to the flow-through section of craft, determined by the closure of throttle

KEY: A -- hp
B -- m^3/sec

various values to the craft elevation h, the coefficients ζ and c_y were determined. Then, by using the values found, the required air volume flow Q and total pressure H were found for different values of the coefficient ζ_δ' of the throttle unit determined by the angle δ of its opening.

Fig. 256 also presents the characteristic of the TsAGI K-06 axial fan equipped with a wheel having the diameter D_ϕ = 3.0 m, with number of blades z = 12, and angle of blade placement θ_k = 20°, for constant wheel angular velocity n = 550 rpm.

When the throttle damper was completely open δ_0 = 0, to which corresponds ζ_δ' = 0, the fan supplies into the network air in the amount Q_0 at total pressure H_0. To this case there corresponds the maximum craft

elevation h_0 above the support surface for a specified fan rpm. With increasing closing of the damper, that is, in the transition from δ_0 to other value of δ, the drag in the flow-through section rises and the fan feeds a smaller amount of air at a greater total pressure. Thus, when the throttle damper is in the position δ_3, the fan supplies into the network air in the amount Q_3 at total pressure H_3. Corresponding to this damper position is the craft elevation h_3. Further closing of the damper leads to a gradual drop in the craft elevation. Here the working point is defined by the intersection of the fan characteristic with the characteristic of the required pressures and volume flows, uniquely related to the network characteristic.

The required N_n and expended N_3 power as functions of air volume flow Q, for a different opening of the throttle damper characterized by the drag coefficient ζ_δ' of the throttle unit, are shown in Fig. 237. Here also are plotted the functions $N_3/N_n = f_1(Q)$, and efficiency $\eta = f_2(Q)$, and craft elevation above the support surface $h = f_3(Q)$. The power was determined via the formulas

$$N_n = \frac{HQ}{75} \quad \text{and} \quad N_3 = \frac{\Delta p_c' V_s}{75},$$

where H and Q were taken from the curves (in Fig. 236), and $\bar{N}$ -- from the curve (in Fig. 235) for the corresponding values of the discharge coefficient α related to the air volume flow Q by Eq. (362).

With increasing closing of the throttle damper leading to a gradual drop in the craft hovering height h (cf. Fig. 237) above the support surface, the expended power N_3 at first decreases somewhat, but then with further increase in the hovering height rises rapidly and becomes greater than the power expended that the maximum hovering height corresponding to total opening of the throttle damper when the required pressure is at its maximum.

By comparing the functions $N_n = f_1(Q)$ and $N_3 = f_2(Q)$, we can conclude that the method of varying craft characteristics by throttling the air stream in the flow-through section is energetically extremely disadvantageous, since it involves a large nonproductive outlay of power in overcoming the additional drag produced by the throttle unit.

98. Varying the Craft Characteristics by Regulating the Fan Stator

One of the possible methods of extensively varying the fan aerodynamic characteristics is the technique based on varying the vane angle placement

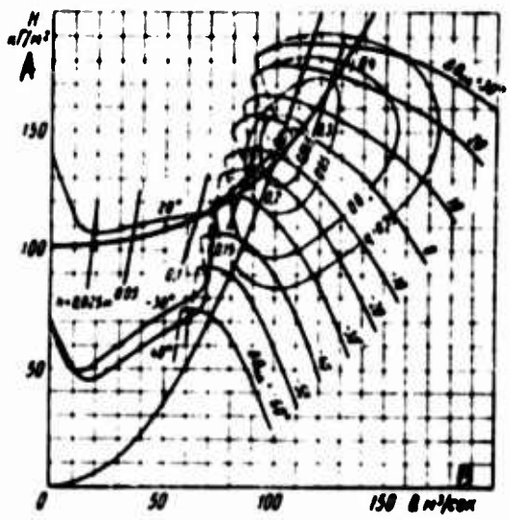

Fig. 258. Variation in air cushion vehicle characteristics caused by regulating fan guide unit (G = 8000 kg; D = 10 m; b = 0.12 m; $\varphi = 45°$; $\zeta_k = 0.5$; $D_k = 5$ m; n = 322 rpm; u = 50.6 m/sec)

KEY: A -- kg/m^2

B -- m^3/sec

of the stator by rotating the vanes. With this regulation, the turning rate of the stream as it enters the impeller is varied, which for a given capacity changes the theoretical pressure of the fan and the pressure losses in it. In a properly designed fan with stator, it is possible to achieve a very broad zone of pressure and falling flow regulation for extremely high fan efficiencies. This method of regulation is quite simple to execute in design.

Let us examine the possibilities of using the vane stator as a device for regulating the hovering regime of an air cushion vehicle above a support surface. Let us assume that a craft with weight G = 8000 kg has a single-pass nozzle installation with diameter D_H = 10 m, nozzle flow-through width b = 0.12 m, and angle of generatrix inclination $\varphi = 45°$. The drag coefficient of the flow-through section ducts extending from the fan outlet to the inlet into the nozzle installation will be taken as $\zeta_k = 0.5$. Let us determine and plot in the coordinates H and Q the characteristic of required total pressures and air volume flows for this craft (Fig. 258).

Let us assume that the TsAGI K-70 meridional fan with stator [9] permitting the vane placement angle this stator to be varied within the range $\Delta\theta_{HA}$ = -60 - 30° is installed in the craft. We take as the design elevation of the craft above the support surface in the free hovering regime to be h = 0.2 m. To this elevation there corresponds the pressure H = 139 kg/m^2 and the air volume flow Q = 100 m^3/sec.

Using the dimensionless aerodynamic characteristics of the fan, let us determine from these design data the fan dimensions and its rpm, assuming that the fan in an air cushion vehicle must operate at the maximum possible efficiency (for the K-70 fan, η_{max} = 0.875 when $\bar{H}$ = 0.44 and $\bar{Q}$ = 0.28). The assumed conditions are satisfied by a fan with diameter D_k = 3 m, with angular velocity n = 322 rpm, and arbitrary vane placement angle in the stator $\Delta\theta_{HA}$ = -11°.

Using the familiar conversion formulas, let us determine for this case the dimensional characteristics of the fan and plot among the characteristic of pressures and volume flows of an air cushion vehicle. Here also we plot the network characteristics corresponding to the representative elevations h of the craft above a support surface.

For the adopted design condition (selection of fan based on maximum efficiency), the use of the possible stability of the fan stator with respect to reducing the air supply into the flow-through section and with respect to the corresponding drop in the craft elevation above the support surface is restricted. Thus, when the vanes of the stator are mounted at the angle $\Delta\theta_{HA}$ = -30°, the working point passes beyond the section of the separation zone of the characteristic and a further slight reduction in the angle $\Delta\theta_{HA}$ causes a jumplike drop in the fan capacity and so intense a drop in the pressure built up by the fan that owing to the air deficiency the nozzle installation is now incapable of producing the required lift to sustain the craft in the air, and the craft makes a hard landing from the elevation determined by the extreme working point on the right branch of the fan characteristic.

The takeoff and climb of a craft to the design elevation is also complicated. For a craft to be able to lift off from the support surface, it is necessary to have $H \geq G/S$ when Q = 0. For the transition to the design elevation it is necessary that the left branch of the fan characteristic passes above the characteristic of the required pressures and volume flows of the craft. For the craft to enter the design elevation, it is necessary to install the stator vanes at the angle $\Delta\theta_{HA}$ = +20°, where in this case also the transition of the working point through the separation zone will be accompanied by the surging regime of fan operation with all of its consequences.

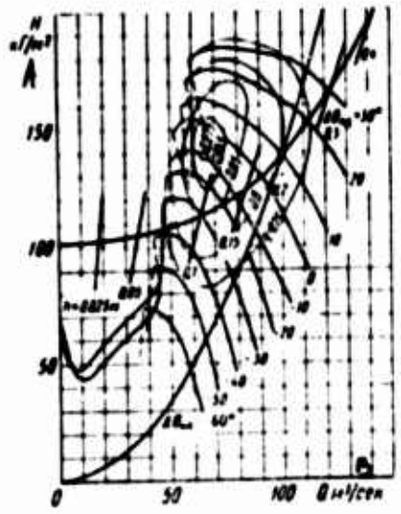

Fig. 259. Variation in air cushion vehicle characteristics by regulating fan guide unit (G = 8000 kg; D_H = 10 m; b = 0.12 m; φ = 45°; D_k = 2.45 m; n = 595 rpm; u = 50.6 m/sec)

KEY: A -- kg/m^2

B -- m^3/sec

The fan stator produces a zone of advantageous changes in H and Q lying along the characteristic of the network drag $H = kQ^2$, where k is a constant independent of pressure H. Therefore, for ordinary commercial fans in which the characteristic of the network drag is simultaneously the characteristic of the required pressures and volume flows, method of regulation by using the stator is very advantageous, since it permits extensive regulation with respect to pressure H and volume flow Q for fairly large fan efficiencies.

In an air cushion vehicle the fan operating regime is determined by the characteristic of the required pressures and volume flows, differing widely from the ordinary network characteristic. The zone of advantageous changes in H and Q produced by the fan stator intersects the characteristic of the required pressures and volume flows of an air cushion vehicle and only partially coincides with it. At small volume flows and pressures, the characteristic of the required H and Q values of a craft departs rapidly to the left from the design values of H and Q, approaching the constant value H = G/S, when Q = 0.

The extent of regulation by a fan stator can be somewhat enhanced if we depart from the particular design condition we have been considering -- selecting a fan by its maximum efficiency. Thus, moving on to larger design values of the dimensionless volume flow $\bar{Q}$ for the same total pressure $\bar{H}$ and the correspondingly smaller fan efficiencies, we can also shift, in the coordinates H and Q, the working branches of the fan characteristic to the left and thus expand the zone of stable regulation, and narrow the zone of surge regimes.

In one of these cases (Fig. 239), the design parameters for fan selection were taken as the following: $\bar{H} = 0.44$, $\bar{Q} = 0.43$, and $\eta = 0.8$, and for the air cushion vehicle $H = 139$ kg/m^2, $Q = 100$ m^3/sec, and $h = 0.2$ m. To these conditions there corresponds a fan with $D_k = 2.43$ m, $n = 395$ rpm, and arbitrary vane placement angle in the stator $\Delta\theta_{HA} = +10°$.

By comparing the corresponding curves (Figs. 238 and 239), we can see that in this case the extent of regulation by means of the stator vanes becomes greater and becomes possible in the range $\Delta\theta_{HA} = +10$ to $-39°$, while in the preceding case $\Delta\theta_{HA} = -10$ to $-30°$. The critical elevation of an air cushion vehicle above a support surface at which the surge fan regime sets in was reduced from $h = 0.14$ m to $h = 0.07$ m, that is, by a factor of two. However, even in this case the transition of the working points through the surge zone of the fan is not precluded.

Note that the better the flow-through section of an air cushion vehicle is from the aerodynamic standpoint, that is, the smaller the detrimental aerodynamic drag of the ducts over the area from the fan to the nozzle installation (receiver and its components), the less advantageous becomes the method of regulating using the stator, since the steepness of the rise in the characteristic of the required pressures and air volume flows of the craft becomes less and thus the range of regulation is also correspondingly narrowed.

These factors strongly limit the effective use of a fan stator as a device for extensive regulation of the takeoff and landing regimes of an air cushion vehicle. The possibility of providing design parameters H and Q for small fan dimensions is a marked advantage of selecting a fan based on large $\bar{q}$ values.

When employing the combined regulation by varying both the stator vane placement angle of a fan as well as the angular velocity of the fan impeller simultaneously in a craft, the air cushion vehicle takeoff and landing process can be executed at relatively low fan wheel rpm values and in a narrow range of elevations in which the surge regime of fan operation is found, which makes the craft takeoff and landing less hazardous. To execute these maneuvers, it is advantageous to mount these stator vanes at the maximum angle $\Delta\theta_{HA}$, and then gradually increase the angular velocity

of the impeller in the case of takeoff, and to reduce it — in the case of landing. Here the angular velocity of the impeller for entering the design regime will be at a minimum.

A marked improvement in regulating air cushion vehicle characteristics can be attained by employing antisurge devices on the fan. However, for large vane placement angles on the fan impeller, these devices do not completely eliminate the trough in the fan characteristic and do not afford the desired solution to the problem.

59. Effect of Fan Blade Placement Angle on Craft Characteristics

One of the effective methods of varying the air cushion vehicle characteristics can be a method based on varying the blade placement angle of the fan impeller at constant rpm. This method permits the following:

to use axial fans of relatively small size on a craft, since the design regimes of the craft for large impeller blade placement angles can be achieved without employing antisurge devices;

avoiding the hazards of surge fan operating regimes in all possible craft operating conditions; and

affording, within wide limits, regulation of fan operation, that is, varying the amount of air fed to the flow-through section, and providing the corresponding reduction in the elevation of the craft above the support surface while retaining quite high fan efficiencies.

In some cases of craft layout, these advantages become decisive and predetermined method of selecting the method of varying craft characteristics. Disadvantages of this method include the marked complexity in fan wheel design, since it must be fitted with a device permitting the blades to be swiveled during operation.

Let us examine this method more closely. Suppose a craft with weight G = 8000 kg has a single-pass annular nozzle with diameter D_H = 10 m, exit width b = 0.12 m, and angle of nozzle generatrix inclination φ = 45°. The drag coefficient of the flow-through section ducts ζ_k = 2.5. An axial TsAGI K-06 fan with impeller diameter D_k = 2.2 m and number of blades z = 12 is mounted on the craft. The fan is equipped with a device that makes it possible to vary the impeller blade placement angle within the range θ_k = 10 - 40°. The motor driving the fan provides a constant angular velocity n = 742 rpm.

The characteristic of required total pressures and air volume flows of this craft is shown in Fig. 240 in the coordinates H and Q. On this

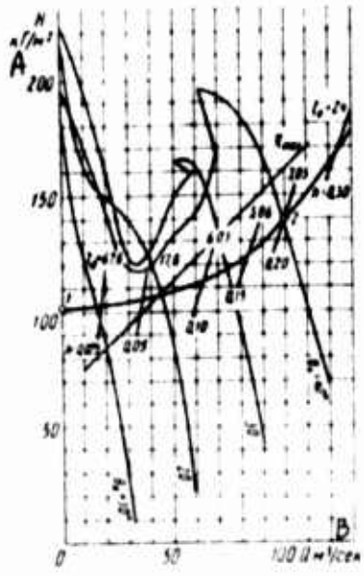

Fig. 240. Effect of fan blade placement angle on air cushion vehicle characteristics (G = 8000 kg; b_H = 10 m; b = 0.12 m; φ = 45°; ζ_k = 0.5; D_k = 2.2 m; [illegible] = 12; n = 742 rpm; [illegible] m/sec)

KEY: A -- kg/m²

B -- m³/sec

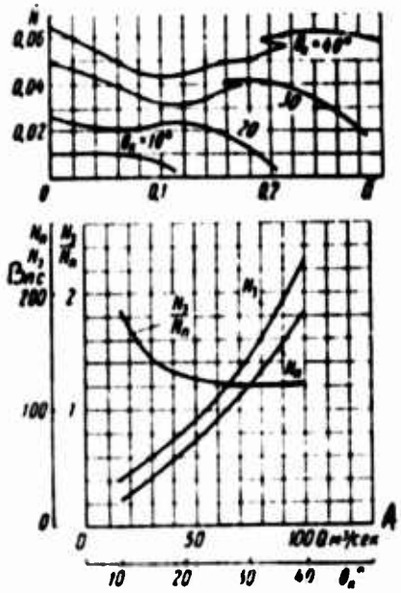

Fig. 241. Required and expended power as functions of air supplied to flow-through section of craft, determined by varying the angle of fan blade placement

KEY: A -- m³/sec

B -- hp

characteristics are plotted the lines determining the elevation of the craft above a support surface and the drag coefficient ζ_0 of the craft flow-through section corresponding to this elevation. Also given in these same coordinates are the dimensional characteristics of the axial K-06 fan for different angles of blade placement on an impeller with diameter D_k = 2.2 m and constant angular velocity n = 742 rpm.

If we assume that the working point on the characteristic for a fan with blade placement angle θ_k = 40° determines the design operating regime to which the elevation h = 0.2 m, air volume flow q_v = 100 m³/sec, and total pressure H = 150 kg/m² correspond, then the craft can be brought into this design regime advantageously as follows.

First, the fan blades are positioned by the angle $\theta_k = 0$ and the impellers driven to n = 742 rpm. Then, by increasing the angle θ_k, the craft is brought into the regime corresponding to the working point 1 at which the instant of craft liftoff from the support surface is reached. With further increase in the angle θ_k, the craft lifts off from the support surface and enters the free hovering regime. To attain the design hovering elevation, it is sufficient to bring the angle of fan blade placement to $\theta_k = 40°$. The variation in the fan operating regime is determined by the section 0-1-2 of the characteristic of the required pressures and volume flows. By this method of bringing the craft to the design hovering height, the presence in the fan characteristic of troughs and discontinuities ordinarily occurring for axial fans for large blade placement angles has no detrimental effect on fan operation.

Knowing the characteristic of the required pressures and volume flows of a craft as well as the characteristics of a fan with discontinuities for large angles θ_k, and varying the impeller diameter and its angular velocity, we can select a fan with impeller diameter and angular velocity for which bringing the craft to the design regime by varying the angle of blade placement can be carried out, bypassing the zone of unstable fan operation and thus not resorting to mounting antisurge devices on the fan.

Dimensionless characteristics of the power $\bar{N} = f(\bar{Q})$ required by the fan, and the dependence of the expended $N_э$ and required $N_п$ power and their ratio $N_э/N_п$ on the air volume flow Q corresponding to varying the fan operating regime while the blade placement angle θ_k on the fan wheel is changed, are shown in Fig. 241. As we can see, as the blade placement angle is reduced, leading to a corresponding drop in the craft elevation above the support surface, the ratio of expended power to required power rises. However, compared with the methods of regulation involving varying the fan angular velocity or throttling the stream in the craft flow-through section, the technique based on varying the blade placement angle is energetically most advantageous. This is because the fan operating regime varies approximately in the zone of H and Q values in which the maximum fan efficiencies lie for different blade placement angles (cf. Fig. 240).

60. Effect of Varying Craft Weight on Its Characteristics With Fan Operating

By using the characteristics of required pressures and volume flows of a craft and the aerodynamic characteristics of the fan installed on it, we can conveniently trace the variation in the craft aerodynamic parameters and craft elevation above a support surface when acted on by variation in craft weight (with additional cargo stowed or with a reduction in total craft weight as fuel is consumed).

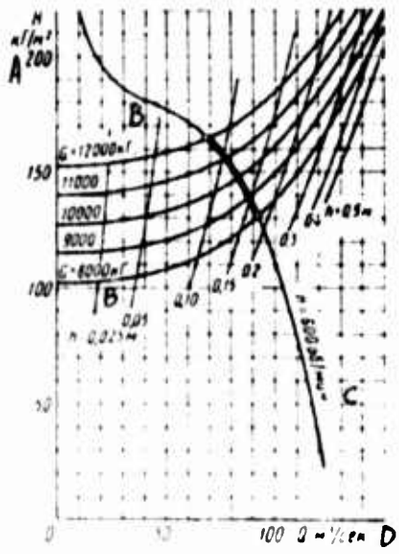

Fig. 242. Characteristics of air cushion vehicle (with fan operating) as a function of craft weight (D_H = 10 m; b = 1.1 m; φ = 30°; ζ_K = 0.5; D_K = 5 m)

Key: a -- kg/m²
b -- kg
c -- rpm
d -- m³/sec

Characteristics of required pressures and volume flows for a craft with specified geometrical parameters of the nozzle installation and flow-through section, for different craft weights, are given in Fig. 242, which also shows the sections of the network drag characteristic determining the craft elevation above a support surface. These characteristics were plotted by Eqs. (359), (358), and (354). Here also are given the characteristic of the K-06 axial fan for constant angular velocity of its impeller.

The fan operating regime in the flow-through section of a craft is determined by the point at which its characteristic intersects the characteristic of the required pressures and volume flows reflecting the characteristics of the network as well as the craft, therefore it is obvious that varying the aerodynamic parameters of the craft under the effect of

variation in craft weight will be defined by the section (shown with a bold line in Fig. 242) of the fan characteristic bounded by the corresponding characteristics of the required pressures and volume flows.

As we can see, as the craft weight is reduced, with constant fan rpm, the amount of air supplied into the flow-through section becomes greater, the total pressure built up by the fan in the network is reduced, and the craft hovering height above the support surface is correspondingly increased.

Thus, for a craft with weight G = 12,000 kg with a single-pass annular nozzle (diameter $D_н$ = 10 m), with exit width b = 0.12 m, and angle of generatrix inclination φ = 45°, at the craft elevation h = 0.085 m above a support surface, the fan supplies air into the flow-through section in the amount Q = 68 m^3/sec at the total pressure H = 165 kg/m^2. As the craft weight is reduced down to G = 8000 kg, the fan will feed air into the network -- at the same rpm -- in the amount Q = 92 m^3/sec at a total pressure H = 131 kg/m^2. The elevation of the craft here will go up to h = 0.175 m.

On inspecting the functions determining the effect that techniques of varying fan operating regime have on the aerodynamic and energy characteristics of air cushion vehicles, we can draw the following principal conclusions.

By varying the fan rpm, over a wide range we can modify the aerodynamic characteristics of an air cushion vehicle. When the fan characteristic shows a trough and discontinuities, bringing the craft into the free hovering regime always involves operating the fan in the surge regimes. As a result, impacts of the craft against the ground and unstable fan operation are possible along with pulsating aerodynamic loads on the fan impeller. Energetically, this method of regulation as applied to air cushion vehicles is uneconomical, but in several cases it can be markedly improved by using antisurge units with the fan.

The method of modifying air cushion vehicle characteristics by throttling the air stream in the craft flow-through section is marked by the simplicity of its design execution. However, it also has the same disadvantages as the method based on varying the fan rpm. Energetically, it is also disadvantageous since it involves the nonproductive outlay of power in overcoming the additional drag introduced by the throttle unit into the craft flow-through section.

Varying the fan operating regime by rotating its stator vanes does not provide extensive regulation of the aerodynamic parameters of air cushion vehicle. This is predetermined by the specific feature of the characteristic of required pressures and volume flows for an air cushion vehicle. The takeoff and landing of a craft when this method of regulation is used involves operating the fan in the surge regimes with all the resulting consequences. One advantage of this method is its marked

simplicity. Regulation characteristics can be improved by using two methods -- swiveling the fan stator vanes and varying the fan impeller rpm.

The method of varying the aerodynamic characteristics of an air cushion vehicle that relies on varying the blade placement angle on the fan impeller is most advantageous both aerodynamically and energetically. This method provides extensive regulation of the aerodynamic parameters in craft takeoff and landing and avoids the zones of unstable fan operation and the corresponding installation of antisurge units in the fan. Here the variation in the fan operating regime occurs in the region of high fan efficiencies. A marked drawback of this method of regulation is the complexity of the fan impeller design, since it must be provided with a device capable of rotating the impeller blades as the fan is operating.

Any given method of varying fan operating regimes for modifying the aerodynamic characteristics of an air cushion vehicle must be chosen based on specific requirements imposed on the craft under construction. Just as in any engineering solution, the method selected is a technical compromise.

Bibliography

1. Avdeyev, G. K., Lipinskiy, V. A., Lyubomirov, I. P., and Khanzhonkov, V. I., "Results of Full-Scale Tests of the Air Cushion Vessel 'Neva'," in: Aero-gidrodinamika Letatel'nykh Apparatov na Vozdushnoy Podushke, Trudy TsAGI (Aero-hydrodynamics of Air Cushion Vehicles, Transactions of the Central Aero-hydrodynamic Institute), No. 976, 1965.

2. Adamiuskiy, S. A., Transportnyye Mashiny na Vozdushnoy Podushke (Air Cushion Vehicles), Moscow, "Nauka", 1964.

3. Andryutin, V. I., Sirotina, G. N., and Zoroastrov, V. K., "Experimental Air Cushion Launch," in: Voprosy Teorii i Proyektirovaniya Korablya, Trudy GIVT (Problems of the Theory and Designing of Vessels, Transactions of the Gor'kiy Institute of Water Transportation Engineers), Moscow, "Vysshaya Shkola," 1969.

4. Benua, Yu. Yu., "Problems of the Propulsion of Air Cushion Vessels," Sudostroyeniye, No. 5, 1961.

5. Benua, Yu. Yu., and Korsakov, V. M., Suda na Vozdushnoy Podushke (Air Cushion Vessels), Moscow, Sudpromgiz, 1962.

6. Benua, Yu. Yu., D'yachenko, V. K., Kolyzayev, B. A., Litvinenko, V. A., Ozimov, I. V., and Smirnov, S. A., Osnovy Teorii Sudov na Vozdushnoy Podushke (Essentials of the Theory of Air Cushion Vessels), Leningrad, Sudostroyeniye, 1970.

7. Biryulin, A. P., "Results of an Experimental Study of the Static Stability of Air Cushion Vehicles," in: Aero-gidrodinamika Letatel'nykh Apparatov na Vozdushnoy Podushke, Trudy TsAGI, No. 689, 1963.

8. Bogdanov, A., "New Air Cushion Passenger Motor Ship," Rechnoy Transport, No. 6, 1964.

9. Brusilovskiy, I. V., "Fans With Meridional Stream Acceleration," in: Promyshlennaya Aerodinamika (Industrial Aerodynamics), No. 24, Oborongiz, Moscow, 1962.

10. Bykov, V. M., "Study of Transitional Processes of Nozzle Type Air Cushion Vehicles for Several External Perturbations," in: Aero-gidrodinamika Letatel'nykh Apparatov na Vozdushnoy Podushke, Trudy TsAGI, No. 976, 1965.

11. Bykov, V. M., "Effect of Restoring and Damping Moments, Moments of Inertia, and Flight Velocity on the Dynamic Stability of Air Cushion Vehicles," op. cit.

12. Vasilkevich, K. P., "Effect of Various Nozzle Installation Parameters on the Aerodynamic Properties of a Plane Air Cushion," ibid., No. 869, 1963.

13. Idem, "Equations of Motion of Air Cushion Vehicles," ibid., No. 976, 1965.

14. Vasilkevich, K. P., Biryulin, A. P., and Zharinova, G. D., "Attitude and Dynamic Characteristics of Forces and Moments of Air Cushion [illegible]," op. cit.

15. Vasilkevich, K. P., and Dolgopolov, A. A., "Efficiency of Monolateral and Bilateral Control of Air Cushion Vehicle Angle of Inclination," op. cit.

16. Vasilkevich, K. P., and Yegorova, L. I., "Control of Flight Vehicle Attitude by Varying the Parameters of the Nozzle Installation Producing the Air Cushion," op. cit.

17. Yegorov, L. A., Pakhter, I. Kh., and Fitterman, B. M., Avtomobili i Drugiye Transportnyye Sredstva na Vozdushnoy Podushke (Trucks and Other Vehicles Based on the Air Cushion), Moscow, TsINTIAM, 1963.

18. Yegorov, L. A., and Fitterman, B. M., "Foreign Air Cushion Vehicles," Avtomobil'naya Promyshlennost', No. 2, 1963.

19. Yegorov, L. A., and Mikhaylov, V. I., "Study of the Lift of a Model Air Cushion Vehicle, Using a Balance," Trudy NAMI (Transactions of the Scientific Research Institute of Motor Vehicles and Automotive Engines), No. 89, 1967.

20. Yegorov, L. A., and Shoyknet, B. M., "Results of Traction Tests of a Full-Scale Model of a Truck With Partial Unloading of Wheels With an Air Cushion," Trudy NAMI, No. 89, 1967.

21. Zharinov, K. V., "Forces and Moments Acting on a Chamber Type Air Cushion Vehicle When Moving Over a Shield," in: Aero-gidrodinamika Letatel'nykh Apparatov na Vozdushnoy Podushke, Trudy TsAGI, No. 976, 1965.

22. Zhukovskiy, N. Ye., "Reaction of Outflowing and Inflowing Fluid," (First Article)," Sobraniye Sochineniy (Collected Works), Vol. 3, Moscow-Leningrad, 1949.

23. Zhukovskiy, N. Ye., "Reaction of Outflowing and Inflowing Fluid, (Second Article)," op. cit.

24. Zhukovskiy, N. Ye., "Theory of Ships Driven by the Reaction Force of Outflowing Water," op. cit.

25. Zlobin, G. P., and Simonov, Yu. A., Suda na Vozdushnoy Podushke (Air Cushion Vessels), Leningrad, "Sudostroyeniye", 1971.

26. Zvonstrov, V. K., "Air Cushion Vessel 'Gor'kovchanin'," Sudostroyeniye, No. 6, 1969.

27. Klichko, V. V., "Hydrodynamic Drag of Air Cushion Vessels," op. cit., No. 5, 1965.

28. Kramer, V. V., and Tabachnikov, V. G., "Experimental Study of Restoring and Damping Moments of the Heeling and Pitching of a Model Air Cushion Vehicle," in: Aero-gidrodinamika Letatel'nykh Apparatov na Vozdushnoy Vodushke, Trudy TsAGI, No. 976, 1965.

29. Korytov, N. V., and Khalfin, M. Ya., "Calculation of the Power Characteristics of Air Cushion Vessels," Sudostroyeniye, No. 9, 1962.

30. Korytov, N. V., Suda i Apparaty na Vozdushnoy Podushke (Air Cushion Vessels and Vehicles), Voyenizdat, 1964.

31. Kocheulov, V. P., and Mikhaylov, V. V., "New Ways of Using the Air Cushion," Avtomobil'nyy Transport, No. 6, 1964.

32. Kurzon, A. G., Grechin, M. A., and Mezheritskiy, A. D., "Capacity of the Power Plants of Air Cushion Vehicles," Sudostroyeniye, No. 9, 1963.

33. Lokshin, I. L., and Solomakhova, T. S., "Centrifugal Fans With Radial Diffusors for Air Cushion Vehicles," in: Aero-gidrodinamika Letatel'nykh Apparatov na Vozdushnoy Podushke, Trudy TsAGI, No. 976, 1965.

34. Lysyakov, A. G., "Pneumatic Devices for Moving Freight," Mekhanizatsiya i Avtomatizatsiya Proizvodstva, No. 5, 1967.

35. Lyubomirov, I. P., Zharinov, K. V., and Petukhov, V. P., "Forces and Moments Acting on Air Cushion Vehicles During Hovering Above a Water Surface," in: Aero-gidrodinamika Letatel'nykh Apparatov na Vozdushnoy Podushke, Trudy TsAGI, No. 889, 1963.

36. Mikahylov, V. V., "Aerodynamic Characteristics of a Chamber-Nozzle Installation for a Truck With Partial Relieving of the Propulsor With an Air Cushion," Trudy NAMI (Proceedings of the Central Scientific Research Institute of Motor Vehicles and Automotive Engines), No. 89, 1967.

37. Nikolayev, N. I., Letayushchiy Vezdekhod (Flying All-Terrain Vehicle), Voyenizdat, Moscow, 1963.

38. Kuznitskiy, Ye. I., Vozdushnyye Vezdekhody (Airborne All-Terrain Vehicles), Moscow, Mashinostroyeniye, 1964.

39. Pyshnov, V. S., "On an Air Cushion," Aviatsiya i Kosmonavtika, No. 2, 1962.

40. Sirota, V., Vozdushnyye Vezdekhody (Airborne All-Terrain Vehicles), Moscow, MOSAAF, 1967.

41. Stepankov, G. Yu., Gidrodinamicheskaya Teoriya Apparatov na Vozdushnoy Podushke (Hydrodynamic Theory of Air Cushion Vehicles), Moscow, Mashgiz, 1963.

42. Stepanov, G. Yu., "Hydrodynamic Calculation of the Jet Curtain Above a Water Surface," Sudostroyeniye, No. 9, 1965.

43. Stepanov, G. Yu., and Arutyunyan, D. B., "Calculation of Air Cushion Vehicles With Partial Unloading," Avtomobil'naya Promyshlennost', No. 9, 1965.

44. Tabachnikov, V. G., "Study of the Moments of Models of Vertical Tail Assemblies for Air Cushion Vehicles," in: Aero-gidrodinamika Letatel'nykh Apparatov na Vozdushnoy Podushke, Trudy TsAGI, No. 889, 1963.

45. Tabachnikov, V. G., and Fingel', A. E., "Operation of the Axial Fan for Jet [illegible] an Arriving Stream," Ibid., No. 976, 1965.

46. Tikhomirov, G. V., "Trends in the Development of Trucks with Partial Relieving of the Propulsor With an Air Cushion," Trudy NAMI, No. 89, 1967.

47. Khanzhonkov, Ye. I., "Streaming of an Annular Jet Over a Shield," in: Promyshlennaya Aerodinamika (Industrial Aerodynamics), No. 23, Moscow, Oborongiz, 1962.

48. Idem., "Life of Air Cushion Vehicles in the Hovering Regime," Sudostroyeniye, No. 12, 1963.

49. Idem., "Aerodynamic and Power Characteristics of Air Cushion Vehicles With Nozzle Installation," in: Aero-gidrodinamika Letatel'nykh Apparatov na Vozdushnoy Podushke, Trudy TsAGI, No. 889, 1963.

50. Idem., "Aerodynamic Characteristics of a Double-Pass Nozzle for Air Cushion Vehicles," in: Aerogidrodinamika Letatel'nykh Apparatov na Vozdushnoy Podushke, Trudy TsAGI, No. 889, 1963.

51. Idem., "Theoretical and Experimental Characteristics of Nozzle Installations in Air Cushion Vehicles," ibid., No. 976, 1965.

52. Idem., "Effect of Planform Shape of Nozzle Installation on the Lift of an Air Cushion Vehicle," ibid., No. 976, 1965.

53. Idem., "Aerodynamic Characteristics of Annular Jets Streaming Over a Shield," in: Promyshlennaya Aerodinamika, No. 27, Moscow, Mashinostroyeniye, 1966.

54. Idem., "Design Parameters of Air Cushion Vehicles With Nozzle Installations, in the Hovering Regime," Rechnoy Transport, No. 6, 1966.

55. Khesin, M. A., and Ginzburg, V. I., Transportnyye Sredstva na Vozdushnoy Podushke, Obzor Inostrannykh Izobreteniy (Air Cushion Transport Vehicles, Review of Foreign Inventions), Moscow, TsNIIPI, 1965.

56. Tsel'nik, D. S., "Theory of Jet Curtain," Trudy MIIT (Transactions of the Moscow Institute of Railroad Transportation Engineers), No. 222, 1965.

57. Idem., "On One Model of a Jet Curtain," Izvestiya AN SSSR, Mekhanika Zhidkosti i Gaza, No. 1, 1966.

58. Tsiolkovskiy, K. E., Soprotivleniye Vozdukha i Skoryy Poyezd (Drag of Air and a High-Speed Train), Kaluga, 1927.

59. Shaydakov, V. I., "Aerodynamic Study of the 'Ducted Propeller' System in the Hovering Regime," in: Issledovaniye v Oblasti Teoreticheskoy i Prikladnoy Aerodinamiki (Research in Theoretical and Applied Aerodynamics), Oborongiz, 1959, (Trudy MAI (Transactions of the Moscow Aviation Institute imeni Sergo Ordzhonikidze), No. 111).

60. Shoykhet, B. M., Yegorov, L. A., and Fitterman, B. M., "Results of a Study of a Full-Scale Model of a Truck With Partial Relieving of Wheels With an Air Cushion," Avtomobil'naya Promyshlennost', No. 11, 1965.

61. Shoykhet, B. M., and Yegorov, L. A., Avtomobili Amfibii za Rubezhom (Amphibious Motor Vehicles Abroad), NIINAvtosel'khozmash, Moscow, 1966.

62. Shoykhet, B. M., "Aerodynamic Tests of the Flow-Through Section of a Full-Scale Model of a Truck With Partial Relieving of the Wheels With An Air Cushion," Trudy NAMI, No. 89, 1967.

63. Berg, S., " 'URBA-4': Moteur Lineaire et Coussin Dair Negatif," Air et Cosmos, March 1968, No. 238.

64. Terence, Ford C., "Air Cushion Monorail Development," Hovering Craft and Hydrofoil, June 1968, Vol. 7, No. 9, pp. 16-21.

65. "Commuting by Overhead URBA Train," Air Cushion Vehicles, February 1969, Vol. 80, pp. 15-19.

66. Marination, M. C., Rechou, I., and Watson, P., "URBA in Business: Some Commercial Aspects of a Suction-Suspended Urban Transport System," Hovering Craft and Hydrofoil, May 1968, Vol. 8, No. 8, pp. 37-46.

67. Boehler, J. D., "Remarks on the Ground-Effect Machine," American Helicopter Society Fifth Annual Western Forum, 25-26 September 1958.

68. Idem., "Aerodynamic Theory of the Annular Jet," IAS Reports, No. 59-77, 28-29 January 1959.

69. Brooks, E. W., "Ground Cushion Research at the David Taylor Model Basin -- A Brief Summary of Progress to Date and a Preliminary Design Technique for Annual Jet GEM's," Symposium on Ground Effect Phenomenon, 21-23 October 1959.

70. Stanton, Jones M., "Some Design Problems of Hovercraft," IAS Paper, No. 61-4, 24-25 January 1961.

71. Stanton, Jones M., "Hovercraft -- Some Design Problems," Aerospace Engineering, Vol. 20, No. 2, February 1961, pp. 16 and 49-57.

72. Turner, M. T., "A Power Plant Man's Look at the Ground Effect Machine," Journal of the American Helicopter Society, Vol. 4, No. 3, July 1959, pp. 4-8.

73. Crewe, P. R., and Eggington, W. J., "The Hovercraft -- a New Concept in Maritime Transport," Quarterly Transactions of the Royal Institution of Naval Architects, Vol. 102, No. 3, July 1960, pp. 315-365.

74. Jaumotte, A., and Kiedrzynski, A., "Theory and Experiments on Air Cushion Vehicles at Zero Speed," Hovering Craft and Hydrofoil, August 1965, Vol. 4, No. 11.

75. Strand, T., "150-Knot GEM Cruise," Aerospace Engineering, April 1962, Vol. 21, No. 4, pp. 38-44.

76. Strand, T., Royce, W. W., and Fujita, T., "Cruise Performance of Channel-Flow Ground-Effect Machines," Journal of the Aerospace Sciences, June 1962, Vol. 29, No. 6.

77. Mair, W. A., "The Physical Principles of Hovercraft," Journal of the Royal Aeronautical Society, October 1964, Vol. 68, No. 646, pp. 683-690.

78. Walker, N. K., "Influence of Fan and Ducting Characteristics of the Stability of Ground Effect Machines," Journal of Aircraft, January-February 1965, Vol. 2, No. 1, pp. 25-32.

79. Alexander, A. J., "The Momentum Equation -- for a Static Hovercraft at Zero Incidence," Journal of the Royal Aeronautical Society, Vol. 70, No. 662, February 1966.

80. Strand, T., "Inviscid-Incompressible-Flow Theory of Static Peripheral Jets in Proximity to the Ground," Journal of the Aerospace Sciences, Vol. 28, No. 1, January 1961.

81. Idem., "Inviscid-Incompressible-Flow Theory of Static Two-Dimensional Solid Jets in Proximity to the Ground," Journal of the Aerospace Sciences, Vol. 29, No. 2, February 1962.

82. Ehrich, F. F., "The Curtain Jet," ibid., Vol. 28, No. 11, November 1961, pp. 859-860, 871.

83. Cohen, M. J., "Peripheral Jets in Proximity of the Ground," Journal of Applied Mechanics, Transactions of the ASME, Vol. 33, No. 4, Series E, December 1966, pp. 721-727.

84. Roche, J. T. D., "The Peripheral Jet Theory," Applied Mechanics Proceedings of the Eleventh International Congress of Applied Mechanics, Munich (Germany), 1964, Berlin and others, 1966, pp. 684-695.

85. Frost, J. C. M., "The Canadian Contribution to the Ground Cushion Story," Canadian Aeronautical Journal, Vol. 7, No. 8, October 1961, pp. 286-302.